

**XXIII INTERNATIONAL CONFERENCE ON
“MATERIAL HANDLING, CONSTRUCTIONS AND LOGISTICS”**

September 18th - 20th, 2019

MHCL 2019

**edited by
Georg Kartnig, Nenad Zrnić and Srđan Bošnjak**

**VIENNA UNIVERSITY OF TECHNOLOGY (TU WIEN)
Institute for Engineering Design and Product Development**

together with

**UNIVERSITY OF BELGRADE
Faculty of Mechanical Engineering**

VIENNA, AUSTRIA, 2019



TECHNISCHE
UNIVERSITÄT
WIEN
Vienna University of Technology



UNIVERSITY OF
BELGRADE
Faculty of Mechanical
Engineering

**XXIII INTERNATIONAL CONFERENCE ON
"MATERIAL HANDLING, CONSTRUCTIONS AND LOGISTICS"**

September 18th – 20th, 2019

MHCL 2019

Edited by

Georg Kartnig, Nenad Zrnić and Srđan Bošnjak

**VIENNA UNIVERSITY OF TECHNOLOGY (TU WIEN)
Institute for Engineering Design and Product Development**

together with

**UNIVERSITY OF BELGRADE
Faculty of Mechanical Engineering**

VIENNA, AUSTRIA, 2019

INTERNATIONAL SCIENTIFIC COMMITTEE

Co-Chairmen:

Prof. Dr. Georg Kartnig, Vienna University of Technology, Austria
Prof. Dr. Nenad Zrnić, University of Belgrade, Serbia
Prof. Dr. Srđan Bošnjak, University of Belgrade, Serbia

Members of Scientific Committee:

Prof. Dr. Bogdevicius Marijonas, Vilnius Gediminas Technical University, Lithuania
Prof. Dr. Bojić Sanja, University of Novi Sad, Serbia
Prof. Dr. Bošnjak Srđan, University of Belgrade, Serbia
Prof. Dr. Ceccarelli Marco, University of Cassino, Italy
Prof. Dr. Chondros Thomas, University of Patras, Greece
Prof. Dr. Clausen Uwe, TU Dortmund, Fraunhofer Institute for Material Flow and Logistic, Germany
Prof. Dr. Čuprić Nenad, University of Belgrade, Serbia
Prof. Dr. Czmochowski Jerzy, Wrocław University of Science and Technology, Poland
Prof. Dr. Dentsoras Argiris, University of Patras, Greece
Prof. Dr. Dragović Branislav, University of Montenegro, Kotor, Montenegro
Prof. Dr. Dukić Goran, University of Zagreb, Zagreb, Croatia
Prof. Dr. Edl Milan, University of West Bohemia, Plzen, Czech Republic
Prof. Dr. Ekren Banu, Yaşar University, Turkey
Prof. Dr. Fottner Johannes, Technische Universität München, Germany
Prof. Dr. Furmans Kai, Karlsruhe Institute of Technology, Germany
Prof. Dr. Gašić Milomir, University of Kragujevac, Kraljevo, Serbia
Prof. Dr. Gašić Vlada, University of Belgrade, Serbia
Prof. Dr. Georgiev Martin, Technical University Sofia, Bulgaria
Prof. Dr. Georgijević Milosav, University of Novi Sad, Serbia
Prof. Dr. Gerhard Detlef, Vienna University of Technology, Austria
Prof. Dr. Golder Markus, Technischen Universität Chemnitz, Germany
Prof. Dr. Guenther Wilibald, TU Munich, Germany
Prof. Dr. Illes Bela, University of Miskolc, Hungary
Prof. Dr. Jančevski Janko, Ss. Cyril and Methodius University Skopje, Republic of Macedonia
Prof. Dr. Jerman Boris, University of Ljubljana, Slovenia
Prof. Dr. Jovanović Miomir, University of Niš, Serbia
Prof. Dr. Kartnig Georg, Vienna University of Technology, Austria
Prof. Dr. Katterfeld Andre, Otto-von-Guericke-Universität Magdeburg, Germany
Prof. Dr. Kessler Franz, Montan University of Leoben, Austria
Prof. Dr. Kosanić Nenad, University of Belgrade, Serbia
Prof. Dr. Kreutzfeldt Jochen, Technische Universität Hamburg, Germany
Prof. Dr. Lerher Tone, University of Maribor, Slovenia
Prof. Dr. Markusik Sylwester, Silesian University of Technology, Gliwice, Poland
Prof. Dr. Mitrović Radivoje, University of Belgrade, Serbia
Prof. Dr. Ognjanović Milosav, University of Belgrade, Serbia
Prof. Dr. Oguamanam C.D. Donatus, Ryerson University Toronto, Ontario, Canada
Prof. Dr. Overmeyer Ludger, Leibniz University Hannover, Germany
Prof. Dr. Park Nam Kyu, Tongmyong Univ. of Information Technology, Busan, South Korea
Prof. Dr. Popović Vladimir, University of Belgrade, Serbia
Prof. Dr. Potrč Iztok, University of Maribor, Slovenia
Prof. Dr. Rakin Marko, University of Belgrade, Serbia
Prof. Dr. Rosi Bojan, University of Maribor, Slovenia
Prof. Dr. Rogić Miroslav, University of Banja Luka, Republic of Srpska, Bosnia and Herzegovina
Prof. Dr. Rusinski Eugeniusz, Wrocław University of Science and Technology, Poland
Prof. Dr. Sari Zaki, University of Tlemcen, Algeria
Prof. Dr. Savković Mile, University of Kragujevac, Serbia
Prof. Dr. Sawodny Oliver, University of Stuttgart, Germany
Prof. Dr. Schmidt Thorsten, Dresden University of Technology, Germany
Prof. Dr. Schott Dingena, Delft University of Technology, The Netherlands
Prof. Dr. Sihn Wilfried, Vienna University of Technology, Fraunhofer Austria, Austria
Prof. Dr. Singhose William, Georgia Institute of Technology, Atlanta, USA
Prof. Dr. Solazzi Luigi, University of Brescia, Italy
Prof. Dr. ten Hompel Michael, TU Dortmund, Fraunhofer Institute for Material Flow and Logistic, Germany

Prof. Dr. Vidović Milorad, University of Belgrade, Serbia
Prof. Dr. Wehking Karl-Heinz, University of Stuttgart, Germany
Prof. Dr. Weigand Michael, Vienna University of Technology, Austria
Prof. Dr. Wimmer Wolfgang, Vienna University of Technology, Austria
Prof. Dr. Wypych Peter, University of Wollongong, Australia
Prof. Dr. Zrnić Nenad, University of Belgrade, Serbia

President of Honorary Scientific Committee and Conference Founder:

Prof. Dr. Đorđe Zrnić, University of Belgrade, Serbia

Members of Honorary Scientific Committee:

Prof. Dr. Babin Nikola, University of Novi Sad, Serbia
Prof. Dr. Hoffmann Klaus, Vienna University of Technology, Austria
Prof. Dr. Mijajlović Radić, University of Niš, Serbia
Prof. Dr. Oser Joerg, Graz University of Technology, Austria
Prof. Dr. Ostrić Davor, University of Belgrade, Serbia
Prof. Dr. Petković Zoran, University of Belgrade, Serbia
Prof. Dr. Severin Dietrich, Technical University of Berlin, Germany
Prof. Dr. Zrnić Đorđe, University of Belgrade, Serbia

ORGANIZING COMMITTEE

Presidents of the Organizing Committee:

Prof. Dr. Georg Kartnig, Vienna University of Technology, Austria
Prof. Dr. Nenad Zrnić, University of Belgrade, Serbia

Vice President of the Organizing Committee:

Prof. Dr. Branislav Dragović, University of Montenegro, Montenegro

Members of Organizing Committee:

Assoc. Prof. Dr. Gašić Vlada, University of Belgrade, Serbia
Ass. Prof. Dr. Gnjatović Nebojša, University of Belgrade, Serbia
Grano Alice, Vienna University of Technology, Austria
Milojević Goran, University of Belgrade, Serbia
Đorđević Miloš, University of Belgrade, Serbia
Milenović Ivan, University of Belgrade, Serbia
Stefanović Aleksandar, University of Belgrade, Serbia
Urošević Marko, University of Belgrade, Serbia
Arsić Aleksandra, University of Belgrade, Serbia
Stanković Vlada, University of Belgrade, Serbia

Reviewers:

Prof. Dr. Dragović Branislav, Montenegro
Assoc. Prof. Dr. Gašić Vlada, Serbia
Ass. Prof. Dr. Gnjatović Nebojša, Serbia
Prof. Dr. Jerman Boris, Slovenia
Prof. Dr. Kartnig Georg, Austria
Prof. Dr. Lerher Tone, Slovenia
Prof. Dr. Zrnić Nenad, Serbia

Publisher:

University of Belgrade, Faculty of Mechanical Engineering

Printout:

SaTCIP d.o.o., Vrnjačka Banja, Serbia

CIRCULATION: 100 copies

ISBN 978-86-6060-020-4

PREFACE

The International Conference on Material Handling, Constructions and Logistics – MHCL is the 23rd event of a series that has been started just 43 years ago, in 1976 by Professor Dr. Đorđe Zrnić. Up to now the Conference gathered together scientists and researchers from all republics (now independent states) of former Yugoslavia (Serbia, Montenegro, Croatia, Slovenia, Bosnia and Herzegovina, and Republic of North Macedonia), as well as from Algeria, Australia, Austria, Bulgaria, China, Croatia, Denmark, Germany, Greece, Hungary, Italy, Japan, Lithuania, Montenegro, Poland, Republic of Korea, Romania, Russia, Slovakia, Switzerland, The Netherlands, Turkey, USA and Vietnam working in the field of Material and Mechanical Handling, Constructions and Construction Machinery, as well as Transport Logistics. Since 2012 MHCL is jointly organized by the University of Belgrade (Faculty of Mechanical Engineering) and Vienna University of Technology (Institute for Engineering Design and Product Development).

The aim of the Conference is to be a forum to exchange views, opinions and experience on MHCL from technical viewpoints in order to track the current achievements, but also to look at to future developments. Most of the authors of contributed papers are experts in MHCL and related topics. Also, one of the main goals of the Conference is to make the scientific/research exchange between similar academic Departments and Institutes from different countries, as well as individual researcher in the field, in order for possible cooperation in applying for international programs or bilateral research and scientific projects.

This year the International Conference MHCL 2019 is held in Vienna at the Vienna University of Technology (Institute for Engineering Design and Product Development) from September 18th - 20th. The Proceedings contain 48 submitted peer-reviewed papers by authors from 13 countries (authors' countries are listed according to the alphabetical order): Austria, China, Croatia, Egypt, Germany, Greece, Italy, Japan, Montenegro, Poland, Serbia, Slovenia and The Netherlands.

The papers are grouped into three sessions A, B and C:

Session A: Hoisting and Conveying Equipment and Technologies - 15 papers

Session B: Constructions, Design Engineering, Mining Equipment and Technologies - 14 papers

Session C: Logistics and Intralogistics Systems - 19 papers

Proceedings also contain 4 invited papers presented in the Plenary Session, from respective professors and scientific and research leaders from German and Slovenian Universities. The invited lectures reflect the wide spectrum of important topics of current interest in MHCL. These Proceedings can also be considered as a kind of handbook on MHCL, and can be inspiring for researchers, graduate students and engineers specializing or addressing attention to MHCL. We truly believe that a reader will take advantage of the papers in these Proceedings with further satisfaction and motivation for her or his work.

We would like to express our sincere thanks to all members of the Scientific and Organizing Committee, Sessions chairmen and reviewers, as well as to all participants including invited speakers for coming in Vienna to present their papers. On this occasion, we are particularly indebted to all people who rendered their help for the preparation of the Conference and publication of the Proceedings.

We are grateful to the authors of the articles for their valuable contributions and for preparing their manuscripts and presentations in time.

Vienna, Austria, September 2019

Editors

Georg Kartnig, Nenad Zrnić and Srđan Bošnjak

DISTINGUISHED PERSON IN THE HISTORY OF THE MHCL CONFERENCE

Prof. Đorđe N. Zrnić, MHCL conference founder in 1976



ZRNIĆ, N. ĐORĐE, full member of the Academy of Engineering Sciences of Serbia (member of Euro-Case), since 2000., was born in Belgrade in 1934. He finished high school and graduated (Dipl.-Ing.), from Faculty of Mechanical Engineering, University of Belgrade 1959. After he was employed in "Serbia - project". Assistant on the FME-UB in decembar 1960, full professor 1982. He received his Dr Sc. at FME-UB. He was the Head of Department of Mechanization (1988 - 1999) and Dean of Faculty (1994 - 1997). Member of the Scientific Society of Serbia since 1996. He is married, wife Ljiljana, son Nenad.

Teaching activity. He lectured Plant Layout Design, Material Handling Systems Design, Optimization Methods in Design. He was supervisor of number of Magister Sc. and eight PhD dissertations. Invited speaker at the Universities in: England, France, Germany, Hungary and Sweden. He was a member of IFAC, IIE, ICAW, since 1980 on invitation, at the Europäische Konferenz der Professoren für Fördertechnik.

Scientific and research activity encompass the development of the theory and practice of designing transport and warehouses systems. He published 177 professional and scientific papers, 82 of them were in international publications and chapters in the monograph, PERGAMON Elsevier Sc 1997 and 1999. He set the theoretical basis of design of storage Large Scale System. He developed a method Total Performance Design, for modeling these systems, and applied it in practice. The work, based on the application of the TPD method presented to IFORS 2002, Edingburgh (Invited section), was one of the 6 awarded works. The results were presented in monograph Manufacturing Systems: Modeling, Management and Control, Ed. P. Kopacek, PERGAMON, Elsevier Sc. 1997. He wrote 10 books, (4 first co-author, total 20 ed.). Book Design of Foundries, total 6 ed. entered in the world bibliography of foundries. In 2016, he published the book Plant layout and Technical Logistics. He received the Annual prize from Belgrade Chamb. of Com. in 1989, for the best technical improvement in the economy, for the project "Central Plant for the Maintenance of the Energy System of Belgrade" (loc. New Belgrade).

Engineering activity. He has designed 93 projects, out of which 59 have been realized in the country and abroad. He designed a series of complex, original material handling machines (especially harbor cranes) in the country and in land (Burma, Indonesia, Bangladesh. Tanzania). All these devices have been manufactured at the "GOSA" Plant, Smederevska Palanka, most of them are innovative.

Innovations: Design of the boogie for motion of harbor cranes (7t /30.5m and 20t /30.5m), on curvilinear rails is an original solution. Construction for boom's outreach changing and level luffing with a rope in the counterweight in the column, for the crane 7t/30,5m, is an original solution. Construction of underwater sweepers with removable knives for TISA excavator (patent), projects sandblasting plants HC-2000 and SHELL-MOULDING for foundry Belgrade. Projects of the Terminal for unloading of barges and transport to the Steel Works, Automatic loading plant for two wagons, capacity of 50 t, Winches for Liesen, Duisburg, Foundries for Burma and Indonesia, Lines for assembling agricultural trailers for Russia, etc. He led the scientific project "Investigation of Contemporary Methods for Designing Complex Systems and Structures in Mechanization" (1996-2000).

CO-PRESIDENT OF THE ORGANIZING COMMITTEE



Univ.-Prof. Dipl.-Ing. Dr. techn. Georg Kartnig was born 1964 in Graz (Austria), where he attended the Akademisches Gymnasium and then the degree programme Mechanical Engineering and Business Economics at the Graz University of Technology. After his graduation in 1989, he worked as an university assistant at the Institute for Machine Elements and Conveying Systems.

In his dissertation, he dealt with the dynamic behavior and positioning precision of Automated Storage and Retrieval Systems (AS/RS). The rigorosum took place in 1993, after which Prof. Kartnig stayed at the institute in order to work on his habilitation dealing with the dynamic behaviour and the throughput optimisation of carousel storage systems. Between 1997 and 1998, he was Department Head of "Machine

Development" at the company KNAPP Logistik Automation. After completing his habilitation in 1998, he returned to the TU Graz as an extraordinary professor. After Prof. Oser retired in 2008, he became Interim Head of the Institute of Technical Logistics at TU Graz. In the same year, he applied for a professorship at the Institute of Engineering Design and Logistics Engineering at the TU Vienna. In 2009, he took over the professorship at this institute and has been in charge of the research area Engineering Design, Material Handling and Ecodesign since then.

Prof. Kartnig's teaching activities cover the areas of fundamentals of engineering design, advanced engineering design, product development, materials handling and technical logistics. In these subjects, he gives lectures and supervises construction exercises and project papers. In addition, he has been involved in the lecture series "Technology and Society" for five years, in which he deals with the topics of technology and ethics as well as the responsibility of engineers. So far, Prof. Kartnig has supervised 83 diploma theses (18 more are in progress) and 5 dissertations (3 more are in progress).

His research activities focus on the calculation of the handling performance of shuttle systems, the modelling and optimisation of the dynamic behaviour of cable cars, the investigation of friction, slip and wear behaviour of wheel-rail systems of bridge and portal cranes as well as the simulation of cohesive and non-cohesive bulk-material simulation. In addition, the development of new products as well as the improvement of existing products play an important role in his research area. In these and other research fields, Prof. Kartnig has led about 30 large-scale projects, many of them funded by the Austrian Research Promotion Agency (FFG).

He published 41 contributions in international journals or conference proceedings (8 of them on the SCI list with IF) and presented 22 lectures at international conferences.

Prof. Kartnig is Chairman of the Standards Committee for Cranes and Hoists of the Austrian Standard Institute. Moreover, he is a member of the Scientific Society for Technical Logistics and of the European Conference of Materials Handling Professors. Since 2012, he has been co-organiser of the MHCL, which was held at the TU Vienna for the first time in 2015.

CO-PRESIDENT OF THE ORGANIZING COMMITTEE



Prof. Dr.-Ing. Nenad Đ. Zrnić was born in 1966 in Belgrade. He graduated from the University of Belgrade - Faculty of Mechanical Engineering (UB FME) in 1992. In 2005 he was elected Assistant Professor at the Faculty of Mechanical Engineering, in 2009 Associate Professor and in 2013 full - tenured professor and head of the Laboratory for logistics/intralogistics and eco-design. He is Corresponding member of the Academy of Engineering Sciences of Serbia since 2015. Since 1st October 2018 he is Vice Rector of the University of Belgrade for international relations, interuniversity cooperation, innovations and technology transfer.

In the period 2012-2015 he was Vice Dean for Academic Affairs at the UB FME and ECTS coordinator, 2015-2018 Vice Dean for International Cooperation and member of HERE (Higher Education Reform Experts) team. He was the president of the Executive Board

of the Association of Mechanical Engineers of Serbia. He is chairman of the Organizing and Scientific Committees of international conferences: MHCL 2006, 2009, 2012 and 2017, held in Belgrade, as well as MHCL in 2015, held in Vienna in cooperation with TU Wien. He is technical expert in Eureka Eurostars program and evaluator of projects H2020 FET OPEN RIA and INNOWWIDE.

Until now he was a supervisor of over 100 MSc and Dipl-Ing. theses, 4 PhD dissertations and currently he is a supervisor of 3 ongoing PhD dissertations. He was a visiting professor at the University of Montenegro – Maritime Faculty in Kotor (2009-2011 and since 2016). He is the author of 2 university textbooks and 2 research monographs (1 in English). He is reviewer in 19 SCI journals and member of editorial board in 5 international journals.

He has excellent multi-year scientific cooperation with the TU Vienna (Institute for engineering design and technical logistics) where he spent a total of 8 months as a visiting researcher. He is a member of several international scientific societies and their bodies: Europäischen Konferenz der Professoren des Fachkreises Foerdertechnik, IFToMM Technical Committee for Transportation Machinery, IFToMM Permanent Commission for History of Mechanism and Machine Science. He was an invited lecturer at foreign universities in Italy - Brescia in 2011 and Greece - Patras, 2013 and at the CEMAT Port Forum in Hannover in 2014.

His scientific research work involves intralogistics and logistics systems, dynamics, strength, integrity and redesign of material handling, conveying and mining machines, eco-design and sustainable logistics, LCA analysis. Among the others he has published 9 chapters in books published by the world's leading publishers (Kluwer, Springer, Wiley, SPH) and 24 papers in international journals on the SCI list with IF. He presented 7 invited plenary papers at international conferences. According to data from Scopus he has got a total of 471 citations, h-index 13, out of which 281 are straight quotes, h-index 10.

He is author of 7 technical and development solutions for industrial purposes, he managed and participated in the realization of 36 projects performed for the purpose of industry, 132 elaborations of as-built design, as well as 26 studies of limited circulation and expertise. He participated in the implementation of 9 projects financed by Serbian Ministry of education, science and technological development, as well as in 13 international projects (1 is FP7 project NEWS, and in international tender he was chosen as the executor of the work package for Serbia WP3 Census of logistic and multimodal platforms in Serbia within the project WATERMODE - Transnational Network for the Promotion of the Water-Ground Multimodal Transport) in 6 among them he was a project manager (since 2017 he is project coordinator of Erasmus+ CBHE project DualEdu), He was an external expert for FP7 project Spider Plus (2013-2015). For the results of his engineering work, he was awarded with a group of authors for the Annual prize of Belgrade Chamber of Commerce for the best technical innovation in 2009.

ABOUT THE MHCL CONFERENCE ORGANIZERS

Vienna University of Technology looks back on a long tradition at the leading edge of scientific research and education: Founded in 1815 as Polytechnisches Institut (Imperial and Royal Polytechnical Institute), it was divided into 5 faculties in 1865. One year later the first freely elected rector was inaugurated. In 1872 its name changed to Technische Hochschule (College of Technology), and in 1902 the first doctorates were awarded. The institution has borne its current name – Technische Universität Wien (Vienna University of Technology) – since 1975. At the Institute for Engineering Design and Product Development the research group Engineering Design for Material Handling and Conveying Systems (Konstruktionslehre und Fördertechnik) is engaged with design principles in mechanical engineering and with material handling as technical as well as logistical tasks. Further key aspects of activities are: rail vehicles, ropeways and supporting structures.

The University of Belgrade is the oldest and largest University in Serbia. Technical Faculty at University of Belgrade was established in 1863, and the first subject in the field of Mechanical Engineering (“Mechanics and Science of Machines”) in 1873. First subject as a forerunner of the Department of Material Handling, Constructions and Logistics (Department of Mechanization) was “Construction Machinery” established in 1897. Starting from 1907 some chapters on hoist machinery (cranes) have been lectured at the academic level. The Department of Construction Machinery and Facilities Layout was established in 1932. In 1948 was established the Department of Industrial Mechanical Engineering, renamed in 1959 to Department of Mechanization (Material Handling and Design Engineering). Up to now the members of Department of Mechanization published several hundred scientific papers in journals, books, and conference proceedings. The Department has an intensive cooperation with industry. That resulted in numerous projects and developed, designed and constructed series of complex, original and modern transporting and construction machines, devices, and systems in the country (former Yugoslavia) and abroad (Burma, Indonesia, Bangladesh, Germany, Russia, Tanzania, Greece and Azerbaijan – former USSR). All these devices have been constructed and functioning for years now and many of them are innovative.

ORGANIZED BY



**TECHNISCHE
UNIVERSITÄT
WIEN**
Vienna University of Technology



**UNIVERSITY OF
BELGRADE**
Faculty of Mechanical
Engineering

SPONSORED BY



LTW INTRALOGISTICS GMBH, AUSTRIA



**SERBIAN MINISTRY OF EDUCATION, SCIENCE AND
TECHNOLOGICAL DEVELOPMENT**



ACADEMY OF ENGINEERING SCIENCES OF SERBIA

IN MEMORIAM



1949 - 2019

Eugeniusz Rusiński graduated in 1975 with a Master of Engineering Degree in Mechanics and Machine Design from the Mechanical Faculty of Wrocław University of Technology. In 1980 he was awarded the Doctor of Science degree. In 1990, the Board of the Mechanical Faculty of Wrocław University of Technology awarded him the degree of Habilitated Doctor of Technical Sciences in machine construction and operation, specializing in theory of machines and mechanisms. In 1993, he was promoted to the position of Associate Professor, and in 1996 awarded with the title of Professor of Technical Sciences (Full Professor). From 1994 he was head of the Department of Computer-Aided Design (CAD) functioning today as the Department of Machine Design and Research of Wrocław University of Science Technology. From 1995 to 1998 deputy head of of the Institute of Machine Design and Operation , 2000-2005 Head of the Institute of Machine Design and Operation, Dean of the Mechanical Faculty (2005-2008) and Vice-Rector for Research and Cooperation with Industry at Wrocław University of Science and Technology (2008-2016). He was author of numerous scientific publications, patents and implemented technical achievements. He developed experience in Poland and abroad including, among others, in Germany, Serbia, USA, India, Austria and Cuba

CONTENTS

PLENARY SESSION – INVITED PAPERS

Katterfeld A., Richter C., Kamps R. FUNCTIONAL ANALYSIS AND MULTILEVEL DEM SIMULATION OF THE INNOVATIVE TUBULAR PUSH CONVEYING PRINCIPLE.....	1
Kreutzfeldt J., Braun P., Schyga J., Hilbrich S., Hinckeldeyn J. PLANNING OF LARGE-SCALE LOGISTICS SITES	7
Golder M., Anders M., Novak G., Eiwani C. NEW APPROACH FOR ISO 16625	17
Lerher T. NEXT GENERATION INTRALOGISTICS: TECHNOLOGIES AND APPLICATIONS.....	23

SESSION A – HOISTING AND CONVEYING EQUIPMENT AND TECHNOLOGIES

Maximow I., Helbig M., Weise S., Golder M. DIRECTLY DRIVEN CONVEYING BELT	31
Burić M., Lučić M., Jokić V., Baucal S., Sekulić A. CALCULATION AND ANALYSIS OF THE STRESS AND DEFORMATION OF CRANE RAIL CLIPS	35
Kondralis F., Dentsoras A. J. CASE-BASED PARAMETRIC DESIGN OF BELT CONVEYORS.....	39
Jovanović M., Pavlović N., Radoičić G., Milić P. DYNAMIC PERFORMANCE OF A DOUBLE-BOOM LEVEL LUFFING CRANE MECHANISM.....	45
Wu F., Xu H., Tang X., Liu E. AMPLITUDE INSPECTION OF THE LARGE CRAWLER CRANE WITHOUT THE MARKER OF TURNING CENTER	51
Tao J., Zeyu D., Hailei R., Guangjun L. STUDY ON AN ELEVATOR EMERGENCY DISPOSAL AND PUBLIC SERVICE PLATFORM.....	55
Pavlović G., Savković M., Zdravković N., Marković G., Gašić M. OPTIMIZATION OF CRANE HOOKS CONSIDERED AS CURVED BEAMS WITH DIFFERENT CROSS-SECTIONS – A COMPARATIVE STUDY USING MATLAB.....	59
Qiu J., Tong Y., Ouyang W. FINITE ELEMENT METHOD SIMULATION AND MULTIFACTOR FAILURE ANALYSIS OF AN IMPORTANT STEPPED SHAFT FRACTURE EVENTS	65
Stölzner M., Kleeberger M., Günthner W.A., Fottner J. CALCULATING THE DYNAMIC BEHAVIOUR OF LATTICE BOOM MOBILE CRANES DURING HOISTING WITH A VIBRATION MODEL.....	69
Solazzi L. DERRICK CRANE SUBJECTED TO REPEATED LOADS.....	75
Solazzi L. GANTRY CRANE SUBJECTED TO PENDULUM LOAD ACTIONS	81
Schmidt T., Müller T. INTEGRATIVE CONCEPT FOR A LIFT MAST OF INDUSTRIAL TRUCKS WITH ELECTRIC DRIVES.....	87

Bizjak L., Hladnik J., Jerman B. STRESS-STRAIN ANALYSIS AND OPTIMIZATION OF UNIVERSAL HYDRAULIC GRAPPLE	99
Paulischin F., Kartnig G. THE LATERAL MOVEMENT OF STEEL PROCESSING BELTS – EXTENDED CONSIDERATION ON BELTS WITH LOW BELT TENSION	105
Đorđević M., Milojević G., Vujičić A., Zrnić N. LIFE CYCLE ASSESSMENT OF THE BELT CONVEYOR IDLER BALL BEARING	111

SESSION B – CONSTRUCTIONS, DESIGN ENGINEERING, MINING EQUIPMENT AND TECHNOLOGIES

Arsić M., Bošnjak S., Grabulov V., Gnjatović N., Milenović I. REPAIR METHODOLOGY FOR THE CARRYING STRUCTURE OF THE REJECTING DRUM OF THE BUCKET-WHEEL RECLAIMER STACKER CONVEYOR AT COAL LANDFILL.....	117
Wen X., Yang Y.Q., Tang X.Y., Wei D.X. CONTROL STRATEGY RESEARCH FOR SUPER -GAUSSIAN RANDOM VIBRATION TEST	123
Lüdemann L., Bona M., Golder M. DEVELOPMENT OF A PRODUCT CATEGORY RULE (PCR) FOR ENVIRONMENTAL PRODUCT DECLARATION (EPD) OF CONVEYOR CHAIN SYSTEMS	127
Kužnar M., Kaczor G., Lorenc A. PANTOGRAPH STRIPS FAILURE ANALYSIS AND ARTIFICIAL INTELLIGENCE PREVENTION METHODS	135
Andruszko J., Moczko P., Pietrusiak D. THE USE OF NUMERICAL METHODS IN CUTTERHEAD DREDGER EXCAVATION UNIT OPTIMIZATION	141
Vladić J., Jojić T., Đokić R., Gajić A. THEORETICAL BACKGROUNDS FOR ZIPLINE ANALYSIS.....	147
Działak P., Karliński J. CRASHWORTHINESS OF PROTECTION STRUCTURES FOR MINING MACHINE OPERATORS: NUMERICAL ANALYSIS AND EXPERIMENTAL VALIDATION USING OPTICAL 3D COORDINATE MEASURING DEVICES	151
Hladnik J., Supej M., Vodičar J., Bizjak L., Jerman B. ROLLING RESISTANCE COEFFICIENT OF PROCESSED ROLLER-SKIS FOR SKATING.....	157
Arsić A., Bulatović S., Mladenović M., Šarkočević Ž., Savić Z. BUCKET-WHEEL EXCAVATOR GEARBOX FAILURE ANALYSIS AND RELIABILITY ASSESSMENT..	161
Mitterlehner T., Kartnig G., Haider M. ANALYSIS OF THE THERMAL RATCHETING PHENOMENON IN PACKED-BED THERMAL ENERGY STORAGE USING DISCRETE ELEMENT METHOD.....	165
Haber A., Kartnig G. DEVELOPMENT OF A NEW DEM CONTACT MODEL FOR HYGROSCOPIC BULK SOLIDS	169
Bošnjak S., Gnjatović N., Milenović I., Stefanović A., Urošević M. MODERNIZATION AND UNIFICATION OF THE EXCAVATING DEVICES OF BUCKET WHEEL EXCAVATORS SRS 2000 DEPLOYED IN SERBIAN OPEN PIT MINES	175
Gašić V., Košanin N., Olszyna G., Arsić A. FEA ASPECTS OF THE LOCAL BENDING STRESSES AT THE HEA-SECTION RUNWAY BEAMS.....	183
Gnjatović N., Bošnjak S., Milenović I., Stefanović A. VALIDATION OF THE NUMBER OF BUCKETS ON THE WORKING DEVICE OF A BUCKET WHEEL EXCAVATOR FROM THE ASPECT OF DYNAMIC BEHAVIOR OF THE SYSTEM	187

SESSION C – LOGISTICS AND INTRALOGISTICS SYSTEMS

Rücker A., Rief J., Fottner J. AN INVESTIGATION OF MEAN ENERGY DEMAND, PERFORMANCE AND REFERENCE CYCLES FOR STACKER CRANES	197
Radoičić G., Jovanović M., Blagojević B., Vojinović M. RC VEHICLE FLEET E-MONITORING IN PRACTICE AND FUTURE.....	203
Kriehn T., Schloz F., Schulz R., Fittinghoff M. ALGORITHM AND ANALYTICAL MODEL TO OPTIMIZE CLASS-BASED STORAGE OF SHUTTLE-BASED STORAGE AND RETRIEVAL SYSTEMS.....	209
Hofmann M. MATERIAL FLOW SYSTEMS AND INTRALOGISTICS COMPONENTS FOR A NON-SEQUENTIAL, FLEXIBLY TIMED AUTOMOBILE PRODUCTION – FIRST PROTOTYPES	217
Servos N., Teucke M., Freitag M. TRAVEL TIME PREDICTION FOR MULTIMODAL FREIGHT TRANSPORTS USING MACHINE LEARNING.....	223
Ernits R.M., Beinke T., Freitag M., Rohde M. AUTOMATIC UNLOADING OF COFFEE SACKS OUT OF SEA CONTAINERS – SPECIAL PILE SITUATIONS AND CHALLENGES FOR GRIPPING.	229
Ortner-Pichler A., Landschützer C. CONCEPTS FOR THE USE OF KNOWLEDGE-BASED ENGINEERING IN INTRALOGISTICS SYSTEM PLANNING	235
Lorenc A., Kužnar M., Lerher T. ARTIFICIAL INTELLIGENCE METHODS FOR SOLVING PRODUCT ALLOCATION PROBLEM (PAP)...	239
Lerher T., Hliš T., Marolt J., Rupnik B., Kovačič M. DESIGN OF AUTOMATED WAREHOUSE FOR LONG AND HEAVY LOAD STEEL BARS	245
Lerher T., Marolt J., Rupnik B., Štor M., Kovačič M. SIMULATION ANALYSIS AND PERFORMANCE MEASUREMENT OF A HEAVY LOAD TRANSPORT VEHICLE IN A STEEL PLANT COMPANY	251
Nishimura E., Kutsuna A., Wei Z. A HEURISTIC APPROACH FOR OPERATING THE MARINE CONTAINER DRAYAGE USING DUMMY NODE CONCEPT.....	257
Pascher R., Ecker C., Sihn W. CONCEPTUAL DESIGN OF A MODULAR, HYBRID SENSOR SYSTEM (DUCK BOX) FOR THE IMPLEMENTATION OF LOCATION-BASED MATERIAL FLOW ANALYSES	263
Ramprecht P., Riester M., Sihn W. MODEL FOR THE CONCEPTUAL DESIGN OF UNIT LOAD WAREHOUSE SYSTEMS THROUGH THE INTEGRATED SOLUTION OF FIVE SUB-PROBLEMS	267
Dukic G., Opetuk T., Cajner H., Gajsek B. INFLUENCE OF PICK TIME DISTRIBUTION ON EXPECTED THROUGHPUT OF DUAL-TRAY VLMS...	271
Egger M., Angleitner K., Steiner W. AUTOMATED STORAGE AND RETRIEVAL SYSTEMS AS LIGHTWEIGHT DESIGN	275
Hassan O., Hamdy Elwany M., El Nagggar M., Fahiem A. MODELLING OF HIGHLY CONGESTED CONTAINER TERMINALS	279

Dragović B., Tselentis V., Zrnić N., Orlandić R., Paladin Z., Perazić K. ENVIRONMENTAL AND OPERATIONAL RISK ASSESSMENT PROCEDURES FOR SUSTAINABLE MARINA: THE CASE OF MARINA BAR	285
Zrnić N., Bojić S., Georgijević M., Urošević M. ANALYSIS OF THE POTENTIAL OF THE PORT OF NOVI SAD TO BECOME A NEW CONTAINER TERMINAL ON DANUBE	293
Dafnomilis I., Duinkerken M. B., Schott D. L., Ley J., Assbrock G. OPTIMIZATION DESIGN OF A FLOATING MODULAR PORT TERMINAL	299
AUTHOR INDEX	309

PLENARY SESSION

André Katterfeld

Professor
Otto-von-Guericke-University Magdeburg
Germany
Faculty of Mechanical Engineering

Christian Richter

Research Associate
Otto-von-Guericke-University Magdeburg
Germany
Faculty of Mechanical Engineering

Rolf Kamps

Senior Lecturer
University of Applied Science Luzern
Switzerland
Faculty of Mechanical Engineering

Functional Analysis and Multilevel DEM Simulation of the Innovative Tubular Push Conveying Principle

The tubular push conveyor, which is developed and marketed by the Bühler AG under the brand name TUBO, is an innovative conveying system for the transport of non-mineral bulk materials. It sets new standards, especially in agricultural and food technology, in terms of flexible conveying routes and simple design. Unlike today's systems, the bulk material is transported in a closed tube without a tension device (rope or chain) but by the help of push elements. The paper will present the general layout of such conveyors as well as the basic calculation approaches for the motion resistances. The calculations will be compared with experimental measurements on an industrial sized test rig. For the further understanding DEM simulations are used to study the detailed motion behaviour of the push elements interacting with the bulk material. To consider the load dependent movement of the push elements, the so-called Multilevel DEM approach was developed.

Keywords: Tubular, Push, Conveyor, TUBO, DEM.

1. INTRODUCTION

Most of today's continuous mechanical conveyors use a traction device to transport bulk materials. Whether it is a chain conveyor, belt conveyor or a bucket elevator, the conveyed material is always pulled to the outlet. In order to transport the goods, an uninterrupted connection of the conveying device – may it be a chain, rope or belt – is always necessary. Most traction conveyors require a minimum traction force for safe, noiseless and low-wear operation and must therefore be pre-tensioned.

When developing and implementing the tubular push conveyor, the so-called TUBO, Bühler AG relies on the completely opposite approach. Instead of pulling the bulk material, it is pushed through a tube. Thanks to this innovative conveying concept, the material has no contact with the drive, which basically leads to better hygiene in the system and at the same time also prevents damage to the conveyed material by the drive. Specially developed push elements, so-called Tubits, serve as conveying device for this purpose. The conveyor is designed to convey especially non-abrasive organic agricultural bulk materials such as grain and flavour.

For a proper functioning of the new conveyor, calculation principles were needed. The classical calculation approach for tube chain conveyors published in [2] and [3] were adopted by Kamps [1]. This allowed the calculation of the force acting on each Tubit depending on the conveyor route and the bulk material properties. Also, experimental investigations were conducted to compare the calculated Tubit forces with measurements.

Here it was found, that particle shape and hardness had significant influence on the Tubit forces due to the so-called gap-effect which is caused by the interlocking of particles between push elements (Tubits) and tube wall.

Computer simulations based on the Discrete Element Method (DEM) were used for a detailed investigation of the movement behaviour of the push elements interacting with the bulk material. The challenge of the simulation is the consideration of the push elements as load-dependent reacting single bodies, whose position in the tube depends on the acting pressure forces in the contact with other push elements but also interacting with the bulk material particles. For this purpose, the so-called multilevel DEM approach was developed. The most important results of this different work packages are summarised in this paper.

2. TUBULAR PUSH CONVEYOR

2.1 Idea

With the support of design methodology combined with variation features, a conveying system can be described as a tube conveyor system that has no closed run, no closed pull rope or chain. The following idea can be developed from this: Bulk material is conveyed via individual push elements in the tube. The required conveying function can therefore be achieved with individual elements (as push elements) which are pushed through the tube. The individual push elements form a closed pressure unit in the "pressure section". However, they remain individual elements which, if they are not brought together in the pressure section, are again individual elements and behave in this way.

Correspondence to: Prof. Dr.-Ing. André Katterfeld
Otto-von-Guericke-Universität Magdeburg
Institute of Logistics and Material Handling Systems
Universitätsplatz 2, D-39106 Magdeburg, Germany
E-Mail: andre.katterfeld@ovgu.de

2.2 Functioning Principle

The tubular push conveyor consists out of the following components which are marked by the number in Fig. 1a:

1. tube as conveying tube,
2. inlet,
3. outlet,
4. tube bends and joints,
5. chain drive station for the imparting motion to the push elements,
6. push elements ("Tubits").

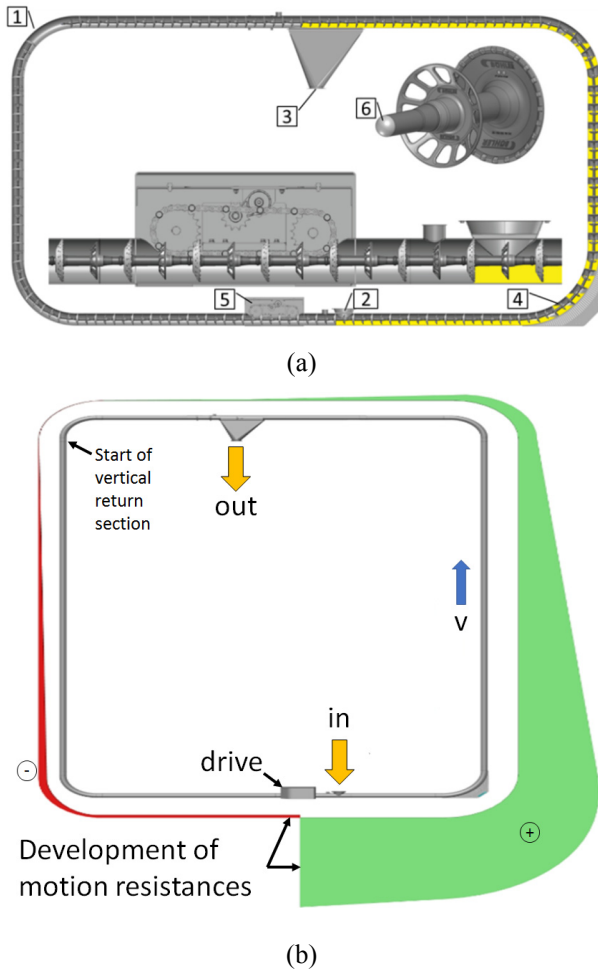


Figure 1. (a) Design and components of the tubular push conveyor TUBO [1], [4], (b) Qualitative development of motion resistances in the tubular push conveyor

Compared to conventional tube chain conveyors (TCC), the drive station can be located in the lower area of the conveyor. In opposition, a TCC drive station must be arranged in the upper area (usually at the outlet) where the highest tensional forces occur. The upper positioning of the TCC drive station makes the statics of the TCC much more complex. The TUBO drive can be mounted at the ground and must be positioned in front of the inlet (seen in the conveying direction), since the conveyed material would cause significant spillage in the drive station. Due to this positioning of the drive, the tube does not have to absorb the usual reaction forces and weight of the drive station and can be designed thinner in wall thickness than comparable TCC. Hence, usual pneumatic conveying tubes can be used for the TUBO. Typically,

no further support construction is necessary. Due to the conveying principle, a tensioning station is not necessary.

Further advantages of the TUBO in comparison to conventional conveyors are according to Kamps [4] low operating costs, flexible 3D conveyor routing, a hygienic conveying with excellent sanitation and a gentle transport.

3. CALCULATION MODEL

The volumetric flow I_V and mass flow rate I_m for the tubular push conveyor (TUBO) is calculated in the same way as for the tube chain conveyor as described in more detail in [2]. The volume which can theoretically be taken up by the bulk material is obtained by subtracting the volume of the push elements V_{PE} from the ideal tube volume V . The ratio of the volume which can actually be filled and the ideal tube volume is referred to as the volumetric efficiency η_V :

$$\eta_V = \frac{V - V_{PE}}{V} \quad (1)$$

For a 6-inch conveying tube with an inside diameter d_{Pi} of 161.9 mm, a push element length L_{PE} of 254 mm and a push element volume of 480 cm³, a volumetric efficiency η_V of 0.9 was obtained. Taking into account the tube cross-sectional area A , the conveying speed of the push elements v , the filling level η_F and the bulk solid density ρ_b , the theoretical mass flow rate I_m is calculated as:

$$I_m = \rho_b \cdot I_V = \rho_b \cdot \eta_F \cdot \eta_V \cdot \frac{\pi}{4} \cdot d_{Pi}^2 \cdot v. \quad (2)$$

In order to describe the conveying behaviour of the TUBO and to calculate the power requirement and the forces acting on the individual push elements, it is necessary to consider the occurring motion resistances. Kamps [1] published a detailed derivation of the equations for the motion resistances based on the theoretical investigations for TCCs, as published in [2], [3]. Accordingly, the calculation of the TUBO corresponds to the calculation of TCC. Only the calculation of the motion resistances in the tube bends changed according to the derived force equilibrium for one push element in the bend. The difference is caused by a reverse force direction: for the TCC the tensional forces increase in conveying direction but due to the conveying principle, the push element forces decrease in the TUBO along the conveying direction. This is shown in Fig. 1b.

It is already known from the investigations on the TCC [2], [3] that the motion resistances in tube bends increase exponentially. These sections of the conveyor route are from essential importance for the entire layout and determine strongly the power consumption. The calculation model for the motion resistances in bends can be traced back to Euler's equation for the calculation of rope forces. According to this theory, the resulting forces in the tension device are only dependent on the coefficient of friction between the tension device and the tube as well as on the bend angle. The forces are independent of the bend radius if a 100% flexible tension device is assumed.

Table 1: Equations of motion resistances for different sections of the TUBO routing

Horizontal sections: $F_h = F_{hPE} + F_{hBM} = L \cdot q_{PE} \cdot \mu_{PE} + L \cdot q_F \cdot (1 + \eta_F / \eta_V \cdot \lambda_a) \cdot \mu_w \quad (3)$ <p> L - the length of the horizontal section, q_{PE} - the meter weight of the push elements, q_F - the meter weight of the bulk material, μ_{PE} - the friction coefficient between push elements and tube, λ_a - the active lateral stress factor, μ_w - the wall friction coefficient of the bulk material </p>
Vertical sections: $F_v = F_{vPE} + F_{vBM} = H \cdot q_{PE} + H \cdot q_F \cdot \frac{d_{Ti}}{4L_{PE}\mu_w\eta_V\eta_F\lambda_a} \left(e^{\frac{4}{d_{Ti}}\mu_w\lambda_a\eta_V\eta_FL_{PE}} - 1 \right) \quad (4)$ <p>H - the height of the vertical sections</p>
Inclined sections: $F_\delta = F_h \cdot \cos \delta + F_v \cdot \sin \delta \quad (5)$ <p>δ - the inclination angle of the section against the horizontal</p>
Vertical bends: $F_B(\psi) = e^{-\mu_{PE}(\psi-\psi_0)} \left[F_B(\psi_0) + \frac{\mathcal{A}(\mu_{PE} \sin \psi_0 - \cos \psi_0)}{\mu_{PE}^2 + 1} + \frac{\mathcal{B}(\mu_{PE} \cos \psi_0 + \sin \psi_0)}{\mu_{PE}^2 + 1} \right] - \frac{\mathcal{A}(\mu_{PE} \sin \psi - \cos \psi)}{\mu_{PE}^2 + 1} - \frac{\mathcal{B}(\mu_{PE} \cos \psi + \sin \psi)}{\mu_{PE}^2 + 1} \quad (6)$ <p>with</p> $\mathcal{A} = \frac{r q_F d_{Ti}}{4 L_{PE} \mu_w \eta_V \eta_F \lambda_a} \left(e^{\frac{4}{d_{Ti}} \mu_w \lambda_a \eta_V \eta_F L_{PE}} - 1 \right) + r q_{PE} \quad (7)$ $\mathcal{B} = r q_F \mu_w \left(1 + \frac{\eta_F}{\eta_V} \lambda_a \right) - r q_{PE} \mu_{PE} \quad (8)$ <p> ψ - the end angle of the tube bend ψ_0 - the start angle of the tube bend </p>

In the absence of a better analytical approach, these assumptions should be used for the calculation, although neither the TCC nor the TUBO have such a flexible tension device. Table 1 summarizes the most important calculation approaches for the motion resistances of the push elements (indices PE) and the bulk material (indices BM) in the TUBO.

Due to the absence of a tensioning station, another main difference in the calculation of TUBO and TCC is that the force on the push elements can only be assumed to be known at one point: at the beginning of the vertical return section. If it is assumed that the tube system is not completely filled with push elements, a single push element falls downwards due to its weight at the beginning of the vertical return section (the so-called free-fall bend). Since gravity acts in the conveying direction, the motion resistance becomes negative at this point as shown in Fig. 1b.

4. EXPERIMENTAL INVESTIGATIONS

In order to validate the results of the calculation model, extensive experimental investigations were carried out on the 6-inch TUBO test rig of the Institute of Logistics and Material Handling Systems (ILM) of the Otto-von-Guericke University Magdeburg. The test rig has a circular conveying route (O-type, see Figure 1) with a horizontal length of approx. 6 m and a conveying height of approx. 7 m.

Initial tests were carried out with slightly cohesive and fine-grained maize semolina. For this bulk material, additional motion resistances due to the gap-effect can be neglected.

In order to measure the motion resistances in the experiment, a push element was equipped with strain gauges and a data logger in cooperation with Bühler AG and IBAF GmbH. This made it possible to record the compression force acting on the push element over the conveying path.

Fig. 2 compares the measurement and calculation results for tests with different filling levels. The experimental investigations were carried out at different conveying speeds due to the limited flow of material through the storage hopper. Although the conveying speed at the test conveyor can be up to 1 m/s - and is thus significantly higher than the conveying speed of many conventional TCC - it can be assumed that the dynamic effects during conveying are negligible. This means that the motion resistances can be assumed to be independent of the conveying speed.

Fig. 2 shows a good agreement between measurement and calculation results. The compression forces on the measuring Tubit reach their maximum as expected in the drive station. As expected, the strongest (exponential) decrease in the compression force occurs in the first tube bend after the drive station. In the subsequent vertical section, a linear decrease in the compressive force can be expected. The real measured values do not show such a clear difference in the decrease between the first bend and the subsequent vertical section. This is probably due to the fact that the polygonal pressure unit of the push elements is not only supported in the bend, but also to some extent in the vertical section.

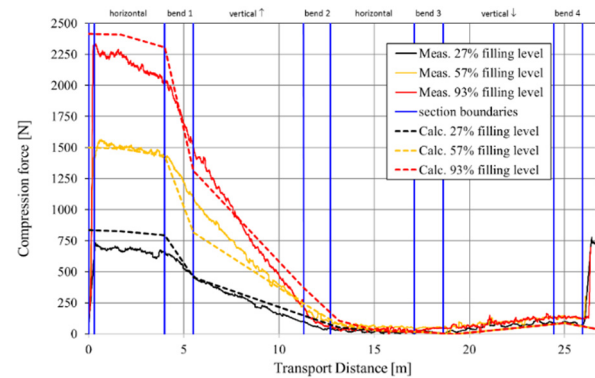


Figure 2: Comparison between measured and calculated Tubit forces for the conveying of fine-grained maize semolina with different filling levels.

For better consideration of the real conditions, investigations with multi-body simulations were carried out in [5]. The motion resistance resulting from the bulk

material interaction was approximated in the multi-body simulation by a constant applied compression force as a boundary condition, which was estimated on the basis of the presented calculation model. In the MBD model, due to modelling problems and due to the high computing effort, no complete push element conveyor could be considered, but only the first bend after the drive station. Although in [5] interesting investigations on the qualitative influence of the tube bend geometry could be carried out on the basis of the MBD model, this approach has strong limitations regarding the detailed analysis of the true interaction between push elements and bulk material. For this reason, an attempt was made to map the entire conveyor including bulk material using the Discrete Elements Method (DEM). Although several DEM couplings to other simulation methods such as FEM [6] or MBD / machine simulation [7] were already developed, for this task a completely different extension of the classical DEM algorithm was necessary. This extended approach was called the Multilevel DEM approach which is described in the following section.

5. MULTILEVEL DEM APPROACH

Particularly in material handling and process engineering, granular material flows are investigated using DEM [8], [9]. In order to consider irregular body shapes in DEM, different methods can be used. It is possible to use non-round particles such as polyhedrons [10], ellipsoids or superquadrics [11]. With these simple geometrically describable bodies, however, not all desired shapes can be represented. Furthermore, the computational effort for contact detection increases strongly with increasing form complexity. For this reason, the multisphere method, also known as clumps, is widely established. Multispheres make it possible to combine spheres into conglomerates (so-called clumps) and to approximate solids of any shape. Thus, it is possible to use the DEM not only for the simulation of granular media, but also for problems that would be classically assigned to multi body simulation (MBD). In [12] it was shown that from a body number of about 90 cubical elements with 6 degrees of freedom the efficient algorithms of DEM for contact detection and contact force calculation are better suited than those in software packages for the classical MBD simulation.

Multispheres have already been used to analyse the behaviour of general cargo in bulk mode [13], [14]. The term "general cargo" can be used, for example, to describe a cuboid package or an arbitrarily shaped, closed loading units. By extending this approach to the so-called multilevel DEM approach, it is possible to consider not only the already mentioned loading units, but also the load carriers (containers, package sleeves, etc.) and other mechanical parts of continuous and discontinuous conveyors, such as the Tubits of a TUBO.

The core of the multilevel DEM approach as shown in Fig. 3 is to consider all interacting bodies through spheres or multispheres.

In the present case, the push elements are simulated by multispheres consisting out of many primary spheres and the bulk material by simple spheres or simple multispheres consisting of a few (<10) primary spheres.

Different levels can be identified, which give the method its name and are decisive for the computing efficiency of the process. The levels can be differentiated according to which entity interacts with each other. In the present case, these are the following contact observation levels:

- 1) Contacts between the bulk material and the push elements / tube walls;
- 2) Contacts between the push elements themselves, between the push elements and the tube wall and between the push elements and the drag chain drive.

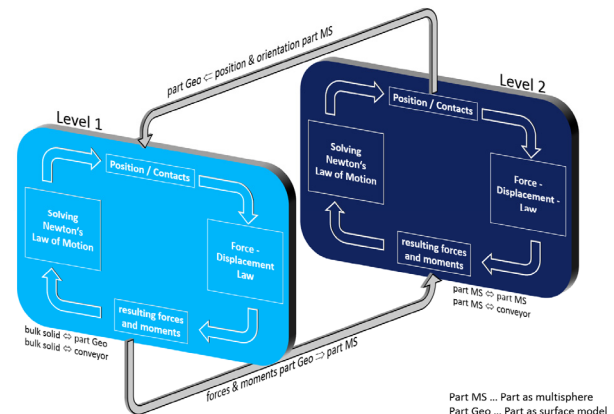


Figure 3: Functioning principle of the Multilevel DEM algorithm.

A detailed description of the Multilevel DEM approach with regards to the simulation of tubular push conveyor can be found in [15].

6. SIMULATION RESULTS

In the DEM simulations geometric simplifications of the bodies are necessary, for example the modelling of the push elements as multisphere bodies. Furthermore, the stiffness parameters must be reduced in order to use a higher critical time step. For a realistic behaviour of the multisphere push elements, their contact parameters must also be calibrated. One of the most important parameters to be calibrated for this special approach is the multisphere wall friction coefficient due to the unrealistic rough surface of the multisphere according to the used primary particle size. For this, a push element was placed in a tube section and the tube was tilted at a constant angular velocity until the push element started to slide. Calibration simulation series analogous to the tilt test but with varying wall friction parameter allowed the determination of the wall friction coefficient which results in a realistic behaviour.

For the TUBO simulation, the tube system of the conveyor is imported directly from the 3D CAD design. The drag chain drive of the drive station is represented by 8 spheres, which move on predetermined paths independent of the load. After the initialization and positioning of the individual push elements in the tube, the DEM calculation cycle begins. The push elements are pushed through the conveying tube by the forces of the drive spheres at a conveying speed of 0.64 m/s and pick up the bulk material at the inlet point. During the simulation, the forces acting on each individual push element are continuously recorded.

The first step was to simulate the empty push element conveyor in order to demonstrate the basic function of the simplified multisphere push elements. Fig. 4 shows the circulation of the push elements.

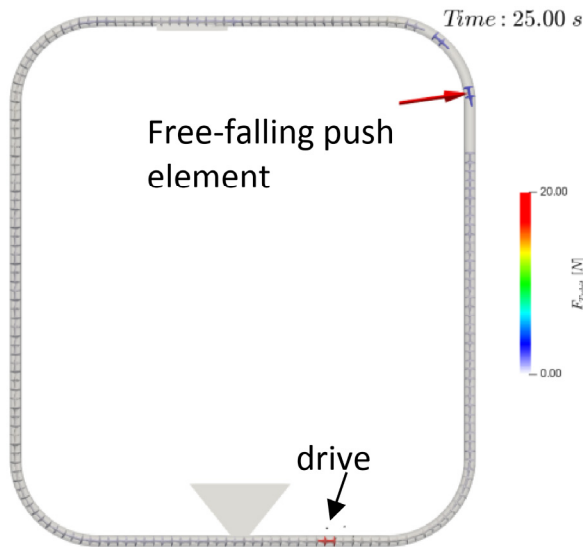


Figure 4: Multilevel DEM simulation of an empty TUBO

The formation of the free fall zone in the upper right tube bend can be seen particularly well. This bend is also known as a free-fall bend. In contrast to the assumption made in section 2 that the pressure section only dissolves at the end of the free-fall bend, it can be concluded from the DEM simulation that this already occurs at the beginning of the free-fall bend. When dissolving the pressure section, it is to be expected that the force on the push element will go towards 0.

The forces of the selected measuring push element can be displayed over the displacement (see Fig. 5). The comparison of simulation data, real measured values and the results from the adapted analytical calculation model in Fig. 5 shows an excellent agreement in terms of quality and quantity.

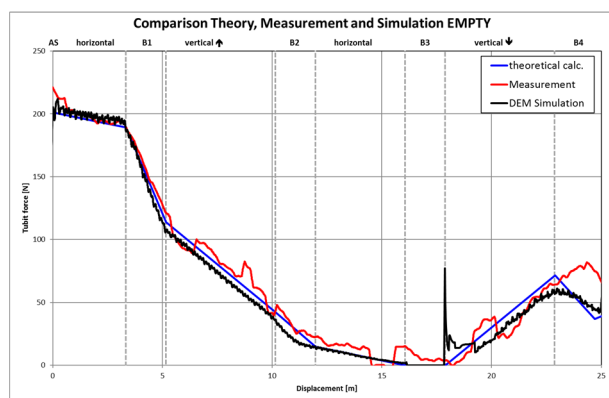


Figure 5: Comparison of the measured, calculated and simulated Tubit forces during the empty run

Fig. 5 shows the resolution of the pressure section in section B3 (force of push element = 0 N). Thus, the multisphere model of the push elements, which is the second observation level in the multilevel DEM approach, works satisfyingly.

As a functional test for the first and second observation level, the push element conveyor in Fig. 4 was filled with virtual bulk material, which was

represented by spherical particles with a minimum diameter of 10 mm. Fig. 6 shows the TUBO simulation with a filling level of approx. 90%. The multilevel DEM approach is working as expected. A quantitative comparison of the Tubit forces is a remaining research task.

The simulated particles are scaled-up by a factor of 3. The spherical representation and the size of the particles prevents their interlocking between push elements and tube. This interlocking (called gap-effect) is strongly influencing the motion resistances and power consumption of the TUBO in reality if coarser material e.g. wheat, rice or beans is transported. For a realistic prediction of the motion resistances in the simulation, this effect needs to be considered.

However, it had to be determined that even when using the University HPC cluster the multilevel DEM simulation is very time consuming. So far, it was only possible to consider scaled-up spherical particles. To consider the gap-effect non-spherical particles with a non-scaled size are mandatory. Because this is only necessary in the spatial surrounding of the gap, it seems to be promising to dynamically change the resolution (degree of details) of the particles during the simulation instead of running the simulation with 100% non-scaled and non-spherical particles.

7. CONCLUSION

This article presents three different perspectives for the investigation of the new conveyor system called tubular push conveyor TUBO:

1. an analytical calculation model based on the tube chain conveyor,
2. experimental investigations on the ILM's experimental push element conveyor and
3. the application of the novel multilevel DEM approach, for the consideration of the interaction of push elements and bulk material.

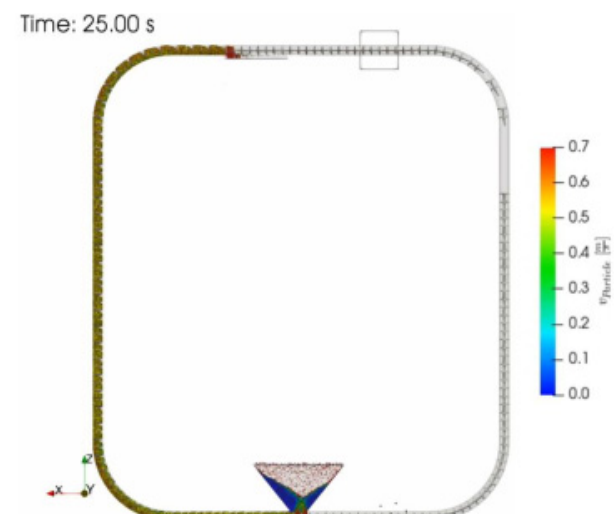


Figure 6: Multilevel DEM simulation of a tubular push conveyor with filling level of approx. 90%

The basic functionality of the calculation model and the developed simulation methodology could be demonstrated. The detailed simulation results allow a better understanding of the compression forces measured in the experimental test and can better explain the

differences between the analytical calculation model and the experimental measured values. Based on the simulation results, the analytical calculation model will be improved. While very good simulation results could be achieved in terms of quality and quantity for the simulation of the empty conveyor, further investigations are necessary for the simulation of the bulk material conveying process due to the very high calculation intensity.

In future work, it will be examined whether how a complete filling of the conveyor and a consideration of the interlocking between particles and push elements can be achieved. The aim of the research work is to simulate even more complex industrial conveyor routings and a realistic bulk material interaction with the help of the multilevel DEM approach.

ACKNOWLEDGEMENT

The presented results regarding the Multilevel DEM Approach in this paper is covered by the research projects "Simulation des Bewegungsverhaltens gefüllter Pakete und Ladungsträger im Pulk (SIMPPL)". The SIMPPL project No. KA1802/2-1 was founded by the German Research Foundation (DFG).

REFERENCES

- [1] Kamps, R.: *Konzept und Realisierung eines Rohrfördersystems mit Schubelementen*, Dissertation, Bergische Universität Wuppertal, 2016.
- [2] Katterfeld, A. and Williams, K.: Functional Analysis of Tube Chain Conveyors Part 1: General Design and Calculation Principles, In: Bulk Solids & Powder - Science & Technology, Vol. 3, No. 1, pp. 23-32, 2008.
- [3] Katterfeld, A. and Williams, K.: Functional Analysis of Tube Chain Conveyors Part 2: Experimental Research and Final Recommendation for the Calculation, In: Bulk Solids & Powder - Science & Technology, Vol. 3, No. 2, pp. 74-82, 2008.
- [4] Kamps, R.: Schubelementeförderer TUBO - neuartiges Förderprinzip der Bühler AG mit einmaligen Möglichkeiten, In: 22. Fachtagung Schüttgutfördertechnik 2017, Magdeburg, 2017.
- [5] Katterfeld, A., Haensel, H., Sawala, T., Stenke, R. and Kamps, R.: Berechnung und Analyse der Bewegungswiderstände in Schubelementeförderern, In: 22. Fachtagung Schüttgutfördertechnik 2017, Magdeburg, 2017.
- [6] Dratt, M. and Katterfeld, A.: Coupling of FEM and DEM simulations to consider dynamic deformations under particle load, Granular matter - Berlin: Springer, Vol. 19, No. 3, Art. 49, pp. 1-15, 2017, <http://dx.doi.org/10.1007/s10035-017-0728-3>
- [7] Heß, G., Richter, C. and Katterfeld, A.: Simulation of the dynamic interaction between bulk material and heavy equipment - calibration and validation, Proceedings of the 12th International Conference on Bulk Materials Storage, Handling and Transportation - ICBMH 2016, edited by David Hastie, The Institution of Engineers, Australia, 11-14 July 2016, Darwin, Australia, pp. 427-436, 2016.
- [8] Katterfeld, A. and Wensrich, C.: Understanding granular media - from fundamentals and simulations to industrial application, Granular Matter, Springer, Vol. 19, No. 4, Art. 81, pp. 1-4, 2017.
- [9] Gröger, T. and Katterfeld, A.: On the Numerical Calibration of Discrete Element Models for the Simulation of Bulk Solids, Computer Aided Chemical Engineering, Vol. 21, pp. 533-538, 2006.
- [10] Chen, W., Donohue, T., Katterfeld, A. and Williams, K.: Comparative discrete element modelling of a vibratory sieving process with spherical and rounded polyhedron particles, Granular Matter, Springer, Vol. 19, No. 4, Art. 81, pp. 1-12, 2017, <https://doi.org/10.1007/s10035-017-0749-y>.
- [11] Podlozhnyuk, A., Pirker, S. and Kloss, C.: Efficient implementation of superquadric particles in Discrete Element Method within an open-source framework, Computational Particle Mechanics, Vol. 4, No. 1, Art. 101, pp. 1-18, 2016, <https://doi.org/10.1007/s40571-016-0131-6>.
- [12] Fritz, M., Wolfschluckner, A. and Jodin, D.: Simulation of parcels in a bulk, Logistics Journal: Not Reviewed - ISSN 1860-5923, Vol. 2013, doi: 10.2195/lj_NotRev_fritz_de_201311_01, 2013.
- [13] Cao, L., Richter, K., Richter, C. and Katterfeld, A.: Simulation of the Peristaltic Conveying of Parcels as Bulk, Logistics Journal: Not Reviewed - ISSN 1860-5923, Vol. 2014, doi: 10.2195/lj_NotRev_cao_de_201409_01, 2014.
- [14] Prims, D. and Katterfeld, A.: Application of Discrete Element Method for Damage Rate Reduction of Parcel Bulk Handling Units, Logistics Journal : Proceedings, Vol. 2017, doi: 10.2195/lj_Proc_prims_de_201710_01, 2017.
- [15] Katterfeld, A., Richter, C., Pusch, M. and Kamps, R.: Tubular Push Conveyor – Functional Analysis and Simulation, Proceedings of the 13th ICBMH, 09-11 July 2019, Gold Coast, Queensland, Australia, 2019.

Jochen Kreutzfeldt

Professor
Hamburg University of Technology
Institute of Technical Logistics

Philipp Braun

Research Assistant
Hamburg University of Technology
Institute of Technical Logistics

Jakob Schyga

Research Assistant
Hamburg University of Technology
Institute of Technical Logistics

Svenja Hilbrich

Research Assistant
Hamburg University of Technology
Institute of Technical Logistics

Johannes Hinckeldeyn

Chief Engineer
Hamburg University of Technology
Institute of Technical Logistics

Planning of large-scale logistics sites

Planning projects of large-scale logistics sites are often characterized by several stakeholders, planning data of limited initial quality and a high number of planning decisions. These specific attributes can lead to uncertainties in terms of stakeholder interests, responsibilities and planning information. Existing methodologies operate mainly in stepwise approaches and cannot always fulfil the requirements of complex plannings and decision-making under uncertainty sufficiently. This paper proposes a new planning framework with regard to insights from several industrial planning projects. The proposed framework starts with a stakeholder analysis and the definition of a planning codex. All subsequent planning decisions are structured in a flexible decision-making network. Lastly, the planning framework is applied to an exemplary planning project.

Keywords: Logistics site planning, warehouse planning, planning uncertainties, stakeholder analysis, planning objectives, planning structures, planning decisions.

1. INTRODUCTION

In a planning project objectives and necessary actions are systematically defined and realized. For logistics sites planning actions include e.g. the designation of processes, site and building surfaces and storage technologies.

There can be various reasons for the planning of a logistics site. Besides the demand for higher capacities, the wish for the optimization of processes, the availability of technical innovations as well as new laws or regulations may result in the requirement for a new or modified logistics site [1].

The planning of a logistics site is a demanding task. Complex company structures, a diversity of involved stakeholders, limitations in the availability and quality of planning data and a broad range of potentially applicable transport and storage technologies lead to uncertainties and challenges in the planning of large-scale logistics sites. To handle this complex task, a structured planning process is required.

Existing planning methodologies for production and logistics sites have shown deficiencies when it comes to deal with the uncertainties of large planning projects. These uncertainties can be driven by new stakeholders entering the project or the integration of new planning data and knowledge in later project phases.

Therefore, based on experiences from industrial projects, an improved approach for the planning of logistics sites was developed. This approach presented in this paper extends the current methodologies to minimize uncertainties and for dealing with them.

It is proposed to form a planning codex at the very beginning of the project. This planning codex is the result

of bringing together and balancing the interests of the project stakeholders identified in a preceding stakeholder analysis.

The planning codex is made up by a vision for the envisaged logistic site and a number of corresponding planning guidelines. For each planning guideline potential realization measures are indicated. At this early project stage, the measures are not decided yet. Their definition serves rather to support an understanding of the defined guidelines and opens the eyes for potential solutions. The project codex shall ensure that the diverse interests of the various stakeholders are taken into account consequently not only at the project start but during the entire project run time.

A dynamic planning framework is proposed integrating both the stakeholder analysis and the planning codex in order to handle uncertainties in planning steps. To identify and evaluate realization alternatives a decision-making process is suggested.

In section 2 an overview on existing methodologies and their limitations is given. This is followed by an analysis of uncertainties in the planning process in section 3. The developed planning framework is described in section 4 and an exemplary planning process based on a selected industrial project presented in section 5. The article is closing with a conclusion in section 6.

2. PRODUCTION AND LOGISTICS SITE PLANNING METHODOLOGIES

The existing literature on the planning of production and logistics sites is extensive.

Today's planning methodologies are mainly based on a hierarchical approach combined with the willingness for an iterative advancement in case unsolvable challenges or unsatisfying results occur on a lower planning level. The well-known methodologies organise the planning process in idealised process steps of project setup, structuring, system design and usually end up with a realization phase.

Correspondence to: Prof. Dr. Jochen Kreutzfeldt
Institute of Technical Logistics,
Theodor-Yorck-Straße 8, 21079 Hamburg, Germany
E-mail: Jochen.Kreutzfeldt@tuhh.de

The actual state of planning methodologies in literature is presented in the succeeding subsections.

Meanwhile, industrial projects have been following agile and iterative procedures different to classical sequential approaches.

2.1 Existing production and logistics site planning methodologies

Production and logistics site planning methodologies are dealing with the design of appropriate processes and storage systems under consideration of various and competing system alternatives. Therefore, planning activities need to be carried out in organizational, technical and economic areas of planning to provide a comprehensive concept [2]. These activities aim at improving current operations and overcoming historically grown structures by developing new solutions [3]. Possible planning situations vary from the design of new sites, extensions, site reconstructions to revitalisations [1]. To select the optimal solution from the pool of alternatives for the different objects and systems within the planning project, the planning should be executed in an iterative and systematic way. Moreover, planning procedures must offer flexible, adaptable and explicit procedures [3].

Figure 1 summarizes actual planning methodologies for production and logistics sites. These can be clustered into the four phases project setup, structuring, system design and realization. The presented methodologies suggest a more or less sequential set of steps for planning projects with varying levels of planning detail.

The first phase is usually described as the project setup phase. The project setup starts with the definition of planning objectives [4], [1]. This includes the definition of tasks included in the scope of the planning. The result is a clear defined project structure supporting

efficient procedures in following project phases [5]. Subsequently, the data analysis aims to determine the starting situation, future performance requirements and boundary conditions. In practice, conducting this data gathering task can be especially time-consuming. Additionally, a feasibility study to further confirm the planning objectives may be conducted [3].

The second project phase is called structuring and aims at creating a holistic concept of the future production or logistics site, which is able to achieve the predefined objectives. Therefore, production and logistics principles, corresponding functional and organizational units and respective processes of the future production or logistics site are to be defined [5]. Surfaces, equipment and personnel requirements must be determined and dimensioned [6]. Under consideration of boundary conditions such as building specifications, system and processes alternatives are generated and evaluated. This phase results in a decision for a future system solution based on a quantitative and qualitative evaluation. Subjective preferences and decisions should be avoided at this planning stage. Therefore, benefit value, profitability and risk analysis are recommended [1].

After selecting a certain system solution based on the outcomes of the systems planning during the structuring phase, the system design follows as the third project phase. In this phase, the detailed planning for the selected system is to be performed. Consequently, the process layout, realization and operating costs must be reassessed and time requirements for the realization of the selected system determined. In the following the industrial engineering and the preparation of calls for tender are performed. This phase delivers a system design planned in detail, if appropriate a selected systems vendor and final calculations of realization costs and time requirements.

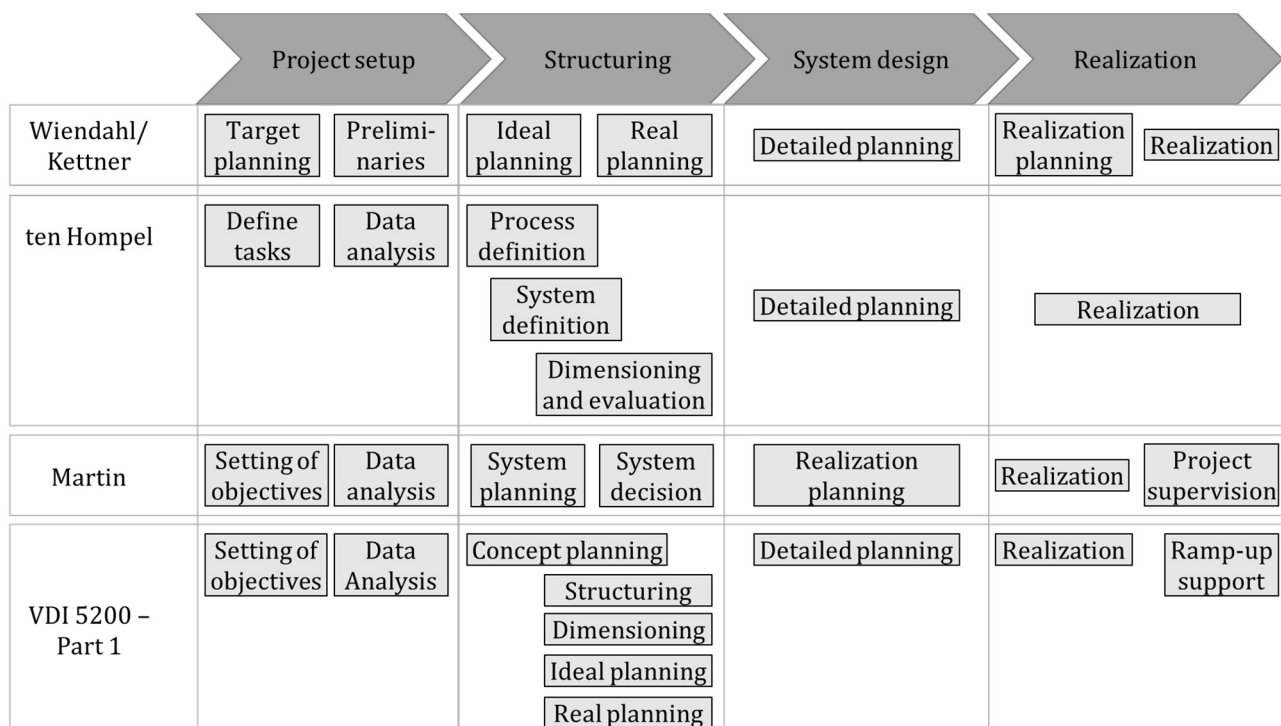


Figure 1: Production and logistics site planning methodologies in the literature [1], [3], [4], [5], [6]

After selecting an appropriate equipment supplier, the realization is carried out in the final project phase. This phase deals with the construction and supervision of all building and system sections, followed by a final project documentation and revision [3].

Most authors point out, that the stepwise planning procedures should not act as a barrier for necessary reiterations within real planning projects.

2.2 Gaps in the recent literature

Insights from several industrial projects showed difficulties in the management of dynamic project procedures. Existing planning methodologies offer sometimes limited support in the management of the practical planning tasks.

Due to the high number of alternatives for system and process solutions, logistics site planning is complex. This entails difficulties in finding an optimal solution [7]. As most authors already pointed out, reiteration is strongly necessary to overcome this problem. However, despite the recommendation for reiteration, the flexible and interrelated way of working in planning projects is not strongly integrated and supported by existing methodologies.

A wide variety of stakeholders is involved in the planning project. Figure 2 shows the exemplary involvement of stakeholders throughout the different steps of planning. All stakeholders must be integrated in the project according to their individual interests, knowledge and responsibilities. During the different steps of the planning project the stakeholders may change to some extent in every step. The dynamic composition of stakeholder groups results in different objectives, information and knowledge leading to additional complexity in the course of planning projects. This aspect has not sufficiently been integrated in current planning methodologies.

An evaluation of the planning alternatives based on qualitative criteria like flexibility and green characteristics is usually applied [1]. A common tool to carry out this evaluation is the benefit value analysis which is chosen in order to obtain objectivity and to avoid personal preferences when assessing qualitative criteria [3]. In practice, the alignment of certain decision criteria to the overall planning objectives is difficult.

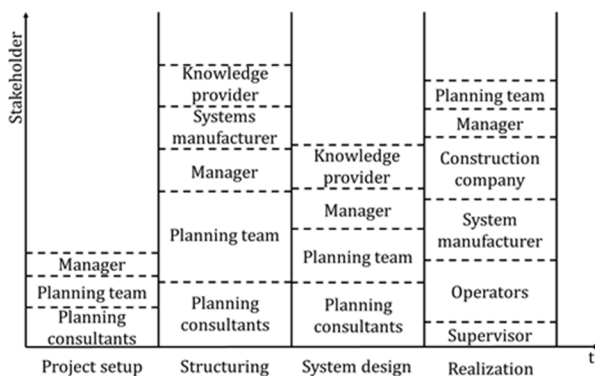


Figure 2: Idealised stakeholders per planning phase

3. UNCERTAINTIES IN PLANNING

The planning of large logistic sites is characterized by a variety of uncertainties leading to excessive time consumption and high costs for planning, nevertheless sometimes to suboptimal results. Number and impact of uncertainties tend to increase with the size and complexity of a planning project. Especially for large logistic sites, it is important to reduce uncertainties and apply methods to deal with them. The aim of this section is to examine the main drivers of uncertainties. Uncertainties are categorized and approaches for minimizing or dealing with them described, which are later on integrated in the developed planning methodology.

3.1 Fields of uncertainty

As in section 2.2 described, many internal and external stakeholders are involved pursuing their own interests.

For example, despite accepted lean management principles a production function may prefer to plan with high stocks of purchased and finished goods. This is especially the case if process variances seem to endanger the aspired fast and flexible deliveries of the right amount of the right objects, packed on the right delivery unit to the right place.

At the same time, the logistics department may aim for lower logistics costs and throughput times through reduced stocks, process standardization and consistent type and quantity of deliveries to and from the logistic site. The procurement in turn wishes to purchase large quantities in high order sizes to reduce administrative efforts and purchase costs.

Furthermore, external parties such as supplier of logistic equipment or consulting companies pursue to generate a high turnover while satisfying the customer. In some cases, there might be logistic service provider involved in order to operate the site.

Partly conflicting interests lead to a wrangle between stakeholders over the influence of the planning project. Furthermore, the individual persons in each interest group cannot be considered fully objective. Their opinions depend not solely on economic principles but also on their personal experience, interests and emotions. With a higher hierarchical position of an individual this factor gains importance. For example, a powerful manager involved in an important decision can tilt the direction of the entire project.

The described uncertainties arising from the wrangle between stakeholders are termed as 'uncertainties of interests'.

Additionally, a project team consisting of various stakeholders can be challenging to coordinate. A lack of clarity in the responsibilities and division of tasks can lead to contradicting or incomplete results and an increasing overall workload. The affiliation of responsibilities to individuals or parties are furthermore matter to change over time. The described driver is termed as 'uncertainties of responsibilities'.

Finally, there is a direct influence through the so-called 'uncertainty of information'. Information can be

derived from data, such as the required storage locations for certain load carriers and boundary conditions, such as the available storage surface or legal requirements. In practice, fully integrated databases are rarely available and the collection of data can be challenging. If certain data is not available assumptions are common. Based on the analysis of existing data, predictions must be made in order to obtain the data that are used to serve as basis for the design of the logistics site. Uncertainty in the data, assumptions and predictions add all up on each other, resulting in the overall uncertainty of the planning data. Various boundary conditions such as laws and regulations or strategic management decisions can lead to further uncertainties as the knowledge of the planner on the issues might evolve over time.

The described uncertainties influence the requirements, the objectives and processes of a decision. Therefore, decisions are often neither definite nor optimal. This makes planning difficult. For the planning of large logistic sites various decisions have to be made, on different levels and from different people. Several actions can follow a decision, finally leading to the planning results. The uncertainties subsequently influence the planning results regarding quality, time and costs. Figure 3 is illustrating the described influence of the identified drivers of uncertainty on the planning results.

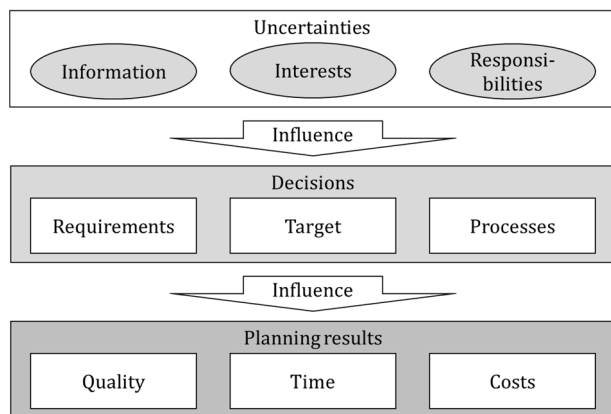


Figure 3: Effects of uncertainties

3.2 Minimizing uncertainties

As previously described, uncertainties in planning increase with the size and complexity of a project. For the planning of large logistic sites, it is therefore particularly important to counteract the uncertainties by applying clear planning methods.

To minimize the uncertainties of interests, good coordination and cooperation between stakeholders is required. Individual planning objectives have to be communicated in an open, transparent and comprehensible way. Clear processes are needed in order to derive common, reliable and consistent planning objectives. The influence of stakeholders in the project needs to be defined by consulting superior managers in order to fundamentally reconcile these determinations with strategic company decisions. The individual planning goals have to be discussed between stakeholders in order to define common goals.

Besides the clear identification of the stakeholders and their responsibilities for decisions and tasks, also tasks and decisions need to be analysed and structured. Overlaps between various decisions and tasks should be avoided. The aim of the decision-/task-structure is to affiliate personal of different fields to support tasks and decisions with their respective competencies. For each individual decision also, a clear decision-making-structure has to be defined and methods applied to increase objectivity. The individual decision-maker need to be defined previously, considering influence of stakeholders on the particular decision and knowledge about the issue.

Significant uncertainties could arise from a lack of information or inaccurate data. Planner are responsible to collect sufficient information to make a certain decision. As described in section 2.1, it is common to carry out an extensive data acquisition before the initialization of a planning project. Since the course of the project is not fully predictable in advance, continuous data acquisition remains necessary during the project. For internal planning data common databases and platforms for communication have to be used to avoid misunderstandings and multiple work. Despite regulations, external information is rarely explicit. Therefore, several internal as well as external knowledge-provider should be consulted in order to build an extensive data pool. Especially, the verification of the data is important as several follow-up decisions and actions depend on them.

3.3 Dealing with uncertainties

Through integration of stakeholders and acquisition of better data, uncertainties in the planning of logistic sites can be minimized but never be fully eliminated. To deal with this issue it is either possible to react to the consequences or to compensate the uncertainties.

Uncertainties can be compensated by applying security margins or introducing redundancy of work. Security margins can be realized by adding extra costs, surfaces, etc. The size of the security margins can be chosen in regard to the estimated uncertainty of the decision. This measure is particularly applicable for the uncertainty of data. To choose reasonable security margins, minimum and maximum values of the planning data can be considered [8].

Redundancy of work is a useful approach if a decision is particularly uncertain. For instance, if two options between which a decision needs to be made are equivalent from a stakeholder point of view. In such cases, several options for the decision can be further investigated. In the course of subsequent planning, each alternative gets further detailed until the primary decision can be made with a sufficient certainty. Up to this point, additional labour has been carried out, but limited project time was wasted in case of a changed decision.

In order to react to uncertainties and the resulting changes of decisions, iteration of planning steps is required. Iteration needs to be possible between different influencing decisions or during a decision-making-process. Every decision-making-process should follow a similar pattern and result in a comprehensible and

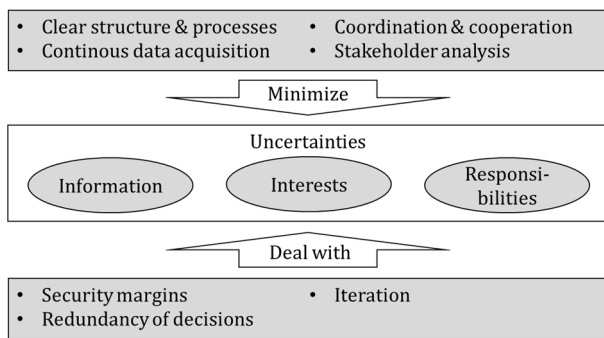


Figure 4: Requirements for planning methods to minimize and deal with uncertainties.

transparent documentation. An approach to realize iteration between influencing decisions is therefore the clear allocation of superordinate and subordinate decisions inside of the previously described top-down decision-structure. In the event that a decision is tipped, all subordinate decisions have to be reconsidered.

Figure 4 summarizes the described measures to reduce the uncertainties in planning. These measures build requirements for the proposed planning framework in order to minimize and deal with uncertainties.

4. PLANNING FRAMEWORK FOR LARGE LOGISTICS SITES

To reduce the risks of uncertainties in planning projects, a new approach is required. A clear identification of stakeholders and planning structures as well as reiterations are highly important. Based on insights from several industrial projects, a planning approach has been developed.

As the analysis of the involved parties, interests and responsibilities is necessary to build common planning objectives, a stakeholder analysis should be the first step of a planning project.

4.1 Stakeholder analysis

The aim of the stakeholder analysis is to create an overview about the involved stakeholders including the project team and external stakeholders [9]. Based on the overview, the technical, economic as well as external interests in terms of sustainable and societal aspects of all parties must be considered for the subsequent definition of planning codex and planning procedure [10].

The members of the project team can be clustered into three main groups according to their role within the planning project (Figure 5). Firstly, the planner are responsible for the conceptual design, processing of planning data and the preparation of decisions within the planning project. The group of planner should be composed cross-functional by members such as internal and external logistics experts, architects and construction experts. Secondly, the knowledge-provider influence the project directly and indirectly by gathering, processing, allocating and provisioning of information on current planning topics. This group consists of internal members such as data analysts and technical experts as well as external members like sales representatives and technical experts of system vendors. The decision-maker are responsible for providing personnel, financial resources and for making a choice for a certain decision alternative. Furthermore, the decision-maker can connect the planner to knowledge-provider and technical experts from different business units. Member of these three groups can be a part of more than one group. For example, planning consultants can be responsible for the actual planning, but they can also contribute their technical expertise as knowledge-provider.

An early and ongoing integration of the decision-maker of the project is crucial for the efficient planning progress and alignment of the potentially different and subjective interests to form a common vision for the future logistics site.

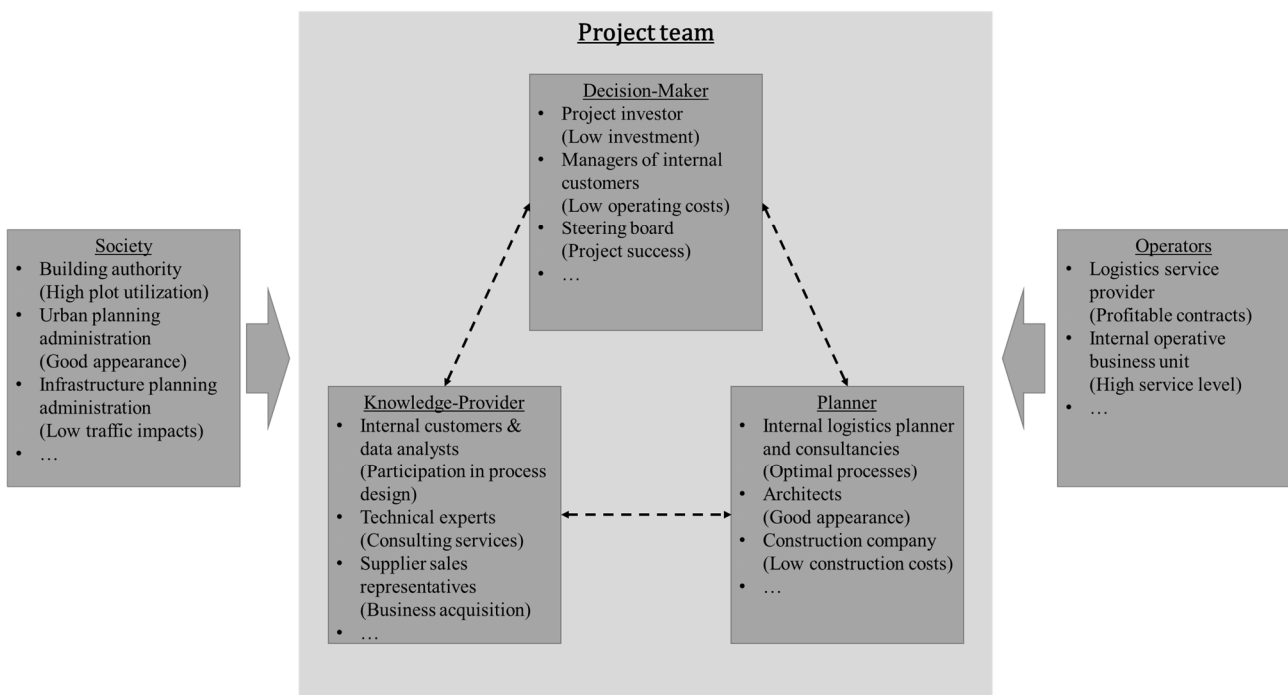


Figure 5: External and internal stakeholder groups and their interests in the planning project

External stakeholders can be clustered into the society and future operators of the logistics site. The interests of the society are mainly represented by regulations, local authorities and administrations, but occasionally also by private initiatives. These actors are primarily concerned about socio-economics and sustainability topics like a high utilization of building plots or a low impact of logistics sites on the traffic situation especially in urban regions [11]. Since the future operation of the logistics site is influenced by all planning decisions, the internal operative business unit or an eventually involved external logistics service provider represent additional stakeholders.

4.2 Definition of the planning codex

After getting a clear view on the stakeholders, their interests and responsibilities, the stakeholders should agree on a corporate planning codex. The planning codex is composed by vision fields and guidelines. The stakeholders who are part of the project team are in charge for defining the vision for the project. Doing so, they are also responsible for taking into account the main interests of external stakeholders such as society's institutions and future site operators next to internal interests. Contradictory interests have to be balanced, resolved or at least decided. The result must be approved by the responsible decision-maker.

The vision should be continuously taken into account for every major decision made during the complete planning process. Moreover, the vision acts as a reminder for the project members in specific situations when planning alternatives or options need to be evaluated. Based on the vision, design guidelines can be derived which later on result in specific measures for the project.

According to Figure 6 the vision definition starts with the vision fields being essential for the representation of all interests within the project team. The vision fields are categories which can still be generic for example like economic benefits or sustainability, because these can be understood as starting points from which more specific guidelines can be derived. At this point of time, these overall principles might be competing, like specific economic benefits and sustainability. Sometimes it may be difficult during the planning phase to combine these aspects without compromises.

Within the next step a set of rules is derived as planning guidelines. These guidelines are object-related, clearly defined and often measurable. For example, these objects can be related to parts of the building structure or used storage technologies. The agreement of all stakeholders and as reliably as possible defined boundary conditions of the project are crucial to ensure the acceptance and usage of the guidelines. Therefore, this combination of steps needs to be performed by all stakeholders which are relevant for the vision definition. The choice of established guidelines should be considered as still mutable in order to act corresponding to these rules but allowing for modifications in order to satisfy new or changed requirements resulting from changes in the data basis or boundary conditions.

The guidelines should be used to determine measures which make the fulfilment of the vision accessible. The

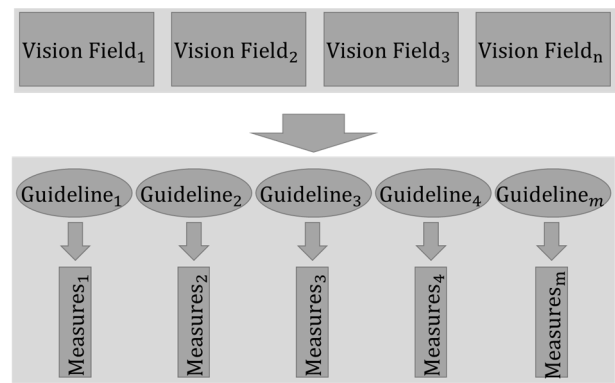


Figure 6: Vision definition process.

measures are formulated by the internal stakeholders. These measures have to be revised in regular intervals, because they are too explicit to be completely determined at the start of the project and in order to work in a flexible way.

4.3 Planning of large logistics sites

In contrast to the recent literature on production and logistics site planning methodologies, the proposed planning procedure is not based on the typical planning stages like project setup, structuring, system design and realization. It is structured like a flexible top-down network of decisions and actions (Figure 7).

In this top-down structure, each decision is followed by actions which lead to decisions on a lower planning level. The decisions on lower levels are determined and derived from decisions on higher levels of the network. In parallel, the influence of a certain decision decreases with the decision level. For example, a possible decision in the beginning of the project could be the proper utilization of the building plot which might lead to a multi-storied logistics site. As a consequence, the storage systems inside the building should also utilize the provided ceiling height. The influence of a certain decision on the entire project decreases with every decision level. But this top-down structure should not be regarded as a barrier for reiteration. For example, higher level decisions can be changed if the data basis of dependent decisions is changing during the planning procedures.

In this structure, the scope of every decision is clearly delimited. This is one more step to minimize uncertainties in the responsibilities, by clearly defined and responsible stakeholders. Therefore, the scope of the decisions on a certain level should not have overlaps with

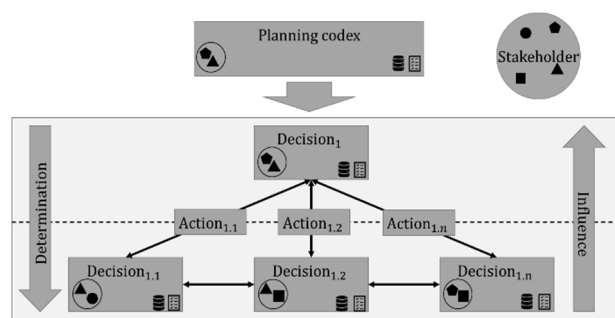


Figure 7: Proposed warehouse planning framework

other decisions on the same level. If a decision in the network shows strong dependencies to other decisions the planning team should consider to merge the mentioned set of decisions to one planning decision. For example, if considerations of the goods receipt processes and storage systems are highly interrelated, a merge of these decisions could be beneficial to combine the competencies of both planning teams and to reduce coordination efforts and interfaces.

4.4 Decision-making steps

Within the presented decision-network, a certain decision is always accompanied by responsible stakeholders and a data basis. The stakeholders are always a subset of the stakeholder pool of the entire project. The database is constantly modified during the course of the project. Every decision must end with a comprehensive documentation for later project demands and overall learnings. The explicit steps in a certain decision of greater importance are illustrated in this section (Figure 8).

The planner have to identify the requirements of the system or object to be designed and to align them to the overall planning codex of the project. On that basis, decision criteria have to be established. Subsequently, possible solutions and scenarios are identified. A morphological box is recommended to build scenarios. According to each process step one or more technical solutions are listed and by the combination of solutions for each step scenarios can be found. This procedure intends to minimize decision biases and ensures a broad decision basis.

During the scenario definition obviously unfeasible technical solutions can be discarded based on decision criteria. From the remaining technical solutions, scenarios will be derived and detailed for further decision-makings. Practical projects have shown a high complexity and time consumption of these steps.

Additionally, during the planning procedures new information can arise, influencing the database of the

decision. Thus, planning iterations are essential to include new insights in further concepts and calculations. Therefore, parameterized spreadsheet models are recommended to perform the calculations [7].

The evaluation of the planning options must be carried out in a qualitative and quantitative way to ensure the feasibility and profitability on the one hand and the alignment of the decisions with the planning codex on the other hand. The qualitative evaluation is performed by revised decision criteria to include priorities from later decision stages of the project. These criteria are incorporated into the benefit value analysis. Capacities, investments and recurring costs are investigated by a quantitative evaluation. Finally, the planning team creates a documentation of the decision which presents the decision scope and the proposed solution. Decision-maker can challenge the proposal and select a certain scenario.

In conclusion, the steps of a decision are highly interrelated while the data basis may still change dynamically. Therefore, the participating stakeholders must be open for reiterations and revisions of basic assumptions even in later planning stages. Thus, parameterized spreadsheets are highly recommended. This way of working should create efficient planning procedures even if redundancies in the procedures are unavoidable.

5. EXAMPLARY PLANNING PROJECT

In order to illustrate the proposed planning framework, results from an exemplary planning project are presented. The project deals with the planning of a logistics site, with the strategic purpose to ensure future demands of the production of a large systems manufacturer. Therefore, existing warehouses are consolidated into a new logistics site, which offers reduced operating costs by simplifications of the processes and reduction of surfaces. The new logistics site should be located as close as possible to the actual production site. Hence, the project is located in an urban

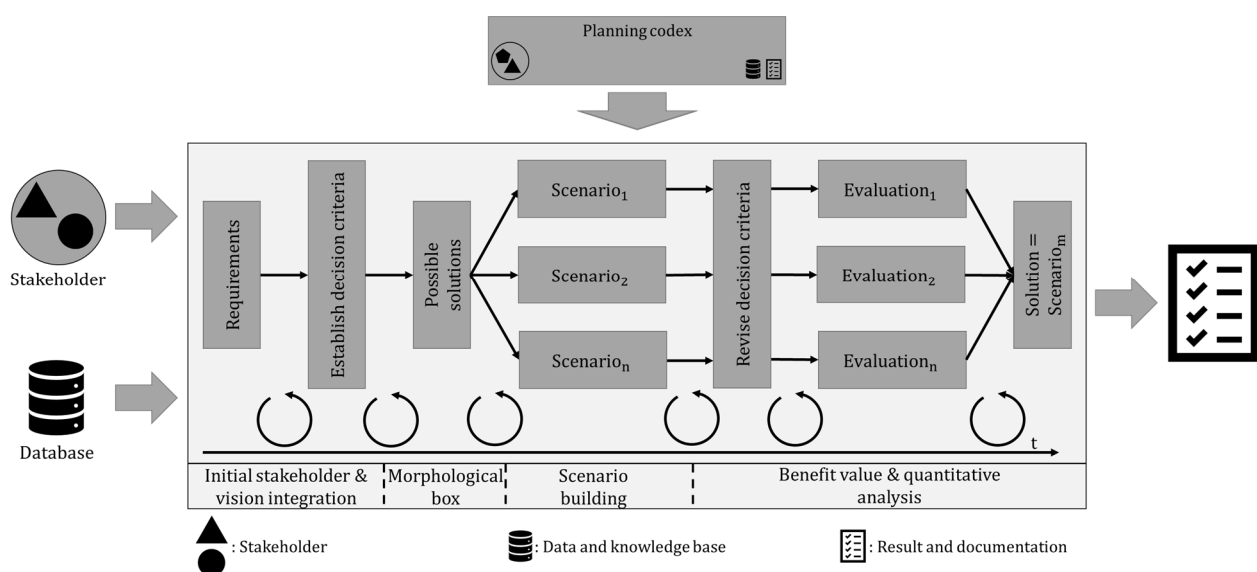


Figure 8: Proposed decision-making steps

environment, leading to the need for an optimal surface utilization avoiding high building plot costs.

5.1 Stakeholder analysis

The core project team consists of some 15 members being responsible for both the design of the building and the planning of the logistics technology. Outside of this core team some 45 stakeholders are identified whose interests have to be considered.

The planner are composed of internal logistics experts from logistics operating and engineering business units. Furthermore, logistics consultants are engaged for the planning of processes, warehouse systems and digital infrastructures. Next to the logistics planner, the construction company is in charge to plan the building of the new logistics site.

These planner are primarily interested in optimal future processes and an overall project success in terms of capital and operating expenditures. Besides this primary interest, internal and external planner may intend to position themselves for future planning and consulting tasks.

Knowledge is provided from over ten stakeholders such as the production, sales representatives of logistics equipment vendors and the current logistics service provider.

The decision-maker are represented by managers with different roles in the corporate organization structure. Thereby, different planning objectives are prevailing within the decision-maker group. The interests of two manager groups have to be integrated. On the one hand, managers who need to bear the subsequent operating expenditures. On the other hand managers being responsible for the project investment who are more concerned about low upfront capital expenditures. Further interests of the society are represented by local authorities which are mainly interested in both an efficient use of land surface and about traffic impact.

The operating logistics service provider of existing logistics sites are mainly integrated as knowledge-provider regarding current material flows and processes.

By the holistic investigation of existing and participating stakeholders inside the planning project the following definition of the planning codex is supported by the comprehensive overview of all interests.

5.2 Vision, guidelines and measures for a large logistics site

For the decision-making in subsequent project phases, interests of some 60 stakeholders need to be included and balanced by the project team. To support the integration, the proposed planning framework recommends the definition of a planning codex. For the actual planning project, this codex is composed out of five vision fields and 13 guidelines which are introduced in the following.

The fields of vision for the planning project address organizational, technological and economic objectives to form a holistic set of rules to align subsequent planning activities with the superordinate planning objectives.

Figure 9 shows two exemplary fields of vision of the project. Economic benefits are mainly generated by the consolidation and reduction of transports, surface requirements and personnel. Furthermore, the use of innovative and adequate technologies can reduce the costs in terms of surface utilization and labour costs. By lean logistics approaches, waste in processes and material demands can be minimized.

The second field of vision for the new logistics site is sustainability in environmental, social and economic

The new warehouse is a logistics site, which ...

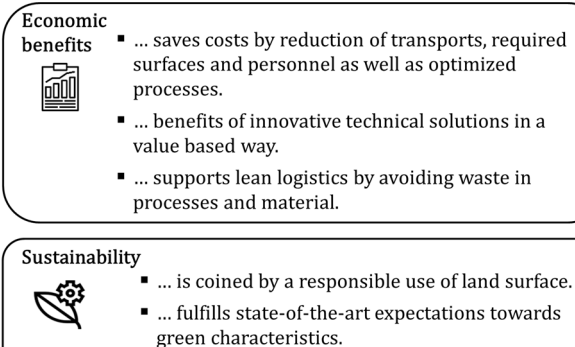


Figure 9: Economic benefits and sustainability as exemplary vision fields

terms. Sustainability especially in terms of building plot utilization is an important topic for logistic projects in urban regions due to expensive and limited building plots for industrial facilities [11]. Further, sustainability must include state-of-the-art technical solutions for green characteristics.

Additional fields of the vision deal with flexible and scalable processes, a good appearance of the logistics facility as well as leadership & human resources focusing on working conditions and responsibilities.

Based on the five vision fields, the project team derives object-related guidelines for certain planning activities. Exemplary guidelines and corresponding measures are given in Table 1. Regarding the building structure, the guidelines could cover the topics high buildings, attractive appearance and extendibility. Potential measures could be to build an at least three-storied logistics facility and to foresee surfaces for future extension. In terms of logistics technologies, potential guidelines could be the usage of innovation and flexible technologies to support a good surface utilization. Furthermore, the separation of value creation and transport leads to dedicated service areas and a specialization of employees responsible for order picking and transport. The installation of mobile shelving racks to reduce aisle surfaces and dedicated service areas for value creating tasks are appropriate measures in terms of logistics technologies.

In investigated industrial projects, the planning codex turned out as an efficient tool for the identification and balancing of the variety of stakeholder interests. Compared to a traditional, extensive requirement specification, the planning code allowed for an earlier identification and documentation of key stakeholder interests. The rather short documentation in the limited number of vision fields and guidelines served as an

important basis for further project work. Due to its compact presentation, the fundamental agreement could be quickly recalled in the discussion of later decisions.

Table 1: Derived guidelines and corresponding measures.

Object	Guidelines & measures
Building structure	<ul style="list-style-type: none"> Rather high than flat <ul style="list-style-type: none"> Usage of at least three floors Efficient usage of the building height with appropriate storage technologies Attractive appearance <ul style="list-style-type: none"> Different pavements for outside surfaces Day light on service areas Building concept allows extensions <ul style="list-style-type: none"> Foresee reserve surface on building plot Roof & wall openings for later equipment installations
Logistics technologies	<ul style="list-style-type: none"> Innovative and flexible logistics technologies <ul style="list-style-type: none"> Mobile shelving systems Automated transports Separation of value creation and transport <ul style="list-style-type: none"> Specific personnel for order picking and transport Well defined material transfer systems

5.3 Scenario building and decision making

To illustrate the described decision-making steps, in the following the decision process for a storage technology for parts with small volume is described. These are parts which can be stored into boxes with 600 mm length and 400 mm width.

The decision for the storage technology of these parts was preceded by the decision of the building height determining the maximum system height of the logistics equipment. Furthermore, the macro material flow was specified beforehand. A coequal but not fully independent decision was the decision of logistics equipment for parts of bigger volume.

The knowledge- and database included e.g. the current number of storage locations, the costs per employee, current production rates or existing fire safety regulations. Requirements for the decision, such as the future number of inbound and outbound transports or storage locations were derived from this database.

Important guidelines and measures for the particular decision from the planning codex were for instance the demand for innovative logistic technologies resulting in the requirement for automated transport. The planning codex was furthermore considered to establish first decision criteria and to build a preselection of possible solutions from an initial morphological box.

While the automated solutions Automatic Storage and Retrieval System (ASRS) and AutoStore are particularly appropriate in terms of picking performance, surface utilization, expandability and operating costs, the manual shelving rack results in the lowest investment costs (Figure 10). The carry pick and manual shelving racks solution were discarded due to the lack of advantages in terms of operating costs and surface requirements. The scenarios always included conveying technology and considered the material flow from the put away process to picking and consolidation. Shelving

racks on three levels with automatic conveyors for material transports, an ASRS and an AutoStore system were selected for detailed considerations.

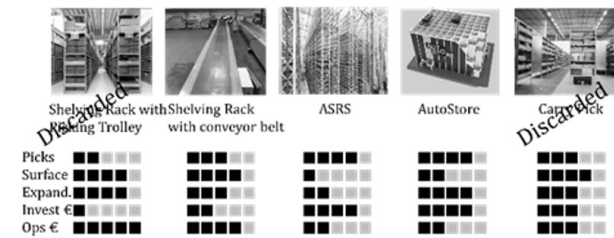


Figure 10: Selected scenarios for further planning

Due to changes in the data base and the requirements for the storage technologies during the planning period, several iterations of the decision-making process became necessary. As a consequence, the AutoStore system was replaced by the scenario storage lifts. Investment costs, operational costs as well as surface requirements were calculated for each scenario. Furthermore, a qualitative analysis was conducted by the project team. Figure 11 shows an abstract of the qualitative evaluation containing three out of ten evaluated criteria. The portfolio diagram from Figure 12 was finally used to compare the scenarios in regard of the total costs for 10 years and their benefit value. As the ASRS shows low total costs and a high benefit it was finally chosen as the preferred solution.

Qualitative evaluation		Scenario 1 - Shelving Rack	Scenario 2 - Storage Lift	Scenario 3 - ASRS Shuttle
Evaluation criteria	Weight	Benefit (0-5)	Benefit (0-5)	Benefit (0-5)
Simple increase of storage locations	8%			
Simple increase of pick rate	7%			
Flexibility of pick rate	7%			
...	x%			
Benefit value:	100%	2.1	2.5	3.8

Figure 11: Benefit value analysis

A high number of knowledge-provider were consulted to gather the required information to develop and evaluate the scenarios.

The logistics experts had a strong influence on the decision process for small volume parts, while architects and building experts were hardly involved. Based on a continuously updated morphological box and investigated

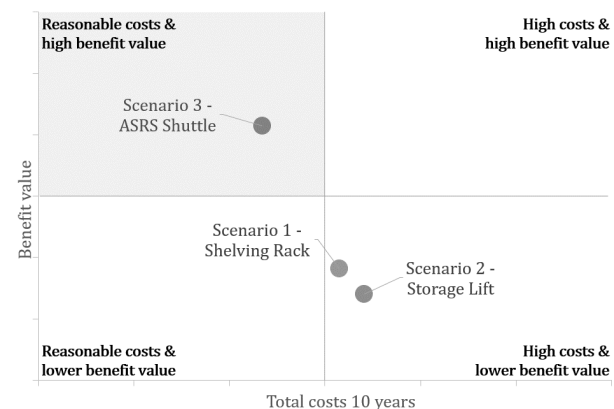


Figure 12: Portfolio diagram of benefit values and total costs

scenarios the decision has finally been made by a group of managers of different departments.

Due to many planning uncertainties a high number of change requests had to be incorporated for a period of 8 months on a weekly basis. The morphological box and a parameterized scenario spreadsheet for the evaluation of competing solutions turned out to be extremely useful during the planning process. Applying these tools, the effects of changes in the planning base could be shown instantly in management meetings and a continuous documentation was maintained.

6. CONCLUSION

Experiences from several industrial projects showed gaps in the applicability of established methodologies for the planning of production and logistics sites. In such a complex planning project various uncertainties exist, which lead to suboptimal planning results in terms of quality, time and cost. This work presents a planning framework for large logistics sites which was developed based on experiences from industrial projects in order to overcome the identified gaps. The proposed framework includes a comprehensive analysis of the involved stakeholders as well as a planning codex to find common agreements between the stakeholders. In contrast to most planning methodologies, which are structured in a fixed

sequence of planning steps, the proposed framework is structured in a network of decisions. This allows a higher flexibility in the planning procedures to react to changing requirements and data. A process for each individual decision is proposed, which includes the creation as well as a quantitative and qualitative evaluation of several planning alternatives. In order to illustrate the developed planning framework, the processes and results from an exemplary planning project are presented.

Overall, the preparation of decisions e. g. the generation of morphological boxes and decision criteria turned out to be highly complex and time consuming in the exemplary project. In addition, the advantages of the method occur only when all stakeholders are well integrated and decisions are not replaced by individual decisions of single stakeholders. Future research should deal with further detailing and validation in order to establish the proposed framework.

The presented work connects academic planning approaches with practical experiences gained in a number of industrial projects. Scientists benefit from this work, as practical limitations and corresponding solutions for academic methodologies are pointed out and insights into practical projects are given. Managers could benefit by introducing the planning framework into their business.

REFERENCES

- [1] ten Hompel, M., Schmidt, T., and Dregger, J.: *Materialflusssysteme*, Springer Berlin Heidelberg, Berlin, Heidelberg, 2018.
- [2] Gudehus, T.: *Logistik*, Springer Berlin Heidelberg, Berlin, Heidelberg, 2010.
- [3] Martin, H.: *Transport- und Lagerlogistik*, Springer Fachmedien Wiesbaden, Wiesbaden, 2016.
- [4] Kettner, H., Schmidt, J., and Greim, H.-R.: *Leitfaden der systematischen Fabrikplanung*, 1984th ed., Hanser, München, 2010.
- [5] Verein Deutscher Ingenieure: *Fabrikplanung*, VDI 5200-1, 2011.
- [6] Wiendahl, H.-P., Reichardt, J., and Nyhuis, P.: *Handbuch Fabrikplanung: Konzept, Gestaltung und Umsetzung wandlungsfähiger Produktionsstätten*, 2nd ed., Hanser, München, 2014.
- [7] Baker, P. and Canessa, M.: Warehouse design: A structured approach, *European Journal of Operational Research*, Vol. 193, No. 2, pp. 425–436, 2009.
- [8] Papadopoulos, C. E. and Yeung, H.: Uncertainty estimation and Monte Carlo simulation method, *Flow Measurement and Instrumentation*, Vol. 12, No. 4, pp. 291–298, 2001.
- [9] Brugha, R. and Varvasovszky, Z.: Stakeholder analysis: a review, *Health policy and planning*, Vol. 15, No. 3, pp. 239–246, 2000.
- [10] Carter, C. R. and Jennings, M. M.: Logistics Social Responsibility: An Integrative Framework, *Journal of Business Logistics*, Vol. 23, No. 1, pp. 145–180, 2002.
- [11] C. Raabe: *Logistikmarkt Deutschland*. [Online] Available: https://www.realestate.bnpparibas.de/upload/docs/application/pdf/2019-07/bnppre-immobilien-logistikmarkt-deutschland-at-a-glance-2019q2.pdf?id=p_1743764 (15.08.2019).

New approach for ISO 16625

Markus Golder

Professor
University of Chemnitz (former Karlsruhe
Institute of Technology)

Martin Anders

Dipl.-Ing.
University of Dresden

Gregor Novak

Dr.-Ing.
University of Stuttgart

Christoph Eiwán

Dipl.-Ing.
Liebherr, Biberach

Since the early 2000s efforts have been made to introduce a new way to calculate the lifetime for a rope in rope drives, nowadays implemented in EN 13001-3-2. This elaborated standard uses a cycle-based approach instead of a time-based approach, previously well-established for many years in DIN 15020-1 for example. Since its introduction, many discussions arose towards the cycle-based approach, especially regarding safety and multi-layer spooling. In 2015, a working group in TC96/SC3 has been established to revise ISO 16625 to adopt the cycle-based approach of EN 13001-3-2 and beyond that to enhance it. The enhancement addresses the special requirements of multi-layer spooling and provides a new foundation for the proof of fatigue strength. This "New Method" for the proof of fatigue strength is based on the Feyrer formula. The "New Method" was developed and verified in a collaboration between the Universities of Karlsruhe, Dresden, and Stuttgart. Combining the "New Method" with the cycle-based approach implemented in EN 13001-3-2 leads to the new approach for ISO 16625. The paper will report the initial situation, the developments of the "New Method" and describes the new approach for ISO 16625 subsequently.

Keywords: ISO 16625, EN13001-3-2, Wire rope, fatigue, bending test

1. INTRODUCTION

ISO 16625, Cranes and hoists – Selection of wire ropes, drums and sheaves, in its current edition from 2013, provides a method to select a design factor Z_p mainly by considering the classification of the hoist mechanism [1]. The classification itself is time-based and refers to ISO 4301-1:1986 [2]. The only "proof of competence" is given by the simple formula $F_{min} \geq S \times Z_p$, where F_{min} is the minimum breaking force of the rope, and S is the maximum rope tension [1]. Modern standards like EN 13001-3-2, Cranes – General design – Part 3-2: Limit states and proof of competence of wire ropes in reeving systems, provide different proof of competences for running and stationary ropes. Furthermore, EN 13001-3-2 distinguishes between a static proof of competence and a fatigue proof of competence. Concerning running ropes, a proof of competence for multilayer spooling is also laid down. It is of particular importance to mention, that the fatigue proof of competence is cycle-based [3]. This concept of EN 13001-3-2 should be transferred to ISO 16625 during a revision. In addition, the proof of fatigue strength for running ropes shall be developed further, based on well-known and scientific proven methods. Two methods are particularly appropriate and will be considered, the stress method Leipzig after Jehmlich/Steinbach [4] and the method Stuttgart after Feyrer [5]. Both methods result in regression models which calculate the amount of bending cycles in dependency of certain parameters like the rope force/stress, the D/d ratio, and the load spectrum. The difference between these two methods is given by the test conditions and the evaluation of the results.

Correspondence to: Prof. Dr.-Ing. Markus Golder
Technical University of Chemnitz, Professorship of
Conveying Engineering and Material Handling
Reichenhainer Str. 70, 09126 Chemnitz, Germany
E-mail: markus.golder@mb.tu-chemnitz.de

2. STRESS METHOD LEIPZIG

2.1 Origin

In the 1970s, extensive bending fatigue tests at the "Institut für Bergbausicherheit Leipzig" formed the basis for the development of the method Leipzig for the mathematical estimation of endurable bending cycles in rope drives. The test evaluation with the help of a mechanical model led to the standard TGL 34022 (statutory standard of the former German Democratic Republic), which regularized the dimensioning of rope drives and the calculation of rope lifetime.

2.2 Basic principle

Starting point is the calculation of the strain of the wires of a wire rope from different oscillating tensile, bending and compressive stresses at the contact areas on the outside and at the inside of a rope construction. The stresses are calculated from parameters of the rope drive (D/d ratios etc.), the operating conditions (rope force or load spectrum etc.) and the design of the rope itself. The mechanical model summarizes the stresses to a combined strain y formula (1). Thus, a single-parameter Wöhler-line-system could be set up with strain y over the bending cycle N , expressed in formula (2), that can be described as the Wöhler-line of the wires of a wire rope (figure 1). With the parameters of the Wöhler-lines for rope discard and strand failure the endurable bending cycles with different failure probabilities can be determined. A specific characteristic of the method Leipzig is the consideration of the contact conditions of the outer wires of the outer strands towards the sheaves and towards the wire rope core for the calculation of the compressive stress. Thereby, it is possible to estimate the inner rope deterioration independent from the visible wire break development.

$$y = \frac{1}{R} \cdot \left(1,04 \cdot \frac{R}{v} + \frac{0,6 \cdot E}{KL^2 \cdot D_G/d} + KL \cdot L \cdot B \cdot \sqrt{\frac{\pi}{4} \cdot \frac{f \cdot R}{v \cdot D_G/d}} \right) \quad (1)$$

$$N^{PA\%} = \frac{H^{PA\%}}{y_{CL}} \quad (2)$$

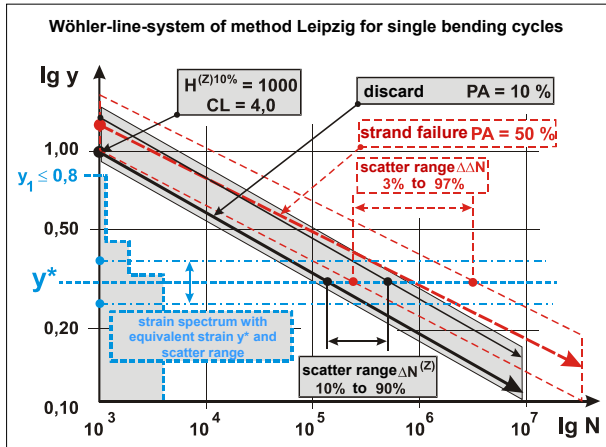


Figure 1: Wöhler-line-system method Leipzig

A detailed description of the method Leipzig with all its parameters can be found in [4].

3. METHOD STUTTGART

3.1 Origin and basic principle

Since the 1980s, several thousand bending tests were performed at the Institute for Material Handling and Logistics (IFT), in the beginning under the supervision of Feyrer. In the lifetime diagram in figure 2, the behaviour of a wire rope is shown. Typically, the lifetime of a wire rope can be represented with a straight best-fit line, which can be separated in two sections. The first section comprises the fatigue strength followed by a sharp reduction of the lifetime - at Donandt point - the short-time strength.

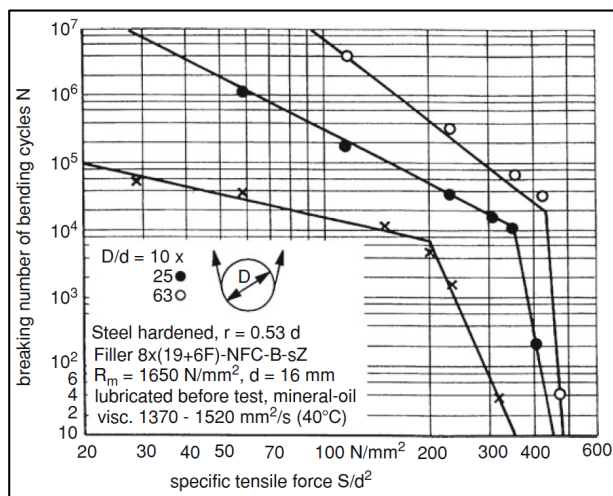


Figure 2: Lifetime diagram of a Filler rope [5]

Feyrer used the results from these several thousand bending tests with different configurations to develop a

linear regression model, which led to the well-known Feyrer-Formula [5]:

$$\begin{aligned} \lg N = & b_0 + \left(b_1 + b_3 \cdot \lg \left(\frac{D}{d} \right) \right) \\ & * \left(\lg \left(\frac{S}{d^2} \right) - 0,4 \right) \\ & * \lg \left(\frac{R_0}{1770} \right) + b_2 * \lg \left(\frac{D}{d} \right) \\ & + \lg(f_d) + \lg(f_L) + \lg(f_C) \end{aligned} \quad (3)$$

Feyrer chose this approach because the actual acting tensions in a rope and pressures on a rope are often unknown or difficult to calculate. Therefore, Feyrer formulated an analogous model, which comprises the main influencing factors. It includes several rope drive related influences like the D/d-ratio as well as regression coefficients b_i for the actual rope construction, e.g. for a rope in Warrington-Seale construction. Depending on the lifetime of interest, different rope coefficients can be chosen, for example to calculate the lifetime until discard with a certainty of 50%. A detailed description of the method Stuttgart with all its parameters can be found in [5].

3.2 Method Stuttgart today

Beside the stress method Leipzig, also the method Stuttgart after Feyrer is an acknowledge procedure to estimate the lifetime of wire ropes and considered in VDI 2358, too. Differences between both methods exist in the test conditions and the evaluation methods [4].

4. THE NEW WAY OF EN 13001-3-2

The standard EN 13001-3-2 has been developed in the early 2000s under the responsibility of CEN/TC 147 Cranes - Safety. From the very beginning, the working group focused on Feyrer's findings and implemented his method into EN 13001-3-2. In particular, the fatigue proof of competence is based on the Feyrer-Formula (3). But, comparative calculations between the methods Leipzig, Stuttgart and EN 13001-3-2:2014 (current edition) revealed that EN 13001-3-2 always "calculates" a higher total amount of bendings for a rope until discard than the other two methods [7, 8]. This circumstance has been criticized heavily [7]. Figure 3 exemplifies the differences in the results for the lifetime of a Filler wire rope calculated by method Stuttgart and according to EN 13001-3-2:2014. Of interest is the area between the vertical lines $Z_p=3,15$ and $Z_p=9$ of the lifetime diagram (figure 3). The range in between usually represents the safety level for ropes in crane applications according ISO 16625. In terms of comparability of the results, dynamic factor, risk coefficient, load spectrum factor and factors for further influences have been set to 1.

The comparative calculations ($D/d=10$) have shown that the ratio in lifetime varies between factor 4 for $Z_p=3,15$ up to factor 10 for $Z_p=9$. The higher calculated lifetimes may lead to safety issues. If a designer would rely on the result of the proof of competence given by EN 13001-3-2 it might happen, that a wire rope would fail in the field prior to its necessary inspection.

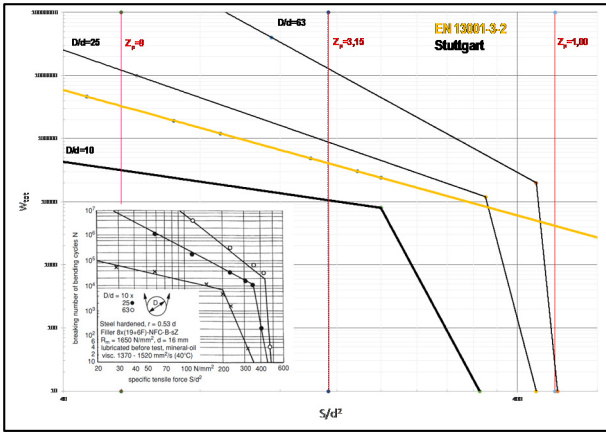


Figure 3: Lifetime diagram of a Filler rope calculated by method EN13001-3-2 and method Stuttgart for D/d=10, based on figure 2 [8]

Detailed studies show why method EN 13001-3-2 leads to such results [8]. In EN 13001-3-2:2014 it is stated:

“According to test results the fatigue strength of ropes in terms of number of bendings (rope force to number of bendings relationship) is approximately inversely proportional to the second power of the applied rope tension force. With the additional requirement that the ratio of the rope bending diameter D to the rope diameter d increases with the number of bendings w_{tot} according to

$$\frac{D}{d} \sim 1,125^{\log_2(w_{tot})} \quad (15)$$

(i.e. D/d increases by 1,125 for increasing w_{tot} by 2), the rope force to number of bendings relationship is closely inversely proportional to the power of 3.” [3, section 6.1].

The assumption stated by formula (15) of EN 13001-3-2 [3, section 6.1] and a constant slope of $m=3$ for the lifetime curve of a wire rope is not correct. The results shown in figures 2 and 3 clearly indicate that the slope changes with the D/d ratio and thus refute the assumption. Furthermore,

“the number of bendings at reference point:

$$w_D = 5 \cdot 10^5 \quad [3, \text{section 6.3.4}],$$

is not selected properly and thus cannot be constant. Also, very critical is the factor f_{f1} that incorporates formula (15) of EN 13001-3-2 and the D/d ratio into one factor:

“The reference ratio value of D/d is calculated by

$$R_{Dd} = 10 \times 1,125^{\log_2\left(\frac{w_{tot}}{8000}\right)} \quad (32)$$

[...] The factor f_{f1} is calculated by

$$f_{f1} = \frac{D/d}{R_{Dd}} \quad (33)$$

[3, section 6.4.2].

It is neither known nor traceable whereof the factor 8000 in the exponent of formula (32) of EN 13001-3-2 [3, section 6.4.2] has been derived from.

As stated, it is possible to “calculate” the amount of bendings until discard by applying the method outlined in EN 13001-3-2, but only implicit. EN 13001-3-2 provides a fatigue proof of competence for running ropes that can be used to derive a unique formula for w_{tot} . The derivation of w_{tot} , starting from the basic proof of competence $F_{Sd-f} \leq F_{Rd-f}$ is shown in figure 4 (see below). In enhancement to EN 13001-3-2 the derivation also implements the Z_p value from ISO 16625 and introduces a variable factor w_{spec} instead of maintaining a fixed value of 8000. Moreover, the explicit formula for w_{tot} introduces a variable factor m instead of a fixed value of 3. Figure 4 highlights the critical parameters. Descriptions of the factors used in EN 13001-3-2 can be found from figure 9 (see below) and [3].

5. “NEW METHOD” TO CALCULATE THE LIFETIME OF A ROPE

The “New Method” is based on the assumption, that the regression calculation given by method Stuttgart, see formula (3), can be conducted even for forces higher than the Donandt force. This assumption seems to be fallacious because a wire rope driven in a reeving system with such high forces will fail after a small amount of cycles. Most likely, that is the reason why such an approach hasn’t been considered yet before. To determine a solution approach which follows the above stated assumption, the straight best-fit lines in figure 2 are extended (figure 5). It becomes apparent, that the extended lines intersect in a common point. This point can be interpreted as a virtual reference point of a specific wire rope, defined by a specific reference force S_{ref}/d^2 and reference amount of bendings w_{ref} . S_{ref}/d^2 and w_{ref} can be determined by using formula (3). For two different D/d ratios, D_1/d and D_2/d , the two equations of formula (3) have to be set equal: $\log(N_1)=\log(N_2)$. The complete derivation with the simplification $D_i = D/d$ is shown in figure 6 (see below).

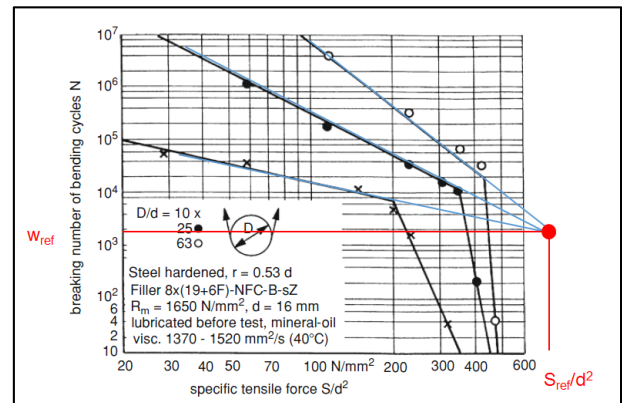


Figure 5: Extension of straight best-fit lines to define a reference point [8]

The derivation of S_{ref} and w_{ref} , with the method Stuttgart, mathematically proves that the virtual reference point would exist, if wire ropes could resist higher forces. Therefore, it is useful to take the reference

point into account that enables a simplified, but equivalent, lifetime calculation of a wire rope. This “New Method” determines the total amount of bendings until discard comparable to the methods of Stuttgart and Leipzig, but in a less complex manner (refer to formula (6)). Thus, such a simplified method is easier to apply and less extensive to adopt into a standard.

$$N = w_{tot} = \left(\frac{S_{ref}}{S} \right)^m \times w_{ref} \quad (6)$$

It can be proven, that formula (6) and formula (3) are equivalent by using the definition of S_{ref} and w_{ref} shown in figure 6 (see below). Further, that the exponent m of formula (6) is given by:

$$m = - \left(\log \frac{D}{d} \times b_3 + b_1 \right) \quad (7)$$

Now, it is possible either to conduct a simplified lifetime calculation by using the regression coefficients b_i from Feyrer based on many tests or to perform wire rope tests for different D/d ratios to determine S_{ref} , w_{ref} and $m(D/d)$. Moreover, it turned out to be useful to relate the reference force S_{ref} with the minimum breaking force F_{min} - in EN 13001-3-2 called ultimate breaking Force F_u - by introducing the parameter γ_{ref} :

$$\gamma_{ref} = \frac{F_{min}}{S_{ref}} = \frac{F_u}{S_{ref}} \quad (8)$$

6. NEW APPROACH FOR ISO 16625

The objective of the revision of ISO 16625 is to combine the partly correct approach of EN 13001-3-2 and the “New Method” introduced in chapter 5 to develop an enhanced, new approach for ISO 16625. As already stated, the factor f_{f1} and $w_{spec}=8000$ shall be eliminated, w_D should be replaced by w_{ref} , γ_{ref} should be introduced, and m should be variable. The result of the combined approach for w_{tot} is shown in figure 7.

Figure 7: Combination of EN13001-3-2 and “New Method” [8]

By introducing $S = (m_{Hr} \cdot x_g) / n_m$ for the rope force and sorting the different parameters in a proper way, w_{tot} can be calculated in a new unique way in accordance with method Stuttgart and the “New Method”, respectively. By setting the dynamic factor Φ° , the risk coefficient γ_{ref} ,

the load spectrum factor k_r and factors for further influences f_{Si} , f_{fi} to 1, w_{tot} can be expressed, like formula (6), in the most basic way, see figure 8.

Figure 8: New approach for ISO 16625 [8]

The exponent m can be calculated according formula (7), but therefore the regression parameters b_i must be known. A simplified possibility is given by the following empiric definition:

$$m = 1.125 \frac{D}{d} \quad (9)$$

Studies show that using formula (6), formula (9) instead of formula (7) in combination with the dynamic factor, risk coefficient, load spectrum factor and factors for further influences will in most cases deliver lower results for the total amount of bendings of a wire rope until discard than real test results [8].

Figure 9 (see below) shows exemplary test results of a Filler rope 8x(19+6) according the method Stuttgart, according EN 13001-3-2:2014 and according the new approach for ISO 16625 for a D/d ratio of 15 and 40. Based on these findings, a clear statement could be made that the new approach of ISO 16625 provides results that are on a safe side. The results for ISO 16625 basic/ “New Method” are almost identical as the results for Stuttgart.

Currently, a revised document of ISO 16625 is under review that contains the new approach introduced in this paper. In this document the parameters $\gamma_{ref} = 0,5$ and $w_{ref} = 1000$ have been predefined. Further studies will clarify, if this setting in general will lead to safe proofs of competence for fatigue strength for all types of wire ropes.

7. CONCLUSION

Combining the partly correct method of EN 13001-3-2:2014 with the “New method” has led to the new approach for ISO 16625, outlined in this paper. This new approach for ISO 16625 is a major step to provide a proof

of competence for fatigue strength of a wire rope in a simplified, unique and safe manner, in particular to calculate the lifetime of a running rope in a reeving system.

REFERENCES

- [1] Cranes and hoists - Selection of wire ropes, drums and sheaves, ISO 16625:2013.
- [2] Cranes and lifting appliances - Classification - Part 1: General, ISO 4301-1:1986.
- [3] Cranes - General design - Part 3-2: Limit states and proof of competence of wire ropes in reeving systems, EN 13001-3-2:2014.
- [4] G. Steinbach, M. Anders, and D. Ryk, "Betriebsdauer in Seiltrieben - Berechnung der Biegewechselzahl - Methode "Leipzig", Hebezeuge Fördermittel, 5, pp. 34-35, 2018.
- [5] K. Feyrer, Wire Ropes, 2nd ed. Heidelberg: Springer-Verlag, 2015.
- [6] O. Gronau and G. Steinbach, "Dimensioning of rope drives and operating time of wire ropes," presented at the Innovative Ropes and Rope Applications: A celebration of 175 years of wire rope, OIPEEC Conference 2009, 3rd International Stuttgart Ropedays, Stuttgart, 2009.
- [7] G. Steinbach, M. Anders, and D. Ryk, "Drahtseile in Seiltrieben nach DIN EN 13001-3-2:2014-12 - Bemessungsbiegewechselzahl und Realbiegewechselzahl; Exklusivbeitrag," Hebezeuge Fördermittel, 11-12, pp. 1-23, 2015.
- [8] M. Golder, "Revision of ISO 16625, new approach for fatigue calculation," Paris, Presentation made during WG 3 Meeting, ISO/TC 96/SC 3/WG 3 - N 23, 16-17 Apr 2018.

$$F_{Sd_f} \leq F_{Rd_f} \quad F_{Sd_f} = \frac{m_{Hr} \cdot g}{n_m} \cdot \phi^{\circ} \cdot f^{\circ} S_2 \cdot f^{\circ} S_3 \cdot \gamma_n \leq F_{Rd_f} = \frac{F_u}{\gamma_{rf} \cdot \sqrt[3]{s_r}} \cdot f_f$$

$$Z_p = \frac{F_u}{\frac{m_{Hr} \cdot g}{n_m}} \geq \frac{\phi^{\circ} \cdot f^{\circ} S_2 \cdot f^{\circ} S_3 \cdot \gamma_n \cdot \gamma_{rf} \cdot \sqrt[3]{s_r}}{f_f} = \frac{\phi^{\circ} \cdot f^{\circ} S_2 \cdot f^{\circ} S_3 \cdot \gamma_n \cdot \gamma_{rf} \cdot \sqrt[3]{s_r}}{f_{f1} \cdot f_{f2} \cdot f_{f3} \cdot f_{f4} \cdot f_{f6} \cdot f_{f7}} = \frac{\phi^{\circ} \cdot f^{\circ} S_2 \cdot f^{\circ} S_3 \cdot \gamma_n \cdot \gamma_{rf} \cdot \sqrt[3]{k_r} \cdot \frac{m}{\sqrt[3]{w_D}}}{\left(\frac{D}{d} \right) \cdot \left(\frac{\log\left(\frac{w_{tot}}{w_{spec}}\right)}{10 \cdot 1.125} \right) \cdot f_{f2} \cdot f_{f3} \cdot f_{f4} \cdot f_{f6} \cdot f_{f7}}$$

In EN 13001-3-2:

w_{tot} is the calculated total number of bendings during the design life of a rope, not to be interpreted as the number of bendings leading to discard of the rope;

$$w_{tot} = \left[\frac{Z_p = \frac{F_u}{\frac{m_{Hr} \cdot g}{n_m}} = f\left(\frac{D}{d}\right)}{f^{\circ} S_2 \cdot f^{\circ} S_3} \cdot \frac{\frac{D}{d}}{10 \cdot \left(\frac{1}{w_{spec}}\right)^{\log(1.125, 2)} \cdot \left(\frac{1770}{R_r}\right)^{0.6} \cdot f_{f3} \cdot f_{f4} \cdot f_{f6} \cdot f_{f7}} \cdot \frac{m}{\gamma_{rf} \cdot \gamma_n \cdot \phi^{\circ} \cdot \sqrt[3]{k_r} \cdot \frac{w_D}{m}} \right]^{\frac{1}{\left(\log(1.125, 2) + \frac{1}{m}\right)}}$$

Now: w_{tot} is the calculated total number of bendings leading to discard of the rope

Figure 4: Derivation of the total number of bendings leading to discard of the rope out of EN 13001-3-2:2014 [8]

$\log(N_1) = \log(N_2)$

$$\left[(b_1 + b_3 \cdot \log(D_1)) \cdot \left(\log\left(\frac{S_{ref}}{d^2}\right) - 0.4 \cdot \log\left(\frac{R_0}{1770}\right) \right) + b_2 \cdot \log(D_1) \right] = \left[(b_1 + b_3 \cdot \log(D_2)) \cdot \left(\log\left(\frac{S_{ref}}{d^2}\right) - 0.4 \cdot \log\left(\frac{R_0}{1770}\right) \right) + b_2 \cdot \log(D_2) \right]$$

Substitution:

$$A = 0.4 \cdot \log\left(\frac{R_0}{1770}\right)$$

$$\log\left(\frac{S_{ref}}{d^2}\right) = \frac{(-b_3 \cdot \log(D_2) \cdot A + b_2 \cdot \log(D_2)) + b_3 \cdot \log(D_1) \cdot A - b_2 \cdot \log(D_1)}{(b_3 \cdot \log(D_1) - b_3 \cdot \log(D_2))} = \frac{(b_3 \cdot A - b_2) \cdot \log\left(\frac{D_1}{D_2}\right)}{b_3 \cdot \log\left(\frac{D_1}{D_2}\right)} = \frac{(b_3 \cdot A - b_2)}{b_3} = \frac{(b_3 \cdot 0.4 \cdot \log\left(\frac{R_0}{1770}\right) - b_2)}{b_3}$$

Result for S_{ref} :

$$\log\left(\frac{S_{ref}}{d^2}\right) = \frac{(b_3 \cdot 0.4 \cdot \log\left(\frac{R_0}{1770}\right) - b_2)}{b_3} \Rightarrow \frac{S_{ref}}{d^2} = 10$$

Use of S_{ref} to get solution for w_{ref} :

$$\log(w_{ref}) = b_0 + \left[(b_1 + b_3 \cdot \log\left(\frac{D}{d}\right)) \cdot \left(\frac{(b_3 \cdot 0.4 \cdot \log\left(\frac{R_0}{1770}\right) - b_2)}{b_3} - 0.4 \cdot \log\left(\frac{R_0}{1770}\right) \right) + b_2 \cdot \log\left(\frac{D}{d}\right) + (\log(f_d) + \log(f_L) + \log(f_C)) \right]$$

$$\log(w_{ref}) = b_0 + \left[(b_1 + b_3 \cdot \log\left(\frac{D}{d}\right)) \cdot \left(\frac{-b_2}{b_3} \right) + b_2 \cdot \log\left(\frac{D}{d}\right) + (\log(f_d) + \log(f_L) + \log(f_C)) \right]$$

Result for w_{ref} :

$$\log(w_{ref}) = b_0 + b_1 \cdot \left(\frac{-b_2}{b_3} \right) + (\log(f_d) + \log(f_L) + \log(f_C)) \Rightarrow w_{ref} = 10$$

Figure 6: Derivation of Sref and wref with method Stuttgart [8]

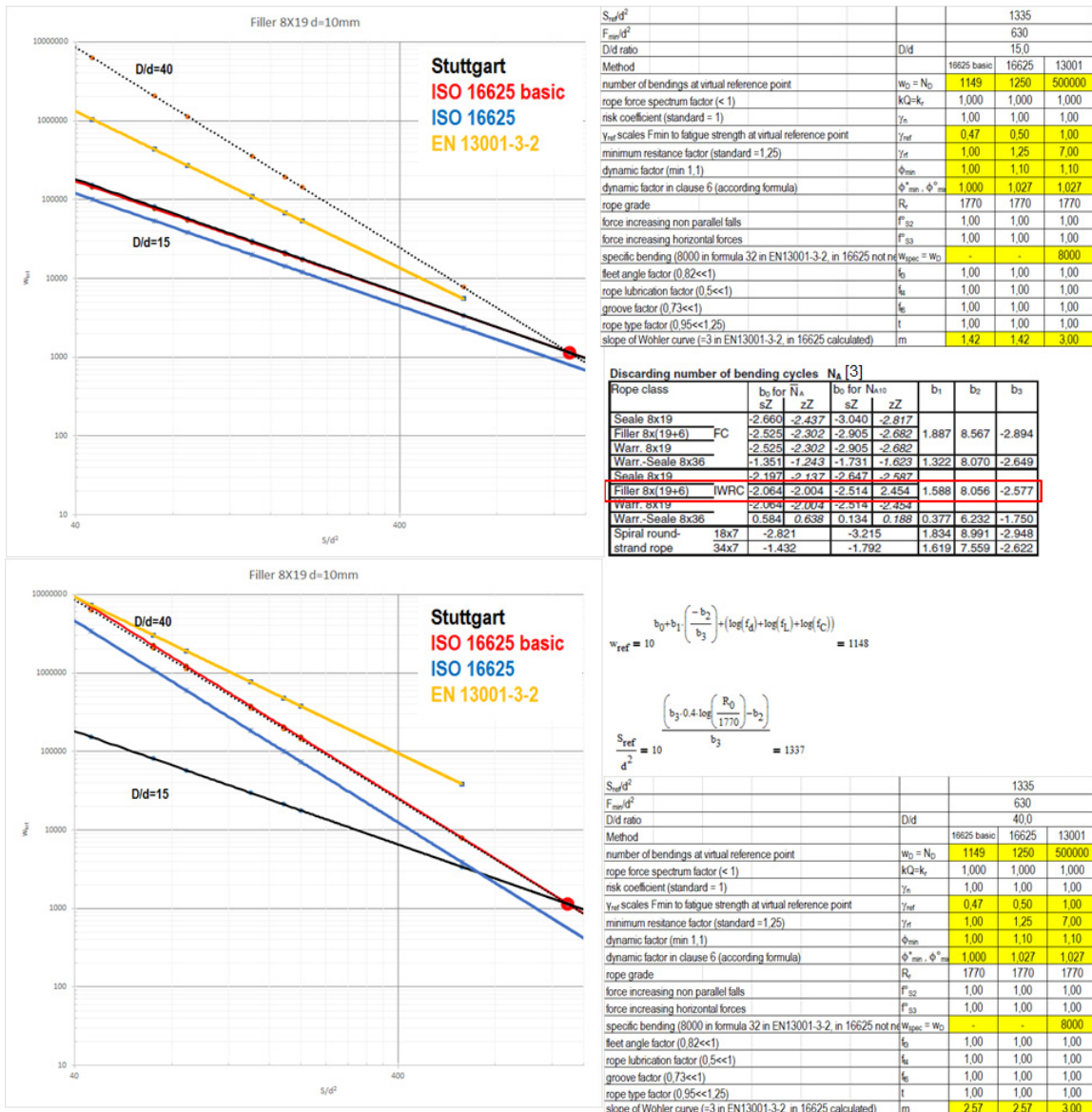


Figure 9: Comparison of the results (D/d=15, 40) calculated by different methods [8]

Next Generation Intralogistics: Technologies and Applications

Tone Lerher

Professor
University of Maribor
Faculty of Logistics
Celje, Slovenia

Logistics can be defined as a science managing the flow of resources through supply chains in terms of distribution logistics (moving goods from the manufacturer through any intermediaries, to the final customer) and intralogistics (moving goods within the walls of a production facility or distribution center) associated with the informational flow. Industry 4.0, internet of Things, Digital Transformation and Digitization, Smart Intralogistics, Intralogistics 4.0 are just some of the phrases, which are used to describe the logistics nowadays. In the framework of the invited paper, trends, technologies and application of the next generation intralogistics will be presented and discussed. Along with the presentation of recent trends, technologies and application in intralogistics, a prototype of an automated guided vehicle developed by the team in the Laboratory of logistics systems on Faculty of Logistics University of Maribor will be presented.

Keywords: Intralogistics, automated warehouses, automated guided vehicles AGVs, design and implementation of AGV.

1. INTRODUCTION

Logistics is part of Supply Chain and represent very important activity on a global scale nowadays. The Council of Supply Chain Management Professionals (<http://www.cscmp.org/>) has defined logistics as "... that part of Supply Chain Management that plans, implements, and controls the efficient, effective forward and reverse-flows, and the storage of goods, services and related information between the point of origin and the point of consumption in order to meet customers' requirements."

Many modern industrial trends like Industrial Internet Consortium (<http://www.iiconsortium.org/>), Smart Manufacturing Leadership Coalition (<http://www.smart-manufacturingcoalition.org/>), European Factories of the Future Research Association (<http://www.effa.eu/>), Industry 4.0 (<http://www.plattform-i40.de/>) and Made in China 2025 (<http://english.gov.cn/>) describe how the logistics along with the production of the future should look like, in order to give a competitive advantage and the sustainable development of society.

An important area of logistics is intralogistics or internal logistics that comprises all technical systems, services and related business involved in the in-house materials handling of production companies. The processes of the intralogistics domain are vital for managing the flows of goods along the entire supply chain as they provide the reliable and predictable flow of physical goods in the nodes of a supply network. The domain of intralogistics spreads in the area of conflict between systems with simple manual operations and few technical solutions adding little value up to highly

automated, complex systems containing several organisational areas and functionally specialised solutions [27]. In the European Union, many companies are investing large financial resources in reconstruction of existing and development of new intralogistics systems (Figure 1), which is shown in a recent study by the European Material Handling Federation (FEM).

Many investments in intralogistics are related to warehouses and internal transport in terms of providing automation and robotization to storage and transportation process. The development trend of warehousing, in a variety of industries, is based on the development of new technologies, the introduction of Information and Communications Technology (ICT), the concept of the "Internet of Things" (IoT) and the concept of Industry 4.0 with the high degree of automation and robotization (the application of industrial and collaborative robots COBOTS). Together with an interdisciplinary scientific approach, they create the conditions of new possibilities and dimensions by using advanced and environmentally friendly technologies.

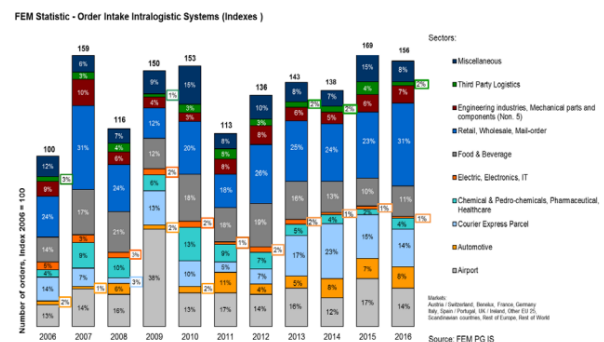


Figure 1. Number of projects of intralogistics systems by years and industrial sectors (Source: https://www.fem-eur.com/wp-content/uploads/2015/12/FEM-IS-PG-Statistic_fact-sheet_2016.pdf).

With the emerge of the e-commerce, companies store millions of unique items in warehouses and handle large

Correspondence to: Dr. Tone Lerher, Professor
University of Maribor, Faculty of Logistics
Mariborska c. 7, 3000 Celje, Slovenia
E-mail: tone.lerher@um.si

and variable daily order volumes. One of the most laborious process in the warehouse is the order-picking process, which often suffers from poor ergonomics, and requires high-quality labour willing to work in shifts, which is often difficult to get. For this reason, warehousing systems and processes are key candidates for automation and robotization.

Warehouse automation dates to 1960s, when the first high-bay unit-load warehouses were established in Germany with aisle-captive cranes driving on rails (Automated Storage and Retrieval Systems; crane-based AS/RS). Many scientific articles were published on the crane-based AS/RS topic, which are listed in a review article published by authors Roodbergen and Vis [32].

In the last decade, warehouse automation has developed rapidly. The Shuttle-Based Storage and Retrieval Systems (SBS/RS) along with Autonomous Vehicle-Based Storage and Retrieval Systems (AVS/RS) have given a big boost in automated warehouses. SBS/RS in AVS/RS consist of storage rack with an elevator that can execute vertical movements of stock keeping units and/or vehicles and vehicles that can execute horizontal movements. Compared to classical crane-based AS/RS, SBS/RS and AVS/RS have several advantages, as high throughput capacity, high flexibility and scalability, small energy consumption, etc. The above-mentioned advantages over crane-based AS/RS are the main generator for choosing and applying SBS/RS in AVS/RS in practice (Figure 2)

Automated Shuttle-Based Storage and Retrieval Systems



Source: SSI Schäfer

The Robotic Mobile Fulfilment System (RMFS)



Source: Amazon Robotics

Collaborative robots COBOTS



Source: Universal Robots

Figure 2. Robotized warehouse and order-picking systems

As for robotization, the use of robots in Intralogistics will expand mainly as distribution operations turn to this technology to automate order-picking, packing, shipping activities, etc. The International Federation for Robotics (<https://ifr.org/>) reports that in 2018 the estimated annual worldwide supply of industrial robots was around 378.000 units with an average growth of 15 % per year (Figure 3). In addition, The International Federation for Robotics predicts that the number of industrial robots deployed worldwide will reach 2.6 million units by the year 2019. (<http://www.invata.com/intralogistics-4-0/>).

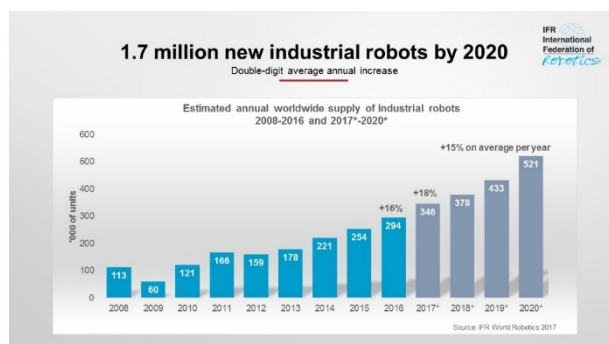


Figure 3. Expected annual supply of industrial robots on a global scale (Source: <http://www.invata.com/intralogistics-4-0/>).

Still, industrial robots are machines that perform automated tasks and not the humanoid robots. Nevertheless, companies are working on humanoid robots that will find their way into Intralogistics. For example, company Rethink Robotics

(<https://www.rethinkrobotics.com/>) has taken a step in the direction of developing a humanoid robot called Baxter (www.youtube.com/watch?v=gXOkWuSCkRI). Humanoid robots could be used to address the challenges inherent to single-item order-picking, which provide process efficiency.



Figure 4. Collaborative (mobile) robots (source: <https://www.nextshiftrobotics.com/>)

Before humanoid robots will be applied in warehouses, they will require the development of fine motor skills for selecting a variety of items along with sophisticated computer visions systems to distinguish object characteristics. Increases in computer power, artificial intelligence, computer vision systems, and sensors will certainly accelerate the development of humanoid robots in the next decade.

Meanwhile new robotic technology known as collaborative (mobile) robots COBOTS is already in use in modern warehouse applications, especially in order-picking process (Figure 4). A collaborative mobile robot COBOT is an intelligent mobile robot that assists humans

in a shared workspace. The main objective of any warehouse is to obtain maximum efficiency in their work processes. A collaborative mobile robot COBOT helps achieve this when it comes to transporting items. In this way, logistics tasks that are repetitive, tedious and/or dangerous (lifting and banding) in warehouses are optimized. An example of the innovative use of collaborative (mobile) robots COBOTS in warehouses are Robotic mobile fulfilment systems (Source: Amazon Robotics), Mobile robots "LocusBots" for automatic order-picking (Source: Locus Robotics), Mobile robots "Pick-and-go" for automatic order-picking (Source: Kollmorgen).

The trend of development and renewal of intralogistics, focusing on warehouses in various industries, is based on the following areas of opportunity:

- Concept Internet of Things (IoT), [14], [27] and [36].
- Concept Industry 4.0, [11], [25] and [31] taking into account ergonomic principles, [28] and [35].
- Concept of increased level of automation by using SBS/RS in AVS/RS, [10], [18], [19], [20], [30] and [34].
- Concept of robotization by using collaborative mobile robots COBOTS (RMFS), [1], [16], [17], [29] and [37].

These concepts along with introduction of support information-communication technology create the conditions for new opportunities and dimension in the framework of smart warehouses. The efforts of researchers on these concepts always strive to increase efficiency and lower the costs and poor quality.

2. PROBLEM IDENTIFICATION IN INTRALOGISTICS

The above-mentioned areas of opportunity (intralogistics, warehouses and robotization) are only partially explored, which is proved by reviewing research field and scientific articles of a newer date, which solve several research questions isolated by individual elements. Intralogistics with emphasis on warehouse robotization has proven to be a potential area for lowering operating costs, raising humanization of work and improvement of environmental and resource management, especially in terms of systemic treatment. The increasing trend of the e-commerce and the increasing customer expectations in terms of speed, reliability and flexibility of services has a significant impact on the demand for effective order fulfilment (order-picking, consolidation and delivery of shipments) in modern warehouses. Many companies integrate their warehouses by using robotization (industrial and collaborative mobile robots COBOTS) to support the process of warehousing and order-picking with the objective to fully meet the increasing trend in speed, reliability and flexibility of their services, and the emerging concept of extremely small orders (Batch size 1). The recent advancement of automation and robotization of transport and storage technology enables the application of many new technologies to increase the efficiency of warehousing activities, such as: Automatic identification with RFID technology, the application of computer and machine vision, the application of

robotization and autonomous vehicles for order-picking, the application of collaborative mobile robots COBOTS, the application of a special workplace with a collaborative robot known as Operator 4.0, etc. Warehouse designers and warehouse managers are thus confronted with many of new techniques and technologies for the application in modern warehouses. This has a significant impact on the appropriate (best) selection of these new technologies in terms of achieving maximum capacity and throughput performance, high reliability and flexibility, good ergonomics and, last but not least, the cost-effectiveness of the warehouse. The objective of this basic research project is the integration of warehouses and order-picking process by using industrial and collaborative robots COBOTS, by creating a model that will enable computer aided design and professional selection of modern transport and storage technologies, analytical and numerical modelling, discrete multi-objective optimization and comparison of various modern transport and storage systems for achieving the maximal performance in order fulfilment in warehouses. In doing so, the project also pursues the social goals of the low-emission economy, since optimization means the rational use of raw materials, while robotized operations means sustainability planning with a low percentage carbon footprint.

Table 1. Problems and their descriptions

Problem	Description
The increasing trend of using the e-commerce	The increasing trend of the e-commerce and the increasing customer expectations in terms of speed, reliability and flexibility of services has a significant impact on the demand for effective order fulfilment (order-picking, consolidation and delivering of the shipment) in modern warehouses. Many companies integrate their warehouses with the application of industrial and collaborative robots COBOTS.
High cost of warehousing as a component of overall logistics cost	The cost of intralogistics, including warehouses, amounts to up to 20% of total product cost. The amount of the cost depends on the type of industry. Companies are not prepared to add additional costs that would result from the continuous renovation of their warehousing systems.
Warehouse systems are rarely renewed in their entirety and therefore inhibit technological development	At the beginning, companies create the required warehouse at a satisfactory level of efficiency. They later add new products and expand their assortment but rarely improve warehouses in parallel. Partial solutions to upgrading warehouses are primarily confined to a single process (Receiving, Storage, Order-Picking, Consolidation and Shipping). As a result, local efficiency is attained at the expense of reducing system efficiency and raising logistics costs.
Companies hesitate regarding technological renovation (automation and	Companies like Amazon, DHL, Schenker and suppliers (integrators) of transport and storage technique and technology (SSI Schäfer, Knapp, Swisslog and others) encourage the

robotization) of warehouses	application of automation and robotization into warehouses. Other companies are showing an interest in implementing these components but hesitate due to a limited familiarity with effects that are impossible to determine without advanced methodological approaches. Due to the complexity of this challenge, companies are searching for an integration model that would effectively lead them through technological renovation of their warehouses.
The growing complexity of warehouse systems	Systems complexity of warehouses is increasing due to the use of advanced technology and the addition of performance indicators. The integration of new technologies in warehouses requires generally useful approaches for the individualized development of basic building blocks that provide customized fit solutions, which are specifically developed for each warehousing system.
The transition from a focus on products to a focus on services	In many cases, product prices are falling, with this difference in price being replaced with advanced or even entirely new services. Logistics is therefore uncovered as the most effective competitive advantage and not as a necessary cost. This involves a major change in mind-set and approach. Academic research has just started to approach the development of new methodologies and models.

3. SURVEY OF THE RELEVANT LITERATURE

Today's logistics represent an important area of businesses effectiveness and competitiveness. Estimates indicate that, depending on the type of industry, at least 25% of the cost of a product is represented by the intralogistics. Therefore, every decision related to the logistics solutions can reduce the logistics cost.

One important area of logistics are automated warehouses known as Automated Storage and Retrieval Systems (AS/RS), Autonomous Vehicle Storage and Retrieval Systems (AVS/RS), Shuttle-Based Storage and Retrieval System (SBS/RS) and Robotic Mobile Fulfilment Systems (RMFS).

Crane-Based AS/RS consist of Storage Racks (SR) along aisles, Storage and Retrieval machines for unit- and mini-loads (S/R machines), Roller conveyors, Input/Output locations (I/O locations), etc. The major advantages of crane-based AS/RS in comparison with conventional warehouses are: high throughput performance, efficient utilization of warehouse volume, high reliability and better control of inventory, improved safety conditions and decrease in damage and shortages. On the other hand, AS/RS are rather expensive and inflexible to future changes in throughput performance and warehouse volume. Crane-Based AS/RS have been studied extensively. We refer to [32] for an extensive overview of the literature on crane-based AS/R systems.

AVS/RS for unit-loads are an upgrade of classical AS/RS and consist of accumulating conveyors, storage racks, lifts (elevators) and autonomous vehicles. Vehicles are completely autonomous and can move inside and outside of the storage rack (non tier-captive system). The vertical movement of autonomous vehicles is facilitated by lifts mounted along the periphery of the storage rack. AVS/RS technology can provide cost effective automation even when transaction volumes change, because it enables the designer to vary the number of autonomous vehicles, [39]. Advances in AVS/RS technology have helped material handling providers to propose the application of autonomous vehicles instead of fixed-path cranes for the unit-load systems. In the last decade, AVS/RS has been the subject of many studies, which are presented in scientific works of the following authors [3-9], [11-13], [15], [21-24], [33] and [39-40].

Due to the need for high throughput performance of mini-load systems (e-commerce), storage system providers present the technology called Shuttle-Based Storage and Retrieval System (SBS/RS). This technology was developed for high throughput performances up to 1000 totes per hour. SBS/RS consists of an elevator with a lifting table, shuttle carriers and storage racks. The elevator with the lifting table is feeding the storage rack. In each tier of the storage rack is a single shuttle carrier (tier-captive system). The performance of the SBS/RS as a whole depends on the throughput performance of the elevator or the shuttle carriers. Most often, the bottleneck of the SBS/RS is the elevator, which is not capable of keeping up with the shuttle carriers and, therefore, works with maximum utilization. On the other hand, shuttle carriers work with relatively low utilization, since they wait in idle mode for tasks to be executed. In the last decade, SBS/RS has been the subject of many studies, which are presented in scientific works of the following authors [18-20], [30] and [34].

The Robotic Mobile Fulfilment Systems (RMFS) represent a modern warehouse technology, in which mobile robots capable of lifting and carrying movable shelves retrieve the storage pods (i.e. Movable shelf racks) and transport them to the pickers, who work in ergonomically designed workstations (Amazon Robotics). Bringing the inventory to the picker instead of the picker traveling to the inventory, can double the order-picking productivity (Wurman et al. 2008). The RMFS consists of three major components:

- Robotic Drive Units: These robots are instructed by the central computer to transport inventory pods to the workstation for restocking or for picking.
- Inventory Pods: Pods are movable shelf racks that contain the stored products. Pods come in two standard sizes. Smaller pods are used for weights up to 450 kg and large pods are used for weights up to 1300 kg.
- Workstation: Ergonomically designed areas where human workers perform pod replenishment, picking and packing functions.

The performance of RMF systems has hardly been studied scientifically. There are some research studies from the following authors [1], [16-17], [29] and [37].

According to the extensive review and analysis of the previous research and relevant literature in scientific

articles in the field of automated warehouses and robotics:

- There is a lack of systemic approach;
- There is relatively few articles on collaborative mobile robots COBOTS and Robotic Mobile Fulfilment Systems (RMFS) in warehouses; in addition to throughput performance, energy

efficiency, good ergonomic solutions and sustainability are rarely found in the models;

- There is no model for the integration of warehouses and order-picking process by using industrial and collaborative robots COBOTS.

Table 2. The differences between models studied in AVS/RS and SBS/RS

Literature	System type	Modelling	Objectives
[2] - Carlo and Vis, 2012	Dynamic storage system	Analytical	Throughput performance
[7] - Ekren et al., 2010a	AVS/RS	Simulation	Design of experiments
[5] - Ekren et al., 2010b	AVS/RS	Simulation	Regression analysis
[3] - Ekren, 2011	AVS/RS	Simulation	Performance evaluation
[6] - Ekren et al., 2011	AVS/RS	Simulation	Performance analysis
[8] - Ekren et al., 2013	AVS/RS	SOQNM	Performance evaluation
[9] - Ekren et al., 2014	AVS/RS	SOQNM	Matrix-geometric solution
[4] - Ekren, 2017	AVS/RS	Simulation	Performance evaluation
[11] - Epp et al., 2017	AVS/RS	QNM	Performance evaluation
[12] - Fukunari et al., 2008	AVS/RS	Simulation	Cycle time analysis
[13] - Fukunari et al., 2009	AVS/RS	QNM	Performance measures
[15] - Kuo et al., 2008	AVS/RS	QNM	Performance analysis
[19] - Lerher et al., 2015a	SBS/RS	Analytical and simulation	Cycle time analysis
[20] - Lerher et al., 2015b	SBS/RS	Analytical and simulation	Throughput performance
[18] - Lerher, 2016	SBS/RS (double-deep)	Analytical	Throughput performance
[21] - Malmberg, 2002	AVS/RS	Analytical	Performance evaluation
[22] - Malmberg, 2003	AVS/RS	Analytical	Cycle time and throughput analysis
[23] - Marchet et al., 2012	AVS/RS	Analytical	Performance evaluation
[24] - Marchet et al., 2013	AVS/RS	Simulation	Design trade-offs analysis
[30] - Ning et al., 2016	Multi-elevator SBS/RS	Simulation	Performance evaluation
[33] - Roy et al., 2012	AVS/RS	SOQNM	Performance analysis
[34] - Tappia et al., 2016	SBS/RS compact storage systems	QNM	Performance evaluation
[39] - Zhang et al., 2009	AVS/RS	Simulation	Transaction waiting times analysis
[40] - Zou et al., 2016	AVS/RS	FJQNM	Performance analysis

4. DESIGN AND IMPLEMENTATION OF AUTOMATED GUIDED VEHICLE (AGV)

An automated guided vehicle (AGV) is a driverless transport system used for horizontal movement of materials. AGVs were introduced in 1955, [26]. The use of AGVs has grown enormously since their introduction. The number of areas of application and variation in types has increased significantly. AGVs can be used in inside and outside environments, such as manufacturing, warehouses, distribution, transshipment and (external) transportation areas, [38].

In Laboratory for logistics systems on the Faculty of Logistics University of Maribor, we have started with an internal project to design and to build an AGV for transporting totes. Our AGV was first design in a computer aided design tool SolidWorks. The next step was to select basic parts of the AGV, as follows.

Driving unit

For the driving unit, we have utilised the assembled wheels with built-in robot brushless servo hub engine, which can be connected to the power supply of 24 or 36 volts (Figure 5). The power range is between 50 and 150 watts. The velocity can be set in the range of 200 to 400 rpm. Ideal current for normal operation is from 3 to 8 amps, as well as a torque of 3 Nm. One wheel is capable of carrying a weight of 60 kg. The wheel diameter is 105 mm.



Figure 5. Four inch robot brushless servo hub motor (source: <https://www.uumotor.com/4-inch-robot-brushless-servo-hub-motor.html>)

Laser scanner

For the laser scanner, we have utilised the RPLIDAR A2M8 360° Laser Scanner (Figure 6). The RPLIDAR A2 360° Laser Scanner is the next generation of 360 degree 2D lidars. The RPLIDAR A2 adopts low cost laser triangulation measurement system developed by SLAMTEC, and therefore has excellent performance in all kinds of indoor environments and outdoor environments without direct sunlight exposure.

It can take up to 8000 samples of laser ranging per second with high rotation speed. And equipped with SLAMTEC patented OPTMAG technology, it breakouts

the life limitation of traditional LIDAR system so as to work stably for a long time (source: <https://www.robotshop.com/en/rplidar-a2m8-360-laser-scanner.html>).



Figure 6. RPLIDAR A2M8 360° Laser Scanner (source: <https://www.robotshop.com/en/rplidar-a2m8-360-laser-scanner.html>)

Magnetic guided sensor

For the magnetic guided sensor we have utilised the MGS1600 of the company Roboteq (Figure 7).

The MGS1600 is a magnetic guide sensor capable of detecting and reporting the position of a magnetic field along its horizontal axis. The sensor is intended for line following robotic applications, using a magnetic tape to form a track guide on the floor.

The sensor uses advanced signal processing to accurately measure its lateral distance from the center of the track, with millimeter resolution, resulting in nearly 160 points end to end.

Applications of the sensor are the following:

- Automatic Guided Vehicles
- Automated warehouses
- Automated shelf restocking systems
- Material conveying robots
- Flexible assembly lines

(source: <https://www.roboteq.com>)

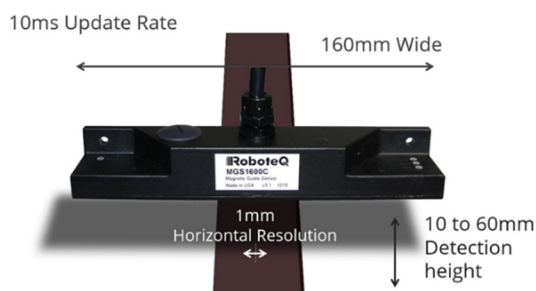


Figure 7. Magnetic guided sensor MGS1600 (source: <https://www.roboteq.com>)

PLC controller

For the PLC controller, we have utilised the STM NUCLEO, which offers 8 analog and 72 digital lines (Figure 8). Our version also has an integrated Ethernet port. The PLC controller can be programed in various environments such as Arduino and others. This controller will initially control the entire AGV via RC control. In the future of our work we would like to implement an additional controller on which the robotic operating system (ROS) will be installed. This will allow the AGV to run autonomously.

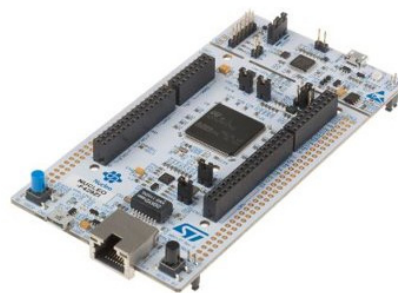


Figure 8. STM NUCLEO (source: <https://www.st.com/en/evaluation-tools/stm32-nucleo-boards.html>)

Digital servo drive

For the digital servo drive we have utilised the Elmo Harmonica (Figure 9). The Harmonica is a series of intelligent compact digital servo drives for DC brush, brushless motors and linear motors. The compact servo drive supports up to 13.3 amps continuous current. The Harmonica is capable of delivering a peak of 2200 W of power and 1100 W of continuous power. Based on Elmo's SimplIQ motion control technology, the Harmonica is capable of operating in position, velocity and current modes and contains a wide range of feedback and I/O options. With Elmo's Composer software, users can easily perform drive setup, configuration, tuning, analysis and programming. The drive operates on DC power. The Harmonica's small case enables efficient, cost saving implementation (source: <https://www.elmomc.com/product/harmonica/>)

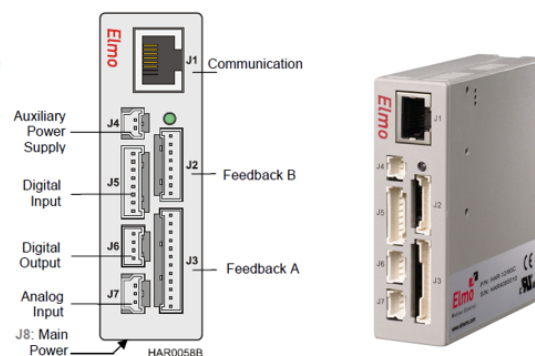


Figure 9. Elmo harmonica (source: <https://www.elmomc.com/product/harmonica/>)

Electrical scheme of the AGV

The electrical scheme of our AGV vehicle would look as follows (Figure 10).

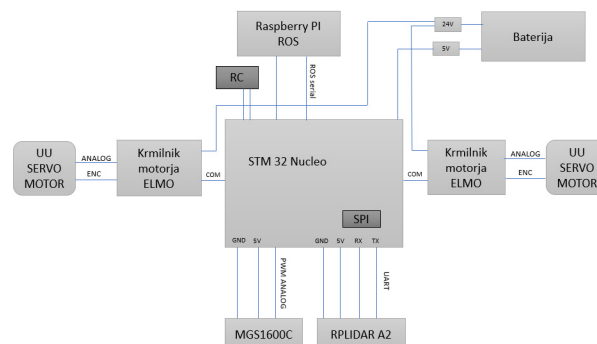


Figure 10. Electrical scheme of the AGV

Design of the AGV

The AGV consists of aluminium profiles of (40 x 40) mm. The final size of the IGV would be in the range of 600 mm in length, 400 mm in width and 270 mm in high, which does not include the height of the auxiliary wheels (Figure 11).

The RP Lidar sensor along with the magnetic sensor will be installed in front of the AGV (Figure 12). Inside of the AGV are two drawers. The bottom drawer is intended to be used for the battery, meanwhile the top drawer will be used for electronics installation.

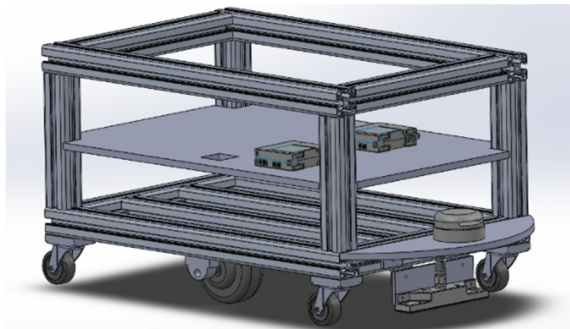


Figure 11. Design of the AGV

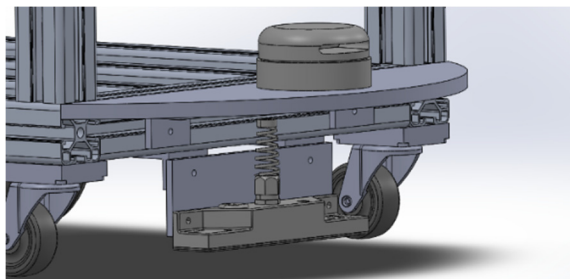


Figure 12. Position of Lidar and magnetic sensor on the AGV

5. CONCLUSION

Intralogistics along with automated and robotized warehouses have proven to be a potential area for lowering operating costs, raising productivity, work humanization, and improving environment and resource management, especially from the systemic approach point of view.

The increasing trend of the e-commerce and the increasing customer expectations in terms of speed, reliability and flexibility of services has a significant impact on the demand for effective order fulfilment (order-picking, consolidation and delivery of shipments) in modern warehouses.

Many companies integrate their warehouses by using robotization (industrial and mobile collaborative robots COBOTS) to support the process of warehousing and order-picking with the objective to fully meet the increasing trend in speed, reliability and flexibility of their services, and the emerging concept of extremely small orders (Batch size 1).

The recent advancement of automation and robotization of transport and storage technology enables the application of many new technologies to increase the efficiency of warehousing activities, such as: Automatic identification with RFID technology, the application of computer and machine vision, the application of

robotization and autonomous vehicles for order picking, the application of collaborative mobile robots COBOTS, the application of a special workplace with a collaborative robot known as Operator 4.0, etc.

Warehouse designers and warehouse managers are thus confronted with many of new techniques and technologies for the application in modern warehouses.

This has a significant impact on the appropriate (best) selection of these new technologies in terms of achieving maximum capacity and throughput performance, high reliability and flexibility, good ergonomics and, last but not least, the cost-effectiveness of the warehouse.

ACKNOWLEDGEMENT

This work was supported by Slovenian Research Agency (ARRS) [Methodology for Building an Integral Model of Transport-Warehouse Processes to Enhance Intralogistics System Efficiency; grant number: L5-8237].

REFERENCES

- [1] Boysen, N., Briskorn, D. and Emde, S.: Parts-to-picker based order processing in a rack-moving mobile robots environment, *European Journal of Operational Research*, Vol. 262, No. 2, pp. 550-562, 2017.
- [2] Carlo, H.J. and Vis, I.F.A.: Sequencing dynamic storage systems with multiple lifts and shuttles, *International Journal of Production Economics*, Vol. 140, No. 2, pp. 844-853, 2012.
- [3] Ekren, B.Y.: Performance evaluation AVS/RS under various design scenarios: a case study, *International Journal of Advanced Manufacturing Technology*, Vol. 55, No. 9-12, pp. 1253-1261, 2011.
- [4] Ekren, B.Y.: Graph-based solution for performance evaluation of shuttle-based storage and retrieval system. *International Journal of Production Research*, Vol. 55, No. 21, pp. 6516-6526, 2017.
- [5] Ekren, B.Y. and Heragu, S.S.: Simulation based regression analysis for the rack configuration of autonomous vehicle storage and retrieval system, *International Journal of Production Research*, Vol. 48, No. 21, pp. 6257-6274, 2010.
- [6] Ekren, B.Y., Heragu, S.S.: Simulation based performance analysis of an autonomous vehicle storage and retrieval system, *Simulation Modelling Practice and Theory*, Vol. 19, No. 7, pp. 1640-1650, 2011.
- [7] Ekren, B.Y., Heragu, S.S., Krishnamurthy, A. and Malmberg, C.J.: Simulation based experimental design to identify factors affecting performance of AVS/RS, *Computers & Industrial Engineering*, Vol. 58, No. 1, pp. 175-185, 2010.
- [8] Ekren, B.Y., Heragu, S.S., Krishnamurthy, A. and Malmberg, C.J.: An approximate solution for semi-open queuing network model of autonomous vehicle storage and retrieval system, *IEEE Transactions on Automation Science and Engineering*, Vol. 10, No. 1, pp. 205-215, 2013.

- [9] Ekren, B.Y., Heragu, S.S., Krishnamurthy, A. and Malmberg, C.J.: Matrix-geometric solution for semi-open queueing network model of autonomous vehicle storage and retrieval system, *Computers & Industrial Engineering*, Vol. 68, pp. 78-86, 2014.
- [10] Ekren, B.Y., Akpunar, A., Sari, Z. and Lerher, T.: A tool for time, variance and energy related performance estimations in a shuttle-based storage and retrieval system, *Applied Mathematical Modelling*, Vol. 63, pp. 109-127, 2018.
- [11] Epp, M., Wiedemann, S. and Furmans, K.: A discrete-time queueing network approach to performance evaluation of autonomous vehicle storage and retrieval systems, *International Journal of Production Research*, Vol. 55, No. 4, pp. 960-978, 2017.
- [12] Fukunari, M. and Malmberg, C.J.: An efficient cycle time model for autonomous vehicle storage and retrieval systems, *International Journal of Production Research*, Vol. 46, No. 12, pp. 3167-3184, 2008.
- [13] Fukunari, M. and Malmberg, C.J.: A network queueing approach for evaluation of performance measures in autonomous vehicle storage and retrieval systems, *European Journal of Operational Research*, Vol. 193, No. 1, pp. 152-167, 2009.
- [14] Holzweissig, P., Kivelä, T., León, S.V. and Golder, M.: HiPi-A concept for a compact, IoT-enabled safety controller, *Logistics Journal*, 2016.
- [15] Kuo, P.H., Krishnamurthy, A. and Malmberg, C.J.: Performance modelling of autonomous vehicle storage and retrieval systems using class-based storage policies, *International Journal of Computer Applications in Technology*, Vol. 31, No. 3/4, pp. 238-248, 2008.
- [16] Lamballais, T., Roy, D. and De Koster, R.: Estimating performance in a robotic mobile fulfillment system, *European Journal of Operational Research*, Vol. 256, No. 3, pp. 976-990, 2017.
- [17] Lamballais, T., Roy, D. and De Koster, R.: Inventory allocation in robotic mobile fulfilment systems, *IIE Transactions*, ERIM Report Series, pp. 1-17, 2019.
- [18] Lerher, T.: Travel time model for double-deep shuttle-based storage and retrieval systems, *Int. J. Prod. Res.*, Vol. 54, No. 9, pp. 2519-2540, 2016.
- [19] Lerher, T., Ekren, B.Y., Dukic, G. and Rosi, B.: Travel Time Model for Shuttle-based Storage and Retrieval Systems, *Int. J. Adv. Manuf. Tech.*, Vol. 78, No. 9-12, pp. 1705-1725, 2015.
- [20] Lerher, T., Ekren, B.Y., Sari, Z. and Rosi, B.: Simulation Analysis of Shuttle Based Storage and Retrieval Systems, *Int. J. Simul. Model.*, Vol. 14, No. 1, pp. 48-59, 2015.
- [21] Malmberg, C.J.: Conceptualizing tools for autonomous vehicle storage and retrieval systems, *Int. J. Prod. Res.*, Vol. 40, No. 8, pp. 1807-1822, 2002.
- [22] Malmberg, C.J.: Interleaving rule dynamics in autonomous vehicle storage and retrieval systems, *Int. J. Prod. Res.*, Vol. 41, No. 5, pp. 1057-1069, 2003.
- [23] Marchet, G., Melacini, M., Perotti, S. and Tappia, E.: Analytical model to estimate performances of autonomous vehicle storage and retrieval systems for product totes, *Int. J. Prod. Res.*, Vol. 50, No. 24, pp. 7134-7148, 2012.
- [24] Marchet, G., Melacini, M., Perotti, S. and Tappia, E.: Development of a framework for the design of autonomous vehicle storage and retrieval systems, *Int. J. Prod. Res.*, Vol. 51, No. 14, pp. 4365-4387, 2013.
- [25] Mičeta, B., Herčko, J., Botka, M. and Zrnić, N.: Concept of intelligent logistic for automotive industry, *Journal of Applied Engineering Science*, Vol. 14, No. 2, Part 1, pp. 233-238, 2016.
- [26] Müller, T.: *Automated Guided Vehicles*, IFS (Publications) Ltd./Springer-Verlag, UK/Berlin, 1983.
- [27] Nagel, L., Roidl, M. and Follert, G.: The Internet of Things: On Standardisation in the Domain of Intralogistics, *First International Conference on The Internet of Things IOT 2008 WORKSHOPS*, Zurich, Switzerland, March 26-28, 2008.
- [28] Niemöller, C., Metzger, D., Fellmann, M., Özcan, D. and Thomas, O.: Shaping the future of mobile service support systems - ex-ante evaluation of smart glasses in technical customer service processes, *Informatik*, pp. 753-767, 2016.
- [29] Nigam, S., Roy, D., de Koster, R. and Adan, I.: Analysis of class-based storage strategies for the mobile shelf-based order pick system, *Progress in Material Handling Research*, 13th IMHRC Proceedings, Cincinnati, Ohio, USA, 2014.
- [30] Ning, Z., Lei, L., Saipeng, Z. and Lodewijks, G.: An efficient simulation model for rack design in multi-elevator shuttle-based storage and retrieval system, *Simulation Modelling Practice and Theory*, Vol. 67, pp. 100-116, 2016.
- [31] Pfeiffer, S.: Robots, Industry 4.0 and Humans, or Why Assembly Work Is More than Routine Work, *Societies*, Vol. 6, No. 2, Article 16, pp. 1-26, 2016.
- [32] Roodbergen, K.J. and Vis, I.F.: A survey of literature on automated storage and retrieval systems, *Eur. J. Oper. Res.*, Vol. 194, No. 2, pp. 343-362, 2009.
- [33] Roy, D., Heragu, S.S., Krishnamurthy, A. and Malmberg, C.J.: Performance analysis and design trade-offs in warehouses with autonomous vehicle technology, *IIE Transactions*, Vol. 44, No. 12, pp. 1045-1060, 2012.
- [34] Tappia, E., Roy, D., De Koster, R., and Melacini, M.: Modeling, analysis, and design insights for shuttle-based compact storage systems, *Transportation Science*, Vol. 51, No. 1, pp. 269-295, 2016.
- [35] Tomasiello, P.: Success in an omni-channel world, *MHD Supply Chain Solutions*, Vol. 46, No. 2, pp. 24-27, 2016.
- [36] Yu, Q. and Wang, K.: Applications of IoT in production logistics: Opportunities and challenges, *WIT Transactions on Engineering Sciences*, 113, pp. 233-240, 2016.
- [37] Yuan, Z. and Gong, Y.Y.: Bot-in-time delivery for robotic mobile fulfillment systems, *IEEE Transactions on Engineering Management*, Vol. 64, No. 1, pp. 83-93, 2017.
- [38] Vis, F.A.I.: Survey of research in the design and control of automated guided vehicle systems, *Eur. J. Oper. Res.*, Vol. 170, No. 3, pp. 677-709, 2006.
- [39] Zhang, L., Krishnamurthy, A., Malmberg, C.J. and Heragu, S.S.: Variance-based approximations of transaction waiting times in autonomous vehicle storage and retrieval systems, *European Journal of Industrial Engineering*, Vol. 3, No. 2, pp. 146-168, 2009.
- [40] Zou, B., Xu, X., Gong, Y.Y. and De Koster, R.: Modeling parallel movement of lifts and vehicles in tier-captive vehicle-based warehousing systems, *Eur. J. Oper. Res.*, Vol. 254, No. 1, pp. 51-67, 2016.

SESSION A

HOISTING AND CONVEYING EQUIPMENT AND TECHNOLOGIES

Ivo Maximow

PhD Student
Chemnitz University of Technology
Faculty of Mechanical Engineering

Markus Helbig

Senior Research Associate
Chemnitz University of Technology
Faculty of Mechanical Engineering

Sebastian Weise

Senior Research Associate
Chemnitz University of Technology
Faculty of Mechanical Engineering

Markus Golder

Full Professor
Chemnitz University of Technology
Faculty of Mechanical Engineering

Directly driven conveying belt

Belt conveyors are very popular due to their low complexity and high flexibility. In the classical drive concept the power of the drive is transmitted via force contact between the belt and the roller. Therefor the belt has to be under tension between the two rollers. By this way of drive the length, the life or the transportation capacity of the conveyor belt is limited. By developing a direct drive, the disadvantages of the classical drive will be avoided. Therefor a belt with an internal copper layer, which is used as moving part of an induction motor as well as the belonging motor stator was developed. In order to obtain a functioning drive, the design of the motor and the structure of the belt must be coordinated. While there is potential to increase the drives efficiency, the dynamic properties of the entire system allow new applications for belt conveyors.

Keywords: linear motor, induction motor, non-contact drive, direct drive, belt conveyor.

1. INTRODUCTION

Belt conveyors belong to the continuous conveyors and represent a widespread "classical" conveyor system. The great popularity is due to the simple structure on the one hand. Essentially, this is limited to a drive and a deflection roller, a frame to which they are attached, the conveyor belt itself and its support. Furthermore, belt conveyors offer a high degree of flexibility with regard to the conveyed goods. Fine bulk material up to heavy general cargo can be transported.

In addition, the requirements on the installation site and the installation costs in comparison to other systems are low. The drive of such a belt conveyor is simple. One of the rollers is driven by a motor. Depending on the requirements of the conveying speed and performance, various drive concepts are used. In industrial applications, however, three-phase induction motors with gearboxes are widespread. The gearbox output drives the drive roller directly. Depending on how the demands on the conveying speed are, the feed of the motors is different. If the conveying speed is always to be constant and if slight differences in speed are negligible, it is sufficient to connect the motor directly to the power grid. If the speed is to be variable or controllable, the motor is fed by a frequency inverter. Of course, other motor types with different types of power supply are conceivable and spread.

Regardless of the principle of how the rollers are driven, the further path of the power flow is the same. The drive power is transferred frictionally from the roller to the conveyor belt. To ensure traction, the conveyor belt must be tensioned. This means that even at standstill, an equally distributed tensile force F_t acts on the conveyor belt. In operation, a load- and location-dependent component F_l is added which is summing up

by the length of the conveyor line till the roller as shown in figure 1.

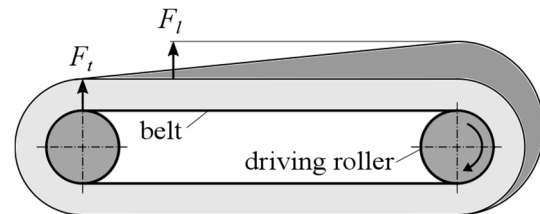


Figure 1. Forces inside conveyor belt

Depending on the needed conveying force, the belt tension must be adjusted accordingly. Decisive for this are the wrap angle α of the roller and the coefficient of friction μ between the belt and the roller. This behavior is described by the Euler-Eytelwein condition (1) [1].

$$F_t \geq \frac{F_l}{e^{\mu \cdot \alpha} - 1} \quad (1)$$

The necessary tension force F_t depends on the load force F_l and the properties of the contact between roller and belt. In addition, there is a security factor to be considered. Furthermore, the conveyor belt must be tensioned for the maximum driving force. In other words, especially for systems with different conveying masses, the belt is unnecessarily tensioned for a large part of the working time. This situation also applies to standstill.

Another aspect which needs to be investigated is the alignment of the belt. In a running system, the belt will move towards the area with the highest friction. The reason therefor is an occurring force due to the reduced speed on the side with higher friction. In an ideal system, the friction along the conveyor line is uniform. This is counteracted primarily by three aspects in industrial use. A non-uniform and off-center loading, belt wear and associated length changes and the state of the equipment in general [2].

As a result, each system requires a belt guide. Usually curved rollers are used to generate an aligning force. This technology is simple to install and common for short conveying lengths. The possible aligning force

Correspondence to: Ivo Maximow, PhD student
Fakultät für Maschinenbau,
Professur Förder- und Materialflusstechnik,
Reichenhainer Straße 70, 09126 Chemnitz, Germany
E-mail: ivo.maximow@mb.tu-chemnitz.de

is limited and the tension over the width of the belt uneven. Other technologies are for example stops for the belts or especially for long distances the use of individually aligned support rollers [2].

The aim of this research is to eliminate the disadvantages described. For this, the driving force should be introduced directly into the conveyor belt, without using a frictional force transmission. This would no longer require a bias to transfer the driving force. As a result, such belts can be loaded with higher conveying masses. Furthermore, it is possible with such a system in addition to the driving force to initiate a variable transverse force. This can implement an active belt guide. In particular, at high belt speeds such a belt can be guided safely. This makes it possible to realize highly dynamic and reversible belt conveyors.

2. APPROACHES FOR IMPLEMENTING A DIRECT DRIVE FOR CONVEYOR BELTS

To realize a direct drive, the conveyor belt itself or parts thereof must be part of the drive motor. The following three motor principles were considered.

The first principle is based on reluctance forces. Representatives of this principle are all switched or synchronous reluctance motors.

The second considered principle is based on the effect of electrodynamic forces. In this case, the magnetic field generated by energized coils interact with permanent magnets. This principle is used in permanent-magnet synchronous motors.

The third considered principle is also based on the effect of electrodynamic forces. In this case, the generated magnetic field interacts with induced eddy currents. This principle is applied to induction motors, also called asynchronous motors.

After a detailed examination of the variants mentioned, the third drive principle was chosen for implementation. The advantage here is that the drive starts itself, no cogging forces occur and no belt forces act in the direction of the stator. Overall, a direct drive can be implemented with this motor principle, which corresponds to the simple and flexible nature of the belt conveyor.

3. DEVELOPMENT OF AN INDUCTION DIRECT DRIVE FOR BELT CONVEYORS

Three-phase induction motors are now the most widely used motors in the industry. Figure 2 shows the cross section schematically.

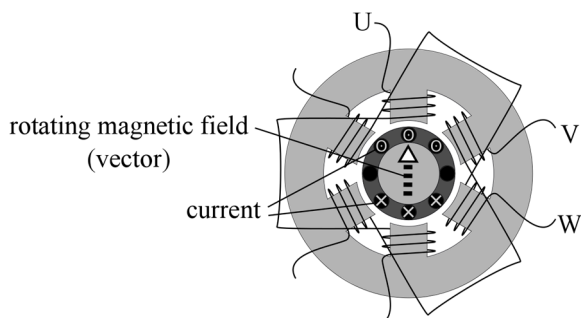


Figure 2. Rotating induction motor

Externally, the motor consists of a stator with the windings U, V, W. These are powered by three-phase current and generate a rotating magnetic field inside. In this field is the rotor, which consists of iron and a copper cage. Due to the electromagnetic induction, a voltage is induced which causes a flow of current in the cage. This current, which is marked as a cross for the flow direction into the figure plane and as a circle with point for the flow direction out of the figure plane, cooperates with the rotating magnetic field of the stator, resulting in the effect of the Lorentz force. This force acts on the copper cage and is directed to transmit torque to the motor shaft.

Based on the findings of the rotating induction motor, a linear motor according to the same principle is shown in figure 3.

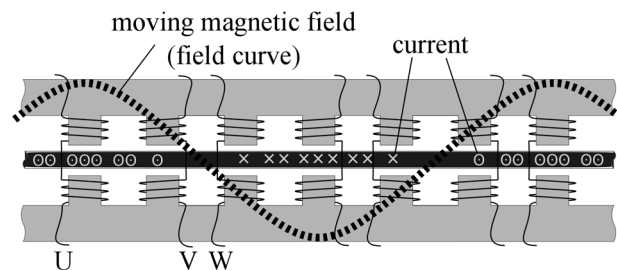


Figure 3. Linear induction motor

In order to implement this principle, it is sufficient to integrate an electrically conductive layer in the conveying plane of the conveyor belt. This layer represents the analogy to the copper cage of the rotating motor, but here the number of conductor loops is infinite. In the figure, only the layer without further components of the belt is illustrated. The conveyor belt must be enforced with a moving magnetic field to induce a voltage in the copper layer which causes a current flow. The current direction is analogous to figure 2. Due to the interaction with the magnetic field, the Lorentz force acts and generates a linear force in the moving direction of the magnetic field. For a significant magnetic field to pass through the layer, the belt must be enclosed by the stator. Therefore, the stator consists of two halves, each with its own stator back. Each tooth and the opposite tooth is wrapped in a coil. Such a drive can be installed only in the lower strand. Alternatively, a one-sided stator with an iron yoke on the opposite side can be used. However, the double stator arrangement is the most effective [3], [4].

3.1 Requirements for the integration of a conductive structure in the conveyor belt

For the motor principle, there is a need for eddy currents to form. The motorically active part of the belt consists only of a copper layer. In this case, the layer resistance plays an important role in generating the resulting driving force. A disadvantage compared to the cage of the rotating motors, the resistance of the layer is high. This has a direct effect on the driving force and can be counteracted by increasing the layer thickness. It should be noted that this cannot be increased arbitrarily, since it also contributes to the total air gap between the two stator parts. Rather limiting are the mechanical

properties. Here, the deflection radius is the decisive criterion for dimensioning of the thickness. The strain in the outer region of the layer must be at the deflection within the elastic range of the electrically conductive material. In this particular case, copper foil is used with a thickness of 0.2 mm due to the mechanical limitation of the application. From an electrical point of view, the foil should be as thick as possible, and as thin as possible from a mechanical point of view.

Another application is examined in [5]. This technology is successfully used to transport electrically conductive sheets without bending them. In this case, the drive will be designed for sheet thickness.

3.2 Requirements for the stator

When designing the motor stator, further restrictions on the use of the conveyor belt must be observed in relation to the rotating motors. It is not possible to install a speed adjustment gear between the belt and the motor. Accordingly, the conveying speed depends on the geometry of the stator, the frequency of the feeding three-phase current and the slip. It should be noted that the teeth of the stator cannot be made arbitrarily small. From a mechanical point of view, small teeth are difficult to manufacture and mechanically unstable. From an electrical point of view, there is the problem that when the teeth are too narrow and the air gap is too large, the magnetic fluxes within a stator half close and do not flood the foil. The air gap cannot be made arbitrarily small, since sufficient clearance for the belt must be present so that it does not tilt in the stator. For the manufactured drive, the stator teeth have a distance (from the center) of 20 mm at a stator air gap of 3.5 mm. The associated synchronous speeds are listed in table 1 and have been determined by the application. This design is already a compromise and causes a reduced efficiency. In general, it can be concluded that a high conveying speed is suitable for realizing the direct drive.

The approach over an increased slip to influence the speed does not make sense. With increasing slip, the efficiency of the induction motor decreases [6]. The reason for this is mainly due to the increased losses in the foil. These losses are converted to heat and can damage the belt. Furthermore, with increased slip, the inductive resistance of the conductive material negatively affects the force. This causes a phase shift between current and voltage [7]. As a result, the maximum current flows locally offset to the maximum field and the Lorentz force is reduced.

3.3 Results of the developed prototype

All measurements are related to the realized prototype shown in Figure 7. A characteristic operating point for induction motors represents the breakaway force. In figures 4 and 5, the measured values are compared with the previously performed simulation. This shows a basically good match. The fact that the values of the simulation are higher is due to longitudinal and lateral effects, which are explained in more detail in [3] and [4] and are not taken into account in the

simulation. The high deviation at 12.5 Hz supply frequency and 200 V supply voltage may indicate saturation effects and must still be investigated.

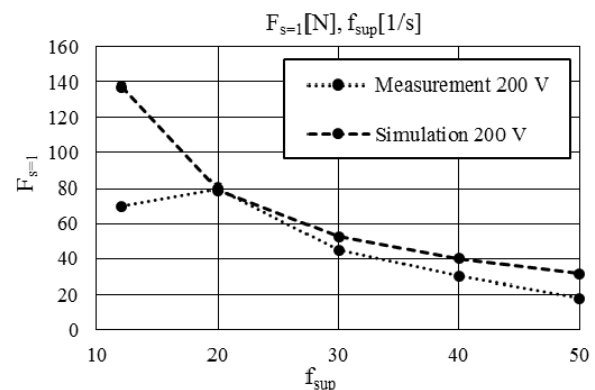


Figure 4. Output force of conveyor belt for slip = 1 at 200 V

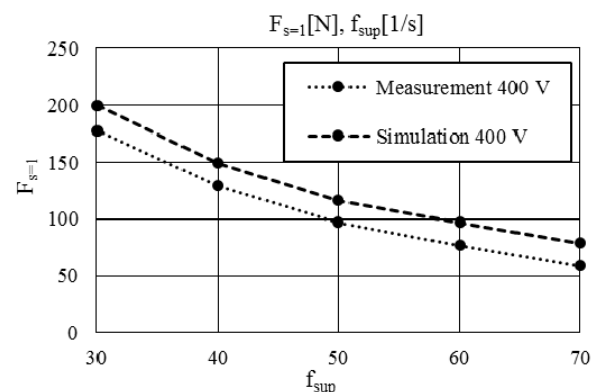


Figure 5. Output force of conveyor belt for slip = 1 at 400 V

In order to investigate the behavior of the belt conveyor system, the power consumption was measured without conveying load and is shown in figure 6. The inverter was operated with a constant voltage / frequency ratio, the parameters are given in table 1.

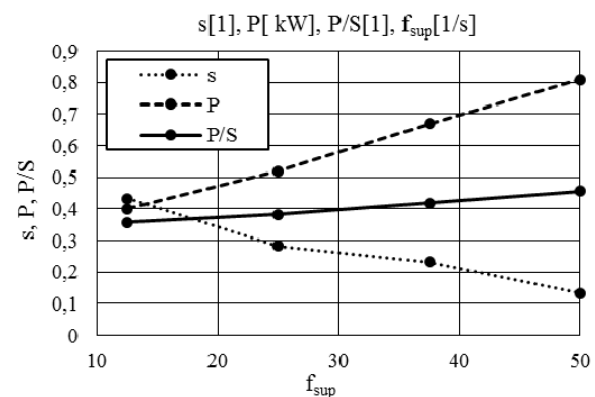


Figure 6. Unloaded belt over constant voltage / frequency

When assessing the efficiency, it must be noted that this is an unloaded conveyor. The consumed active power is mainly composed of the frictional resistance of the belt, the power required to deflect the copper foil, the inverter losses and the motor losses.

While the conveying speed according to table 1 more than sixfold, doubled only the active power consumed. This is due to the current heat losses. Since the impressed current is almost constant, the current heat losses of the stator are constant and are approximately 280 W. These losses dominate especially

at low speeds. This is typical for motors operating outside their rated point. The linear increase of the active power over the feed frequency is due to the increased frictional losses and deflection losses and must be further investigated. The P/S power factor increases slightly due to the increased mechanical load at faster speeds. However, to determine the characteristic power factor at the nominal point, the load must be increased in a defined manner. For this purpose, the installation of a variable load is planned for the future.

Table 1. Parameters of the test run

Parameter	Supply frequency (1/s)			
	12.5	25	37.5	50
Voltage (V)	100	200	300	400
Current (A)	5.5	5.63	5.68	5.7
Belt speed (m/s)	0.85	2.15	3.45	5.2
v_{syn} (m/s)	1.5	3	4.5	6

It should be noted that the diagram shown represents only one attempt. The engine can be greatly changed in electrical properties. In addition, the feed can be adjusted via the inverter. The results presented here are the first tests and will be extended by a variety of following experiments to determine the characteristics of the drive and the system.

4. CONCLUSION

It could be proven that the driving force can be introduced into a conveyor belt contactless via the principle of an induction motor. This technology is particularly suitable when very high conveying speeds are to be achieved. Due to the directed introduction of force, the guidance of the belt can be actively regulated. Thus, a highly dynamic and reversing belt conveyor can be realized. In further research, such a system should be implemented and the achievable dynamics determined. Since no bearings are installed, the motor can be encapsulated and is insensitive to external influences.

The achievable efficiency of this drive is well below that of the rotating motor. On the one hand, this is due to the stator, where magnetic fields have to be built up and dismantled, while the fields rotate harmoniously with rotating motors. On the other hand, the air gap is very large and the belt free of iron. As a result, the reactive power consumption is very high. This leads to increased current heat losses. On the supply side, the effect of reactive power can partly be compensated by using an inverter.

For further research, the integration of the conductive layer and its mechanical properties should be improved. The more flexible the layer, the narrower the deflection radius of the belt can be and the lower are the bending losses. At the same time, the conductivity should be improved to achieve higher efficiency. For this purpose, an investigation with woven copper structures is aimed at.

ACKNOWLEDGMENT

The project was made possible by the Federal Ministry for Economic Affairs and Energy (BMWi) within the framework of a ZIM project on the basis of a resolution of the German Bundestag.

REFERENCES

- [1] Sumpf, J.: *Lecture "Fundamentals of Conveyor Technology - Belt Conveyors"*, TU Chemnitz, 2016.
- [2] Martin Engineering: *Foundations*, Druckstudio Gallé GmbH, Klein-Winternheim, 2011.
- [3] Luda, G.: *Three-phase asynchronous linear drives*, Vogel-Verlag, Würzburg, 1981.
- [4] Budig, P.-K.: *Three-phase linear motors*, VEB Verlag Technik, Berlin, 1982.
- [5] Teichrib, S.: *Electromagnetic feed system for electrically conductive sheets*, PZH Verlag, Garbsen, 2016.
- [6] Müller, G. and Ponick, B.: *Basics of electrical machines*, WILEY-VCH Verlag, 2014.
- [7] Schröder, D.: *Electrical drives*, Springer-Verlag, 2007.

NOMENCLATURE

f_{sup}	supply frequency
F_l	belt force caused by the load
$F_{s=1}$	belt force at slip = 1
F_t	belt force caused by belt tension
P	active power
S	slip
S	apparent power
v_{syn}	synchronous speed

Greek symbols

α	wrap angle
μ	coefficient of friction

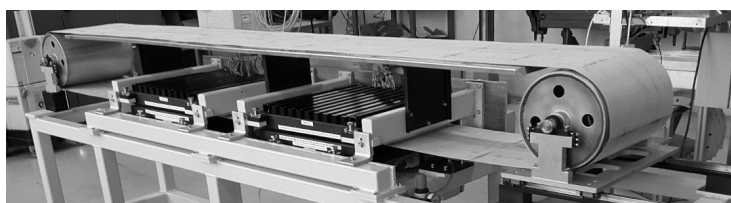


Figure 7. Prototype of the directly driven conveyor belt

Milorad Burić

Professor
University of Montenegro
Faculty of Mechanical Engineering

Marko Lučić

Teaching Assistant
University of Montenegro
Faculty of Mechanical Engineering

Vlastimir Jokić

Research Trainee
University of Montenegro
Faculty of Mechanical Engineering

Stanko Baucal

Research Trainee
University of Montenegro
Faculty of Mechanical Engineering

Aleksandar Sekulić

MSc Economics
BSc mechanical
Aluminium Plant Podgorica

Calculation and analysis of the stress and deformation of crane rail clips

This paper deals with the calculation and analysis of the stress and deformation of crane rail clips which are located on the bridge crane in the Aluminium Plant in Podgorica, using the finite element method using ANSYS software. Although they are exposed to high impact loads and high temperatures, these crane rail clips have been in operation for more than 20 years. However, some crane rail clips are deformed and also deformation of the crane rails. The cause for the formation of these deformations was obtained after the analysis of the obtained results. A new crane rail clip was designed and calculated. Analysis of the results of the calculation shows that the shape and dimensions of the new crane rail clip have eliminated the causes of the occurrence of the above deformations.

Keywords: crane rail clips, overhead crane, bridge crane, crane rail, finite element analysis.

1. INTRODUCTION

In the industrial halls of the Aluminium Plant Podgorica shown in Figure 1, in 1999, the replacement of the broken crane rails was performed, as shown in Figure 2, by which the bridge cranes move. On that occasion, new crane rail clips were built on the basis of the Project [1]. These crane rail clips are shown in Figure 3.



Figure 1. Industrial halls of the Aluminium Plant Podgorica

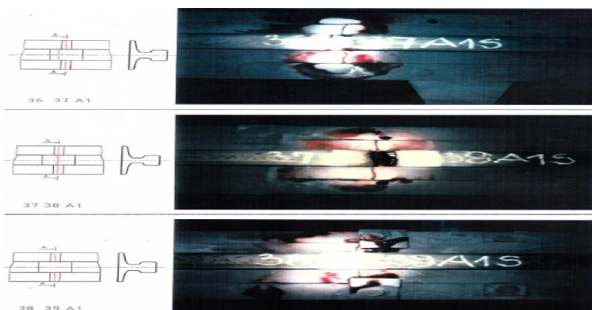


Figure 2. Crane rails that are broken

Correspondence to: Dr Milorad Burić, Professor
Faculty of Mechanical Engineering,
Džordža Vašingtona bb, 81000 Podgorica, Montenegro
E-mail: mburic@ucg.ac.me

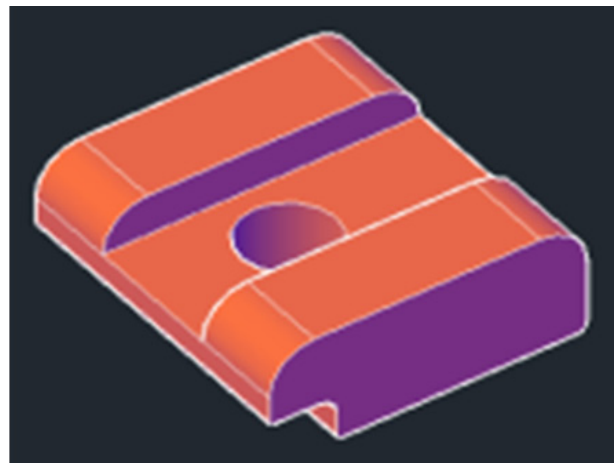


Figure 3. Crane rail clip used in the Aluminium Plant Podgorica.

After 20 years of exploitation, the state of most of these crane rail clips is still satisfactory even though they are exposed to strokes and high temperatures. Figure 4 shows the wheel of a crane with a rail and a crane rail clip.



Figure 4. Wheel of a crane with a rail and a crane rail clip

However, a smaller number of crane rail clip and crane rails are deformed at the points of connection of

the crane rails with crane rail clips, as shown in Figure 5.



Figure 5. Deformed crane rail

2. CALCULATION AND ANALYSIS OF THE STRESS AND DEFORMATION OF CRANE RAIL CLIPS

In order to check the strain-deformation status of this crane rail clip, we made a 3D model of the crane rail with commercial name A65 and the “T” beam in AutoCAD software. This 3D model is shown in Figure 6 and Figure 7.

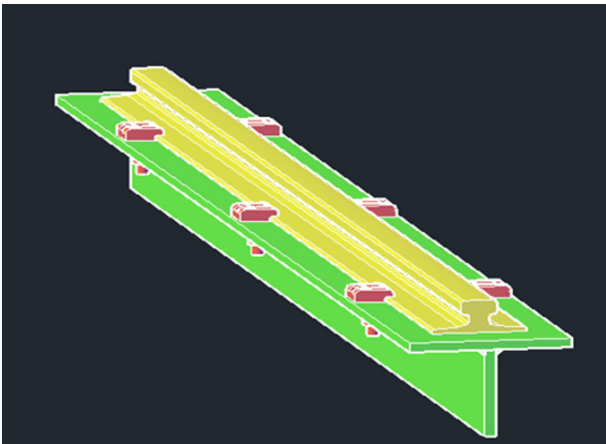


Figure 6. Isometric view of 3D model in AutoCAD interface

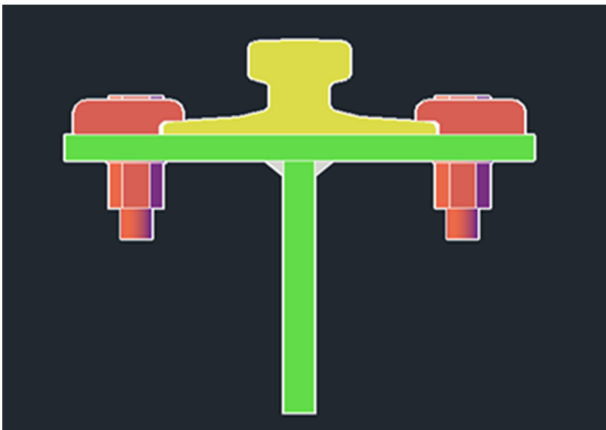


Figure 7. Side view of 3D model in AutoCAD interface

We have defined one of the possible real loads on the crane rail so that it causes high stress in the crane rail clip. We have taken the combination of vertical and horizontal force on the crane rail. The vertical force has a probability of 193750 N and is the result of the weight of a crane with a nominal load. The horizontal force has a value of 28050 N and is the result of the action of the inertial force that occurs when stopping the crane trolley with the load. The load of the 3D model is shown in Figure 8.

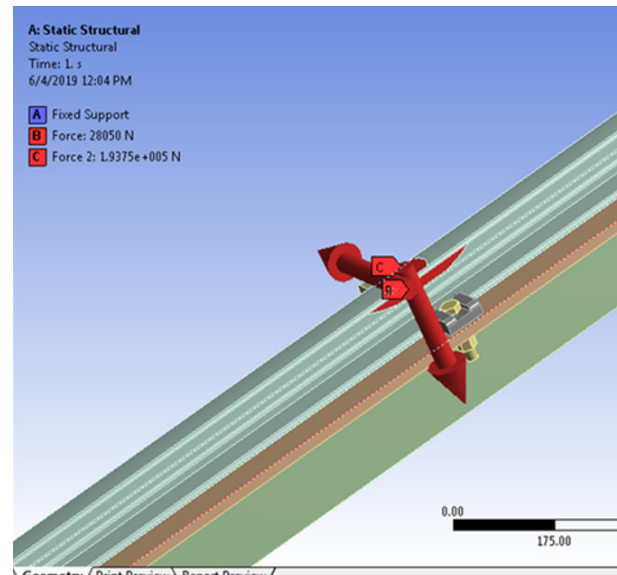


Figure 8. Load on the crane rail

The calculation was done using the Finite Element Method (FEM) in the ANSYS software. We have set boundary conditions that there is no movement in the points of the bottom and front cross sections of the “T” beam.

Figure 9 shows a mesh of finite elements, and Figure 10 shows the location of the fixed support.

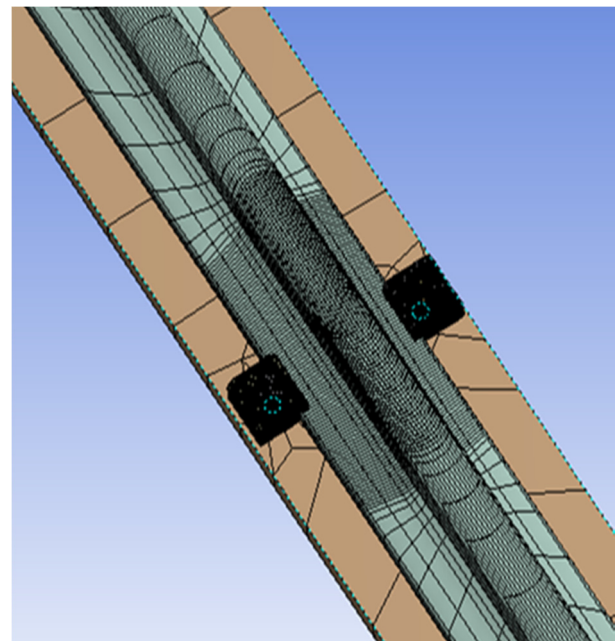


Figure 9. Mesh of finite elements

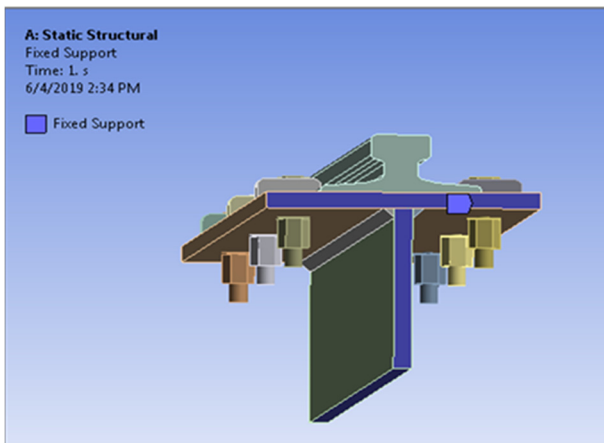


Figure 10. Location of the fixed support

Graphical display of the results of the Von-Mises stress on the crane rail, crane rail clip and “T” beam is shown in Figure 11. Graphical display of the results of the Von-Mises stress on isolated crane rail clip is shown in Figure 12.

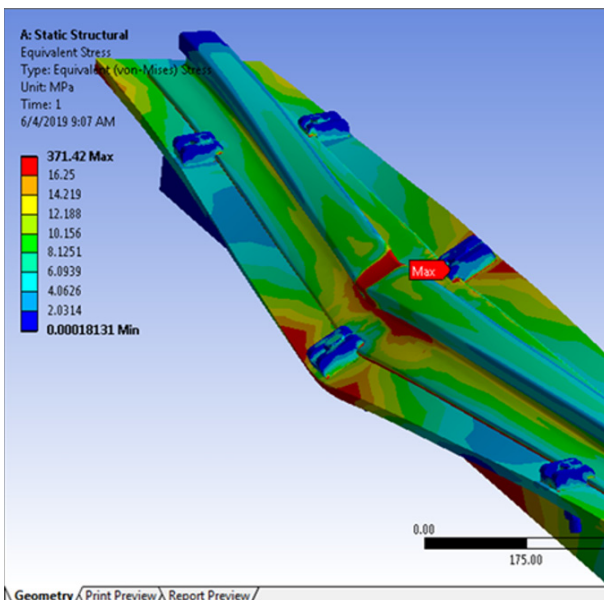


Figure 11. Von-Mises stress on the crane rail, crane rail clip and “T” beam

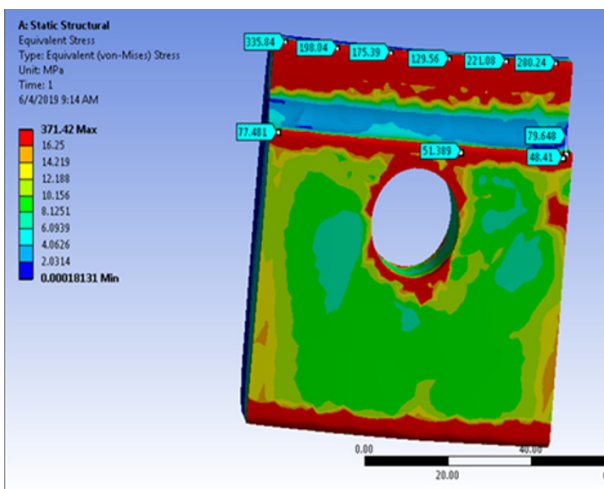


Figure 12. Von-Mises stress on the crane rail clip

Figure 13 shows total deformations on the crane rail, crane rail clip and the “T” beam and in Figure 14 the values of some total deformations on the crane rail clip and “T” beam.

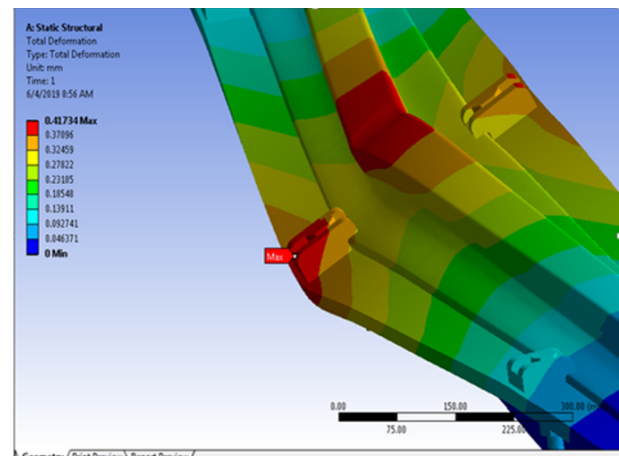


Figure 13. Total deformations on the crane rail, crane rail clip and the “T” beam

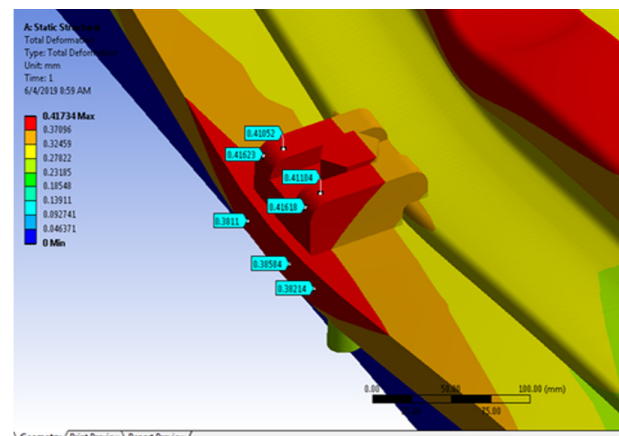


Figure 14. Values of some total deformations on the crane rail clip and “T” beam

In addition to the many good features that this crane rail clip has, his disadvantage is that his edges that fit on the crane rail are heavily loaded and, in time, they become more cluttered and deformed the crane rail as shown earlier in Figure 5. The relatively large Von-Mises stress on this edge can be seen in Figure 12.

For this reason, we designed a new crane rail clip shown in Figure 15.

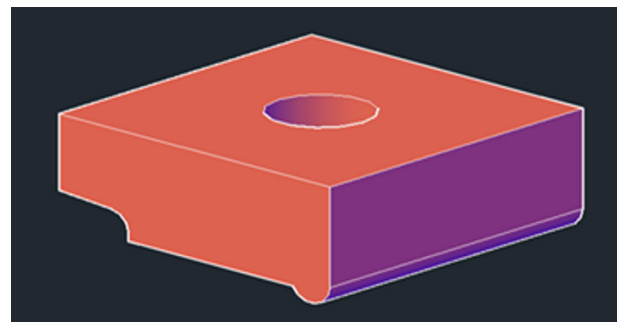


Figure 15. New design of crane rail clip

The tracking of the rail is shown in Figure 16.

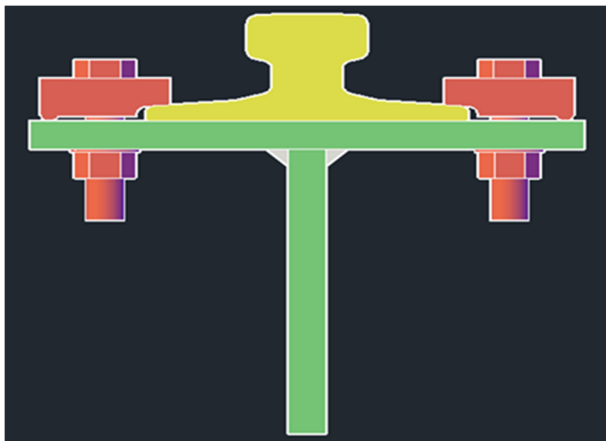


Figure 16. The position of the new crane rail clip on the crane rail

This design and the position of the new crane rail clip lead to a great reduction in the Von-Mises stress, as can be seen in Figure 17 and Figure 18.

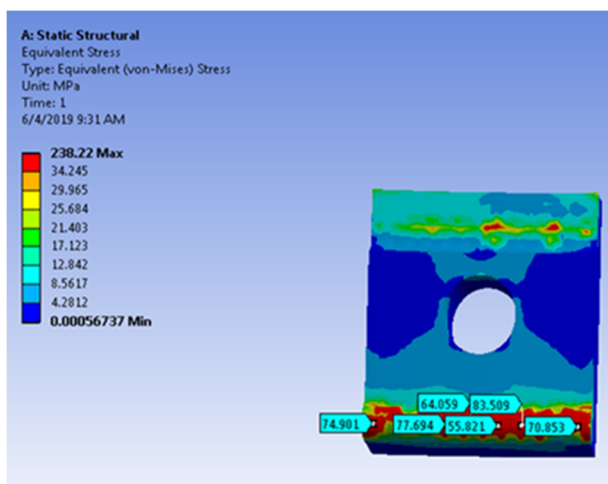


Figure 17. Von-Mises stress on the new designed crane rail clip

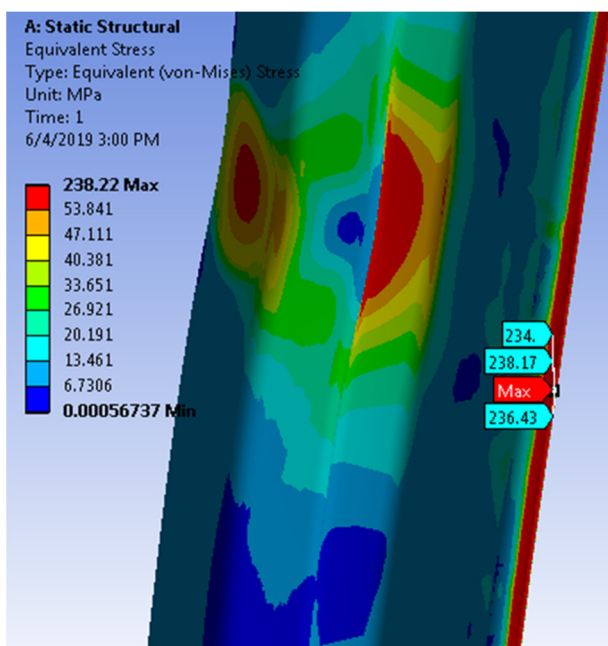


Figure 18. Von-Mises stresses on the crane rail

3. CONCLUSION

With the new designed crane rail clip, the Von-Mises stress have decreased considerably. While in the old crane rail clip, the maximum Von-Mises stress had a value of 371.42 MPa (Figure 12) for a new designed crane rail clip, it is only 77.70 MPa (Figure 17). Therefore, the maximum Von-Mises stress is less than about 79% of the previous crane rail clip.

The maximum Von-Mises stress of the crane rail clip and crane rail is transferred from the crane rail clip to the crane rail.

The crane rail clip in industrial hall of Aluminium Plant Podgorica is made of structural steel (ST 52-3-DIN) with a ultimate tensile strength of 500 MPa and a tensile yield strength of 330 MPa. The maximum Von-Mises stress of 371.42 MPa is higher than the tensile yield strenght, which explains the occurrence of deformation on the crane rail clip. With a new designed crane rail clip, the maximum Von-Mises stress of 77.70 MPa is far less than the tensile yield strenght. Namely, the degree of security is 4.25 for him and is significantly higher than the minimum required which is 1.5.

REFERENCES

- [1] Burić, M., Čulafić, V., Savićević, S. and Filipović, B.: The project of replacing old and installing new crane rails in industrial halls A1, A2 and B1 and rehabilitation of crane rails in the hall B2 of the Aluminium Plant Podgorica, 1999, Faculty of Mechanical Engineering, Podgorica.

Case-based parametric design of belt conveyors

Fotis Kondralis

M.Sc.
Olympic Mechanical SA,
Design Dept.

Argyris Dentsoras

Professor
University of Patras,
Dept. of Mech. Eng. & Aeronautics,
Machine Design Lab

Artificial intelligence (AI) offers methods that can provide efficient solutions to complex, non-conventional problems. Among those methods, Case-Based Reasoning (CBR) provides tools that give solutions to new problems based on past cases, an approach that – in the field of engineering design - is known as Case-Based Design (CBD). The present paper studies the application of (CBD) for designing belt conveyors. In general, designing belt conveyors is considered as a routine process where many parameters participate. These parameters may acquire their values by combining AI-based exhaustive design space search, generic design methods and case-specific calculation and selection procedures. The present approach exploits a set of past solutions (cases) and by using proximity metrics, retrieves and adapts a past case to create a new solution that satisfies the posed requirements. A case study of a belt conveyor design exemplifies the method and presents its advantages in terms of efficiency and computational cost.

Keywords: design parameters, parametric design, case-based design, belt conveyors.

1. INTRODUCTION

During the last decades, in the field of artificial intelligence (AI), a multitude of methods have emerged that provide efficient solutions to complex, non-conventional design problems [11], [1]. Starting from design knowledge representation issues and ending up to machine learning processes, (AI) has addressed many design subjects such as generation of concepts and solutions, reasoning and decision-making, evaluation of alternatives, optimization of proposed solutions, design for assembly and manufacturing, etc. [1], [13].

At most of the cases, designers use their experience, acquired skills and knowledge and rely on earlier design cases to solve new design problems. Within the field of (AI), case-based reasoning (CBR) [8], [12]- as a form of analogical reasoning [18] - has provided tools that give solutions to new problems based on past designs (cases), thus forming an approach that is now known as Case-based Design (CBD) [19], [9], [1].

The design of conveying systems has benefited from the advances in the field of engineering design and the development of new materials and manufacturing processes. This is valid also for belt conveyors which, among all systems used in industry, logistics and services, hold the largest proportion due to their structural simplicity, high service reliability and performance and low functional cost.

Parametric design is considered as one of the design phases where major design tasks are implemented [6]. Analytical, empirical and experimental methods are used

mainly for providing values to design parameters, verifying compliance with design constraints and assessing operational performance and efficiency. The design process of a belt conveyor is considered as parametric where, usually, a great number of parameters participate in order to provide a unique final solution that satisfies the posed requirements. These parameters acquire their values by combining generic design methods and techniques [6], [4] and case-specific calculation/selection procedures originated from the belt conveyor design theory and practice [2], [3], [5], [7], [14].

The present paper studies the application of (CBD) for performing parametric design of belt conveyors. First, the most important parameters that determine the structural and functional features of the belt conveyor are determined. Then, each parameter is characterized as independent or dependent [17]; for independent parameters, their importance indices are calculated [4]. Next, a base of solutions (cases) is created through twenty-five (25) calculation formulas and procedures where all parameters participate. The so created case-base is stored according to attribute-value pair paradigm [9] and subsequently used for performing (CBD) by following the typical cyclic process “retrieve-rank-adapt-store” [9]. The retrieval process uses Euclidean distances as proximity metrics [10] in the parameter space and the adaptation process is applied on an “if-needed/if-changed” basis [18]. The final so formed case is added to the case-base for future use.

The implementation of the case-based parametric design of belt conveyors has been done in Microsoft Excel[®] by extensive use of Visual Basic for Applications (VBA)[®].

Correspondence to: Dr Argyris Dentsoras, Professor
Machine Design Lab., Dept. of Mech. Eng. & Aeronautics
University of Patras, 26500, Patras, Greece,
E-mail: dentsora@mech.upatras.gr

2. CASE-BASED PARAMETRIC DESIGN OF BELT CONVEYORS

Belt conveyor case-based design may be considered as a stepwise executable procedure that leads to a solution for a new problem. Figure 1 shows schematically the proposed approach. Starting with the new problem and its requirements, the latter should be mapped to the appropriate independent parameters which – according to the set of associative relationships that represent the parametric belt conveyor design process - provide the rest, dependent parameters (see section 2.1 below).

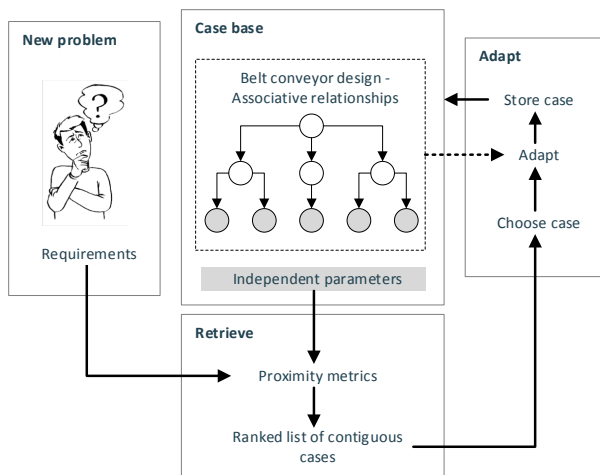


Figure 1. Case-based parametric design of belt conveyors

The application of proximity metrics for all the cases will finally provide a ranked list of contiguous cases (see section 2.2). The closest of those cases will be subsequently adapted (see section 2.3) and will finally become the solution for the new problem. Then, it will be stored in the case base and will be available for any new case-based design in the future.

2.1 Independent and dependent parameters – Associative relationships

The parameters that participate in a design problem form associative relationships which – under a certain formalism – consist a representation of the available relevant knowledge. The amount of details so represented depends on the availability of data, information and knowledge. It is obvious that if the design proceeds to the later phases (parametric design, detailed design), the degree of availability increases.

For the present work, a formalism based on the Design Structure Matrix (DSM) [16] is adopted for representing the associative relationships among design parameters. These associative relationships have been extracted from different sources containing calculation formulas, tables, empirical rules, etc. [2], [3], [5], [7], [14], [15]. Below, an example of a list of thirty-five (35) parameters in total that participate in the design of a belt conveyor that conveys bulk material is given:

1. Material
2. Material density (γ) (t/m³)
3. Surcharge angle (ϕ_i) (o)
4. Number of rollers ($NumTrRol$)
5. Trough angle (atr) (o)

6. Capacity factor (c_f)
7. Maximum allowed inclination angle (β_{max}) (o)
8. Maximum inclination angle along conveyor (β) (o)
9. $ccos$
10. IS 8730 coding
11. Maximum lump size ($alump.max$)
12. Belt width (B) (mm)
13. Required Capacity (Q_{req}) (t/h)
14. Required Volume Capacity (Q_v) (m³/h)
15. Material Type
16. Minimum speed (v_{min}) (m/sec)
17. Nearest Capacity (Q_{near}) (m³/h)
18. Design Capacity (Q_{des}) (t/h)
19. rq
20. Final speed (v_{fin}) (m/sec)
21. Transportation Length (L) (m)
22. Kg
23. Horizontal Length Projection (L_h) (m)
24. Load Weight per meter (W_m) (kgf/m)
25. Weight of load section rollers ($W_{u.s}$) (kgf/m)
26. Weight of return section rollers ($W_{l.s}$) (kgf/m)
27. Weight of belt per meter (W_b) (Kgf/m)
28. Conditions (C_w)
29. Resistance coefficient for load section (ω_u)
30. Resistance coefficient for return section (ω_l)
31. Load Elevation (H) (m)
32. Maximum total resistance ($Stot$) (Kgf)
33. Adhesion margin between belt and pulley (K_a)
34. Total efficiency of drive unit (η)
35. Required power (N) (Kw)

	1	2	3	4	5	6	7	8	9	10
1	x									
2	✓	x								
3	✓		x							
4				x						
5					x					
6			✓	✓		x				
7	✓						x			
8							✓	x		
9								✓	x	
10	✓									x
11										✓
12										
13										
14		✓								
15										✓
16										
17			✓	✓	✓					
18					✓	✓				
19										
20				✓	✓					

Figure 2. Design Structure Matrix of conveyor design parameters (partial representation)

After parameter rearrangement and under the assumption that there are not dependency loops among them, the DSM gets the form of a lower triangular rectangular matrix. A part of the reformed DSM is shown in figure 2. Here, the original parameter names have been substituted by their numbering indices in the previous parameter list.

The underlined parameters in the previous list are *independent*. This means that their values are assigned by

the designers, while the other parameters depend upon them and their values are determined with respect to them through the appropriate formulas, expressions, rules, etc. As an example of that dependency, figure 3 shows a tree that represents the associative relationships for the dependent parameter *Design Capacity*. Similar tree representations may be formed for all dependent parameters.

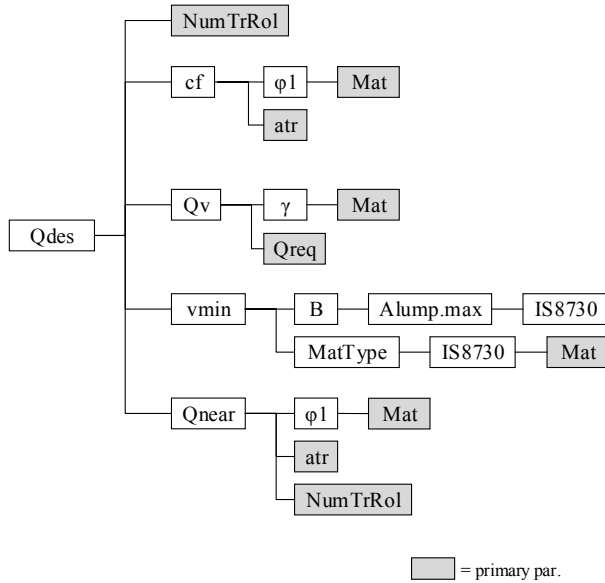


Figure 3. Tree representation of associative relationships for the dependent design parameter *Design Capacity*.

In parametric design, the associative dependencies among the parameters represent the available design knowledge for the subject under consideration. They dictate the value assignment priorities and sequences and they should not be violated in any case and for any reason during the design process. Regarding each independent parameter, it may participate – through the appropriate relationships – to the value assignment of one or more dependent parameters and its impact will relatively depend upon the exact number of those participations [4].

For the present approach it is assumed that the requirements for a new design case design problem can be expressed as values assigned by the designer to independent parameters that represent those requirements. The list of independent parameters can then be reordered decreasingly with respect to the number of participations of each of its members to value assignments for all dependent parameters. Following that ordered list for creating a design solution implies that the most important of the independent parameters will lead to the generation of the maximum of design information in early design time. Additionally, for case-based design, the case retrieval stage may benefit if the suggested order is strictly followed. In other words, the proximity calculations will start from the most critical independent parameter.

2.2 Application of proximity metrics - Ranked list of cases

If c_n is a *new case* and C is the case base that contains m past cases, then the *proximity index* between case c_n and case c_j , $j = 1, 2, \dots, m$ is defined through the

Euclidean distance in the space formed by the independent design parameters as follows:

$$r(c_n, c_j) = \sqrt{\sum_i \left(\frac{p_{n,i} - p_{j,i}}{p_{n,i}} \right)^2} \geq 0 \quad (1)$$

where $p_{n,i}$ and $p_{j,i}$ are expressions for the values of parameter p_i for the two cases respectively. The calculation of proximity index can be performed for independent parameters in both the new and past (existing) case. This fact implies that as design advances and more parameters acquire their values, there will be repeated index calculations and for each new calculation it is expected that the number of participating parameters will contribute to more realistic estimation of the proximity among cases.

It may be assumed that the design process takes places in *design cycles*, with *each cycle corresponding to possible value assignments and/or actions*. So, at a certain design cycle k , m proximity index calculations will be possible for all m members of case base C for that set that will form a list R_k of index values. Arrangement in ascending order of all values will finally provide a sorted case list C_k . In that list, the first element will be the case closest to the new case. It will also be a candidate for adaptation, a process that is discussed in the next section.

2.3 Adaptation of the closest case

In case-based design, the case adaptation process must be guided by and be always compliant with the field knowledge and the formalism used for its representation [9]. This means that any assignment of values to the design parameters that comes as a result of adaptation should not violate the quantitative and qualitative relationships that are expressed by the proper formulas, expressions, rules, etc.

Case-based design can start by forming the list P_{or} of ordered independent parameters (see section 2.1). Next, it may be assumed that, at a certain design cycle k , the designer sets the value $p_{n,i}$ for independent parameter p_i for the new case. This assignment will trigger the following actions:

1. *Action 1*: Determination of values of one or more dependent parameters whose instantiations depend upon p_i . The realization of the action will be possible only if $p_{n,i}$ is the only missing parameter for the completion of that determination and will follow an “if-needed/if-changed” approach [18]. For example, if p_i is *atr* (see figure 3), then parameter *Qnear* will be instantiated if both the rest two (*Mat*, *NumTrRol*) of the three parameters in total that affect its instantiation have been already instantiated. The output of action 1 will be a list of valued dependent parameters $P_{n,v}$.
2. *Action 2*: Formation of lists R_k and C_k for the current design cycle and normalization of their values with respect to the maximum value

3. *Action 3*: By consulting list C_k , choice of an already existing case c_r . This will be the case that presents the lowest value of proximity in that list
4. *Action 4*: Assignment - in new case c_n - of values for all independent parameters from case c_r that correspond to still non-instantiated independent parameters according to list P_{or} . It is important to note that the values of the rest parameters of the retrieved case will not be affected.
5. *Action 5*: Determine the values of all dependent parameters whose instantiations depend upon the newly assigned independent parameter values. The process is like the one followed in action 1
6. *Action 6*: Store the adapted case in the case base for future use. Now case base now contains $m + 1$ cases

Figure 4 shows schematically the above procedure.

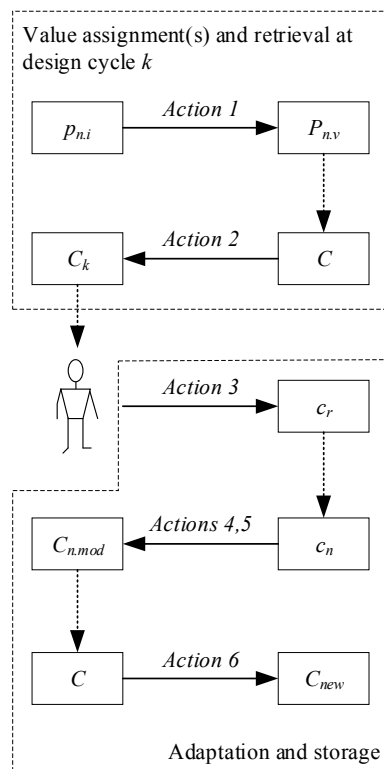


Figure 4. Actions for adapting past cases and storing new cases to case base.

The adaptation actions may take place at any design cycle except the first one since it is assumed that at least one value should be assigned to an independent parameter and at least one cycle of proximity calculations should be performed so that the designer is able to choose a past case to be adapted from those contained in list C_k .

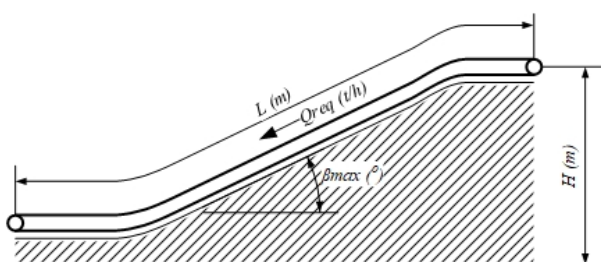


Figure 5. Transportation of dry gravel along an inclined part.

2.4 A case study: Case-based design of a belt conveyor

In order to exhibit the capability of the proposed approach for performing efficiently belt conveyor design, a case study is provided for a system that will convey dry gravel along an inclined path (see figure 5).

The case base contains seventy (70) previous cases. For the new design, the designer must initially form the ordered list of independent parameters P_{or} which has the following elements:

1. *Material*, 2. *atr*, 3. *NumTrRol*, 4. β , 5. *Qreq*, 6. *L*, 7. *Cw*, 8. *H*, 9. *Ka*, 10. η

According to this list, for the new case, the designer must initially assign the value "dry gravel" for parameter *Material*. This value assignment will trigger actions 1 and 2 (see section 2.3) and will provide values for the following parameters:

Table 1. Parameters instantiated by *Material*

Material	Gravel dry
Material density (γ) (t/m ³)	1.52
Surcharge angle (ϕ_1) (°)	25
Maximum all. incl. angle (β_{max}) (°)	12
IS 8730	C
Maximum lump size ($\alpha_{lump.max}$)	10
Belt width (<i>B</i>) (mm)	400
Material Type	Granular
Minimum speed (<i>vmin</i>) (m/sec)	1.60

The assignment of the value to parameter *Material* triggers a search in the case base and locates twenty (20) of them that are cases of belt conveyors that convey dry gravel. By following the recommendations set by the list, the design process continues with parameters *atr* (*atr* = 30 (°)) (trough angle) and *NumTrRol* (*NumTrRol* = 3) (number of trough rollers). Continuing with next independent parameter β and the assignment of a value of 7 (°) to it, further relative reduction of the proximity index values is observed for almost all cases.

Figure 6 below shows proximity index values for all twenty (20) cases at the third and fourth design cycles. At third design cycle (black bars), the lowest value of proximity index is equal to 0.882 and is possessed by more than one cases. At fourth design cycle (grey bars), that value becomes equal to 0.767 and is possessed by case C68.

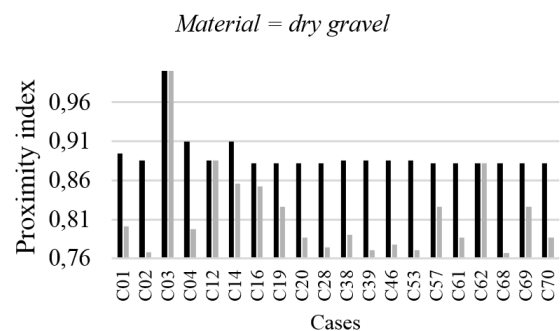


Figure 6. Average proximity values at third and fourth design cycles.

The assignment of a value of 210 (t/h) to Q_{req} changes the proximity values as it is shown in figure 7. Now it is case C53 that presents the lowest proximity index value and seems to be very close to the new case that is currently being configured. At this point, there are two (2) options for the designer. The first is to continue assigning values to the independent parameters that form the ordered list and the second is to choose the closest case (here case C53) for adaptation so that eventually he/she gets the solution to the initial problem. The first option is trivial. The second one implies that the designer accepts the transfer of all rest values of list P_{or} from case C53 to the new case. This will trigger actions 3 and 4 (see section 2.3 and figure 4).

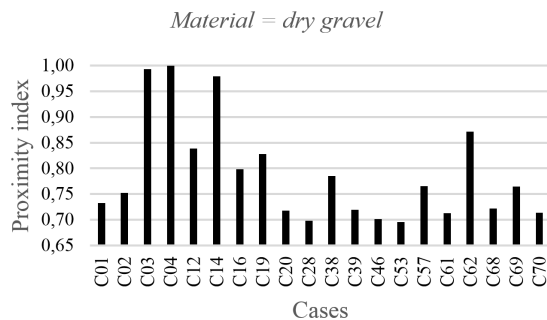


Figure 7. Proximity values for the fifth design cycle and for the independent parameter Q_{req} .

Action 3 sets case C53 as retrieved case. This case presents the following image regarding the values of its parameters:

Table 2. Instantiated parameters of case c_n at retrieval

<u>Material</u>	Gravel dry
Material density (γ) (t/m ³)	1.52
Surcharge angle (ϕ_1) (°)	25.00
<u>Number of rollers (NumTrRol)</u>	3.00
<u>Trough angle (atr)</u> (°)	30.00
Capacity factor (cf)	1.01
Max. all. inc. angle (β_{max}) (°)	12.00
<u>Max. incl. angle along conv.path (β) (°)</u>	7.00
ccos	0.99
IS 8730	C
Max. lump size ($alump.max$)	10.00
Belt width (B) (mm)	500.00
<u>Required Capacity (Q_{req}) (t/h)</u>	210.00
Required Capacity (Q_v) (m ³ /h)	138.16
Material Type	Granular
Minimum speed (v_{min}) (m/sec)	1.60
Nearest Capacity (Q_{near}) (m ³ /h)	139.66
Design Capacity (Q_{des}) (t/h)	212.28
rq	1.01
Final speed (v_{fin}) (m/sec)	1.60
Load Weight (W_m) (N/m)	80.00
Weight of load sec. rollers ($W_{u.s}$) (N/m)	2.12
Weight of return sec. rollers ($W_{l.s}$) (N/m)	79.24
Weight of belt (W_b) (N/m)	36.46

In table 2, the underlined parameters are independent and their values have been set by the designer. The rest are values of dependent parameters calculated according to the associative relationships that represent the available design knowledge.

Next, actions 4 and 5 are triggered. The result is an instantiation of all remaining parameters as it is shown in table 3 below (column 3). Here the values of the independent parameters (underlined) have been transferred from C53 (see column 2 in the same table) and the rest have been calculated with respect to them and to all previously value assignments made in the new case. One must notice the significant difference for the required power between case C53 and the new case. This is mainly due to the lower value of required capacity for the latter.

Table 3. Parameter values for case C53 and case $c_{n.mod}$ after adaptation

Parameter	C53	$c_{n.mod}$
<u>Transp. length (L) (m)</u>	80.00	80.00
Kg	2.12	2.12
Hor. Length Projection (L_h) (m)	79.24	79.24
<u>Conditions (C_w)</u>	heavy	heavy
Resist. coef. for load section (ω_u)	0.035	0.035
Resist. coef. for return section (ω_l)	0.03	0.03
<u>Load Elevation (H) (m)</u>	-11.00	-11.00
Total inclination angle (β_{tot}) (°)	-7.90	-7.90
Max. total resistance ($Stot$) (N)	1241.78	932.48
<u>Adhesion margin belt-pulley (K_a)</u>	1.14	1.14
<u>Total efficiency of drive unit (η)</u>	0.86	0.86
Required power (N) (Kw)	32.3	19.4

Figure 8 shows the variation of proximity index with respect to design cycles. There is a high reduction of its value that occurs when independent parameter L gets its value at cycle 6. This happens because that parameter is the one that causes high approximation among the two cases.

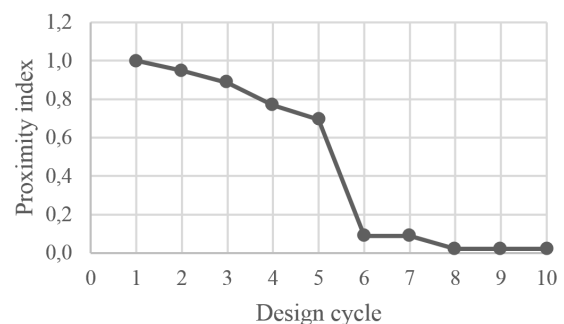


Figure 8. Variation of Euclidean distance with respect to design cycles between new case and case C53.

The final action 6 (see section 2) stores the adapted case in the case base for future use. Now the case base contains $m + 1$ cases.

The approach discussed in the present section is restricted to parameters that are related to the most significant functional features of a belt conveyor (material, belt, conveyor geometry, support rollers,

conditions and power). In fact, the number of the parameters that should be considered for obtaining a detailed final design documentation for a belt conveyor is much higher. This implies that in real world situations, when the adaptation of a case commences, much more independent and dependent parameters will be transferred from the past case being adapted to the new one.

3. CONCLUSION

The design process of a belt conveyor is considered as routine where, usually, many parameters participate in order to provide a unique final solution that satisfies the posed requirements. These parameters acquire their values by combining generic design methods and techniques and case-specific calculation/selection procedures originated from the belt conveyor design theory and practice.

According to the proposed approach, an exhaustive search of the design space may lead to a categorization of the parameters into independent and dependent. As design involves, the dynamic use of a heuristic function (Euclidean distance) for calculating proximity indices between new case and past cases in a multidimensional space formed by the independent parameters may lead to a choice of a past case for adaptation. So, at a certain design cycle and quite automatically, values for the rest non-instantiated independent and dependent parameters may be provided. These value assignments are in full agreement with the associative relationships among the parameters.

The presented case study shows that the proposed approach exploits efficiently and in a structured way the available knowledge and creates new belt conveyor designs based on verified past design solutions. It may also reduce the time needed for performing all necessary design tasks and for providing values to design parameters. Especially in design problems, where large number of parameters are involved, this time reduction is of high importance. What is also important is the fact that the parameters being transferred to a new case from an existing one will be probably standardized to their greatest percentage and their values would have been previously tested for reliability in real world situations.

REFERENCES

- [1] Avramenko, Y. and Kraslawski, A.: *Case Based Design: Applications in Process Engineering*, 2008 edition, Springer, Berlin, 2008.
- [2] Brown, D.C.: Artificial intelligence for design process improvement, in Clarkson, J. and Eckert, C. (eds.) *Design process improvement: A review of current practice*, Springer, London, pp. 158-173, 2005.
- [3] The Conveyor Equipment Manufacturers Association: *Belt Conveyors for Bulk Materials*, 5th Edition, Conveyor Equipment Manufacturers Association - Engineering Conference, 1997.
- [4] Fenner - Dunlop: *Conveyor Handbook*, 2009.
- [5] Dentsoras, A.J.: Information generation during design: Information importance and design effort, *AI EDAM*, Vol. 19, No. 1, pp. 19-32, 2005.
- [6] Dentsoras, A.J.: *Material Conveying Machines*, University of Patras, Patras, 2009 (in Greek).
- [7] Eggert, R.J.: *Engineering Design*, Upper Saddle River, N.J: Prentice Hall, 2004.
- [8] Fayed, M.E., Skocir T.S.: *Mechanical Conveyors: Selection and Operation*, CRC Press, 1996.
- [9] Kolodner, J.: *Case-Based Reasoning*. San Mateo, CA: Morgan Kaufmann, 1993.
- [10] Maher, M.L., Balachandran, M.B. and Zhang D.M.: *Case-Based Reasoning in Design*, 1st edition, Mahwah, N.J: Psychology Press, 1995.
- [11] Mc Adams, D.A. and Wood, K.L.: A Quantitative Similarity Metric for Design-by-Analogy, *J. Mech. Des.*, Vol. 124, No. 2, pp. 173-182, 2002.
- [12] Noor, A.K.: AI and the Future of the Machine Design, *Mechanical Engineering*, Vol. 139, No. 10, pp. 38-43, 2017.
- [13] Richter, M.M. and Weber, R.: *Case-Based Reasoning: A Textbook*, Berlin Heidelberg: Springer-Verlag, 2013.
- [14] Saridakis, K.M. and Dentsoras, A.J.: Soft computing in engineering design - A review, *Advanced Engineering Informatics*, Vol. 22, No. 2, pp. 202-221, 2008.
- [15] Shah, K.P.: *Construction and Maintenance of Belt Conveyors for Coal and Bulk Material Handling Plants*, <https://practicalmaintenance.net>, Accessed: April 2019.
- [16] Spinakovsky, A. and Dyachov, V.: *Conveying Machines*, Moscow: Mir Publishers, 1985.
- [17] Steward, D.V.: The Design Structure System: A Method for Managing the Design of Complex Systems, *IEEE Transactions on Engineering Management*, Vol. EM-28, No. 3 71-74, 1981., <https://doi.org/10.1109/TEM.1981.6448589>.
- [18] Summers, J.D. and Shah, J.J.: Mechanical Engineering Design Complexity Metrics: Size, Coupling, and Solvability, *J. Mech. Des.*, Vol. 132, No. 2, pp. 021004-1 - 021004-11, 2010.
- [19] Vlahavas, I., Kefalas, P., Bassiliades N., et al: *Artificial Intelligence*, 3rd Edition, Publisher: University of Macedonia Press, Greece, 2011. (in Greek).
- [20] Watson, I. and Perera, S.: Case-based design: A review and analysis of building design applications, *Artificial Intelligence for Engineering Design, Analysis and Manufacturing AIEDAM*, Vol. 11, No. 1, pp. 59-87, Cambridge University Press, New York, 1997.

Miomir JovanovićProfessor
University of Niš
Faculty of Mechanical Engineering**Nenad Pavlović**Professor
University of Niš
Faculty of Mechanical Engineering**Goran Radoičić**Research Associate
University of Niš
Faculty of Mechanical Engineering**Predrag Milić**Assistant Professor
University of Niš
Faculty of Mechanical Engineering

Dynamic performance of a double-boom level luffing crane mechanism

The design of large-mass supporting crane structures carries the risk of sensitive parts of construction. Sensitivity is often expressed as a dynamic phenomenon in the larger oscillation amplitude and longer period of deceleration. This paper presents one such study of dynamic behavior of a 400-tonne structure of a double-boom shipyard crane (with joint connected parts). Investigations of dynamic phenomena in the level-luffing mechanism also include the study the random influence caused by large cargo oscillations. Research was conducted using the experimental method and FEM. Dynamic behavior of the crane was analyzed to determine in which luffing operation the amplitude of the dynamic forces increases. This research will provide an answer to the question on the field of the occurrence of larger dynamic forces in the wipp mechanism for luffing changes in largest cranes.

Keywords: Double-boom crane, Shipyard crane, Transient dynamic analysis, Luffing mechanism, FEM.

1. INTRODUCTION

Shipbuilding cranes have evolved into specific forms in the last 100 years, characterized by large structures, a long jib and a tall rotary column.

Their level luffing systems with double-booms (jibs) are in theory (TMM) known as a four-bar mechanism. Dimensions of these systems reach a height of 80 m and the crane's own weight exceeds 500 t, and they represent one of the largest cranes today. The construction of these cranes requires: heavy duty ability, good dynamic behavior, high operational reliability and precision of cargo control. Experimental investigations into double-boom cranes have been published in the papers by Eiler [1-1965], Pielorz [2], Jovanovic [3]. A picturesque description of these technical systems, by Weinreich, can be seen on the Internet, [10]. By experimental testing [3], it was observed that the dynamic amplitudes of the forces during the operation of a four-bar mechanism are unequal at different levels. The measurements of the mechanical torque were performed on the level-luffing drive for the horizontal transfer of load on the rope. By disturbing the load from the state of rest – the swinging of the load is caused. It is shown that the amplitude of the dynamic torque for the level luffing drive is visibly higher at a lower reach (range).

This question was studied theoretically by a numerical simulation model of the crane on which the experiment was performed (Pula-Croatia, 1987). This paper confirms the experimental findings of the theoretical model.

2. CHOICE OF THE SIMULATION MODEL

Shipbuilding cranes are characterized by strong elastic deformations of long members (25÷80 m), caused by the limited load capacity of track (paths) and light (optimized) structure.

Large elastic deformations of the structure cause a disproportionate change in the position of discrete masses. Because of this, a large elastic displacement was introduced into the dynamic model using the method of non-linear analysis. The complexity of the topology of the cranes led to the choice of analysis in the numerical domain. The research of Sadler and Sandor [4], which deal with the kineto-elastodynamic analysis of a four-bar mechanism with an elastic coupling (rocker arm), indicates that the harmonic analysis produces complex solutions of differential equations, which are in such form unsuitable for analytical solution. Therefore, many studies in the field of applied mechanisms introduce the finite element method [5], in order to replace the "rigid" design with elastic properties. That is why the finite element method (FEM) is chosen here as well. To make the model of the transient dynamic analysis more efficient, the authors proposed the usage of the technique of modal superposition. Nonlinear analysis of the supporting structure was carried out by conventional - variational formulation and finite element deformation method (FEM) [8]. For the solution of forced oscillations (vibrations) of a discrete mechanical system structure with a double-boom (four-bar level luffing mechanism) in these studies, the differential equation of motion is used:

$$[M] \{\ddot{u}\} + [C] \{\dot{u}\} = \{f_{\text{ext}}\} - \{f_{\text{int}}\} \quad (1)$$

where $[M]$ and $[C]$ are the mass and damping matrices, $\{f_{\text{ext}}\}$ and $\{f_{\text{int}}\}$ the external (excitation) and internal (elastic) forces of the set of finite elements, and u, t (left index) is the time when the quantity is observed (i.e. acceleration, damping, velocity, and force).

The procedure of nonlinear analysis is described in detail in reference [11]. Geometric non-linear analysis requires the application of direct integration methods. Here, the implicit method of solving differential

Correspondence to: Dr Miomir Lj. Jovanović, Professor
University of Niš, Faculty of Mechanical Engineering,
Aleksandra Medvedeva 14, 18000 Niš, Serbia,
E-mail: miomir@masfak.ni.ac.rs

equations (1) was used. Neumark's time integration is applied. The equation system (1) can be written for time $t+\Delta t$ by equation (2):

$$\begin{aligned} [M]^{t+\Delta t} \{\ddot{u}\}^{(k)} + [C]^{t+\Delta t} \{\dot{u}\}^{(k)} + [K_T]^{t+\Delta t} \{u\}^{(k)} &= \{f_{ext}\}^{t+\Delta t} - \{f_{int}\}^{(k-1)} \\ \{u\}^{(k)} &= \{u\}^{(k-1)} + \Delta t \{\dot{u}\}^{(k-1)} + \frac{\Delta t^2}{2} \{\ddot{u}\}^{(k-1)} \end{aligned} \quad (2)$$

where $[K_T]$ denotes the tangential matrix of stiffness, Δt the increment of time, and k the number of iterations. The tangential stiffness matrix with the increment of displacement allows the assessment of internal forces at time $t+\Delta t$. The frame structure considered in this paper is modeled by means of beam and bar elements.

3. DEVELOPMENT OF THE SIMULATION MODEL

The dynamic simulation model of the crane was tested on the simple model shown in Figure 1, [3]. It is characterized by 36 nodes, 53 beam class elements and 212 degrees of freedom (DOF). This model is enhanced by later research (3D) and contains 225 finite elements and 135 nodes with a total of 810 degrees of freedom [12]. The coefficient of overall structural damping $G = 0.05$ is taken from the experimental study of the frame structure [13] (frame structure and tall crane). Nonlinear static, modal, and transient FE structural analysis were performed using the PLM SIEMENS software (FEMAP, 2018). The model has certain simplifications: the inertial resistance of rotating masses and energy of rotation of drive masses are ignored. Elastic supports of the portal are defined by spring finite elements describing the resilience of soil, wheels and balancers. The stiffness of soil was taken from an experimental test (experiments), [3].

The experimentally determined rigidity of the track was used: $c_z = 3018750$ (kN/m). Geometry modeling was performed according to the technical documentation of the 060270000 MIN-Niš crane. Masses of box-like structure members are reduced in their weight points. Thus, 15 concentrated masses were obtained, Figure 1. The reduction was performed by the *Rely* method (1894). Dynamic equation (3) of the free undamped oscillation of the structure in FEM was used to determine the eigenvalues of the dynamic system:

$$[M] \cdot \{\ddot{q}\} + [K] \cdot \{q\} = 0 \quad (3)$$

where $\{q\}$ is the generalized node coordinates of the model. The initial task of this process is to determine the natural frequencies (ω_i) of the undamped system, by solving the characteristic determinant (4):

$$P(\omega^2) = \det([K] - \omega^2 \cdot [M]) = 0 \quad (4)$$

The frequency equation was determined by the method of iteration of the sub-space (repeated application of the *Ritz* method). Low rotational frequency of the model corresponds to the oscillation pivotally coupled to the top rope $\omega_{FEM(1)}$ rocker arm, and the second frequency corresponds $\omega_{FEM(2)}$ to the swaying of the payload like a pendulum. These frequencies are used to select the oscillation attenuation rate as this is the case of viscous friction in the model [14].

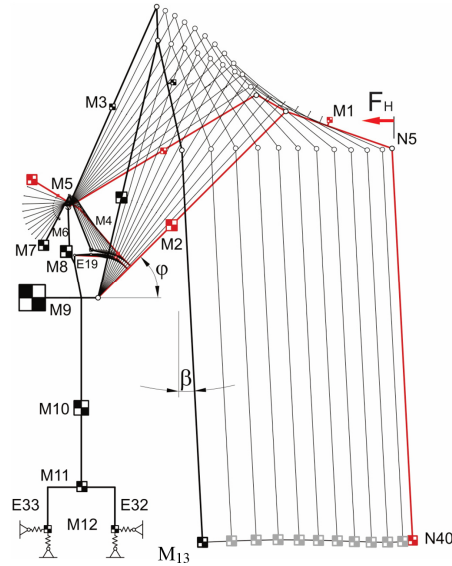


Figure 1. FEM model of the four-bar mechanism type shipbuilding crane in 12 characteristic reaches (levels)

4. TRANSIENT FEM ANALYSIS

STARTING TASK: Drawing on the criteria for the design of shipyard crane structures, a fundamental question was raised: Can a sudden swing of a rated load (on a long rope) designed for angle $\beta \pm 3^\circ$ (Figure 1) cause critical phenomena, jeopardizing the stability of the whole and damaging the supporting structure?

As this is a case of forced dynamic work, with damping in the material and joints and with a variable position of an oscillating load, the solution is sought in the application of the nonlinear FEM dynamic analysis. Since the analysis observed a transitory dynamic behavior, the transient mechanical analysis was applied. Transient response analysis was performed by numerical integration of the equation of motion. Transient response analysis is most commonly applied to structures with linear elastic behavior. The nonlinearity of the elastic deformation of the structure was treated by the *Newton-Raphson* method. The analysis includes the total structural dynamic damping forces proportional to displacement q and the recommended structural dynamic coefficient $G=0.05$ [8].

Two additional parameters were used in transient response analysis to convert structural damping to equivalent viscous damping, parameter ω_3 and parameter ω_4 . The speeds of frequency damping in the first (modal) analysis for the respective position of the crane reach (double-boom mechanism) were $\omega_2=0.42 \div 0.47$ Hz, $\omega_3=0.93 \div 0.74$ Hz, $\omega_4=1.40 \div 0.92$ Hz.

Since the oscillation of the cargo on the crane was slow, the 300-second observation period was chosen.

$N_{step} = 30,000$ increments with a time increment $\Delta t_{incr} = 0.01$ sec (speeds of crane lifting speed for shipbuilding were 10 m/min^4) were adopted for the nonlinear procedure. Such integration controls the behavior of the model in the current 300 sec. In the *Newton-Raphson*

nonlinear model, the integration is limited to maximum $N_{\text{iter}} = 25$ steps with convergence tolerance $\varepsilon = 0.001$.

This study observed the drive member for changing the reach (element E-19) and portal structure (elements E32 and E33 are portal legs through which the stability of the mech. system was monitored). The movement of the cargo (node - N40) and the movement of the top of the rocker arms node (N5) were observed, Figure 1.

HIGHER LEVEL TASK: In the case of free oscillation of loads on a long rope, it is interesting to note the position (reach) of cranes in which a larger internal dynamic force is generated on the drive member. The response was obtained by a series of nonlinear transient analyses: The double-boom system was set up in 12 successive positions (Figure 1) for which the response of the free-motion oscillating load ($M = 12$ t) was required. The simulation scenario implied all analyses of the same initial conditions of the load position.

The time period of the disruption force (T_1 , Figure 2) was determined to be sufficient to decelerate the oscillation of the individual crane mass, which ended in the first 150 seconds. During this period, the external disruption forces were statically held by a mass of 12 t under the angle of 3° vertical displacement. The disturbance function had the form of a spring ramp function with the characteristic of the momental termination after the end of the T_1 calming period (Figure 2). Then the oscillation of the load began on the long rope hanging from the rocker arm that connects the double-boom luffing mechanism. The choice of the 3° angle under which the oscillation starts is consistent with the classical design procedures under which the resistance of the luffing mechanism [15] is calculated. This angle gives offset loads of 2.46 m from the equilibrium position when using a rope of 47 m (starting position).

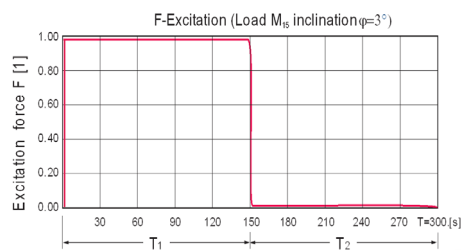


Figure 2. Excitation force in transient analysis - Ramp force ($T=300$ s)

SOLUTION OF ANALYSES: The drive-member to change the reach (luffing) was observed, due to its importance and the smallest dimension (marked as element E19 in the model, Figure 1). The obtained transient analysis solutions (the law of the change of the internal axial force in drive-member E19) are presented in Figure 3. The figure shows the dynamic response of

the crane construction (axial force S_{E19}) in drive-member E19, which performs a change of range (level) with three characteristic dampings (limit and medium).

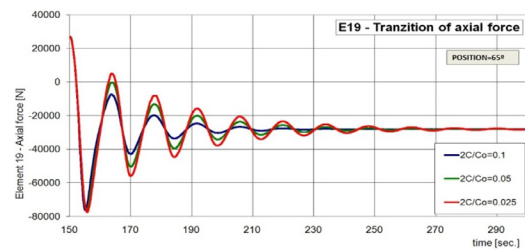


Figure 3. Dynamic forces in the member of level luffing mechanism at three characteristic dampings (lightning angle $\varphi = 65^\circ$)

If the static structural analysis of the double-boom mechanical system is performed by the procedure of linear and nonlinear solution, the difference between the two methods can be noticed. Figure 4 shows the solutions of the static linear and nonlinear force analysis in the drive-member of the luffing mechanism (two blue central curves). These curves show a permanent (static) resistance of the luffing range in the working range (the angle of major boom inclination is between 45° and 77°). Differences in the results of linear and nonlinear analysis are the consequence of elastic deformations of long members and changes in the position of their center of gravity - determined by the second order theory [12].

Figure 4, in six typical reaches (i.e. main boom inclination φ), displays the results of the individual dynamic forces of the driving-member (red curve). These forces are due to rocking loads of 12 t at the top of the rocker arm hung at an angle of 3° .

Discrete dynamic forces were obtained by nonlinear transient analysis of a simple model from Figure 1. Based on these six individual diagrams, it is possible to identify the dynamically deployed internal forces in the drive at different reaches and to the same external excitation. Equal external dynamic effects on the structure caused by horizontal forces are produced in the drive member - greater axial force at smaller reaches (at higher angles of inclination of the main boom $\varphi = 77^\circ$). Horizontal forces can cause the wind or towing loads on the ground. Determining the occurrence of larger internal dynamic forces in the drive-member at lower reaches points to an area of increased sensitivity of the mechanical system. Therefore, dynamic analysis is recommended just at the smallest reaches of the crane.

5. EXPERIMENTAL VERIFICATION OF THE MODEL

The modeling quality of the crane¹ was verified through several criteria: First, the elastic properties of the structure were verified.

above which a tower is mounted on a compact rotary platform. The tower houses the main members for the reach change: tie rod, jib and rocker. The drive device for the reach change is made with a helical screw, which acts on the main jib. The drive mechanism for the reach change is driven by an asynchronous motor. Boom balancing is carried out by the structure in the form of a four-bar linkage mechanism - a lever and balancer with a mass of 21 (t). Balancing of the entire crane is carried out by a fixed weight of 100 (t) on the rotating platform.

¹ Experimental verification of the models was performed on the crane in the "Uljanik" shipyard - Pula (Croatia). Crane PULA MIN-2 is characterized by a structure of 67 (m) in height, the maximum reach of 40 (m), with a base of the portal 6x8 (m), and a total weight of 400 (t). The crane has a system for the reach change in the form of a four-bar linkage mechanism, and members and a rocker connected with joints. The payload is 25/15/5 (t), the reach 27/37/40 (m), the lifting height 45 + 10 (m), the rate of reach change 10 (m / min) and the working drive class 3. The crane is formed on the column with the height of 30 (m)

Verification of elastic properties: The FEM model properties were controlled by comparing the experimental properties of the real structure (used for verification). The rocker arm path was determined experimentally using a geodetic - nivelman method (optical method). Measurement results are shown in Figure 5. It combines analytical, numerical and experimental results, shown simultaneously. The experimental results are given in discrete points (marked with square symbols) for working with cargo-weight M_{15} . The theoretical (numerical) results of the direction (elastic line) of the rocker arm movement, obtained by the FEM method, are given with a black continuous curve. The second (gray) continual curve shows the theoretical trajectory of the rigid mechanical model. The differences between the extreme values of the deflection from the numerical and experimental tests are maximally 10.2% in the luffing range, [3]. In doing so, the differences in the results are not only the consequence of elastic deformations, but include other non-idealities of trails and coast. The accuracy of the optical equipment (nivelman methods) for the moving rocker is defined by 0.01 m.

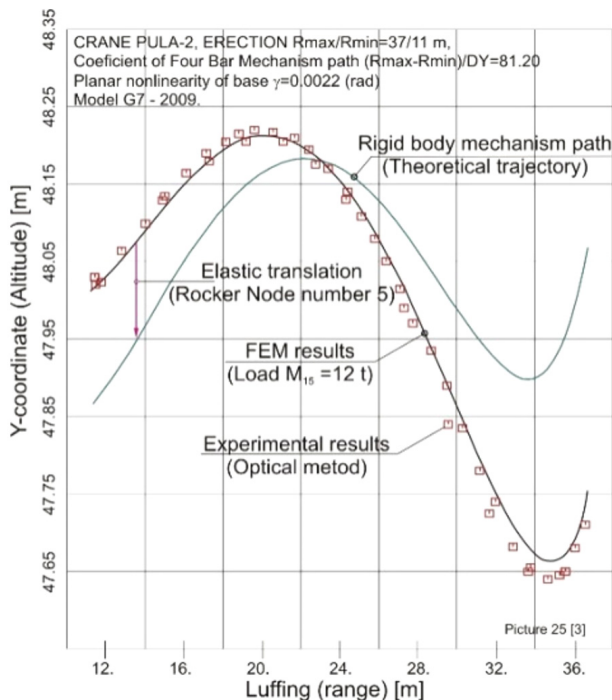


Figure 5. Comparative overview of numerically determined translations (FEM) and experimental elastic translations ² of the crane [3]

Dynamic verification was performed by comparing the experimental results of the oscillation of the crane (oscillation period) in the same modes of operation with and without loads. Thus, the impact of the load (cargo) oscillation frequency on the long rope was separated (from the other frequencies present) at the change of the reach.

Analytically, the oscillation of a cargo as a mathematical pendulum (with a suspension height of $L = 47$ m and gravity $g = 9.81$ m/s²) has a solution of the oscillation period by equation:

$$T_{MAT} = 2 \cdot \pi \cdot [L/g]^{0.5} = 2 \cdot \pi \cdot [47/9.81]^{0.5} = 13.75 \text{ (sec)} \quad (5)$$

This analytically obtained value is compared with the experimental results from the measurement. Figure 6 shows the results of experimental tests of the driving system for changing the reach (luffing system) of the crane 060270000 built in the MIN-Niš factory.

In Figure 6, the central (purple) curve shows the tensometrically determined drive moments of the luffing mechanism (on the spindle - member E19). This experimental curve easily shows the pendulum impact loads, the presence of 7-8 wave periods $T_{EXP(2)}$ approximately equal to the period of the lowest natural frequency of the FEM modal analysis.

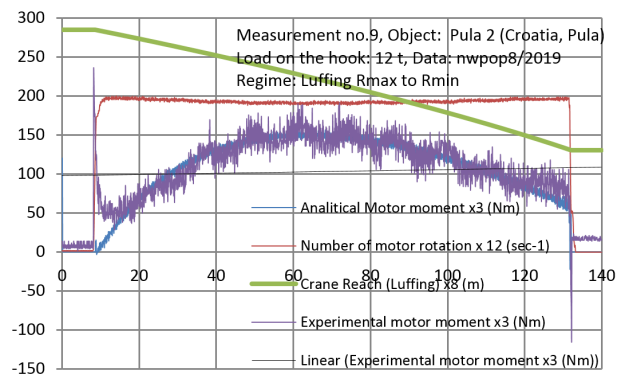


Figure 6. Results of experimental testing of the drive system of change of the reach (level) of crane [3]. Moment, reach, engine speed.

The red curve shows the number of engine revolutions. The green curve shows an analog reach. Modal (numerical) FEM analyses give the periods of oscillation loads of M_{15} (Figure 1), for a series of separately observed consecutive crane admissions: $T_{FEM(2)} = 13.454 \div 14.680$ sec. The measured average oscillation experimental period, from the diagram (Figure 6), is $T_{EXP(2)} = 13.85$ sec. Comparing the analytical ($T_{MAT} = 13.75$ sec), (5) and numerical ($T_{FEM(2)} = 13.454 \div 14.680$ sec) period of the model oscillation with the experimentally determined period of oscillation (on a long rope $T_{EXP(2)} = 13.85$ sec), the periods (fields) of swinging coincide.

Verification of the support stiffness: The rigidity of the support of the portal crane is determined by the stiffness of the path and stiffness of the roller coaster of the portal. The average experimentally measured stiffness of the path was obtained by measuring the deflection rail operation by a known control force. The stiffness of the path was determined from the force and defect rate: $c_{SR} = 1620000$, kN/m. The rigidity of the roller coaster was determined by computational FEM analysis of the roller assembly (balancers), which is a reliable category given the simplicity of the model (elastic isotropic materials). The deflection of a group of the roller coaster balancers is $f_{BAL} = 0.00028$ m, at the effect of force $F^1 = 1000$, kN. From this deflection the stiffness of the balancer (portal system) is calculated as $c_{BAL} = 3571000$ (kN/m). It is now possible to determine the stiffness of the support of the portal, adding rigidity of the paths and rigidity of the balancers (series connection of springs). The total rigidity of the path and balancers ($c^* = 1116000$, kN/m), with which the portal is elastically supported, was obtained.

6. DYNAMIC SENSITIVITY

Below are presented the results of the dynamic simulation of the luffing drive (for change in the reach of the crane). Using FEM nonlinear transient analysis, dynamic responses were obtained for cranes with the elastic construction.

The dynamic phenomenon was induced by the external force which is a statically balanced swinging of cargo (the given initial rope angle). By examining the crane, a similar situation caused by the oscillation of a suspended load was considered. In Figure 6, curve IiIa (in the middle of the diagram) shows the measured moments for change (decrease) of the reach. With this torque (moment), the engine (at the output from the gear unit) generates an active force for luffing over member E19 (Figure 1). A group of dynamic analyses of the supporting structure of the cranes (in all discrete ranges) yielded a common area of dynamic forces on drive E19. It is shown in Figure 7.

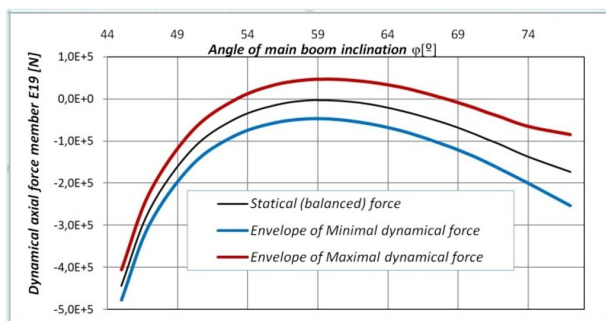


Figure 7. Dynamic forces in the member of the level luffing syst.

Figure 7 shows the lower and upper limit (envelope) amplitude of the dynamic forces on member E19, due to swinging of suspended cargo with all successive ranges. Both curves obtained are based on splines. The middle curve shows the value of resistances, which correspond to the equilibrium state at rest of the drive for luffing the reach (with the weight). Envelopes indicate the area of higher amplitude of oscillation at large angles of the main boom inclination. This indicates that the largest internal dynamic force in the drive member (helical spindle) occurs at a minimum reach of the crane.

These observations of the dynamic properties of a concrete crane have a general character for all cranes with a double boom and four-bar jointed mechanism. This phenomenon derives from the obviously different angles of the luffing mechanism (From TMM) in different reaches. Larger internal dynamic forces are generated at small reaches. The area of small reaches can be considered as a zone of greater dynamic sensitivity of the crane to external horizontal forces.

In the present case the internal dynamic force on the driving member (double amplitude) are higher no fewer than 2.35 times in the minimal reach in relation to the force (double amplitude) in the maximal reach ($168555/71635 = 2.35$).

7. CONTROL OF THE MECHANISM SENSITIVITY

The dynamic sensitivity of the luffing system was determined from numerous transient analyses. The scope of these dynamic analyses raises the question: Is there a simpler dependence of internal luffing forces than the one on external forces? Such an analysis is done based on the model with a horizontal force F_H on the top of the rocker arm (Node N5, Figure 1).

By observing the luffing system, it was found that the kinematic transmission ratio of the luffing mechanism is not constant. This variability can be seen from the speed of the rocker arm at a constant speed of the spindle drive. Therefore, the generalization of these analyses was found in the static relationship of model members. Therefore, a test horizontal force F_H was introduced at the top of the rocker in the model (Figure 1). The static FEM analysis now solves the structure response at the operating member (E19) of the F_H force. The resistance of the luffing drive at the same external force F_H was obtained in all discrete reaches of the crane. Static analysis can be done with or without load ($M13=12$ t) for all discrete reaches ($m=12$). The difference between the drive forces (E19) with and without load (M13) for all positions is shown in Figure 8.

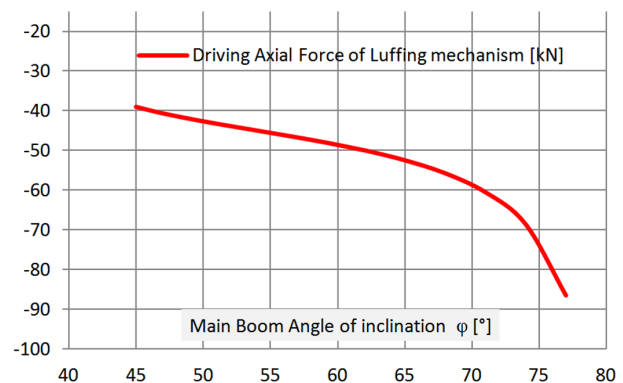


Figure 8. The growth of the static forces in the drive member under the control horizontal static force on the top of the rocker arm

8. CONCLUSION

Dynamic analyses have shown the position of the greater sensitivity of the luffing system with a double-boom - at larger angles of the main boom ϕ (at the same external horizontal excitation), Figure 7.

On the other hand, in the large reaches of the crane, the maximum static resistances of the drive appear (caused by their masses and useful load), Figure 4. A collective effect of the minimal (from dynamics) and maximal (from mass) resistances is a convenient combination.

Therefore, it can be said that technical solutions, the design of a shipbuilding crane with a double-boom, will still remain in use. Dynamic simulations can improve the kinematic properties of transport machines and increase their capacity.

ACKNOWLEDGMENT

The dynamic study was carried out with the funds from the Ministry of Science of the Republic of Serbia, within the project TR35049 in 2011-2019. The authors would like to thank the Ministry on their trust and financial support.

REFERENCES

- [1] Eilor, P.: *Über Massenkräfte an dreh und Wippdreh Kranen*, Technischen Hochschule München, 1965.
- [2] Pielorz, J.: *Wyzaczenie obciazen dinamicznych w okresie hamowania mechanizmu zmiany wisiegu na wybranym przykladzie zurawia jedno czlonow.*, Praca doktorska, Politechnika Wroclaw, 1975.
- [3] Jovanović, M.: *Supporting structure level luffing system and driving mechanisms resistance of portal-jib cranes optimization*, Ph.D. Thesis, University of Niš, Faculty of Mechanical Engineering, 1990.
- [4] Sadler, P.J. and Sandor, N.G.: Kineto-elastodynamic Harmonic Analysis of Four-bar Path Generating Mechanisms, ASME Paper No. 70-Mech-61, 1971.
- [5] Thompson, S.B. and Sung, K.C: A Survey of Finite Element Techniques for Mechanism Design, Mechanism and Machine Theory, Vol. 21, No. 4, pp. 351-359, 1986.
- [6] Jovanović, M., Radoičić, G. and Milić, P.: Dinamic Sensitivity research of Portal-rotating Cranes, XIX International Conference MHCL 2009, University of Belgrade, Faculty of Mechanical Engineering, 15th - 16th 2009., Belgrade, pp. 61-66, 2009.
- [7] Lipinski, J.: *Fundamente und trag-konstruktionen fur Maschinen*, Bauverlag GMBH, Viesbaden, 1972.
- [8] MSC Nastran: *Basic Dynamic Analysis*, User Documentation - Version 68, Santa Ana (CA), USA, 2004.
- [9] Timoshenko, S. and Young, D.H.: *Advanced Dynamics*, McGRAW-HILL, 1948.
- [10] Weinreich, D.: *Slew Cranes in Shipyards: A Study*, M.A.N. - Wolffkran, Heilbronn Emscor Inc., Houston, Texas, 1985, <https://apps.dtic.mil/dtic/tr/fulltext/u2/a453172.pdf>
- [11] Radoičić, G., Jovanović, M. and Marinković D.: Non-linear incidental dynamics of frame structures, Structural Engineering and Mechanics, Vol. 52, No. 6, pp. 1193-1208, Techno-Press Ltd., ISSN: 1225-4568 (Print), 1598-6217 (Online), DOI: <http://dx.doi.org/10.12989/sem.2014.52.6.000>, 2014.
- [12] Radoičić, G.: *Dynamic behavior of certain classes of transport machinery in terms of incidental events*, Ph.D. Thesis, Vol. 1, p. 195, University of Niš, Faculty of Mechanical Engineering, 2016.
- [13] Radoičić, G. and Jovanović, M., Experimental identification of overall structural damping of system, Strojniški vestnik – Journal of Mechanical Engineering, , Vol. 59, No. 4, pp. 260-268, 2013.
- [14] Marinković, D., Milić, P. and Marinković, Z.: The Idea of Combined Linear – Geometrically Nonlinear FEM Modeling with Application on a Tower Crane, The XI International Conference SAUM 2012, Faculty of Electronics, Faculty of Mechanical Engineering, University of Niš, 2012. ISSN 978-86-6125-072-9, pp. 282-285, 2012.
- [15] Mijajlović, R., Jovanović, M. and Domazet, D.: Beitrag zur erforschung der geometrie eines doppeltenker systems und ihres einflusses auf den widerstandsverlauf im wippwerk, Conference Proceedings, 7. International Tagung für Fördertechnik, Dresden, 1984.

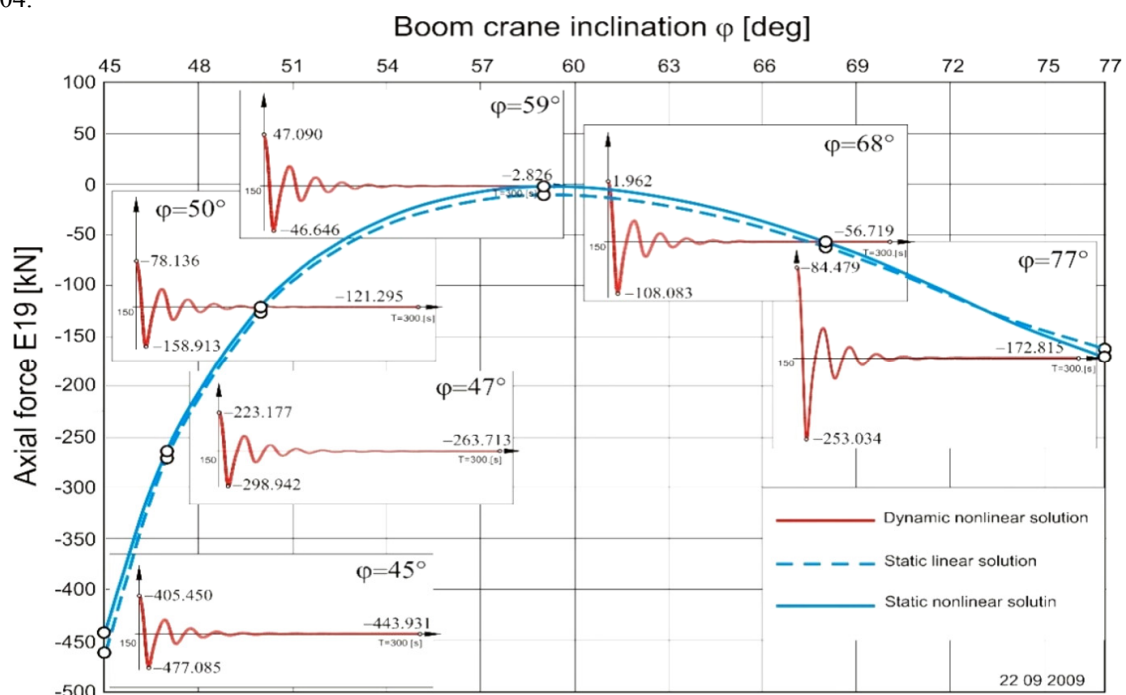


Figure 4. Comparative static and dynamic forces in a member to change the reach of cranes at different ranges (level). Dynamic curves (six smaller individual curves) are caused by a load deflection angle of $\pm 3^\circ$.

Amplitude inspection of the large crawler crane without the marker of turning center

Wu Fengqi

Professor Senior Engineer
Shanghai Institute of Special Equipment
Inspection & Technical Research,
Shanghai, China

Xu Haixiang

Senior Engineer
Shanghai Institute of Special Equipment
Inspection & Technical Research,
Shanghai, China

Tang Xiaoying

Associate Dean
Shanghai Institute of Special Equipment
Inspection & Technical Research,
Shanghai, China

Liu Enpin

Senior Engineer
Shanghai Institute of Special Equipment
Inspection & Technical Research,
Shanghai, China

According to the requirement of monitoring and management system for large lifting machinery in the national safety inspection regulations, safety monitoring and management system should be installed for crawler crane with a capacity of exceeding 100 tons. There is an inspection requirement for the amplitude accuracy of the crawler crane. It requires that the sensors should be tested accurately during operation and within the allowable range of the operation instructions. However, it is difficult to measure the amplitude without the marker of turning center on the spot. as the crawler crane has been assembled, the revolving center is covered by the end cover, etc. Therefore, it is necessary to consider other ways to test the relevant parameters. In this paper the method is resorted to the technical and precision advantages of the Total Station, so as to obtain the key amplitude plane and turning center level. The amplitude is calculated by MATLAB programming, and more accurate measurement values are obtained. This method is universal in use, which can thoroughly solve the problem that the amplitude of large equipment cannot be accurately detected, and the accuracy is relatively high.

Keywords: Slewing Cranes, Safety Monitoring and Management system, Amplitude inspection

1. INTRODUCTION

In recent years, along with the continue expansion of domestic construction scale, the demand of large crane is increasing. As an indispensable equipment for loading and unloading in construction works, crawler crane plays an important role in infrastructure construction and social development. However, crane accidents have brought many negative effects because of their frequent occurrence. So, crane safety work becomes one more noticeable problem. Additionally, the national special equipment safety supervision bureau also in the book of the supervision and inspection of hoisting machinery regulations proposes it should be equipped with safety monitoring devices for some large crane, such as, the crawler crane hoisting weight exceeding 200t should be installed safety monitoring device.

2. PRINCIPLE OF VARIABLE AMPLITUDE MONITORING SYSTEM

Crawler crane is a special operation equipment used in large-scale construction and industrial control occasions. It is not only necessary to accurately realize the functional action required by the system, but also an important prerequisite to ensure the safety of people and equipment. Therefore, its safety and reliability are the premise of all functions. Only under the premise of ensuring safety, can functional design be carried out. Therefore, the crane luffing monitoring system is an important part of the crane control system.

Correspondence to: Dr Wu Fengqi, Prof. Senior Engineer
Shanghai Institute of Special Equipment Inspection &
Technical Research Room 1001, No. 915 Jinshajiang Road,
Putuo District, Shanghai, 200062, China
E-mail: wufq@ssei.cn

It mainly monitors the amplitude change system in real time, transforms and analyses the necessary data, and then displays them on the monitoring equipment. At the same time, there are faults which need real-time alarm output. Under the premise of perfect system communication, the ability to solve some faults remotely is realized.

The realization steps of the variable amplitude monitoring system are as follows:

(1) Sensor signal acquisition

This part mainly collects all kinds of signals through sensors. The signal of angle sensor is analog signal, and the signal of height limit switch is switching signal.

Angle sensor (mounted on the bottom arm) - Real-time measurement of the working angle of the boom.

Height Limit Switch - Real-time limit the maximum lifting height of heavy objects.

(2) Data processing and calculation

The measured signal is input to the PLC controller. The PLC controller calculates the real-time load and moment percentage of the crane according to the data collected by the sensor, the parameters required for the crane's amplitude change are preset by the system, the crane's working principle and moment calculation formula, and stores the calculated data.

(3) State display alarm

The alarm and parameter setting of status display are realized by display and buzzer. The parameters of crane, such as structure, working condition, alarm and so on, are set by human-computer interaction interface on the touch screen display. In order to be easy to understand, these parameters are displayed graphically. The buzzer is mainly used to realize sound and light alarm under different working conditions.

(4) Output safety protection control signal

The actual load is compared with the rated load, and the percentage of comparison is divided into four sections. Different color icons are shown on the display of different sections, which is divided into four states: normal operation, yellow warning, orange warning and cut-off dangerous action.

(5) System Communication

The system communication between the controller, PC and other serial devices is realized by RS232. The field bus communication between Profibus devices is realized by Profibus bus.

The purpose of inspecting the amplitude monitoring system is to verify whether the system's indication and accuracy of the amplitude are correct and meet the requirements of the national hoisting machinery regulations.

3. THE CHARACTERISTICS AND MEASURING PROCESS OF LEICA TPS1200

After doing some reference research on the domestic and foreign existing crane safety protection monitoring devices, based on current inspection method of crane safety monitoring system stability, reliability and precision and system function of the shortage, this paper puts forward an amplitude inspection method based on Leica TPS1200 Total Station system.

At present, in the process of crane debugging and testing, manual tape is often used to measure the amplitude, which requires visual measurement of the corresponding position and reading data, so that the measurement accuracy is poor and the efficiency is low. moreover, visual measurement of the corresponding position by manual tape requires that when the crane is debugging the lifting weight, people work under the boom, which has a great potential safety hazard. In order to accurately measure the amplitude, improve the efficiency. and eliminate potential safety hazards, Leica TPS1200 Total Station system can be used to accurately measure the crane's amplitude with an accuracy of $2\text{ mm} + 2\text{ ppm}$ [1].

3.1 Characteristics of TPs 1200

The TPS1200's precision angle-measurement system operates continuously to provide instant horizontal and vertical circle readings that automatically corrects for any "out of level" by a centrally located twin-axis compensator. Leica TPS1200 instruments is shown in the Figure 1.



Figure 1. Leica TPS1200 instruments

Distance Measurement (aver. atmos. condit.)
Range Round prism (GPR1): 3000 m

Range 360° reflector (GRZ4): 1500 m
Range Mini prism (GMP101): 1200 m
Shortest measurable distance: 1.5 m
Accuracy (standard deviation, ISO 17123-4):
Standard mode: $2\text{ mm} + 2\text{ ppm}$
Measurement Time: $\sim 1.5\text{ s}$
Display resolution: 0.1 mm
Method: Phase measurement (coaxial, invisible infrared laser)

3.2 Measurement and calculation methods

(1) Obtaining geometric dimension data of side steel structure based on instructions.

The crawler crane is tested for amplitude is shown in the Figure 2. First, we should read the instructions of the crawler crane, each crawler crane should have the operating manual, geometric dimension data of side steel structure can be obtained from the technical description pages of instructions. The dimension data is shown in the Figure 3.



Figure 2. The crawler crane

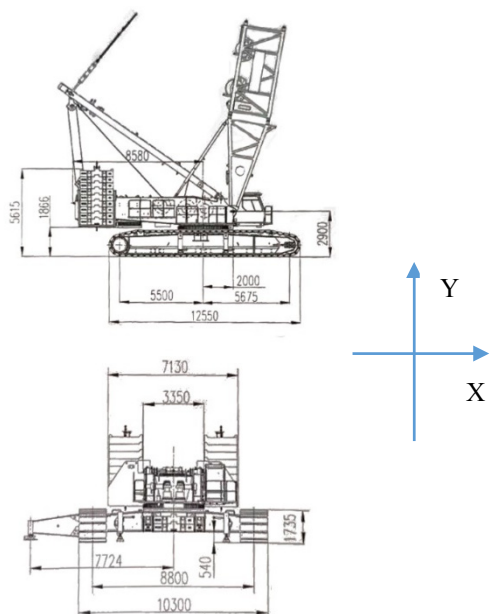


Figure 3. Geometric dimension data of side steel structure of the crawler crane

(2) Determining the measuring points of ①, ②, ③, ④

The geometric dimension data of the crawler crane are known. We can determine the middle point ① of the

steel structure of the crawler traveling mechanism. This point has the same X coordinate value as the revolving center of crawler crane, which is the key point and shown in the Figure 4, then we can find a point ③ of Plane of steel structure, which is in the vertical direction of ①. Ensuring the plane composed of the line of ① and ③ points and the revolving center of crawler crane is consistent with the normal plane of the side of tracked steel structure. the points of ② and ④ are arbitrarily decided side plane of steel structure, which is to determine and verify the lateral plane of this steel structure.

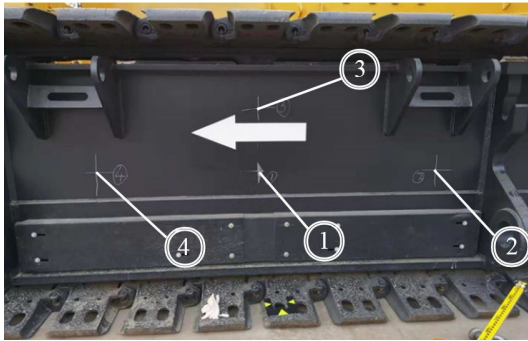


Figure 4. Determining the measuring points of the crawler crane

(3) Gauging data of points ①, ②, ③, ④ & Lifting point with Total Station.

Gauging data of points ①, ②, ③, ④ (This point is a reserve checkpoint, which is the same function of ②) is obtained with Leica TPS1200 Total Station. The measurement process is as follows:

It is very important to level the instrument after installing it. If the Total Station is not leveled correctly, measurements will not be continued. The bubble level above the keyboard can be used to make the major adjustment, which is realized by using the thumbscrews on the tribrach to locate the bubble in the center. The fine adjust must be done using the Total Station. First, press the SHIFT key. After pressing SHIFT arrow in the lower right portion of the display which should be solid. Then press <F12>, which will display the Level & Laser Plummet screen.

Use the thumbscrews to locate the bubble as precisely in the center as possible.

After leveling the instrument the various settings related to the acquisition of targets should be checked.

Select the Config menu from the main menu.

Scroll down to General Settings (or press the number key 3). Press <ENTER>.

Scroll down to Units & Formats (or press the number key 3). Press <ENTER>. The default options for Units & Settings will display.

Next, check the EDM (Electronic Distance Measuring Device) and ATR (Automatic Target Recognition) configuration options and adjust them if necessary.

Select the Config menu from the main menu.

Press <ENTER>.

The first option EDM & ATR Settings should be selected, if not then use the scroll keys to select it (or press the number 1 on the numeric keypad).

Check the other settings including EDM Mode, Automation and ATR Settings to make sure they match the screenshot shown at right. The default settings are shown, adjust as needed.

The initial Survey screen shows the current telescope position. We will need to point the telescope at the prism we wish to measure. Use the crosshair spotting tool at the top of the telescope to more precisely locate the prism or view the prism through the telescope itself. Align the crosshairs of the telescope with the center of the target. It does not have to be an exact alignment because the ATR of the instrument will locate the prism precisely once it's engaged. Use the knobs on each side for fine horizontal and vertical adjustments.

Note the DIST button at the bottom of the display. Use the stylus to select this button or press <F2> to engage the ATR and actively locate and measure the target prism position.

Auto will utilize the ATR system to automatically locate the Target within the search window defined previously, measure the distance using the EDM system and update the Hz, V and distance values.

If the ATR is unable to locate the reference you will need to sight the telescope more precisely and press <F2> again. If unsuccessful after a few attempts then check section 4 for troubleshooting help.

Record the Hz and V values for entry in the MultiLogger Configure Total Station Targets form. The Horiz Dist measurement value can also be recorded but it is not used for configuring the automation.

As a new technology in the field of Surveying and mapping, Prism-free surveying technology is applied to production, and its accuracy is the most concerned problem. For this reason, we collect two sets of data in IR state with infrared light and prism ranging and RL state (no prism measurement) where the field of vision is wide and the reflective medium is good. Because the measured distance is not more than 500 m, the meteorological correction, multiplication constant correction, tilt correction and projection correction of oblique distance are all very small, and their effects can be neglected.

Measure points are used by the Prism-free measurement technology of Total Station. The measuring points coordinate values are shown :

A=[14.0748, 36.4558, 5.2339] of point ①;

B=[14.0740, 36.4562, 5.6192] of point ③;

C=[13.4379, 37.4143, 5.2236] of point ②;

The equation of plane A,B,C is as follows:

$$Ex + Fy + Gz + H = 0 \quad (1)$$

Then the normal vector of the plane is $\overrightarrow{(E, F, G)}$, which could be solved by the determinant equation,

$$\begin{vmatrix} i & j & k \\ (A-B)_x & (A-B)_y & (A-B)_z \\ (C-B)_x & (C-B)_y & (C-B)_z \end{vmatrix} = 0 \quad (2)$$

Then the coefficients of i,j,k are corresponds to E,F,G respectively, and H can also be obtained by introducing the coordinate value of point A into the equation of plane ABC.

(4) From the content of spatial analytic geometry, we know that the determinant of D equals zero, which is a plane equation [2], $D = [\text{ones}(4,1), [x,y,z]; A; B; C]$. The basic principles are as follows:

If three points p_1, p_2, p_3 are known, the plane equation is obtained, $p_1 = [x_1, y_1, z_1]$; $p_2 = [x_2, y_2, z_2]$; $p_3 = [x_3, y_3, z_3]$; then the following matrix Q determinants are solved: $q = [\text{ones}(4, 1), [x, y, z]; p_1; p_2; p_3]$; $\text{DET}B = \det(q)$; finally, $q = 0$.

The solution here is the determinant of the fourth-order matrix, which can be solved from the determinant of the third-order matrix. That is the conventional solution method: the system of equations is written as $[p_1; p_2; p_3] = D$, where $D = [d, d, d]$ represents the constant term of the plane equation, and first the determinant of $q = [p_1; p_2; p_3]$ is obtained, then the determinant of the third-order matrix composed of D and three coordinates is set as q_1, q_2, q_3 respectively. The four parameters of the plane equation are $A = q_1/q$; $B = q_2/q$; $C = q_3/q$; $D = d$; and the result multiplied by q/d is essentially the determinant solution of the fourth-order matrix above.

(5) Creating a symbolic matrix

$\text{dett} = \det(D)$; which returns the determinant of square matrix D.

(6) Getting the coefficients of geometric equation

$G = \text{coeffs}(\text{dett})$; which returns a structure containing the coefficients of the discrete-normal vector in the Side Plane of Steel Structures.

(7) Coefficient assignment

$a = G(4)$; $b = G(3)$; $c = G(2)$; $d = G(1)$;

$\text{vpa}(a)$; $\text{vpa}(b)$; $\text{vpa}(c)$; $\text{vpa}(d)$;

The basic effect of VPA function is as follows:

$\text{vpa}(x)$ uses variable-precision floating-point arithmetic (VPA) to evaluate each element of the symbolic input x to at least d significant digits, where d is the value of the digits function. The default value of digits is 32.

Assignment of Lifting point is measured by Leica TPS1200 Total Station. The coordinates of the hoisting point are as follows:

$p(1) = 38.3101$; $p(2) = 8.1980$; $p(3) = 30.0578$;

(8) Solving the Normal Vector of a Plane Passing Points of ① & ③

$a1 = [(A(1)-B(1)) (A(2)-B(2)) (A(3)-B(3))]$; which is the vertical vector in the Side Plane of Steel Structures.

$b1 = [a \ b \ c]$, which is the normal vector in the Side Plane of Steel Structures.

$c1 = \text{cross}(a1, b1)$; which returns the cross product of $a1$ and $b1$.

$a1$ and $b1$ are matrices or multidimensional arrays, then they must have the same size. In this case, the cross function treats $a1$ and $b1$ as collections of three-element vectors. The function calculates the cross product of corresponding vectors along the first array dimension whose size equals 3.

(9) Solving the amplitude from point to plane by Point of ① & the Normal Vector.

$La = \text{abs}(u \times (A(1)-p(1)) + v \times (A(2)-p(2)) + w \times (A(3)-p(3))) / \sqrt{u^2 + v^2 + w^2}$

Where, $u = c1(1)$; $v = c1(2)$; $w = c1(3)$. (3)

Distance calculation from hanging point to normal plane, the amplitude is 36.9983m.

4. SYSTEM VALIDATION

Let's change the point of ② to the reserve checkpoint of ④, the amplitude is 36.9919m. The error is 6.4 mm, which is acceptable, because the error is the result of system measurement and calculation.

Considering the sag and measurement error of tape in long distance, it can be considered that tape can be replaced within the allowable range of error, and the accuracy is higher than that of tape. Installation of test equipment depends on tooling, and special tooling for installation of test equipment is developed independently, which greatly saves installation time.

5. CONCLUSION

Aiming at the problem of measuring range in the debugging test of crawler crane, this paper completes the measurement of crane amplitude by means of Total Station measuring system. This method has the advantages of high measuring efficiency and high accuracy in practical application, eliminating the hidden safety hazards of manual tape measurement, and achieves the expected effect. Prism-free measurement technology has many advantages, but it is not omnipotent. Especially for harsh observation conditions in the field, the instrument can not change it, nor can it fully adapt to the conditions in the field. Therefore, operators should fully understand the characteristics of this new technology, take necessary measures to enhance their strengths and avoid weaknesses, in order to better play to the advantages of its advanced technology and equipment, and achieve good observation results. Through surveying and mapping practice, we put forward the following two suggestions for improvement:

(1) In view of the fact that Prism-free measurement is limited by obstacles and easy to cause errors in object surveying, it is suggested that the reflective function of Prism-free ranging range should be enhanced on equipment, and the visual estimation ability of surveyors should be fully utilized. If the object at 500m is to be measured and the range of ranging is set, the refractive object at 300m will not be mismeasured. When the object within 400-500m is to be surveyed, the best place for the line of sight to leave the obstacle is more than 1.5m in the range of 400-500m.

(2) In order to avoid eye damage caused by laser radiation in measurement operation, the author suggests that the instrument manufacturer add a high-power visible light "quasi-star" system.

ACKNOWLEDGMENT

This work is supported by the National Key R&D Program of P.R.C (Research on Typical Fault Prediction Technology of Mechatronic Special Equipment Based on Multi-source Data Analysis).

REFERENCES

- [1] TPS1200 Total Station User's Guide.
- [2] <https://www.mathworks.com/help/matlab/index.html>

Tao Jiang

Senior Engineer
Shanghai Special Equipment Supervision
and Inspection Technological Research
Institute

Zeyu Duan

Masters Candidate
School of Mechanical Engineering
Tongji University

Hailei Ruan

Senior Engineer
Shanghai Special Equipment Supervision
and Inspection Technological Research
Institute

Guangjun Liu

Professor
School of Mechanical Engineering
Tongji University

Study on an elevator emergency disposal and public service platform

Shanghai is an emerging financial center in Asia with skyscrapers throughout the city. With the rapid development, internet technology has been widely used in the field of public services in Shanghai, which is a technology-innovative city. This paper proposes a new elevator emergency disposal and public service platform for the area of elevator rescue public services. The main functions of the elevator emergency disposal and public service platform include equipment information management, personal information management, alarm failure event information reporting and disposal, statistical information analysis, reminder information release, and information reporting. Also, it can set the priority, preferentially forward the alarm, trapped signals, and voice signals. The main functions of the elevator emergency disposal and public service platform can efficiently analyze emergencies and link rescue companies and federal rescue agencies.

Keywords: Public service platform, Elevator accident, Mechanical and electrical safety, Smartlift, People trapped

1. INTRODUCTION

The number of skyscrapers may be one of the barometers in showing the economic power of the country. Such powerful nations continue to build high-rise buildings with various facilities for comfort and safety, based on advanced technologies[1]. As transportation means in such structures are mainly elevators, the strict "Safety Standards" for them are provided. It is because the bins in the high-rise buildings have high potential energy enough to take away the lives of elevator-passengers. Shanghai is an emerging financial center in Asia with skyscrapers throughout the city. With rapid development, internet technology has been widely used in the field of public services in Shanghai, which is a technology-innovative city. This paper proposes a new elevator emergency disposal and public service platform for the area of elevator rescue public services.

The main functions of the elevator emergency disposal and public service platform include equipment information management, personal information management, alarm failure event information reporting and disposal, statistical information analysis, reminder information release, and information reporting. Also, it can set the priority, preferentially forward the alarm, trapped signals, and voice signals. The emergency disposal process of the service platform is to immediately start an emergency response after receiving the emergency disposal information, launch an emergency rescue, and relieve the passengers within the prescribed rescue time. If it does not respond in time, the elevator

emergency response public service platform will notify the elevator emergency rescue enterprise to dispose of it, and decide whether the federal rescue agency needs to be linked according to the situation. After the disposal, the disposal situation will be put into the elevator emergency disposal public service platform in time.

2. ELEVATOR EMERGENCY DISPOSAL AND PUBLIC SERVICE PLATFORM SOFTWARE SYSTEM

The construction of Shanghai elevator emergency disposal and public service platform can meet the requirements of Shanghai elevator safety supervision and the five-year elevator market incremental development. The platform is easy to operate, stable, secure, maintainable, scalable, open, and advanced[2]. Elevator emergency disposal and public service platform is a specific method of using information technology to improve the effectiveness of safety supervision. It is also an important platform to ensure the safe operation of elevators and implement safety publicize.

2.1 The functions of the elevator emergency disposal and public service platform

The elevator emergency disposal and public service platform have the following functions:

a) Supervision function

The platform has a monitoring function for emergencies, and can timely understand and trace the incident handling process through the enterprise platform, and can timely understand the situation on the spot through mobile Internet, mobile communication and other technical means. At the same time, it has the supervision function of the emergency rescue responsibility of the maintenance enterprise, and can automatically collect the data of the enterprise platform

Correspondence to: Dr Guangjun Liu, Professor
School of Mechanical Engineering
Tongji University, 1239 Siping Rd., Shanghai 200092, China
E-mail: gjliu@126.com

through the interface to timely understand the disposal situation. And it is connected with public platforms such as the municipal government, fire protection, public security, etc., and traces the complaints and reports.

b) Emergency treatment function

The platform has the functions of monitoring and emergency dispatching for emergencies such as elevators. It has the functions of dispatching, monitoring, and disposing of the elevator maintenance unit and emergency rescue unit of this city. For the emergency disposal personnel, it has a dynamic tracking function and has an image real-time acquisition and transmission function for the emergency disposal site. It has real-time calling and video functions for public rescue agencies.

c) Public service function

The platform provides the public with basic elevator information inquiry through an app, WeChat, etc., including manufacturer information, maintenance enterprise information, inspection organization information, and inspection results. At the same time, it provides elevator safety and passenger knowledge and basic knowledge of elevator safety policies and regulations.

d) Statistics and warning functions

When an accident occurs, the platform can have a statistical analysis of the elevator trapped incident, and statistical analysis of the specified elevator fault, event, alarm, operation, and complaint suggestion information. At the same time, the platform can capture, track, and analyze the elevator accidents and events (including public opinion reports), and analyze the statistical data for big data, and provide early warning information and auxiliary decision-making.

e) Platform display function

The platform has geographic information display, regional maintenance unit communication, and display, public service display, emergency treatment process display (equipment basic information, emergency disposal scene video display, emergency disposal personnel online display, disposal status display, emergency process retrieval, and Playback display) function.

2.2 Platform system composition

The elevator emergency disposal and public service platform mainly include the following subsystems: dynamic information management, emergency command system, call center system, electronic map system, analysis, and early warning system, public service system (APP, WeChat, SMS, etc.), emergency rescue mobile terminal.

a) Dynamic information management

The platform obtain all kinds of information of the elevator from the elevator safety monitoring platform (national, city, district level 3), inspection platform (the agency responsible for elevator inspection in this city), including the necessary information of the elevator

(manufacturer, brand, date of manufacture, technical parameters, etc.), status information (test validity period, overhaul, renovation, update, etc.), use unit information, maintenance unit information, inspection unit information, monitoring status information, etc.

b) Emergency treatment system

According to the telephone call or the Internet of Things, the automatic alarm, the system can complete the acceptance, command, and coordination according to the provisions of the emergency disposal process. And send the information data to be disposed of to the user unit, elevator maintenance unit (emergency disposal service platform) through the information exchange platform, Elevator emergency rescue enterprises, public rescue agencies, etc., provide fast and timely emergency response information services for elevator emergencies. The system's workflow chart is shown in Figure 1.

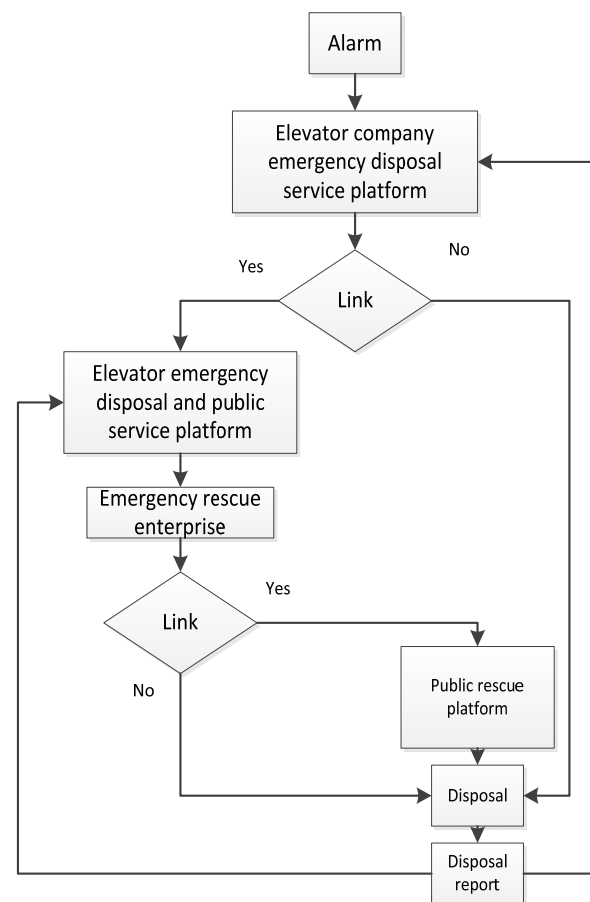


Figure 1. The platform system's workflow chart

c) Electronic map system

Using GIS technology, establish a geographic information system for Shanghai elevator emergency disposal and public service platform, and use a variety of essential GIS geographic information services to combine interfaces and functions in an emergency response system to integrate geographic information systems. With positioning, query, mark, zoom, move, ranging, and other features [3].

The cooperation between the systems of the elevator emergency disposal and public service platform forms an overall operation and improves the safety and reliability of the platform.

3. ELEVATOR EMERGENCY DISPOSAL AND PUBLIC SERVICE PLATFORM HARDWARE SYSTEM

The hardware system of the elevator emergency disposal and public service platform is composed of a call system, an extensive screen display system, a computer network system, an integrated wiring system, an uninterruptible power supply system, a lightning protection grounding system, and an access control system. Computer network systems, integrated wiring systems, and uninterruptible power systems should provide good line and power protection for call systems and large-screen display systems. At the same time, the hardware system can meet the corresponding protection requirements, such as stable operation and anti-interference.

3.1 Call system

The call system should include at least a core access platform system, a computer voice integration system, a synchronous recording system, an automatic voice navigation server, and a seat telephone. The calling system should have at least the following features:

a) The automated call distribution function shall support the display of the calling and called numbers, the location of the call-in-call number, and the retrieval of the number data;

b) The computer telephony integration function should support intelligent answering (incoming call, automatic voice answering), multi-party calling, softphone, caller information pop-up, synchronous full-call recording, outbound call, etc., and can provide network telephone interface;

c) The automatic voice navigation function should support personalized voice navigation, electronic telephone transfer, and customized voice flow;

d) The synchronous recording function should support the full recording and can make online inquiry according to the caller's caller number, outgoing number, incoming call time, agent number, extension number, etc.; the call record is kept for at least one year.

e) The report customization function should support the daily work report of the customer service (online time, break time, busy time, etc.), traffic data report (call record, call duration, peak point, post-processing time, connection rate, etc.), Customization of business processing reports (elevator disposal records, business summary reports, etc.).

3.2 A large screen display system

The emergency response agency shall establish a large-screen display system to coordinate elevator emergency rescue. The large-screen display system should at least include a display unit splicing wall, a multi-screen processor system, a matrix switcher, and a video matrix switcher[4].

The large screen display system should have at least the following features:

a) The information receiving function shall support the receiving of graphic and video information displayed

by the network computer and support information conversion;

b) The information display function should support resolutions above 1920*1080;

c) The preview and switching function should realize at least eight channels of video signals and one channel of computer RGB signals in the real-time display by window opening, which should be scaled, moved, and superimposed.

3.3 Electrical line system

The electrical line system consists of a computer network system, an integrated wiring system, and an uninterruptible power supply system. Ensure the overall operation of the system.

a) Computer network system

The computer network system undertakes information access and output of methods such as call systems, large-screen display systems, and elevator Internet of Things. The system includes switches, routers, servers, storage, hardware firewalls, and carrier lines. The various devices in the computer network system can ensure the overall stable operation of the system.

b) Integrated wiring system

The integrated wiring system can realize the application requirements of voice, data, and video, and can provide connection channels for computer networks, large-screen display systems, call systems, voice calls, and the like. The system includes at least the following five subsystems:

(1) Workspace subsystem: consists of the connection of the terminal equipment to the information outlet, which shall consist of the assembly cord, the connector and the extension cord required for the link, and the connection between the terminal equipment and the I/O;

(2) Horizontal subsystem: implements the relationship between the information outlet and the management subsystem (distribution frame). Twisted pair should be used for the output point of voice and data;

(3) Backbone subsystem: A connection between computer equipment, switches, and management subsystems. It is advisable to use large logarithmic cables, optical fibers, etc.

(4) Management area subsystem: realize wiring management, use tracking and jumper operation by using color coding;

(5) Inter-device subsystem: Provides the hardware environment and interface between the backbone and the network. There are a large number of hardware devices in the subsystem, and a large number of communication trunks are concentrated.

c) The uninterruptible power supply system

The uninterruptible power system consists of a host, battery, battery box, and battery pack connection cable. The uninterruptible power supply system shall provide the power supply with reliable operation of the equipment, eliminate the power pollution caused by power failure and voltage fluctuation, protect the weak electrical equipment, prevent the loss of essential data,

and ensure the reliable operation of the material under power failure.

3.4 Equipment information collection and transmission system

The hardware system of the elevator emergency disposal public service platform is connected, and the software system is organically combined to form a complete elevator emergency disposal public service platform. The equipment information collection and transmission system architecture are shown in figure 2.

4. CONCLUSION

Elevator safety is an integral part of public safety. Establishing an elevator emergency service rescue system is an important way to ensure the safe use of elevators and an important measure to improve the elevator emergency service disposal capacity. The public service platform for elevator emergency response proposed in this paper is a specific method to improve the efficiency of safety supervision by using information technology, and it is also an important platform to ensure the safe operation of elevators and implement safety publicity. The platform organically combines software and hardware systems, integrates the cooperative relationship between public rescue agencies and

enterprise rescue agencies, and will effectively improve elevator safety.

ACKNOWLEDGMENT

The authors would like to acknowledge the support of the Fundamental Research Funds for the Central Universities.

REFERENCES

- [1] Lim, H.S., Krishnan, R. and Lobo N.S.: Design and control of a linear propulsion system for an elevator using linear switched reluctance motor drives, IEEE Transactions on Industrial Electronics, Vol. 55, No. 2, pp. 534-542, 2008.
- [2] Liang, Z.: Construction of Provincial Elevator Emergency Rescue and Disposal Service System, Computer Knowledge and Technology, Vol. 14, No. 19, pp. 257-258, 2018.
- [3] Han, S., Ma, S., Li, Z., Li, W., Liu, S. and Yuan, J.: Research on city elevator emergency rescue system and mechanism, Journal of Safety Science and Technology, Vol. 9, No. 2, pp. 145-150, 2013.
- [4] Kong, W.: Analysis of Countermeasures and Suggestions of Improving the Capacity of the Elevator Safety Regulation, Quality and Technical Supervision Research, Vol. 5, pp. 56-60, 2014.

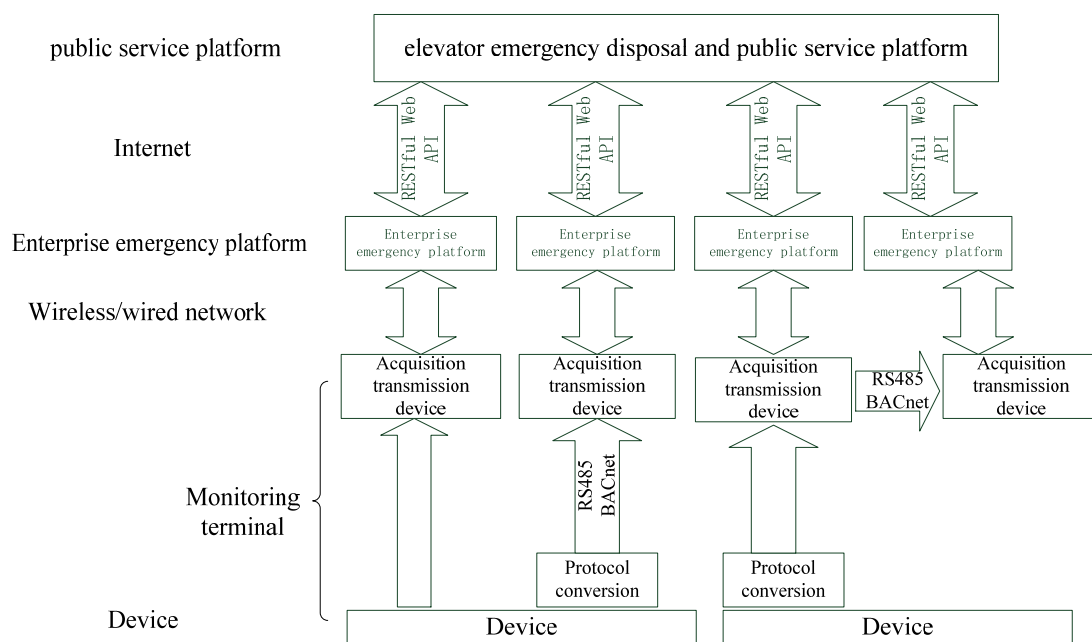


Figure 2. Equipment information collection and transmission system architecture

Goran PavlovićResearch Associate
R&D Centre Alfatec Ltd**Mile Savković**Professor
University of Kragujevac
Faculty of Mechanical and Civil Engineering
in Kraljevo**Nebojša Zdravković**Assistant Professor
University of Kragujevac
Faculty of Mechanical and Civil Engineering
in Kraljevo**Goran Marković**Assistant Professor
University of Kragujevac
Faculty of Mechanical and Civil Engineering
in Kraljevo**Milomir Gašić**Professor
University of Kragujevac
Faculty of Mechanical and Civil Engineering
in Kraljevo

Optimization of crane hooks considered as curved beams with different cross-sections – a comparative study using MATLAB

This paper presents the analysis and the optimization of the geometric parameters of different crane hook cross-section types. The study included trapezoidal, rectangular, square, elliptic, circular and T cross-section. The reduction of hook critical cross-section area was set as the primary goal for the optimization process. The criterion of maximum permissible stress is set as the constraint function, while the maximum stress values at the characteristic points were calculated according to Winkler-Bach theory, considering the hook as a curved beam. The optimization procedure was conducted using some metaheuristic optimization methods, in conjunction with known MATLAB functions. The goal of this research was to determine the optimum geometric parameters of mentioned cross-section types and to compare them in order to gain some conclusions and choice recommendations.

Keywords: Crane Hook, Optimization, Metaheuristic algorithms, MATLAB, Winkler-Bach theory

1. INTRODUCTION

Crane hooks are the means for lifting the heavy loads and are an integral part of different types of hoists. By proper use of the hoisting equipment, heavy loads can be effectively manipulated, while reducing manual handling operations. On the other side, the use of hoisting equipment and hooks with inadequate geometry and characteristics can lead to malfunctions and heavy accidents. Therefore, the proper choice and usage of this equipment is of great importance.

In this research, obtained optimization results were compared to standard crane hooks according to [1]. The reduction of hook critical cross-section area was set as the primary goal for the optimization process.

Stress and strain analysis of a crane hook and the optimization of its cross-sections were the subject of research of numerous authors, so there are many published papers on this issue [2-12]. The most frequently used approach for such analysis and optimization was finite element method (FEM) [2-9]. Rectangular, trapezoidal, triangular and circular cross-sections were analysed in ANSYS software in [2]. Similarly to previous, rectangular, trapezoidal and circular shapes were analysed in [3], using the same software and for the different payload. Recently, T-section has frequently been included in the analysis. For example, [4] showed the advantage of that cross-section type over circular and trapezoidal type, with various materials used. Similar to this research, the author in [5]

presented how maximum stress values are changed in different types of cross-sections while maintaining the same cross-sectional area. Besides stress and strain, the fatigue is frequently used for analysis and optimization of such structure types, as presented in [6, 7]. Also, many authors combined FEM analysis and various numerical optimization procedures [8, 9]. In [8], genetic algorithm (GA) was used to optimize geometric parameters of trapezoidal cross-section, and the verification was done in ANSYS package. Particle Swarm Optimization (PSO) method was used to obtain an optimum shape of a crane hook through a multi-criteria optimization process in [9]. The same method was applied in [10], determining optimum T-section geometric parameters. In [11, 12], the optimization of crane hook cross-sections was done by the analytical approach and some optimization algorithms. Optimized values of cross-sectional areas for trapezoidal, circular, rectangular, triangular, T and I shape were compared in [11], where the authors presented optimization algorithm in detail. Comparative analysis and optimization of various types of cross-sections were conducted in [12], where, besides common types, parabolic and elliptic type were additionally considered. Lagrange multiplier and GRG2 algorithm were used as optimization methods.

The publications mentioned above indicate the significance and justification of the analysis and optimization of these structures. Hence, the goal of this research was to determine the optimum geometric parameters of mentioned cross-section types and to compare them in order to choice recommendations.

2. OPTIMIZATION PROBLEM

Static analysis of the crane hook critical cross-section was conducted (Fig. 1). The criterion of

Correspondence to: Dr Goran Pavlović, Research Associate
R&D Centre Alfatec Ltd,
Bulevar Nikole Tesle 63/5, 18000 Niš, Serbia
E-mail: goran.pavlovic@alfatec.rs

maximum permissible stress is set as the constraint function, while the maximum stress values at the characteristic points were calculated according to Winkler-Bach theory, considering the hook as a curved beam, [13]. Also, some geometric constraints were taken into account.

The crane hooks within payload range between 5 and 16 tonnes were considered. The study included T (Fig. 2), trapezoidal (Fig. 3), rectangular, square, elliptic (Fig. 4) and circular cross-section. The rectangular and square sections were considered as special cases of trapezoidal shape, while the circular section was considered a special case of elliptic shape.

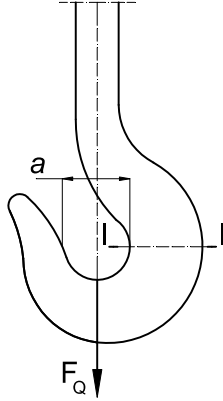


Figure 1. Crane hook

The optimization is based upon stress criterion, according to Winkler-Bach theory, for cross-section characteristic points 1 and 2, (1):

$$\sigma_{1,2} = \frac{F_Q}{A} \pm \frac{M_{\max}}{S_x} \cdot \frac{h_1}{R_1} \leq \sigma_d \quad (1)$$

The permissible stress is taken within the interval $\sigma_d = 8 - 10 \text{ kN/cm}^2$, for the case of stress check in a model where the hook curvature is not considered. Since the curvature of the hook makes the equivalent stress increase for 20 – 30 %, the permissible stress will also be increased by 20 % in further analysis (adopted value is $\sigma_d = 9,6 \text{ kN/cm}^2$).

The parameters which figure in (1) are calculated in (2-6).

In all cases it is $R_1 = a/2$, $F_Q = Q \cdot g$, $M_{\max} = F_Q \cdot R_c$, $S_x = A \cdot y_o$.

$$r = \frac{A}{\int_A \frac{dA}{\rho}} \quad (2)$$

$$h_1 = r - R_1 \quad (3)$$

$$h_2 = R_2 - r \quad (4)$$

$$R_c = R_1 + e_1 \quad (5)$$

$$y_o = R_c - r \quad (6)$$

All necessary relations for calculation of geometric properties for each cross-section type are presented in the following text.

2.1 T cross-section geometric properties

Fig. 2 shows T cross-section with all necessary geometric parameters.

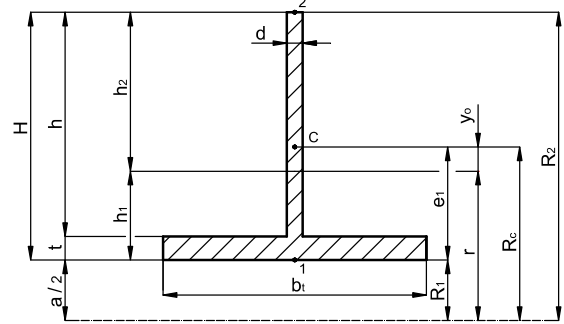


Figure 2. T cross-section

$$A = b_1 \cdot t + h \cdot d \quad (7)$$

$$r = b_1 \cdot \ln \frac{a + 2 \cdot t}{a} + d \cdot \ln \frac{a + 2 \cdot H}{a + 2 \cdot t} \quad (8)$$

$$e_1 = \frac{b_1 \cdot t^2 + 2 \cdot h \cdot d \cdot t + h \cdot d^2}{2 \cdot A} \quad (9)$$

2.2 Trapezoidal cross-section geometric properties

Fig. 3 shows trapezoidal cross-section with all necessary geometric parameters.

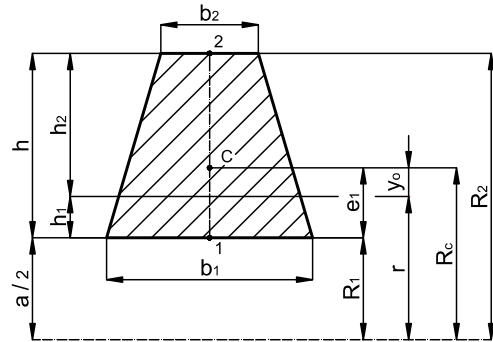


Figure 3. Trapezoidal cross-section

$$A = (b_1 + b_2) \cdot h / 2 \quad (10)$$

$$r = \frac{A}{\left(b_2 + R_2 \frac{b_1 - b_2}{h_1} \right) \cdot \ln \frac{R_2}{R_1} - (b_1 - b_2)} \quad (11)$$

$$e_1 = \frac{h}{3} \cdot \frac{b_1 + 2 \cdot b_2}{b_1 + b_2} \quad (12)$$

The rectangular cross-section is a special case of trapezoidal section, where $b_1=b_2=b$. Square cross-section is a special case of rectangular section, where $b=h$.

2.3 Elliptic cross-section geometric properties

Fig. 4 shows elliptic cross-section with all necessary geometric parameters.

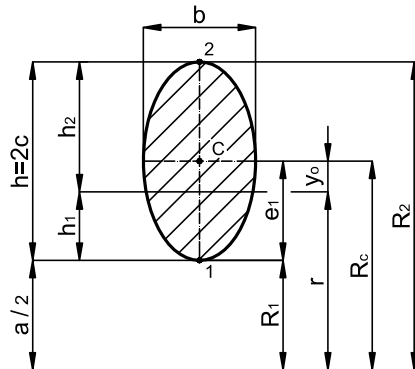


Figure 4. Elliptic cross-section

$$A=b \cdot c \cdot \pi / 2 \quad (13)$$

$$r = \frac{b \cdot \pi}{c} \cdot \left(R_c - \sqrt{R_c^2 - c^2} \right) \quad (14)$$

The circular cross-section is a special case of elliptic section, where $2c = b$.

3. NUMERICAL REPRESENTATION OF THE OBTAINED RESULTS

The optimization procedure was conducted using some metaheuristic optimization methods, e.g. Firefly Algorithm (FA), Cuckoo Search algorithm (CS), Simulated Annealing (SA) and Harmony Search (HS), in conjunction with known MATLAB functions *fmincon* and *pattern search*. It should be mentioned that the metaheuristic algorithms were utilized in their source form, without any modifications.

Geometrical data for the cross-sections of the crane hooks are given in Table 1, according to [1].

Table 1. Crane hooks geometrical data

Q	a	b ₁	h _s	b ₂	A
5	8	7.1	9	2.84	44.73
6.3	9	8	10	3.2	56.00
8	10	9	11.2	3.6	70.56
10	11.2	10	12.5	4.0	87.50
12.5	12.5	11.2	14	4.48	109.76
16	14	12.5	16	5.0	140.00

As the constraints within the optimization process, it was taken that the heights and the widths of the cross-sections must be less than standard profile height h_s (Table 1). Also, it was taken that the variables cannot be less than 1 cm.

The values of optimized variables are given in [cm] and cross-sectional areas are given in [cm²]. In addition, a percentage deviations between optimized and standard areas are given in the last column, according to [1].

The following tables (Table 2 - Table 7) present the optimization results for T cross-section.

Table 2. T cross-section optimization results (FA)

Q	b _t	t	d	h	A	%
5	9.00	1.41	1.81	7.59	26.38	41.0
6.3	10.00	1.80	1.87	8.20	33.35	40.4
8	11.20	2.21	2.00	8.99	42.80	39.3
10	12.42	2.15	3.32	9.77	59.23	32.3
12.5	14.00	2.56	2.70	11.44	66.73	39.2
16	16.00	2.90	2.79	13.10	82.85	40.8

Table 3. T cross-section optimization results (CS)

Q	b _t	t	d	h	A	%
5	9.00	1.61	1.53	7.39	25.76	42.4
6.3	10.00	1.85	1.82	8.15	33.31	40.5
8	11.20	2.10	2.10	9.10	42.66	39.5
10	12.50	2.37	2.37	10.13	53.61	38.7
12.5	14.00	2.63	2.63	11.37	66.66	39.3
16	16.00	2.90	2.79	13.10	82.84	40.8

Table 4. T cross-section optimization results (SA)

Q	b _t	t	d	h	A	%
5	8.96	1.65	1.52	7.35	25.91	42.1
6.3	10.00	1.78	1.91	8.22	33.47	40.2
8	11.18	2.12	2.11	9.07	42.82	39.3
10	12.50	2.44	2.31	10.06	53.74	38.6
12.5	13.99	2.59	2.68	11.41	66.75	39.2
16	15.98	2.88	2.83	13.12	83.05	40.7

Table 5. T cross-section optimization results (HS)

Q	b _t	t	d	h	A	%
5	8.94	1.75	1.44	7.25	26.1	41.6
6.3	10.00	1.77	1.91	8.23	35.52	36.6
8	11.20	2.21	2.16	8.80	44.00	37.6
10	12.50	2.35	2.39	10.15	53.74	38.6
12.5	14.00	2.50	2.78	11.50	66.91	39.0
16	16.00	2.73	2.98	13.27	83.23	40.6

Table 6. T cross-section optimization results (fmincon)

Q	b _t	t	d	h	A	%
5	9.00	1.61	1.53	7.39	25.76	42.4
6.3	10.00	1.85	1.82	8.15	33.31	40.5
8	11.20	2.10	2.10	9.10	42.66	39.5
10	12.50	2.36	2.38	10.14	53.61	38.7
12.5	14.00	2.63	2.63	11.37	66.66	39.3
16	16.00	2.90	2.79	13.10	82.84	40.8

Table 7. T cross-section opt. results (pattern search)

Q	b _t	t	d	h	A	%
5	9.00	1.69	1.46	7.30	25.89	42.1
6.3	10.00	2.11	1.64	7.89	33.98	39.3
8	11.20	2.17	2.11	9.03	43.29	38.6
10	12.45	2.55	2.62	9.54	56.79	35.1
12.5	13.96	2.99	2.40	11.01	68.10	38.0
16	15.94	3.18	2.59	12.82	83.94	40.0

The following tables (Table 8 - Table 13) present the optimization results for trapezoidal cross-section.

Table 8. Trapezoidal cross-section optimization results (FA)

Q	b ₁	b ₂	h	A	%
5	7.69	1.50	9.00	41.38	7.5
6.3	9.06	1.33	10.00	51.92	7.3
8	10.66	1.05	11.20	65.57	7.1
10	11.81	1.32	12.50	82.08	6.2
12.5	11.92	3.10	13.96	104.89	4.4
16	13.83	2.66	16.00	131.91	5.8

Table 9. Trapezoidal cross-section optimization results (CS)

Q	b ₁	b ₂	h	A	%
5	8.11	1.00	9.00	41.00	8.3
6.3	9.35	1.00	10.00	51.75	7.6
8	10.71	1.00	11.20	65.56	7.1
10	12.12	1.00	12.50	82.01	6.3
12.5	13.53	1.10	14.00	102.43	6.7
16	15.11	1.20	16.00	130.50	6.8

Table 10. Trapezoidal cross-section optimization results (SA)

Q	b ₁	b ₂	h	A	%
5	8.11	1.00	9.00	41.01	8.3
6.3	9.36	1.00	9.99	51.76	7.6
8	10.71	1.00	11.20	65.57	7.1
10	12.07	1.06	12.50	82.02	6.3
12.5	13.58	1.05	14.00	102.43	6.7
16	15.02	1.30	16.00	130.52	6.8

Table 11. Trapezoidal cross-section optimization results (HS)

Q	b ₁	b ₂	h	A	%
5	8.46	1.42	8.45	41.79	6.6
6.3	9.10	1.27	10.00	52.06	7.0
8	10.29	2.81	10.43	68.32	3.2
10	11.67	1.48	12.50	82.23	6.0
12.5	12.38	2.42	14.00	103.59	5.6
16	14.31	2.07	16.00	131.05	6.4

Table 12. Trapezoidal cross-section optimization results (fmincon)

Q	b ₁	b ₂	h	A	%
5	8.11	1.00	9.00	41.00	8.3
6.3	9.35	1.00	10.00	51.75	7.6
8	10.71	1.00	11.20	65.56	7.1
10	12.12	1.00	12.50	82.01	6.3
12.5	13.53	1.10	14.00	102.43	6.7
16	15.11	1.20	16.00	130.50	6.8

Table 13. Trapezoidal cross-section optimization results (pattern search)

Q	b ₁	b ₂	h	A	%
5	8.11	1.00	9.00	41.00	8.3
6.3	9.35	1.00	10.00	51.75	7.6
8	8.84	3.57	11.20	69.47	1.5
10	10.07	3.71	12.50	86.10	1.6
12.5	13.62	1.01	14.00	102.43	6.7
16	14.00	2.44	16.00	131.54	6.0

The following tables (Table 14 - Table 19) present the optimization results for rectangular cross-section.

Table 14. Rectangular cross-section optimization results (FA)

Q	b	h	A	%
5	5.64	9.00	50.79	-13.5
6.3	6.41	10.00	64.12	-14.5
8	7.26	11.20	81.32	-15.2
10	8.13	12.50	101.7	-16.2
12.5	9.08	14.00	127.06	-15.8
16	10.17	15.95	162.23	-15.9

Table 15. Rectangular cross-section optimization results (CS)

Q	b	h	A	%
5	5.64	9.00	50.79	-13.5
6.3	6.41	10.00	64.11	-14.5
8	7.26	11.20	81.32	-15.2
10	8.14	12.50	101.70	-16.2
12.5	9.08	14.00	127.06	-15.8
16	10.13	16.00	162.15	-15.8

Table 16. Rectangular cross-section optimization results (SA)

Q	b	h	A	%
5	5.64	9.00	50.79	-13.5
6.3	6.41	10.00	64.12	-14.5
8	7.26	11.20	81.33	-15.3
10	8.14	12.49	101.72	-16.3
12.5	9.08	13.99	127.07	-15.8
16	10.14	16.00	162.16	-15.8

Table 17. Rectangular cross-section optimization results (HS)

Q	b	h	A	%
5	7.08	7.45	52.72	-17.9
6.3	7.83	8.44	66.13	-18.1
8	7.30	11.15	81.44	-15.4
10	9.26	11.19	103.78	-18.6
12.5	11.23	11.70	131.29	-19.6
16	12.97	12.98	168.44	-20.3

Table 18. Rectangular cross-section optimization results (fmincon)

Q	b	h	A	%
5	5.64	9.00	50.79	-13.5
6.3	6.41	10.00	64.11	-14.5
8	7.26	11.12	81.32	-15.2
10	8.14	12.5	101.70	-16.2
12.5	9.08	14.00	127.06	-15.8
16	10.13	16.00	162.15	-15.8

Table 19. Rectangular cross-section optimization results (pattern search)

Q	b	h	A	%
5	5.75	8.86	50.91	-13.8
6.3	7.05	9.21	64.99	-16.1
8	8.10	10.12	82.59	-17.0
10	8.17	12.47	101.83	-16.4
12.5	9.08	14.00	127.06	-15.8
16	10.13	16.00	162.15	-15.8

Since there is only one variable for square cross-section, by solving (1) it is obtained (Table 20):

Table 20. Square cross-section optimization results

Q	b	A	%
5	7.27	52.85	-18.2
6.3	8.16	66.62	-19.0
8	9.18	84.36	-19.6
10	10.27	105.49	-20.6
12.5	11.48	131.81	-20.1
16	12.98	168.383	-20.3

The optimization of the elliptic cross-section has given no results because of set geometric constraints. Without them, the following results are obtained (Table 21 – Table 26):

Table 21. Elliptic cross-section optimization results (FA)

Q	b	c	A	%
5	6.80	6.46	69.05	-54.4
6.3	8.21	6.73	86.91	-55.2
8	9.50	7.39	110.37	-56.4
10	10.15	8.66	137.98	-57.7
12.5	11.48	9.56	172.45	-57.1
16	12.50	11.25	220.92	-57.8

Table 22. Elliptic cross-section optimization results (CS)

Q	b	c	A	%
5	7.32	6.00	68.98	-54.2
6.3	8.20	6.75	86.91	-55.2
8	9.37	7.50	110.36	-56.4
10	10.46	8.40	137.95	-57.7
12.5	11.71	9.37	172.44	-57.1
16	13.38	10.50	220.73	-57.7

Table 23. Elliptic cross-section optimization results (SA)

Q	b	c	A	%
5	7.34	5.98	68.98	-54.2
6.3	8.25	6.70	86.91	-55.2
8	9.31	7.55	110.36	-56.4
10	10.47	8.39	137.95	-57.7
12.5	11.70	9.38	172.44	-57.1
16	13.40	10.49	220.73	-57.7

Table 24. Elliptic cross-section optimization results (HS)

Q	b	c	A	%
5	7.52	5.84	68.99	-54.2
6.3	7.12	7.79	87.25	-55.8
8	6.45	11.21	113.70	-61.1
10	14.36	6.22	140.33	-60.4
12.5	13.35	8.25	172.98	-57.6
16	14.86	9.47	221.17	-58.0

Table 25. Elliptic cross-section optimization results (fmincon)

Q	b	c	A	%
5	7.32	6.00	68.98	-54.2
6.3	8.20	6.75	86.91	-55.2
8	9.37	7.50	110.36	-56.4
10	10.46	8.40	137.95	-57.7
12.5	11.71	9.37	172.44	-57.1
16	13.38	10.50	220.72	-57.7

Table 26. Elliptic cross-section optimization results (pattern search)

Q	b	c	A	%
5	4.83	9.43	71.61	-60.1
6.3	7.13	7.79	87.24	-55.8
8	5.62	13.26	117.07	-65.9
10	7.21	12.54	142.08	-62.4
12.5	7.60	15.04	179.64	-63.7
16	13.26	10.69	222.66	-59.0

Since there is only one variable for circular cross-section, by solving (1) it is obtained (Table 27):

Table 27. Circular cross-section optimization results

Q	R	A	%
5	4.88	74.82	-67.3
6.3	5.41	92.05	-64.4
8	6.04	114.50	-62.3
10	6.70	140.94	-61.1
12.5	7.45	174.18	-58.7
16	8.39	221.24	-58.0

4. CONCLUSION

The optimization procedures were successfully applied in the considered case, in order to decrease the cross-sectional area of the crane hook at its critical section.

It can be noted that the smallest cross-sectional area was obtained for T section, for given conditions and constraints. Savings are up to 42,4 % (Table 2 – Table 7), which is almost identical with achieved savings in the paper [10], for somewhat different considered conditions and the same geometric constraints. As in the paper [10], the *fmincon* method gave the maximum savings.

Less savings are achieved with trapezoidal cross-section due to geometric constraint, and they are up to 8,3 % (Table 8 – Table 13). In comparison with the results from paper [12], it can be seen that, for certain ratios b_2/b_1 , the same saving value is achieved by usage of GRG2 method.

The rectangular cross-section, due to the geometric constraints, yielded greater areas in relation to considered areas (Table 14 – Table 19), where cross-sectional area exceeded the limit by 3,5 – 20,3 %. For the same geometric constraints, with somewhat different conditions and utilization of GRG2 procedure, this overrun was 13,1 % in paper [12]. The square cross-section gave a little higher area values than rectangular cross-section (Table 20).

The elliptic cross-section gave very unfavourable results, both with height and the area of the cross-section (Table 21 – Table 26). For the considered conditions, the overruns are even 65,9 %. In the paper [12], for somewhat different conditions, the value of crane hook cross-sectional area is also high. The circular cross-section yields even worse results in comparison to the elliptic one (Table 27).

The most favourable results for the considered optimization problem are obtained with the appliance of CS method and *fmincon* function. A bit worse results are achieved with HS method, as well as with *pattern search* function, depending from the case. Quite good results are obtained by usage of FA method and SA method. For these types of structures, T and trapezoidal cross-sections (and similar shapes such as triangular shape) should be exploited.

Further researches should include all potential cross-sectional shapes and materials as well, in order to get lighter crane hooks. Aside the stress states, the deformations and the fatigue of the crane hooks can be analysed.

ACKNOWLEDGMENT

A part of this work is a contribution to the Ministry of Science and Technological Development of Serbia funded projects TR 35038 and III 44006.

REFERENCES

- [1] DIN 15 401: Lifting hooks for lifting appliances – Single hooks - Unmachined parts, Deutsches Institut für Normung, Berlin, 1982.
- [2] Nagaraju, B., Roy, M.R., Reddy, P.V. and Satyanarayana, K.: Stress Analysis of Crane Hook Using FEA, IJCESR, Vol. 2, No. 2, pp. 126-131, 2015.
- [3] Mehendale, S.A., Wankhade, S.R.: Design and Analysis of EOT Crane Hook for Various Cross Sections, IJCESR, Vol. 3, No. 12, pp. 53-58, 2016.
- [4] Krishnaveni, M.N.V., Reddy, M.A. and Roy, M.R.: Static Analysis of Crane Hook with T-Section using ANSYS, IJETT, Vol. 25, No. 1, pp. 53-58, 2015.
- [5] Sundriyal, R.: Stress Analysis of Crane Hook with Different Cross Sections using ANSYS, IJSR, Vol. 6, No. 8, pp. 1363-1368, 2017.
- [6] Chunkawan, Y.B., Subramaniam, R.S.: Static structural analysis of crane hook, IRJET, Vol. 4, No. 7, pp. 2265-2274, 2017.
- [7] Singh, A., Rohilla, V.: Optimization and fatigue analysis of a crane hook using finite element method, IJMECH, Vol. 4, No. 4, pp. 31-43, 2015.
- [8] Vanpariya, K.B., Pandya, V. and Koisha, J.: Design Analysis and Weight Optimization of Lifting Hook, JETIR, Vol. 3, No. 12, pp. 81-85, 2016.
- [9] Muromaki, T., Hanahara, K., Nishimura, T., Tada, Y., Kuroda, S. and Fukui, T.: Multi-Objective Shape Design of Crane-Hook Taking Account of Practical Requirement, AIP Conference Proceedings, Vol. 1233, No. 1, pp. 632-637, 2010.
- [10] Pavlović, G., Savković, M., Zdravković, N., Marković, G. and Stanojković, J.: Analysis and Optimization of T-Cross Section of Crane Hook Considered as a Curved Beam, IMK – 14, Research&Development in Heavy Machinery, Vol. 24, No. 2, pp. 53-60, 2018.
- [11] Bhasker, R.S., Prasad, R.K., Kumar, V. and Prasad, P.: Simulation of Geometrical Cross-Section for Practical Purposes, IJETT, Vol. 4, No. 3, pp. 397-402, 2013.
- [12] Savković, M., Pavlović, G., Stanojković, J., Zdravković, N. and Marković, G.: Comparative Analysis and Optimization of Different Cross-Sections of Crane Hook Subject to Stresses According to Winkler-Bach Theory, Proceedings of IV International Conference "Mechanical Engineering in the 21st Century – MASING 2018", pp. 135-140, 2018.
- [13] Dedijer, S.: *Transportation equipment I*, Institute for Mechanization of the Faculty of Mechanical Engineering of the University in Belgrade, Serbia, 1986.

Finite Element Method Simulation and Multifactor Failure Analysis of an Important Stepped Shaft Fracture Events

Qiu Jun

Senior Engineer
Shanghai Institute of Special Equipment
Inspection and Technical Research

Tong Yaoting

Engineer
Shanghai Institute of Special Equipment
Inspection and Technical Research

Ouyang Weiping

Engineer
Shanghai Institute of Special Equipment
Inspection and Technical Research

Aiming at a fracture event of an important stepped shaft parts, finite element method was used to simulate and analyze. Results show that the stress concentration is serious at the step and the maximum stress occurs at the transition corner, which exceeds the yield strength limit of the material under the most unfavorable condition. Scanning Electron Microscope and X-ray Energy Spectrum analysis shows that fracture of the shaft is a fatigue fracture initiated by multiple sources. Design analysis states that the initiation is mainly related to the small turning radius of the step, which caused stress concentration factor increase. Besides, the higher shoulder height caused sudden change of the section size and aggravated stress concentration effect. Furthermore, machining quality analysis indicates that the rough surface with micro-defects may be the origin of fatigue crack initiation. Heat Treatment process quality analysis indicates that improper control of quenching and tempering process had a negative impact on the initiation of crack. Working conditions analysis shows that the actual load state, which exceeded the design standard load spectrum, accelerated the fatigue damage.

Keywords: stepped shaft, fatigue fracture, finite element, failure analysis

1. INTRODUCTION

Finite Element Method (FEM) is a common method for the design and stress analysis of stepped axle, especially for stress concentration analysis[1-3]. In application of finite element method, mesh generation is a key step. Researchers need to select the appropriate mesh size according to the purpose of analysis [4-5]. In this paper, the finite element method is applied to fracture analysis of an important stepped shaft, while other failure analysis methods are synthesized, to find out the real cause of the fracture of the stepped shaft.

A 450t shipbuilding gantry crane in a company, which has been in operation for 3 years, is used in large lifting operation. Due to the breakage of the drum shaft of the lifting mechanism, the lifting objects fall to the ground and the crane is damaged.



Figure 1. Drum shaft of lifting mechanism of the crane

The fracture region was found locating at the step of

the stepped shaft. By observing and analyzing extra features of the damaged area, investigators believed that the macro morphology of the section is fatigue fracture, and the final fracture zone is small (about 40mm).

2. GEOMETRY AND LOADING ANALYSIS OF SHAFT

Geometric sketch of the shaft was drawn, which shown that the fracture occurred at the turning corner of $\phi 180\text{mm}/\phi 220\text{mm}$ steps.

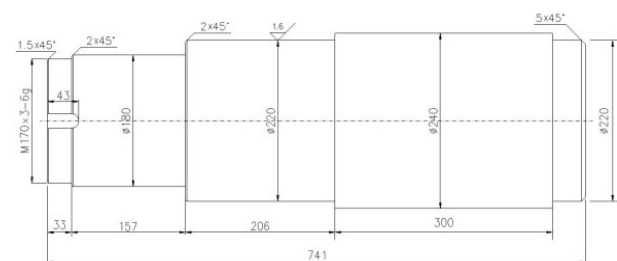


Figure 2. Geometric sketch of the shaft

According to the working conditions of the crane, the force analysis sketch of the drum structure was drawn, and the bearing support reaction of the drum shaft was solved, with the results shown in Table 1.

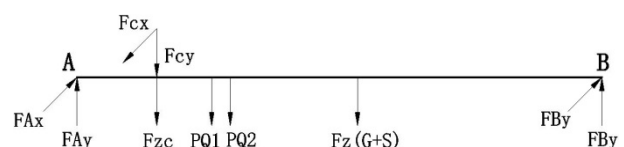


Figure 3. Diagram of force analysis of drum structure

Correspondence to: Qiu Jun, Senior Engineer
Shanghai Institute of Special Equipment Inspection and
Technical Research, JinShaJiang Road915, China
E-mail: qiuju@ssei.cn

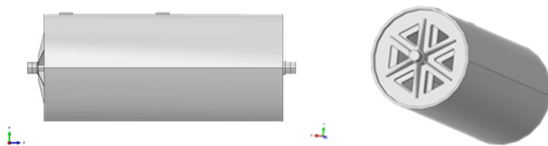
Table 1. Bearing support reaction on drum shaft

F_{AX}	F_{AY}	F_{BX}	F_{BY}
242.1kN	682.2kN	14.7kN	141.3kN

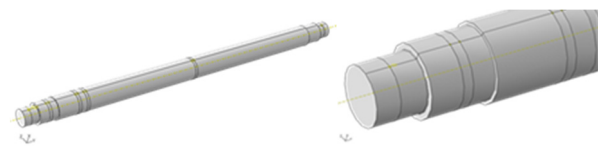
3. FINITE ELEMENT SIMULATION

3.1 Model Establishment

The geometric model of the whole drum structure was established in CATIA.

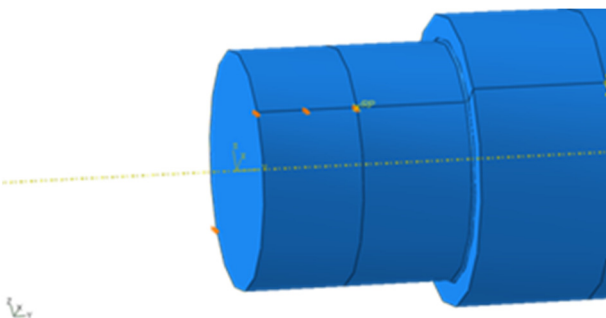
**Figure 4. Geometric model of drum structure**

As the fracture of the mechanism occurs on one side of the shaft only, so that it's unnecessary to apply the finite element analysis for the whole model. In finite element software ABAQUS, the drum part can be replaced by a through shaft ($D=240\text{mm}$), than both two ends of the mechanism can be connected together, thus the model can be easily calculated, while the bending moment and the force at the fracture will not change. The simplified model is shown in Figure 5.

**Figure 5. ABAQUS simplified finite element model**

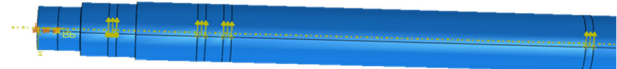
3.2 Material properties and constraints

The base material of the shaft is No.35 steel, whose Young's modulus is 212,000MPa, Poisson's ratio is 0.31, yield stress is 315MPa, and ultimate stress is 530MPa. The parameters are input into the material library of the finite element software, and the material properties are assigned to the components. As the hoisting mechanism used a self-aligning bearing, the shaft does not bear additional bending moment, so that the two fixed ends of the shaft are constrained by XYZ displacement in three directions, one end is constrained by YZ displacement in two directions, and the shaft is not constrained by rotation. The constraint diagram is shown in Figure 6.

**Figure 6. Constraint diagram of the model**

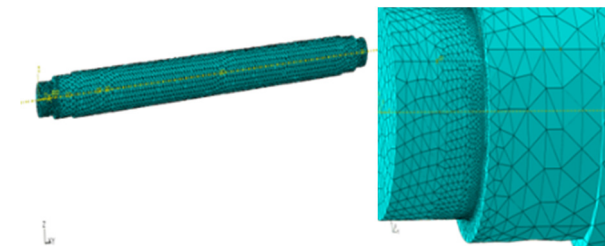
3.3 Loading

Through analysis of the most unfavorable working conditions of the drum shaft, it can be concluded that the force acting on the drum single rope is X-direction $p=210.8\text{kN}$, and the tangential force, radial force and ring weight projected to the XZ plane respectively are, $F_{X1}=281.2\text{kN}$, $F_{Z1}=256.8\text{kN}$, and the total $F_{X2}=120.6\text{kN}$ of the drum and the wire rope on it. Due to the singularity of stress in local area under concentrated load, the calculation results will be deviated. Therefore, the concentrated load is converted into volume force in the model, eliminating unnecessary errors caused by loading. The loading diagram is shown in Figure 7.

**Figure 7. Load distribution of drum shaft**

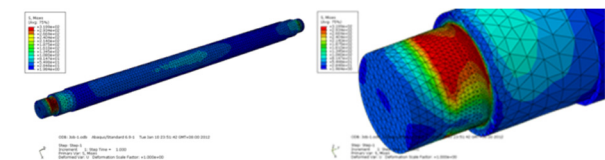
3.4 Finite Element Mesh

According to the size of the model and the requirement of calculation accuracy, entity unit and the mesh refinement was employed to the model, and the mesh is divided and refined at the corner transition of R2 (the mesh size set as 1.5mm). As the mesh size of different regions in the model varies greatly, tetra shaped elements was chosen.

**Figure 8. Model meshing and encryption**

3.5 Results

After checking correctly, the model is submitted to ABAQUS software for post-processing calculation, and the calculation results are shown in Figure 9.

**Figure 9. Stress distribution of the shaft and its left end**

From Figure 9, it shows that the stress concentration occurs at the fracture site of the shaft under rated load. The stress distribution phase diagram of its left end is analyzed. Maximum stress occurs at the transition point of R2 fillet. The maximum stress value is 319.9MPa, which exceeds the yield strength limit of the material $R_{el}=315\text{MPa}$. In order to stereoscopically reflect the stress state of this section, the section is cut off along R2 rounded cross section, XY plane and YZ plane, and the stress distribution diagram is shown in Figure 10.

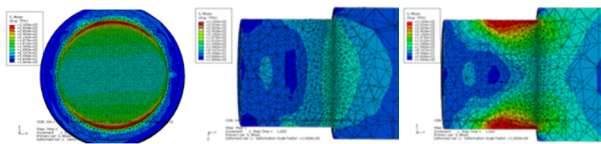


Figure 10. Stress distribution diagrams of cross section, xy section and yz section at R2 round corner at axis fracture

4. MULTIFATOR FAILURE ANALYSIS

4.1 Design Analysis of Shaft

The design structure diagram shows that the radius of transition corner $R=2\text{mm}$ at the step shaft $\phi 180\text{mm} / \phi 220\text{mm}$ is less than the national standard value, and it is quite different from the industry standard value. If the radius of transition corner is too small, the stress concentration factor will increase. The shoulder height is higher which cause the sudden change of the section size, and will aggravate the stress concentration effect.

4.2 Quality Analysis of Heat Treatment Process

According to the technical requirements of the shaft (35 steel), the hardness after quenching and tempering should reach 170HB-200HB. Brinell hardness was measured from surface to interior on longitudinal of the shaft at $\Phi 220\text{mm}$ fracture section. Physical and chemical test results show that the actual near surface hardness (220HB) exceeds the technical requirements, and the effective quenching layer depth is shallow, which has a certain impact on fatigue strength.

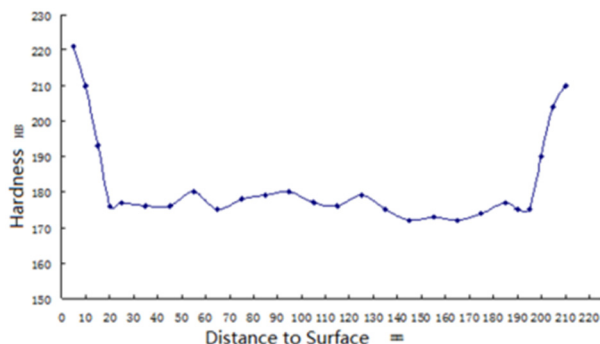


Figure 11. Hardness gradient on longitudinal section of shaft at $\Phi 220\text{mm}$ fracture zone

4.3 Quality Analysis of Metal Processing

There are obvious turning marks on the surface of the shaft near the fracture section. Compared with the roughness sample, the surface quality of the shaft is between $3.2\mu\text{m}$ and $6.3\mu\text{m}$, and the roughness of the surface does not meet the design requirement $Ra 1.6\mu\text{m}$. Surface state coefficient β has certain influence on fatigue fracture [6-7], and surface micro-defects may be the origin of fatigue crack initiation.

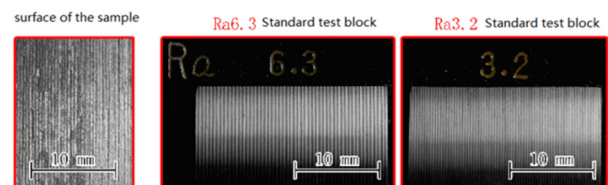


Figure 12. Comparisons of surface roughness in turning

4.4 Scanning Electron Microscope and X-ray Energy Spectrum Analysis

The fatigue fracture of shafting can be clearly confirmed by scanning electron microscopy (SEM) analysis of the fracture surface of shafting. On the outer surface of the shaft, there are rough bamboo-shaped metal processing marks and transverse stretch-like stripes with nodal spacing distribution; at higher magnification, the morphology shows that the processing cracks open and turn, and extend to the edge of the section, which is related to the beginning of the section; at the edge of the section, there are parallel and dense fatigue stripes. Parallel fatigue growth fringes and intergranular secondary cracks can be seen in the sub-edge region, showing brittle morphology.

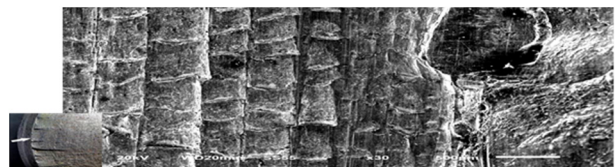


Figure 13. Machining traces of rough surface of axis and sub-layer fatigue glow

4.5 Working Conditions Analysis

Statistical data of hoisting mechanism operation show that the actual load state exceeds the L2-intermediate level of the design standard load spectrum, and it is easy to accelerate the fatigue damage of mechanical parts. At the same time, the fatigue fracture surface accounts for about 85% of the area of the cross-section, and the potential hazard cannot be found in daily use.

5. CONCLUSION

According to ABAQUS finite element simulation calculation, the maximum stress of local stress concentration exceeds the yield strength limit of material under the most unfavorable conditions at the transition corner of the shaft's $\phi 180\text{mm} / \phi 220\text{mm}$ step.

During the design of shaft, the selection of transition corner radius at fracture is too small and the selection of shoulder height is too large, which makes the stress concentration factor too high, and has adverse effects on the fatigue life of shaft.

The surface roughness and surface hardness of the fracture zone of the shaft do not meet the technical requirements, which will greatly reduce the toughness and fatigue resistance of the corner zone. The use beyond the design level has a negative impact on the initiation of cracking.

A large proportion of the fatigue growth zone on the cross section indicates that there is a period from crack initiation to final fracture, but the fatigue crack cannot be found in the daily maintenance of the crane during this period, which indicates that there is a blind area in the daily maintenance of the crane.

The fracture of the drum shaft is a fatigue fracture initiated by multiple sources. The initiation of the drum

shaft is mainly related to the small transition fillet in the step area and the high stress concentration effect. It is easy to initiate fatigue cracking under impact load, which eventually leads to the overall failure, the drum losing its restraint, and high-speed rotation under the gravity drag of the suspender until the suspender falls to the ground and damaged.

ACKNOWLEDGMENT

This paper is support by The National Key Research and Development Program of China No.2017YFC0805705.

REFERENCES

- [1] Zhang, J., Chen, X.Y. and Wang, L.: Journal of Anhui university of science and technology (natural science), Vol. 37, No. 3, pp. 56, 2017.
- [2] Jiang, B., Zhang, Q. and Cui, W.: Machine design and manufacturing engineering, Vol. 47, No. 7, pp. 11, 2018.
- [3] Liang, K.S.: Machinery, Vol. 55, No. 10, pp. 67, 2017.
- [4] Wang, M.Q., Zhu, Y.M. and Lu, W.X.: Machinery design & manufacture, 1:22, 2004.
- [5] Wang, Y., Lu, L. and Li, W.T.: Hoisting and conveying machinery, 3:52, 2014.
- [6] Cai, Y.: Internal combustion & parts, 21:128, 2018.
- [7] Sun, J.L. and Jiang, D.Z.: Journal of Yancheng institute of technology (natural science), Vol. 15, No. 4, pp. 21, 2002.

Manuel Stölzner

Research Assistant
Technical University of Munich
Faculty of Mechanical Engineering
Chair of Materials Handling,
Material Flow, Logistics

Michael Kleeberger

Senior Research Assistant
Technical University of Munich
Faculty of Mechanical Engineering
Chair of Materials Handling,
Material Flow, Logistics

Willibald Günthner

Professor
Technical University of Munich
Faculty of Mechanical Engineering
Chair of Materials Handling,
Material Flow, Logistics

Johannes Fottner

Professor
Technical University of Munich
Faculty of Mechanical Engineering
Chair of Materials Handling,
Material Flow, Logistics

Calculating the dynamic behaviour of lattice boom mobile cranes during hoisting with a vibration model

Lattice boom mobile cranes are mainly used to move heavy payloads with a large hoisting radius. During this work, crane motions cause dynamic forces on the crane's structure. In order to guarantee the safety of cranes, exact calculations are absolutely essential for the boom system. The calculation standards stipulate the use of special dynamic factors to estimate the dynamic loads. Several research projects have shown, that the standards often describe the dynamic effects only approximately. In order to calculate the dynamic behaviour accurately without a disproportionate increase in computing time, special vibration models have been developed in a current research project. This paper presents a new vibration model for the process of hoisting suspended loads. The model is based on the response spectrum method and describes the dynamic effects in an exact way.

Keywords: mobile crane, dynamic calculation, finite element method, modal reduction, hoisting, vibration model.

1. INTRODUCTION

Lattice boom mobile cranes typically have a hoisting capacity of more than 1000 metric tonnes and a maximum hoisting radius of around 200 meters. Mobile cranes are set up with long, elastic lattice booms and acute-angled suspensions. Their fundamental motions are hoisting, slewing and luffing. The slender boom system has become more and more complex due to increasing load capacity.

Each working process causes dynamic forces on the supporting structure of a crane. In order to avoid security risks, the exact calculation of the boom system is an important task in the development of cranes. One main objective of the calculation is to reproduce the system's realistic dynamic behaviour. According to current standards [3-5, 8, 9], stress calculations for mobile cranes are carried out using static approaches. The dynamic effects are considered in the calculation by means of special dynamic factors. The factors are often based on the experience of the crane manufacturers or, alternatively, they can be taken from tables in the standards. The cranes' dynamic behaviour is analysed in several publications [10, 11, 18] and some previous articles have shown, that the calculation standards often describe the dynamic effects only approximately for the motions of slewing, luffing and hoisting grounded loads [2, 11, 14, 15]. For this reason, the standards also allow the use of other methods to calculate dynamic effects. One way to characterize the dynamic behaviour of cranes very accurately is to use the nonlinear dynamic finite element calculation. The main disadvantage of this

method is the much higher computing time needed compared to a static calculation. Furthermore, there is no reasonable way to take the standards' partial safety factors into consideration. These are the two main reasons why the dynamic analysis is very rarely used by crane manufacturers, even though it allows exact and reliable calculations. In order to achieve a more exact calculation of the dynamic behaviour of cranes without a disproportionate increase in computing time, special vibration models have been developed in a current DFG-research project. This paper presents a new vibration model for the process of hoisting suspended loads. The results of the model are compared to those of the nonlinear dynamic finite element calculation to verify the accuracy of the developed model. Furthermore, a comparison between the results of the calculation according to the current European standard for mobile cranes [3] and other methods is referenced and the advantages of the proposed calculation process are presented.

The applicability of the model and the calculation standard is shown for mobile cranes with various set-ups, different loads and different boom positions. The comparison takes various accelerations and velocities of the hoisting drive into account to verify the accuracy of the model.

2. BASICS

The stress calculation for cranes follows the rules of the European standard DIN EN 13001 [4, 5] or international standard ISO 8686 [8, 9]. The European standard refers to the standard DIN EN 13000 [3] for calculating mobile cranes. In the standards, the approach for considering dynamic loads is based on a rigid body kinetic analysis and uses quasi-static calculation methods. A previous project has shown that these methods are often inappropriate to reproduce the dynamic effects on mobile cranes. However, the standard

Correspondence to: Manuel Stölzner, Research Assistant
Faculty of Mechanical Engineering
Chair of Materials Handling, Material Flow, Logistics
Boltzmannstr. 15, 85748 Garching, Germany
E-mail: manuel.stoelzner@tum.de

ISO 8686 'expressly permits the use of more advanced methods (calculations or tests) to evaluate the effects of loads and load combinations, and the values of dynamic load factors, where it can be demonstrated that these provide at least equivalent levels of competence' [8]. The European standards DIN EN 13001 and DIN EN 13000 contain similar remarks concerning other possible calculation methods. The nonlinear dynamic finite element calculation and the vibration model presented here are two of the aforementioned advanced methods.

In order to compensate uncertainties, the standards prescribe the use of partial safety factors. However, this paper does not consider any safety factors because only the accuracy of the loads generated with the vibration model and the standards is verified. The objective of the current research project is to depict the dynamic effects on cranes in an exact way and not to assess the quality of the safety factors. Nevertheless, partial safety factors can be considered in the vibration model presented here in the same way as stipulated in the calculation standard. The following sections describe the calculation standard and the basics of the newly developed vibration model.

2.1 DIN EN 13000

The standard DIN EN 13000 is currently used by crane manufacturers in Europe to do the stress calculation of mobile cranes. This standard refers to the guideline FEM 5.004 [6] for calculating loads and load combinations on the supporting structure. Unlike DIN EN 13001, it does not distinguish between hoisting grounded loads and hoisting suspended loads. In order to take the dynamic effects into consideration, a factor Φ is proposed for the process of hoisting suspended loads. This factor is dependent on the hoisting speed v_h and is calculated with the equation

$$\Phi = 1.1 + 0.133 v_h. \quad (1)$$

The minimum permissible value of Φ is 1.1, the maximum value is 1.3. For the proof of security, the weight force of the payload is multiplied by this factor and used in a static calculation.

2.2 Vibration model

Some publications have shown, that the dynamic effects during the process of slewing and hoisting grounded loads can be depicted by the static approach with great precision if suitable quasi-static loads are applied [12, 13, 17]. The following paragraph contains a new calculation method for the process of hoisting suspended loads. This vibration model offers a more exact method to generate quasi-static loads than the regulation proposed by the standard. Consequently, the dynamic effects can be depicted with greater accuracy in a static calculation.

The model is based on the response spectrum method. It uses a linearized approach of the nonlinear equation of motion and the method of modal reduction. This approach is very similar to the calculation method described in [12, 17] for the process of slewing.

To reproduce the cranes' dynamic behaviour, the vibration model has to replace the equation of motion

$$M\ddot{\mathbf{u}} + D\dot{\mathbf{u}} + K(t)\mathbf{u} = \mathbf{r}. \quad (2)$$

In Eq. (2) M , D and $K(t)$ are the mass, damping and stiffness matrices. The vector \mathbf{r} contains the externally applied loads and \mathbf{u} , $\dot{\mathbf{u}}$, $\ddot{\mathbf{u}}$ are the vectors of displacement, velocity and acceleration [1]. To take the damping into consideration, we assume Rayleigh damping of the type

$$D = \alpha M + \beta K \quad (\alpha, \beta \in \mathbb{R}). \quad (3)$$

The vector \mathbf{r} in (2) only contains the inertia force $m_{pl}a_{pl}$ acting on the payload, where m_{pl} is the payload's mass and a_{pl} is the acceleration of the load. The external forces on all other degrees of freedom are zero. In a first step the equation is linearized so that the stiffness matrix is only calculated in the initial state. The model is consequently based on the assumption that $K(t)$ remains constant throughout the whole working process.

The matrices M , D and $K(0)$ are symmetric and positive definite and thus can be diagonalised with the eigenvectors of the autonomous conservative system. A modal transformation into the modal coordinates \mathbf{q} is performed using the equation

$$\mathbf{u} = \Phi \mathbf{q}, \quad (4)$$

where Φ is the modal matrix containing the mass-normated eigenvectors as columns. This modal transformation results in the mass-normated equation of motion

$$\ddot{\mathbf{q}} + D_{mod}\dot{\mathbf{q}} + \Omega \mathbf{q} = \Phi^T \mathbf{r}. \quad (5)$$

In this equation the matrix $\Omega = \Phi^T K \Phi$ contains the squares of the eigenfrequencies and $D_{mod} = \Phi^T D \Phi$ is the matrix of modal damping. As the matrices Ω and D_{mod} are diagonal, the differential equations in (5) are decoupled and can be solved analytically. Consequently, there is no need for any numerical method to solve these equations of motion so that the proposed method needs only slightly more computing time than the calculation methods proposed by the standards.

The crane's vibrations caused by the working process contain only few eigenfrequencies. This is why the method of modal reduction can be used as a very exact approximation. With this method, only a certain number of n equations is considered in (5). Consequently, even less time is needed for the calculation.

In a next step, an approximate solution of (2) is calculated using the analytical solution of (5). The solution of the physical displacements related to the m -th modal coordinate is computed using the equation

$$\mathbf{u}_m(t) = \Phi_m q_m(t), \quad (6)$$

which contains the eigenvector Φ_m and the modal displacement q_m . The superposition

$$\mathbf{u}(t) = \sum_{m=1}^n \Phi_m q_m(t) \quad (7)$$

results in an approximate solution of $\mathbf{u}(t)$. This solution describes the dynamic displacements of every degree of freedom of the finite element model.

The final stress calculation should still be based on the results of static calculations, as specified in the standards. For this reason, appropriate quasi-static loads

have to be generated that reflect the worst state of elastic deformation in the same way as the dynamic calculation. The nodal forces related to the m -th modal coordinate $R_{Q,m}$ are calculated with the equation

$$R_{Q,m} = M\phi\ddot{q}_{m,\max} \quad (8)$$

which contains the maximum value $\ddot{q}_{m,\max}$ of the modal acceleration $\ddot{q}_m(t)$.

The quasi-static load for every degree of freedom i is generated with the equation

$$R_Q^i = \sqrt{\sum_{m=1}^n (R_{Q,m}^i)^2}. \quad (9)$$

This method to generate quasi-static loads is also used in a similar way in the field of civil engineering to calculate the effect of earthquakes on high-rise buildings [16]. In a static calculation these loads depict the worst state of elastic deformation in a much more accurate way than the loads based on the calculation standard.

3. NUMERICAL ANALYSIS

The nonlinear dynamic finite element calculation is the most realistic calculation method for cranes. For this reason, the results of the vibration model and the calculation standard are evaluated by comparing them with the results obtained with the dynamic calculation method. To verify the accuracy of the model, the comparison takes various accelerations and velocities of the hoisting drive into account. The following sections describe the modelling of the analysed cranes and the calculation results.

3.1 Modelling

The analysis of the dynamic behaviour is based on two cranes with a maximum hoisting capacity of around 500 and 1000 metric tonnes. In order to investigate the applicability of the vibration model for different lattice boom systems, the evaluation comprises different complexities of the boom system and various crane set-ups (see Figure 1). Furthermore, different hoisting radii of every crane configuration are analysed.

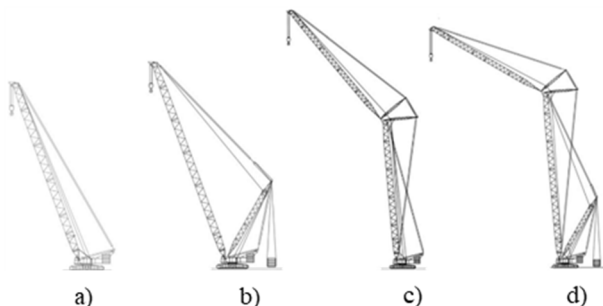


Figure 1. Analysed crane configurations: a) M-configuration (only main boom), b) MD-configuration (main and derrick boom), c) ML-configuration (main and luffing boom), d) MDL-configuration (main, derrick and luffing boom)

The method of finite tower elements is applied to model the lattice boom structure [7]. This modelling method replaces each lattice boom component by a beam

element with equivalent stiffness and mass. The payload's position was chosen close to the ground. In the numerical investigations no damping was considered because the objective of the project is not to analyse the influence of damping on the supporting structure. However, it would be possible to consider the damping of the structure as presented above (3).

The finite element program NODYA was used to carry out the calculations. This software was developed for the dynamic and static calculation of lattice boom mobile cranes and provides special elements for the crane calculation such as a rope element [11].

The calculation comprises the phases of acceleration and constant velocity as shown in Figure 2. At the beginning, there is a linear increase in the velocity of the payload followed by the phase of constant velocity. In the calculations three different velocities (0.7 rad/s, 1.4 rad/s, 2.1 rad/s) and three different accelerations (0.42 rad/s², 0.56 rad/s², 0.7 rad/s²) of the hoisting drum are considered. Furthermore, the investigation comprises different values for the rope reevings, resulting in different hoisting parameters of the payload. A simulation time of 60 s was chosen to detect the maximum modal acceleration. Numerical investigations have shown that a number $n = 10$ of modal coordinates is sufficient for the calculation of all analysed boom systems.

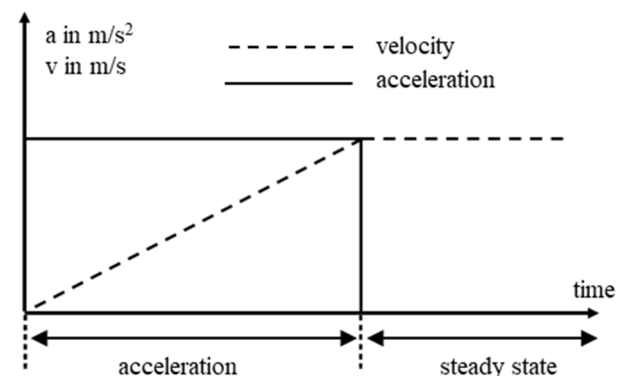


Figure 2. Variation of acceleration and velocity over time

3.2 Results

All of the comparisons collate the results obtained using the vibration model and the dynamic finite element analysis.

In a first step, the results of the vertical displacements of different nodes are considered. Figure 3 shows the time course of the vertical displacement of the payload for a crane set-up d) depicted in Figure 1 by way of example. The considered crane configuration M72D42L72 (72 meters main boom, 42 meters derrick boom and 72 meters luffing boom) was analysed with a hoisting radius of 120 meters. In the upper diagram, the displacement result obtained by the vibration model after superposition (7) of all considered modes is compared with the results of the dynamic finite element calculation. The result of the vibration model duplicates the results of the nonlinear dynamic finite element method in a good approximation. Both the amplitudes and the frequencies of the two signals are almost exactly matched. The

second diagram of Figure 3 shows all 10 modal components $u_1 - u_{10}$ of the physical displacement solution (6). It becomes very clear that the vibration is influenced mainly by one modal coordinate. The influence of the other modal coordinates is of only secondary importance. Altogether only the fourth, sixth and eighth modal coordinate contribute to the shown motion. Consequently, it would be possible to consider only three modal equations in (5) to calculate the dynamic behaviour of this crane system. Even though the number of eigenfrequencies in the crane motions changes with different crane configurations. For this reason, it is impossible to generalize the number of relevant modes on every crane system. Furthermore, it can be clearly seen that the influence of many modal coordinates is zero, as these modes can be assigned to horizontal motions of the crane and thus do not influence the process of hoisting. As for the motion depicted and a comparison of the results for other crane systems, it can be said that a number of $n = 10$ eigenfrequencies and modes is sufficient to describe hoisting motions of mobile cranes.

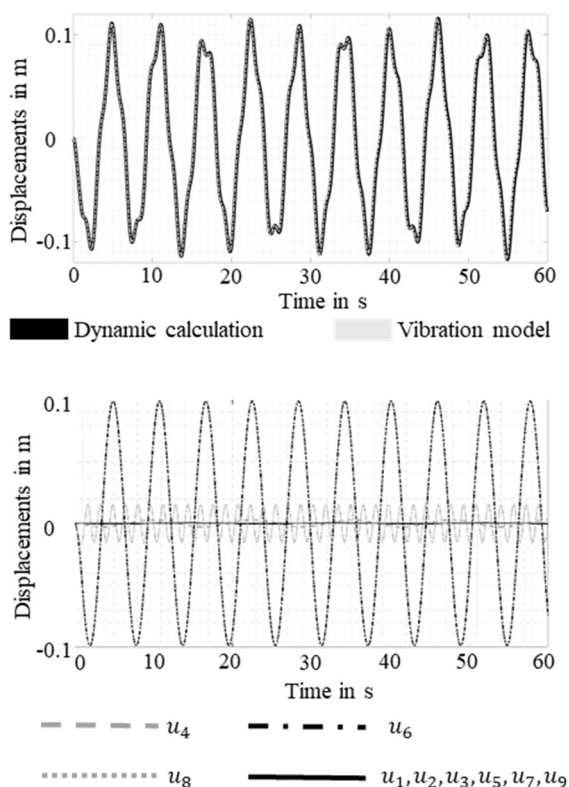


Figure 3. Displacements of the payload (M72D42L72) top: dynamic calculation and vibration model, bottom: displacements of every modal coordinate in physical coordinates

In order to carry out further comparisons, stress calculations of different systems were considered. The following figures show comparisons of the nonlinear dynamic finite element calculation, the vibration model and the standard DIN EN 13000. In the vibration model's approaches, the quasi-static loads were generated with (9). The stresses were calculated in the four corner posts of every lattice boom section.

Figure 4 shows the variation of stresses over time for the crane configuration M60L87 under consideration with a hoisting radius of 76 m. The diagram shows the

dynamic part of the stress value for the luffing boom section, where the maximum absolute stress value occurs. Comparing the results of the dynamic finite element analysis and the calculation standard, it can easily be seen that the static approach in the calculation standard leads to a much too conservative approximation of the dynamic stress. This diagram clearly shows that the quasi-static loads generated with the vibration model can reproduce the dynamic effects of the crane in a very accurate way. However, the vibration model's results are also slightly conservative and consequently still enable a safe sizing of cranes.

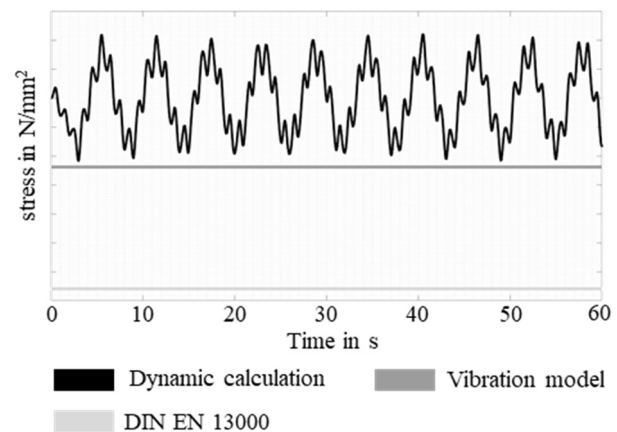


Figure 4. Variation of stresses over time, comparison of static calculation methods and nonlinear dynamic finite element calculation (M60L87, hoisting radius: 76 m)

In Figures 5 and 6, the results of the crane component's utilization is shown for the different considered calculation methods. The utilization is defined as the ratio of the compressive stress and the limit of the compressive design stress. Figure 5 shows the utilization of the different components for the considered crane configuration M90D36. In the diagram shown here, the maximum utilization is located in the derrick boom. The vibration model can accurately reproduce the results of the dynamic finite element calculation in every lattice boom section. Conversely, the calculation standard cannot describe all components of the crane with the same precision. The standard's approach can depict the low level utilization in a good approximation whereas utilization of the derrick boom is overestimated.

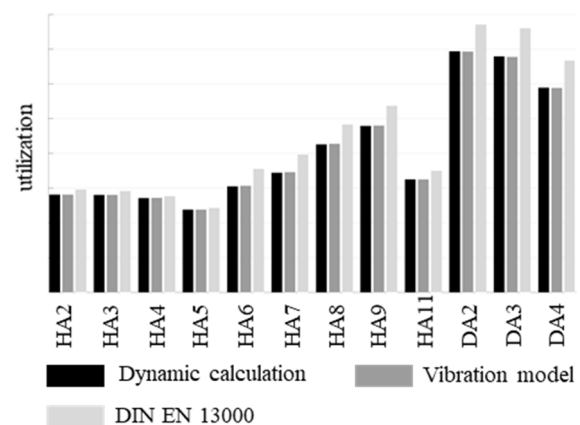


Figure 5. Utilization of different components, comparison between static calculation methods and nonlinear dynamic finite element calculation (M90D36, hoisting radius: 52 m)

The overview in Figure 6 shows a comparison of the higher lifting capacity crane in different crane configurations. Each bar of the chart depicts the lattice boom section with maximum utilization in the analysed crane configuration. This diagram shows the results for two analysed hoisting radii respectively.

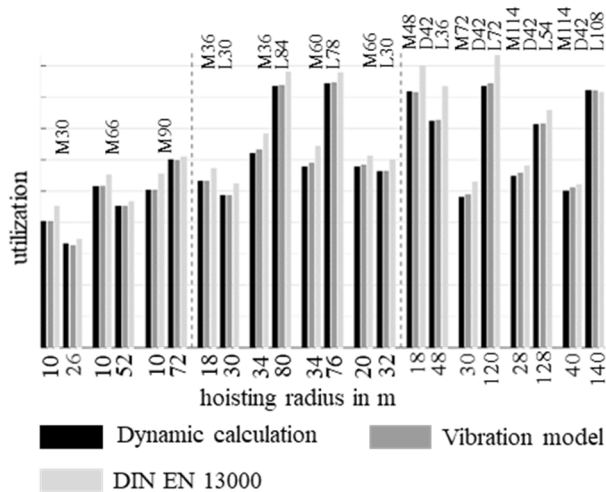


Figure 6. Maximum utilization of various crane configurations, comparison between static calculation methods and nonlinear dynamic finite element calculation

The purpose of this diagram is to compare the outcome of the calculation methods relating to different complexities of the boom system. The results presented in this figure confirm those of the other charts. In almost every crane configuration, the utilization calculated using the approach in the calculation standard leads to higher values than if the nonlinear dynamic finite element calculation is used. A dependency of the inaccuracy on any crane configuration is not apparent. Contrary to the calculation standard, the vibration model follows the results of the nonlinear dynamic finite element calculation very accurately. Most of the results are only slightly too conservative or even equal to these results. This diagram shows clearly that the linearized approach of the vibration model is applicable to different boom systems of mobile cranes.

4. CONCLUSION

This paper presents a vibration model that reproduces the dynamic behaviour of lattice boom mobile cranes during the process of hoisting suspended loads. The model enables an effective analysis of the dynamic behaviour of boom systems with any kind of configuration. Thanks to linearized formulations and the method of modal reduction, the computing time decreases compared to the dynamic finite element calculation whilst maintaining a similar accuracy. Furthermore, it is possible to consider the partial safety factors stipulated in the calculation standards.

This paper compares the results of the calculation standard, the vibration model and the dynamic finite element calculation. The approach in the standard often leads to great inaccuracies compared to the dynamic finite element calculation. One important aspect is that the vibration model presented here reproduces the dynamic effects in a more exact manner than the methods

commonly used by the standards. For this reason, the use of the new calculation method could lead to improvements in crane safety in future.

Measurements are currently being carried out to obtain further comparisons regarding the accuracy of the vibration model. In future, it will also be necessary to develop a model that depicts the dynamic effects of loader cranes during the process of hoisting suspended loads. The forces on the supporting structure of loader cranes during this motion are fundamentally different from those on mobile cranes. Another important objective is to consider the combination of the working processes hoisting and slewing in an additional model and to develop a further model which describes the dynamic effects during luffing motions of mobile cranes.

ACKNOWLEDGMENT

The research project is funded by the German Research Foundation and is being carried out in collaboration with the companies Liebherr-Werk Ehingen GmbH and Palfinger Europe GmbH.

REFERENCES

- [1] Bathe, K.-J.: *Finite Element Procedures*, Prentice Hall, 1996.
- [2] Celiktas, M. and Kleeberger, M.: Dynamische Belastung beim Lastheben: Ein Vergleich von dynamischer und quasistatischer Berechnung (en: Dynamic loads during hoisting: Comparison between dynamic and static calculation), F+H Fördern und Heben, Vol. 47, No. 6, pp. 56-61, 1997.
- [3] DIN Deutsches Institut für Normung e.V.: Cranes - Mobile Cranes, DIN EN Standard No. 13000, 2014.
- [4] DIN Deutsches Institut für Normung e.V. Cranes - General Design – Part 1: General principles and requirements, DIN EN Standard No. 13001 Part 1, 2015.
- [5] DIN Deutsches Institut für Normung e.V.: Crane safety – General design – Part 2: Load actions, DIN EN Standard No. 13001 Part 2, 2014.
- [6] Federation Europeene de la Manutention: Rules for the design of the steel structures of general use, FEM – guideline 5.004, second edition, 1994.
- [7] Günthner, W.A.: *Statische Berechnung von Gittermast-Auslegerkränen mit Hilfe finiter Turmelemente unter Berücksichtigung der Elastizität des Kranwagens und von Messungen* (en: Static calculation of lattice boom cranes with finite tower elements considering the elasticity of the crane truck and measurements), PHD Dissertation, Technical University of Munich, 1985.
- [8] ISO International Organization for Standardization Cranes-Design: principles for loads and load combinations – Part 1: General, ISO Standard No. 8686 Part 1, 2012.
- [9] ISO International Organization for Standardization Cranes-Design: principles for loads and load combinations – Part 2: Mobile cranes, ISO Standard No. 8686 Draft Part 2, 2016.

- [10] Ju, F., Choo, Y.S. and Cui, F.S.: Dynamic response of tower crane induced by the pendulum motion of the payload, *International Journal of Solids and Structures*, Vol. 43, No. 2, pp. 376–389, 2006.
- [11] Kleeberger, M.: *Nichtlineare dynamische Berechnung von Gittermast-Fahrzeugkranen* (en: *Nonlinear dynamic calculation of lattice boom mobile cranes*), PhD Dissertation, Technical University of Munich, 1996.
- [12] Kleeberger, M. and Günthner, W.A.: Abbildung der dynamischen Beanspruchungen von Gittermast-Fahrzeugkranen mit komplexen Auslegersystemen in quasistatischen Berechnungen (en: Calculation of dynamic loads of mobile cranes with complex boom systems in quasi-static calculations), Conference Proceedings 23. Kranfachtagung. Dresden, 2015.
- [13] Kleeberger, M. and Günthner, W.A.: Methoden zur Abbildung der dynamischen Beanspruchungen von Fahrzeugkranen in quasistatischen Berechnungen (en: Methods to calculate dynamic loads of mobile cranes in quasi-static calculations), Conference Proceedings 25. Kranfachtagung. Magdeburg, 2017.
- [14] Kleeberger, M., Schneidler, S. and Günthner, W.A.: Untersuchung der dynamischen Beanspruchungen von Gittermast-Fahrzeugkranen und Vergleich mit der quasistatischen Auslegung der Norm (en: Investigation of the dynamic loads of lattice boom mobile cranes and comparison with the static approach of the standard), Conference Proceedings 22. Kranfachtagung. Magdeburg, 2014.
- [15] Schneidler, S., Kleeberger, M. and Günthner, W.A.: Vergleich der dynamischen Beanspruchungen von Gittermast-Fahrzeugkranen mit den Ergebnissen der quasistatischen Auslegung nach DIN EN 13001 (en: Comparison of the dynamic loads of lattice boom mobile cranes with the quasi-static loads according to the standard DIN EN 13001), Conference Proceedings, 20. Kranfachtagung. Dresden, 2012.
- [16] Schweizerhof, K. and Fleischmann, N.: Erdbebenberechnung von Hochbauten mit Antwortspektrenverfahren-Überlagerungsregeln, Grenzen einfacher Modelle (en: Earthquake calculation of high-rise buildings with the response spectrum method-overlapping rules, limits of simple models), *Beton- und Stahlbetonbau*, Vol. 82, No. 5, pp. 117-122, 1987.
- [17] Stölzner, M., Kleeberger, M., Günthner, W.A. and Fottner, J.: Schwingungsmodell zur Abbildung der dynamischen Beanspruchung von Gittermast-Fahrzeugkranen und Lkw-Ladekranen (en: Vibration model to describe the dynamic behaviour of lattice boom mobile cranes and loader cranes), *Proceedings Logistics Journal*, 2018.
- [18] Trąbka, A.: Dynamics of telescopic cranes with flexible structural components, *International Journal of Mechanical Sciences*, Vol. 88, pp. 162-174, 2014.

Derrick crane subjected to repeated loads

Luigi Solazzi

Associate Professor
University of Brescia
Department of Mechanical
and Industrial Engineering

The goal of this research is the numerical study of a derrick crane subjected to repeated load conditions. The numerical analyses were carried out considering two different geometrical crane configurations, and two different rope lengths. After a preliminary analysis in order to evaluate both static and dynamic crane performance, many different analyses were carried out applying different load sequences. These actions were characterized by several impulse load. Two parameters define the impulse load i.e. the impulse duration and the delay between two successive impulses. This load condition, which isn't present in the crane design standards, was checked during the use of the crane itself in the marble quarry where it was installed. The results show that in particular crane configurations and with a specific load sequences both the vibration and the displacement magnitude increase in time inducing high stress value in the crane components that can collapse the crane itself.

Keywords: Dynamic Loading, Impulse Loading, Structural Vibration, Moving Load, Derrick Crane.

1. INTRODUCTION

The main action that acts on the crane structure is due to the payload. In particular, in addition to the payload, it is very important to consider also the inertia action induced by moving load that act on the crane [1,2,3], on the excavator [4], on the lifting equipment [5,6] and on the trailers [7]. In general, these actions are evaluated by a specific coefficient that multiplies the nominal load value; through this simple procedure it was estimated a load spectrum applied to the lifting machine [8]. The crane mechanical behaviour is completely different if we compare the actions induced by an earthquake or by the wind, with the action induced by moving load; in fact, in general the earthquake and wind actions are random and affect all crane parts [9,10,11]. The application of a repeated load on the crane shows a completely different mechanical behaviour, especially for displacement magnitude, compared to the load application and release, also sudden [5,12,13].

The focus of this research regards the effect on the structure of the same crane reported in [12] subjected to a repeated impulse load. A typical repeated actions appears when a jackhammer is applied to an arm machine. In this case many repeated load were applied to the machine structure itself [14]. This action type is frequent when it is necessary to position a component; in fact, in this case, in order to achieve a correct position many impulse loads were applied by the machine drive.

For example, in civil engineering, to build a structure it is necessary to locate a component in a specific position; in this case it is necessary to apply many repeated actions for lifting and lowering the load. In this

research many different impulse load sequences (impulse duration, delay between two successive impulses, impulse number, etc.) were numerical implemented to a derrick crane.

These actions were implemented in derrick crane with different geometrical configurations: the main arm in horizontal and in vertical position. In this numerical study also the ropes were implemented because these components influence both the dynamic factor (due to the lifting operations) and the friction coefficient [15]. For each geometrical configuration two different rope lengths were assumed.

The problem can be solved by analytical methods [16-17-18-19] however the crane object of this research is very complex, and the adoption of an analytical method could lead to excessive approximations.

In this research, the problem was solved by many numerical analyses especially by finite element method technique. As reported in the results section, this phenomenon is very important and dangerous; in fact, the displacement might diverge and, as a result, increase in time, so both the maximum stress value in the crane elements and the overturning moment increase. In addition to these aspects, the repeated impulse load induces vibrations and fatigue phenomenon in the crane components [20,21,22].

For these aspects, the focus of this research is on studying the derrick crane subjected to a specific load condition, not included in the standard procedures for crane design, but the effects can be very dangerous for this type of lifting machine.

2. CRANE DESCRIPTION AND FEM MODEL

The object of this research is a very large derrick crane; very briefly, it was composed of an arm with a length equal to 75 m, a central tower with a height equal to 45 m and two struts whose length depends on the site where the crane was installed. In general, the angle of

Correspondence to: Dr Luigi Solazzi, Associate Professor
University of Brescia, Department of Mechanical and
Industrial Engineering,
Via Branze 38, 25123 Brescia, Italy
E-mail: luigi.solazzi@unibs.it

inclination is 45° and so the length is approximately 60 m.

All the structural elements are obtained by assembling elementary blocks made of a reticular structure. More details on a very similar crane are present in [12]. Figure 1 represents the crane object of this research.



Figure 1. Derrick crane used in this research.

The geometrical configurations shown in this paper are two i.e. the crane with the arm angle equal to 85° (vertical position) and with the arm angle equal to 5° (horizontal position). In the first configuration the payload is equal to 60 t, while in the second configuration, this value is 30 t.

For each configuration two lengths of the load lifting ropes were considered, in particular a length equal to 0 m, that is modelling the payload positioned at the arm end, and a length of the rope such as to be able to have the load at -10 m from the support plane of the machine. For the 85° configuration the rope length is equal to 90 m while for the other configuration this length is approximately 15 m.

The rope to move both the arm and the payload is 6x36 Warrington-Seale with a diameter equal to 24 mm. According to the equivalent number of rope sections, the equivalent stiffness was evaluated by (1):

$$k_i = \frac{E \cdot A}{L_i} \quad (1)$$

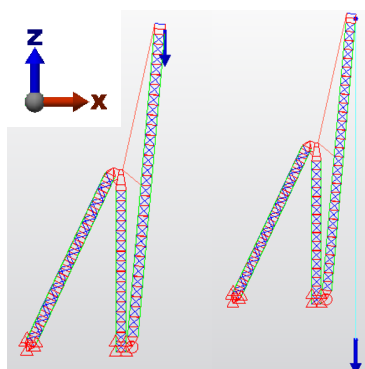


Figure 2. FEM model with arm position at 85°.

Once the rope stiffness value was determined, in the finite element model (FEM), it was modelled with beam-spring type elements.

The FEM models are shown in figures 2 and 3, they are made by means of quadratic formulation beam

elements for a total of about 100,000 elements. The analyses were carried out with Autodesk Simulation® software.

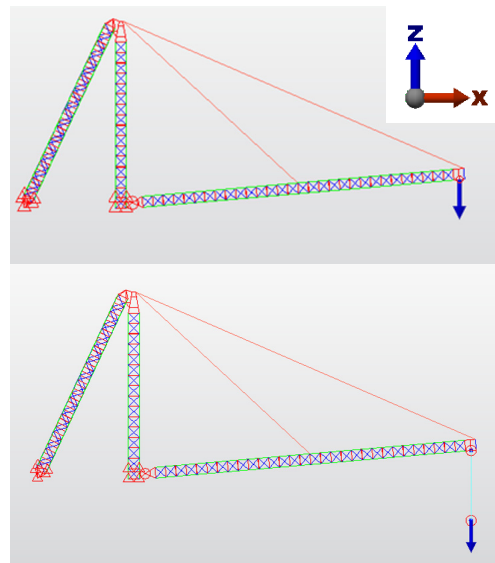


Figure 3. FEM model with arm position at 5°.

3. STATIC ANALYSES RESULTS

The load applied to the crane at 85° geometrical configuration is 78 t. This value derives from the payload (equal to 60 t) to which must be added the weight of the accessories (ropes, hook, pulleys) equal to 5 t, all multiplied by a dynamic factor set to 1.2. In the case of geometrical crane configuration at 5° the load applied to the crane is equal to 42 t.

Figure 4 shows the crane displacement for the two geometrical configurations. The maximum displacement value for 85° geometrical configuration is equal to 318.9 mm (-60.1 mm in z direction and 313.4 mm in y direction), while for 5° geometrical configuration it is 432.7 mm (-19.1 mm in x direction and -432.2 mm in z direction).

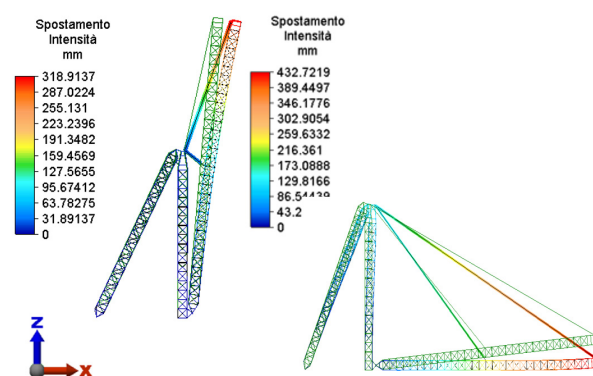


Figure 4. Crane displacement results for two geometrical configurations.

4. MODAL ANALYSES RESULTS

Figures 5, 6 and 7 show the structure displacement at the 85° geometrical configuration. They refer to the first two vibration modes with the largest mass percentage in the three directions (x, y and z). Table 1 shows the values

for the 85 ° configuration while Table 2 reports the values for the 5 ° configuration. For both configurations the sum of the participating mass involved in the vibration modes considering the first 60 natural frequencies is greater than 85% of total mass.

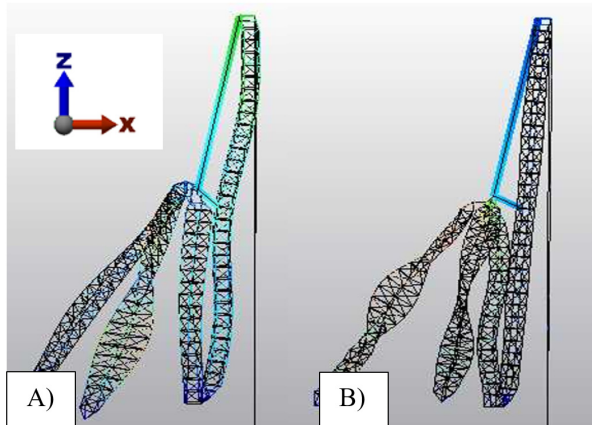


Figure 5. FEM model deformation in z direction: A) 11.96 Hz; B) 22.47 Hz..

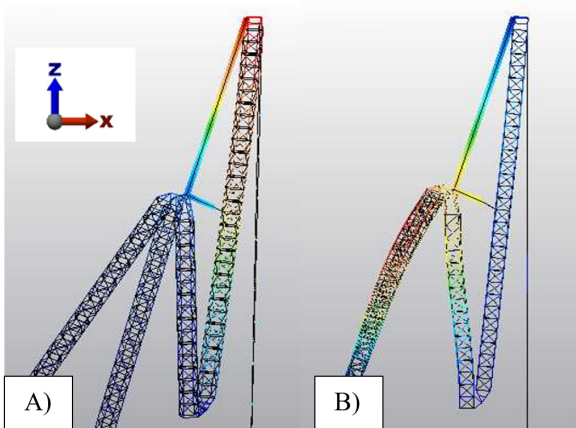


Figure 6. FEM model deformation in x direction: A) 0.816 Hz; B) 2.81 Hz.

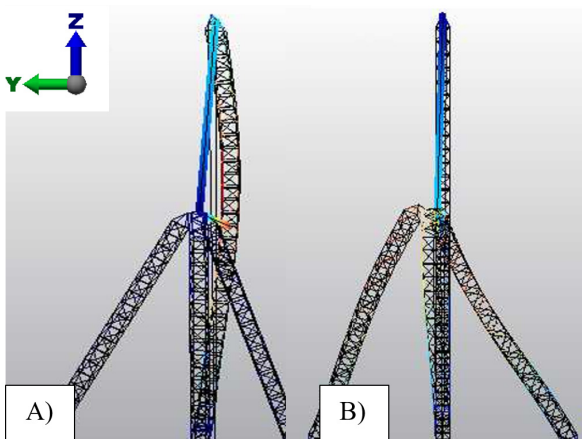


Figure 7. FEM model deformation in y direction: A) 1.619 Hz; B) 2.730 Hz..

From the values of the natural frequencies reported in the tables 1 and 2, it emerges that the structure presents distinct vibration modes in the three directions. From the comparison of the natural frequency values with and without a rope for payload moving, it emerges that, in general, the rope induces further vibration modes. These

natural frequencies are associated with a low mass rate because the weight of the rope constitutes a small percentage of the total weight crane.

Table 1. Natural frequencies and mass rate at 85° geometrical configuration.

Mode	Freq. [Hz]	X_Mass [%]	Y_Mass [%]	Z_Mass [%]
2	0.816	34.31	0.00	0.05
3	1.619	0.00	25.61	0.02
6	2.730	1.14	32.08	0.18
7	2.811	35.88	0.72	2.52
32	10.257	0.04	0.00	11.96
53	17.760	2.49	0.01	22.47

Table 2. Natural frequencies and mass rate at 5° geometrical configuration.

Mode	Freq. [Hz]	X_Mass [%]	Y_Mass [%]	Z_Mass [%]
2	1.094	3.00	0.00	34.90
3	1.669	0.00	25.91	0.00
5	2.732	0.01	33.06	0.02
8	3.481	22.14	2.68	0.14
32	10.820	21.52	0.01	0.05
47	17.435	2.72	0.02	28.25

5. DEFINITION OF LOAD CONDITIONS AND NUMERICAL ANALYSIS PROCEDURE

In the event that a component needs to be moved to a specific position, it often happens that the operator repeatedly executes the commands in order to reach the desired position. This load condition is not present in the crane design standards and its definition is quite approximate as a consequence of the fact that it depends both on the operator assigned to the machine, on the lifting device and on the load to be handled.

Through a series of experimental tests, it was noted that the time of the operator's action is very short and that the pause between one command and the next is variable.

These observations were conducted both in the marble quarry where the derrick crane is present, and in a mechanical firm where similar operations were checked for positioning a steel block on a work centre by means of an overhead crane.

For this reason, it was decided to study this effect with a load sequence composed by three load impulse whose duration is the same for all, i.e. $A = 0.1$ s while the delay between two repeated operations is variable and in particular $B = 0.3, 0.5$ and 0.8 s (figure 8).

All numerical analyses were conducted in the linear elastic range using Autodesk Simulation® software. The procedure adopted to resolve the dynamics equations is

direct integration method; what is fundamental for this technique is the integration step parameter which was assumed after a series of analyses performed in order to achieve the convergence of the numerical solution obtained. This value was assumed equal to 0.0005s.

Another fundamental parameter is the damping value which was assumed equal to 5% of the critical damping (plausible value for these types of structures). The damping value (2) in the matrix [C] depends on the parameters α and β which multiply both the mass matrix [M] and the stiffness matrix [K]. These parameters α and β are the Rayleigh coefficients whose values vary, depending on the geometric configuration of the crane and the presence or absence of the rope; in particular, the α value changes in the range 0.06-1.6 while the β value varies in the range 0.0006-0.0008.

$$[C] = \alpha[M] + \beta[K] \quad (2)$$

The load applied to the crane is equal to the 25% of the working load limit for each specific configuration; in particular for 85° geometrical configuration, the load is equal to 15 t, while the value is equal to 7.5 t for the second configuration.

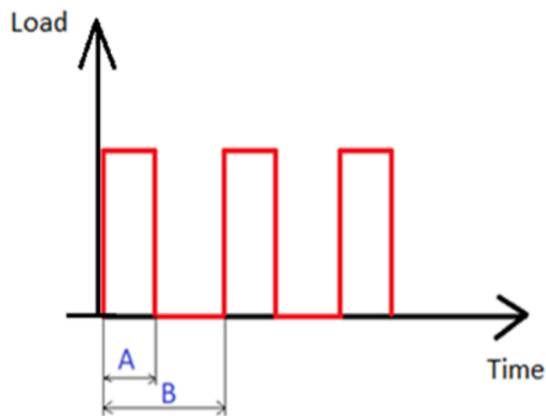


Figure 8 Schematization of the repeated impulse load applied to the crane.

6. RESULTS AT 85° GEOMETRICAL CONFIGURATION

The next paragraphs report the main numerical results acquired by FEM analyses.

6.1 85° Geometrical configuration

Figure 9,10 and 11 report the displacement in x direction acquired at the arm end for three different load sequences. The results concerning the configuration without the rope for fixing the payload.

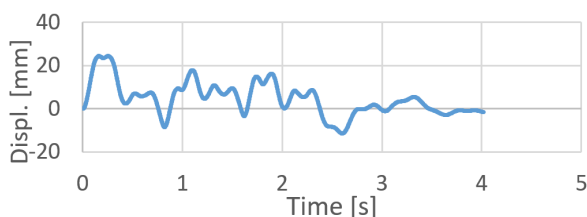


Figure 9. End arm x-displacement: A=0.1 s and B=0.8 s.

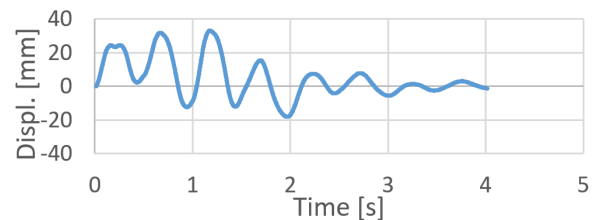


Figure 10. End arm x-displacement: A=0.1 s and B=0.5 s.

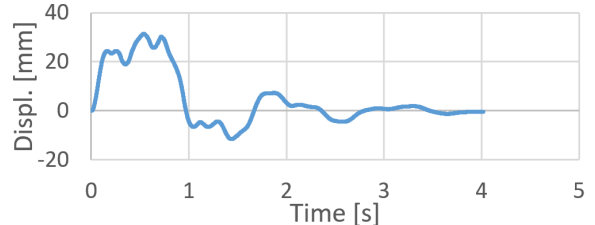


Figure 11. End arm x-displacement: A=0.1 s and B=0.3 s.

6.2 5° Geometrical configuration

Figure 12,13 and 14 report the displacement in z direction acquired at the arm end for three different load sequences. The results concerning the configuration without the rope for fixing the payload.

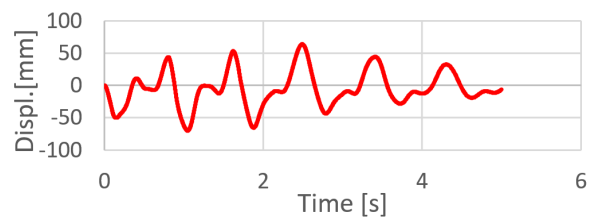


Figure 12. End arm z-displacement: A=0.1 s and B=0.8 s.

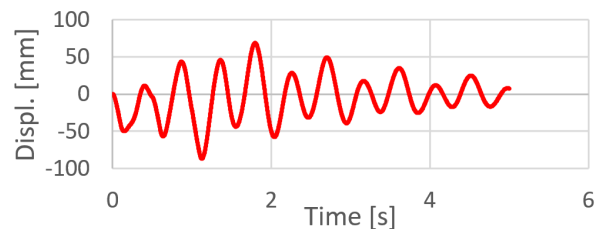


Figure 13. End arm z-displacement: A=0.1 s and B=0.5 s.

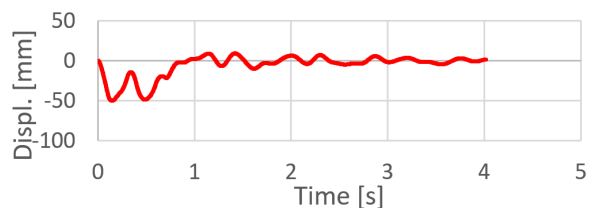


Figure 14. End arm z-displacement: A=0.1 s and B=0.3 s.

6.3 Remarks

The results for the two geometrical configurations show a progressive increase of displacement especially for A=0.1s and B=0.5s parameters for 85° configuration and for A=0.1s and B=0.8s and 0.5s for 5° configuration. It is possible also to observe that the displacement value, in some load conditions, changes in sign.

7. ROPE LENGTH EFFECT

Figures 15 and 16 show the displacement in z direction for the 85° geometrical configuration with $A=0.1$ s and $B=0.5$ s parameters with and without the rope for fixing the payload.

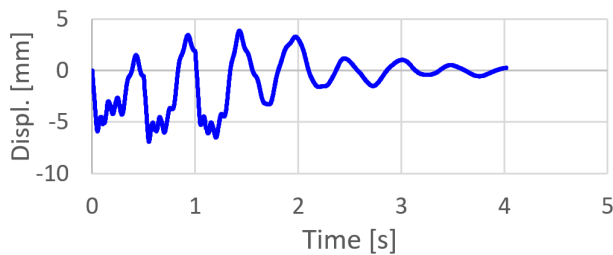


Figure 15. End arm z displacement: $A=0.1$ s and $B=0.5$ s, without rope.

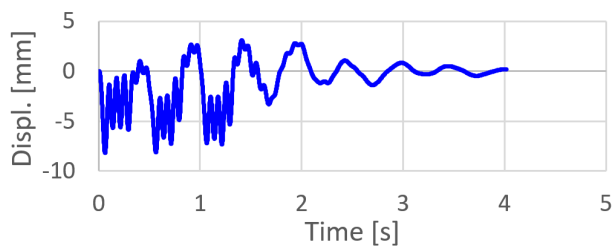


Figure 16. End arm z displacement: $A=0.1$ s and $B=0.5$ s, with rope.

By comparing of these figures is evident that the rope presence induces more vibrations in the crane structure (in this case the rope length is equal to 90m) respect to the situation without the rope.

8. RELATION BETWEEN IMPULSE LOAD ACTIONS AND CRANE NAURAL FREQUENCIES

Table 3 shows the correlation between the parameters A and B which define the load sequences with the first crane natural frequency for both 85° and 5° geometrical configurations without the rope.

Table 3. Natural frequencies and A e B parameters.

	85° Geometrical configuration	5° Geometrical configuration
Freq. [Hz]	1.346	0.719
A [s]	0.1857	0.3479
B [s]	0.7430	1.3916

Figure 17 and 18 show the displacement at the end arm for a derrick crane for these specific load conditions, which depend on the A and B parameters. The results concern a sequence composed by ten impulse load. It is important to highlight that this load condition can be really applied in the normal operation while using a crane. From the graphs, it is possible to underline that the displacement continuously increases in time.

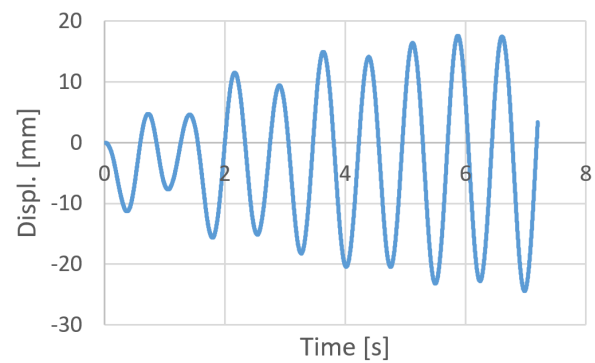


Figure 17. End arm z displacement, 85° configuration.

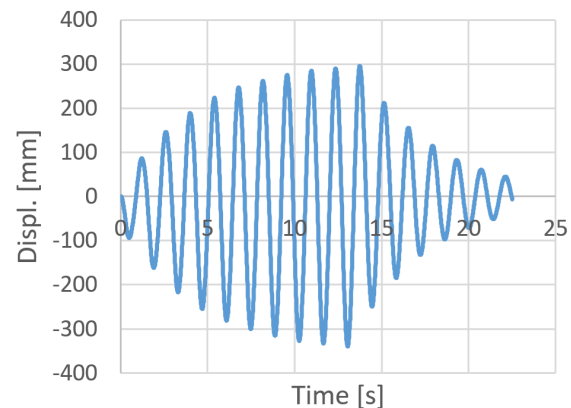


Figure 18. End arm z displacement, 5° configuration.

9. CONCLUSION

The present work reports the results of numerical analyses carried out using the finite element technique on a particular high performance derrick crane. The purpose of this research was to evaluate the dynamic behaviour of the crane which was subjected to a series of impulse loading. This load condition is not present in the crane design standards but may occur operationally during its use. To respond to the research purpose, 4 different crane configurations were studied, that is with a 85° and a 5° arm position and with or without a load moving rope.

The crane was characterized both statically and dynamically (by modal analysis) also evaluating the influence of the presence or not of lifting rope.

The operation by means of a impulse load, defined by the impulse duration and by the temporal delay between two consecutive pulses, generates in the crane a series of vibrations whose magnitude is dependent on the crane configuration and the sequence of impulse loading.

In the configuration in which the load sequences parameters bring the external action with the frequency near to the crane ones (absolutely plausible in-service load condition), it is possible to observe a progressive increase in displacements and their divergence over time.

This aspect induces obvious by an increase in the stresses values, on all the machine components (structure, ropes, winches, motors and gearbox) which can also lead to the collapse of the machine itself. Based on these results it emerges that the load condition given by a series of impulse load must be further investigated also on other lifting devices.

The objective of future researches is to correlate the lifting equipment natural frequencies with the parameters that characterize the load sequences, in order to avoid these load conditions (for example by a specific driver electronic control) that are very dangerous for the crane.

REFERENCES

- [1] Yildirim, Ş. and Esim, E.: A new approach for dynamic analysis of overhead crane systems under moving loads, *Lectures Notes in Electrical Engineering*, Vol. 402, pp. 471-481, 2017.
- [2] Rupar, D., Hladnik, J. and Jerman, B.: Loader crane inertial forces, *FME Transactions*, Vol. 44, No. 3, pp. 291-297, 2016.
- [3] Solazzi, L., Incerti, G. and Petrogalli, C.: Estimation of the dynamic effect in the lifting operations of a boom crane. *Proceeding of the 28 European Conference on Modelling and Simulation*, Brescia, Italy, pp. 309-315, 27-30 May 2014.
- [4] Solazzi, L., Assi, A. and Ceresoli, F.: Excavator arms: numerical, experimental and new concept design, *Composite Structures*, Vol. 217, pp. 60-74, 2019.
- [5] Solazzi, L.: Experimental and analytical study on elevating working platform, *Procedia Engineering*, Vol. 199, pp. 2597-2602, 2017.
- [6] Solazzi, L.: New design concept for lifting platform made of composite material, *Applied composite materials*, Vol. 20, No. 4, pp. 615-626, 2013.
- [7] Solazzi, L.: Applied research for Weight Reduction of an industrial Trailer, *FME Transactions*, Vol. 40, pp. 57-62, 2012.
- [8] Rahbar-Ranji, A.: Dynamic magnification factor in a box shape steel girder, *Journal of the Institution on Engineers (India): Series C*, Vol. 95, No. 1, pp. 11-18, 2014.
- [9] Solazzi, L.: Ship to shore crane subject to earthquake, *Procedia Engineering*, Vol. 10, pp. 2690-2695, 2011.
- [10] Wang, D., Wang, G., Xiong, Y. and Hu, J.: Analysis of nonlinear dynamic second order effect of a large scale container crane under seismic excitations, *Mechanisms and Machine Science*, Vol. 23, pp. 889-899, 2015.
- [11] Solazzi, L.: Stochastic wind loading applied to container crane, *FME Transactions*, Vol. 46, pp. 299-305, 2018.
- [12] Solazzi, L. and Zrnić, N.: Design of a high capacity derrick crane considering the effects induced by load application and release, *Journal of Applied Engineering Science*, Vol. 15, No. 1, pp. 15-24, 2017.
- [13] Haniszewski, T.: Preliminary modelling studies of sudden release of a part of the hoist load with using experimental miniature test crane, *Vibroengineering Procedia*, Vol. 13, pp. 193-198, 2017.
- [14] Jiong, L., Yu, W., Kai, Z., Zhiqiao, W. and Jixiang, L.: Design analysis of demolition robot arm based on finite element method, *Advance in Mechanical Engineering*, Vol. 11, No. 6, pp. 1-9, 2019.
- [15] Yang, S., Fang, X., Zhang, J. and Wand, D.: Dynamic behaviour of bridge erecting machine subjected to moving mass suspended by wire ropes, *Applied Mathematics and Mechanics*, Vol. 37, No. 1, pp. 741-748, 2016.
- [16] Lin, G.Y., Li, Z. Y., Wang, Z. G., Li, K.X.: A calculation of the crawler crane boom system's dynamic load in the lifting process, *Dongbei Daxue Xuebao Journal of Northeast University*, Vol. 36, No. 5, pp. 699-703, 2015.
- [17] Lin, G.Y., Cao, S.Q. and Guo, C.J.: analysis and control the influence factors on the dynamic load coefficient of the crawler crane working mechanism, *Advanced materials research*, Vol. 945, 626-632, 2014.
- [18] Posiadala, B., Warys, P., Cekus, D. and Tomala, M.: The dynamics of the forest crane during the load carrying, *International journal of structural stability and dynamics*, Vol. 13, No. 7, 2013.
- [19] Liu, J., Zhou, G. and Han, G.: Simulation model for in service rig derrick based on finite dynamic model, *Shiyou Xuabao, Acta Petrolei Sinica*, Vol. 30, No.5, pp. 788-792, 2009.
- [20] Zaretsky, A.A. and Shapiro, H.I.: Overturning stability of a free standing crane under dynamic loading. *SAE Technical Papers*, International Off Highway and Powerplant Congress and Exposition, Milwaukee, WI, 8-10 September 1997.
- [21] Ogrinec, P., Slavič, J., Cesnik, M. and Boltežar, M.: Vibration fatigue at half sine impulse excitation in the time and frequencies domains, *International Journal of Fatigue*, Vol. 123, pp. 308-317, 2019.
- [22] Li, X., Yan, X., Shuai, F. and Shen, Y.: Study on estimating fatigue life of main girder of portal crane, *Proceedings of 2018 Prognostics and system health management conference PHM*, Chongqing, China, pp. 1132-1237, 4 January 2019.

Gantry crane subjected to pendulum load actions

Luigi Solazzi

Associate Professor
University of Brescia
Department of Mechanical
and Industrial Engineering

The purpose of this research is to study the dynamic behaviour of a real gantry crane subjected to the actions induced by the trolley and payload movement. A specific numerical procedure was implemented in numerical analyses performed by finite element method in order to simulate the trolley movement on the crane's main beam. The study was conducted considering different trolley movement laws.

From the results, it is clear that the displacement, especially the longitudinal one, is strongly dependent on the acceleration both in the starting phase and in the stopping phase to which the trolley is subjected during its movement on the crane main beam. The last part of this research simulates the sudden stop of the trolley movement and subsequent payload swinging; in this case, the length of the rope that fixed the payload to the trolley has a fundamental role on the longitudinal crane displacement value.

Keywords: dynamic load, load movement, dynamic behaviour, dynamic analyses, lifting equipment, crane, finite element analyses.

1. INTRODUCTION

Lifting equipment are machines subject to many loading conditions, in particular the actions induced by the load movement. The dynamic effects assume a fundamental role regards the actions acting on the structure [1,2,3,4,5]. Obviously these actions are completely different to the other loading conditions such as seismic or wind actions which are applied to the whole structure and not only to the payload [6,7]. The vertical dynamic actions, which are obtained by multiplying (with a coefficient that in general varies from 1.2 to 2) the nominal load or working load limit of the lifting equipment [4,8], are particularly important. With these considerations, even the weight of the structure plays an important role, in fact the lightening of the machine structural components implies an increase in the performance of the machine as a consequence of the fact that the inertia actions are reduced [9,10,11]. In gantry cranes, in addition to lifting actions, also the actions induced by trolley movement are very important. These actions generate an oscillatory movement of the load and vibrations on the structure [12]. The magnitude of the oscillations and vibrations is highly dependent on the load handling law and especially also on the trolley movement speed [13,14,15,16]. It is obvious that the oscillation of the load must be limited in order to minimize the time required for coupling and uncoupling the payload [17,18]. For example, waiting for reduction the load oscillation before releasing the payload implies increasing the time necessary for loading and unloading a cargo-ship, which involves an increase in costs. The evaluation of the payload angle oscillation can be estimated both analytically and numerically [19,20].

It is possible to adopt methods based on concentrated parameters (lumped parametric system) [21,22,23], calculation methods that also take into account the elasticity of the structure [24], based on spectral methods [25], developed on logics of control "fuzzy" [26,27,28] or neural networks [29].

Other techniques are founded on making certain specific paths for payload in order to reach the final position without load oscillation [30]. The present research does not focus on the load or on the determination and control of its movement, but the actions that the translation of the trolley and subsequent pendulum of the payload generate on the structure. These actions, in general, are not provided in standards; however, from the numerical analyses carried out it emerges that they are very important. The present work is developed through a specific numeric procedure formulated and implemented in finite element analyses in order to simulate the trolley movement with different motion laws. The research also focuses on the phase when there is also the payload oscillation or load pendulum as a consequence, for example a sudden stop of the trolley translation, after which the payload starts swinging.

2. NUMERICAL PROCEDURE

One of the purposes of this research is the definition of a numerical procedure to be implemented in a finite element analyses (using a specific software) in order to simulate the trolley and payload movement. This procedure was implemented and applied to a specific and real crane.

2.1 Crane

The crane geometry structure, on which the innovative numerical procedure for the simulation of the trolley movement and payload swinging by using finite elements was implemented, is reported in the paper [23].

Correspondence to: Dr Luigi Solazzi, Associate Professor
University of Brescia, Department of Mechanical and
Industrial Engineering,
Via Branze 38, 25123 Brescia, Italy.
E-mail: luigi.solazzi@unibs.it

Specifically, and very briefly, the crane is a classic portal crane, the maximum payload is 60 t, the span is 40 m and the crane height is 15 m. On one side there is a leg realized by a rectangular section while on the other side the support of the main horizontal beam is made by two circular section legs. Numerical analyses were conducted with SolidWorks® and Autodesk Simulation® software. The fine element model is made by means of plate elements with a quadratic formulation for a total of about 10,000 elements.

At the base the crane columns were constrained with hinges. Figure 1 shows the photo of the crane used in the present research, while figure 2 shows the deformation of the crane in correspondence with the first two natural frequencies. The first value is 1.801 Hz while the second value is 4.788 Hz; they are very close to those reported in [23], which were estimated by analytical method.

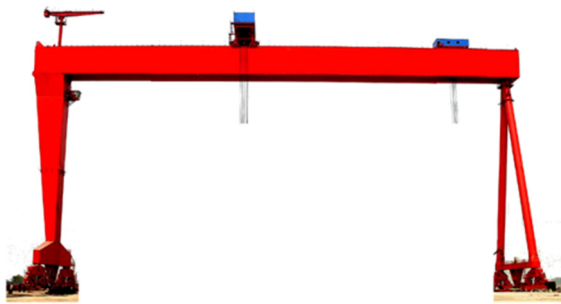


Figure 1. Crane.

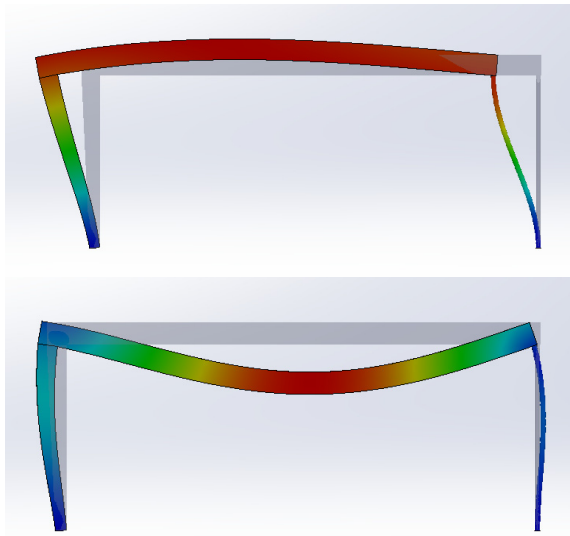


Figure 2. Main displacement in correspondence with the first two vibration modes.

2.2 Numerical Procedure

The definition of the calculation procedure to simulate a moving load is described in the following points.

The trolley moves with a defined law on the main crane beam. On this beam there are a series of forces whose intensity is equal to the maximum load generated by the trolley on the beam.

Each force is fixed in the space but linearly variable over time. The force at point n grows from zero when the trolley is at point $n-1$, the value is equal to the maximum

value when the trolley is at point n and returns to zero (in linear way) when the trolley moves to the point $n+1$. This schematization is shown in figures 3,4,5 and 6.

Obviously this procedure presupposes that the trolley action can be schematized with a single force, otherwise as in the case, two coupled forces should be adopted in order to simulate the trolley wheels. Another important aspect to underline is the fact that the forces must be applied in correspondence with the nodes of the mesh with which the beam was discretized.

In order to correctly assess the dynamic crane behaviour it is important to consider, in addition to the vertical forces, horizontal inertial forces that arise on the beam during start and stop phases of trolley movement.

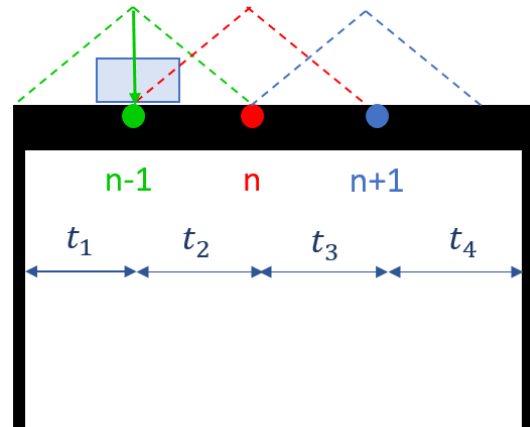


Figure 3 . The trolley is at $n-1$ point.

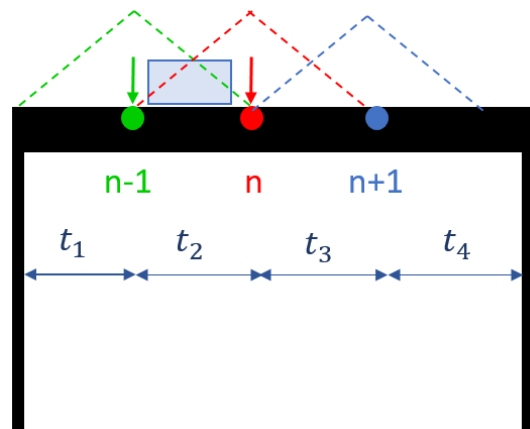


Figure 4. The trolley is at the middle point between $n-1$ and n .

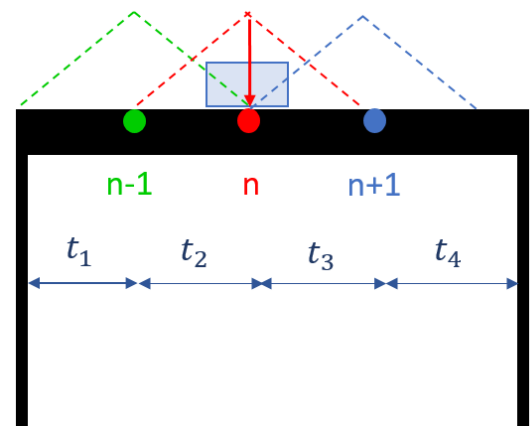


Figure 5. The trolley is at n point.

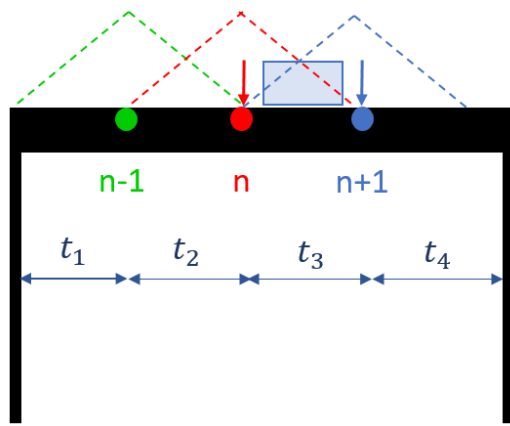


Figure 6. The trolley is at the middle point between n and $n+1$.

3. DIFFERENT TROLLEY MOVE LAWS

For the purpose of this research, different trolley movement laws were implemented. All these laws were characterized by a different value of the maximum acceleration imposed on the trolley. This value is the same both in the start and in the stop movement. Figure 7 refers to an acceleration equal to 0.6 m/s^2 (travel time = 16.7 s); figure 8 at 0.12 m/s^2 (travel time = 33.7 s), figure 9 at 3 m/s^2 (travel time = 12.7 s); while figure 10 refers to the implementation of a polynomial law in order to minimize the trolley acceleration (travel time = 23.1 s).

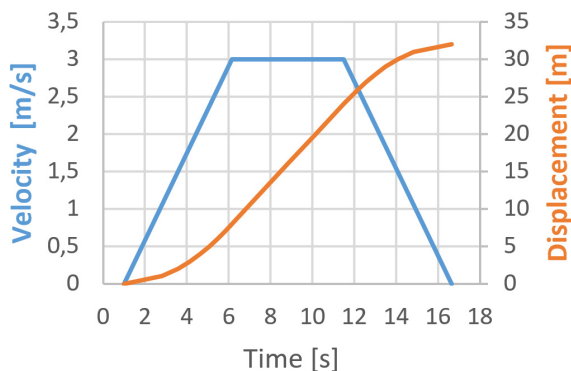


Figure 7. Trolley acceleration equal to 0.6 m/s^2 .

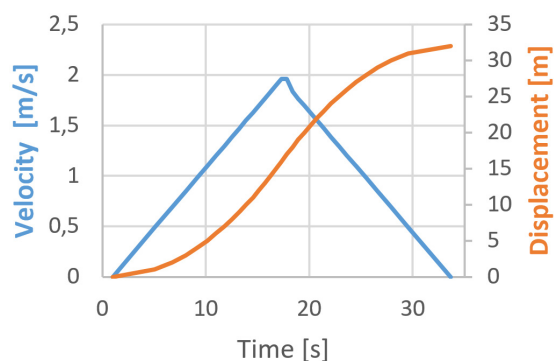


Figure 8. Trolley acceleration equal to 0.12 m/s^2 .

Figure 11 shows the displacement values for the midpoint or the horizontal beam in case when the trolley is moved with a law having an acceleration equal to 0.6 m/s^2 (figure 7). The maximum values are fully in

agreement with what reported in [23] where these values were determined by a discrete analytical solution.

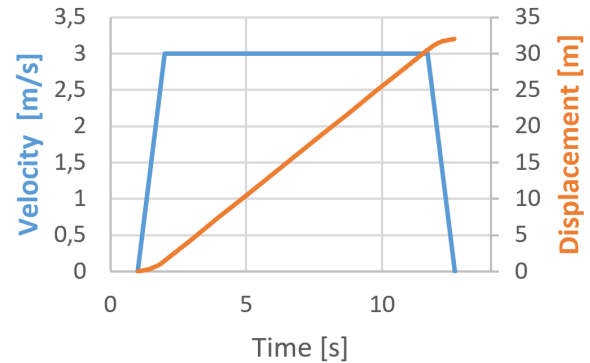


Figure 9.3. Trolley acceleration equal to 3 m/s^2 .

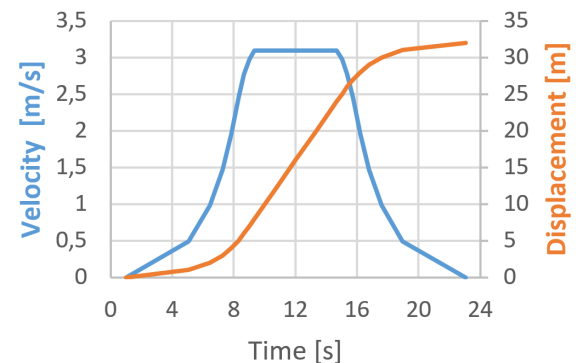


Figure 10. Trolley movement by polynomial law.

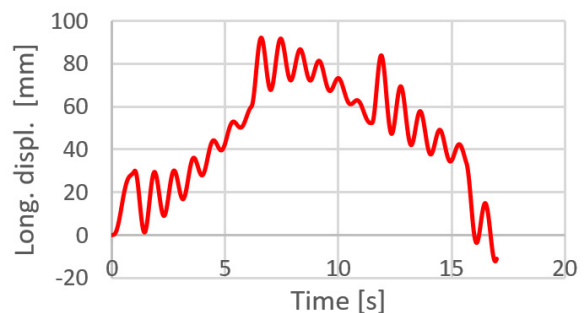
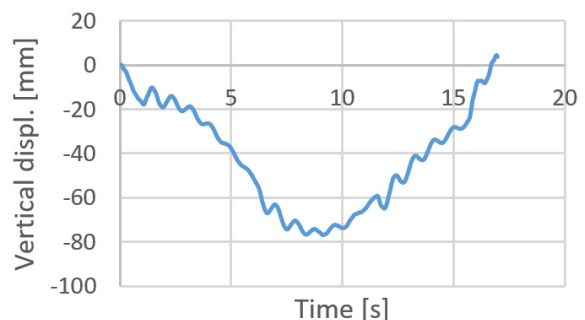


Figure 11. Displacement of the midpoint crane beam both in the vertical direction and in the longitudinal direction. The trolley was moved with an acceleration equal to 0.6 m/s^2 .

Figures 12 shows the displacements of the crane; from these graphs it is clear how the displacement both vertical and longitudinal is correlated to the maximum acceleration to which the trolley is subjected both in the start and stop phase movement. The solution of moving the trolley with a polynomial law (with the travel time

value is between the trolley movement laws one with acceleration equal to 0.12 m/s^2 , and second with acceleration equal to 0.6 m/s^2 leads to the minimum displacement of the crane main beam.

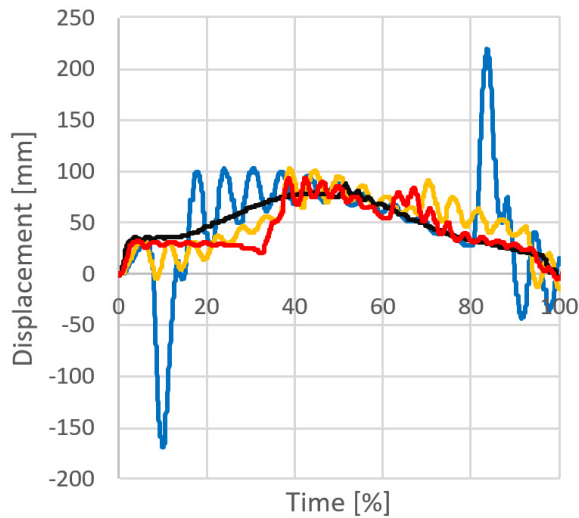


Figure 12. Longitudinal displacement for the middle beam point for different trolley moves laws. Blue acceleration= 3 m/s^2 , yellow acceleration = 0.6 m/s^2 , black acceleration = 0.12 m/s^2 , red polynomial law.

The results also show that the longitudinal displacement, especially in the phase of starting and stopping movement, is greater than the vertical one.

4. ARREST OF TROLLEY MOVEMENT

Based on the previous elaborations, it was decided to study the phenomenon in which the trolley movement is stopped abruptly when it is at the middle point of the crane horizontal beam. This loading condition corresponds, for example, to emergency stop of the trolley movement. Braking occurs with an acceleration of 5 m/s^2 . This value was determined assuming that the braking torque is equal to 1000 Nm and that it acts on the four wheels that support the trolley.

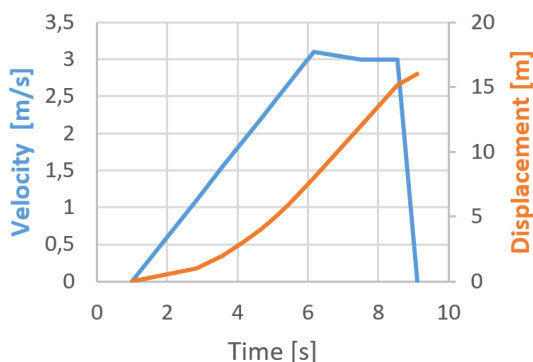


Figure 13. Trolley move law with abrupt stop.

Figure 13 shows the motion law applied to the trolley.

The payload distance from the trolley was simulated with the presence of ropes having different lengths as a consequence of the fact that, for example, a suitable damping coefficient is also associated with the rope presence [31,32].

4.1 Elaboration model

Figure 14 shows the schematization for this load configuration. In particular, the payload it was schematized like a point element. The motion of the pendulum is described by (1), while the expressions (2) and (3) show the values of tangential and centrifugal forces.

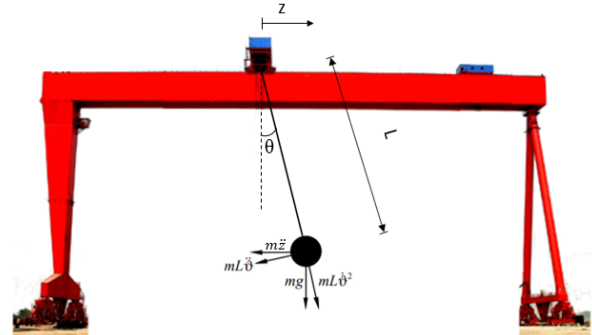


Figure 14 Payload schematization.

The equation that governs the motion of the pendulum can be determined in different ways, such as through the energy balance or Lagrangian method.

In any case, the angular position θ can be estimated by solving the following differential equation.

$$\ddot{\theta}(t) + b * \dot{\theta}(t) + \frac{g}{L} * \theta(t) = \frac{-\ddot{z}(t)}{L} \quad (1)$$

Tangential force is:

$$F_t = m * L * \ddot{\theta} \quad (2)$$

Centrifugal force is :

$$F_c = m * L * \dot{\theta}^2 \quad (3)$$

The pendulum natural frequency is

$$\omega = \sqrt{\frac{g}{L} - \frac{b^2}{4}} \quad (4)$$

Once the tangential and centrifugal forces were determined as a function of the position of the θ angle and as a function of time, they were decomposed into a horizontal and a vertical component. These forces were applied on a crane beam in correspondence with the position in which the trolley was stopped, which is equal to $1/2$ of the length of the crane main beam.

4.2 Rope length effect

In order to study this effect, three different rope lengths 0.216 m , 3 m and 17 m were simulated. It was assumed that the rope length was equal to 0.216 m (physically not feasible), in order to make the natural pendulum swing frequency equal to the crane one. The payload value adopted is equal to 15000 kg .

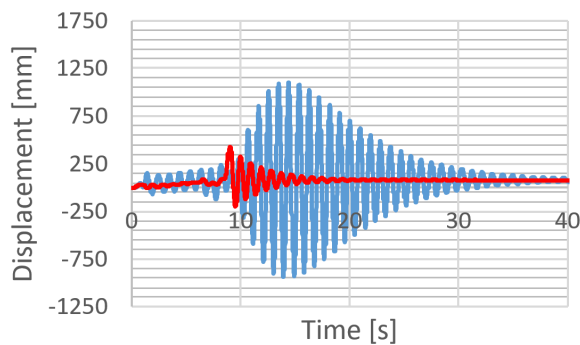


Figure 15 Longitudinal displacement, rope length =0.216m, blue with swinging load, red without swinging load.

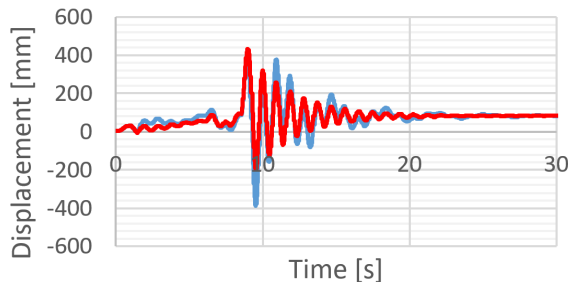


Figure 16 Longitudinal displacement, rope length =3m, blue with swinging load, red without swinging load.

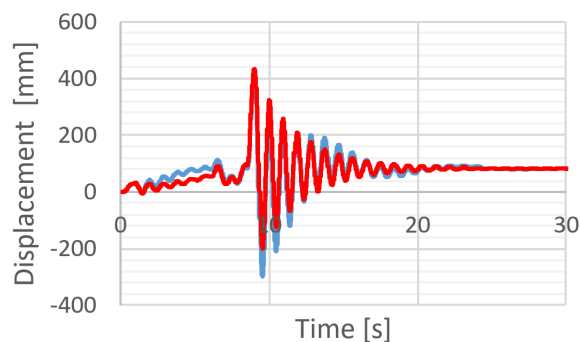


Figure 14 Longitudinal displacement, rope length =17m, blue with swinging load, red without swinging load.

Figures 16, 17 and 18 show the displacements of the midpoint of the horizontal beam for all three rope lengths. In particular, each graph shows the displacements considering and not the payload swinging.

The graphs show how the maximum longitudinal crane displacement in the configuration in which the rope length is 3 m and 17 m is close to 400 mm and that the effect of the payload swinging is particularly evident on the displacement magnitude at the second peak. In the theoretical case in which the rope length is equal to 0.216 m, the displacements diverge up to the values close to the 1 m (obviously considering the presence of the pendulum of the load) making this result absolutely physically unacceptable.

The sudden trolley stop movement accompanied by the swinging of the payload is therefore one of the most severe load conditions to which these types of lifting equipment can be subjected.

The present work reports the main results of numerical analyses carried out on a real gantry crane with working load limit equal to 60t subjected to the actions induced both by the trolley movement and by the payload swinging. To resolve this problem, a specific numerical

procedure was developed and was implemented in numerical analysis performed by finite elements.

The results obtained with the trolley acceleration equal to 0.6 m/s^2 , are reflected in the existing literature [23]. Different trolley move laws were implemented. The results show how the longitudinal displacement is strongly dependent on the acceleration with which the trolley is moved. In the case in which a polynomial law is adopted, the longitudinal displacement value is the minimum.

The work develops further as it also considers the effect of the swinging payload, which is evident when there is a sudden stop of the trolley movement. From the numerical results, it is important to highlight that the rope length that fixed the payload to the trolley is a fundamental variable that characterizes the longitudinal crane displacement.

On the basis of the analyses performed, it is therefore clear that the crane longitudinal displacement is absolutely not negligible nor are the actions induced on the structure.

The future developments concern the implementation of the numerical procedure described to other lifting machines in order to deepen the study of the interaction between the structure, the movement of the trolley and the payload swinging. Given the importance of this loading condition and in particular the sudden stop of the trolley movement, it is not excluded that this load condition can be proposed in the standards committee in order to include these actions in the rules for lifting equipment or crane design.

REFERENCES

- [1] Yildirim, S. and Esim, E.: A new approach for dynamic analysis of overhead crane systems under moving loads, *Lecture Notes in Electrical Engineering*, Vol. 402, pp. 471-481, 2017.
- [2] Solazzi, L. and Zrnić, N.: Design of a high capacity derrick crane considering the effects induced by load application and release, *Journal of Applied Engineering Science*, Vol. 15, No. 1, pp. 15-24, 2017.
- [3] Rupar, D., Hladnik, J., Jerman, B. and Yoo, S.C.: Loader crane inertial forces, *FME Transactions*, Vol. 44, pp. 291-297, 2016.
- [4] Solazzi, L., Incerti, G. and Petrogalli, C.: Estimation of the dynamic effect in the lifting operations of a boom crane, *Proceeding of the 28 European Conference on Modelling and Simulation*, Brescia, Italy, pp. 309-315, 27-30 May 2014.
- [5] Solazzi, L.: Experimental and analytical study on elevating working platform, *Procedia Engineering*, Vol. 199, pp. 2597-2602, 2017.
- [6] Solazzi, L.: Ship to shore crane subject to earthquake, *Procedia Engineering*, Vol. 10, pp. 2690-2695, 2011.
- [7] Solazzi, L.: Stochastic wind loading applied to container crane, *FME Transactions*, Vol. 46, pp. 299-305, 2018.
- [8] Kiviluoto, S., Eriksson, L. and Koiva, H.N.: Modelling and control of vertical oscillation in

- overhead cranes, Proceedings of the American Control Conference, pp. 1290-1295, 2015.
- [9] Solazzi, L., Assi, A. and Ceresoli, F.: Excavator arms: numerical, experimental and new concept design, Composite Structures, Vol. 11, pp. 60-74, 2019.
- [10] Solazzi, L. and Scalmana, R.: New Design Concept for a Lifting Platform made of Composite Material, Applied Composite Materials, An International Journal for Science and Application of Composite Materials, Vol. 20, No. 4, pp. 615-626, 2013.
- [11] Solazzi, L.: Applied research for Weight Reduction of an industrial Trailer, FME Transactions, Vol. 40, pp. 57-62, 2012
- [12] Maximov, J.T. and Dyunchev, V.P.: Investigation of dynamic response of "bridge girder telfer-load" crane system due to telfer motion, Coupled Systems Mechanics, Vol. 7, No. 4, pp. 485-507, 2018.
- [13] Korytov, M.S., Shcherbakov, V.S. and Titenko, V.V.: Comparative analysis of methods of cargo vibration damping moved by overhead crane, Journal of Physics: conference series, Vol. 1050, No. 1, 2018.
- [14] Osmanaj, S., Simnica, A.K., Limani, M. and Kabashi, Q.: The sensitivity of the hoist system in crane applications from speed control methods at induction motor, Elektrotechnik und Informationstechnik, Vol. 135, No.2, pp. 195-203, 2018.
- [15] He, W.: Vertical dynamics of a single –span beam subjected to moving mass suspended payload system with variable speeds, Journal of Sound and Vibration, Vol. 418, pp. 36-54, 2018.
- [16] Gašić, V., Zrnić, N., Obradović, A. and Bošnjak, S.: Consideration of moving oscillator problem in dynamic response of bridge cranes, FME Transactions, Vol. 39, pp. 17-24, 2013.
- [17] Zrnić, N., Petković, Z. and Bošnjak, S.: Automation of ship to shore container cranes: a review of state of the art, FME Transactions, Vol. 33, pp. 111-121, 2005.
- [18] Singhouse, W., Peng, K., Garcia, A. and Ferri, A.: Modelling and control of crane payload lift-off and lay down operations, FME Transactions, Vol. 44, pp. 237-248, 2016.
- [19] Ohtomo, S. and Murakami, T.: Experimental evaluation of estimated sway angle of payload in crane systems, IECON Proceedings Industrial Electronics Conference, pp. 146-151, 2014.
- [20] Ghafoori, E. and Younesian, D.: Dynamic analysis of gantry crane subjected to a moving trolley hoisting a swinging object, Eurodyn: European Conference on Structural Dynamics, Southampton, United Kingdom, 2008.
- [21] Bajer, C.I. and Dyniewicz, B.: *Numerical analysis of vibration of structures under moving inertial load*, Springer, 2012
- [22] Gašić, V., Zrnić, N. and Milovančević, M.: Considerations of various moving load models in structural dynamics of large gantry cranes, FME Transactions, Vol. 41, pp. 311-316, 2013.
- [23] Zrnić, N., Gašić, V., Bošnjak, S. and Đorđević, M.: Moving loads in structural dynamics of crane: bridging the gap between theoretical and practical researches, FME Transactions, Vol. 41, pp. 291-297, 2013.
- [24] Kimmmerle, S.-J., Gerdt, M. and Herzog, R.: Optimal control of an elastic crane trolley load system a causes study for optimal control of coupled ode pde systems, Mathematical and Computer Modelling of Dynamic Systems, Vol. 24, pp. 182-206, 2018.
- [25] Shu-Rui, W., Yhi-Jing, W. and Nian-Li, L.: High precision solution to the moving load problem using an improved spectral element method, Acta Mechanica Sinica / Lixue Xuebao, Vol. 34, No. 1, pp. 68-81, 2018.
- [26] Omar, H.M.: Developing anti swing fuzzy logic controller for suspended loads by genetic algorithms, International Journal of Applied Engineering Research, Vol. 9, No. 16, pp. 3455-3468, 2014.
- [27] Pal A.K. and Mudi, R.K.: An adaptive fuzzy controller for overhead crane, Proceedings of the 2012 IEE International Conference on Advanced Communication Control and Computing Technologies, Ramanathapuram, India, pp. 300-304, 2012.
- [28] Ding, Y., Wei, J. and De Cai, L.: Study on overhead crane anti swing system with self-adjustable fuzzy control, Applied Mechanics and Materials, Vol. 128-129, pp. 1050-1053, 2012.
- [29] Abe, A.: Anti-sway control for overhead cranes using neural networks, International Journal of Innovative Computing Information and Control, Vol. 7, No. 7B, pp. 4251-4262, 2011.
- [30] Habibi, H. and O'Connor, W.: Payload motion control of rotary gantry and luffing cranes using mechanical wave concepts, Transactions of the Institute of Measurement and Control, Vol. 39, No. 11, pp. 1649-1662, 2017.
- [31] Kim, C.W., Hong, K.S. and Lodewijks, G.: Anti-sway control of container cranes as a flexible cable systems, Proceeding of the IEE International Conference on Control Applications, Taipei, Taiwan, pp. 1564-1569, 2-4 September 2004.
- [32] Bartolini, G., Orani, N., Pisano, A. and Usai, E.: Load swing damping in overhead cranes by sliding mode technique, Proceeding of the IEE International Conference on Decision and Control, Sydney, Australia, pp. 1697-1702, 12-15 December 2000.

Thorsten Schmidt

Professor
Technische Universität Dresden
Faculty of Mechanical Engineering
Institut of Material Handling
and Industrial Engineering

Tobias Müller

Research Assistant
Technische Universität Dresden
Faculty of Mechanical Engineering
Institut of Material Handling
and Industrial Engineering

Integrative concept for a lift mast of industrial trucks with electric drives

As part of a pre-competitive research project, a concept for an industrial truck lift mast is being developed that consists of only a few wear parts and is powered exclusively by electrical components. An energy recovery takes place in the lowering mode. This requires a new approach in the design of lift frame profiles. The lift mast should be operated purely electrically, consist of few components and have a compact design. Furthermore, it should be able to produce a telescopic stroke of approx. two meters with a payload of one ton. A preferred variant resulted from different concepts, which is shown in a simulation model and which is used for a theoretical energy analysis.

Keywords: lifting mast, industrial truck, push chain, energy recovery.

1. INTRODUCTION

Current lift masts are dominated by hydraulic drives, which realize all lifting, lowering and sideshift as well as tilting movements. Hydraulic systems are proven, robust, compact and flexible. Furthermore, hydraulics offers a previously unattainable power density. What has been solved so far by compact actuators must be compensated by elimination of the hydraulic system. This is achieved with the help of electrical and mechanical components which previously required larger dimensions. Disadvantages of hydraulic systems are short maintenance intervals as well as the inefficient energy recovery of the potential energy during the lowering processes due to the multiple energy conversion. Current electrical systems have a significantly more efficient energy recovery and higher efficiency with much more maintenance-friendly operation. Although many industrial trucks have an electric traction drive, a purely electrical operation of the lifting mast is not yet known. Attachments are also increasingly being electrically powered, e.g. the electric tine arm position of KAUP. Approaches to electrically controlling lifting masts are provided, e.g. by the patents DE1020008022487A1 [1] and US2514563A [2], in which the two non-telescopic mast arms are designed as threaded spindles. An energy recovery in this way is not possible. In addition, there are pure mechanical operating variants, but these are predominantly hand-guided and non-telescopic, see DE2403181A1 [3].

This article presents concepts for an electric mast. The preferred variant from the concepts is illustrated in a simulation model and compared to a theoretical energy consideration.

2. CONCEPT ANALYSIS

Lift masts consist of the essential components drive, lifting frame and traction mechanism, which are available

in different versions. In hydraulically operated systems, compact actuators control the lift mast. The hydraulic pump used as drive provides the necessary hydraulic pressure, valves control the movement of the lift frame and also take over the load holding function as well as a protection against uncontrolled lowering in case of

leakage. The concept of the electric lift mast by definition eliminates the hydraulics. Thus all functions of hydraulic components are replaced by electrical and mechanical components. This has an effect on the lift mast design, in particular the design of the mast frames, the load-holding function and the drive concept, which influence each other. The design objective is to integrate as many components as possible inside the lifting frame to protect them from external interference and environmental influences.

2.1 Safety consideration

Lift masts are used exclusively for the movement of goods and are not subject to the relevant safety restrictions of passenger transport. In passenger transport, e.g. in elevator areas according to [4], safety gears are required to prevent the cabin from falling. In addition, the service brakes and the traction equipment are redundant. All these requirements are not relevant for the lifting gear, nor are buffers or dampers mandatory. In conventional lifting frames, the traction devices, e.g. roller or Fleyer chains, are dimensioned with a sufficiently large safety factor. Hydraulic actuators involved in the lifting process must limit the lowering process to 0.6 m/s in the event of a leak [5] in order to prevent uncontrolled lowering. Even in current industrial trucks, there are no redundant safety measures for the breakage of hydraulic lines, chains or other components. They are subject to regulated maintenance intervals.

2.2 Selection of lifting frame

Lifting frames exist in different profile structures as well as constructions with different characteristics, especially with regard to telescope design. Current lifting masts have a fixed, outer lifting frame (fixed mast) on which an internal, movable mast is supported (traction mast). Both lifting frames are usually made of steel and

Correspondence to: Dr Thorsten Schmidt, Professor
Technische Universität Dresden, Institut of Material
Handling and Industrial Engineering,
Georg-Schumann-Bau, A312, 01062 Dresden, Germany
E-mail: thorsten.schmidt@tu-dresden.de

thus contribute to a high deadweight at an unfavorable position of the industrial truck. Previously, lightweight construction was not implemented in industrial trucks. Only the concept study cubeXX by STILL introduces a mast made of carbon components. Another approach to a lightweight solution is provided by DE102009039218A1 [6]. The research project pursues the approach that an outer movable lifting frame is supported by a fixed inner frame. The outer lifting frame has a larger profile than the inner one. Larger profiles possess greater stiffness and can therefore be lighter designed. Figure 1 shows the described approach with an sample cross section. The cavities between the lifting frames could be used for brakes, cables, sensors or the lifting frame guide, while the inside of the lifting frame is available for the mechanical components and traction equipment.

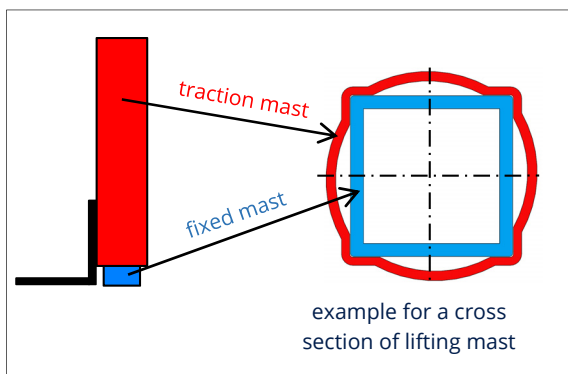


Figure 1. Approach for the mast concept with an exemplary cross-section

The design of the lifting frame is initially designed for a single-mast construction. The results can be transferred to a two-mast design, as it is common in industrial trucks. Further examples of this approach to the lift frame design can be seen in Figure 2.

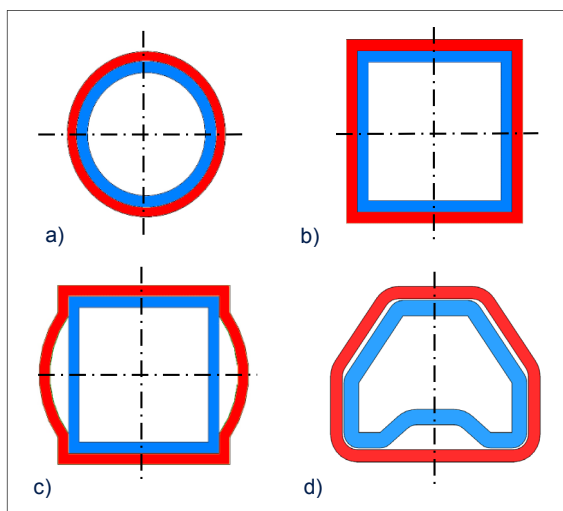


Figure 2. Further examples of lifting frame cross-sections

Figure 2 a) shows pipe profiles for the lifting frame cross section, which must be secured against rotation of the lifting frames in the one-mast design. Figure 2 b) is the angular counterpart to the above-mentioned profile, which can be found in the telescopic arms of telescopic handlers or cranes. Profiles c) and d) again have gaps which could be used for elements to secure and guide the lifting frames and to carry cables and sensors. Nevertheless,

they are much more expensive to produce and less compact, which restricts visibility more. For these reasons the profile in Figure 2 b) should be favoured.

2.3 Concepts for load holding

When holding the payload and the mass of the frames, the first question is how the braking function works. The following possibilities for brake design exist: Locking brake, release brake, service brake with or without redundancy. A locking brake closes when actuated, a release brake behaves contrary to the locking brake. A service brake allows a malfunction that has no serious consequences. E.g. the spring-applied brake closes in the event of a power failure and the sufficiently dimensioned spring packs hold the effective mass without any problems and prevent a load crash. With additional redundancy, a malfunction is permitted without affecting the function of the brake. Using the example of a dual-circuit spring-applied brake, another circuit runs through the brake coil, so if one circuit fails, another circuit can take over. For use of the electric mast in small forklift trucks and high-platform trucks, the holding functions of the fork carrier dominate. A raised fork carrier is used, e.g. for the ergonomic loading of goods and also during the transport process, see Figure 3. For this reason, the holding function by means of the currentless spring packs of the service brake is the most energy-efficient solution. Redundancy of the service brake is not required for transport of goods and is therefore not considered.



Figure 3. Frequent applications for holding the load in operation with industrial trucks

2.3.1 Load holding function on the drive engine

Holding the mass of the telescopic components of the lift frame can be done in different ways. Electromechanical spring-applied brakes, which brake the load directly at the elevator door, are known from elevator construction. This possibility could also be realized on the extended drive shaft of the electric motor in the electric mast, see Figure 4. Whereby a lower torque has to be braked, which reduces the dimensions.

A disadvantage of this arrangement is that the load is held by the drive train of the lifting frame. In the event of a traction mechanism crack or gear damage, the brake would become inoperative.

Another application of the spring-applied brake in direct braking action on separate rails of the lifting frame results in a very large dimension of the brakes, which would miss the goal of a compact lifting frame. Pneumatic brakes are considerably more compact than

electromechanical brakes of the same power. Pneumatic links represent an additional medium in the lifting mast that requires greater effort. This is why they are not analysed in detail.

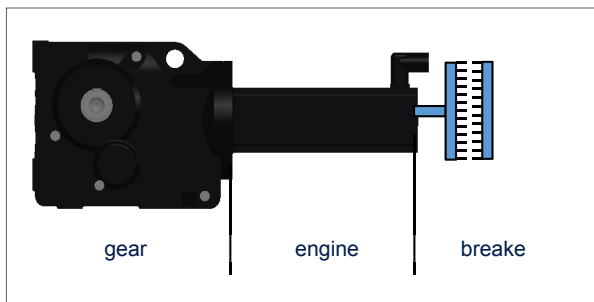


Figure 4. Spring-applied brake on the extended drive shaft of the electric engine

2.3.2 Load holding functions by piston brakes

Another option for an electromagnetic load holding function is the piston brake. This design would not secure the traction mechanism, but directly the outer lifting frame. The piston rod is connected to the outer lifting frame, the piston brake to the inner lifting frame, see Figure 5. This would not secure the fork carrier, so that a further load-holding function is required. Piston brakes achieve greater braking forces than the usual spring-loaded brakes. Nevertheless, several piston brakes are required for the expected holding force. Although these piston brakes do not have to be lifted, they occupy a lot of the space inside the stroke frame, which limits the dimensioning of the frames.

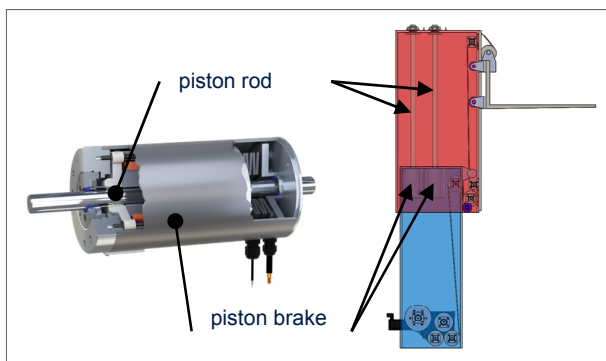


Figure 5. Piston brake using a CAD model as an example

2.3.3 Load holding function through form-closure

Due to the high dimensions of the electromechanical brakes, an alternative brake solution is being searched for. This can be e. g. in the form-closure by saw tooth as well as eccentrically mounted pinions. Figure 6 shows an example of a form-closure connection between a brake rail with toothed rack located on the inner lifting frame and a counterpart mounted on the outer lifting frame. This load holding function can also be used on the fork carriage. It is actuated by so-called lifting magnets. Figure 7 shows a similar load holding function in which the form-closure is realized by an eccentric operated by rotary magnets with the toothed rack.

Advantages of this type of load-holding function are the low power requirement for control as well as a safety

device independent of the traction mechanism. In the case shown, the load would also be held in the event of a power failure because the spring force permanently secures the form-closure.

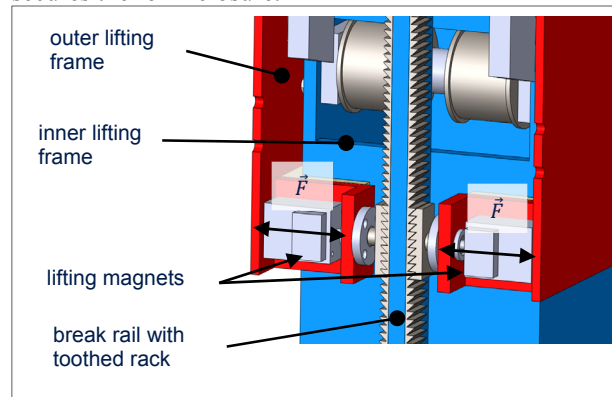


Figure 6. Load-holding function by saw-tooth gearing, actuated by lifting magnets

Disadvantages are the abrupt stopping process, which is accompanied by a slight position shift. The suitable gearing may not be found immediately or the eccentric needs a way to activate the form-closure due to the rotation. Furthermore, lifting of the lifting frame is unavoidable to release the load holding function.

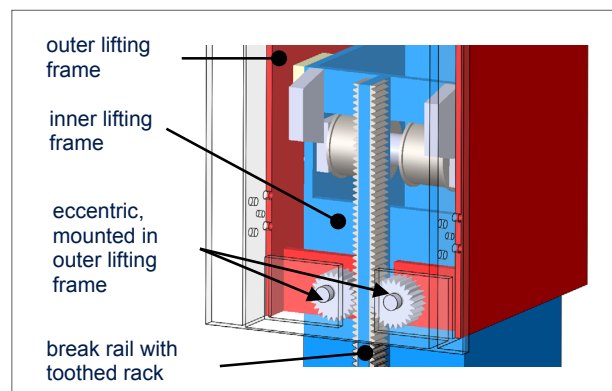


Figure 7. Load holding function by eccentric, actuated by rotary magnets

With saw-tooth gearing, the moving mass of the lifting frame rests on the individual tooth flanks and the intentionally small dimensioned lifting magnets would not release the friction between the tooth flanks of the saw-tooth gearing without lifting. If the eccentric is used, it has to be unscrewed from the gearing, which also requires lifting of the lifting frame. The positioning accuracy is quite important for lifting masts, so that an application in operation would not be realizable without further effort, but is conceivable as a concept study for a mast that is as energy-efficient as possible.

2.3.4 Load holding function by jamming the traction mechanism

Another possibility of the load-holding function is the fasten of the traction mechanism, as it is known, e. g. from winch technology. Two symmetrically arranged wedges are supported on a fixing, the traction mechanism runs in the middle, see scheme in Figure 8. The greater the force of the traction mechanism, the greater the contact force of the wedges on the traction mechanism.

Each wedge is controlled by a linear drive. Linear drives transmit the high tensile and compressive forces required to release the wedge from the load-holding function. The advantage of this load-holding function is the simple design inside the lifting frame. Disadvantages are the required linear drives, which not only require a high power requirement, but whose control is slower than with hoist drives. Furthermore, the traction mechanism is subject to high wear due to direct contact with the wedges and the associated pressure and relative movement.

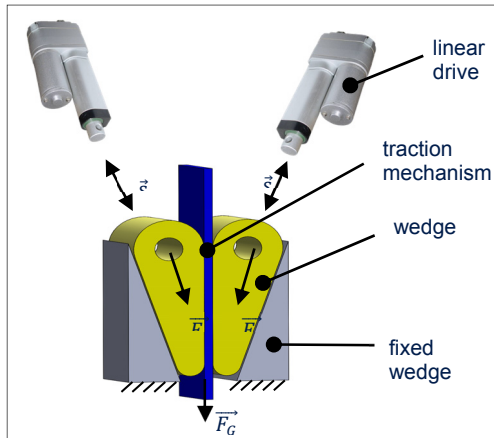







Figure 8. Load-holding function by wedges on the traction mechanism, controlled by linear drives

2.3.5 Evaluation of the load holding function

The load holding function is evaluated by a weighted point rating according to [8]. The highest priority is the power requirement for controlling the load holding function, which should be as low as possible. The securing of the traction mechanism has the lowest priority, because a securing of the traction means is not required for the transport of goods. From these considerations, the spring-applied brake on the extended drive shaft achieves the best result and is selected for the lifting mast concept. Table 1 shows the result of the evaluation.

Table 1. Evaluation of the load holding concepts

						
	power for brake control	4 x 126 W	4 x 30 W	4 x 7 W	2 x 30 W	1 x 85 W
	mass of the brake	4 x 26.000 g	4 x 1300 g	4 x 85 g	2 x 85 g	1 x 30.000 g
weigh- ting	criteria	piston brake	to jam the traction mechanism	braking with form closure through sawtooth gear	braking with form closure through eccentric	spring loaded brake on the engine
0.65	compact design	1	4	3	3	4
0.39	dead weight	1	4	5	5	3
0.47	reaction rate	5	2	4	4	5
0.71	positioning accuracy	5	2	2	1	5
0.88	handling during operation	5	1	3	2	5
0.47	constructive effort	3	5	3	3	5
0.06	securing the traction mechanism	5	1	5	5	1
0.18	wear traction mechanism	5	1	5	5	3
1.00	spent power	1	3	5	4	4
sum		14.8	12.6	16.9	14.4	20.7

2.4 Traction mechanism analysis

Various traction mechanism can be used for the vertical movement of the lifting mast. E.g. due to their maintenance-free operation, their high tensile strength at low mass and their long lifetime, timing belts are already being used successfully in hoist drives of storage and retrieval machines [9,10,11] and represent a viable alternative for chain drives. The efficiency of both enveloping drives is almost the same and is between 0.95

and 0.98 [10,12]. Similar efficiencies are also achieved by wire rope drives. Wire ropes and timing belts require larger sheave diameters than chains or flat belts for a long lifetime. Belts generally require less maintenance because chains or ropes have to be relubricated regularly. In addition, gear solutions using cardan shafts or gear racks are also conceivable. Known from stage technology, push chains or folding spindles, also known under the name Spiralift, are also possible variants.

With folding spindles, the spindle is formed as a tube from a horizontal and vertical spiral belt. In the lowered state, both belts are pushed together in a package like a spiral spring. In the lifting process, the two belts are form closed and helically connected to a column. The push chain consists of block-shaped links which interlock in a form closed manner and thus straighten up into a lifting column. This lifting column can only be bent in one direction. Push chains and folding spindles compete in the field of stage technology because they have similar lifting speeds [13]. There is currently no comparison of the wear behaviour between the two lifting mechanisms. The mechanism of the folding spindle shows if the belts start to wear, the form closure between the belts provides less support and the risk increases that the payload will suddenly fall down. Furthermore, a minimum compressive force must always be available for the functionality of the folding spindle, otherwise the form closure between the horizontal and vertical belts will be lost [13]. This minimum compressive force cannot be guaranteed when operating industrial trucks, as the fork carriage with the forks also lie on the ground during storage. For this reason, folding spindles are not considered as a further alternative to the lift frame concept. Push chains can absorb tensile and compressive forces and always form a form-closer structure, so that the payload can be held securely even when wearing occurs. Theoretically, a scissor lift inside the lifting frame is also conceivable. This would require a very large amount of space, so that this variant will not be pursued any further. The use of the traction mechanism depends on the drive concept, which is presented below.

2.5 The drive concept

The design of the drive concepts depends on the selected traction mechanism and the lifting frame profile. Not every variant is suitable for the free lift that required by industrial truck users.

2.5.1 Drive concept with gears

Figure 9 shows a drive concept with gears for power transmission. It consists of tube profiles. In the interior runs a cardan shaft with gears. The engine torque is transmitted to a cardan shaft by a bevel gear. It is then transmitted to a differential gear. Due to the characteristics of differential gears, the outputs can be shifted in different ways so that a free lift is possible by controlling the gear accordingly. Up to the first lift stage, the differential gear distributes the transmittable torque exclusively on the shaft to the wrapping storage, so that only the fork carriage is moved by the traction mechanism. After the second lift stage, the output of the

differential is additionally distributed to the pinions for the rack. The outer lifting frame is moved while the drive train to the fork carriage continues to be loaded. The slipping clutch compensates excessive tensile forces for the fork carriage and keeps it under tension, as the path of this traction mechanism changes during the movement of the outer lifting frame. In the lowering mode, the traction mechanism for the fork carriage must continue to be kept under tension, e.g. by braking the wrapping storage.

If this drive concept were considered without free lift, its design would be considerably easier, because a simple bevel gear is sufficient and the clutch and the wrapping storage are no longer required. By moving the outer lifting frame, the fork carriage would be moved simultaneously by the traction mechanism, which is fixed on the inner lifting frame. The round cross-section of the profiles provide a high degree of stiffness, but the mounting of shafts or bearings on uneven surfaces is difficult. The free lift variant is complex in terms of control and due to the differential gear with clutch and wrapping storage requires a large amount of space at high mass in the upper area of the inner lifting frame, which is unfavourable for stability.

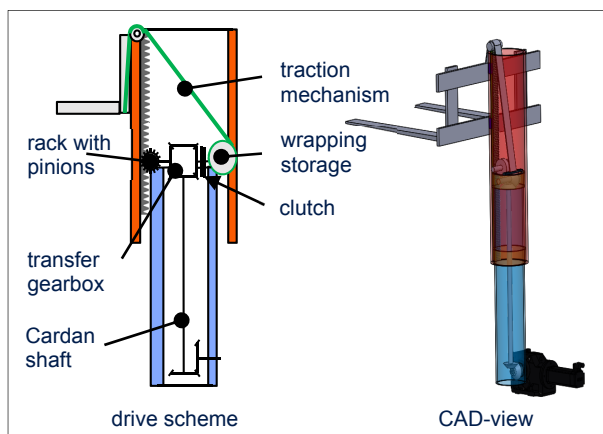


Figure 9. Drive concept with gears and cardan shaft (not to scale)

2.5.2 Drive concept with a loose pulley

Figure 10 shows a drive concept in which the traction mechanism of a wrapping storage moves a loose pulley displacing the lifting frame and fork carriage in the same way as other traction mechanisms. The traction mechanism of the loose pulley is attached to the lower ends of the outer lifting frame and is supported by the inner lifting frame. The loose pulley not only halves the load on the traction mechanism, it also compensates for any tensions that may be caused by the load on the fork carriage. Therefore, the outer lifting frame is always lifted synchronously.

The fixation of the traction mechanism for the fork carriage at the inner lifting frame ensures that the outer lifting frame and fork carriage extend simultaneously. A free lift is not possible with this variant. This option has a simple structure with very few components. The wrapping storage ensures a variable speed of the traction mechanism, which must be compensated by a corresponding motor control. Especially for using a loose

pulley, the length to be stored for the wrapping storage is very large.

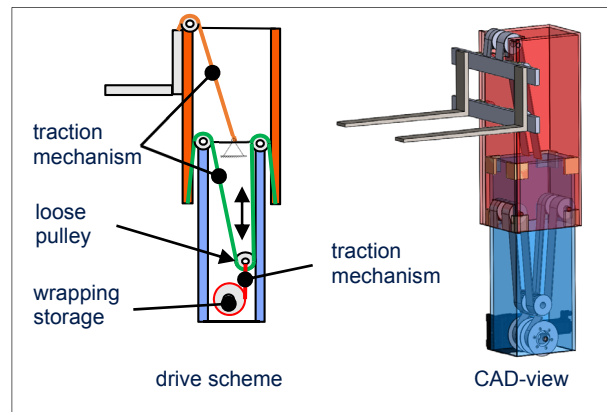


Figure 10. Drive concept with loose pulley (not to scale)

A large diameter variation in the wrapping storage results in a variable engine torque. The engine needs to be dimensioned correspondingly large.

2.5.3 Drive Concept with omega drive

The drive concept, shown in Figure 11, solves the problem of varying engine torque with an Omega drive. Not only the two ends of the timing belt are connected to the carriage, but also the outer lifting frame. By driving the timing belt, the slide slips past the inner lifting frame and moves the outer lifting frame. The fork carriage is fixed as in the previous drive concept and moves simultaneously with the outer lifting frame. Free lift is not possible with this drive concept either. This drive concept is more complex than the loose pulley, but due to the Omega drive it has a low-maintenance drive with always the same torque. The deflection pulleys are larger when using a timing belt when using a flat belt. This drive concept is slightly larger in terms of dimensions.

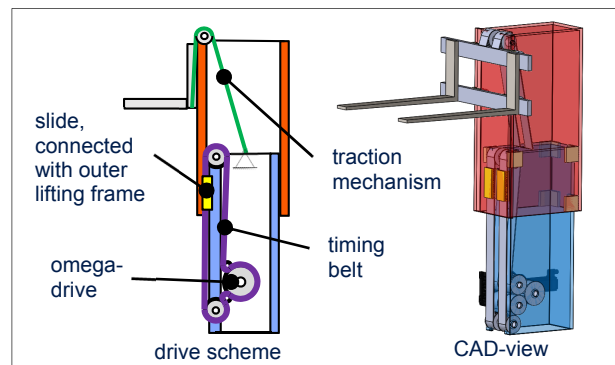


Figure 11. Drive concept with omega drive (not to scale)

2.5.4 Drive concept with circumferential traction mechanism

Figure 12 shows a drive concept with circumferential traction mechanism, preferably flat belts, which is supported by the respective lifting frame. This concept has already been published in publication DE 2403181 [14]. A practical implementation is not known.

The approach provides a free lift by first moving the fork carriage and then the outer lift frame with fork carriage. This function is only fulfilled if the payload with

fork carrier is smaller than the mass of the outer lift frame.

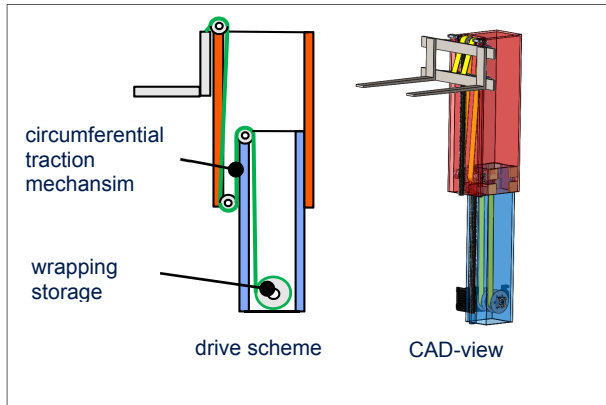


Figure 12. Drive concept with circumferential traction mechanism (not to scale)

The system strives to balance the mass between the fork carriage and the outer lifting frame by means of the circumferential traction mechanism, as shown schematically in Figure 13.

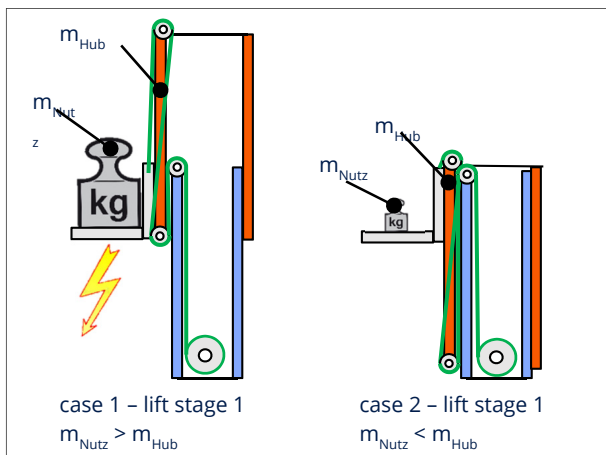


Figure 13. Problem of mass balancing with different payloads

In the case that the mass of the fork carriage and the payload is greater than the weight of the outer lifting frame, as shown in case 1, the fork carriage would extend in the first lift stage together with the outer lifting frame. In the reverse variant, as shown in case 2, a free lift is possible. In practice, it is not possible to differentiate between light and heavy masses, but the mast must always extend reliably. This is not the case in this variant, especially as working in narrow spaces is impossible or even dangerous in case 1. This variant offers solutions. One solution is the design of a loose pulley on the fork carriage, as shown in case 3 in Figure 13. The danger of mass balancing is reduced by a factor of two by granting the free lift with twice the payload compared to the mass of the outer lifting frame. However, the danger of mass balancing is not solved.

In the second approach, mass balancing can be prevented by locking the lifting frames and the fork carriage in each other's positions, as shown schematically in Figure 14.

Lock 2 between the lifting frames is active when lifting to the first lift stage. If the first lift stage is

exceeded, the locking device 1 between the fork carriage and the outer lift frame must first be closed and then the locking device 2 released, otherwise there is a risk of mass balancing.

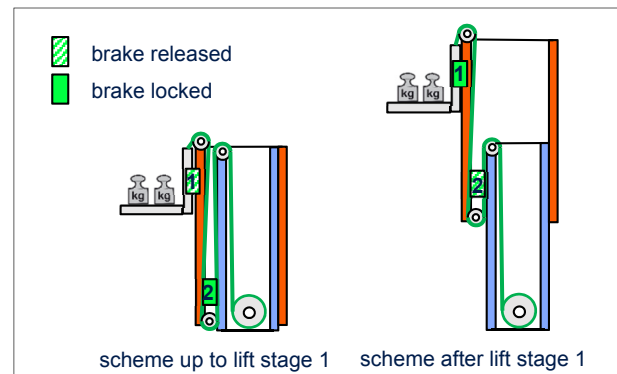


Figure 14. Preventing mass balancing by locking the lifting frame and fork carriage

When lowering from the second lift stage to the first, lock 2 must first be closed, then lock 1 can be released. The description shows that the operation must be interrupted briefly between the change of lifting stages, which causes delays. The locking device could be designed similar to the load-holding function like Figure 6, whereby the gearing must be a square, as the loads on both sides act on the gearing, caused on the one hand by the working mass and on the other hand by the mass balance. The disadvantage of this locking mechanism is that it requires an additional distance between the lifting frame as well as between the outer lifting frame and the fork carriage. In addition, with this drive concept the traction mechanism runs between the lifting frames, which means that the mast is approx. 25 % longer. This distance, which also represents a leverage effect, must be guided in a complex manner. There is also the danger that the contact tooth flanks of the profile rail and counterpart may lead to high friction for the release process during load holding or mass balancing. This requires strong linear drives, which need a great power requirement and also a high dead weight, which must always be lifted.

2.5.5 Drive concept with push chain

Figure 15 shows another variant for an electric drive concept with a push chain. Push chains in lifting masts have already been published in EP3106421B1 [14] and DE102012100356A1 [15], whereby the latter patent application refers directly to an industrial truck, but has not yet been implemented in practice.

The push chain is driven by a pinion and is attached at one end to the fork carriage. Thereby the fork carriage is moved first and a free lift is realized. The outer lifting frame is slotted on the side of the fork carriage so that it can be guided through it. A cross beam in the lower area and the stop for the fork carriage in the upper area connect the outer lifting frame. At the transition from the first to the second lifting stage, the fork carriage moves against the stop of the outer lifting frame and telescopes it. The push chain is stored inside the lifting frame. By attaching the other end of the push chain to the inner lifting frame, it is stacked inside and deflected again.

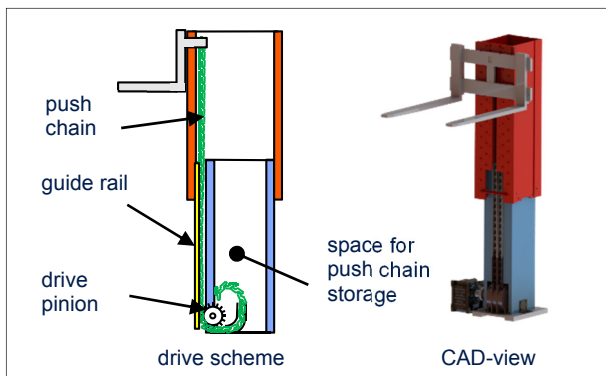


Figure 15. Drive concept with push chain (not to scale)

The push chain is additionally guided through a sheet metal up to the height of the inner lifting frame. In the telescoped state, the chain is guided through the outer lifting frame. As the push chain can only bend in the direction of the forks, a guide to the inside of the lifting frame is not necessary.

The functional principle of this drive concept is similar to that of hydraulically operated lifting frames. It has a free lift in a relatively simple design with a small number of assemblies and a small space requirement. The disadvantage is the maintenance, because the chains have to be lubricated regularly, as well as the lower efficiency compared to the other drive concepts. In [16] an efficiency of 0.8 to 0.9 is given, in [17] it is given in connection with a storage in magazines of 0.65.

2.5.6 Evaluation of drive concepts

The evaluation of the individual drive concepts is performed analogous to the evaluation procedure of the load holding function. From a requirements matrix, the individual requirements are compared with each other. The result is the weighting. Particularly important requirements are the free lift, the expected dimensions of the outer lifting frame and the complexity of the entire drive concept. The estimated dead weight, the constant drive torque and the maintenance of the traction mechanism used are considered less important. On the basis of this weighting and the evaluation of the individual concepts, an evaluation matrix is created in which the drive concept with push chain is preferred. Table 2 shows the results of the evaluation of drive concepts.

Table 2. Evaluation of the drive concepts

	concept 1	concept 2	concept 3	concept 4	concept 5
criteria	gears	loose pulley	omega drive	circumferential belt	push chain
previous cross section of outer lifting frame	ca. 400 mm	ca. 370 mm x 500 mm	ca. 500 mm x 600 mm	ca. 378 mm x 670 mm	ca. 340 mm x 504 mm
weighting					
0.867 Dimensions	3	5	1	2	5
1.000 free lift	5	1	1	5	5
0.200 constant drive torque	1	1	5	5	5
0.400 maintenance	2	5	5	3	2
0.667 complexity	2	5	3	1	5
0.067 estimable deadweight	2	5	3	3	2
0.667 number of parts	2	4	3	1	5
0.400 efficiency traction mechanism	3	4	5	5	2
sum	11.2	13.3	8.8	10.5	17.5

2.6 Design of the preferred variant

The lifting frames of the preferred variant are designed in the form of the thrust field support construction. The fixed mast is closed by an U-profile. The inside of the fixed mast is used for chain storage. The

push chain is in the form of a double push chain and has lateral rollers for guidance in the recess of the fixed mast through the U-profile. The rollers of the pivot bolts are guided by means of corresponding webs which are attached to the fixed mast as well as the traction mast. This also ensures a chain guide in the extended position, which prevents the push chain from bending during operation. The lifting frames are separated laterally and on the unloaded side by plastic sliding blocks. In the range of the fork carriage, the lifting frames are mounted on roller bearings in relation to each other. The fork carrier is guided vertically by support rollers and laterally on the mast by combination rollers. In the upper range of the mast there is the stop, where parts of the fork carriage push when extending. The lower part of the mast is closed by a T-profile. Figure 16 shows a side cut of the preferred variant with stored push chain. Figure 17 shows the preferred variant in plan view and illustrates what is described.

A permanent servomotor with gears is used as drive. This motor design optimally combines power and dimensions. In addition, geared motors are not only lighter than gearless motors, they can also be mounted more flexible.

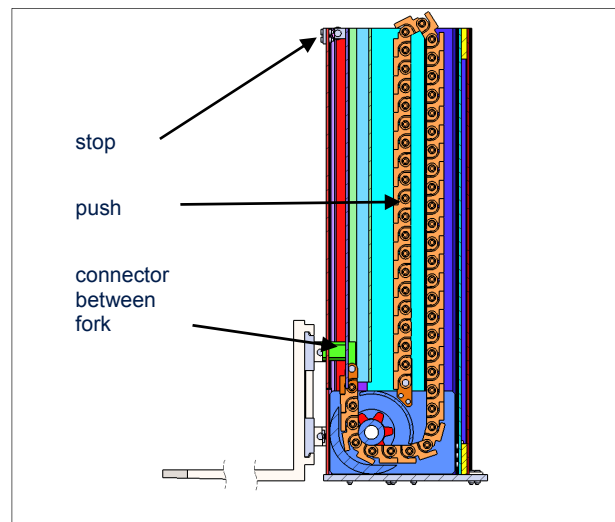


Figure 16. Preferred variant in lowered state in lateral cut

3. DYNAMIC SIMULATION

A detailed CAD model exists for the manufacturing of the lifting frame. This model has been considerably simplified for simulation in order to save computing time and effort, e.g. screw connections have been modified or omitted. The thrust field support construction was combined and the fork carriage was also replaced from one component. The push chain was not considered for the moment, because its simulation, with its many individual links, is too complex and time-consuming.

The dynamic simulation was performed with Inventor Professional 2019. All elements are considered as rigid bodies. For the simulation, the individual components were combined into assemblies so that the model consists of the following components: outer and inner lifting frame, base plate, fork carriers and support rollers. The lifting frames contain the sliding blocks, the base plate the attachment for the fixed mast, the fork carriage the

connector and the support rollers the attachment to the frame. The model is shown schematically in Figure 18.

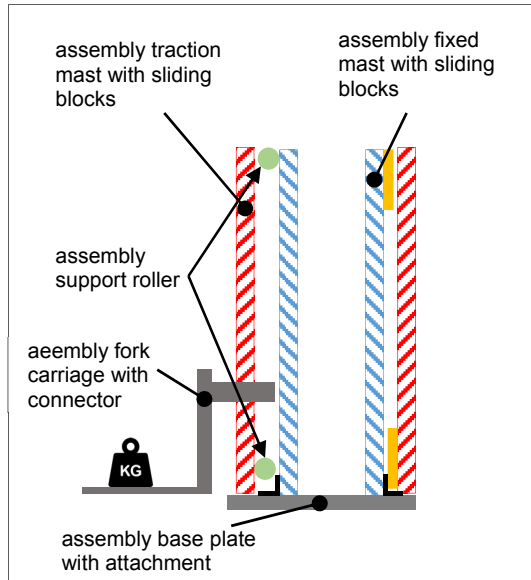


Figure 18. Schematic illustration of the structure of the simulation model

The effective mass is 100 kg, the lifting and lowering speed is 300 mm/s, the lifting height is 2 m. The coefficient of friction between steel materials for rolling friction is 0.1. In contact with the sliding blocks, this coefficient of friction is also assumed because the sliding surfaces between the steel and the material POM for the sliding blocks are lubricated. The damping for the joints is assumed to be 10 N*s/mm, because at lower damping values the mast jumps on the fork carriage connector during lifting, which cannot be explained physically. Figure 19 shows a lifting operation. It shows the impact that occurs at the transition between the lifting stages. Despite the damping, the impact causes 2.5 times the effective mass to be lifted. It can be seen that after the second lifting stage the load is higher due to the additional weight of the mast. The moving loads for the time of the maximum load are transferred to a finite element analysis to determine the deformation of the lifting frames and the connector, see Figures 20 to 22.

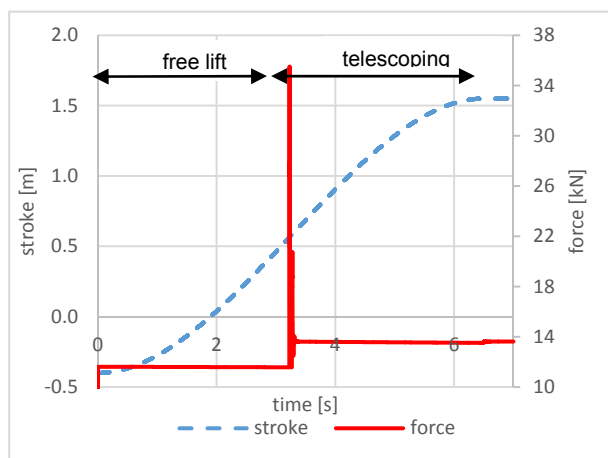


Figure 19. Impact load in the stroke movement at the crossing of the lifting stage

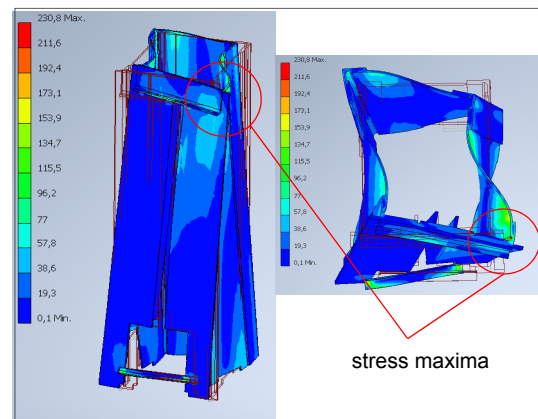


Figure 20. Stresses at the traction mast at the crossing of the lifting stage (increased strain condition)

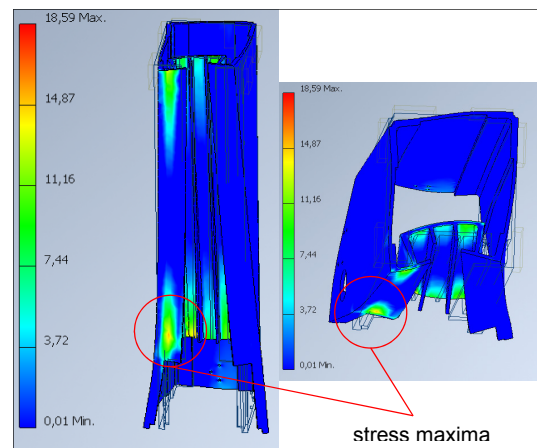


Figure 21. Stresses at the floor mast at the crossing of the lifting stage (increased strain condition)

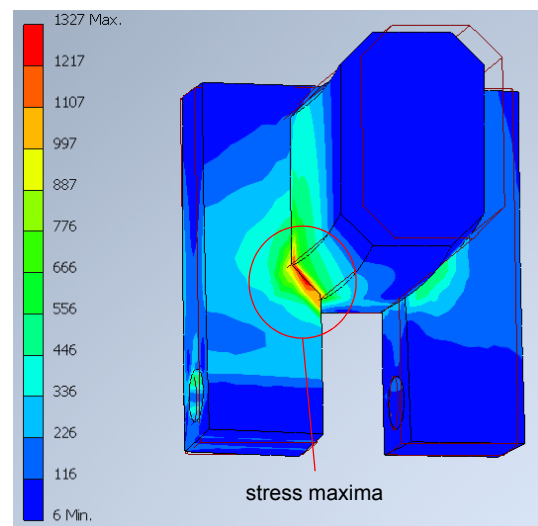


Figure 22. Stresses at the connector at the crossing of the lifting stage (increased strain condition)

The lifting frames are not symmetrically constructed due to mounting holes or recesses for the drive shaft. Furthermore, the analysis was based on an asymmetrical load on the forks (7000 N and 3000 N) in order to consciously assume no ideal load. Accordingly, asymmetric stresses are also expected.

The traction mast is rotated about its longitudinal axis and is subjected to the highest stress in one of the thrust field supports in the upper range. The slotted mast tries to split the mast, but the L-profile at the top and the T-

profile at the bottom of the mast prevents it. In the cross-section, see Figure 20 (right), it can be seen that the mast buckles inwards at the sides. The mast is also buckled inwards at the sides in the upper range, and strongly twisted in the fork carriage range. The mast is subjected to the greatest stress on a thrust field support used to guide the push chain. In all cases, the stresses are below the yield strength, so that there is no danger to the lifting mast. Only in the connector, see Figure 22, are the stresses considerably higher, but they are caused by instability of the mesh at a sharp notch. All other areas have non-critical stresses. The connector achieves its greatest stress when the lines of force are deflected from horizontal to vertical. Stress-reducing radii or chamfers allow more homogeneous transitions to the lines of force action. These were adapted according to the construction data.

When extended, the lifting frames overlap by 500 mm. The slotted design of the traction mast is subjected to particular stress, which is why the maximum stress occurs on the lower cross plate, see Figure 23. The stresses are lower overall than in the case of impact, and the twists are not as great either. The same applies to the fixed mast, see Figure 24.

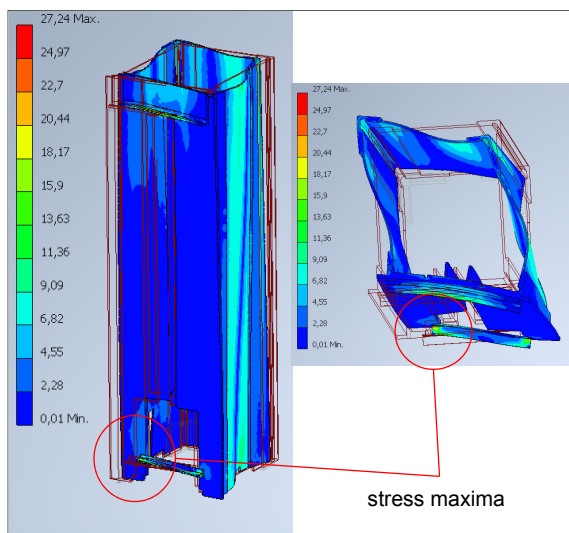


Figure 23. Stresses for the extended traction mast (increased strain condition)

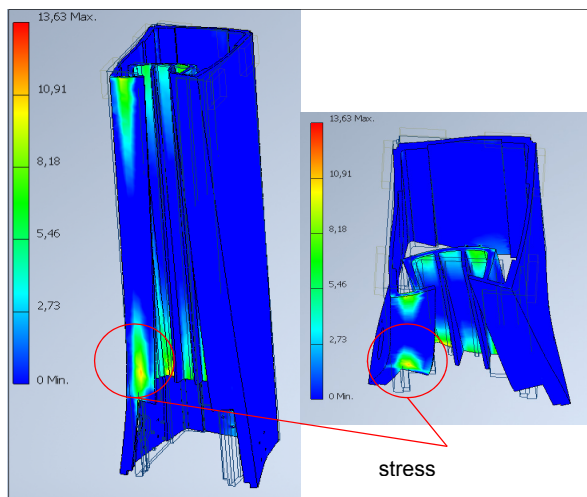


Figure 24. Stresses for the fixed mast in the extended state of the lifting mast (increased strain condition)

The dynamic simulation was also used to investigate emergency stop situations. The fork carriage with mast lowers at 300 mm/s and is abruptly stopped shortly before the second lift stage. This impulse can be seen in Figure 25 at approx. 2.5 seconds, which is 2.8 times higher than the usual stress. According to this, the emergency stop situation is roughly comparable to the impact of the transition in the lift stage. This situation describes in practice, e.g. the operation of the emergency stop switch or a power failure.

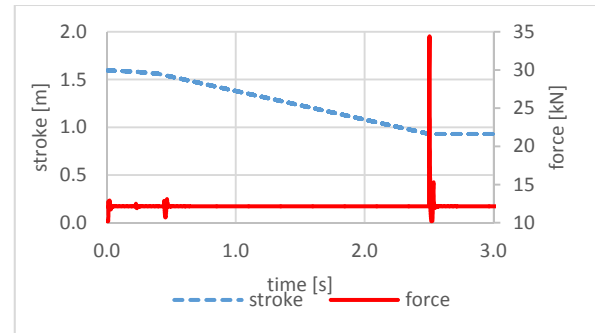


Figure 25. Emergency stop situation with the telescoped lifting mast

4. ENERGY EFFICIENCY CONSIDERATION

In view of constantly increasing energy costs [18], increasing competition among industrial truck manufacturers, research into an efficient mast is of great importance as lifting mast systems determine the handling capacity of an industrial truck to a great extent. Energy recovery in particular increases the energy efficiency of a system.

Up to now, energy recovery has only been carried out on electro-hydraulic lifting frames by using the hydraulic pump as a motor and the electric machine as a generator during the lowering process [19]. Another possibility of recovery in hydraulic systems is the collection of the hydraulic medium in pressure storage tanks.

The idea of using potential energy for recovery has been discussed in past publications regarding elevators [20], excavators [21,22], cranes [23] and forklift trucks [24,25].

[26] demonstrates the recovery in form of regenerative lowering by means of a hydraulically operated forklift truck which can be telescoped twice. Instead of a conventional valve control the lift system is controlled directly by an electric servomotor and a hydraulic pump which can also operate as a hydraulic motor if energy recovery is possible.

The measurement results show that approx. 14 % of the total mass is required to overcome the hydraulic system losses before energy recovery can begin. In addition to the payload, the degree of recovery also depends on the lowering speed and the electrohydraulic energy conversion [27]. [28] shows that the amount of recovery energy is approximately proportional to the payload and approximately inversely proportional to the fork speed and the speed of the permanent magnet synchronous motor. A comparison of battery set operation with and without energy recovery showed that storing the recovery energy while lowering the payload

reduces the degree of battery discharge. This makes it possible to reduce the size of the battery or extend the life of the battery at the same size. In [29] energy recovery in the regenerative lowering process was increased to 40% which results in an improvement of 16% compared to conventional hydraulic systems. This result was achieved by improving the pump, the electric motor and the energy storage system while maintaining the optimum viscosity of the hydraulic medium.

In the planned electric lifting mast there are only electro-mechanical components. This eliminates the need for electro-hydraulic energy conversion.

In principle, there are four ways to transfer the recovered energy:

- into the local power supply system
- into a battery preferably a battery for industrial trucks
- into a capacitor
- by heat conversion into a braking resistor

One aim of the test bench concept is to reproduce the recovery as realistically as possible. It makes sense to choose an industrial truck battery as an energy storage device. Their handling in the recovery process, however, is complicated due to their specifications, e.g. CAN bus codes. For this reason, a system solution from SEW is used, which enables the energy from the generator to be stored in a capacitor by means of a converter. This alternative may be unsuitable for operational use as the capacitor discharges itself. But it is completely sufficient for research purposes and for measuring the recovery power.

These consumers result in small losses which, however, are negligible in relation to the mechanical losses, e.g. in the geared motor, the sliding friction caused by the sliding elements between the lifting frames, the rolling friction caused by the supporting and combination rollers between the lifting frames and the fork carriage. The biggest weak point considering energy efficiency is the push chain, in particular its storage, as it provides the most friction contacts. The theoretical consideration for the lifting process provides for a calculation of the potential energy, in which the masses per lift are described by

$$E_{pot,Hub} = \sum_{i=1}^n E_{pot,i} = \sum_{i=1}^n m_i \cdot g \cdot h_i \quad (1)$$

i, n : summation index

m_i : vertically moved mass

g : gravitational constant

h_i : control variable depending on height

In the lowering process, the efficiencies of the individual electromechanical components are added to (1). These are

$$\eta_{engine} = 0,85 \text{ [30]}$$

$$\eta_{push\ chain} = 0,65 \text{ [17]}$$

$$\eta_{sliding\ block} = 0,9$$

$$\eta_{roller\ guidance} = 0,9 \text{ [31]}$$

The efficiency for the sliding blocks results from the consideration that the contact surface between the sliding blocks and the lifting frame is lubricated. Otherwise this value would be 0.7 [32]. All individual efficiencies

multiplied add up to 0.447. Assuming a payload of 1000 kg and a mass of the traction mast of 250 kg, the energy to be used for the standard lifting mast is 22.1 kJ and yield about -10 kJ of recovered energy. In a study this mast was weight-optimised with a reduction of 87.7 kg in dead weight. The spent and recovered amount of energy for the optimized lift mast are slightly lower. In summary the weight reduction allows an increase in energy efficiency of just under 4 %. Figure 26 shows the curves of the two different mass of the lifting frames. The curve for the lowering process has an offset for the expended energy.

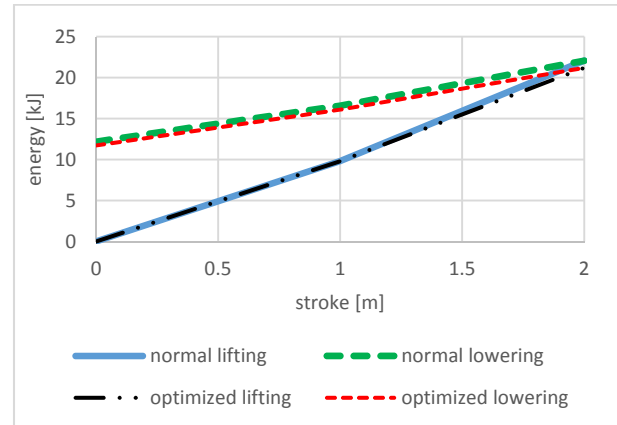


Figure 26. Theoretical energy consideration of the preferred alternative

The theoretical consideration calls for an experimental validation, which is not yet feasible due to the fact that the test bench is still under construction, through comparison to the existing literature is possible. The stated value for the recovery in [29] is about 5 % less the calculated value of the preferred variant.

5. CONCLUSION

The substitution of hydraulic links by electrical and mechanical components requires a new design of the lifting frames. Since industrial trucks are used to transport goods, they are not subject to the relevant restrictions for passenger transport. This means that redundancies in the holding functions can be eliminated, which simplifies dimensioning. In this article concepts for the holding function are presented ranging from classic spring-applied brakes to alternative form-closure brakes. The result is a weighted point evaluation which favoured a spring-applied brake on the extended shaft train of the geared motor. This is followed by further concepts for the drive, which includes already published concepts, but had not yet been implemented into practice. A weighted point evaluation showed that the drive concept using a push chain was the favourite. The preferred concepts result in the preferred variant, which was converted into a CAD model and finally into a dynamic simulation. The dynamic simulation analyses a load case with asymmetrically loaded forks (7000 N and 3000 N). The multiple magnification of the distortion state shows that both lifting frames are most strongly deformed in the area of the fork carriage, the load side. In these areas the greatest stresses are achieved. In a study, the weight of the mast was optimized and a theoretical energy analysis was carried out to calculate

the lifting and lowering process, including recovery. The results showed that the optimized traction mast leads to an energy saving of 4 %. Including the efficiency rates of the producers in the energy balance, 44.75 % can theoretically be recovered for the electric lifting mast with a lift of 2 metres and a payload of 1000 kg.

APPENDIX

This AiF research project is funded by the Federal Ministry of Economics and Technology as part of the program for the promotion of industrial community research (IGF), on the basis of a resolution of the German Bundestag.

REFERENCES

- [1] DE102008022487A1, Flurförderzeug mit einem Hubmast, 2009.
- [2] US2514563A, Electric hoist structure, 1946.
- [3] DE2403181, Mechanische Hubvorrichtung, 1973.
- [4] DIN EN 81-3: Sicherheitsregeln für die Konstruktion und den Einbau von Aufzügen – Teil 3: Elektrisch und hydraulisch betriebene Kleingüteraufzüge, Jun 2011.
- [5] DIN EN ISO 3691-1: Sicherheit von Flurförderzeugen – Sicherheitsanforderungen und Verifizierung – Teil 1: Motorkraftbetriebene Flurförderzeuge mit Ausnahme von fahrerlosen Flurförderzeugen, Staplern mit veränderlicher Reichweite und Lastentransportfahrzeugen, December 2012.
- [6] DE102009039218A1, Hubgerüst für Flurförderzeuge, 2011.
- [7] <https://hiveminer.com/User/Crown%20Lift%20Trucks%20Ltd>, Mai 2019
- [8] VDI 2225-3: Konstruktionsmethodik – Technisch-wirtschaftliches Konstruieren – Technisch-wirtschaftliche Bewertung, November 1998.
- [9] EP2565148A1, Regalbediengerät mit flaschenzugartig angetriebenem Hubschlitten, 31.08.2012.
- [10] Nagel, T.: *Zahnriemengetriebe – Eigenschaften, Normung, Berechnung, Gestaltung*, München: Hanser, 2008.
- [11] Perneder, R.: *Handbuch Zahnriementchnik – Grundlagen, Berechnung, Anwendungen*, Berlin, Heidelberg: Springer, 2009.
- [12] Hagl, R.: *Elektrische Antriebstechnik*, München: Hanser, 2013.
- [13] Grösel, B.: *Bühnentechnik*, 5. Auflage. Oldenburg: De Gruyter, 2015.
- [14] EP3106421B1, Teleskopstange, 2015.
- [15] DE102012100356A1, Flurförderzeug mit einem Hubgerüst, 2013.
- [16] Teleskopischer Hubmast mit Schubkettentechnik. www.serapid.com, May 2019.
- [17] Heinrich Wolf Antriebs- und Steuerungstechnik GmbH & Co. KG: Linear Chain, Technische Dokumentation. www.wolf-eutin.de, Mai 2019.
- [18] Statista 2018: Index zur Entwicklung des Industriestrompreises in Deutschland in den Jahren 1998 bis 2018 (1998 = Index 100), BDEW - Strompreisanalyse Januar 2018, Seite 4, 2018.
- [19] Grote, K.-H. and Feldhusen, J.: *Dubbel – Taschenbuch für den Maschinenbau*, Berlin, Heidelberg: Springer, 2014.
- [20] Yang, H., Sun, W. and Xu, B.: New investigation in energy regeneration of hydraulic elevators, IEEE/ASME Transactions on Mechatronics Journal, Vol. 12, No.5, 2007.
- [21] Lin, T., Wang, Q., Hu, B. and Gong, W.: Research on the energy regeneration systems for hydraulic excavators, Automation in Construction, Vol 19, No 8, pp. 1016-1026, 2010.
- [22] Yoon, J.I., Kwan, A.K., Truong, D.Q.: A study on an energy saving electro-hydraulic excavator, IEEE Proceedings of the International Joint Conference ICROS-SICE, pp. 3825–3830, (Fukuoka, Japan), 2009.
- [23] Liang, X. and Virvalo, T.: An energy recovery system for a hydraulic crane, Conference Proceedings of the Institution of Mechanical Engineers, Part C: Journal of Mechanical Engineering Science, Vol. 215, No. 6, pp. 737–744, June 2001.
- [24] Andersen, T.O., Hansen, M.R., Pedersen, H.C. AND F. Conrad: Regeneration of potential energy in hydraulic forklift truck, Proceedings of the 6th International Conference on Fluid Power Transmission and Control, Hangzhou, pp. 302–306, 2005.
- [25] Rydberg, K.-E.: Energy efficient hydraulic systems and regenerative capabilities, Conference Proceedings of the Ninth Scandinavian International Conference on Fluid Power SICFP, pp. 2–5 (Linköping), 2005.
- [26] Minav, T.A., Laurila, L. and Pyrhönen, J.: Analysis of electro-hydraulic lifting system's energy efficiency with direct electric drive pump control, Automation in Construction, Vol. 30, pp. 144–150, 2013.
- [27] Sinkkonen, A. et al.: Energy usage in mast system of electrohydraulic forklift, Ventil (Ljubljana), Vol. 17, No. 6, pp. 500-506, 2011..
- [28] Minav, T.A., Murashko, K., Laurila, L. and Pyrhönen, J.: Forklift with a lithium-titanate battery during a lifting/lowering cycle: analysis of the recuperation, Automation in Construction, Vol. 35, pp. 275–284, 2013
- [29] Minav T.A. et al.: Towards a better energy efficiency through a system approach in an industrial forklift system, Proceedings of the Institution of Mechanical Engineers Part D Journal of Automobile Engineering, Vol. 228, No. 8, 2014.
- [30] Kegelradgetriebe: hoher Wirkungsgrad und dauerfeste Verzahnung. www.sew-eurodrive.de, May 2019.
- [31] Decker, K. et. al: *Decker Maschinenelemente*, 20. Auflage, Carl Hanser, 2018.
- [32] Licharz technische Kunststoffe, Konstruieren mit technischen Kunststoffen, Firmenschrift, http://www.ktw-gornau.de/tl_files/ktw/Inhalte/Downloads/Broschuere_Kunststoffe_Gleitlager.pdf, Mai 2019

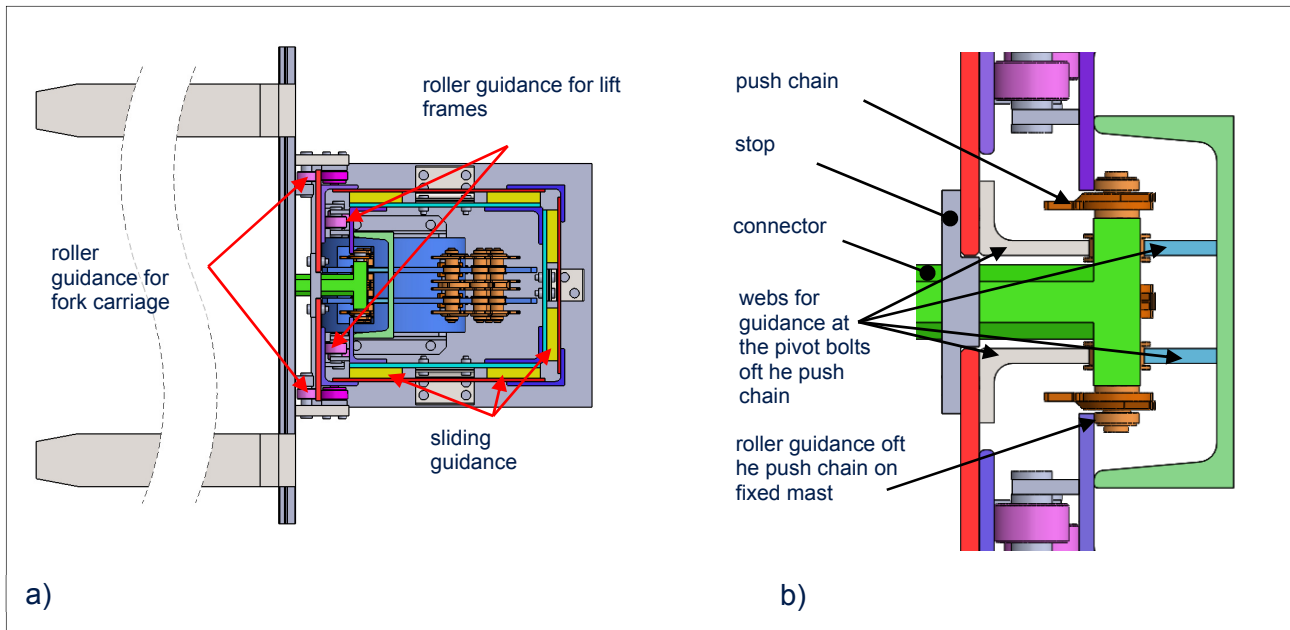


Figure 17. Preferred variant in top view: a) Overview b) connector with guide for push chain

Stress-strain analysis and optimization of universal hydraulic grapple

Luka Bizjak

Researcher
University of Ljubljana
Faculty of Mechanical Engineering

Jurij Hladnik

Teaching Assistant
University of Ljubljana
Faculty of Mechanical Engineering

Boris Jerman

Assistant Professor
University of Ljubljana
Faculty of Mechanical Engineering

Hydraulic grapples are used on various construction and material handling machines. Important characteristic of each grapple is its mass. Grapple's mass represents the load acting on manipulation device. As load-capacity of each manipulation device is limited, grapple's mass permanently decreases mass of actual burden. Therefore users and manufacturers are favouring lighter grapples. In this paper optimisation of universal hydraulic grapple is presented, the purpose of which is grapple's mass reduction. In order to efficiently reduce grapple's mass it is necessary to understand its stress-strain state. For these purpose grapple's finite element method (FEM) models were prepared and calculations were performed. By analysing calculations results, possibilities for topology optimisation were recognized. Further, topology optimisation of least-stressed grapples elements was performed. Topology optimization results were used to perform optimisation adaptations of grapple's geometry. Considering adaptations, new FEM models were prepared and new calculations were performed. By comparing two sets of FEM calculations results, grapple optimisation adaptations were evaluated. With optimisation adaptations mass of grapple was reduced by 8,5 kg, while acceptable stress state of grapple, obtained prior optimisation process, was preserved.

Keywords: Hydraulic grapple, finite element method, stress-strain analysis, topology optimisation, mass reduction.

1. INTRODUCTION

Hydraulic grapples are devices used on various construction and material handling machines such as excavators, skidders, forwarders, cranes etc. [1] In the past many different types of grapples were developed with the purpose to improve manipulation of broad spectrum of burdens. Specially shaped grapples intended to handle bulk materials, logs, large stones, barrels, etc. are well known and extensively used in everyday practice. Wang [2] studied effects of different tong shapes on hydraulic grapple's performance in loading and unloading operations.

The object of our research is universal hydraulic grapple which differs from other grapples by fully enclosed hydraulic mechanism in central housing and possibility of rapid arm change. These constructional attributes, together with the possibility of synchronous and asynchronous arm movements make this grapple highly efficient.

Grapple has significant impact on loading efficiency, as shown in productivity and time consumption analysis by Väättäinen et al. [3] and Nurminen et al. [4] Beside handling efficiency the important characteristic of grapple is its mass. According to Wang et al. [1] grabbing force is closely related to the structural parameters of the grapple, the weight of the grapple, and the weight of the grabbed burden. Additionally

grapple's mass represents the load acting on manipulation device. As load-capacity of each manipulation device is limited, grapple's mass permanently decreases mass of actual burden. Therefore users and manufacturers are favouring lighter grapples.

The aim of our research was to firstly detail analyse different stress-strain states of universal hydraulic grapple that occurs during its use. Based on findings of the analysis it was our further aim to perform optimization of grapple with the purpose to reduce its mass.

For these purpose appropriate geometrical and finite element method (FEM) models of grapple were developed. Further, load cases to be investigated were defined. Using developed models and defined load cases, first set of FEM calculations was performed. Analysing results of FEM calculations, different stress-strain states of grapple were recognized. Findings on stress-strain states were used at topology optimization of grapple. Topology optimisation is typically employed when design is at the conceptual stage [5], while in papers [6] by Tsavdaridis et al. and [7] by Chung and Lee reports the use of topology optimisation also in later design stages, when it is used to improve existing structures. Topology optimization results were used to perform optimisation adaptations of grapple's geometry. Adaptations were incorporated in previously developed geometrical model. On the basis of adapted geometrical model new FEM models were developed. Using new models and previously defined load cases, second set of FEM calculations was performed. By comparing two sets of FEM calculations results, grapple optimisation adaptations were evaluated.

Correspondence to: Dr Boris Jerman, Assist. Professor
Faculty of Mechanical Engineering,
Aškerčeva 6, 1000, Ljubljana, Slovenia
E-mail: boris.jerman@fs.uni-lj.si

2. STRESS-STRAIN ANALYSIS OF GRAPPLE

2.1 Geometrical and numerical models

Grapple's structure consist of three major sets; central housing, shafts and hands (Figure 1). Two shafts are positioned inside the central housing. One hand is mounted to each shaft. Grapple's drive is provided by two hydraulic cylinders inside the central housing. Each hydraulic cylinder is mounted to the central housing and to the shaft by connecting pins. Bearing inner ring and rotational motor's flange are bolted to the central housing. By bearing and flange grapple is connected to the linkage element which further connects grapple to the construction or handling machine.

To form geometrical model of grapple, we modelled its major sets. Each set consist of several parts connected by welds. All the parts and welds were modelled. Additionally to the grapple's major sets, bearing ring, motor's flange, connecting bolts and pins were also modelled. These parts were added to the geometrical model in order to apply as realistic boundary conditions as possible to the FEM models (see Section 2.2). Structurally unimportant features were simplified or removed from geometrical model in order to ease finite element mesh generation.

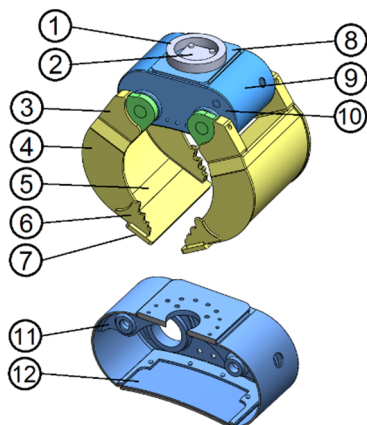


Figure 1. Grapple's geometrical model. Major sets are coloured: BLUE central housing, GREEN shafts, YELLOW hands. Numbered parts are: (1) bearing ring, (2) motor's flange, (3) hand's connecting ear, (4) hand's side plate, (5) hand's shell plate, (6) reinforcement, (7) blade plate, (8) base plate, (9) housing's shell plate, (10) housing's side plate, (11) support element, (12) housing's bottom.

On the basis of grapple's geometrical model three FEM models were prepared (Figure 2). FEM models differs by grapple's hands position. At the first and third model hands are in almost closed and fully open position. At the second model position of hands is used at which hydraulic mechanism inside central housing generate highest gripping force. For meshing 20-node hexahedral finite elements were used. Beside hexahedral elements contact and beam finite elements were also used in FEM models. Bonded-type contact elements were used to model connections between welds and parts. Friction type contact elements were used to model connections between grapple's sets. Use of beam elements is presented in Section 2.2.

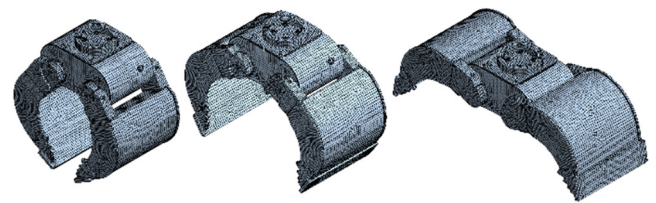


Figure 2. Grapple's numerical models.

2.2 Load cases and boundary conditions

FEM calculations were performed for two different load cases. Loads acting on grapple when purposely used were considered at the first load case. These loads are force due to mass of grapple and burden as well as grapple's gripping forces. Force due to mass of grapple and burden was estimated using maximum load capacity of 8 ton excavator.

$$Q = m_{L,max} \cdot g = 4715 \cdot 9,81 = 46254 \text{ N} \quad (1)$$

Grapple's gripping forces are provided by hydraulic cylinders inside central housing. Gripping forces were estimated considering cylinder's geometry and maximum pressure of hydraulic system.

$$F = p \cdot \frac{\pi \cdot d^2}{4} = 350 \cdot 10^{-1} \cdot \frac{\pi \cdot 90^2}{4} = 222660 \text{ N} \quad (2)$$

At the second load case, loads acting on grapple when non-purposely used were considered. As non-purpose we considered use of grapple for excavator self-lifting. Loads acting on grapple when non-purposely used were estimated using mass and dimensions of 8 ton excavator (Figure 3).

$$G = m_E \cdot g = 8600 \cdot 9,81 = 84366 \text{ N} \quad (3)$$

$$R = G \cdot \frac{b}{a+b} = 84366 \cdot \frac{2815}{940 + 2815} = 63246 \text{ N} \quad (4)$$

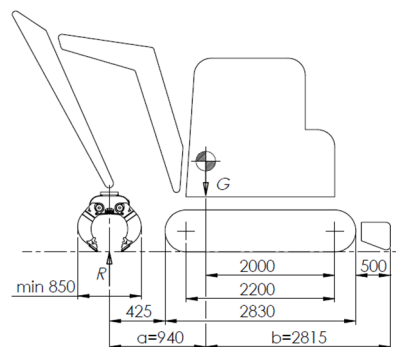


Figure 3. Excavator's dimensions.

In addition to the listed loads, pretension of bolts connecting bearing ring (M12) and motor's flange (M16) with central housing was considered at both load cases.

$$F_{P,M12} = v_1 \cdot A_{C,M12} \cdot \sigma_{Y,8.8} = 0,8 \cdot 76,2 \cdot 640 = 39014 \text{ N} \quad (5)$$

$$F_{P,M16} = v_1 \cdot A_{C,M16} \cdot \sigma_{Y,8.8} = 0,8 \cdot 144 \cdot 640 = 73728 \text{ N} \quad (6)$$

Listed loads were applied to the FEM models as follows. At the first load case beam elements connecting grapple's hands were added to the FEM models (Figure 4). Force due to mass of grapple and burden was applied to red-coloured beam elements. Gripping forces were applied to the connecting pins.

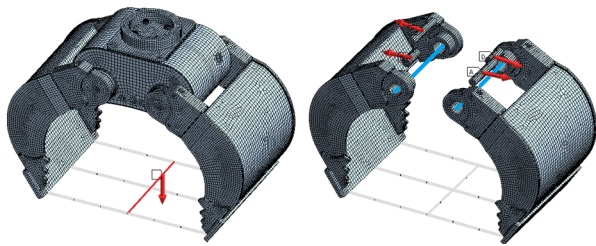


Figure 4. First load case's loads on FEM model.

At the second load case, beam elements connecting pairs of connecting pins were added to the FEM models (Figure 5). Reaction force on grapple due to mass of excavator was applied to the red-coloured edges of grapple's hands.

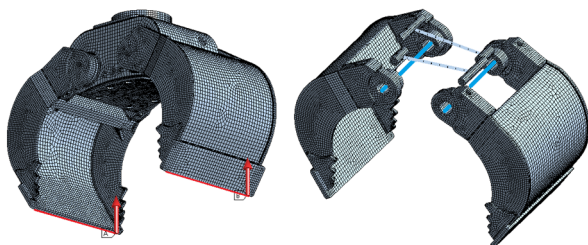


Figure 5. Second load case's loads on FEM model.

Grapple's displacements were limited at red-coloured surfaces of bearing ring (in ring's radial direction) and motor's flange (in all the directions).

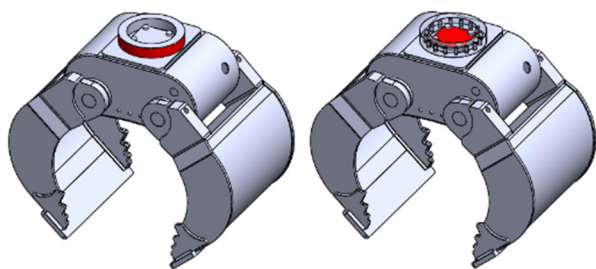


Figure 6. Red coloured surfaces at which grapple's displacements were limited.

On Figures 4 and 5 shafts are shown only symbolically. Actual shaft's construction presents competitive advantage of studied grapple and therefore should not be shown.

2.3 Material properties

Several materials listed in Table 1 are used for grapple's parts. At the FEM calculations bilinear material characteristics were considered for most of the parts. To define these characteristics values listed in Table 1 were used. For additionally modelled parts (bearing ring, motor's flange, connecting bolts and pins) simple linear material characteristic was considered as stress-strain state of these parts wasn't in our interest.

Table 1. Material properties of grapple's parts.

material	σ_Y E E_T [MPa]			ν [/]	sets / parts
S355	345	210000	1100	0,3	central housing
20MnCr5	540				hands shell plates
40CrMnMoS8-6	850				hands side plates
HARDOX 450	1200				shafts
			hands connecting ears		
			shafts connecting ears		
					hands blade plates
					hands reinforcements

Global and local stresses achieved at various hands positions and various load cases were studied and compared. Places at which high local stresses constantly occurs were marked and causes for these stresses were examined. Highest local stresses achieved on grapple's central housing and hands are presented in Tables 2 and 3.

It was found that similar grapple's stress states are achieved at various hands positions and various load cases (Figure 7). At both load cases generally highest stresses are achieved on grapple when hands are in fully open position and lowest when hands are in almost closed position.

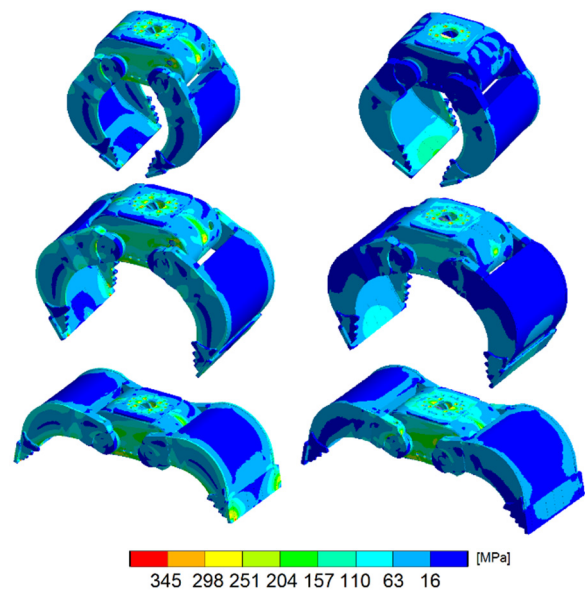


Figure 7. Equivalent stresses on grapple. Left: first load case, right: second load case.

Greatest differences in stresses achieved were discovered on the grapple's central housing (Figure 8). On central housing highest global stresses occurs on side plates. These stresses occurs, due to bending of shafts and connecting pins, mounted to the housing. At shafts and connecting pins mounting points high local stresses also occurs (see places marked with B, C, E and F). These stresses are consequence of local bending of side plates and deformations of mountings. Due to similar reasons high local stresses also occurs on two support elements inside housing (see placed marked with H and I). On central housing high local stresses

also occurs on shell plates (see places marked with L and M) and base plate (see places marked with J and K). These stresses are consequence of inadequate load transfer from support elements to the plates. At the second load case moderate global stresses also occurs on base plate, due to plate bending around X axis.

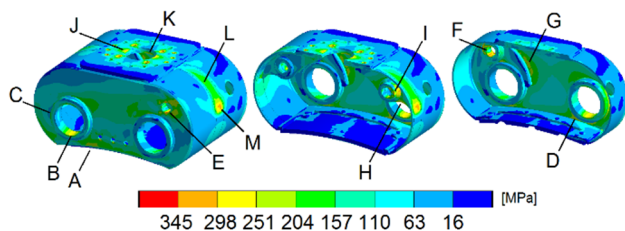


Figure 8. Equivalent stresses on central housing (FEM model 2, load case 1).

Table 2. Highest local stresses achieved on grapple's central housing prior optimisation.

place	σ_{EQ} [MPa]	FEM model	load case
A	267	3	1
B	297	3	1
C	196	3	1
D	287	1	1
E	379	1	1
F	280	1	1
G	264	3	1
H	362	3	2
I	301	2	1
J	367	3	2
K	309	3	2
L	225	3	1
M	345	3	2

On grapple's hands higher global stresses occurs on edges of side plates (Figure 9). Beside them local stresses also occurs on side plates. At the place marked with A local stresses are consequence of local bending. At the place marked with B teeth are shaped on side plate that causes stress concentrations. Local stresses also occurs on connecting ears due to their stretching (see place marked with C) and due to contacts with shaft's ears (see placed marked with E and F).

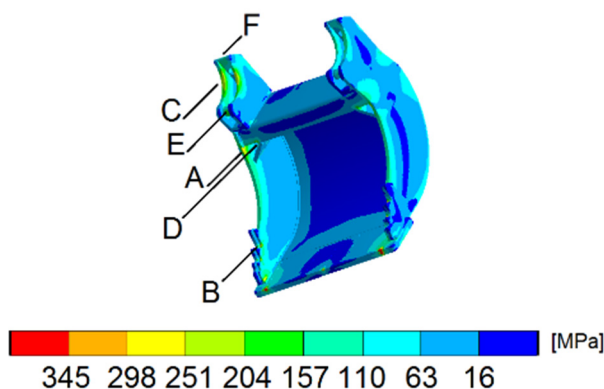


Figure 9. Equivalent stresses on grapple's hand (FEM model 2, load case 1).

Presented stress state of grapple is acceptable and was used as reference when evaluating optimisation results (Section 3.3).

Table 3. Highest local stresses achieved on grapple's hand prior optimisation.

place	σ_{EQ} [MPa]	FEM model	load case
A	345	3	1
B	388	3	1
C	259	3	2
D	274	3	1
E	213	3	2
F	233	3	2

3. OPTIMISATION OF GRAPPLE

3.1 Topology optimisation

Based on findings of stress-strain analysis we performed optimisation of grapple with the purpose to reduce its mass.

Firstly, topology optimisation on grapple's parts that were previously recognized as least-stressed was performed. On central housing, shell plates and housing bottom was optimised and on grapple's hands, shell plates and side plates were optimised. For listed elements we required 50 % mass reduction, while retaining rigidity of housing and hands as high as possible. Two calculations were performed, using third FEM model and loads of both load cases separately.

On Figure 10 results of topology optimisation on central housing are shown. From red-coloured areas material can be removed with minimal impact on housing's stiffness. On grey-coloured areas material should be retained. On the housing bottom similar pattern is obtained at both load cases. According to the pattern material should be retained in area between two pairs of diagonally positioned bolts that connects bottom to the housing. Outside of these area material can be partly and at some places (theoretically) fully removed from housing's bottom.

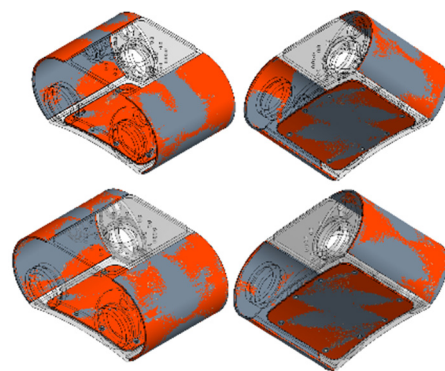


Figure 10. Results of topology optimisation on central housing. Top: first load case, bottom: second load case.

Patterns obtained on shell plates also share some similarities. Material should be retained in areas where support elements are welded to the plates and in areas below these elements. According to the results obtained at the second load case, material should also be retained on joints between shell plates and base plate. Outside of listed areas material can be partly removed from shell plates.

Results of grapple's hand topology optimisations are shown on Figure 11. It is seen that part of shell plate can

be (theoretically) fully removed from hand's back side. Additionally vertical part of shell plate between hand's ears can also be removed. Horizontal part of shell plate between ears should be retained as well as part beside hand's blade plate. From hand's side plates only small amount of material can be removed.

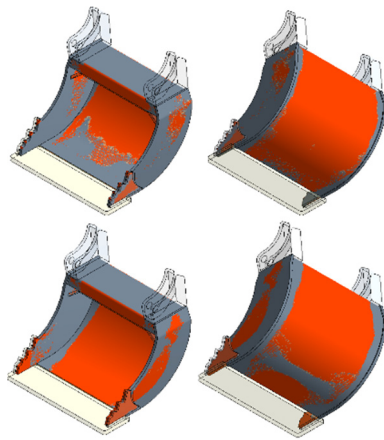


Figure 11. Results of topology optimisation on grapple's hand. Top: first load case, bottom: second load case.

3.2 Geometry adaptation

On the base of topology optimisation results we performed optimisation adaptations on grapple's geometry. Thickness of shell plates on grapple's central housing and hands was reduced by 1 mm. Therefore, for housing's shell plates thickness of 5 mm and for hands shell plates thickness of 4 mm is used. Additionally shape of support elements inside the housing was changed and thickness reduced (Figure 12). New shape should provide more uniform transfer of loads from support elements to the shell plates. Thickness was reduced from 15 mm to 12 mm.

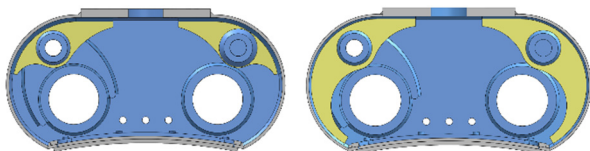


Figure 12. Left: support element's old shape, right: support element's new shape.

Despite optimisation potential of housing's bottom shown (Figure 10), optimisation wasn't performed, as non-structural characteristics of bottom would be worsened by material removal.

By listed optimisation adaptations mass of grapple was reduced by 8,5 kg. Adaptations were incorporated in grapple's geometrical model and three new FEM models were prepared. With new models FEM calculations were performed for both load cases.

3.3 Optimisation results

Results of FEM calculations performed with new models were compared to the results obtained prior grapple optimisation (Section 2.4). Global as well as high local stresses achieved on previously marked places were compared, in order to determine the influence of optimisation adaptations on various

grapple's stress states. Highest local stresses achieved on grapple's central housing and hands are presented in Tables 4 and 5.

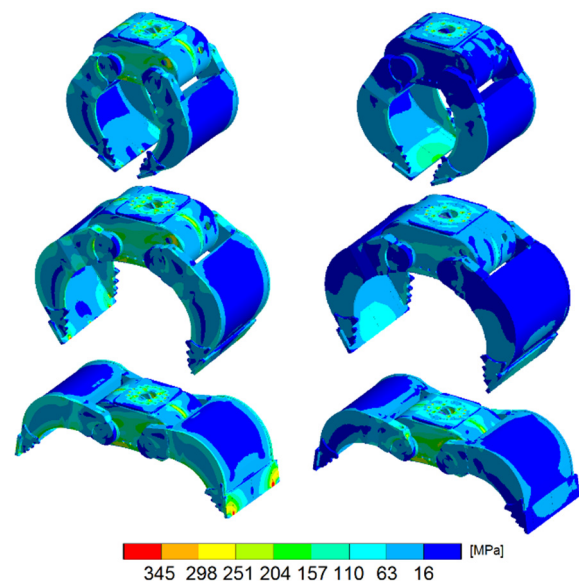


Figure 7. Equivalent stresses on grapple. Left: first load case, right: second load case.

It was found that despite optimisation grapple's global stresses didn't change (Figure 7). At the local stresses some differences were discovered. On central housing lower local stresses were obtained on base and shell plates. Higher local stresses were obtained on side plates and on support elements inside housing. Lower stresses are consequence of support elements new shape. Due to new shape transfer of load from support elements to the shell plates is more uniform. On the other hand higher local stresses are consequence of support elements reduced thickness. Due to reduced thickness bending of connecting pins mounted to the housing is more intense, causing higher local stresses. Local stresses on grapple's hands remains similar despite optimisation.

Grapple optimisation was performed so that acceptable stress state of grapple obtained prior optimisation process (Section 2.4) was mostly preserved. Due to optimisation only some local stresses were slightly augmented. This doesn't change acceptability of grapple's stress state.

Table 4. Highest local stresses achieved on grapple's central housing.

place	σ_{EQ} [MPa]	FEM model	load case
A	288	3	1
B	299	3	1
C	202	3	1
D	299	3	1
E	299	3	1
F	381	2	1
G	253	3	2
H	254	3	1
I	371	3	2
J	370	2	1
K	280	2	1
L	258	3	1
M	231	3	2

Table 5. Highest local stresses achieved on grapple's hand prior optimisation.

place	σ_{EQ} [MPa]	FEM model	load case
A	343	3	1
B	389	3	1
C	256	3	2
D	223	3	1
E	206	3	2
F	187	3	2

4. CONCLUSION

At the grapple similar stress states are achieved at various hands positions and various load cases. Generally highest stresses are achieved on grapple when hands are in fully open position and lowest when hands are in almost closed position. Highest global stresses occurs on side plates of central housing and hands. At the second load case moderate global stresses also occurs on housing's base plate as well. High local stresses also occurs on grapple as consequence of local phenomes (local bending, mountings deformation, contacts) due to load transfer between grapple's segments. Places at which high local stresses constantly occurs were marked. Based on the results of stress-strain analysis following parts were chosen for topology optimisation: housing bottom, hands side plates and shell plates of hands and housing. Topology optimisation shown that material can be partly removed from all the shell plates and housing bottom. As non-structural characteristics of bottom would be worsened by material removal, changes were made only to the shell plates. Thickness of shell plates on grapple's central housing and hands was reduced by 1 mm. Additionally shape of support elements inside the housing was changed and thickness reduced by 3 mm. By optimisation adaptations mass of grapple was reduced by 8,5 kg. Results of re-executed FEM calculations shown that optimisation was performed so that acceptable stress state of grapple was obtained.

ACKNOWLEDGEMENT

This research was supported by Modularis Teh d.o.o., Ljubljanska c.11, SI – 1270 Litija, Slovenia. We are grateful for their kind assistance.

REFERENCES

- [1] Wang, J., LeDoux, B.C. and Wang, L.: Modeling and Validating the Grabbing Forces of Hydraulic Log Grapples Used in Forest Operations, *International Journal of Forest Engineering*, Vol. 16, No. 1, pp. 77-85, 2005.
- [2] Wang, J.: Effects of Tong Shapes on Hydraulic Log Grapple's Performance in Loading and Unloading Operations, *International Journal of Forest Engineering*, Vol. 14, No. 1, pp. 59-66, 2003.
- [3] Väättäin, K., Ala-Fossi, A., Nuutinen, Y. and Röser, D.: The Effect of Single Grip Harvester's Log Bunching on Forwarder Efficiency, *Baltic Forestry*, Vol. 12, No. 1, pp. 64-69, 2006.
- [4] Nurminen, T., Korpunen, H. and Uusitalo, J.: Time Consumption Analysis of the Mechanized Cut-to-length Harvesting System, *Silva Fennica*, Vol. 40, No. 2, pp. 335-363, 2006.
- [5] Gunwant, D. and Misra, A.: Topology Optimisation of Continuum Structures using Optimality Criterion Approach in ANSYS, *International Journal of Advances in Engineering & Technology*, Vol. 5, No. 1, pp. 470-485, 2012.
- [6] Konstantinos, T., Kingman, J. and Toropov, V.: Application of Structural Topology Optimization to Perforated Steel Beams, *Computers & Structures*, Vol. 158, pp. 108-123, 2015.
- [7] Chung, J. and Lee, K.: Optimal design of rib structures using the topology optimization technique, *Proceedings of the Institution of Mechanical Engineers, Part C: Journal of Mechanical Engineering Science*, Vol. 211, No. 6, pp. 425-437, 1997.

NOMENCLATURE

a	distance from grapple to the excavator's mass centre
$A_{C,M12}$	core cross section of M12 bolt
$A_{C,M16}$	core cross section of M16 bolt
b	distance from excavator's mass centre to its tipping point
d	diameter of hydraulic piston
E	Young's modulus
E_T	tangential modulus
F	gripping force
$F_{P,M12}$	pretension force of M12 bolt
$F_{P,M16}$	pretension force of M16 bolt
g	gravitational acceleration
G	force due to mass of excavator
m_E	mass of excavator
$m_{L,max}$	maximum load capacity of excavator
p	maximum pressure of hydraulic system
R	reaction force on grapple due to mass of excavator
Q	force due to mass of grapple and burden

Greek symbols

ν	Poisson's ratio
ν_1	safety factor
σ_{EQ}	equivalent stress, von Misses
σ_Y	yield strength
$\sigma_{Y,8.8}$	yield strength of bolts material 8.8

Franz Paulischin

Teaching Assistant
Vienna University of Technology
Faculty of Mechanical and Industrial
Engineering
Institute for Engineering Design and
Product Development

Georg Kartnig

Professor
Vienna University of Technology
Faculty of Mechanical and Industrial
Engineering
Institute for Engineering Design and
Product Development

The lateral movement of steel processing belts – extended consideration on belts with low belt tension

Due to the system behaviour, the tracking of steel processing belts is typically performed by the feedback controlled pulley adjustment. There is an analytical model available to describe the lateral running behaviour of the belt, but it was developed for highly tensioned belts. As the belt tension decreases, the model becomes invalid and ultimately unusable. After a presentation of this model the calculated lateral moving behaviour is compared with the results of measurements on a test rig for steel processing belts. In this way, the limits of use for the analytical model with respect to belt tension are shown. Finally, it is demonstrated how the lateral running of a belt can be simulated, especially by means of the discrete element method.

Keywords: steel processing belt, belt conveyor, belt misalignment, tracking, DEM

1. INTRODUCTION

Steel processing belts are special conveyor belts which use a steel belt with a thickness of one to a few millimetres. These conveyors are required, for example, in the chemical industry or in the production of bakery products. Due to the high stiffness of the steel belt, many track guidance systems known from rubber belts cannot be used here. Consequently, steel belts are guided on cylindrical, position-controlled pulleys. The controller is based on a belt model that currently only works satisfactorily for highly-tensioned belts. However, the following applications require low-tensioned belts. Therefore, suitable models are being searched for these low tensioned belts.

- during the start-up-phase of the system starting with the totally untensioned belt e.g. during belt production or the first installation of a belt machine
- in the operation of refurbished plants, when a new belt with larger dimensions (width b , thickness h) runs on existing pulley stations. The maximum permissible belt tensile force is limited by the existing design. The system must be operated with reduced belt tension.

This paper starts with the modelling of the steel belt. After a presentation of existing models for high tensioned belts, the geometric situation at the point of contact is examined more closely. Based on this, ideas for a new approach for low tensioned belts are presented. Finally, this article deals with simulations of the lateral movement of the belt. After a short presentation of an existing FEM model, a new approach in DEM is presented.

2. PULLEY ADJUSTMENT VIA YAW ANGEL β

The regulation of the belt position in y-direction is typically achieved by the inclined position of the tail pulley TP. The yaw angle occurring in this case ranges from a few hundredths to tenths of a degree. In order to be able to clearly illustrate this angle and the resulting effects, the following sketches are shown strongly larger in relation to the yaw angle. The two ends of the axis of the tail pulley TP (Figure 1) are moved in x-direction in the opposite direction by the distance Δx . As a result, the tail pulleys axis yaws by the angle β .

$$\beta = \tan^{-1} \frac{2 * \Delta x}{d} \approx \frac{2 * \Delta x}{d} \quad (1)$$

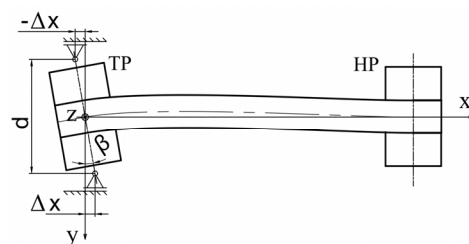


Figure 1. Pulley adjustment in vertical axis

Figure 2 shows a characteristic belt moving curve for the upper span (Figure 3) of a highly tensioned belt. The duration of the transient phase and the amplitudes occurring depend on the belt dimensions and the belt tension.

The following characteristic values can be obtained from the steady-state range:

- steady-state velocity: slope of the curves in the steady-state situation:

$$\dot{y}_1 = \dot{y}_4 = \frac{\Delta y_1}{\Delta x_1} = \frac{\Delta y_4}{\Delta x_4} \quad (2)$$

- steady-state offset: distance in y-direction between the run-up point and the run-off point of a belt span

Correspondence to: Dipl. Ing. Franz Paulischin, Teaching Assistant, Technische Universität Wien, Getreidemarkt 9/307-1, 1060 Vienna, Austria
E-mail: franz.paulischin@tuwien.ac.at

$$\Delta y_{1-4} = |y_1 - y_4| \quad (3)$$

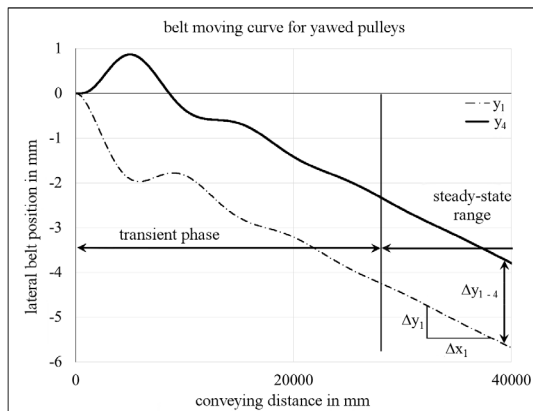


Figure 2. Characteristic belt moving curve

3. MODELLING

In this chapter, the geometric conditions at the point of contact of a flexible rope and a belt on a cylindrical pulley, which is yawed by β , are examined in detail. Thus the lateral moving behaviour of the run-up point of a rope or a belt at a pulley can be determined. Next, a closed rope on a belt conveyor with two cylindrical pulleys is considered. With the help of the rope model - a limp, highly tensioned rope on two pulleys - the movements at the run-up and run-down points (Figure 3, points 1, 3 and 2, 4) as well as the interaction between these points are described. Finally, the beam model [1] [2], a mathematical model for highly tensioned steel processing belts, is presented.

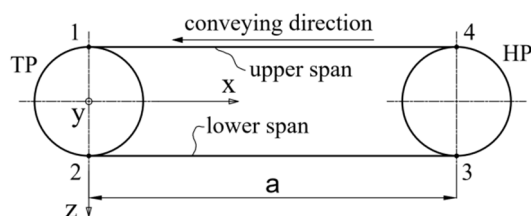


Figure 3. Nomenclature of run-up and run-off points

4.1 Highly tensioned belt: the rope model

Due to the missing bending stiffness and under the assumption of perfect static friction [2], the run-up and run-off points of both spans are connected in a straight line. As long as the pulleys are aligned parallel, the rope on the pulleys runs at a constant y-position. If, however, the tail pulley TP is yawed by the angle β , the rope begins to move sideways. A closer look at a run-up point (Figure 4) reveals the direction of the movement. From this, the chronological sequence of the lateral running (Figure 5, I - VI) and the interactions between the run-up and run-off points can be shown. The corresponding diagram with the position of these points is shown in Figure 6.

After yawing the tail pulley by the angle β (Figure 5, I), the direction of the rope deviates from the normal of the tail pulley (Figure 4). The angle difference between the direction of the rope and the normal direction of the pulley, the contact angle β_0 , corresponds to the yaw

angle β . When the head pulley is driven and the rope moves by the distance Δx , the point 1_0 runs sideways by the distance Δy_1 to its new position 1_1 .

$$\Delta y_1 = \Delta x * \beta_0 \quad (4)$$

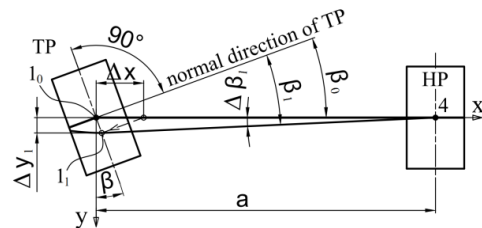


Figure 4. Geometric situation at the run-up point

The direction of the upper rope span is determined by connecting the new run-up point 1_1 in a straight line with the unchanged run-off point 4 (Figure 5, II). This reduces the contact angle by $\Delta\beta_1$ (Figure 4). The new contact angle β_1 can be calculated.

$$\beta_1 = \beta_0 - \Delta\beta_1 \quad (5)$$

$$\Delta\beta_1 = \frac{\Delta y_1}{a} \quad (6)$$

After half a revolution of the pulleys (Figure 5, III) the run-off point 2 begins to move sideways. The y-position of the run-off point 2 is the same as the y-position of the run-up point 1 a half pulley revolution earlier.

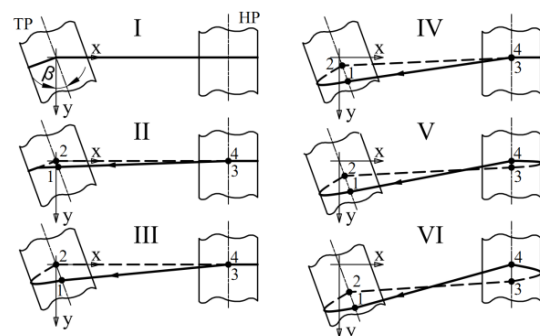


Figure 5: lateral movement of the rope

At the next step (IV) the lower rope span also begins to deflect, and the situation at the point of contact 3 of the head pulley HP begins to change gradually. As the deflection of the lower rope span increases, the contact angle at the run-up point 3 increases and the lateral travel speed of this point increases (V).

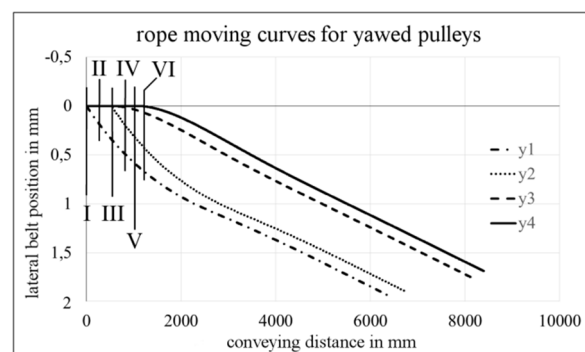


Figure 6: moving curves of a limp rope on yawed pulleys

A full pulley revolution after starting to revolute, the run-off point 4 begins to move (VI). From this time on, all four points (1 - 4) move sideways and affect each other.

The duration of the resulting stabilization process (Figure 6) depends on the geometry of the belt conveyor machine. With the dimensions of the test rig (centre distance $a = 2$ m, pulley radius $R = 170$ mm and yaw angle $\beta = -0.042^\circ$), the oscillation decays after a few pulley revolutions and all four points move sideways at the same speed. Finally, the rope always runs sideways in the direction of the lower belt tension [2] (Figure 7).

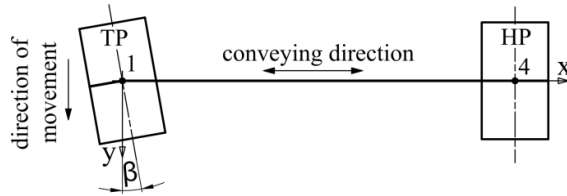


Figure 7: direction of the rope movement

4.2 Highly tensioned belt: the beam model

The lateral moving behaviour of a highly tensioned steel processing belt is also based on the geometric effects mentioned above. However, the additional bending stiffness of the belt changes the geometric conditions at the run-up point. A linear connection of the run-off point with the run-up point, as assumed in the rope model, is no longer realistic. The beam model, a mathematical model for a highly tensioned belt span consisting of a simple bending beam on two supports, is able to take this effect into account. Its bending line is used to calculate the lateral running behaviour. Due to the high tension, it is assumed that the deformation of the belt span takes place only in the belt plane and no buckling occurs. The validity of this assumption was confirmed for highly tensioned belts by measurements on a test stand [1]. With the following boundary conditions at the run-up and run-off points (7) of a belt located centrally on the pulleys and the tail pulley yawed by β

$$y(0) = 0 \quad y(a) = 0 \quad y'(0) = \beta \quad y'(a) = 0 \quad (7)$$

the equation of the bending line can be written for each belt span.

$$y'' = \frac{-M}{E * I} - \frac{\chi * q}{G * A} \quad (8)$$

For the calculation of the bending moment in the belt span, 1st order theory (Th 1. O) as well as 2nd order theory (Th 2. O) can be used [1]. The bending moment M in the belt span is calculated according to Th 1. O and Th 2. O:

$$M = M_{Th\ 1.0} = -M1 - Q1 * x \quad (9)$$

$$M = M_{Th\ 2.0} = -M1 - Q1 * x - F_v * (y(x) - y1_0) \quad (10)$$

If Th 1. O is applied, the equilibrium conditions on the undeformed beam are considered. When working according to Th 2. O, the deformed beam (Figure 8) is used. This makes it possible to include the preload force

F_v in the equation for the bending moment. The calculation of the lateral belt position is basically done in the same way as for the rope model. In addition, the belt shape has to be considered according to the bending line. The difference between the gradient of the bending line in the run-up point and the normal direction of the pulley represents the angle of contact at this point. For the next step a new contact angle has to be calculated using the curvature of the bending line. The following process considerations for the upper belt span explain this statement in detail.

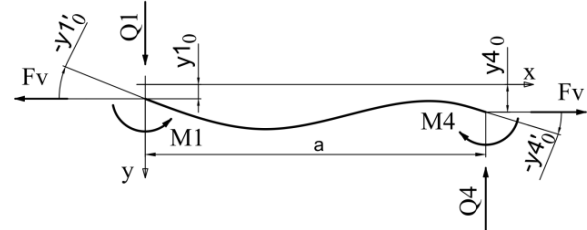


Figure 8: the beam model

Starting with the central arrangement of the undeformed belt span on the pulleys and a yaw angle β , the following situation arises for the run-up point 1_0 at timestep 0.

$$y1_0 = 0 \quad y1'_0 = 0 \quad y1''_0 \neq 0 \quad (11)$$

$$y4_0 = 0 \quad y4'_0 = 0 \quad y''4_0 \neq 0 \quad (12)$$

Since perfect static friction is assumed, the contact angle $y1'_0$ at timestep 0 equals zero. After a belt feed by Δx , the run-up point remains on its y -position.

$$y1_1 = y1_0 + y1'_0 * \Delta x = 0 \quad (13)$$

Due to the curvature $y1''_0$ of the belt span at the run-up point 1 at the timestep 0 and to the belt feed by Δx , the contact angle $y1'_1$ for the timestep 1 is different from zero.

$$y1'_1 = y1'_0 + y1''_0 * \Delta x \quad (14)$$

Only in the second step the lateral movement of the run-up point 1 starts.

$$y1_2 = y1_1 + y1'_1 * \Delta x \quad (15)$$

In that way, the lateral belt movement of the belt span can be calculated for the first half pulley revolution. Then the run-off point 4 begins to move in y -direction. The bounding conditions of the beam at the run-off point will change continuously furthermore. In the next step after the mentioned half revolution, the belt leaves the pulley at point 2 at the y -position $y1_1$ with the contact angle $-y1'_1$ and deflects the lower belt span. The same situation happens at point 4, with the past conditions of point 3. With these considerations, the lateral movement of the belt can be calculated analytically.

4.3 Comparison of models

To compare the models to each other, the y -position of the run-up point 1 of a steel process belt ($b = 200$ mm, $h = 0.3$ mm) with the geometry data of the test rig (centre distance $a = 11.28$ m, pulley radius

$R = 170$ mm and twist angle $\beta = -0.042^\circ$) (Figure 11) can be calculated and visualized in a diagram (Figure 9). It can be seen that the curves of the rope model as well as those of the beam model according to Th 1. O delimit an area in which all the curves of the beam model according to Th 2. O are located. At low belt tensions the Th 2. O model behaves like the beam model according to Th 1. O. If the belt tensions are assumed to be very high, it behaves like the rope model. Consequently, the approach according to Th 2. O includes the information of the rope model and the Th 1. O beam model.

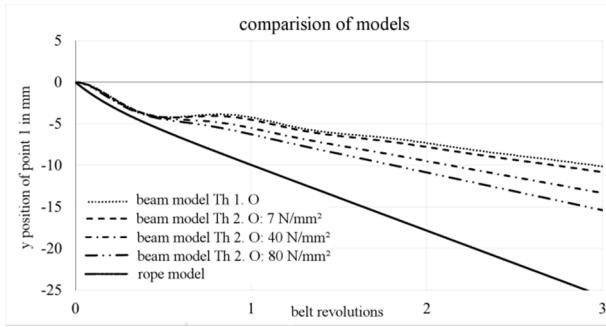


Figure 9: comparison of models

4.4 Low-tensioned belts

In order to be able to describe the effect of the decreasing tension force on the lateral running behaviour of the steel processing belt, Ritzinger [3] made fundamental considerations. The belt span is reduced theoretically to the two belt edges, which are defined as two independent ropes. Each of the ropes is loaded with half the weight of the belt span in the form of a rectangular distributed load. When the pulley gets yawed by β , the distances between the run-up and run-off points of the two ropes differ. This results in different sag. These saggings as well as the tension forces F_1 , F_2 in the two ropes are calculated over the catenary curve. From the two tension forces and the width b of the belt a torque T_{requ} is calculated, which is required to yaw the pulley.

$$T_{requ} = (F_1 - F_2) * \frac{b}{2} \quad (16)$$

A highly tensioned belt span (width b , thickness h , length a) counteracts the yawing of the pulley by β with the torque T_{belt} .

$$T_{belt} = -\frac{4 * E * I * \beta}{a} = -\frac{4 * E}{a} * \frac{b^3 * h}{12} * \beta \quad (17)$$

Using the quotient of these two torques, the steady-state running velocity \dot{y}_{ext} of a low-tensioned belt is calculated [3].

$$\dot{y}_{ext} = \dot{y}_{Th 1.0} * \frac{T_{requ}}{T_{belt}} \quad (18)$$

These considerations according to Ritzinger provide similar results for the steady-state velocity at medium belt tensions as the beam model according to Th 2. O. If the belt tension continues to decrease, a significantly lower lateral moving speed is obtained from (18).

A new approach is to extend the existing model by considering the real position of the run-up and run-off points instead of the highest pulley position (Figure 10). With increasing the sag, the four points 1-4 move further and further away from the original position and the influence of the yaw angle β decreases. On the other hand, the influence of the roll angle from the rope's point of view increases more and more. In order to be able to include these considerations in a belt model, a suitable analytical description of the free belt spans must be found.

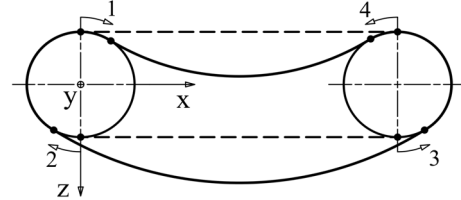


Figure 10: real position of points 1 – 4 at low belt tension

5. BEAM MODEL VS. MEASUREMENT

Before the development of further mathematical models for low-tensioned belts can be started, the behaviour of the system must be studied. The first step is to identify how the steel belt ($b = 200$ mm, $h = 0.3$ mm) actually behaves on the test rig (Figure 11: centre distance $a = 11.28$ m, pulley radius $R = 170$ mm and yaw angle $\beta = -0.042^\circ$) when the tension is reduced.

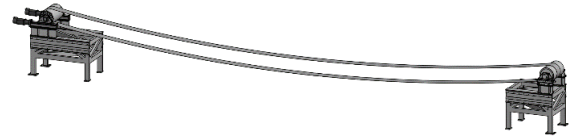


Figure 11: test rig: center distance $a = 12$ m

According to the beam model Th 2. O (Figure 9), the velocity of lateral movement of the run-up point decreases with lower belt tension. This behaviour could only be partially confirmed by the measurements on the test rig. At a belt tension of 40 N/mm², the measured behaviour differs significantly from the calculated belt moving curve, but both show the same behaviour (Figure 12). If the belt tension is decreased further, two unexpected changes occur. First, the belt responds more and more slowly after yawing the pulley. The curves start less inclined (Figure 12, curve 7 and 10 N/mm²). If, however, the lateral movement has started, its speed increases unexpectedly strongly. Compared to the highly tensioned belt, the steady-state velocity of the low-tensioned belt is a lot higher.

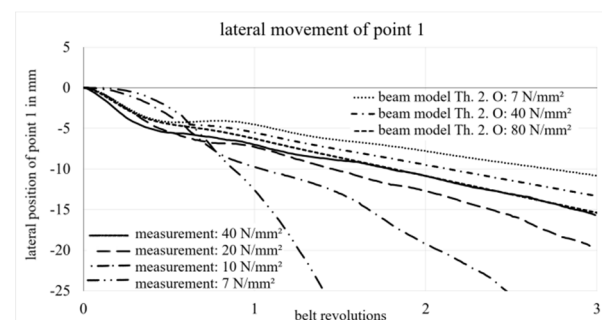


Figure 12: comparison of models and measurement

Figure 13 shows the measured values of the steady-state velocities as well as those calculated using models according to Th 1. O and Th 2. O as a function of the belt tension for the above mentioned belt with a yaw angle of $\beta = -0.042^\circ$ for the run-up point 1.

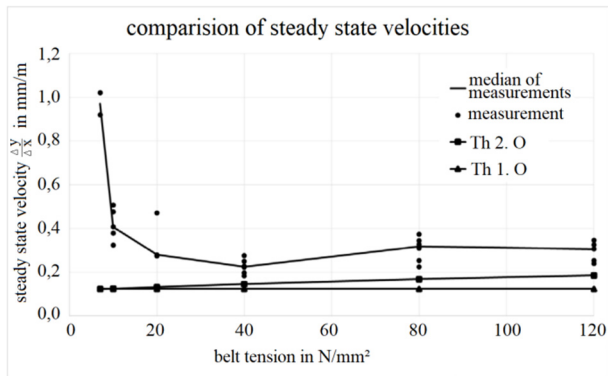


Figure 13: comparison of steady-state velocities

At a belt tension in the range of 20 to 40 N/mm², the Th 2.O model still provides quite realistic results for the steady-state velocity. If the belt tension decreases further, the characteristics of the belt will change significantly, so that the simplification of the belt deformation in one plane loses its validity. At belt tensions below 20 N/mm², its catenary is clearly visible. In addition to the known sideways deflection of the belt, yawing the pulley also results in a tilt in the cross-section of the belt (Figure 14).

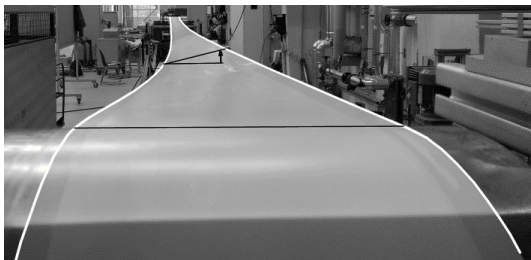


Figure 14: low tensioned belt on test rig at 10N/mm², extrem belt deformation after yawing the pulley

6. SIMULATION

In addition to analytical modelling and measurements on the test rig, the simulation of the belt movement is another method for determining the lateral running behaviour of a steel processing belt. In addition to the already mentioned parameters such as belt tension and yaw angle, the geometry of the belt machine and the belt itself can also be changed.

6.1 Finite Element Method

Koller [4] introduced an Abaqus FEM model for highly tensioned belts. He used a flat strip, meshed with S4R shell elements and rolled it into a ring so that its ends could be joined together. The pulleys were inserted into the belt ring, driven and slowly moved apart so that the belt was stretched into the correct shape. With this FEM model, the behaviour of strongly tensioned process belts was correctly visualized. Therefore these considerations as well as the procedure are continued.

The aim is to be able to also describe low tensioned belts using FEM.

Otto [5] also used the finite element method to describe belt misalignment in belt conveyors. He primarily investigated the effects of geometric errors in the arrangement of the idler stations on the lateral movement of the belt.

6.2 Discrete Element Method

A new kind of simulation arises from the atypical use of the discrete element method (DEM) with the software LIGGGHTS. While DEM is typically used to describe the behaviour of bulk materials, here the belt itself is modelled from particles and placed over the pulleys of the belt machine. Since the connections between the particles can also transmit tension forces, this approach is possible. One of the aims of the DEM simulation is to create a model that can be calculated much faster than the FEM in order to predict the lateral running behaviour of a lightly tensioned belt.

ROPES:

Basic tests with high and low tensioned particle chains on two cylindrical pulleys provide the known behaviour for the rope. Figure 15 shows the movement of a highly tensioned rope and a yawed pulley at three different points in time.

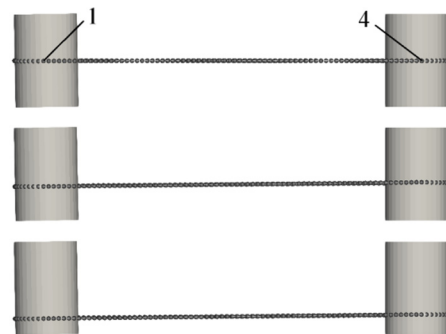


Figure 15: lateral movement of a particle chain

The corresponding diagram for the upper belt span with the run-up point 1 and the run-off point 4 is shown in Figure 16. The simulation shows the known effects such as transient oscillation, steady-state velocity and steady-state offset. Since the ropes have not yet been calibrated, a direct comparison with the analytical models at this point is not yet effective.

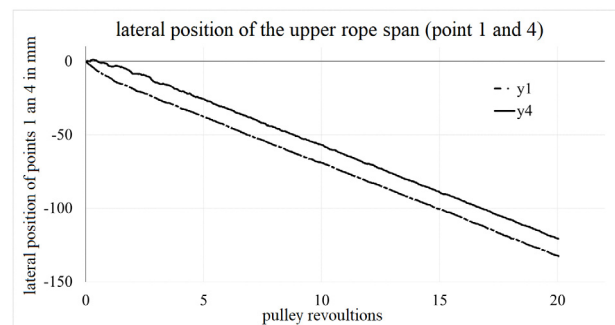


Figure 16: moving diagram for upper rope span

By increasing the rope length, low-tensioned particle chains are created. Figure 17 shows two of these chains,

each after 20 pulley revolutions. It can be seen that the position after the run is approximately the same.



Figure 17: high and low tensioned particle chains on two pulleys, shown simultaneously

BELTS:

If two or more particle chains are arranged next to each other and linked by bonds, a particle belt is formed. It can be placed on the pulleys under high tension (Figure 18) or low tension (Figure 20, above).

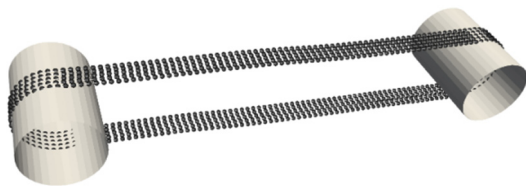


Figure 18: high tensioned particle belt

The simplest way to create the belt is to join the particles together longitudinally and transversely. This makes the connection of the particle chains very weak with respect to shear stresses (Figure 19). If the particles are additionally joined diagonally, the shear strength of the belt is significantly increased.

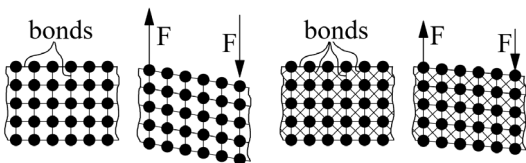


Figure 19: different types of bond arrangement

Based on these considerations, high tensioned as well as low tensioned belts can be operated on two pulleys. (Figure 20).

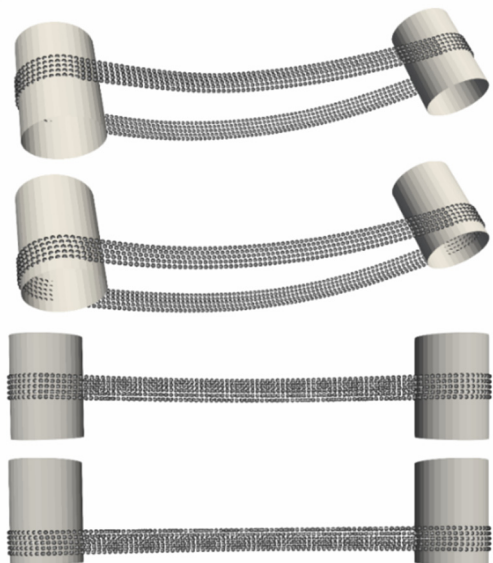


Abbildung 20: low tensioned particle belt

The corresponding belt moving diagram shows the expected behavior. Since the belt models were not yet calibrated at the time this article was written, a comparison with the analytical models or the measurement at this point is not yet meaningful. Consequently, no reliable statement can be made about the behaviour of the belt when the belt tension changes.

7. SUMMARY AND OUTLOOK

The lateral movement behaviour of a highly tensioned steel processing belt can be calculated with the beam model according to 2nd order theory. Measurements have shown that this model loses its validity with decreasing the belt tension. In order to be able to make reliable statements for low-tensioned belts, new models have to be developed. By the positions of the run-up and run-off points and with an analytical description of the belt geometry between these points, the lateral running behaviour at lower belt tension should be calculated according to the known geometric effects.

To estimate the range of validity of the known beam model with respect to belt tension, further measurements on the test rig with belts of different geometries would be desirable. In addition, the measurement results should be used to validate a mathematical model for the low-tensioned belt. In a further step, the considerations made by Koller [4] during the creation of the FEM simulation are taken up again and applied to belts with lower tension. Also the simulation with DEM seems to be helpful for the description of the lateral running behaviour of the steel belt. The work on the described models will be continued. The calibration of these DEM models is in progress.

REFERENCES

- [1] Egger, M.: *Seitliches Laufverhalten des Fördergurtes beim Gurtbandförderer*, TU Wien, PHD Thesis, 2000
- [2] Gabmayer, T.: *Untersuchung der Effektivität verschiedener Steuereinrichtungen zur Beeinflussung des seitlichen Laufverhaltens von Edelstahlprozessbändern*, TU Wien, PHD Thesis, 2011.
- [3] Ritzinger, P.: *Seitliches Bandlaufverhalten von langsam laufenden Metallbändern auf zylindrischen Trommeln*, TU Wien, PHD Thesis 1997
- [4] Koller, M.: *Simulation des seitlichen Verlaufs von endlosen Stahl-bändern*, TU Wien, Master Thesis 2009
- [5] Otto, H. and Katterfeld, A.: Prediction and Simulation of Mistracking of Conveyor Belt, The 8th International Conference for Conveying and Handling of Particulate Solids, Tel-Aviv, Vol. 8, 2015.

Miloš Đorđević

Research Assistant
University of Belgrade
Faculty of Mechanical Engineering

Goran Milojević

Teaching Assistant
University of Belgrade
Faculty of Mechanical Engineering

Andrija Vujičić

Member of the Council
University of Belgrade
Faculty of Mechanical Engineering

Nenad Zrnić

Professor
University of Belgrade
Faculty of Mechanical Engineering

Life Cycle Assessment of The Belt Conveyor Idler Ball Bearing

This paper deals with the LCA of a ball bearing used in belt conveyor idler. Previous work had shown that ball bearing is manufacture intensive product. Therefore herein conducted LCA is cradle-to-gate analysis and it was focused on the production stage of the ball bearing. Chromium steel and stainless steel were considered as ball bearing materials. Results had shown that chromium steel from the ball bearing has the highest environmental impact in all impact categories, followed by processes related to machining of the chromium steel and forging. Change of the lubricant harmed the environmental properties in this case. Future work should consider different materials for raceways and balls.

Keywords: LCA, ball bearing, manufacturing, lubricant, environmental impact).

1. INTRODUCTION

This paper deals with the LCA of the conveyor roller ball bearing. Simplified LCA analyzes of the ball bearing have already been done in [1-3]. In those analyzes, the ball bearing was treated in different ways.

Ball bearings are recognized as very important parts of belt conveyors. Most of the belt conveyors consist of idlers with built-in ball bearings. Usually, two ball bearings are constituent parts of each idler. As previously explained in [1, 2], idlers are one of 5 major groups of belt conveyor components [1, 2]. In previous papers related to this issue [2, 3], ball bearings were treated as components made of a single material - steel. Besides that, the influence (environmental impact) of lubricant used in ball bearings was investigated.

Terminology and terms related to the life cycle, LCA (Life Cycle Assessment), sustainable development, Ecodesign and LCT (Life Cycle Thinking) were explained in [2-6].

The first part of the paper summarizes previous work and conclusions related to ball bearings. Since the production stage of the ball bearing is recognized as the most significant stage of the ball bearing life cycle, the second part of the paper deals with cradle-to-gate LCA, focused on this issue.

This analysis is important for future work which is related to the development of the LCA methodology for short type belt conveyors.

2. PREVIOUS WORK

Previous work, related to ball bearing and its LCA analyzes was published in several scientific papers. Most of the LCAs were conducted in EA (Ecodesign Assistant) and EP (Ecodesign PILOT - Product Investigation, Learning and Optimization Tool) software tools,

available at [7], and explained in [2-4] and [8]. The exception was the last paper from this series [5]. This last LCA was conducted using SimaPro 8 Educational software package [9].

The first of these papers was [3], followed by [1], [2] and [5].

2.1 Simplified LCA of the belt conveyor idler [3]

The functional unit of the idler roller was defined as: "Carrying and aligning conveyor belt at 500 rpm rotational speed for 30,000 h". Functional unit and bearing life (as well as idler life and belt conveyor life) were determined based on L_{10} bearing life. Having that in mind calculated bearing life was 6.23 years for a belt speed of 3.5 m/s and 5.45 years for a belt speed of 4 m/s. " L_{10} bearing life is commonly used and accepted for bearing life calculations and rating. While bearing life is often used as an indicator of idler life, it must be recognized that the effect of other variables (e.g., seal effectiveness) may be more important in determining idler life than the bearings. Nevertheless, since bearing rating is the only variable for which laboratory tests have provided standard values, CEMA uses bearing L_{10} life as a guide for establishing idler ratings." [10].

Grease FOR LPD 2, used for lubrication of ball bearings, was recognized as environmentally hazardous material. The estimated input per use was 4×10^{-4} kg. It consists of EP based mineral oil and Li-soap as thickener [11].

The lubricant was considered as a part in the raw materials stage or as auxiliary material in the product use stage. Both approaches gave the same result.

Ball bearing was considered a part made of steel.

2.2 Simplified LCA of the belt conveyor [1]

To conduct simplified LCA using EA and EP this paper brought several assumptions and simplifications:

- The belt conveyor was divided into 5 major groups of parts.
- All idler ball bearings are presumed to be 6310 C3 type.

Correspondence to: Miloš Đorđević, Research Assistant
Faculty of Mechanical Engineering,
Kraljice Marije 16, 11120 Belgrade 35, Serbia
E-mail: mddjordjevic@mas.bg.ac.rs

- Ball bearings were presumed to be made of steel. (Analysis conducted in EA and EP had justified this assumption)

This analysis has also shown that the most significant stage in ball bearing life cycle is its production stage - too many production processes involved. This is presented in more detail in [2].

Lubricating grease was considered in a same manner as in [3]: 1. as product part in raw materials stage and 2. as auxiliary material in product use stage. Both options gave the same result.

Since lubricants and most of the auxiliary and process materials are marked as hazardous waste, their replacement with renewables contributes to sustainable development by reducing their environmental impact. Like stated in [3]: "mineral oil based lubricant can be replaced with vegetable oil, ionic liquid or synthetic ester based lubricant resulting in similar or even better tribological and better environmental properties at the same time.". There is also stated that: "Consumption of process and/or auxiliary materials can be reduced through recycling coolants, lubricants and process water.".

2.3 LCA of a belt conveyor and its application [2]

In this monograph chapter in addition to the conducted simplified analyses of the complete belt conveyor and its main components, three more simplified analyses are conducted to verify previously obtained results. These analyses included simplified LCA of ball bearing 6310 C3.

In accordance with L10 bearing life minimum service life of the belt conveyor was presumed to be 5 years. It is calculated. Actual life span of a belt conveyor is considerably longer and it equals 25 to 30 years. Therefore, ball bearings are to be replaced at least 5 to 6 times during the conveyor lifetime. Ball bearings are parts that are most often changed as spare parts. They are becoming worn-out mostly because of inadequate lubrication, harsh working condition and improper installation.

Simplified LCA of the ball bearing 6310 C3 type, conducted with EA and EP, showed that it is B type product. All assumptions made in [1] and [3] related to ball bearings were retained. Four iterations were conducted during the analysis. Different cage materials and lubrication in two different life cycle stages were considered. Regardless input changes throughout iterations, result form remained the same. "Too many production processes such as machining, multiple stages grinding, polishing, washing, cutting, die punching and furnace hardening alongside with use of water-based and oil-based lubricants, kerosene and other process materials results in manufacturing intensive product, see Table 1." [2].

Here is explanation why change in type of the product (considering ball bearing) did not affect the result of the analysis conducted in [1]: Although the ball bearing belongs to B type products, its production energy, multiplied by the number of ball bearings installed in the belt conveyor, is negligible in comparison with energy consumption of the belt conveyor in the use stage.

Therefore, this fact did not change the outcome of the conducted analysis described in 1].

Table 1. Ball bearing parts and most of their production processes and process materials

Product part	Manufacturing process	Process material
Raceways	Machining	
	Grinding	Water-based lubricant
	Polishing	Oil-based lubricant
	Washing	Oil and kerosene
Balls	Steel wire cutting	
	Die-punching	
	Grinding (3÷4 stages)	
	Hardening (furnace)	
	Washing	
Cage	Die-punching	
	Machining	
Automatic assembly machine	Testing	
	Quality control	
	Laser marking	

"Ecodesign PILOT's improvement strategies are also the same for each iteration. All of the improvement strategies are primarily focused on the manufacturing stage and thus on the reduction of energy consumption in the production process and optimizing type and amount of process materials followed by reducing waste and ecological procurement of external components." [2].

Lubricating oils and greases can be replaced with more environmental friendly lubricants such as SKF biodegradable, low-toxicity, synthetic ester-based greases using a lithium-calcium thickener or with environmentally adapted lubricants (EALs).

"EALs are based on biodegradable base fluids with a high degree of renewable content. Lubricants that reduce the environmental impact are generally technically as good as regular ones and fulfill the same requirements. A 60% biodegradation within 10 days is the requirement for readily biodegradable lubricants. Renewability is becoming increasingly important due to worldwide oil depletion. A source is considered renewable if it can be renewed within approximately 100 years. Vegetable oils and synthetic esters are more readily biodegradable than base oils originating from crude oil. Vegetable oils have excellent lubricating properties, are biodegradable and renewable, and are in general low toxic. However, the oxidation stability is low and they have limited cold flow properties [12]." [2].

"Lubricants age when being used. This implies that additives are being used and that base oils degrade. In addition, the lubricant may have become contaminated

with water, dissolved contaminants or particles. After a while, the lubricant is not suitable in the application and needs to be replaced. However, the used lubricant can be re-refined by purification, removal of water, particles and soluble contaminants. Any mineral-based lubricant or industrial oil that is not suitable to be used should be re-refined rather than burnt [12].” [2].

“When considering the selection of lubricant it should be kept in mind that the purpose of lubrication is: 1. wear/friction reduction, 2. heat dissipation and 3. protection against corrosion and environmental influences.” [2].

2.4 LCA of the Manufacturing Stage of the Laboratory Belt Conveyor [5]

Conducted LCA represents a cradle-to-gate analysis. The analysis was focused on the production stage of the belt conveyor. The use phase and the end of life phase were not modeled.

Since global warming, climate change and other environmental impacts are more and more gaining on importance, energy efficiency, energy saving, and resource usage become more and more relevant. This paper does just that by emphasizing the importance of improving energy efficiency and resource use.

The analysis had shown that if the system contains components that are built-in as finished products, it is important to investigate their composition to determine if any of the environmentally problematic substances are present. There is a lot of literature talking about this issue, especially when it comes to applying the “cut-off” rule. Process and auxiliary materials are often hazardous substances. Following previously stated, the nature and amount of these additional materials should be inspected. However, in this case specifically, there were no many process and auxiliary materials so they were excluded from the analysis. On the other hand, copper from the EM was considered a problematic substance and its influence is shown in the paper.

3. GOAL AND SCOPE OF THE LCA

3.1 Description of the product

The product that is the subject of analysis is the ball bearing 6310 C3 type, Figures 1-2 and Table 2.

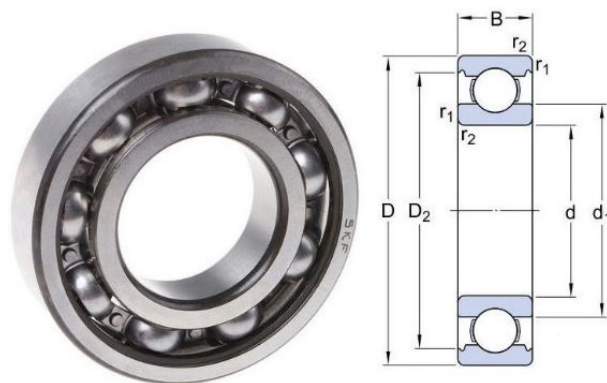


Figure 1. Ball bearing 6310 C3 type

Table 2. Ball bearing details

Dimensions [mm]		Characteristics	
Outer diameter	D = 110	RPM	8,500 ÷ 13,000
Inner diameter	d = 50	C	65 kN
Width	B = 27	C ₀	38 kN
Ball diameter	≈ 20	Mass	1.1 kg



Figure 2. Packaging of the ball bearing 6310 C3 type

3.2 Goal and scope definition

As well as in [5], this LCA also is intended for internal screening at the Faculty of Mechanical Engineering at the Department for Material Handling, Constructions and Logistics and academic population.

Functional unit is defined as: “Producing one 6310 C3 ball bearing”.

4. LCI PHASE

Having in mind analysis of the ball bearing described in [2] and reintroduced in Chapter 2.4, the following parts, materials, and processes will be considered in this LCA, see Table 3.

Table 3. Ball bearing 6310 parts, materials and processes

Part	Material and process material	Process
Ball bearing (finished product)	Chromium Steel (raceways and balls) Lubricating Oil (0.1 kg) Cardboard (packaging)	Assembly Inspection Laser Marking Transport
Raceways -inner (m = 0.3 kg) -outer (m = 0.5 kg)	Chromium Steel Water Oil Thick Oil Kerosene	Hot Forging 4-stage Grinding Heat Treatment Turning Polishing Cleaning
Balls (m _B = 0.2 kg)	Chromium Steel Water Oil Thick Oil Kerosene	Steel Wire Cutting Die-punching 3-4 Stage Grinding Hardening Polishing Cleaning

Chromium steel will be considered as ball bearing material for both raceways and balls. Cage will be neglected since it is noticed that the cage does not influence on the analysis. Due to its small mass, it can also be removed by the “cut-off” rule.

Due to the lack of data, water used for different production processes will not be considered in this analysis, as well as polishing and cleaning processes. Steel wire cutting together with die-punching processes are replaced with forging. Grinding is replaced with chromium steel removed by milling. Since there is no adequate process found in the database for the heat treatment of the steel parts, electric energy consumed by the furnace is used instead [15]. Oil and thick oil used for grinding, polishing, and quenching are replaced with lubricating oil. Due to the lack of data, one more petty rough assumption is made: consumption of lubricating oil for the above-mentioned processes is estimated to be

10% of the finished product mass. Transportation of the finished product is assumed to be 500 km, which is presented with 0.575 tkm.

Therefore materials and processes can be summarized as in Table 4.

Table 4. Summarized materials and processes

Material and process material	Process
Chromium Steel	Forging
Lubricating Oil	Turning
Kerosene	Milling
Cardboard (packaging)	Electricity
	Laser machining (marking)
	Transport

Calculations are in more detail presented in Figure 3.


Name Ball Bearing - summarized	Image 	Comment
Status None		
Materials/Assemblies	Amount	Unit
Corrugated board box (GLO) market for Alloc Def, S	0,05	kg
Lubricating oil (GLO) market for Alloc Def, S	0,21	kg
Steel, chromium steel 18/8 (GLO) market for Alloc Def, S	1	kg
Kerosene (Europe without Switzerland) market for Alloc Def, S	0,11	kg
Vegetable oil, refined (GLO) market for Alloc Def, S	0	kg
(Insert line here)		
Processes	Amount	Unit
Carton board box production, with offset printing (GLO) market for Alloc Def, S	0,05	kg
Chromium steel removed by turning, average, computer numerical controlled (GLO) market for Alloc Def, S	0,43	kg
Chromium steel removed by milling, average (GLO) market for Alloc Def, S	0,29	kg
Electricity, medium voltage (RS) market for Alloc Def, S	0,376	kWh
Forging, steel (GLO) market for Alloc Def, S	1,337	kg
Laser machining, metal, with YAG-laser, 30W power (CA-QC) laser machining, metal, with YAG-laser, 30W power A	0,0014	hr
Transport, freight, lorry >32 metric ton, EURO3 (GLO) market for Alloc Def, S	0,575	tkm
(Insert line here)		

Figure 3. Inputs in SimaPro for ball bearing [9], [13-15]

5. LCIA PHASE

Impacts on the environment have been calculated using the Ecoinvent 3 database and CML-IA baseline V3.02 method. Impact assessment has been done through several iterations.

The first iteration summarized all similar processes as shown in Figure 4.

In all impact categories, chromium steel has the highest impact, followed by impacts related to its processing, that is operations of milling and turning of the chromium steel. Forging of the steel has visible influence also, while kerosene and lubricating oil realize significant impact only in ODP (Ozone layer Depletion Potential) and ADP (Abiotic Depletion Potential) impact categories. Electricity realizes the noticeable impact in MAEP (Marine Aquatic Ecotoxicity Potential), POCP (Photochemical Oxidation Creation Potential), AP (Acidification Potential), and especially in EP (Eutrophication Potential). All other materials and processes realize negligible impacts.

In the second iteration, lubricating oil is replaced with vegetable oil to reduce environmental impact. However,

its use has an increasing environmental impact, to a considerable extent, Figure 5.

6. CONCLUSION

Following previous work it can be concluded that bearings can be improved from different points of view:

- Reducing friction losses
- Bearing temperature monitoring
- Bearing lubrication
- Energy-saving bearings

Improving operation and maintenance can be done by monitoring bearings vibrations and temperature and timely replacement of the worn-out bearing [10] and [16].

Options for environmental improvement:

- Slider bearings made of plastics
- Eco-friendly lubricants
- Energy-saving bearings

Higher bearing quality reduces resistances and provides higher energy efficiency.

Besides, if one considers the result presented above, which, by changing the lubricant, produces a worse effect, it follows that special care should be taken to

select the appropriate lubricant for each purpose to minimize environmental impact. Additional iterations are needed to find the lubricant with the best (or at least better) environmental characteristics.

And finally, future research should consider different materials for rolling paths and balls. Thereafter, the results should be compared with these and the conclusions regarding the rolling bearings made.

ACKNOWLEDGMENT

This work is a contribution to the Ministry of Education, Science and Technological Development of Republic of Serbia funded project TR 35006.

REFERENCES

- [1] Đorđević, M., Zrnić, N. and Jerman, B.: Simplified life cycle assessment of a belt conveyor, Proceedings of the 21st International Conference on Material Handling, Constructions and Logistics - MHCL 2015, ISBN: 978-86-7083-863-5, University of Belgrade, Faculty of Mechanical Engineering, September 23rd - 25th, Vienna, Austria, pp. 199-206, 2015.
- [2] Đorđević, M., Zrnić, N. and Bošnjak, S.: LCA of a Belt Conveyor and its Application, in: Borut, J. (Ed.): *Next Generation Logistics: Technologies and Application*, Scientific Monograph, Scientific Publishing Hub, Chapter 8, pp. 175-197, 2017.
- [3] Đorđević, M., Zrnić, N. and Pantelić, M.: Simplified life cycle assessment of a return belt conveyor idler, Proceedings of the 11th International conference on accomplishments in Electrical and Mechanical Engineering and Information Technology - DEMI 2013, Banja Luka, BiH, May 30th - June 1st, University of Banja Luka, Faculty of Mechanical Engineering, ISBN 978-99938-39-46-0, pp. 201-206, 2013.
- [4] Zrnić, N. and Đorđević, M.: *Ecodesign: Sustainable Product Development* (in Serbian: *Dizajn i Ekologija: Održivi Razvoj Proizvoda*), ISBN 978-86-7083-772-0, University of Belgrade, Faculty of Mechanical Engineering, Belgrade, Serbia, p. 526, 2012.
- [5] Đorđević, M., Mladenović, G., Zrnić, N. and Bošnjak, S.: LCA of the Manufacturing Stage of the Laboratory Belt Conveyor, FME Transactions, Vol. 46, No. 3, pp. 410-417, 2018.
- [6] EN ISO 14040: 2006.
- [7] www.ecodesign.at
- [8] Wimmer, W. and Züst, R.: *Ecodesign PILOT - Product Investigation, Learning and Optimization Tool for Sustainable Product Development*, Kluwer Academic Publishers, ISBN 1-4020-0965-8, Dordrecht, The Netherlands, p. 99, 2003.
- [9] SimaPro Life Cycle Analysis version 8.0.4.7 (software) by Pre Consultants.
- [10] *Belt Conveyors for Bulk Materials*, 6th Edition, USA, CEMA, ISBN 1-89117-59-3, p. 600, 2007.
- [11] FOR LPD 2 / EP Lubricant, from <https://fam.co.rs/art/246/mazive-masti-i-specijalna-aziva/specijalna-maziva-za-dugotrajno-podmazivanje/for-lpd-2.html>, accessed on 2019-07-10.
- [12] Torbacke, M., Rudolphi, A.K. and Kassfeldt, E.: *Lubricants, Introduction to Properties and Performance*, John Wiley & Sons Ltd, ISBN: 9781118799741, United Kingdom, 2014.
- [13] Kalpakjian, S. and Schmid, R.S.: *Manufacturing Processes for Engineering Materials*, 5th Edition, Pearson Prentice Hall, New Jersey, 2007.
- [14] https://www.alibaba.com/product-detail/Full-automatic-bearing-assembly-machine_60462234882.html?spm=a2700.7724857.normalList.1.47d43277yObS0V&s=p, accessed on 2019-07-10.
- [15] <http://ba.zdfurnace.com/quenching-furnace/pit-type-quenching-furnace/high-temperature-pit-type-hardening-furnace.html>, accessed on 2019-07-10.
- [16] Đorđević, M., Zrnić, N. and Jerman, B.: Simplified life cycle assessment of a belt conveyor electric motor, Proceedings of the 14th International conference "Research and Development in Mechanical Industry – RaDMI 2014", Topola, Serbia, September 18th - 21st, SaTCIP, Vrnjačka Banja, ISBN 978-86-6075-047-3, pp. 671-678, 2014.

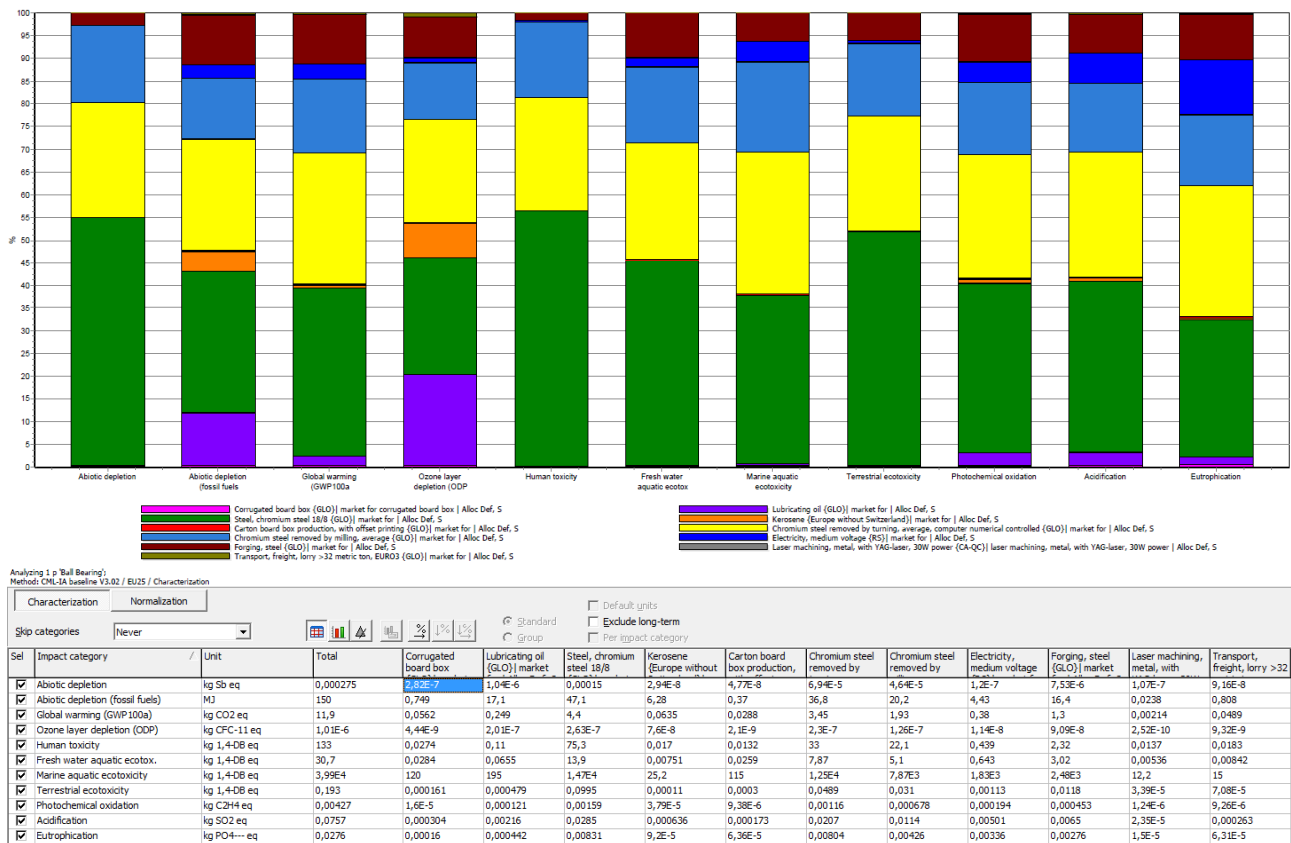


Figure 4. Characterization of the first iteration [9]. Chart and Table representation

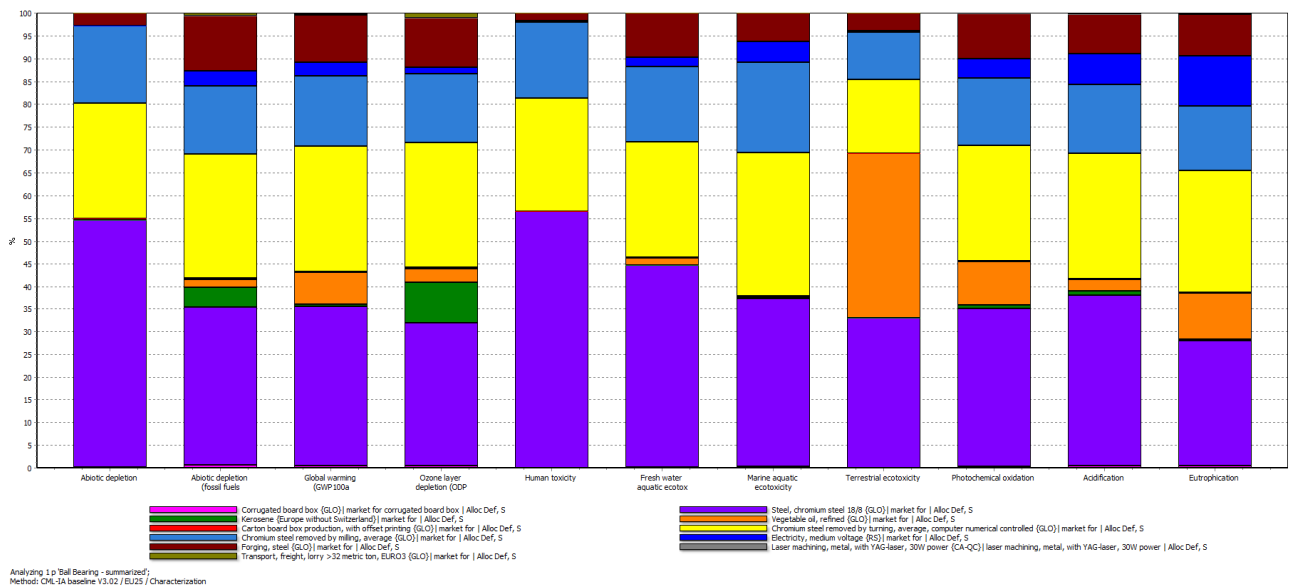


Figure 5. Characterization of the second iteration [9]. Lubricating oil is replaced with vegetable oil

SESSION B

CONSTRUCTIONS, DESIGN ENGINEERING, MINING EQUIPMENT AND TECHNOLOGIES

Miodrag ArsićPrincipal Research Fellow
Institute for materials testing
Belgrade**Srđan Bošnjak**Professor
University of Belgrade
Faculty of Mechanical Engineering**Vencislav Grabulov**Principal Research Fellow
Institute for materials testing
Belgrade**Nebojša Gnjatović**Assistant Professor
University of Belgrade
Faculty of Mechanical Engineering**Ivan Milenović**PhD Student
University of Belgrade
Faculty of Mechanical Engineering

Repair Methodology for the Carrying Structure of the Rejecting Drum of the Bucket-Wheel Reclaimer Stacker Conveyor at Coal Landfill

Damaging of the carrying steel structure and embedding of the rejecting drum of the stacker conveyor occurred during the exploitation of the bucket-wheel reclaimer with the belonging stacker. The analysis of the cause and level of damaging led to the conclusion that damaged parts should be replaced by new ones and that methodology of repair should be based on the application of a suitable welding technology. This paper presents the methodology of repair welding performed during the replacement of the damaged carrying structure and embedding of the rejecting drum of the stacker conveyor which consist of steel sheets and profiles that's based on the conceptual solution for damage repair through the use of program package 'Catia' – V5 that enabled the creation of models and graphic documentation of structural parts that should be replaced by new ones. It should also be noted that geodetic survey of the lower belt of the stacker structure was performed after the substitution of damaged parts of the structure.

Keywords: spreader, open pit surface mine, welded structure, damage, repair

1. INTRODUCTION

At the coal landfill of the thermal power plant 'Nikola Tesla A' in Obrenovac (Serbia) two bucket-wheel reclaimers with internal designations DU1 and DU2, manufactured by french company 'Ameco', are in service. They are moving along the circular track (the so called polar track), and it should be noted that there are only 3 bucket-wheel reclaimers of that type in Eastern Europe. The third bucket-wheel reclaimer manufactured by 'Ameco' operates at the coal landfill that belongs to thermal power plant 'Nikola Tesla' in Obrenovac.

Bucket-wheel reclaimer with the belonging stacker [1] is presented in figure 1, while damages that occurred at the support steel structure and embedding of the stacker conveyor rejecting drum before repair are shown in figure 2. Figure 3 shows the condition of the support steel structure and embedding of the stacker conveyor rejecting drum after temporary repair has been carried out.



a) Bucket-wheel reclaimer (DU1);



b) Appearance of the bucket-wheel reclaimer (view from the side);



c) Appearance of the bucket-wheel reclaimer (view from behind)

Figure 1. Appearance of the bucket-wheel reclaimer with internal designation DU1 and of the boom of the belonging stacker at the coal landfill.

2. REPAIR TECHNOLOGY FOR THE CARRYING STRUCTURE OF THE REJECTING DRUM OF THE BUCKET-WHEEL RECLAIMER DU1 STACKER CONVEYOR

Through the analysis of damages and executed temporary repair of the support steel structure and embedding of the rejecting drum of the bucket-wheel reclaimer stacker conveyor, shown in figures 2 and 3, it can be concluded that temporary repair has not been successful, because figure 3 clearly shows that welded joints have not been executed properly, as well as that

geodesic deviation between the carrying steel structure and embedding of the rejecting drum of the stacker conveyor occurred. Only by replacing the complete section of the damaged structure its integrity and service life could be maintained.

After the determination of the cause and amount of damage that occurred at the steel structure of the rejecting drum of the bucket-wheel reclaimer stacker conveyor during service it was concluded that repair methodology should be based on the application of adequate welding technology.



a) Damage that occurred on the carrying structure of the drum (right side);



b) Damage that occurred on the carrying structure of the drum (left side);



c) Detail that indicates the cause of geodesic deviation of parent material during the repair of carrying structure;



d) Damage at the structure of an embedding of the stacker conveyor rejecting drum – detail;



e) Damage at the carrying structure of an embedding of the stacker conveyor rejecting drum – side view;

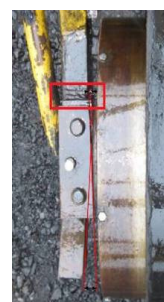


f) Damage and a crack at the carrying structure of an embedding of the stacker conveyor rejecting drum

Figure 2. Appearance of damages that occurred at the carrying structure and embedding of the stacker conveyor rejecting drum.



a) Appearance of the rejecting component of the stacker and of the last repair carried out in the area of the damage that occurred at the carrying structure of the drum;



b) Badly executed welded joint and repair carried out in the area of the damage that occurred at the carrying structure of the stacker conveyor rejecting drum

Figure 3. Appearance of the carrying steel structure of the stacker conveyor rejecting drum after temporary repair.

On the basis of the design solution for the repair which relied on program 'CATIA' – V5 the models and graphic documentation which refer to components that should be replaced were created, figure 4.

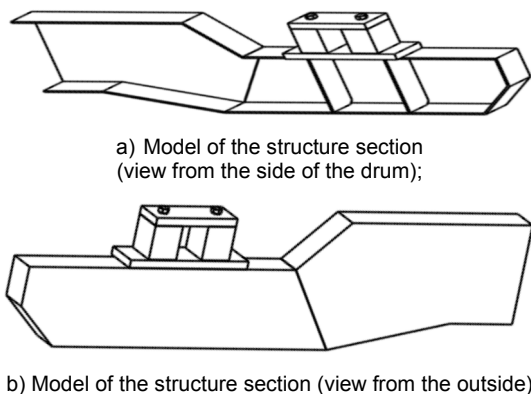


Figure 4. Model of components that should be replaced by new ones at the carrying structure of the rejecting drum of the bucket-wheel reclaimer stacker conveyor.

3. TECHNOLOGY OF WELDING OF NEW COMPONENTS AT THE CARRYING STRUCTURE OF THE REJECTING DRUM OF THE WHEEL RECLAIMER DU1 STACKER CONVEYOR

Complete welding of new components at the carrying structure of the rejecting drum of the bucket-wheel reclaimer stacker conveyor at the coal landfill located near thermal power plant 'Nikola Tesla A' in Obrenovac which were joined by butt and/or fillet welds formed between steel sheets and profiles made of structural steel should be carried out in accordance with technology presented in reference [2].

Taking into account the fact that the user of equipment does not possess project and technical documentation, creators of the welding technology assumed that structural steels S235J2G3 and S355J2G3 (in accordance with standard EN 10025-2 [3]) were used, which are often being applied for the making of steel structures of bucket-wheel reclaimers and stackers.

3.1 Introductory considerations

Properties of parent material and profiles made of structural non-alloyed steels S235J2G3 and S355J2G3 (in accordance with standard SRPS EN 10025-2:2011) [3] are presented in tables 1 and 2.

Table 1. Chemical composition in accordance with [3]

Steel	C (%)	Si (%)	Mn (%)	P (%)	S (%)	Cu (%)
S235J2G3	≤ 0.19	-	≤ 1.50	≤ 0.045	≤ 0.045	≤ 0.60
S355J2G3	≤ 0.23	≤ 0.60	≤ 1.70	≤ 0.045	≤ 0.045	≤ 0.60

Table 2. Mechanical properties in accordance with [3]

Steel	Yield strength YS (N/mm ²)	Tensile strength TS (N/mm ²)	Elongation A5 (%)
S235J2G3	235	360 - 510	24
S355J2G3	355	470 - 630	22

3.2 Weldability of parent material (sheets and profiles)

Weldability of sheet and profile material can be operative, metallurgical and structural. Ability of material to be joined by welding (technological process of material joining) is being determined by material equivalent CEV, which is being calculated on the basis of chemical composition. Equations from which the CEV could be obtained are as follows:

According to the International Institute of Welding (IIW)

$$CEV = C + \frac{Mn}{6} + \frac{Cr + Mo + V}{5} + \frac{Ni + Cu}{15} (\%) > 0.45 \quad (1)$$

According to Ito-Bessyo

$$CEV = C + \frac{Si}{30} + \frac{Mn + Cu + Cr}{20} + \frac{Ni}{60} + \frac{Mo + V}{15} + \dots + 5B (\%) > 0.45 \quad (2)$$

According to HCS (Hot Cracking Sensitivity)

$$HCS = \frac{100C \cdot \left(S + P + \frac{Si}{25} + \frac{Ni}{100} \right)}{3Mn + Cr + Mo + V} (\%) \leq 4.5 \quad (3)$$

- Through the use of HCS equation (Hot Cracking Sensitivity) it was determined that the material is not prone to hot cracking, due to the fact that obtained result is smaller than 4.5 (boundary value for the occurrence of hot cracks in steels with tensile strength $TS < 700 \text{ (N/mm}^2\text{)}$)
- For chemical compositions of materials presented in table 1 and in the case of the least favourable content of hydrogen in weld metal ($H = 6 \text{ ml/100 grams}$) preheating at temperatures up to 100°C is required;
- Maximum hardness in heat-affected zone (HAZ) for shown chemical compositions of parent material can not be higher than 350 HV, which means that materials are not prone to cold cracking;
- Critical cooling rate at which purely martensitic structure which would cause cold cracking occurs should be lower than 32°C/sec , which means that no delayed cooling is necessary;
- Taking into account the fact that tensile strength of profile material is $TS < 700 \text{ N/mm}^2$, hot cracking is not likely to occur.

3.3 Selection of the process and filler material for repair welding of new components

By the analysis of parameters on which the selection of the process of repair welding depends (weldability of material, energetic possibilities of welding processes, geometric complexity of the structure, economic indicators) it was determined that process 111 is the most appropriate process for application. Due to limited possibilities of execution of preheating and heat treatment after repair welding, the most optimal solution was to use Mo alloyed basic electrodes EVB Mo (Jesenice), classified in accordance with standard [4]. Chemical composition of pure weld metal is shown in table 3, while mechanical properties are presented in table 4.

Table 3. Chemical composition

Electrode	C (%)	Si (%)	Mn (%)	Mo (%)
EVB Mo	0.10	0.50	0.80	0.50

Table 4. Mechanical properties of pure weld metal

Electrode	Yield strength YS _{0.2%} (N/mm ²)	Tensile strength R _m (N/mm ²)	Elongation A ₅ (%)	Impact energy KV _{300/2} (J/cm ²)
EVB Mo	> 450	530 - 630	> 22	> 47 (- 20 °C)

3.4 Rules that should be abided during the execution of welding

Rules that should be abided during the execution of welding are presented due to the fact that no welding technology qualification for sheets and profiles was predicted:

- Preparation of grooves and surfaces for welding should be performed by grinding. All requirements defined in the specification of welding technology have to be met;
- Allowed deviation regarding the parallelness of surfaces and constituting elements with respect to the welding axis is 1-2 mm;
- Allowed deviation of verticality of the position of constituting elements with respect to the welding axis is 1°;
- Allowed deviation of the position of constituting elements with respect to the welding axis is 1 mm;
- Edges of segments of constituting elements should be thoroughly cleaned from the outside at a length of 15 mm from the edge of the segment;
- Prior to processing edges of constituting elements have to be degreased and clean;
- Number of passes n (including the roots) for welding is the constituting part of the welding technology specification;

Butt welds (depending on the thickness of parent material):

$$n = \frac{A_{ov} - A_r}{A_f} - 1 \quad \text{- for one-sided welding} \quad (4)$$

where:

- n - number of welding passes (including the root)
- A_{ov} (mm²) - overall area of the weld defined with respect to the groove shape
- A_r (mm²) - area of the root weld
 $A_r = (4 \div 6) \cdot d_e$
- A_f (mm²) - surface of the weld fill
 $A_f = (6 \div 9) \cdot d_e$
- d_e (mm) - diameter of the electrode

Fillet welds (depending on the cathetus of the 'k' weld)

$$n = \frac{A_{ov}}{A_f} \quad A_{ov} = (0.6 \div 0.65) \cdot k^2 \quad (5)$$

for grooves with area smaller than 20 mm² value 0.65 is being adopted, while value 0.6 is being adopted for grooves with area higher than 20 mm².

- Filler material has to respond to parent material regarding the chemical composition and mechanical properties;
- Quality and dimensions of filler material are listed in the welding technology specification for every single welded joint;
- Welding electrode has to be completely dry and devoid of dirt and grease;
- Designations and types of filler material are integral parts of the welding technology specification, in accordance with the appropriate standard;
- Welding should be executed only by welders with an adequate certificate, in accordance with standard SRPS EN 287-1 [5];
- Tacking of profiles and sheets should be performed with length of 10 mm. Taking into account the fact that tacking edges remain integral parts of the root weld they have to be flawless;
- Electric arc used for tack welds is being generated by pulling in front of the starting point of the weld, in the section of the groove which would subsequently be welded. The establishment of the arc should not be executed on the surface of parent material;
- Welded joints should be executed without interruption, in the most convenient position;
- Welded joints need to have well penetrated roots and mild transition into parent material;
- Welding should be executed with reinforcement as low as possible.

3.5 Preparation of New Components for Welding and Appearance of the Carrying Structure of the Drum After Welding

Figure 5 shows the preparation of new components for welding, while figure 6 offers the appearance of the rejecting drum of the bucket-wheel reclaimer stacker conveyor after welding.

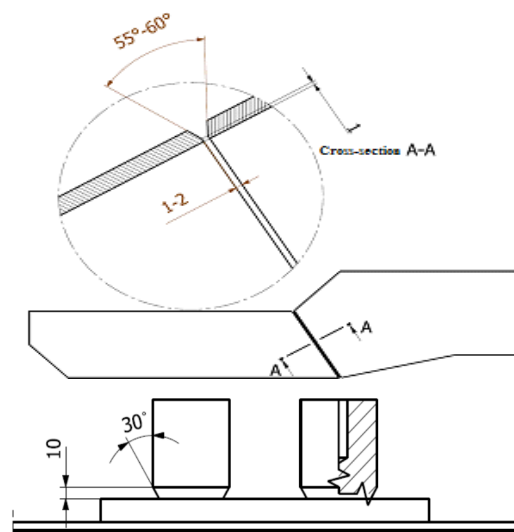


Figure 5. Appearance of the preparation of new components for welding at the carrying structure and embedding of the rejecting drum

During and after welding testing of welded joints by non-destructive methods was carried out (visual testing [5], magnetic particle testing [6], penetrant testing [7] and ultrasonic testing [8]). Geodetic survey was also performed in order to determine if the carrying steel structure and embedding of the rejecting drum were brought to an adequate position and therefore restored functionality.



Figure 6. Appearance of the rejecting drum after the installation of new components at the carrying structure

4. GEODETIC SURVEY OF THE LOWER BELT OF THE STACKER STRUCTURE AFTER THE REPAIR OF THE CARRYING STRUCTURE AND EMBEDDING OF THE REJECTING DRUM

Results of the geodetic survey of the condition of the welded carrying structure and embedding of the rejecting drum after the repair are presented in figures 7 and 8, as well as in tables 1 and 2.

Results of the geodetic survey carried out in order to establish the condition of the lower belt of the welded lattice structure of the stacker boom after the repair of the carrying structure and embeddings of the rejecting drum show that there is no significant deviation from predetermined geodetic values.

CONCLUSION

Integrity of structures is a relatively recent scientific and engineering discipline which in a broader sense comprises state analysis, behaviour and loosening diagnostics, service life evaluation and refurbishment of structures which means that, beside the usual situation in which it is necessary to evaluate the integrity of a

structure when a flaw is detected by means of non-destructive tests, this discipline also comprises structural stress state analysis.

Calculation of the stress state and strength of the carrying structure of the stacker conveyor rejecting drum of the bucket-wheel excavator DU1 at the landfill of the thermal power plant 'Nikola Tesla A' in Obrenovac showed that the integrity of the lattice structure of the stacker as a whole was not jeopardized after the installation of new components.

ACKNOWLEDGMENT

The authors acknowledge the support from the Serbian Ministry of Education, Science and Technological Development for project TR 35006.

REFERENCES

- [1] Available documentation regarding the bucket-wheel reclaimers at the open pit surface mine of the thermal power plant "Nikola Tesla A" in Obrenovac (Serbia), internally labelled DU1 (1971.) and DU2 (1974.), manufactured by "Ameco", France.
- [2] Arsić, M., and Veljović A.: Rehabilitation project of the support steel carrying structure of the rejecting drum of the bucket-wheel reclaimer DU1 stacker conveyor at coal landfill of TPP 'TENT A', Obrenovac, Institute for materials testing, Serbia, 2015.
- [3] EN 10025 - 2: Hot rolled products of structural steels - Part 2: Technical delivery conditions for non-alloy structural steels, European Committee for Standardization, 2004.
- [4] EN 499: E 42 2 Mo B 42, Welding consumables. Covered electrodes for manual metal arc welding of non alloy and fine grain steels, Classification, European Committee for Standardization, 1995.
- [5] EN ISO 17637: Non-destructive testing of welds - Visual testing of fusion-welded joints, European Committee for Standardization, 2016.
- [6] EN ISO 17638: Non-destructive testing of welds - Magnetic particle testing, European Committee for Standardization, 2016.
- [7] EN ISO 3452-1: Non destructive testing - Penetrant testing - Part 1: General principles, European Committee for Standardization, 2013.
- [8] EN ISO 13588: Non - destructive testing of welds - Ultrasonic testing - Use of automated phased array technology, European Committee or Standardization, 2012.

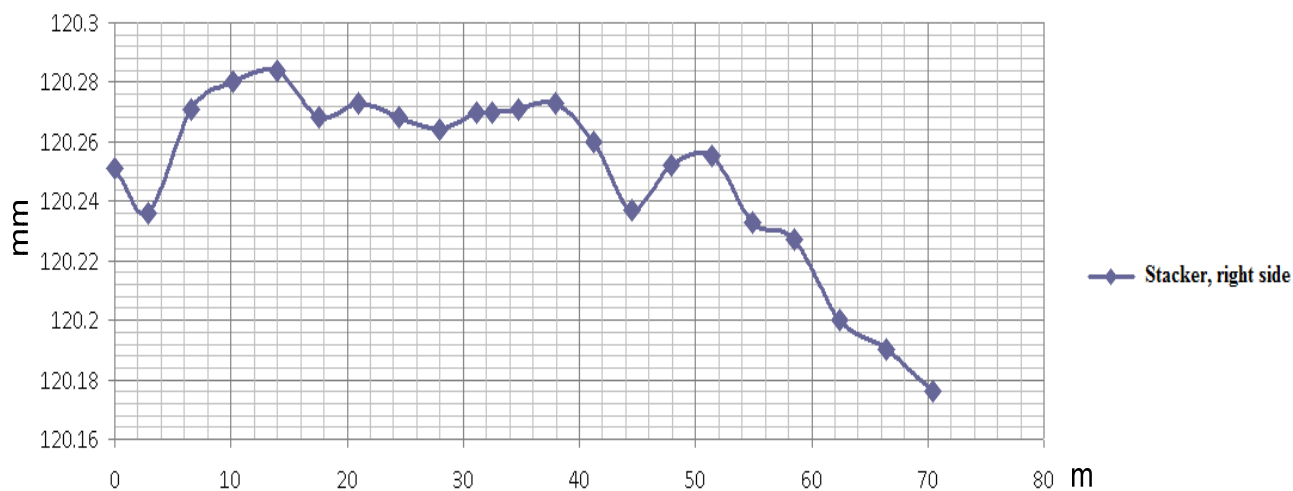


Figure 7. Appearance of results of geodetic survey that refer to the right side of the lower belt of the stacker structure

Table 1. Results of the geodetic survey of the condition of the right side of the lower belt of the stacker structure

Right side of the lower belt of the lattice structure of the stacker																						
RS	0	2.82	6.52	10.23	13.92	17.61	20.98	24.47	27.97	31.21	32.49	34.70	37.94	41.21	44.20	47.94	51.64	54.97	58.46	62.46	66.42	70.42
RGL	120.3	120.3	120.3	120.3	120.3	120.3	120.3	120.3	120.3	120.3	120.3	120.3	120.3	120.3	120.2	120.2	120.2	120.2	120.2	120.2	120.2	120.2

* RS – Right side of the stacker boom; ** RGL – Relative ground level of the stacker boom

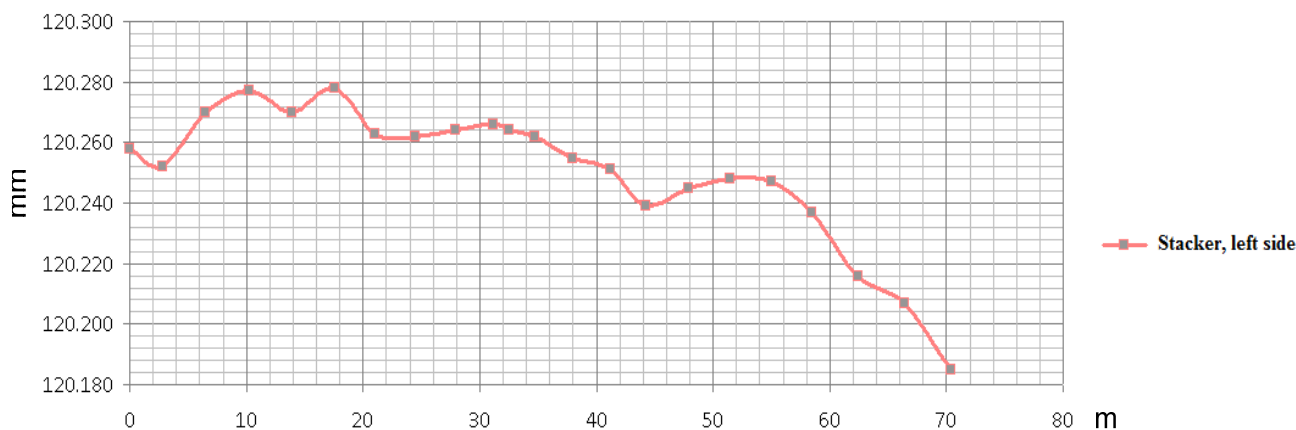


Figure 8. Appearance of results of geodetic survey that refer to the left side of the lower belt of the stacker structure

Table 2. Results of the geodetic survey of the condition of the left side of the lower belt of the stacker structure

Left side of the lower belt of the lattice structure of the stacker																						
LS	0	2.82	6.52	10.23	13.92	17.61	20.98	24.47	27.97	31.21	32.49	34.70	37.94	41.21	44.20	47.94	51.64	54.97	58.46	62.46	66.42	70.42
RGL	120.3	120.3	120.3	120.3	120.3	120.3	120.3	120.3	120.3	120.3	120.3	120.3	120.3	120.3	120.2	120.2	120.2	120.2	120.2	120.2	120.2	120.2

* LS – Left side of the stacker boom; ** RGL – Relative ground level of the stacker boom

Xiang Wen

Engineer
Shanghai Institute of Special Equipment
Inspection and Technical Research

YuQing Yang

Senior Engineer
Shanghai Institute of Special Equipment
Inspection and Technical Research

XiaoYing Tang

Professor
Shanghai Institute of Special Equipment
Inspection and Technical Research

DaoXiang Wei

Engineer
Shanghai Institute of Special Equipment
Inspection and Technical Research

Control strategy research for super - Gaussian random vibration test

Compared with Gaussian random vibration testing, the super-Gaussian random vibration test is preferably designed to simulate practical environment. The super-Gaussian random signal generation principle is studied, what is more, drive signal required for the control system is generated by use of Poisson process and filtering theory. The simulation and experiment tells that the method to generate super-Gaussian random signal is correct, meanwhile, based on the proposed super-Gaussian random vibration control strategy, the high accuracy of output power spectrum and kurtosis can be realized, which satisfies the requirement in practical. At the end, super-Gaussian random vibration control system is applied into the Highly Accelerated life Testing(HALT) in terms of fans, the comparison results indicate that super-Gaussian random vibration excitation signal can obviously speed up the fatigue failure process of fans, which improves test efficiency, reduces the cost and shortens the development cycle of products.

Keywords: random vibration test, super-Gaussian random signal, Kurtosis, vibration control, HALT

1. INTRODUCTION

Vibration test is defined as the process where test piece is exposed to the designated vibration environment created by exciter equipment, and desired aims can be realized. Since majority of products are subject to the random vibration during the process of manufacture, transportation and usage, the detailed random vibration test regulation has been published in vibration test standard home and board, and random signal generated from vibration control system conforms to Gaussian distribution in the regulation mentioned. In practice, although some of products may pass through examination in the traditional random vibration test, certain potential faults still exist. We have seen the truth that these products are apt to fail to work when they experience the super-Gaussian random vibration test, which affects the product performance. To simulate Gaussian random vibration environment with given power spectrum is easy thing while to simulate super-Gaussian random vibration environment with given power spectrum so far is still confronting with some problems in technique.

Smallwood from US Sandi National lab gets the required super-Gaussian random signal through carrying out non-linear transformation to the Gaussian random signal by making use of Zero Memory Nonlinearity [1, 2], (ZMNL). Scholar Alexander from New Zealand realizes environment simulation to non-Gaussian random signal by using polynomial function transformation [3, 4, 5]. Doctor Jiang Yu from national defense university of technology in China investigates

super-Gaussian random vibration control and achieves control to super-Gaussian random vibration test by using quadratic phase modulation. Based on looking up the material home and aboard, Gaussian random signal produced from Poisson Process is applied into vibration control in this study, which provides technical support to the development of random vibration test system.

2. VIBRATION CONTROL PRINCIPLE

2.1 Super-Gaussian random signal

Gaussian signal is defined as random signal whose amplitude probability density conforms to Gaussian distribution while non-Gaussian signal is defined as random signal whose amplitude probability density dose not conform to Gaussian distribution. Non-Gaussian signal which is described by former fourth order accumulation statistical quantity during the random process contains sub-Gaussian signal and super-Gaussian. the first order central moment in random process describes the signal mean value μ , the second order central moment in random process describes the signal variance σ , the third order central moment in random process describes the signal skewness degree S , the fourth order central moment in random process describes the signal kurtosis K , the relation between skewness degree and kurtosis can be expressed as (1), (2).

$$S = \frac{E[X - E(X)]^3}{E[X - E(X)]^{3/2}} \quad (1)$$

$$K = \frac{E[X - E(X)]^4}{(E[X - E(X)]^2)^2} \quad (2)$$

Correspondence to: Dr Xiang Wen, Engineer
Shanghai Institute of Special Equipment Inspection and
Technical Research
JinShaJiang Road915, Shanghai, China,
E-mail: Wenxiang3567755@163.com

The characteristics of Gaussian random signal can be described by mean value and variance, skewness degree of Gaussian random signal is a constant 0 and Kurtosis value is also a constant 3. At least one of them for skewness degree and kurtosis value of non-Gaussian random signal is different from those of Gaussian signal.

Skewness degree describes the degree that random signal distribution deviates from symmetrical distribution, kurtosis describes waveform characteristic parameters of random signal amplitude. Kurtosis value of Gaussian signal is considered as a benchmark, where non-Gaussian signal with Kurtosis value less than 3 is called sub-Gaussian signal and non-Gaussian signal with Kurtosis value greater than 3 is called super-Gaussian signal. The central region of amplitude probability density of super-Gaussian signal is relatively narrower than that of Gaussian signal, and margin region tail of amplitude probability density of super-Gaussian signal is relatively longer than that of Gaussian signal. Jiang Pei's investigation indicates that super-Gaussian signal has a greater impact on the accumulation fatigue damage of testing piece comparing with Gaussian and sub-Gaussian, therefore, the faults of products can be adequately excited. This paper mainly investigates the super-Gaussian random signal with skewness degree 0, and super-Gaussian random vibration test control is also realized on the shaker.

2.2 Basic control principle

Super-Gaussian random vibration test control is relatively more complicated in technique than traditional random vibration test control since the former have to introduce Kurtosis control except for implementing power spectrum equalization.

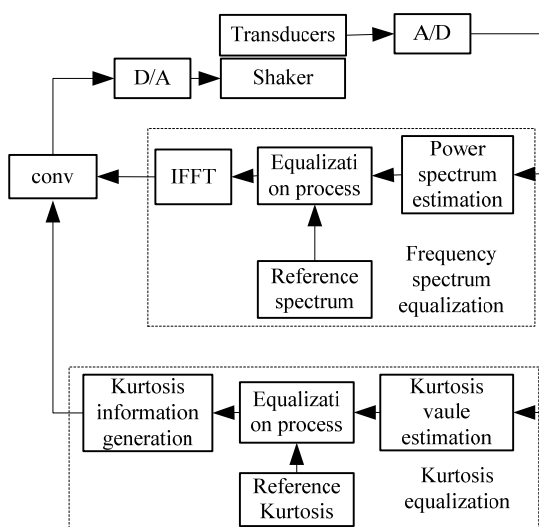


Figure 1. super-Gaussian random vibration test control

Figure 1 shows the flow chart of super-Gaussian random vibration test control, vibration response signal taken from the transducer is converted into digital signal through A/D converter and transferred to DSP, then the frequency spectrum equalization and kurtosis equalization are carried out respectively, two signals after equalization are implemented convolution

operation so as to obtain the drive signal contained reference spectrum and reference kurtosis, in the end, the drive signal is sent to the D/A converter to drive the shaker. Error between power spectrum and reference spectrum for control response signal is in the allowable range, so does the error between kurtosis value and reference kurtosis value.

3. GENERATION PRINCIPLE FOR SUPER-GAUSSIAN RANDOM SIGNAL

It is clearly seen in Fig. 1 that system control signal is divided into two signals, one of them is output signal $h(n)$ after frequency spectrum equalization, the other is output signal $A(n)$ after Kurtosis equalization, ultimately, two signals are carried out convolution operation to produce the drive signal $x(n)$ to excite the shaker. The relation among signals can be described by linear time invariant system, shown in Fig. 2.

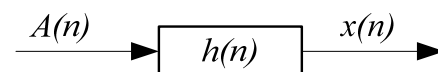


Figure 2. Relation among signals

The signal of super-Gaussian random vibration control can be modulated according to the relation among signals shown in Fig. 2, which results in the control to the vibration test system.

4. SIMULATION AND EXPERIMENT

The simulation search is carried out by using Matlab so that validity of super-Gaussian random signal generated from Poisson Process is able to be verified, Fig. 3 shows the piece of the super-Gaussian random signal in time domain, the probability density function of super-Gaussian random signal is calculated and comparison with probability density function of Gaussian random signal is made, probability density of super-Gaussian random signal has dense value scope nearby the mean value and has a relatively longer tail, partial signal value is even beyond the range 3σ and some signal value reaches 6σ , which satisfies the requirement of control system

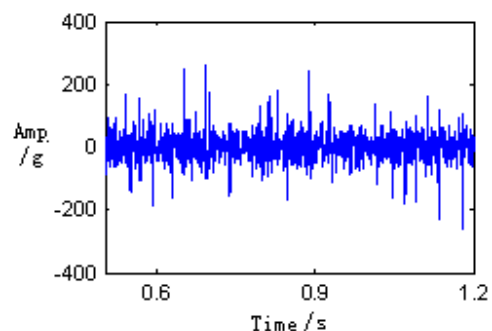


Figure 3. Super-Gaussian random signal

The experiment of super-Gaussian random vibration test is conducted in order to verify the control strategy. Since the vibration test system is constantly accompanied with non-linear and noise signal, which actually better bears out effectiveness and practicability of the control strategy. The hardware and software

related to the super-Gaussian random vibration test are provided by Hangzhou Econ Technologies Co., Ltd. The vibration experiment is done in the lab, Fig. 4 shows the on-site scene. Fig. 5 shows the interface of the software of the vibration control system, Fig. 6 shows the result of power spectrum control ranging 5HZ to 2000HZ, control response spectrum is approximately same with reference spectrum and high control accuracy is achieved, which satisfied the requirement of $\pm 3\text{dB}$ in engineering. Fig. 7 shows the control response output signal of vibration test system in time domain. Fig. 8 shows the probability density of control response signal, Fig. 9 indicates that kurtosis value is fluctuating around reference value in the whole range of time with respect to kurtosis control, which satisfies the requirement of high accuracy in engineering.



Figure 4. Vibration experiment on site

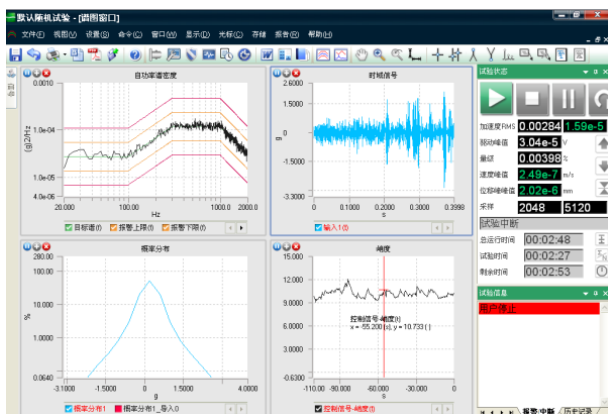


Figure 5. Interface of software of control system

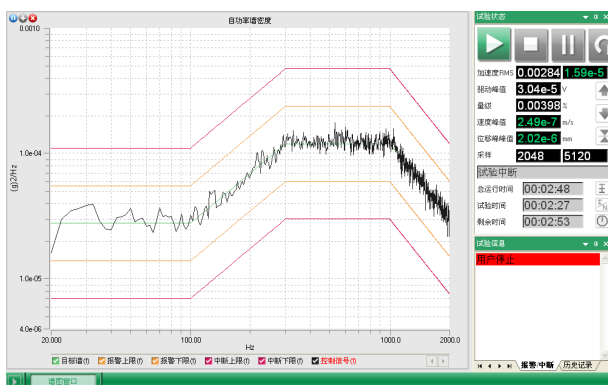


Figure 6. Result of power spectrum control

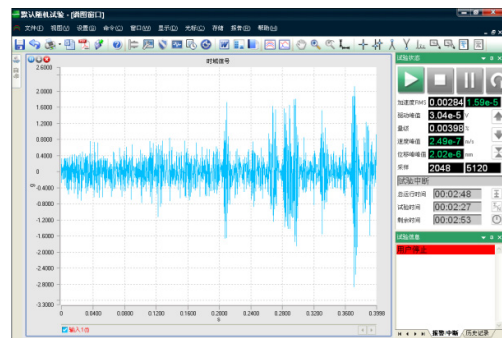


Figure 7. Control response output signal of test system in time domain

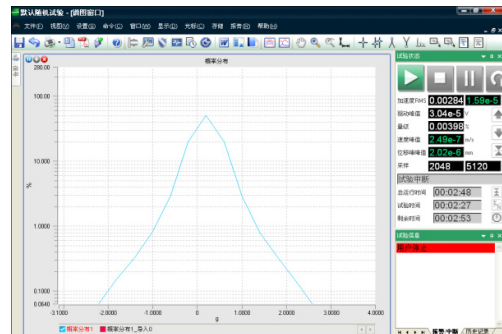


Figure 8. Probability density of control response signal

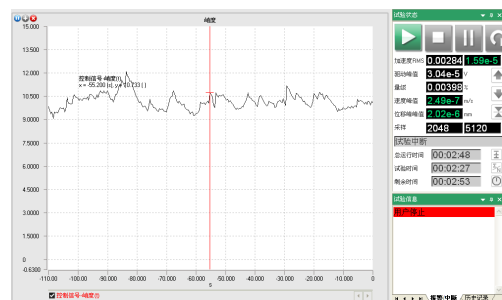


Figure 9. Kurtosis of control response signal

5. APPLICATION IN THE HIGHLY ACCELERATED LIFE TESTING (HALT) FOR SUPER-GAUSSIAN RANDOM VIBRATION TEST

Figures are to be inserted in their proper place throughout the paper and not to be grouped together. Please use only drawings and photographs of excellent quality. It is especially important that all numbers and characters appearing in your figures are of good quality and well-readable size ($\approx 8\text{-}10\text{ pt}$), i.e. approximately the same size as your text. Figure axis labels are often a source of confusion. Axes labels must be clearly denoted. Figure labels should be legible, approximately 8 to 10 point type.

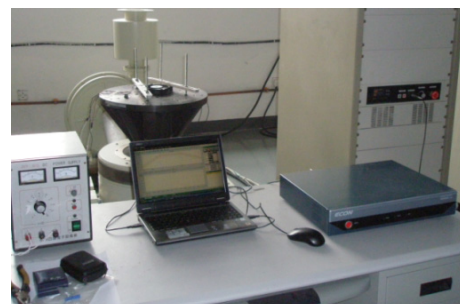


Fig. 10. Strenuous vibration test on site

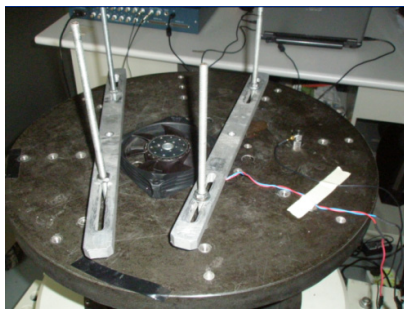


Fig. 11. Fan installation

There are two groups of fans in the first experiment, each group consists of two fans, the first group is conducted Gaussian random vibration test, the second group is conducted Super-Gaussian random vibration test. Fig. 11 shows that fan is fastened by a pair of clamps on the electromagnetic shaker.

Mean square root of vibration excitation signal in two experiments is set as 20g, and frequency ranges from 5HZ to 500HZ, kurtosis value in Super-Gaussian random vibration test is set as 7, both of experiments are carried out until the pins or weld of the fans appear fatigue failure, the experiment results are showed in Tab. 1.

Table 1. Results comparison between two experiments

Vibration environment	Gaussian Random	Super-Gaussian Random
Testing piece I (min)	98	68
Testing piece II (min)	92	74
Mean time (min)	95	71

Results comparison between super-Gaussian and Gaussian experiment indicates that super-Gaussian random vibration comparing with Gaussian random vibration can dramatically speed up the fatigue failure process for products when both of them have the same mean square root value and frequency band.

There are three groups of fans in the second experiment, each group also consists of two fans, super-Gaussian random vibration tests with different kurtosis value are conducted when Mean square root of vibration excitation signal in each experiment is set as 20g, and frequency ranges from 5Hz to 500Hz, the experiment results are shown in Tab. 2.

Table 2. Results comparison for different kurtosis value

kurtosis value	3	7	10
Testing piece I (min)	103	68	57
Testing piece I (min)	95	74	45
Mean time (min)	99	71	56

Experiment results in different super-Gaussian random vibration test indicate that kurtosis value of response signal will gradually increase with the increasing kurtosis value of excitation signal if super-Gaussian random vibration signal in each case has the same mean square root value and frequency band, which makes super-Gaussian distribution characteristic of response signal more evident that accelerates the fatigue failure of testing pieces, that is to say, products

fatigue failure will gradually increase in company with the increasing kurtosis value.

6. CONCLUSION

Based on the research about control theory for the super-Gaussian random vibration test home and abroad, The super-Gaussian random signal generated from Poisson process is applied into vibration control system. The control principle of super-Gaussian random vibration test is investigated in this paper. Super-Gaussian random signal, which is taken as drive signal of control system, is modulated by making use of digital filter theory. Furthermore, the required filter is designed by using power spectrum, amplitude of Poisson points generating from Poisson process are assigned as Gaussian distribution, then, both power spectrum and kurtosis for super-Gaussian random vibration test are simultaneously and independently controlled through the convolution operation between signals. The simulation and experiment indicates that the high control accuracy of output power spectrum and kurtosis based on the proposed super-Gaussian random vibration control strategy can be achieved, which satisfies the requirement in engineering.

In conclusion, super-Gaussian random vibration control system is applied into the Highly Accelerated life Testing (HALT) for certain fans, and a comparison between super-Gaussian random vibration test and traditional Gaussian distribution random vibration test is made, the comparison results prove that super-Gaussian random vibration excitation signal comparing with Gaussian distribution signal can markedly speed up the fatigue failure process for fans, fan fatigue failure will gradually increase with the increasing kurtosis value if super-Gaussian random vibration signal in each case has the same mean square root value and frequency band. Application of Super-Gaussian random vibration test in the Highly Accelerated life Testing (HALT) improves test efficiency, reduces the cost and shortens the development cycle of products.

REFERENCES

- [1] Smallwood, D.O.: Generating non-Gaussian vibration for testing purposes [J], Sound and Vibration, Vol. 39, No. 10, pp. 18-23, 2005.
- [2] Smallwood, D.O.: Generation of partially coherent stationary time histories with non-Gaussian distributions [R], Sandia National Labs., Albuquerque, NM (United States), 1996.
- [3] Steinwolf A.: Closed-loop shaker simulation of non-Gaussian random vibrations [J], Test Engineering and Management, Vol. 68, No. 3, pp. 10-16, 2006.
- [4] Steinwolf A.: Random vibration testing beyond PSD limitations [J], Sound and Vibration, Vol. 40, No. 9, pp. 12-21, 2006.
- [5] Jiang, Y., Chen, X., Tao J., etc.: The technique of generating super-Gaussian and quasi-random vibration excitation signal [J], Journal of vibration engineering, Vol. 18, No. 2, pp. 179-183, 2005.

Development of a Product Category Rule (PCR) for Environmental Product Declaration (EPD) of Conveyor Chain Systems

Lynn Lüdemann

Research Assistant
(Plastic Components and Tribology)
Technical University of Chemnitz
Faculty of Mechanical Engineering

M. Bona

Research Assistant
(Plastic Components and Tribology)
Technical University of Chemnitz
Faculty of Mechanical Engineering

Markus Golder

Professor
Technical University of Chemnitz
Faculty of Mechanical Engineering
Professorship of Materials Handling,
Conveying and Conveying Engineering

Environmental Product Declarations are a form of sustainability performance measures, because they provide information about environmental aspects. They are based on results of Life Cycle Assessment (LCA), which is an international standardized method for the assessment of environmental impacts of products within their life-cycle. [4] Nowadays it is usual to adopt the life-cycle-thinking, which has its roots in biological science, on every material, product or activity. By building up a "Reference Conveyor System", which conveys goods over a length of about 5 meters and includes one L-curve we were able to examine a first Life Cycle Assessment. The results of the LCA can be used for choosing the Rules of Product Categories to develop the requested Environmental Product Declaration. Furthermore it is interesting to have a closer look on the different Impact Categories, (Global Warming, Acidification etc.) which results differ between the phases of the life cycle (up-stream, core, down-stream). Of importances is as well the influence of velocity, good-load and useful lifetime. By including the last into the functional Unit, the comparability between different technological solutions is assured. Processess of recycling were not taken into account because it would exceed the goal of the examination for the moment. The results of the examination are uninspected and have to be discussed.

Keywords: Environmental Product Declaration, Life Cycle Assessment, Conveyor Chain Systems

1. INTRODUCTION

"Warming from anthropogenic emissions [...] will continue to cause further long-term changes in the climate system, such as sea level rise." This is one of the most relevant theses from the latest special report "Global Warming of 1,5°C" published by the Intergovernmental Panel of Climate Change (IPCC) [1]. The IPCC is an organization of the United Nations which provides reliable scientific information concerning the climate change and measurements of mitigation and adaption for policy makers in all countries [2].

To avoid an excessive use of the earth resources it is necessary to live sustainable. However, you can only manage, what can be measured - so the question is "how to measure sustainability?". First of all, it is necessary to take a life cycle perspective. Life Cycle Assessment (LCA) is one of the common scientific methods to estimate the environmental impact of products, people and organisations. It offers this perspective, because it analyses the whole life cycle of the researched object [3].

Our focus concerns the ecological dimension (the two others are: social and economic) of sustainability of products, in our special case conveyor chain systems.

Products normally have a life cycle, with several phases like extraction of raw materials, production, assembly, use and disassembly at the end of life. Every phase has impacts on the environment, e.g. reducing of natural resources or using non-renewable energy sources. It is not helpful to reduce the effect in one phase by moving it into another phase (so called shifting). To minimize the entire environmental impact, it is important to examine the whole life-cycle [4].

The results of an LCA show the environmental impact in different categories: Global Warming Potential (GWP), Eutrophication, Land-Use etc., for the observed product (life cycle). By publishing the results in an Environmental Product Declaration (EPD) it is possible to make an environmental choice for users of the product. How EPDs are created and what the results can tell, will be object of this paper.

2. PRODUCTS, ECODESIGN AND POLITICAL BACKGROUND

2.1 Political background

In 2001 the European Commission (EC) promoted its "Integrated Product Policy" as an instrument to push eco-friendly products, energy, fuel consumption and chemicals [8]. Environmental labels and declarations measure the performance of sustainability. Furthermore, they provide the information to non-environmental experts to serve their decision to more eco-friendly products [3]. In Germany the Blue Angel was one of the

Correspondence to: Dipl.-Ing. Lynn Lüdemann, research assistant

Faculty of Mechanical Engineering,
Technical University of Chemnitz
E-mail: lynn.luedemann@mb.tu-chemnitz.de

first environmental labels developed in 1978 by the Government. After the UN conference on environment and development in 1992 a lot of countries have promoted green labelling to achieve the target concerning sustainable development [3].

2.2 Products and their influence on the environment

Every product has got influence on the environment during its life-cycle. This influence results from the chosen materials, production sites and ways, the transport and its use. It is possible to distinguish products between passive and active ones, concerning their use-phase. Furthermore, you can divide products by their energy demand in the different phases of life. Figure 1 illustrates this with using the energy fraction.

As the energy fraction is a simple indicator for environmental stress and also easy to monitor, it is useful for distinction of products at this point. Following Lafuente [10] you can differentiate between :

- I. Energy producing products (e.g. solar modules)
- II. Energy using products for one user, dependant on the behaviour of their user (like houses, cars)
- III. Energy using products for a group of users, an prediction is difficulty, scenarios could be made (trains, aircrafts)
- IV. Energy using products designed for one application, it can be optimized for it (e.g. conveyor systems, lifts)

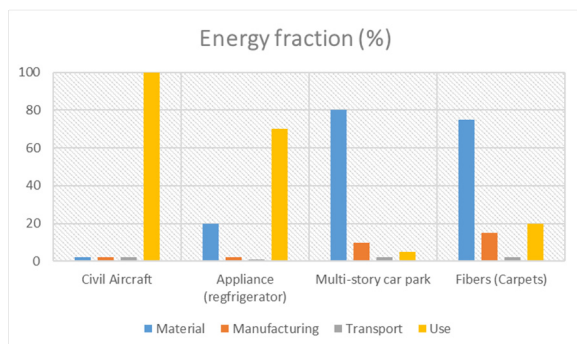


Figure 1. Approximate values for energy consumed at each phase, without disposal [4]

In every phase of the life-cycle you can optimize the design for reducing the energy/CO₂ emissions. This process is called ecodesign. At the first glance, conveyor systems belong to category IV, which means that the optimization has to be targeted to the use phase. Furthermore, the manufacturing phase should have an influence on the environmental impact, valuable measurements could be minimizing process energy and in the use phase reducing losses by friction [4]. If this assumption is right will be shown by the Life Cycle Assessment and detailed examinations hereafter.

2.3 Ecodesign for Products

As explained before life-cycle-perspective is one of the main features concerning eco-labelling, EPDs, LCA and more. Recently the After-Use or End-of-Life phase becomes more and more in the focus of the researcher. Regarding the huge amount of waste coming from the industrial nations, new odds are demanded. Figure 2

shows the different possibilities for the end-of-life of industrial products. All these measurements like re-use or re-engineering have to be foreseen in the design-phase and do therefore belong to the eco-design.

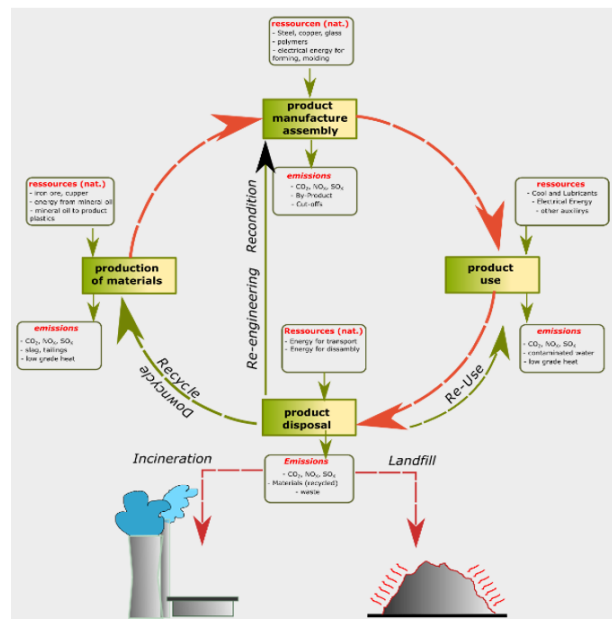


Figure 2. Potential materials life-cycle including end-of-life options for industrial products, like conveyor systems [4]

There is another conflict for energy using products like conveyor chains: finding a useful lifetime, between “renewing because of increased efficiency” and “re-use because of resource reduction”. EPDs include information about the end-of-life phase and are therefore a useful instrument for being aware of this conflict.

3. ENVIRONMENTAL LABELLING, PRODUCT CATEGORY RULES AND ENVIRONMENTAL PRODUCT DECLARATIONS (EPDS)

3.1 Environmental Labels

On the website “the Ecolabel Index” (www.ecolabelindex.com) there are more than 400 different labels from 199 countries and 25 industry sectors listed. You can find labels concerning single issues, like “animal-friendly” or sector labels like “sustainable forest management” useable for different kinds of products.

Environmental labels measure sustainability performance of product (-systems) or organisation. Their intention is to inform and influence the consumer or purchaser. By developing the standards of ISO 14020ff the International Organization for Standardization (ISO) wanted to tackle down misuse of labels for “greenwashing”. They developed three types of Label-categories, which are regulated by ISO 14021, ISO 14024 and ISO 14025. Type I labels point out products and services with an overall environmental preferability, Type II labels are self-declarations and are published by the organisation itself and are therefore often misused. Type III labels are based, as Type I, on Life Cycle Assessment [3].

3.2 Environmental Product Declarations (EPDs)

Creation and publishing of so called Typ III declarations are standardized by ISO 14025. EPDs are primarily intended to B2B communication and enable the comparison between products, fulfilling the same function. In the introduction of the International Standard [11] the main requirements for publishing EPDs are pointed out: provided by one or more organizations; based on independently, verified LCAs (according to ISO 14040 [6] and ISO 14044 [7]) and administrated by a program manager.

In Germany one program manager for EPDs is the "Institut für Bauen und Umwelt" (Institute for Construction and Environment (IBU)). It provides more than 1.700 EPDs in the construction sector. Therefore a specific standard was developed, which declares the core rules of the product category of construction products [13]. As part of green building programmes like BREEAM® they are often used in the construction sector [17].

In her masterthesis M. Mageroy examines eleven different international EPD systems, five of them publish EPDs in the construction sector, two in the electronic and one only in the food sector [17]. Only the International EPD System environdec® settled in Sweden offers the possibility to publish EPDs for different product categories. We decided to follow the rules of environdec® for developing the PCR and conducting the LCA.

3.3 Product Category Rules (PCRs)

PCRs are one of the mandatory requirements for calculating and publishing an EPD. Rules for developing PCRs are declared in a specific standard [18] but also in specific rules provided by the program operators of the EPD System. The above mentioned IBU for example divides a PCR into two parts, part A for the standard calculation rules concerning every PCR and than specific rules concerning only one product in Part B. The international EPD system, environdec® provides own "General Programm Instruction – GPI", which concerns all information about publishing and producing verified Typ III declaration.

PCRs have to be developed for each product group and are meant to enable transparency and comparability between EPDs. In PCR you find information concerning the functional unit, allocation rules, system boundaries and more. The development of PCR requires open consultation involving interested parties [3]. As there exist more than one programme operator, aligning and harmonising different EPD schemes is a challenge for today. In practice it is difficult to use EPDs for comparison of products coming from different programmes [3].

4. LIFE CYCLE ASSESSMENT (LCA)

4.1 Introduction

PCRs and EPDs have to be developed in accordance with the results of a conducted LCA. That's why we performed a Life Cycle Assessment of a part of a

Conveyor Chain System, which we called Reference-Conveyor-System (RCS) and used the results to continue our research. After a short summary of the theoretical background of LCA, the results of the conducted LCA are presented.

4.2 Phases of an LCA

LCA is a technique developed for better understanding and addressing the possible impacts of products on the environment [6]. LCA calculates the impacts of a product throughout its entire life, from the cradle to the grave. It forms the basis of an EPD and has to be performed according to the standard [17]. Figure 3 shows the four phases of an LCA, each of them interacting with the other, the box in the right shows the application of LCA.

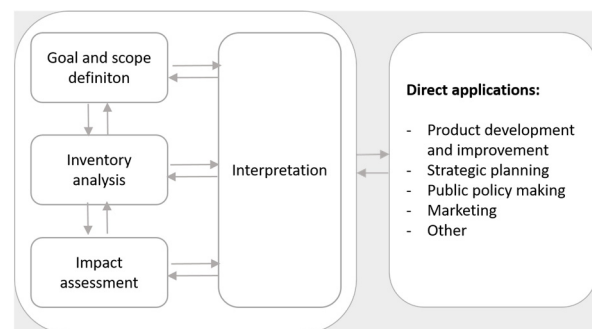


Figure 3. The four phases of an LCA [4]

One of the key characteristics of an LCA is its relative nature, due to the functional Unit (fU) feature of the methodology [6].

4.3 Goal and Scope Definition

The first phase of an LCA is the definition of goal and scope. The goal is composed of six aspects, which are (1) Intended applications of the results, (2) Limitations due to methodological choices, (3) Decision context and reasons for carrying out the study, (4) Target audience, (5) Comparative studies to be disclosed to the public, (6) Commissioner of the study and other influential actors [21]. The scope determines what product system will be assessed and how. In the ILCD Handbook you find nine scope items, but the ISO defines fourteen. The most important items effect to the definition of the object of the assessment and its functions. An important result is the specification of the functional unit and the reference flow [7].

The functional Unit represents the main function of the product, which is a simple example to illustrate its conception [20]. If you want to calculate an LCA to compare plastic bottles with glass bottles, you have to declare as functional Unit "transport and supply of 1.000 Liter water" instead of comparing 1 plastic bottle to 1 glass bottle. For fulfilling the above mentioned function, you need to select the right reference flow, which means the amount of materials and auxiliaries to fulfill the choosen function. In the example you need therefore 1.000 bottles made from plastics and 100 bottles made from glass. Furthermore you need ressources to produce, to transport and to wash the bottles.

According to the standard, the scope should be sufficiently well defined to ensure that the goals of the study can be achieved. The scope covers system boundaries, allocation procedures, the selected impact categories, data requirements.

4.4 Life Cycle Inventory Analysis

In the 2nd step, the Life Cycle Inventory Analysis (LCI) - the flow model of the product system with all input and output flows for each unit process is built. The LCI involves data collection and calculation procedures to quantify inputs and outputs of the product system. As it is interactive, the results can lead to changes of scope. Data collections can be headed under four major groups: inputs (energy, raw materials, auxiliary etc); outputs (products, co-products and waste); emissions (air, water, soil); other environmental aspects. For the data recording several methods are useful: measuring, estimating, calculating. Data can be original (measured at the production site) or generic, which means that they come from databases as ecoInvent and are representative for a process. Afterwards the data have to be splitted to the different life cycle stages, such as up-stream, core and down-stream. All data have to be referred to the chosen fU.

4.5 Life Cycle Impact Assessment

The Life Cycle Impact Assessment (LCIA) is in the first instance the last phase of the LCA. By using LCA software it is automated in practice, but to understand the results and for right interpretation – the practitioner should well understand the methodology behind [3].

The results of the LCIA have to be fit and consistent impact categories, category indicators and characterisation models for the given goal of the study. The indicators should i.a. have environmental relevance and be traceable. A lot of LCIA methods have been developed since the 1984. In the used software more than hundred methods are available. By explaining the most common impact category “Global Warming (GW)/ Climate change” – the conception of environmental impact should be explained. GW is a midpoint impact category, which is caused by the anthropogenic greenhouse effect. Global warming means the phenomenon of rising surface temperature across the planet averaged over longer periods of time. It is caused by emissions of greenhouse gases, like carbon dioxide, methane or nitrous dioxide. These emissions result from activities like heat production, construction of buildings, transport and other. There are other impact categories, such as stratospheric ozone depletion and acidification – which also belong to midpoint categories. Beside the midpoint impact categories, also endpoint impact indicators could be defined. Typical endpoints are human health, ecosystem quality, natural resources. This conception allows more condensed information to consider for a decision, while still being transparent.

Normalization and weighting are mandatory steps of an LCIA and could also help for better understanding. The results of the LCIA are the core of the EPD and are presented in the next chapter. The choice of LCIA

categories is predetermined by the international EPD system.

5. DEVELOPMENT OF PCR AND EPD FOR CONVEYOR CHAIN SYSTEMS

5.1 Introduction

In the next paragraphs the present status of our research is described. Goal of the project is the development of a PCR for conveyor chain systems. As mentioned above several steps are required: conducting an LCA, defining functional Unit and reference flow, defining product category rules and so on. The chosen starting point is a closer research concerning existing PCR – to define the fU and RF, afterwards an LCA on a Reference Conveyor System (RCS) will be examined. All results will be aggregated for perception of next research steps.

5.2 PCR Development

The international EPD System uses the UN classification Central Product Classification (CPC) for sorting the examined products. The CPC constitutes a comprehensive classification of all products, including goods and services, it presents categories for all products that can be the object of domestic or international transactions or that can be entered into stocks [26]. Following the CPC system the appropriated PCR category for the examined conveyor chains is

4355 Pneumatic and other continuous action elevators and conveyors, for goods or materials

Whereas the 4 stands for the section (here metal products), the 3 for the division (machinery), the 5 for the group (lifting and handling equipment) and the 5 for the class of product (continuous handling equipment).

After choosing a fitting PCR number, the next steps following the General Program Instruction (GPI) from environdec® and the given information on their website, are

- Definition of the Product Category (primary and secondary functions of product; fitting UN/CPC Code)
- Consideration of other available PCR (from environdec® or other EPD programmes)
- Appointing a PCR moderator
- Seeking for cooperation with other parties to take part in the PCR committee
- Planning the PCR development; Announcement of the PCR development

At present we focus our research on the first two points of the list above. In literature no PCR for conveyor chains exists. Table 1 shows eight selected EPDs/PCR for examination of functional Unit and the reference flow.

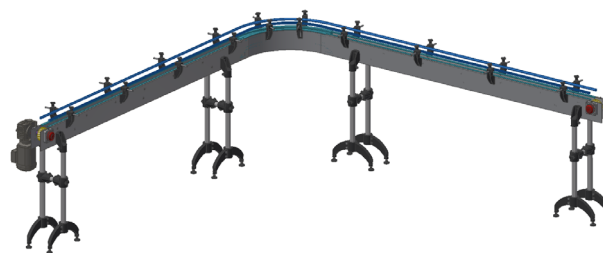
Table 1. Examples of examined PCR for the Development

Nr	Product (system)	Functional Unit (fU)	Reference flow	Source
1	Forklift (Jungheinrich)	1 LifeCycle (operation time 10.000h for each reference car)	Averaged weight of the reference car (product cluster weighted with sales ranking)	The Jungheinrich environmental label [22]
2	Lifts (elevators)	Transportation of a load over a distance, expressed in tonne[t] over a kilometre [km] travelled, i.e. tonne-kilometre $FU = \%Q \times S_{RSL}$	1 lift (specific) or „generic“ lift	Envirodec PCR: UN CPC 4354 [23]
3	Machines for filling and packaging of liquid food	1000 litres of filled product delivered by the machine (independent from the packing size)	Not specified	Envirodec PCR: UN CPC 43921
4	Road transport service of freight of food products and meals	1 kg of delivered food transported from the loading to the unloading site	Not specified	Envirodec PCR: UN CPC 6511
5	Pump for liquids, liquid elevators mixers	1 kW hydraulic power at best efficiency point, 1 N (for mixers)	Not declared (one pump, one mixer)	Envirodec PCR: UN CPC 4322
6	Machine tools for drilling, boring or milling metal	One product unit (Declared Unit) from the core including packaging	Reference flow of the use phase: 1 working hour reference service life: 62.400 hours	Envirodec PCR: UN CPC 44214
7	Rolling stock	1 passenger over 1 km (total number of passengers calculated according to EN 15663)/ 1 ton above 1 km	Not specified	Envirodec PCR: UN CPC 495
8	Plastic waste and scrap recovery	Declared unit: 1 kg of recycled material		Envirodec PCR: UN CPC 8942

As mentioned above the chosen functional unit should represent the function of the product system. Examples therefore could be found in selected PCRs, having an active use phase (all exclude 8). Some of the examined PCRs included the lifetime in their calculation (1, 2, 6). Jungheinrich calculated their LCA over a reference forklift, which was done by product cluster weighted with sales ranking.

5.3 Goal and Scope of Life Cycle Assessment

In our research we decided to build up a Reference Conveyor System (RCS) like Jungheinrich. Figure 4 shows the chosen RCF, which consists of four pillars, a five meter long chain, one curve and the necessary drive unit. The chain can be made of plastic or steel, in the last case parts for providing cooling and lubrication have to be foreseen.

**Figure 4. Reference Conveyor System**

Following the above described instruction, it is necessary to define the scope and goal of the study. The six aspects of the goal are:

- (1) Intended applications of the results → development of PCR rules for conveyor chain systems
- (2) Limitations due to methodological choices → only estimated values, coming from catalogues and databases
- (3) Decision context and reasons for carrying out the study → gaining deeper knowledge about the research topic
- (4) Target audience → for intern discussion, readers of the article, other researchers
- (5) Comparative studies to be disclosed to the public → not for the moment
- (6) Commissioners of the study and other influential actors → authors of the article.

This means that the study is first of all intended to get closer knowledge about the life cycle of conveyor chain systems, the results should help to identify the next research steps.

To find out the exact fU of the RFC, it is necessary to look at the functions of a conveyor chain system. The primary function is the transportation of goods over a defined route in a defined time span. Additional functions are protecting, sorting, accelerating or others procedures concerning the good. Normally the transportation of goods goes continually, concerning velocity and load, so no “use-scenario” has to be foreseen, as it has to be at the lifts, which often have diverse uses.

In a previous publication, the material throughput in kg per second was chosen as fU [25]. With the perceptions about the examined PCR, it becomes clear, that is not widespread enough. It is obviously to include the useful lifetime into the fU. For the goal of comparability of two different systems of conveyor chains, e.g. chains made of plastic and chains made of steel, it is necessary to include the useful lifetime, because steel chains are durable and also easier to recycle than plastic chains.

To complete the scope definition it's necessary to choose the fitting LCIA categories for the last phase of the LCA. Publishing the EPD by the international EPD System on the website of envirodec® is targeted. On its website envirodec proposes at least the following LCIA categories to be included in EPD and PCR.

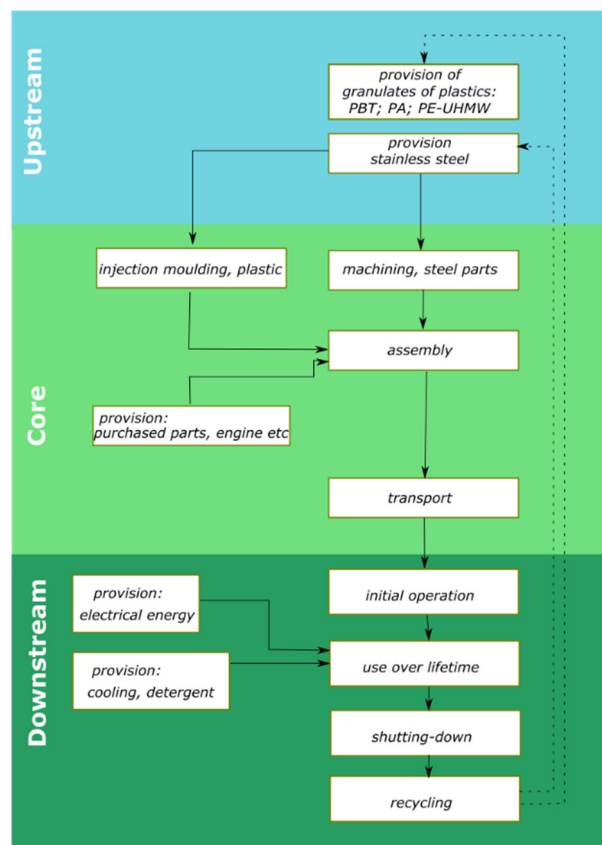
Table 2. Examples of LCIA categories proposed from the International EPD syste

Impact category (Unit)	Characterisation factors	Original reference(s)
Global warming potential (kg CO ₂ eq.)	GWP100, CML 2001 baseline V.: Jan 2016.	IPCC (2013)
Acidification potential (kg SO ₂ eq.)	AP, CML 2001 non-baseline, V.: Jan 2016.	Hauschild & Wenzel (1998)
Eutrophication potential (kg PO ₄ -eq.)	EP, CML 2001 baseline, Version: January 2016.	Heijungs et al. (1992)

At this point of research, we decided to examine only the first three categories – to explain all features would be go beyond the scope for the moment. The other will be examined in the next step.

5.4 LCI and LCIA of the Reference Conveyor System

The next step in the LCA-procedure is to conduct the Life Cycle Inventory, this means for the different processes (modules) of the RCS the necessary data have to be collected and split on to the life cycle phases. To identify processes for the LCI model it is useful to detail the coarse initial system picture (Figure 2) into a diagram by incorporating the scope and the goal of the study.

**Figure 5. Processes and life cycle phases of Reference Conveyor System****Table 3. Some of the processes of the examined RCS**

	Process module	Part	Flow in open LCA	Amount	Unit
Upstream	providing POM-granulat	chain link	Polyoxymethylene (POM)	31.16	kg
	providing PE-UHMW- granulat	guiding profile, side guidance, slide rail	Polyethylene high density granulate (PE-HD)	7.18	kg
Core	injection moulding	chain link, leveller, bipod	injection moulding	49.47	kg
	extrusion	guiding profile, side guidance, slide rail	extrusion, plastic film	7.18	kg
Downstream	energy input	Electricity supply	electricity mix, 230 V, Germany	15.848	KWh

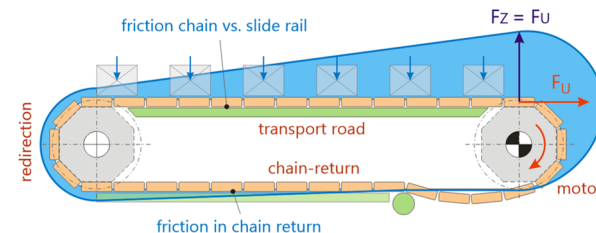
The life cycle is separated in three phases, the upstream comprises all processes before the conveyor purchaser (cradle-to-gate), the core process all steps done by the purchaser (gate-to-gate) and the downstream all processes after the finishing of the conveyor (gate-to-grave/cradle). For every process the fitting flows/processes of the databases were researched and the product system was built up in open LCA.

The presented amounts were taken from catalogues or calculated considering physical formulas. For the transport the weight of the RCS (150 kg) was multiplied with 500 km. Cooling/lubrication is only needed when the examination concerns a chain made of steel. The next step is calculating the energy use in the downstream-phase.

5.5 Energy-Use of the Reference-Conveyor-System

Under presumption that the use phase is the most important one for the whole life cycle assessment of a

conveyor system, its examination is crucial. By using a conveyor chain system made of plastic (like POM), the friction coefficient could be lowered to amounts near 0.2. Together with the less dead load of the chain (one-third compared to steel), the energy consumption declines significantly. There are two main methods to get the energy consumption of the RCS, measuring or calculating. Below the last one is presented.

**Figure 6. Force progression in a conveyor chain system**

As shown in the figure the maximum chain force occurs near the power unit in the upper run. The

calculation of the maximum force follows along the system, at every point of change (direction, accumulation, load) a new force is calculated which is cumulated to the last force.

$$F_n = F_{n-1} + F_i \quad (1)$$

On a straight section, without accumulation or vertical curve the tensile force is a result of multiplication of the weight with the friction coefficient.

$$F_n = F_g \cdot \mu \quad (2)$$

If the chain has to follow a horizontal sliding arch, the curve friction causes an exponential increase in the chain tensile force compared to a linear increase in straight and curved wheels. At the end of the calculation the maximum chain force can be used to continue the calculation of the energy consumption.

With the following given parameters

- Specific weight of the chain = 1.01 kg/m [m_{ch}]
- Maximum chain Force = 356.44 N [F_{max}]
- Number of working hours/year = 5.760 [Numb]
- Coefficient of friction = 0.2 [μ]
- Reference Life-time = 10 year [RSL]
- Velocity of chain = 30 m/min = 0.5 m/s [v_{ch}]
- Losses cause of inefficiency = 0.499 [η_{all}]
- Absolute losses in the periphery = 8 W [E_{per}]

it is calculated as follows

$$P_{operating} = F_{max} \cdot v_{ch} \quad (3)$$

$$P_{losses} = P_{operating} \cdot \eta_{all} \quad (4)$$

$$P_{total} = P_{operating} + P_{losses} + P_{per} \quad (5)$$

The total of Power can be calculated as follows

$$P_{total} = (356.44 \cdot \frac{30}{60}) \cdot (1 + 0.499) + 8$$

$$P_{total} = 275.15 \text{ W}$$

$$P_{Use_RSL} = \frac{P_{total}}{1000} \cdot Numb \cdot RSL \quad (6)$$

$$P_{Use_RSL} = 15.848 \text{ kWh}$$

Following this calculation the energy-input is 15.848,69 kWh. All the amounts were put into the software and than product system was built up. After setting-up the LCI model in open LCA the calculation of the LCIA results can be made.

5.6 Results of the LCIA

As mentioned before only three categories (global warming, acidification, eutrophication) are examined. They all can be find in the method CML2001. This collection of LCIA factors is published by the Centrum

of Milieukunde Leiden, which is a very well know environmental research institute.

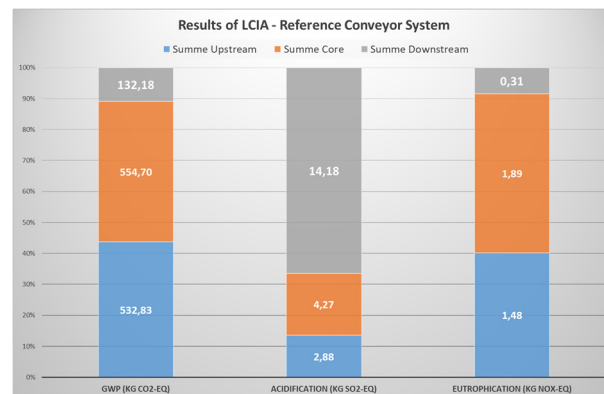


Figure 7. Results of the LCIA of RCS

Figure 77 shows the result of the examination for the three categories separated after Upstream, Core and Downstream. The results are not as expected. For the categories global warming and eutrophication the upstream and core phase have the most impact (about 90%), the use phase (downstream) only contributes to 10%. Concerning acidification the use phase has the most impact (about 70%), which is due to the emission of sulfur dioxide by burning down fossil energies like coal or oil.

In chapter 3 it was stated that conveyor chain systems belong to product category IV (energy using products) and that the use phase has the greatest impact on the LCIA. The results negate this results. On the contrary, despite acidification the upstream and core processes contribute to the most impact. The next step will therefore be the validation of the results, on one hand the energy use has to be measured and on the other hand a sensitive analysis has to be conducted.

6. CONCLUSION

Environmental Product Declarations, which are needed to publish the results of a Life Cycle Assessment are appropriate to show the environmental impact of product systems like conveyor chain (systems) over their life cycle. The research of our institute concerns the development of EPDs for this product category. Therefore rules (PCR) and a publishing program manager are needed. The international EPD system environdec® is suitable. Furthermore the goal and scope of the examination has to be defined. A suitable functional Unit and the division of the life cycle into stages was examined. It is inevitable to include the lifetime into the functional Unit. The results are not as expected, because the use phase has not such an important impact as assumed. The next steps has to be a validation of the results and an implementation of the end-of-life phase. Also a comparison with LCA results of conveyor chains made of steel is foreseen, this will help to better understand the presented results and to continue the research.

ACKNOWLEDGMENT

We want to acknowledge the Röchling Foundation, which helps to finance this project.



REFERENCES

- [1] Masson-Delmotte, V., Zhai, P., Pörtner, H.-O., Roberts, D., Skea, J., Shukla, P.R., Pirani, A., Moufouma-Okia, W., Péan, C., Pidcock, R., Connors, S., Matthews, J.B.R., Chen, Y., Zhou, X., Gomis, M.I., Lonnoy, E., Maycock, T., Tignor, M. and Waterfield T.: Summary for Policymakers, Global Warming of 1.5°C, An IPCC Special Report on the impacts of global warming of 1.5°C above pre-industrial levels and related global greenhouse gas emission pathways, in the context of strengthening the global response to the threat of climate change, sustainable development, and efforts to eradicate poverty, World Meteorological Organization, Geneva, Switzerland, pp. 32, 2018.
- [2] www.ipcc.ch: About the IPCC, website, last access 15.05.2019.
- [3] Hauschild, M., Rosenbau, R.K. and Olsen, S.I.: *Life Cycle Assessment, Theory and Practice*, Springer International Publishing, 2018.
- [4] Ashby, M.F.: *Materials and the Environment*, Elsevier Inc., 2012.
- [5] UN: <https://www.un.org/sustainabledevelopment/sustainable-development-goals/>, Zugriff, 03.06.2019.
- [6] DIN EN ISO 14040:2006, Environmental management - Life Cycle Assessment – principles and framework (ISO 14040:2006), German and English version (EN ISO 14040:2006).
- [7] EN ISO 14044: 2006, Environmental management – Life Cycle Assessment – requirements and guidelines (ISO 14044:2006 + Amd:1-2017), German Version EN ISO 14044:2006+A1:2018.
- [8] European Commission: Products – labelling rules and requirements, https://ec.europa.eu/info/energy-climate-change-environment/standards-tools-and-labels/products-labelling-rules-and-requirements_en, letzter Zugriff, 15.05.2019.
- [9] UN WCED: *Our Common Future*, Oxford University Press, Oxford, 1987.
- [10] Lafuente A.-M.: *Life Cycle Analysis and Energy Modeling of Lifts*, Doctoral Thesis, University de Zaragoza, Sep. 2013.
- [11] Rehfeld, K.-M., Rennings, K. and Ziegler, A.: Integrated Product Policy and Environmental Product Innovations: An Empirical Analysis, Elsevier, Ecological Economics, Vol. 61, No. 1, pp. 91-100, 2007.
- [12] DIN EN ISO 14020: Umweltkennzeichnungen - und Deklarationen, Allgemeine Grundsätze, Februar 2002.
- [13] DIN EN ISO 14021: Umweltkennzeichnungen und – deklrationen: Umweltbezogenen Anbietererklärungen, (Umweltkennzeichnung Typ II), Juli 2016.
- [14] DIN EN ISO 14024: Umweltkennzeichnungen und – deklrationen, Umweltkennzeichnung Typ I: Grundsätze und Verfahren, Juli 2018.
- [15] DIN ISO 14025: Umweltkennzeichnungen und – deklrationen, Grundsätze und Verfahren, Oktober 2011.
- [16] DIN EN 15804: Nachhaltigkeit von Bauwerken: Umweltproduktdeklarationen, Grundregeln für die Produktkategorie Bauprodukte, Juli 2014.
- [17] BRE: Building Research Establishment, REEAM (Building Research Establishment Environmental Assessment Methodology), www.breeam.com, last access 11.06.2019.
- [18] DIN CEN/ISO TS 14027, DIN SPEC 35805, Umweltkennzeichnungen und – Deklarationen, Entwicklung von Produktkategorieregeln, April 2018.
- [19] Mageroy, M.: *The communication of environmental impacts through environmental product declarations*, Master thesis at Norwegian University of Science and Technology, 2011.
- [20] Genossenschaft Deutscher Brunnen eG: Ökobilanz – Vorsprung für Mehrweg, 2008, Bonn, www.gdb.de
- [21] EC-JRC.: European Comission – Joint Research Centre – Insitute for Environment and Sustainability: *International Reference Life Cycle Data System (ILCD) Handbook – General Guide for Life Cycle Assessment – Detailed Guidance*, Publications Office of the European Union, Luxemburg, 2010.
- [22] Heigl, M.: Das Jungheinrich-Umweltprädikat, In C. Deckert, CSR und Logistik, pp. 227-245, Berlin Heidelberg: Springer, 2016.
- [23] International EPD System environdec®: PCR Search on website, <https://www.environdec.com/PCR/>, last access 11.06.2019.
- [24] International EPD System ®: Default Impact assessment categories, 2018-06-08, <https://www.environdec.com/Creating-EPDs/Steps-to-create-an-EPD/Perform-LCA-study/Characterisation-factors-for-default-impact-assessment-categories/>.
- [25] Nendel, K., Lüdemann, L. and Weise, S.: Energieeffizienzbetrachtungen logistischer Systeme, Logistics Journal, Vol. 2013., 2013 (urn:nbn:de:0009-14-37717).
- [26] Global Inventory on Statistical Standards: website, https://unstats.un.org/unsd/iiss/_Central-Product-Classification-CPC.ashx, last access 10.06.2019.

Pantograph Strips Failure Analysis and Artificial Intelligence Prevention Methods

Małgorzata Kuźnar

Research Assistant
Cracow University of Technology
Institute of Rail Vehicle, Poland

Grzegorz Kaczor

Research Assistant
Cracow University of Technology
Institute of Rail Vehicle, Poland

Augustyn Lorenc

Assistant Professor
Cracow University of Technology
Institute of Rail Vehicle, Poland

In rail transport, reliability and operational safety in large part depends on the correct reception of power from the catenary by a traction vehicle. In this paper, a special attention was paid to consumption of sliding strips of a current collector (AKP-4E and SZL type), measured during periodic reviews of locomotives EU07 and EU09. Pantograph data, collected during periodic technical reviews, was provided by one of the biggest railway carrier in Poland. To investigate the reliability assessment of the selected pantograph strips a non-destructive degradation analysis was carried out. On the basis of the wear measurements of the strips and the critical value of wear, the failure distribution model was developed. It was used to obtain the selected reliability characteristics and to predict the lifetime of the strips. In next step, failure analysis was conducted. Such analysis was carried out for two variants to compare the effectiveness of Artificial Intelligence Prevention method. In the first variant, analysis was based on data selected during standard technical review of a pantograph. Second variant considered Artificial Intelligence method to predict and prevent cases of pantograph strip damage. Applied and tested methods of artificial intelligence were mainly related to classification algorithms. For this purpose was used techniques such as: decision trees (Complex Tree Medium Tree, Simple Tree), supporting vector machines (Linear SVM, Quadratic SVM, Cubic SVM, Fine Gaussian SVM, Medium Gaussian SVM, Coarse Gaussian SVM), method of nearest neighbors (Fine KNN, Medium KNN, Coarse KNN, Cosine KNN, Cubic KNN, Weighted KNN) or classifiers (Boosted Trees, Bagged Trees, Subspace Discriminant, Subspace KNN RUS Boosted Trees). The results of conducted analyzes may be used to build a preventive maintenance strategy of the pantographs. The applied reliability models of wear propagation can be extended by the parameters of the cost and repair time becoming the basis for estimating the costs of operation and maintenance.

Keywords: Reliability Assessment, Failure Distribution Model, Pantograph Strip, AI Methods, Machine Learning, Artificial Neural Network, Damage Prevention

1. INTRODUCTION

Reliability and safety during technical operation of the rail vehicles depend largely on the correct power reception from the catenary system by a traction vehicle. Currently, there are many scientific papers regarding the pantograph-overhead catenary system. These works concern mainly numerical methods of simulation of dynamic phenomena [1-7], analysis of contact force [8-15], as well as wear of sliding strip material [16-24]. The papers focus particularly on material properties depending on the composition of the strip. A wide interest in the problems of the pantograph-overhead

catenary system results from the desire to ensure the best cooperation and reduce the operating costs.

Technical condition of pantograph is checked on every technical review. According to the preventive maintenance strategy related to the pantograph, we distinguish the following activities:

- control reviews (every 2 - 4 days),
- periodic reviews (once a month),
- large reviews (every 250 thous. km \pm 10%),
- smaller repair (every 500 thous. km),
- bigger repair (every 1000 thous. km),
- major repair (after the course of 4000 thous. km).

During each review, among other things, a visual inspection of a current collector is made which takes into account checking the current collector components without disassembly.

A component which is in direct contact with contact wire of overhead catenary line is a carbon sliding strip. Because of that, when strip is damaged, it can cause danger and expensive damages to catenary line. The problem associated with the correct determination of the

Correspondence to: MSc Małgorzata Kuźnar, Research Assistant

Cracow University of Technology
Institute of Rail Vehicle,
al. Jana Pawła 37, 31-864 Cracow, Poland
E-mail: malgorzata.kuznar@mech.pk.edu.pl

technical condition is therefore very important. In this paper, a special attention was paid to consumption of sliding strips of a current collector (AKP-4E and 5ZL type), measured during periodic reviews of locomotives EU07 and EU09.

2. PANTOGRAPH SLIDING STRIPS

A verification of slides state is performed on every technical review. At the time of examination it should be remembered that sliding strip exchange can be caused by three types of destructive processes – wear and small failures caused by wear; failures of a sliding strip; and changes in pantographs' regulations.

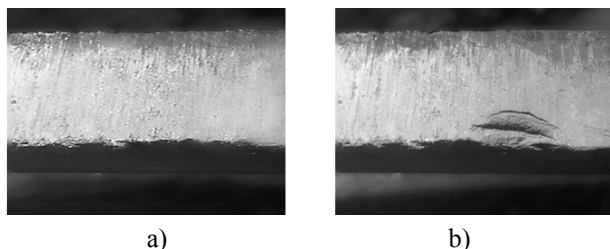


Figure 1. Damages of the edge of carbon sliding strip: a) minor surface damages; b) major surface damages

In case of wear a reduction in the thickness of strip may be noticed, as a result of the abrasion processes and electro-eroding phenomena. The wear process has approximately monotonous change in the thickness of the sliding strip. The reason for replacing the sliding strip in this case is exceeding the recommended strip thickness. If some small defects will occur during which do not cause loss of the strip ability of current collection – e.g. wear of the edge of the strip – there is no need to replace the strip (Fig. 1a).

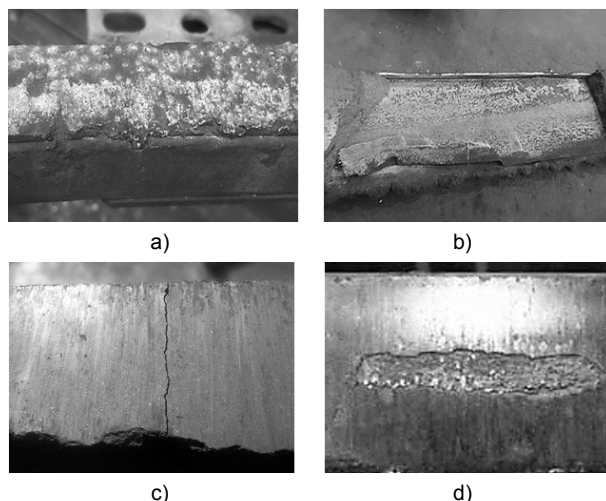


Figure 2. Wear of sliding a) material melting as a result of arcing; b) detachment of piece of carbon strip; c) crack of a strip; d) peeling off the top layer of a strip [25]

Such failures are caused by impact on the hard points of catenary and it is often assumed that minor surface damage may not exceed 30% of the surface of the carbon strip. However, if there is one major damage (Fig 1b), the strip should be replaced, because it may damage the overhead line.

In case of replacement caused by damage, there are undertaken steps aimed at evaluating criteria such as:

- material melting as a result of arcing and damages caused by arcing (Fig. 2a),
- detachment of a piece of carbon strip (Fig. 2b),
- cracks of a sliding strip (Fig. 2c),
- peeling off the top layer of a carbon strip Fig. 2d).

During maintenance there are also some changes in pantograph regulations, which can caused uneven wear of sliding strips. In such case, if the difference in strip thickness is big, the strips should be replaced. If the thickness is different in a strip but acceptable, then then the slide should be turned 180 degrees.

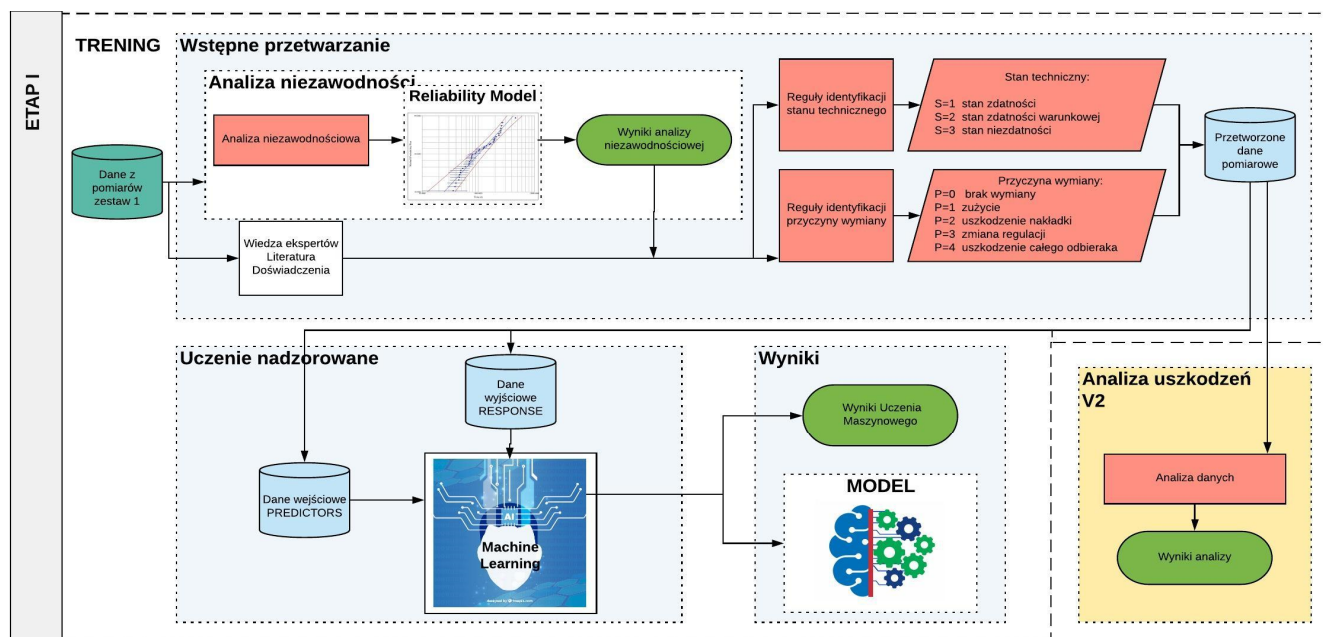


Figure 3. Methodology first step – Machine Learning and failure analysis for variant I

3. METODOLOGY

In order to reduce the number of damage to the strips, a model based on Machine Learning was developed. In order to develop such a model, it was necessary to process archival data, train data by the supervised learning method, and then select and implement the best predictive model for simulation.

This method is presented in detail in Figure 3 and 4. Figure 3 shows the first stage in which, apart from training, damage analysis was made according to archival data (Variant I). The second stage presented in Figure 4 contains the prediction of the technical condition of the current collector and the damage analysis for the data modified in accordance with the prediction results (Variant II). In Step I there is also assumed Reliability assesment in order to process the data correctly.

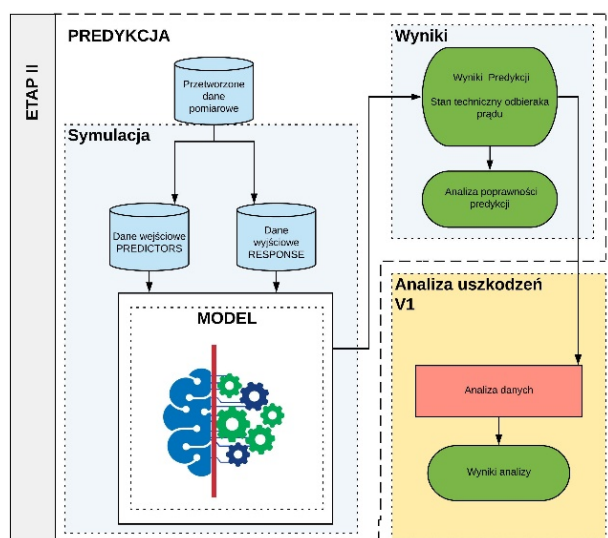


Figure 4. Metodology second step – Prediction and failure analysis for variant II

3.1 Reliability Assesment

Based on the technical reviews of locomotives EU07 and EU09, the empirical data were collected which correspond to the failures of the selected pantograph types. These data were analysed according to the Weibull analysis [IEC 61649:2008 Weibull analysis] and the parameters of 2-p Weibull distribution were obtained, as shown in the Table 1. The Weibull parameters were obtained using the Maximum Likelihood Estimation

method included in Reliasoft Weibull++ software, which allows to take into account confidence bounds.

Table 1. Parameters of Weibull distribution for the analysed types of pantograph

Parameters of Weibull distribution	DSA-150	AKP-4E	5-ZL
β	1.470337	1.153632	1.329664
η (days)	74.619087	119.655763	134.032580

Goddness of fit for the considered Weibull distribution with two sided confidence bounds on reliability with significance level of 0.05 for the selected pantograph types are shown in the Fig 6a-c.

Probability density function for the Weibull distribution is given as follows (1):

$$f(t) = \frac{\beta}{\eta^\beta} t^{\beta-1} \exp \left[-\left(\frac{t}{\eta} \right)^\beta \right] \quad (1)$$

Based on the calculated parameters of a Weibull distribution, a probability density function may be plotted in order to compare the time at which the probability of occurrence of failure reaches the maximum, $t_{f=\max}$ (Fig. 5). This will be the basis for the further failure analysis and supervised machine learning.

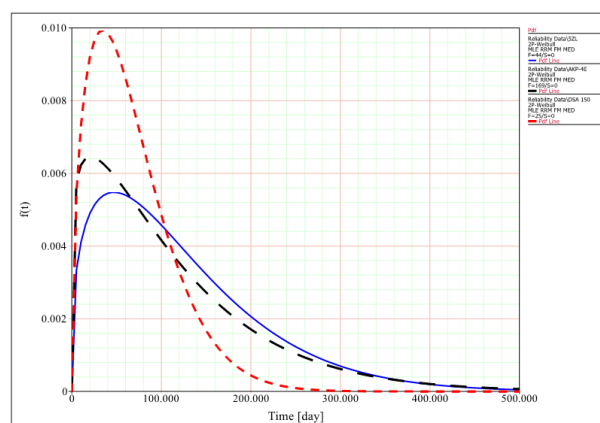


Figure 6. Probability density function for th selected types of pantograph: a) DSA-150, b) AKP-4E, c) 5-ZL

where:

β – shape parameter

η – scale parameter

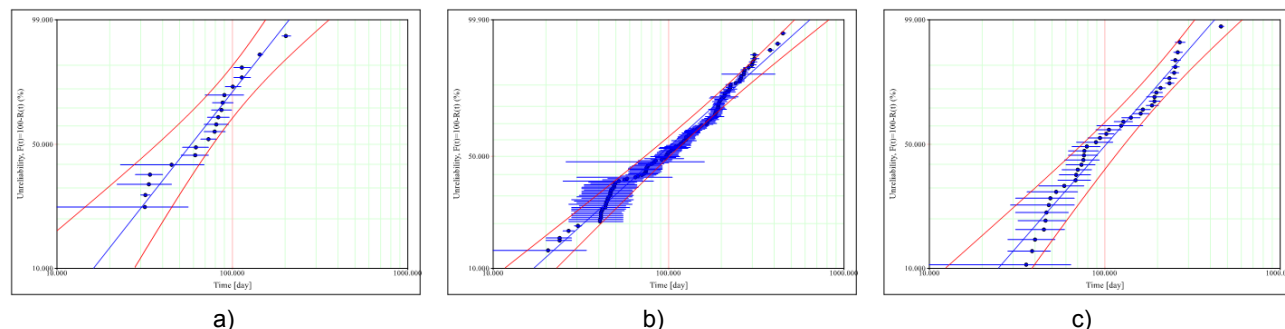


Figure 5. Weibull Probability plot for th selected types of pantograph: a) DSA-150, b) AKP-4E, c) 5-ZL

Based on the probability density function, a mean time to failure may be calculated as:

$$MTTF = \int_0^{\infty} t \cdot f(t) dt \quad (2)$$

The values of MTTF and $t_{f=\max}$ are presented in the Table 2.

Table 2. Calculated MTTF and $t_{f=\max}$ parameters for the selected types of pantographs

Type of pantograph	MTTF (day)	$t_{f=\max}$ (day)
DSA-150	67.53	35
AKP-4	113.77	21
5-ZL	123.25	48

The obtained results indicate that the lowest value of MTTF is for the DSA-150 pantograph, which may suggest its lowest durability. However, it should be taken into account that the calculated MTTF values refer to the theoretical mean value of time at which the failure may be observed, according to the approximation of Weibull distribution. Therefore, the more important information is the value of operation time at which the failure occurrence is the most probable. From the practical purposes such a value may indicate the actual durability of the pantograph. This approach may indicate the worst durability for the AKP-4 pantograph.

3.2 Data preparation for the Machine Learning

Reliability assessment and knowledge of experts allowed to prepare identification algorithms for technical condition and for replacement causes. The exemplary algorithms are shown below.

$$Wop = 1 \Leftrightarrow \quad (2)$$

$$Nl_{i+1} = Nl_i \wedge (Top_{i+1} \neq Top_i \vee Nop_{i+1} \neq Nop_i)$$

$$Wn = 1 \Leftrightarrow \quad (3)$$

$$(Nl_{i+1} = Nl_i) \wedge (Top_{i+1} = Top_i) \wedge (Cop_i \neq 1) \wedge ((Gn1_i - Gn1_{i+1} < 0) \vee (Gn2_i - Gn2_{i+1} < 0))$$

$$N_1 = 1 \Leftrightarrow \quad (4)$$

$$Nop = 1 \wedge N_3 = 0 \wedge (Gn1 < 32 \vee Gn2 < 32)$$

$$N_2 = 1 \Leftrightarrow \quad (5)$$

$$Nop = 1 \wedge (N_1 + N_3 = 0) \wedge ((Gn1 > 33) \vee (Gn2 > 33))$$

$$N_3 = 1 \Leftrightarrow \quad (6)$$

$$Nop = 1 \wedge (|Gn1 - Gn2| \geq 2)$$

Developed algorithms, in turn, allowed to prepare input data for machine learning. Learning data - predictors, are presented in Table 3.

Table 3. Machine Learning Predictors

Name	Symbol
Review number	i
A new measuring cycle	C_{new}
The number of days since the replacement	D
The quarter of the year	Q
Current collector type	Top
Front / rear current collector	Cc
Difference in the N1 thickness between reviews	$Th1$
Difference in the N2 thickness between reviews	$Th2$
Earlier technical condition	S
The reason for the replacement	N

3.3 Prediction model

Machine learning is currently used in many fields. In the article, the predicted model is based on the algorithms for the classification of machine learning. For the development of the predictive model, it was decided to use the MATLAB environment due to its strengths associated with machine learning.

It has a high quality function library. The algorithms are compliant with industry standards, while reducing the time required to develop solutions to the minimum. Also the tools used to validate the model are embedded in the application so the developed model can be easily evaluate.

In order to develop the best predictive model, the following methods were tested:

decision trees (Complex Tree, Medium Tree, Simple Tree), supporting vector machines (Linear SVM, Quadratic SVM, Cubic SVM, Fine Gaussian SVM, Medium Gaussian SVM, Coarse Gaussian SVM), method of nearest neighbors (Fine KNN, Medium KNN, Coarse KNN, Cosine KNN, Cubic KNN, Weighted KNN) or classifiers (Boosted Trees, Bagged Trees, Subspace Discriminant, Subspace KNN, RUS Boosted Trees).

Among the methods of classifying machine learning, the method of decision trees proved to be the best. Below, Figure 5 presents a graphic representation of the Complex Tree model. The tree in this form reflects how the classification decisions were made on the basis of attributes.

In proposed model, the maximum number of splits was 100; it was applied Gini's Diversity Index as a split criterion, and there was none surrogate decision split.

The analysis of errors in the assignment to different classes was made with the help of a confusion matrix. The (3×3) matrix, where the lines correspond to the correct decision classes, and the columns with the decisions predicted by the classifier are shown in Figure 6. At the intersection of the row i and columns j is the number of examples originally belonging to the i -th class, and included in the j -class.

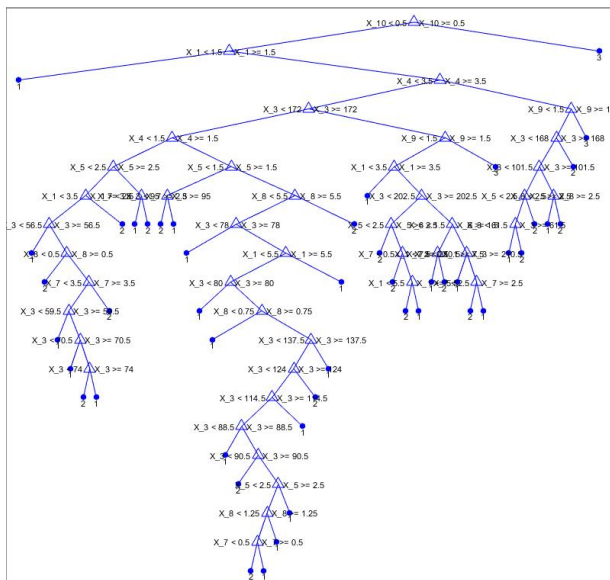


Figure 7. Complex Tree

As it results from the evaluation of the developed model, the correctness of the classification is about 81%. However, the prediction of the damage itself is key to reducing sliding strips damage. In the model it was defined as conditional technical condition (class 2). It means that in the next time interval it will be necessary to replace the sliding strip. The prediction of this state thus makes it possible to reduce damage to the overlays.

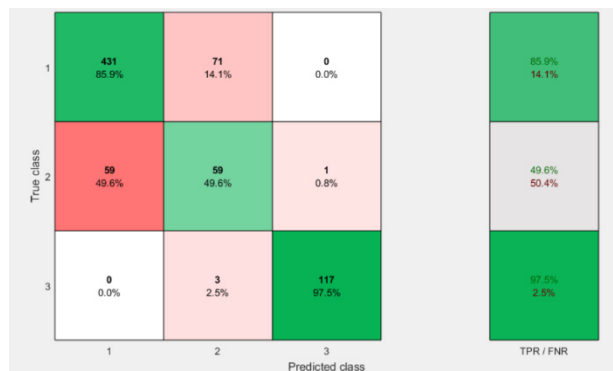


Figure 8. Confusion Matrix for Decision Tree

4. FAILURE ANALYSIS

Damage analysis included two variants. Variant I was based only on processed archival data. For the analysis of Variant II, data from technical reviews modified by the predictive model were used. The structure determined during the preliminary data processing in stage I was also used in stage II, thanks to which it was possible to compare the results.

Below, Figure 7 shows the correctness of the classification of technical states. The three technical states used mean as follows:

- 1 - possibility of further use,
- 2 - limited possibility of further use, it will be necessary to replace the overlay for the next inspection
- 3 - no use, it is necessary to replace the overlay

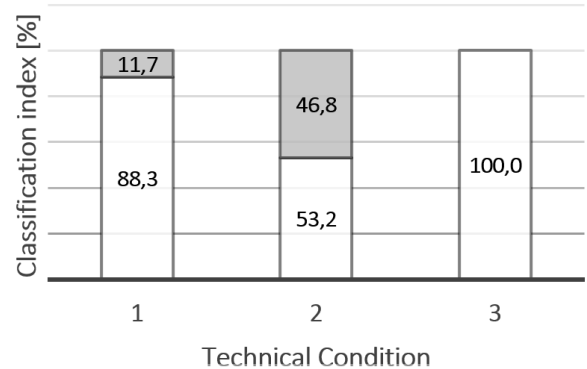


Figure 9. Correctness of classification of technical condition

Analyzing the data in Variant I, there were 47 damages to the cap or to the collector. In Variant II (after machine learning), only 23 were noted. The use of the presented model allows to reduce damage by about 50%.

5. CONCLUSION

In conclusion, the presented methodology is based on Artificial Intelligence. Failure analysis is necessary to properly prepare input data for both variants. Variant I concerns the analysis only of data obtained during the technical review, when Variant II is based on the classification machine learning method developed under this article.

Results show that prediction of a technical condition can reduce sliding strip damages by about 50%. Therefore, also the costs related to the repair of damaged railway infrastructure caused by the poor technical condition of the collector can be significantly reduced. The application of the developed method would also enable the reduction of railway delays caused by damage to the current collector system - the traction network. Further research will focus on the development of a predictive model that allows 100% prediction of damage so that its negative effects can be eliminated.

REFERENCES

- [1] Abbott, M.: Numerical method for calculating the dynamic behaviour of a trolley wire overhead contact system for electric railways, The Computer Journal, Vol. 13, No. 4, pp 363-368, 1970.
- [2] Aboshi, M.: Estimation method of contact line unevenness using dynamic simulation, IEEJ Transactions on Industry Applications, Vol. 126, No. 7, pp. 983-988, 2006.
- [3] Wąkatroba, P., Duda, S. and Gąkasiorek, D.: Symulacje numeryczne zjawisk dynamicznych w układzie pantograf-sieć jezdna, Modelowanie Inżynierskie, Vol. 23, pp. 94-100, 2015.
- [4] Wilk, A., Karwowski, K., Judek, S. and Mizan, M.: A new approach to determination of the two-mass model parameters of railway current collector, TTS Technika Transportu Szynowego, Vol. 10, pp. 212-218, 2015.

- [5] Judek, S., Karwowski, K., Mizan, M. and Wilk, A.: Modelowanie współpracy odbieraka prądu z siecią trakcyjną, *Przegląd Elektrotechniczny*, Vol. 1, No. 11, pp. 248–253, 2015.
- [6] Wilk, A., Karwowski, K., Judek, S. and Mizan, M.: Modelowanie i symulacja dynamiki ruchu trakcyjnego odbieraka prądu, *Przegląd Elektrotechniczny*, Vol. 1, No. 10, pp. 245–260, 2016.
- [7] Rusu Anghel, S., Miklos, C. and Averseng, J.: Control system for catenary—Pantograph dynamic interaction force, *Computational Cybernetics and Technical Informatics (ICCC-CONTI)*, 2010.
- [8] Aboshi, M. and Manabe, K.: Analyses of contact force fluctuation between catenary and pantograph, *Quarterly Report of RTRI*, Vol. 41, No. 4, pp. 182–187, 2000.
- [9] Mokrani, N. and Rachid, A.: A robust control of contact force of pantograph-catenary for the high-speed train, *2013 European Control Conference (ECC)*, Zürich, Switzerland, July 17–19, 2013.
- [10] Abdullah, M.A., Michitsuji, Y., Nagai and Miyajima, N.: Integrated simulation between flexible body of catenary and active control pantograph for contact force variation control, *Journal of Mechanical Systems for Transportation and Logistics*, Vol. 3, No. 1, pp. 166–177, 2010.
- [11] Piga-Carboni, A., Pisano, A. and Usai, E.: Robust control of the contact force of an asymmetric pantograph, *Eighth International Conference on Computers in Railways. Computers in Railways VIII*, Lemnos, Greece, pp. 223–232, 2002.
- [12] Makino, T., Yoshida, K., Shinji, S. and Makino, K.: Running test on current collector with contact force controller for high-speed railways, *JSME International Journal Series C Mechanical Systems, Machine Elements and Manufacturing*, Vol. 40, No. 4, pp. 671–680, 1997.
- [13] Abdullah, M.A., Michitsuji, Y., Nagai and Miyajima, N.: Analysis of contact force variation between contact wire and pantograph based on multibody dynamics, *Journal of Mechanical Systems for Transportation and Logistics*, Vol. 3, No. 3, pp. 552–567, 2010.
- [14] Pappalardo, C.M., Patel, M., Tinsley, B. and Shabana, A.A.: Contact force control in multibody pantograph/catenary systems, *Proceedings of the Institution of Mechanical Engineers, Part K: Journal of Multi-body Dynamics*, Vol. 230, pp. 307–328, 2016.
- [15] Pisano, A. and Usai, E.: Contact force regulation in wire-actuated pantographs via variable structure control, *International Journal of Control*, Vol. 81, No. 11, pp. 1747–1762, 2008.
- [16] Yuan, H., Wang, C.G., Lu, W.B. and S. Zhang: Preparation and Tribological Behavior of Carbon Fiber Reinforced Pantograph Slide Plate, *Advanced Materials Research*, Vol. 430, pp. 378–382, 2012.
- [17] A. ROJEK and W. MAJEWSKI, Materiały nakładek ślizgowych pantografów, VI Lubuska Konferencja Naukowo-Techniczna - i-MITEL, 2010.
- [18] Ding, T., Yuan, J., Fan, Y., Yang, Y and Xiong, W.: Tribology Behaviors of Carbon Strip/Copper Contact Wire of Pantograph/Catenary System Under Electric Current, *3rd International Conference on Applied Mechanics and Mechanical Automation (AMMA 2017)*, 2017.
- [19] Ding, T., Li, Y., Xu, G. and Yang, Y.: Friction and Wear Behaviors with Electric Current of Carbon Strip/Copper Contact Wire for Pantograph/Catenary System, *2017 Asia-Pacific Engineering and Technology Conference (APETC 2017)*, 2017.
- [20] W.J.-M. Review and undefined 2003, Current Status and Future Trends of Research on Pantograph Slide, en.cnki.com.cn.
- [21] QIAN, Z., SHENG, W., ZHANG, GU, Z. S., J.Z.-E.D.: Development of carbon contact strips and research progress in china, en.cnki.com.cn.
- [22] Kubo, S. and Kato, K.: International and undefined 1999, Effect of arc discharge on the wear rate and wear mode transition of a copper-impregnated metallized carbon contact strip sliding against a copper disk, *Tribology International*, Vol. 32, No. 7, pp. 367–378, 1999.
- [23] Ding, T., Chen, G.X, Bu, J. and Zhang, W.H.: Effect of temperature and arc discharge on friction and wear behaviours of carbon strip/copper contact wire in pantograph–catenary systems, *Wear*, Vol. 271, No. 9–10, pp. 1629–1636, 2011.
- [24] He, D.H. and Manory, R.: A novel electrical contact material with improved self-lubrication for railway current collectors, *Wear*, Vol. 249, No. 7, pp. 626–636, 2001.
- [25] Sitarz, M., Adamiec, A. and Mańka, A.: Uszkodzenia węglowych nakładek stykowych pantografów kolejowych stosowanych w Polsce, *TTS Technika Transportu Szynowego*, Vol. 23, No. 1–2, pp. 70–74, 2016.

Jakub Andruszko

PhD Researcher
Wrocław University of Technology
Faculty of Mechanical Engineering
Department of Machine
Design and Research

Przemysław Moczko

Associate Professor
Wrocław University of Technology
Faculty of Mechanical Engineering
Department of Machine
Design and Research

Damian Pietrusiak

Associate Professor
Wrocław University of Technology
Faculty of Mechanical Engineering
Department of Machine
Design and Research

The use of numerical methods in cutterhead dredger excavation unit optimization

Authors presented a numerical approach for assessing the efficiency of the cutterhead dredger. To assess the efficiency parameters, it was necessary to determine the boundary conditions such as the geometry of the cutterhead, which was obtained by 3D laser scan and operational parameters of the dredger. Based on that numerical model was prepared to and numerous analyzes conducted that allowed authors to verify their thesis regarding the improvement of the machines efficiency, proposing the correct teeth geometry on the cutterhead and at the same time gave the opportunity to determine their optimal alignment for a specific work technology.

Keywords: : dredger, Rigid-Body Dynamic, 3D scanning

1. INTRODUCTION

Mining, rock/raw materials processing or material handling is dominated by the underground and surface mining technologies. One should also be aware that exploration of minerals or earth moving is undertaken also under water. It can be very demanding and sophisticated deep, open water mining but also removing, collecting or relocating material from relatively shallow water which is called dredging. Dredging is the process which is very often a part of maintaining the ports, channels and other water passages to keep them accessible. However, as already mentioned, collecting of sediments, but also more hard or cohesive soils are run that way.

As the dredging is used in different basins and for different type of minerals, dredgers – the special type of floating excavators, differ in construction of the floating unit and working/excavating unit.

From the point of view of the floating unit, the main type division is for self-propelled and stationary. Self-propelled units are similar to regular vessels which are able to change the location in long distance, seagoing. However, for the change of the local position while operating piles and anchored ropes are in use.

Stationary, non-propelled are the barge floating structures which requires independent units engagement in purpose to relocate. Mostly, those units are smaller. The local change of the position, while operating, is provided by piles and anchored ropes or anchored ropes only.

The classification with respect to the working unit is strongly related to the collected material and its resistance for excavation. Both the factors will influence the collection/suction method and dislodgement method. For the purpose of this article only the excavating units for hard minerals will be discussed.

While facing with the cohesive soils or hard mineral a cutterhead must be installed. Cutterhead function is similar to all mining equipment cutting tools where hard rock or soil must be excavated.

Most common cutterhead is the *crown type*. Crown design will differ with respect to the resistance of the excavated material. A *wheel type* cutter is similar with its construction to all bucket wheel excavator/reclaimers operating on the surface. A modification of this type is closely spaced bucket wheel which works like milling cutter or cutting blade [4].

In the presented paper, investigations of technological parameters with respect to the production output of the non-propelled dredger will be discussed. Excavating unit of the machine is bucket type cutterhead, however of special two side/blade with closely spaced buckets. As a result the cutting tool is closer with is function to milling type cutting blade. In figure 1, the barge on which the system is installed is presented with the cutting blade in the foreground.



Figure 1. View of the dredger

The manoeuvrability is provided by sets of anchored (at the dry shore) ropes operate by winches. Two of the ropes are assemble to the dredger ladder providing slewing. Set of three ropes running to the common point localised at stern, creates the fixed point of rotation. For location change in big range, external self-propelled unit must be used. Presented machine is used for underwater sand excavation.

Correspondence to: M.Sc.Eng. Jakub Andruszko,
PhD Researcher

Department of Machine Design and Research,
Łukasiewicza 7/9, 50-371 Wrocław, Poland
E-mail: jakub.andruszko@pwr.edu.pl

2. PROBLEM IDENTIFICATION

It is common problem that the underwater sand excavation faces two main problems related to wear of the cutterhead and relatively low output. Both issues are more present in heavy operational conditions (high excavation/cutting resistance). Despite such a heavy conditions, the conventional dredging technique with cutter head is still used as more economically efficient instead of blasting based technique. This is due to the fact that not all sand deposits are characterised by high cutting resistance that can be excavated with satisfactory output and equipment wear ratio. However more and more deposits, which are scheduled for excavation lately, are these, where abrasive wear and low output play an important role in the total cost of operation. Therefore it is important to design new and optimise existing dredging equipment to enable operation in the wider range of excavation resistance with economically justified costs. For this purpose investigations of cutting tools wear process based on operational data, experimental tests and numerical simulations were conducted. Based on the results of investigations, optimisation recommendations of cutting process are given. The presented approach is applied for dredger described in the first chapter of the paper however it can be used at any dredging equipment as well.

2.1 Cutting tool wear process

In the described dragger, which is equipped with two bucket wheels on which chisel type teeth are installed, the wear process occurs on the cutting edges of teeth at the most and on the bucket wheel as well. Example of teeth wear process is shown in figure below.



Figure 2. Typical wear of cutting teeth

The abrasive wear of teeth is typical for sand excavation and accelerated by higher excavation resistance of deposit. In order to improve teeth usage intervals all areas, which are prone to such abrasive wear are hardfaced (around 60 HRC hardness is obtained). The same technique is used to prevent wear of the bucket wheel in teeth fixing areas and buckets edges as well. The wear rate of teeth is significantly high and requires replacing of around 20-30 % of teeth per 24 hours of operation. Teeth are then repaired by hardfacing of cutting edges. Teeth wear is unequal and the higher wear rate is observed on the corner located teeth and also on the teeth fixing areas (Figure 3).



Figure 3. Unequal wear of teeth and bucket wheel wear areas

Unequal and asymmetric wear observed on the cutter head indicates improper design of cutting geometry such as locations, numbers and angles of teeth. In order to analyse this phenomena in details, the 3D laser scanning, loads identification and further numerical simulations were conducted.

2.2 Laser scanning

Due to the need to accurately simulate the dredging process, a virtual model of cutterhead was developed [1]. The model was created using a 3D scanning technique. The overall scanning accuracy was 3 mm at 50 m and angular accuracy of 8 "horizontally and 8" vertically. Scans were made in five positions: 0°, ±45°, ±90° in relation to the cutterhead boom longitudinal. An example view on the scanning object and equipment is shown in Figure 4 and 5.



Figure 4. First scanning position - 90°



Figure 5. Second scanning position - 45°

Based on the surface model, generated from the cloud of points, a solid model of the cutterhead was developed. This 3D scan model of the cutterhead was compared with the virtual 3D model created with consideration of technical documentation. Comparison of both models is shown in Figure 6. Significant differences were found, which means that the existing cutting wheel has not been

built as per design, which is caused by low quality or errors of casting process of the cutting wheel.

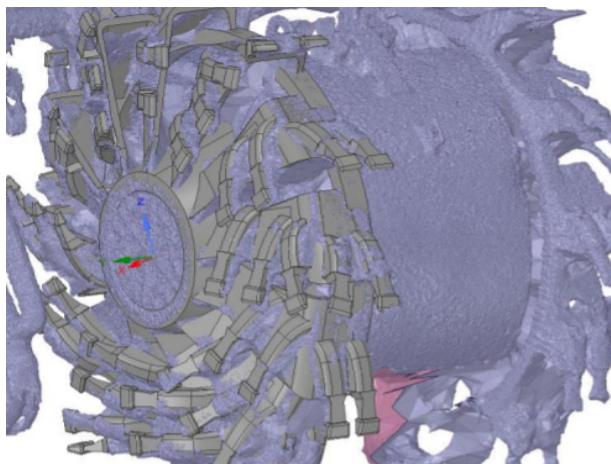


Figure 6. Comparison of 3D scan and the model created with consideration of technical drawings

The model obtained thanks to 3D scanning has been implemented for further numerical calculations as a reference to the real object. On the basis of this model, a kinematic analysis of the cutterhead and ladder was made. The trajectory of tooth movement during the dredging process were determined as well [14].

2.3 Loads identification

The main operational loads are generated by slewing (movement generated by two winches which ropes are attached to the ladder in the proximity of cutterhead) and cutting wheel rotation. Both drives are powered by hydraulic system of maximum operational pressure of 200 bars.

In Figure 7 trace of the cutting wheel pressure and output (tonnes per hour) is presented. One can observe that output drops and rise are not correlated directly with the pressure increase, with exception to the time band 400-600s where cutterhead is out of the excavated deposit.

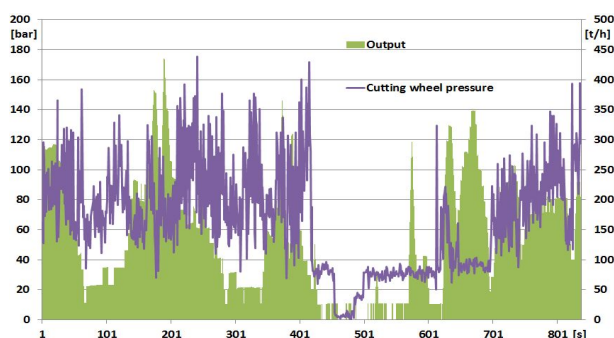


Figure 7. Cutterhead pressure and output trace

Analysis of Figure 8 allows to observe that nevertheless the slewing force (generated by the hydraulic winch) is kept relatively constant, there is no constant value of output observed. The only relation observed in two cycles, is increase of the output with pressure increase (with small phase shift), but only in the end of slew cycle (~190s., ~290s).

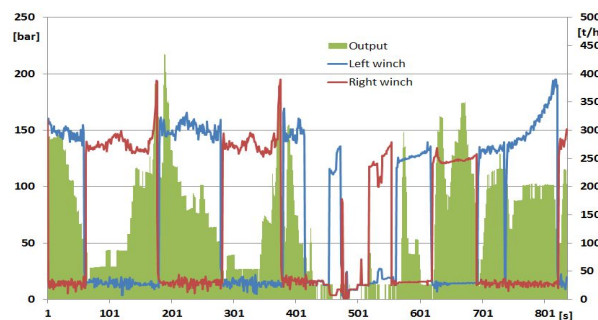


Figure 8. Cutterhead winch pressure and output trace

In Figure 9 where pressure of slewing and cutting is compared, it is possible to point that alternations of cutting wheel pressure are close to harmonic and not reaching the maximum value. Different observation is done in case of the slewing winch pressure which is rather constant, but rapid increase of the pressure (up to the maximum value) are observed occasionally.

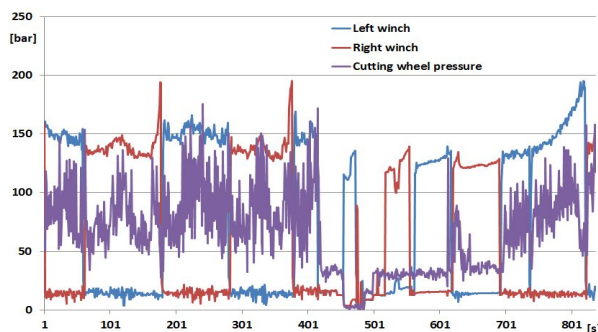


Figure 9. Cutterhead winch pressure and cutting wheel pressure trace

The analysis of diagrams described above, drives the conclusion that process of operation is not stable. Fluctuations of resistance increase, not correlated with the output increase, implies the difficulties with excavation process. Rapid pressure rise at the slewing winches, confirms problems with operation – emergency stops. The expected output (300 t/h) is reached only occasionally.

Measurements of forces on the winches ropes indicated that forces during normal operation oscillates around the value of 60-70 kN. When overload, the force in rope reaches about 80 kN. If assuming that the nominal excavation torque on the wheel (21kNm) corresponds with the maximum hydraulic pressure of the wheel drive, the average operational torque equals 7.9 kNm.

3. NUMERICAL SIMULATIONS

In author's method, in order to determine the efficiency of the dredger, numerical methods were implemented [16][17]: Discrete Element Methods (DEM) and Rigid Body Dynamics (RBD). Authors proposed to determine the efficiency of the dredger as a measure of the change in the load of the cutterhead, thus changing the loads on the cutterhead and the ladder.

By means of the RBD analysis, the trajectories of the teeth were determined [9]. The simulation was carried out in accordance with the parameters of the real object [2], [7], [8] and [10]. Thanks to the implementation

of the Discrete Elements Method, excavated material model has been built [11], [12] and [15]. The correctness of this model was verified by means of a comparative analysis of numerical simulation loads and operational loads described in subchapter 2.3 [5] and [6]. The values of the loads from the simulation were compared with values measured on the real object [3], [13]. Parameters related to the contact between discrete elements have been adjusted to properly calibrate the numerical model [18]. As a result the validated numerical model was used as a reference to subsequent numerical DEM-RBD simulations, allowing to determine the method of improving the dredger's efficiency. The RBD and DEM model described above is shown in Figure 10, where dredging process is simulated.

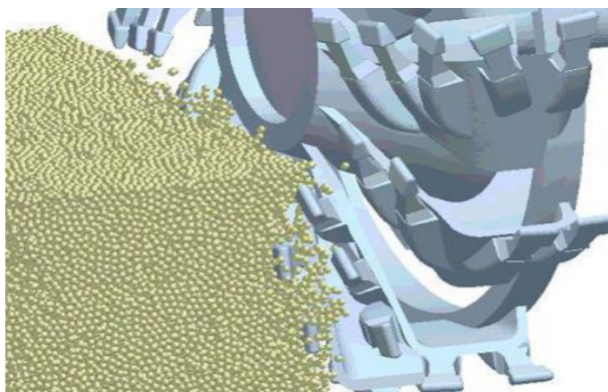


Figure 10. Simulation of RBD-DEM

Figure 11 presents examples of teeth trajectories obtained from simulations as well.

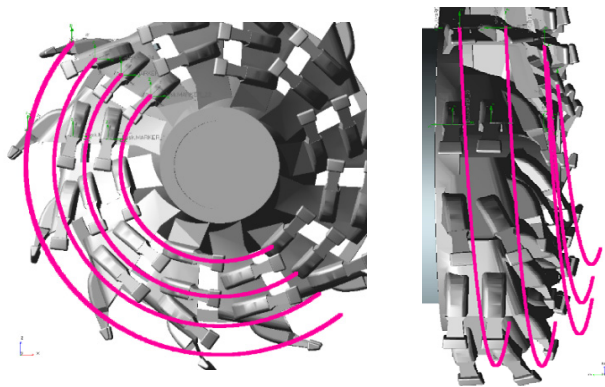


Figure 11. Teeth trajectories of RBD-DEM model

3.1 Currently used cutterhead

Numerical simulation with current teeth geometry were performed. Diagrams of torque loads measured on the cutterhead shaft and ladder are shown in Figures 12 and 13.

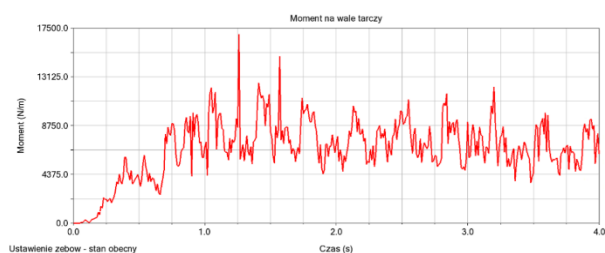


Figure 12. Torque load of the cutterhead shaft

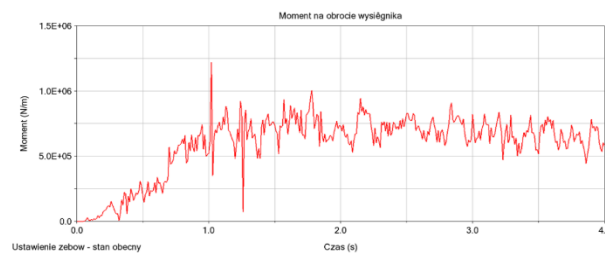


Figure 13. Torque load of the ladder

The effective reference values of the obtained characteristics were determined. Torque on the cutterhead shaft equals (1):

$$RMS_{S0c} \cong 8447 \text{ Nm} \quad (1)$$

Torque on the ladder equals (2):

$$RMS_{S0L} \cong 783220 \text{ Nm} \quad (2)$$

3.2 Optimisation of the cutterhead

Based on the numerical simulations of the existing design, the new geometry of teeth locations and angles were developed (Figure 14), and numerical simulation were performed to obtain optimal solution. Diagrams of torque loads for the cutterhead shaft and the ladder for the existing and new model are shown in Figures 15-16.

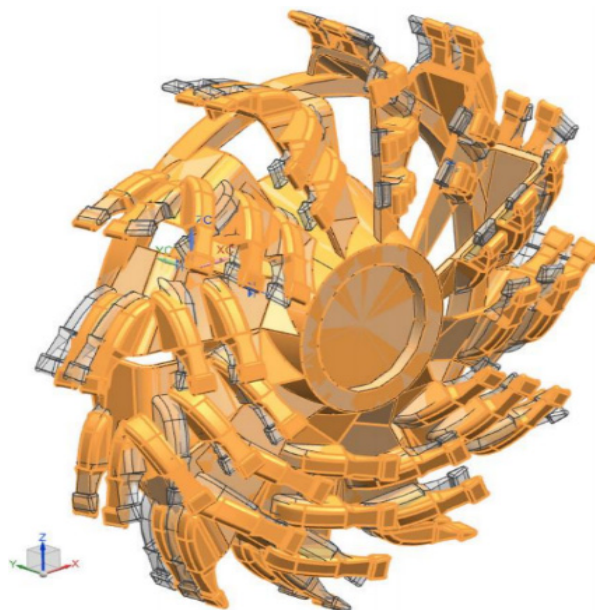


Figure 14. The new model (orange) compared to the existing one

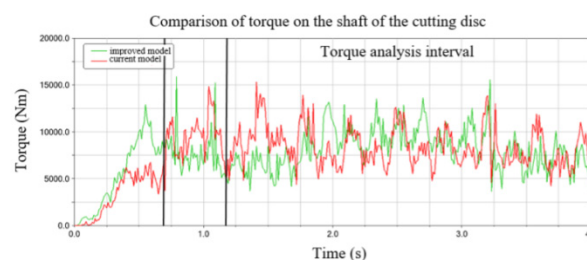


Figure 15. Comparison of existing and new design of teeth geometry- torque loads on the cutterhead shaft

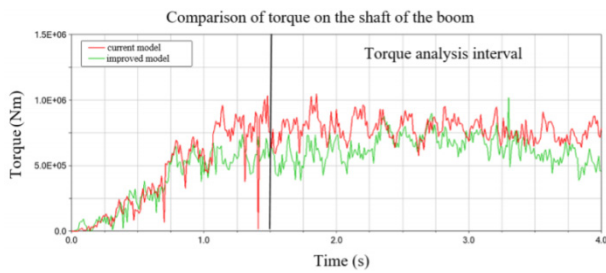


Figure 16. Comparison of existing and new design of teeth geometry- torque of loads on the ladder

The effective reference values of the obtained characteristics for the new geometry were determined. Torque on the cutterhead shaft equals (3):

$$RMS_{S1c} \cong 8691 \text{ Nm} \quad (3)$$

Torque on the ladder equals (4):

$$RMS_{S1L} \cong 641070 \text{ Nm} \quad (4)$$

4. EXPECTED INCREASE OF THE DREDGER OUTPUT

As per simulations results, the significant drop of torque loads (~18%) on the ladder was observed for the new design in comparison to the existing one, while the load on the cutterhead shaft remains almost unchanged. With such a results it is possible to increase slewing speed of the ladder and obtain output increase as well within existing torque limits of the dredger. Increase of the dredger output can be assumed as volume of the material being excavated while slewing of the ladder in the unit of time for the existing and higher slewing speed.

In order to obtain optimal geometry of the new design, numerical simulations with different position angles of teeth in relation to the model exhibiting lower resistance forces, were performed. It was decided to deviate the teeth in the positive and negative angles in relation to the corrected model to. This approach enabled finding the minimum torques loads on the ladder and cutterhead shaft and thus the optimal angle of tooth position on the bucket wheel of the cutting disc. The obtained results for three different teeth angles allowing to determine the optimal value are shown in Figures 17 and 18.

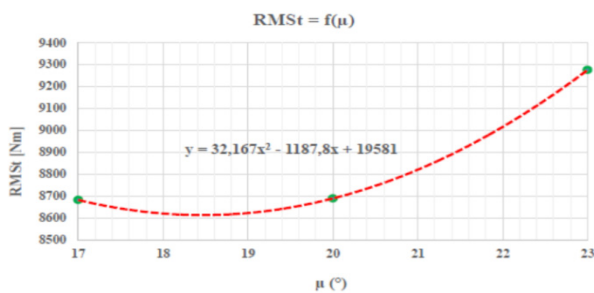


Figure 17. Teeth angle vs cutterhead shaft torque

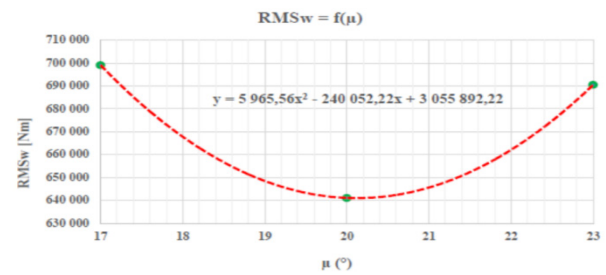


Figure 18. Teeth angle vs ladder torque

The obtained torque loads results were approximated with the quadratic polynomial. The function minimum for cutterhead torque equals 18.5°, while for the ladder torque it is 20°.

In the next step similar type of simulations were performed with increased slewing speed of the ladder for 18%. Both ladder and cutterhead torques were checked for the constant teeth angle of 20°. As per obtained results the torque on the cutterhead shaft equals (5):

$$RMS_{S1c} \cong 9487 \text{ Nm} \quad (5)$$

Torque on the ladder equals (6):

$$RMS_{S1L} \cong 658330 \text{ Nm} \quad (6)$$

Based on the results it was confirmed that optimized teeth geometry enabled to increase output of the dredger without significant loads of the machine. Expected increase equals 15%.

5. SUMMARY AND CONCLUSIONS

Dredging of mineral deposits faces problems related to wear process of cutting tools. Such problems are accelerated by excavation of deposits characterised by high excavation/cutting resistance, which directly impacts production output. In order to improve this situation it is possible to design new technical solutions or optimise existing ones. Authors of this paper present numerical and experimental approach to optimise geometry parameters of dredger's cutterhead in order to increase output and reduce unequal wear of cutting equipment.

The analyses conducted for the existing design pointed out that actual geometry of cutting tool is not suited for the operational conditions. Maximum capacity of the side winches is reached repeatedly with no dredger output increase. Additionally, problems with rapid cutting teeth wear and its insecure assembly, increase the machine downtime. As a result, the total output is far from the expected. In order to improve this situation, the new optimised geometry of cutter head was developed. In the new design locations and teeth angles were modified and numerically tested with the use of Discrete Element Methods (DEM) and Rigid Body Dynamics (RBD) methods.

In the presented in the paper case of the sand dredger and with consideration of the results of the numerical simulation it was possible to estimate that the potential of the output of the dredger is not achieved. By implementation of the optimised design of cutting tools, it is expected to increase the excavation efficiency for

even up to 20% and at the same time to increase output of the dredger significantly within existing drive limits.

As a result of the performed investigations the following conclusions can be given:

1. Dredging of new deposits, with more difficult excavation conditions, results in many problems such as higher wear rate of cutting tools and lower output, which may lead to a situation where existing technique use is not economically justified anymore.
2. In such a case optimisation of existing technique may extend operational limits significantly.
3. The design of the cutting tools should be customised with respect to the material type (characteristics, resistance) and the technical capabilities of the dredger.
4. Numerical methods are efficient tools to simulate, and investigate cutting process and thus enable to obtain optimised solutions.

REFERENCES

- [1] Blouin, S., Hemami, A. and Lipsett, M.: Review of resistive force models for earthmoving processes, *Journal of Aerospace Engineering*, Vol. 14, No. 3, pp. 102-111, 2001.
- [2] Bošnjak, S. M., Oguamanam, D. C. D. and Zrnić, N. Đ.: The influence of constructive parameters on response of bucket wheel excavator superstructure, *Archives of Civil and Mechanical Engineering*, Vol. 15, No. 4, pp. 977-985, 2015.
- [3] Bošnjak, S., Petković, Z., Simonović, A., Zrnić, N. Đ and Gnjatović, N.: Designing-in failures and redesign of bucket wheel excavator undercarriage, *Engineering Failure Analysis*, Vol. 35, pp. 95-103, 2013.
- [4] Bray, R. N., Bates, A. D. and Land, J. M.: *Dredging: A Handbook for Engineers*, Butterworth-Heinemann, 1996.
- [5] Czmochoński, J., Moczko, P., Pietrusiak, D., Przybyłek, G. and Rusiński, E.: Selected Aspects of Technical Condition State Assessment of Spreaders Operating in Lignite Mines, *Proceedings of the 13th International Scientific Conference Computer Aided Engineering*, pp. 89-98, 2016.
- [6] Danicic, D., Sedmak, S., Ignjatovic, D. and Mitrovic, S.: Bucket wheel excavator damage by fatigue fracture - case study, *Procedia Materials Science*, Vol. 3, pp. 1723 - 1728, 2014.
- [7] Derlukiewicz, D.: Application of a Design and Construction Method Based on a Study of User Needs in the Prevention of Accidents Involving Operators of Demolition Robots, *Applied Science*, Vol. 9, No. 7, 2019.
- [8] Derlukiewicz, D., Kowalczyk, M., Moczko, P. and Smolnicki, T.: Selected Aspects Of Loads Identification In Caterpillar Undercarriage Of Bucket Wheel Excavator, *25th Danubia-Adria Symposium On Advances In Experimental Mechanics*, pp. 55-56, 2008.
- [9] Flores, F. G., Kecskeméthy, A. and Pöttker, A.: Workspace analysis and maximal force calculation of a face-shovel excavator using kinematical transformers, *Proceedings of the 12th IFToMM World 454 Congress in Mechanism and Machine Science*, pp. 375-381, 2007.
- [10] Gnjatovic, N.: *Influence of constructional parameters and parameters of excitation on response of the bucket wheel excavator with two masts in the out-of-resonance region*, PhD Thesis, University of Belgrade, 2016.
- [11] McKyes, E.: Agricultural engineering soil mechanics, *Developments in Agricultural Engineering, Soil and Tillage Research*, Vol. 10, No. 3-4, pp. 393-394, 1992.
- [12] Perumpral, J. V., Grisso, R. D. and Desai, C. S.: A soil-tool model based on limit equilibrium analysis, *478 Transactions of the American Society of Agricultural Engineers*, Vol. 26, No. 4, pp. 991-995, 1983.
- [13] Pietrusiak, D., Moczko, P. and Rusiński, E.: Recent achievements in investigations of dynamics of surface mining heavy machines, *24th World Mining Congress: mining in a world of innovation - proceedings*, pp. 295-308, 2016.
- [14] Rashi, T., Jeremy, K. and George, D.: Bucket trajectory classification of mining excavators, *Automation in 470 Construction*, Vol. 31, pp. 128-139, 2013.
- [15] Reece, R.: The Fundamental Equation of Earth-Moving Mechanics, *Proceedings of the Institution of Mechanical Engineers Conference*, Vol. 179, No. 6, pp. 16-22, 1964.
- [16] Rusinski, E., Cegiel, L., Michalczyk, A. et al.: Investigation and modernization of buckets of surface mining machines, *Engineering structures*, Vol. 90, pp. 29-37, 2015.
- [17] Rusiński, E., Czmochoński, J., Moczko, P., Pietrusiak, D.: Challenges and strategies of long-life operation and maintenance of technical objects, *FME Transactions*, Vol. 44, pp. 219-228, 2016.
- [18] Swick, W.C., Perumpral J. V.: A model for predicting soil-tool interaction, *Journal of Terramechanics*, Vol. 25, No. 1, pp. 43-56, 1988.

Theoretical backgrounds for zipline analysis

Jovan Vladić

Professor
University of Novi Sad
Faculty of Technical Sciences

Tanasije Jojić

Teaching Assistant
University of Novi Sad
Faculty of Technical Sciences

Radomir Đokić

Assistant Professor
University of Novi Sad
Faculty of Technical Sciences

Anto Gajić

Associate Professor
Mine and Thermal Power Plant
Ugljevik

This paper defines theoretical backgrounds for the zipline analysis. Considering that these systems are relatively new, and that there are still no valid regulations or drafts for them, the production of such systems is still left to the enthusiasts. For quality design it is necessary to perform a detailed analysis of persons kinematic parameters dependence from a range of influential sizes such as person's weight, tensile rope force, position during lowering, wheel resistance, wind, etc. Procedure for computational model forming is based on the catenary theory. The analysis are made by computer simulations for concrete conditions of zipline whose installation was planned on Fruška Gora. Conditions for mentioned zipline are characteristic due to the relatively large length (≈ 1500 m), small inclination angle ($\approx 3.50^\circ$) and the "shallow" terrain. Analysis results are given through diagrams that shows the person's reach, velocity or acceleration in dependence of time or travelled distance.

Keywords: Zipline, Catenary, Computation Model, Computer Simulation, Motion Resistance, Velocity, Deflection, Wind.

1. INTRODUCTION

The term "zipline" represents a system of tightened steel rope by which the person is carried by high speed travelling trolley. The trolley and person are moving under the influence of their own weight. The main aim is causing increased excitement, so-called adrenaline sport. They expanded over the past two decades, with construction in various locations such as hilly areas, parks, lakes, bridges, the city cores, etc., [1].

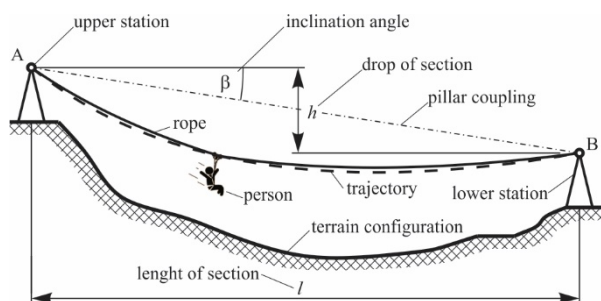


Figure 1. Schematic representation of zipline

From usage and safety viewpoint, the most interesting kinematic parameters are maximum velocity and acceleration, travelling time, range and velocity at the end of the section (velocity at limiter). The most significant size that influences those parameters is the inclination angle (β). For inclination angle larger than 10° , high velocities are achieved at the section, but also at the entry of lower station which is a significant problem for safe stopping of the person. In cases of inclination angles lower than 5° , there is a problem with arriving to the lower station, especially in cases of

unfavorable wind direction or changes of the area exposed to the air flow (body position, spreading of hands, etc) during movement. For such cases, there is often a need for "pulling out" the person from the section.

2. THEORETICAL BACKGROUND AND COMPUTATIONAL MODEL FOR ZIPLINE ANALYSIS

Figure 2 shows a schematic representation of zipline with main notions and convenient mechanical model as background for computational model defining, [2], [3].

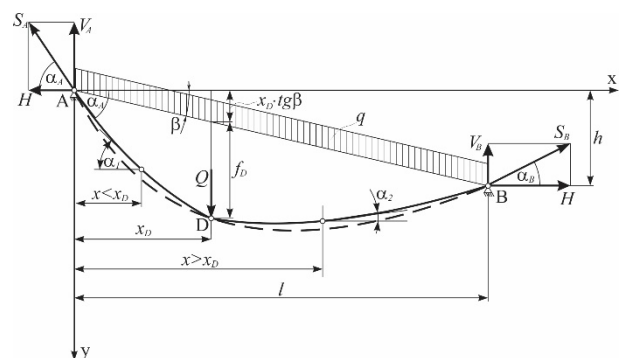


Figure 2. Mechanical model of zipline

The computational model is based on the catenary theory which represents an elastic flexible thread freely suspended between two supports located on the horizontal (l) and vertical (h) distance and loaded with its own weight [4].

The catenary equation, in a well-known form, is:

$$y = C \cdot \operatorname{ch}\left(\frac{x}{C}\right) \quad (1)$$

where catenary parameter:

$$C = \frac{H}{q} \quad (2)$$

Correspondence to: Tanasije Jojić, Teaching Assistant
Faculty of Technical Sciences,
Trg Dositeja Obradovića 6, 21000 Novi Sad, Serbia
E-mail: tanasijejojic@uns.ac.rs

The usage of hyperbolic functions is relatively complicated, so the catenary is replaced by the appropriate parabola in the engineering practice. Errors which are made by this parabola are about $2 \div 3\%$.

In case of steel rope, whose supports are at different heights, loaded with its own weight and concentrated loads, the equation of the trajectory of person can be represented as:

$$y = x \cdot tg\beta + f_x \quad (3)$$

where the deflection at a distance x_D at which the load is acting is represented as:

$$f_D = \frac{x_D}{l \cdot H} \cdot \left[Q \cdot (l - x_D) + \frac{q \cdot (l - x_D) \cdot l}{\cos\beta} \cdot \frac{1}{2} \right] \quad (4)$$

Usually, for short ziplines, both ends of the rope are anchored, but for ziplines with larger spans, the ropes are anchored at one end and tightened with weight at other.

Realization of zipline with both-sided anchorage is easy, which is the reason why it is often applied for short ziplines (from "tree to tree") but it represents a statically indeterminate system. For such case, the tension rope force changes considerably with the load moving, and additionally depends on the rope elasticity and current temperature [5]. This are main reasons why the case of a rope that is anchored at one end, and tightened with weight at other is generally more favourable, but the solution requires more space on the pillar and the system is more expensive which is justifiably only for large span ziplines.

The relevant computational model will be formed by neglecting small quantities of high order. The so-called static trajectory of movement is determined by expressions (3) and (4). Rope oscillation in vertical plane is, according to [6], [7] and [8], relatively small and can be neglected in case of "shallow" terrain and a system where the rope is anchored at one end and tensioned with weight at other.

Person connected with trolley forms a mathematical pendulum. If the length of the connecting belts is small, the effect of the swing can also be neglected as well as the influence of the centrifugal force due to the large radius of the trajectory curvature.

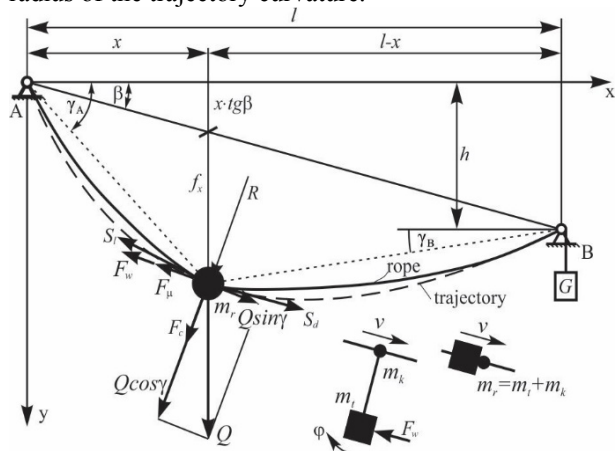


Figure 3. Computational model of zipline

In accordance to that, the computational model, shown on figure 3, can be represented as the movement of a concentrated mass along the trajectory determined

for static conditions, [9] and [10]. The air resistance and rolling resistance are acting on the concentrated mass while moving. The direction of resistances is always opposite to the direction of movement.

Every wheel that is rolling along deformable surface has a resistance component due the friction in wheel bearings and due to deformation of contact surfaces. Wheel that is rolling along the rope (Figure 4) has additional resistance component due the rope stiffness. Unlike the perfectly flexible rope, the real rope will not take the position of the tangents behind and in front of the wheel, which can be seen as a "wrinkling" of rope in front of the wheel.

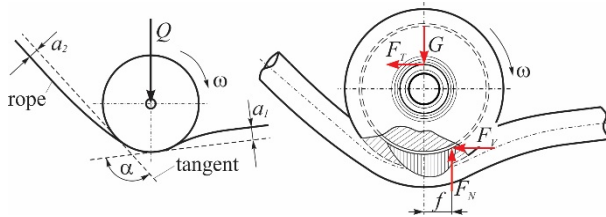


Figure 4. Model of wheel rolling along steel rope

Movement resistance of wheel that is rolling along steel rope can be determined by the expression:

$$F_\mu = \mu \cdot \Sigma G = \left(\mu_0 \cdot \frac{d}{D} + 2 \cdot \frac{f}{D} \right) \cdot \Sigma G \quad (5)$$

As the person traveling on zipline typically generates high velocity, the air resistance has a significant impact on all driving parameters. The air resistance is calculated according to [11]:

$$F_W = c_W \cdot A \cdot \frac{\rho \cdot (v \pm v_v)^n}{2} \quad (6)$$

where the dimensionless exponent depending on velocity (n) has values of:

- $n=1$ for velocities smaller than 1 m/s,
- $n=2$ for velocities between 1 m/s and 300 m/s,
- $n=3$ for velocities greater than 300 m/s,

and values of drag coefficient (c_W) are determined experimentally. According to [12], the values for different lowering positions are:

- $c_W=0,6$ - for sitting position,
- $c_W=0,4$ - for half-sitting position,
- $c_W=0,2$ - for lying position.

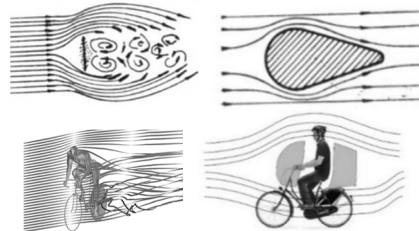


Figure 5. Turbulent or laminar flow cases

Areas exposed to air (A) are depending on the persons size and the body position. For person weighting 100 kg, they are approximately defined as:

- $A=0,4 \text{ m}^2$ for sitting position,
- $A=0,3 \text{ m}^2$ for half-sitting position,
- $A=0,2 \text{ m}^2$ for lying position.

Areas are proportional larger or smaller for persons weighting more or less than above mentioned mass.

3. RESULTS OF THE ANALYSIS

This heading presents analysis results for a concrete example of a zipline with a section length of 1467 m and drop of 99 m (therefore with inclination angle of $3,86^\circ$). Following diagrams shows the dependence of range, velocity and acceleration on person's weight, tensile rope force, position during lowering and wind direction.

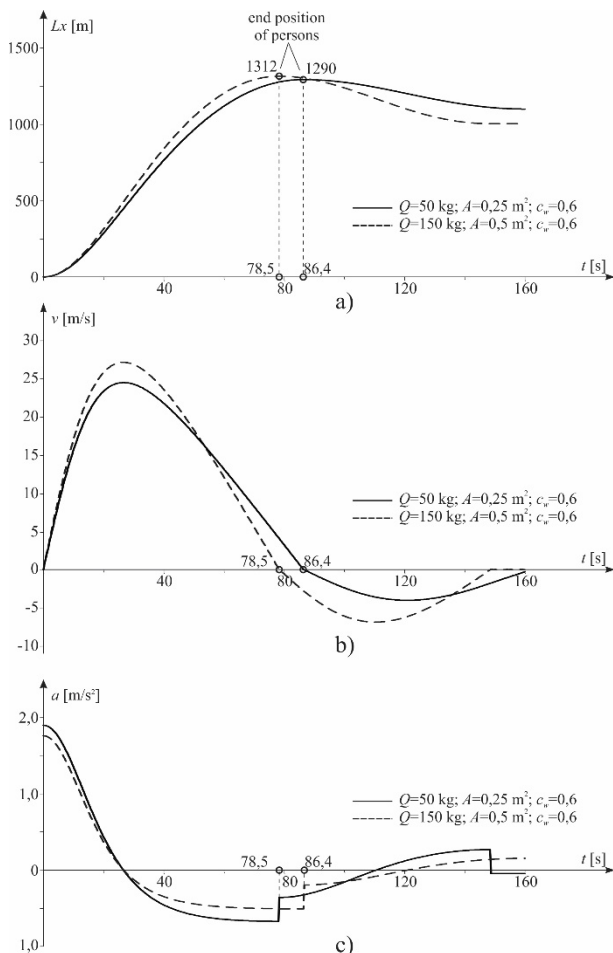


Figure 6. Diagram of the change in reach, velocity and acceleration for different values of person's mass

Diagram shown on figure 6 represents reach, velocity and acceleration as function of time for persons weighting 50 kg and 150 kg.

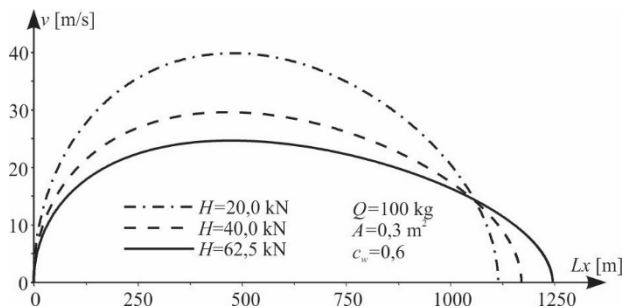


Figure 7. Diagram of velocity for different values of tension rope force

Diagram shown on figure 7 represents velocity as function of the horizontal distance between pillars for

different values of tensile rope force. It is notable that the reach is increasing with tension rope force increasing.

Diagram shown on figure 8 represents velocity as function of the horizontal distance between pillars for different lowering positions, where it is notable that lowering in sitting position can't be applied. On the other hand, case of lowering in lying position requires caution due the high velocity of arrival at lower station.

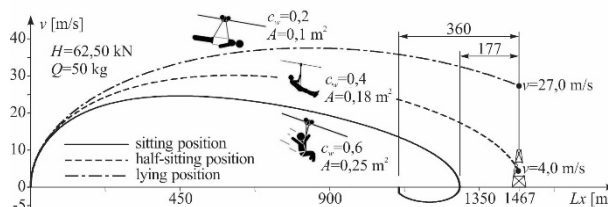


Figure 8. Diagram of velocity for different lowering positions

Diagram shown on figure 9 represents velocity as function of the horizontal distance between pillars for different directions of wind.

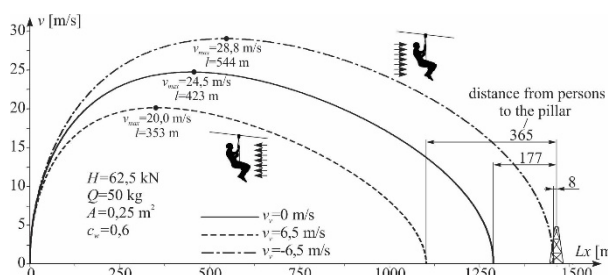


Figure 9. Diagram of velocity for different wind directions

4. CONCLUSIONS

For quality design, production and safe use of zipline, it is necessary to perform a detailed analysis of persons kinematic parameters dependence from a range of influential sizes. It is essential to form a relevant computational model which allows the simulation and determination of so-called "driving" characteristics" for concrete conditions.

For small inclination angles, the problem with person's arrival to the lower station occurs, especially in the case of "headwind" for light persons, which requires an appropriate solution for "pulling out" from the line. It is necessary to minimize movement resistance for such cases. Reducing trolley movement resistance can be achieved by an appropriate selection of wheels, rope construction and larger rope tension. In real conditions, air resistance can be reduced by reducing the area exposed to obstruction, or by correct selection of person's lowering position. The "half sitting" and "lying" lowering positions ensures arrival of persons to the lower station even for small inclination angles, whereby it is necessary to determine the arrival velocity and selection of appropriate safe stopping equipment.

Here are presented the analysis results by varying person's weight, tensile rope force, position during lowering, and wind direction. More detailed results are given in [13].

REFERENCES

- [1] Jojić, T., Vladić, J. and Đokić, R.: Specific machines and devices with horizontal rope as carrying element – zipline, Proceedings of the Faculty of Technical Sciences, Vol. 33, No. 1, pp. 13-16, 2018.
- [2] Alamoreanu, M. and Vasilescu, A.: Theoretical Aspects of Zip Line Analysis, Proceedings of VIII Triennial International Conference Heavy Machinery - HM 2014, pp. 131-136, 2014.
- [3] Vladić, J.: The Parametric of Equation of a Catenary Line and Theoretical Foundations for Static Analysis a Ropeway, Proceedings of XV European Conference of Material Handling Teaching Professors, pp. 170-178, 2004.
- [4] Czitary E. *Ropeways*, Springer-Verlag, Wien, 1962.
- [5] Mungan, C. E. and Lipscombe, T. C.: Traveling along a zipline, Latin-American Journal of Physics Education, pp. 5-9, 2011.
- [6] Vladić, J.: *Calculus and experimental methods for static and dynamic analysis of ropeways*, Faculty of Technical Sciences, Novi Sad, 1991.
- [7] Vladić, J.: *Development of calculation methods for analyzing the static and dynamic behavior of the ropeways*, Faculty of Technical Sciences, Novi Sad, 1989.
- [8] Vladić, J., Živanić, D., Džinčić, I., Đokić, R. and Gajić, A.: Application of the numerical methods for dynamic analysis of transport systems with rope, Proceedings of VIII Triennial International Conference HEAVY MACHINERY - HM 2014, pp. A.37-42, 2014.
- [9] Kožar, I., Torić, M. N.: Analysis of body sliding along cable, Coupled Systems Mechanics, Vol. 3, No. 3, pp. 291-304, 2014.
- [10] Kožar, I. and Štimac, I.: Dynamic Analysis of Loads Moving Over Structures, 4th International Congress of Croatian Society of Mechanics, 2003.
- [11] Janković, A.: *Car dynamic*, Faculty of Mechanical Engineering, Kragujevac, 2008.
- [12] Mun, H. K., Abdulkareem, S. and Mahdi, A.: Calculation of Aerodynamic Drag of Human Being in Various Positions, Proceedings of EURECA 2013, pp. 99-100, 2013.
- [13] Vladić, J., Đokić, R. and Jojić, T.: *Elaborats I, II i III - Analysis of the zipline system in Vrdnik*, Faculty of Technical Sciences, Novi Sad, 2017.

NOMENCLATURE

β	inclination angle /°/
h	section drop /m/
l	section length /m/
H	horizontal component of rope force /N/
q	own weight of rope /kg/m/
μ	total resistance coefficient /-/
μ_0	bearing friction coefficient /-/
d	bearing diameter /mm/
D	wheel diameter /mm/
f	lever arm of rolling torque /mm/
$\sum G$	sum of vertical forces /N/
c_w	drag coefficient /-/
A	frontal area /m ² /
ρ	air density /kg/m ³ /
v	person velocity /m/s/
v_v	component of wind velocity in the direction of movement /m/s/;
n	dimensionless exponent depending on velocity

Crashworthiness of protection structures for mining machine operators: numerical analysis and experimental validation using Optical 3D Coordinate Measuring Devices

Paulina Działak

Research Assistant
Wrocław University of Science and Technology
Faculty of Mechanical Engineering

Jacek Karliński

Assistant Professor
Wrocław University of Science and Technology
Faculty of Mechanical Engineering

The aim of the work was to perform comparative tests based on strength analysis and experimental research of the structure protecting the operator of the self-propelled mining machine. The first stage was to develop a numerical model of the protection structure in accordance with the technical documentation provided by the manufacturing company and to analyse it with the use of finite element method. The analysis was conducted in the dynamic range, taking into account material and geometric non-linearity. Performed calculations included simulation of the strength test of a protective structure's impact with falling mass in accordance with PN-92 / G-59001 (RSPS - Rock slide protective structures). Basing on the documentation, geometric and then discrete model were developed and the numerical calculations were performed. Then, in order to verify the computer simulation, experimental tests of the analysed cabin were carried out.

Keywords: protective structure, photogrammetry, finite element method, high speed camera, strain gauge measurements, comparative testing

1. INTRODUCTION

Assessment of the self-propelled machine operators safety by numerical methods in order to obtain approval for sale and usage of the machine is related to the experimental validation of the method used. The most often performed procedures are FOPS (Falling Object Protective Structure) and RSPS (Rock Slide Protective Structures) tests. They are a means of testing the characteristics of the structures used to protect the operator from localized impact penetration and, indirectly, of the load-carrying capacity of the supporting structure to resist impact loading [1]. The experiment consists in dropping the object with mass and shape defined in standards onto the cab roof from height, which will provide the required impact energy (FOPS-11.6 kJ, RSPS - 60 kJ). The evaluation of the protective structure after the test consists in the measurement of the deflection of the roof by a simple ruler in the area where the machine operator is located. The authors of the paper decided to go one step further and perform more accurate measurement of the cab structure before, after and during the impact of the falling object [2]. Additionally, the measurement of other elements of the protective structure was made.

The research was carried out using innovative measurement methods based on photogrammetry. Finally, they were compared to the results obtained from numerical analysis.

2. NUMERICAL CALCULATION

The objective of the study was the strength analysis of the protective structure with the use of numerical method, in the dynamic range, considering material and geometrical nonlinearity. The analysis encompassed a simulation of the impact test of the protective structure with the falling object in compliance to norm PN-92/G-59001 (RSPS - Rock slide protective structures).

On the basis of the technical data of the cab received from the manufacturing company, geometrical and then discrete models were built. Strength calculations were performed with use of finite element method (FEM) [3]. Impact energy was equal 60 kJ.

From the structural analysis contours of the displacement, stress and strain were obtained.

The entire research encompassed the following issues:

- building a geometrical model of the cab on the basis of the technical documentation (Fig. 1)
- creating a discrete model of the protective structure (Fig. 2)
- nonlinear strength calculation of the load-bearing structure with the use of FEM in the dynamic range [4],
- discussion of the results.

Correspondence to: Paulina Działak, Research Assistant
Faculty of Mechanical Engineering,
Lukasiewicza 7-9, 50-371, Wrocław, Poland
E-mail: paulina.dzialak@pwr.edu.pl

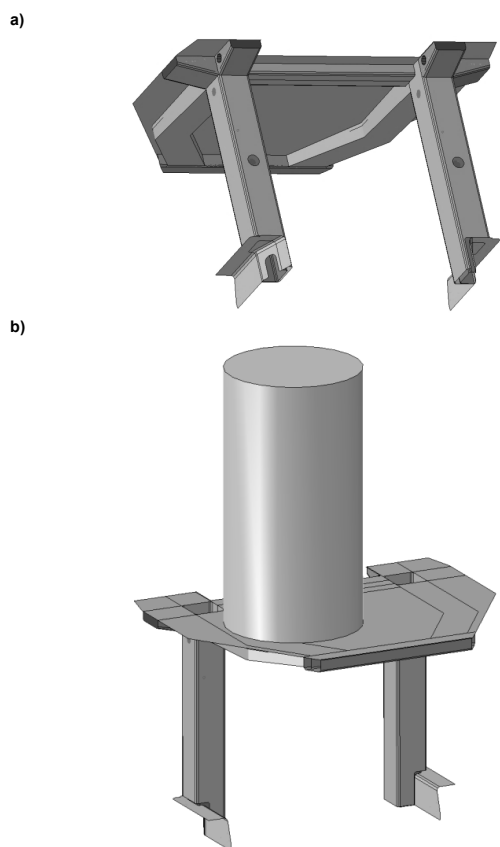


Figure 1. Geometrical model of the cab (a) and assembly with platform and falling mass (b)

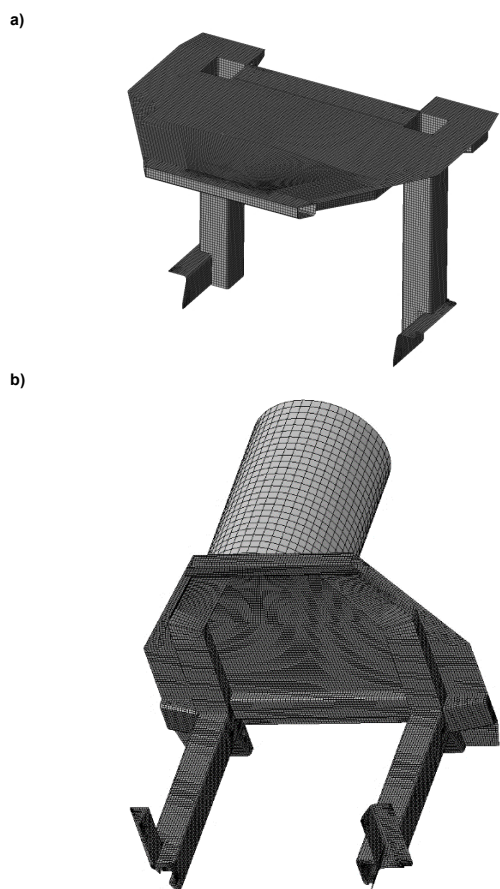


Figure 2. Discrete model of the cab (a) and assembly with platform and falling mass (b)

The results of the simulation are presented in figure 3.

Verification of the structure according to the standard is based mainly on the results of the roof deflection above the operator's head. Tests are considered positive when the operator model (DLV) remains intact by any element puncturing the protective structure and by any deformation of the structure in elastic and plastic range [5]. DLV is situated inside the cab, in the location of real operator, with the same seat index point (SIP) position.

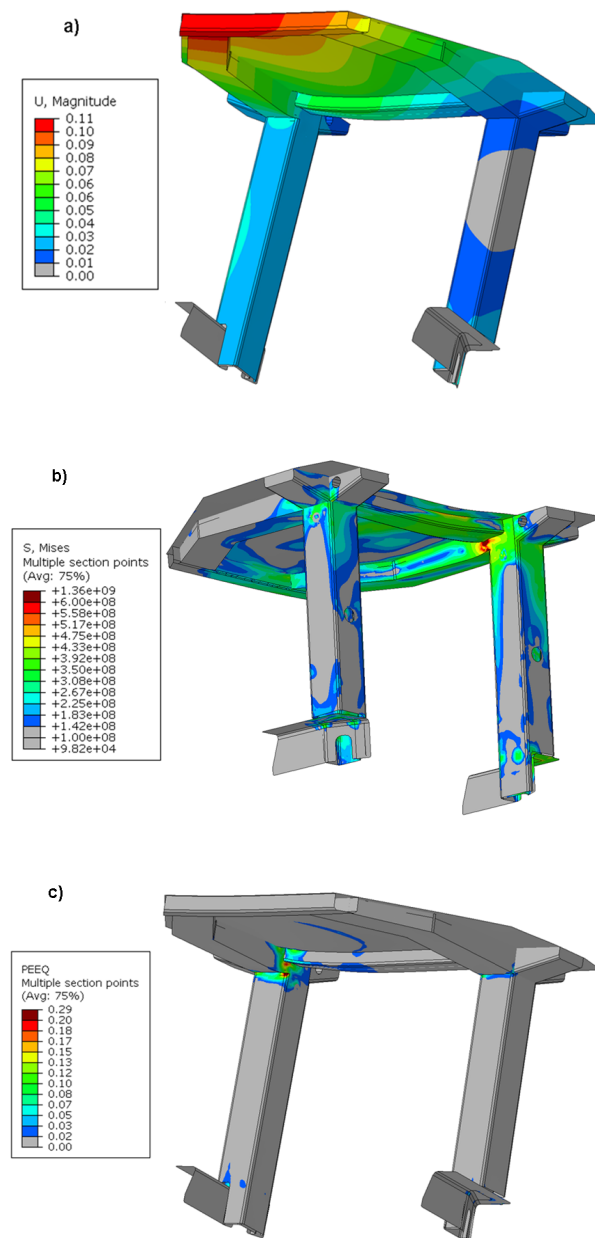


Figure 3. Results of the numerical simulation; a - displacement, b - HMM stress, c - plastic strain

For the purpose of numerical calculations, measuring points above the operator were selected in nodes of finite elements for which courses of displacement were determined (Fig. 4).

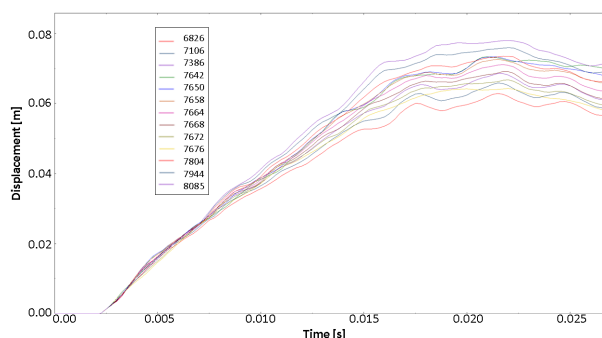
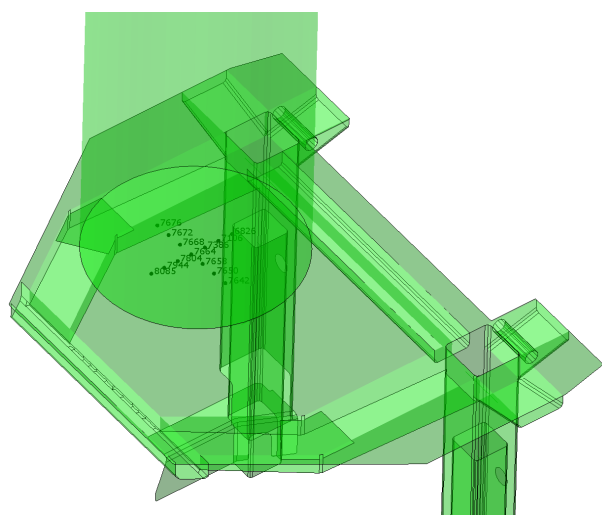


Figure 4. Deflection courses for selected measuring points above the machine operator

3. EXPERIMENTAL TESTING

In order to verify numerical calculations performed within the accredited laboratory, authors are obliged to carry out experimental validation of the computational method once a year. Beside standard measurements with the simple measuring devices (ruler, tape measure) more complex methods were used [6].

3.1 High speed camera

One of the proposed methods to verify the numerical calculations were high speed camera measurements [7].

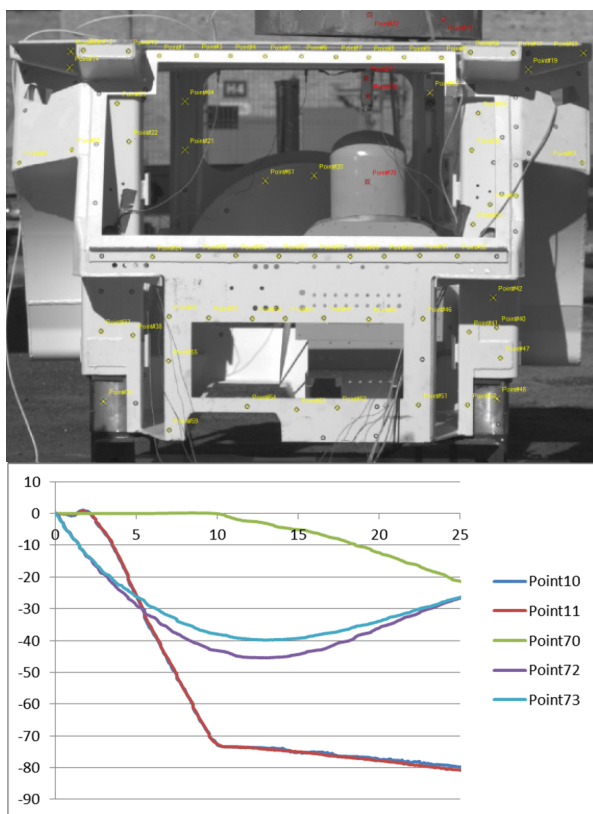


Figure 5. Vertical displacement courses for selected sampling points (10, 11, 70, 72, 73)

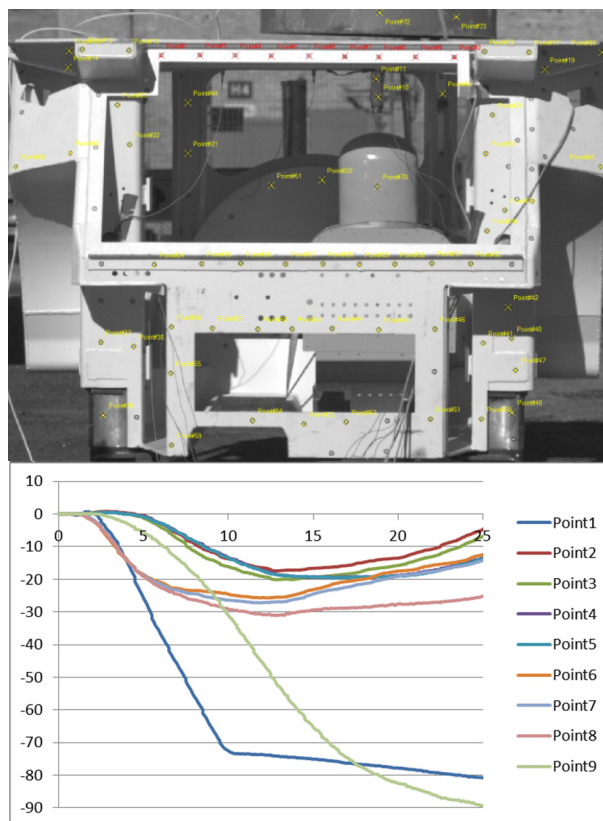


Figure 6. Vertical dynamic displacement courses for selected sampling points (1-9)

The experiment was recorded using the VISION research high speed monochrome digital camera Phantom V12 to determine the dynamic vertical deflection of the cab roof (Fig. 5 and 6).

3.2 TRITOP measurements

The protective structure was also measured before and after the test by means of the GOM's TRITOP device used for quick and precise measurements of the coordinates of three-dimensional objects [8]. The system accurately defined the 3D coordinates of the object points. As a result, the cloud of the sampling

points and the deflection of the protective structure were obtained (Fig. 7).

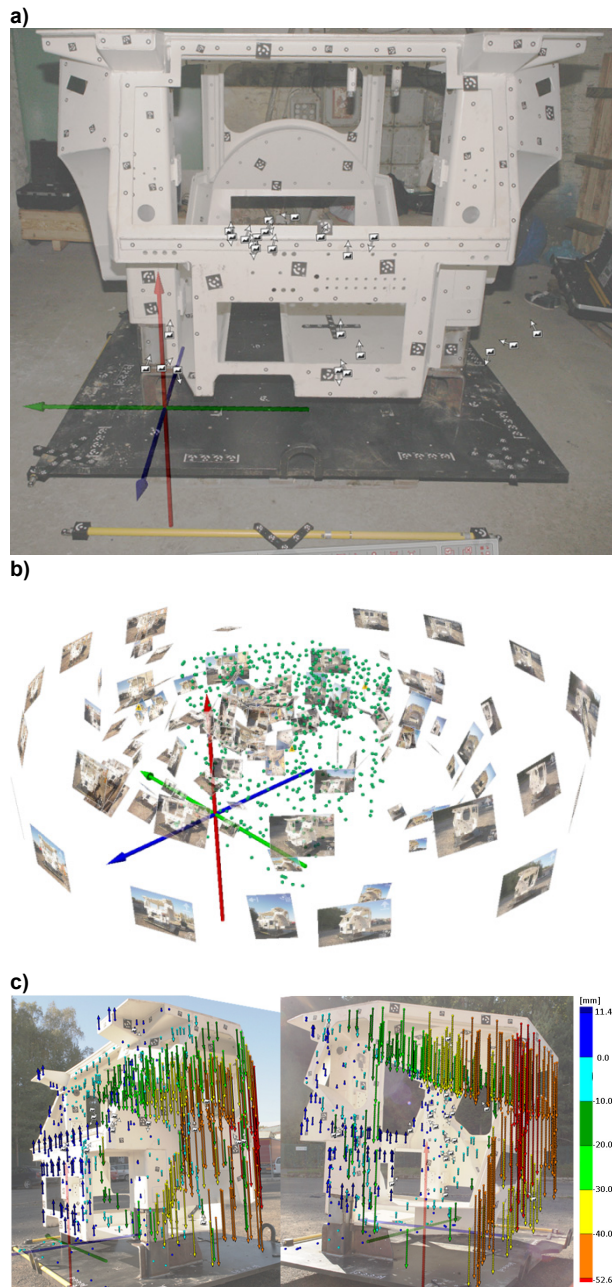


Figure 7. TRITOP measurements; a – sampling points, b – cloud of points, c – vertical permanent displacement of the sampling points (1-9)

3.3 Strain gauge measurements

On the basis of strength calculations, sampling points where the strain gauges should be located to measure cab deformations during the test were selected. Target points for acceleration sensors were also determined. Eventually, three points were chosen to measure deformations and six points to measure accelerations [9]. Figure 8 present sampling points on the protective structure.

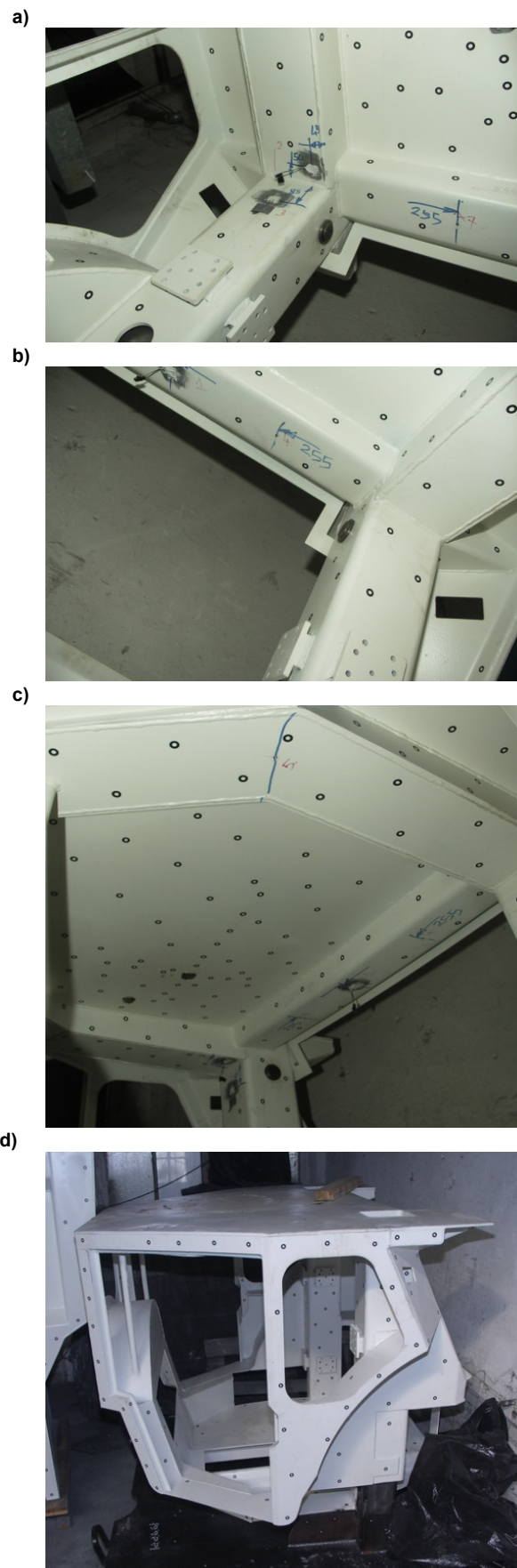


Figure 8. Sampling point for strain and acceleration measurements, points 1-3 – strain gauges, points 4-9 – accelerometers; a – points 2, 3, 7, b – points 1, 4, c – points 1-5, 7, 8, d – protective structure (side view)

Results from strain gauges are shown in figure 9.

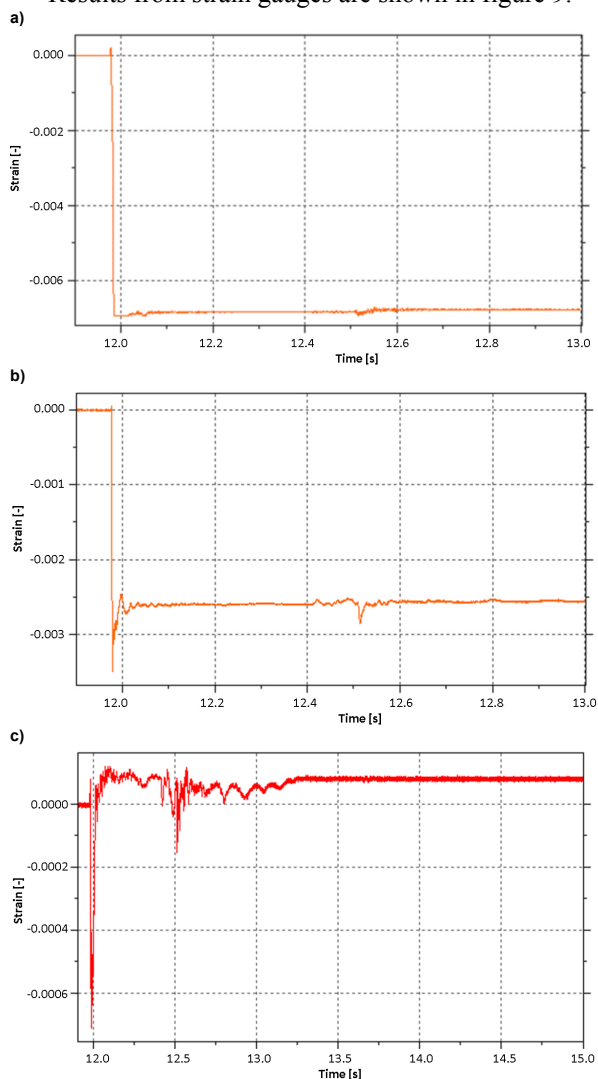


Figure 9. Strain results recorded during the experiment; a – point 1, b – point 2, c – point 3

4. RESULTS COMPARISON

Results obtained from the experiment were compared with the numerical simulation.

Table 1 presents comparison of the permanent and maximal dynamic deflection. Measurements of the permanent deflection were taken after the experiment and it arises from yielding of the structure. The dynamic deflection on the other hand was recorded throughout the entire duration of the experiment. For the comparison, maximal value of the dynamic deflection was taken into consideration.

It may be seen that the relative error in case of permanent deflection is approximately 18-19% and for maximal dynamic deflection it is about 8-9%.

Table 1. Comparison of the deflection results obtained from simulation and experiments

Permanent deflection [mm]		Maximal dynamic deflection [mm]	
Simulation	Experiment	Simulation	Experiment
39	33	77	73

Visual overview of the methods used to analyse the deflection of the cabin is shown in figure 10.

Comparison of the strain results is shown in table 2. It was measured in three most loaded points, selected based on previously performed numerical calculations. The values in table presents maximal obtained strain during entire simulation (ϵ_{\max}) and residual strain after yielding of the protective structure and removing the falling object ($\epsilon_{\text{after yield}}$). Compared values appeared to be within the same or similar orders of magnitude.

Table 2. Comparison of the strain results for selected sampling points (1-3)

	ϵ_{\max} [-]		$\epsilon_{\text{after yield}}$ [-]	
	Simulation	Experiment	Simulation	Experiment
Pt 1	0.0062032	0.0069317	0.007025	0.006756
Pt 2	0.005254	0.00346	0.004019	0.002568
P 3	$8.4414 \cdot 10^{-4}$	$7.1108 \cdot 10^{-4}$	$1.1027 \cdot 10^{-4}$	$8.4426 \cdot 10^{-5}$

5. CONCLUSION

Validation of the computer analysis with the use of photogrammetry enabled the authors to verify the numerical simulations of the protective structure of the mining machine operator [10]. The results obtained from the simulation are consistent with the experiment.

Using three different measuring methods allowed the authors to verify many different results obtained during the experiment and also precise validation of the numerical model.

TRITOP device enabled accurate measurement of the 3D coordinates of sampling point selected on the analysed structure. On this basis permanent deflection of the cab was determined.

High speed camera Phantom permitted to obtain dynamic deflection of the protective structure in near real-time as an experiment was running.

Finally, strain gauge measurements enabled to determine strain (and then stress) values on the most loaded areas of the structure.

Additionally, values received from the numerical model are slightly higher, thus meaning that the computational calculations provided a safety margin in the structure examination.

REFERENCES

- [1] Kalita, M.: Konstrukcja ochronna operatora ładowarki górniczej w świetle przepisów i badań niszczących, *Maszyny Górnicze*, 1, pp. 16-21, 2013.
- [2] Saska, P., Czmochoński, J., Iluk, A. and Piterusiak, D.: Application of high speed camera to determine the blast impulse generated by a small explosive charges, *Modelling in Engineering*, Vol. 21, No. 52, pp. 186-192, 2014.
- [3] Hughes, T.J.R.: *The finite element method: linear static and dynamic finite element analysis*, 2012.

- [4] Sun, J.S., Lee, K.H. and Lee, H.P.: Comparison of implicit and explicit finite element methods for dynamic problems, *Journal of Materials Processing Technology*, Vol. 105, No. 2, pp. 110-118, 2000.
- [5] Karliński, J., Rusiński, E. and Smolnicki, T.: Protective structures for construction and mining machine operators, *Automation in Construction*, Vol. 17, No. 3, pp. 232-244, 2008.
- [6] Clark, B.J., Thambiratnam, D.P. and Perera, N.J.: Analytical and experimental investigation of the behaviour of a rollover protective structure, *The Structural Engineer*, Vol. 84, No. 1, pp. 29-34, 2006.
- [7] Dziopa, Z., Stefański, K.: Using the high-speed camera as measurement device in the dynamic material tests, *Journal of Vibroengineering*, Vol. 14, No. 1, pp. 22-26, 2012.
- [8] Koutecký, T., Paloušek, D. and Brandejs, J.: Method of photogrammetric measurement automation using TRITOP system and industrial robot, *Optik - International Journal for Light and Electron Optics*, Vol. 124, No. 18, pp. 3705-3709, 2013.
- [9] Czmochoowski, J., Maślak, P., Przybyłek, G. and Stańco, M.: Numerical and experimental identification of crack in the stacker construction, *Materials Today: Proceedings*, Vol. 5, No. 13, pp. 26642-26647, 2018.
- [10] Koruba, Z., Osiecki, J.: The operator protective structures testing for mining machines, *Solid State Phenomena*, Vol. 165, pp. 256-261, 2010.

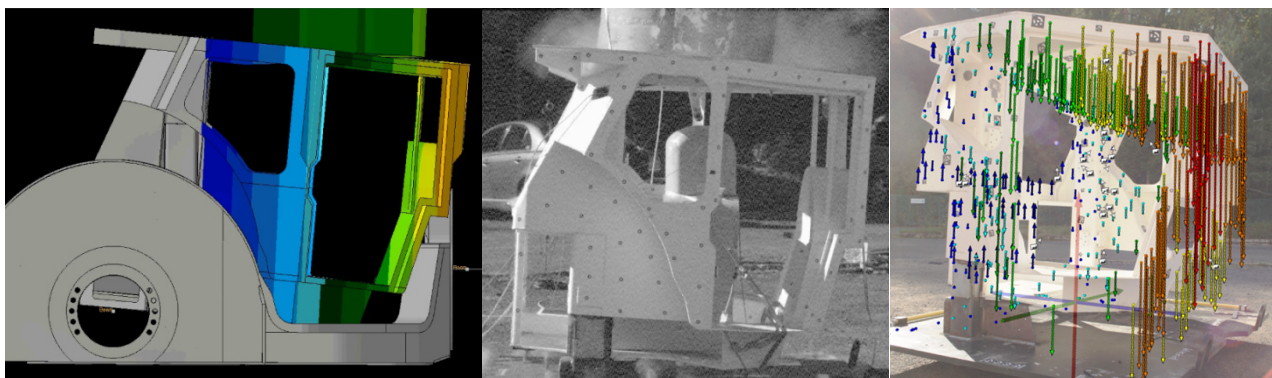


Figure 10. Overview of the methods measuring the deflection of the protective structure

Jurij Hladnik
Teaching Assistant
University of Ljubljana
Faculty of Mechanical Engineering

Matej Supej
Professor
University of Ljubljana
Faculty of Sport

Janez Vodičar
Assist. Professor
University of Ljubljana
Faculty of Sport

Luka Bizjak
Researcher
University of Ljubljana
Faculty of Mechanical Engineering

Boris Jerman
Assist. Professor
University of Ljubljana
Faculty of Mechanical Engineering

Rolling resistance coefficient of processed roller-skis for skating

For accurate calculations of the resistance forces and other work-energy calculations during skate roller-skiing on a treadmill the rolling resistance coefficient μ of the roller-skis needs to be determined in dependency of the normal force F_n . In the skating technique the skier rolls side-to-side alternating on one and the other roller-ski, and thus always rolls on a different part of the treadmill surface, which needs to be considered in the measurement of μ .

In this study μ of unique processed roller-skis for measurement of the ground reaction forces during skate roller-skiing was measured (a) over time at constant F_n and (b) in dependence from F_n , by towing a trolley with attached roller-skis on a treadmill. Changes of μ over 70 minutes resulted in maximally 12%. μ in dependence from F_n rose for 57% for F_n ranging from 141 N to 724 N per roller-ski.

Keywords: Cross-country skiing, roller-skiing, friction, treadmill, warm-up time.

1. INTRODUCTION

Rolling resistance has been recognized as an important parameter on the energy efficiency of roller-skiing. This resistance yields mainly from the resistance caused by the deformation of the wheels and the rolling surface, and the resistance caused by the bearings. In previous studies it has been found out that the rolling resistance coefficient μ of the roller-skis significantly depends from the roller-ski warm-up time [1] and the normal force F_n to the roller-skis' upper surface [1, 2], while the speed [1, 2] and inclination of the track [1] have non-significant influence. However, some less relevant studies [3] found just the opposite; that μ is not dependant from F_n , and is dependant from the velocity.

In the laboratory LASOK at the Faculty of Mechanical Engineering in Ljubljana unique processed roller-skis for measuring the ground reaction forces during skate roller-skiing were developed [4]. These roller-skis measure the ground reaction forces normal to the skis' upper surface and the forces in the axial wheel direction at each wheel. For full determination of the ground reaction forces acting on the roller-skis, their rolling resistance coefficient needs to be known.

The aim of the study was to determine the rolling resistance coefficient μ in dependence of F_n and the warming-up time of the roller-skis, respectively the rolling resistance coefficient μ in dependence from the rolling time.

2. METHODS

In the present study the rolling resistance coefficient μ of unique processed roller-skis (Alpina I.I.c., Žiri,

Slovenia) [4] for measurement of the ground reaction forces during skate roller-skiing was investigated. The following measurements of μ in dependence from:

- (a) rolling time at constant F_n , speed and inclination of the track and
- (b) F_n at constant speed and inclination of the track

were performed in a similar manner as in the study of Ainegren et al. [1]. For these measurements the analysed roller-skis were accurately fixed to a purposely built trolley from standard aluminium profiles (Figure 1). This trolley was then placed on a 3.5 x 2.5-m treadmill (RL 3500, Rodby Innovation AB, Vänge, Sweden) with an upper slider bed and fixed to a freely supported force sensor (HBM S9M, 2 kN, Hottinger Baldwin Messtechnik GmbH, Darmstadt, Germany; sampling frequency 100 Hz, Butterworth low-pass filter, cut-off frequency 0.01 Hz) by a rope. The measurements were performed at belt speed 3 m/s (10.8 km/h) and inclination of 8° at 24°C and 40% of relative humidity. The rolling resistance coefficient was calculated as:

$$\mu = \frac{F_r - m \cdot g \cdot \sin \alpha}{m \cdot g \cdot \cos \alpha} \quad (1)$$

where F_r is the measured force in the rope, m the mass of the trolley including weights and roller-skis, g the gravitational acceleration and α the inclination of the track.

2.1 The rolling resistance coefficient over time

In the preliminary measurements of μ over time it was discovered, that for relevant measurements the rolling track of the roller-skis for skating needs to be changed, as this is done during skate roller-skiing where the skier rolls side-to-side alternating on one and the other roller-ski, and thus always rolls on a different part of the treadmill surface, whereas in classic roller-skiing

Correspondence to: Dr Jurij Hladnik, Teaching Assistant
Faculty of Mechanical Engineering, University of Ljubljana,
Aškerčeva 6, 1000 Ljubljana, Slovenia
E-mail: jurij.hladnik@fs.uni-lj.si

the roller-skis roll mostly on the same part of the treadmill belt. These rolling-track changes were performed by manually shifting the force sensor, to

which the trolley was fixed, transversally to the belt rolling direction.

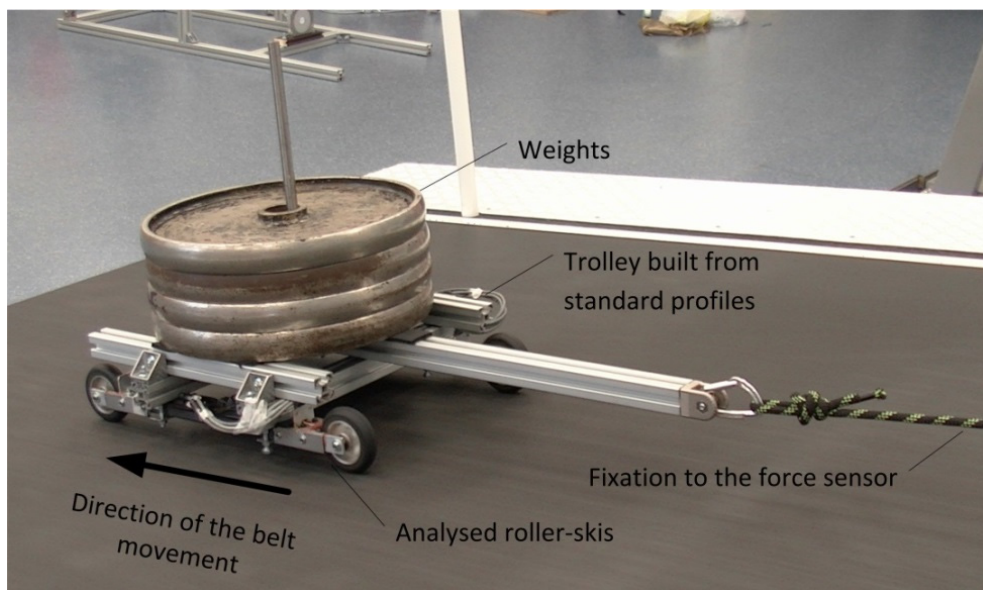


Figure 1: Measurement setup for measurement of the rolling resistance coefficient of the roller-skis.

The preliminary measurements of μ over time lasted for 80 minutes and the trolley was shifted per 20 minutes. The normal force F_n per roller-ski was taken 432.4 N (approximate half weight of an average roller-skier), similarly as in [1]. Here, μ was calculated as the average value over each minute.

Upon the findings obtained in the preliminary measurements, new measurements of μ over time were performed. In these measurements the trolley was shifted once per minute in the first 10 minutes, and once per five minutes in the following 55 minutes. μ was then calculated as the average value of the 10th second after the shift, when the possible dynamic effects were already stabilized.

2.2 The rolling resistance coefficient in dependency of the normal force

The rolling resistance coefficient dependency from F_n was obtained by sequentially reducing the overall mass of the trolley from 149 to 29 kg in 20-kg steps. At each load the trolley was shifted four times, which gave four reference points from which the average μ was calculated. Individual μ was calculated as the average of the 10th second after each shift.

3. RESULTS

From the preliminary measurement results shown in Figure 2 it can be seen that μ of the processed roller-skis rises with a digressive trend after each shift and at the beginning of the measurement. The rolling resistance coefficient seems to stabilize after the 20-minute periods. The rises in μ after the 2nd and 3rd shift are similar size of 10% μ . For these rises mostly the changes in the track conditions are to be blamed. The rolling resistance coefficient in the first 20-minute interval rises for only 6%. This smaller rise-up can be

attributed to simultaneous warming-up of the roller-skis, which decreases the roller-ski's μ .

The rolling resistance coefficient in dependence from the rolling time is shown in Figure 3, a. In the first three minutes μ falls rapidly for app. 10%. From here on, in the next 7 minutes μ rises up for 9% and falls back down for 5%. Between the 15 minute of rolling and the end of the measurement maximal changes of 6% in μ appear. The average μ in this time range amounts to 0.0211.

In Figure 3, b the dependence of the rolling resistance coefficient from the normal force F_n is shown considering the changing rolling track. Also the approximation curve with its function and mean quadratic deviation (R^2) is shown. The rolling resistance coefficient increased for 57%, while increasing F_n from 141 to 724 N.

4. DISCUSSION

The rolling resistance coefficient μ of the roller-skis is dependant from the interaction of the roller-skis and the rolling surface. The main finding of this study is that for relevant measurements of μ of the roller-skis for the skating technique used on a treadmill the rolling track needs to be changed, as this is done during skate roller-skiing. So far, none of the existing studies that investigated μ of skating roller-skis on a treadmill considered this fact.

When rolling on the treadmill the roller-ski wheels need to deform the rolling track, which additionally increases μ . If the roller-skis roll on the same rolling track of the treadmill, someone could expect that μ would decrease, since the rolling track is already deformed and the track is more and more strengthened, similar as by trudging through the snow. But the results in Figure 2 show the opposite, that μ increases by

rolling on the same rolling track. The logical explanation of this phenomenon is, that by rolling on the same rolling track, the belt heats at that part and the

track becomes softer, which causes higher rolling resistance. However, for the proof of this assumption further investigations are necessary.

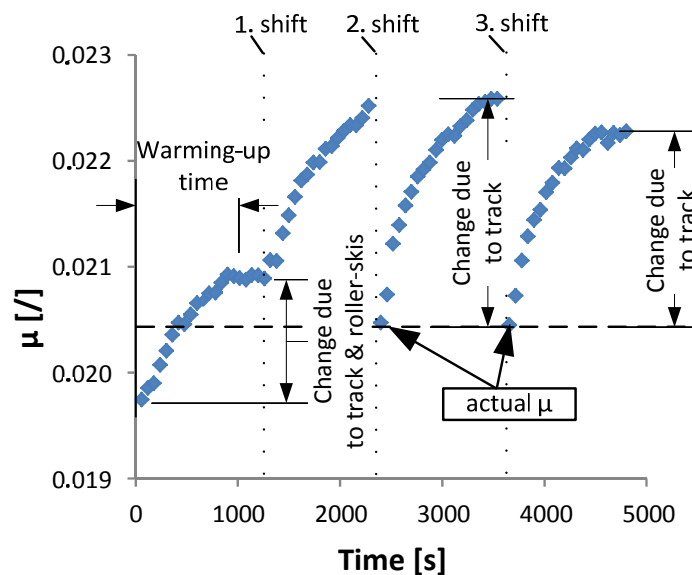


Figure 2: Results of the preliminary measurements of the rolling resistance coefficient μ of the processed roller-skis over time. Black dotted vertical lines present shifts of the trolley, blue squares present the average μ over 10 seconds read out for each minute. After each shift μ begins to rise due to changes of the permanent track. The rise in μ before the first shift is smaller than the following rises due to simultaneous warming-up of the roller-skis. The actual μ of the warmed-up roller skis for the skating technique is marked as the first μ of the 2nd and 3rd trolley shift.

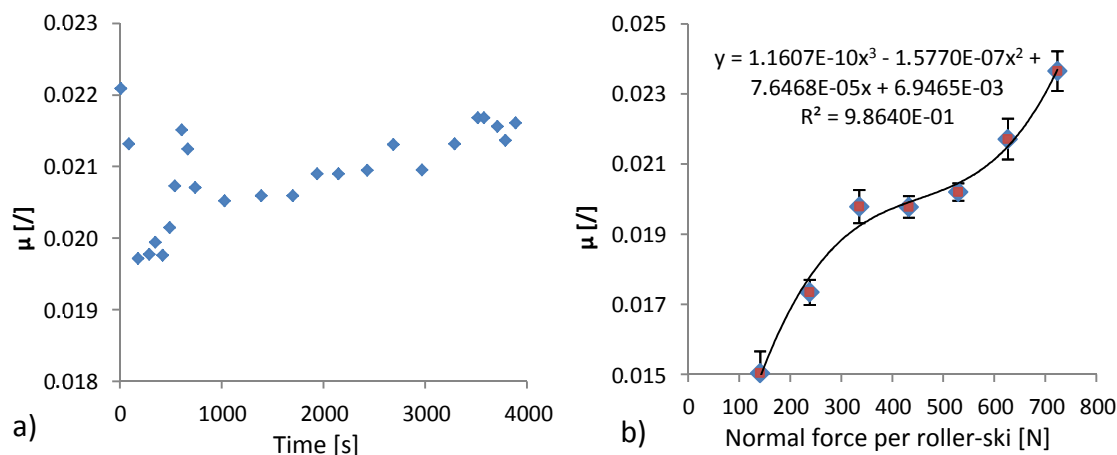


Figure 3: Rolling resistance coefficient μ of the processed roller-skis in dependence of: a) rolling time and b) normal force per roller-ski. In b) also the approximation curve with its function and mean quadratic deviation (R^2) is presented.

From the changes of μ through time (Figure 3, a) a warming-up time of at least 15 minutes is suggested (considering similar conditions as in the measurement), since the changes of μ after this time were maximally 5%. This warming-up time is shorter than suggested in [1], where a 30 minute warming time was suggested.

Generally μ increased with F_n (Figure 3, b) by an average factor of $1.287 \cdot 10^{-5} N^{-1}$, which is in agreement with the findings of other studies [3], where this factor was calculated to be $0.731 \cdot 10^{-5} N^{-1}$, disregarding the track changes. In the present study μ increased for 57%, while increasing F_n from 141 to 724 N.

In case the $\mu(F_n)$ dependency is not considered, the rolling resistance force of an 88 kg person at level

roller-skiing on a treadmill amounts to 17.1 N. Here, μ was taken 0.0198, which corresponds to μ at F_n of half of this person's weight acting on individual roller-ski.

Regarding the $\mu(F_n)$ curve (Figure 3,b), the greatest error in the rolling resistance force is made when the roller-skis are unequally loaded, respectively when all the load is applied on one roller-ski. In case the rolling resistance force accounts to 26 N, which is 53% more, than when neglecting the $\mu(F_n)$ dependency. This comparison shows how important it is to consider μ as a function of F_n .

Some μ values are still difficult to explain; e.g. the lower values of μ in the first 20 minutes of the preliminary measurements (Figure 2) and some of the changes in μ during its time dependency measurement

(Figure 3, a). Suspicion exists that such deviations appeared due to minor displacements of the roller-skis' fixation on the trolley when the trolley shifts were executed. For more accurate measurements of μ , the roller-skis' fixation to the trolley should enable them to settle in a position with minimal rolling resistance and with uniform load distribution per wheels.

The presented results are directly valid only for the analysed roller-skis. Other roller-skis may have different characteristics. For higher reliability of the results repetition of the measurements is suggested and usage of different roller-skis.

ACKNOWLEDGMENT

The authors would like to thank Alpina Ltd. for providing the roller-skis employed in this study and the laboratory personnel at the Institute of Sport (Faculty of Sport, University of Ljubljana) for their help with carrying out the measurements.

REFERENCES

- [1] Ainegren, M., Carlsson, P. and Tinnsten, M.: Rolling resistance for treadmill roller skiing, *Sports Engineering*, Vol. 11, pp. 23–29, 2008.
- [2] Hoffman, M. D., Clifford, P. S., Bota, B., Mandli, M. and Jones, G. M.: Influence of body-mass on energy-cost of roller skiing, *Int J Sport Biomech*, Vol. 6, No. 4, pp. 374-385, 1990.
- [3] Hoffman, M.D., Clifford, P.S., Watts, P.B., O'Hagan K.P. and Mittelstadt, S.W.: Delta efficiency of uphill roller skiing with the double pole and diagonal stride techniques. *Can J Appl Physiol*; Vol. 20, No. 4, pp. 465-479, 1995.
- [4] Hladnik, J., Supej, M. and Jerman, B.: Force measurement system for roller-ski skating, *Teh Vjesn*, Vol. 25, No. 5, pp. 1291-1297, 2018.
- [5] Ainegren, M.: *Roller skis' rolling resistance and grip characteristics-influences on physiological and performance measures in cross-country skiers*, PhD Thesis, Department of Engineering and Sustainable Development, Mid Sweden University, Östersund, p. 74, 2012.
- [6] Sandbakk, Ø., Ettema, G. and Holmberg, H.-C.: Efficiency in cross-country skiing. A brief review, In: *Science in skiing V*, editors: Müller L., Stöggl. T., Vol. 5, Meyer & Meyer Sport (UK) Ltd., St. Christoph/Arlberg, Austria, pp. 557-567, 2012.

Miodrag Arsić

Principal Research Fellow
Institute for materials testing
Belgrade

Srđan Bulatović

PhD
Institute for materials testing
Belgrade

Mladen Mladenović

Expert associate
Institute for materials testing
Belgrade

Živče Šarkočević

Assistant Professor
Technical Faculty
Kosovska Mitrovica

Zoran Savić

Expert associate
Institute for materials testing
Belgrade

Bucket-wheel excavator gearbox failure analysis and reliability assessment

This paper presents the analysis of failure causes and reliability assessment executed for the gearbox of the bucket-wheel excavator SRs 470.20/3 "TAKRAF" (produced by "Lauhhammer", Germany), which is engaged in overburden excavation at the surface mine 'Kostolac' (in Serbia). In order to determine during which phase the error was made (during the design process, production or exploitation), failure analyses and assessments of reliability have been performed for gearbox elements through the use of Pareto analysis, FTA - Fault Tree Analysis, reliability allocation and failure intensity. For the calculation of reliability allocation and failure intensity an adequate program package was developed. Through the use of the above mentioned procedures data necessary for the identification of most important elements for the analysis regarding the maintenance process and failure prevention measures have been collected.

Keywords: bucket-wheel excavator, bucket-wheel drive gearbox, failure analysis, reliability

1. INTRODUCTION

Continuous technological process of excavation, transport and disposal of overburden at the surface mine is being executed through the use of the compact system which consists of the bucket-wheel excavator, rubber band conveyors and spreader. Bucket-wheel excavator SRs 470.20/3 and the excavation subsystem which consists of the electromotor (1), couplers (2, 3), drive gearbox (4), bearings (5), bucket-wheel shaft (6) and wheel (7) with buckets (8) are shown in Figure 1. Bucket-wheel excavator SRs 470.20/3 is engaged in overburden excavation at the surface mine 'Kostolac' and possesses the following technical and technological properties:

- theoretical capacity $Q_t = 1688 \text{ [m}^3/\text{h]}$,
- maximum depth of the cut $L = 3 \text{ [m]}$,
- maximum height of the cut $H = 20 \text{ [m]}$,
- drive power of the bucket-wheel $N = 400 \text{ [kW]}$,
- bucket-wheel diameter $D_r = 6.3 \text{ [m]}$,
- number of buckets and interbuckets (intercutters) $z = 8$
- number of interbuckets (intercutters) $z_m = 8$,
- number of bucket unloads $n_s = 58 \text{ [min}^{-1}\text{]}$,
- overall drive efficiency coefficient $\eta = 0.92$,
- cutting rate $V_r = 2.4 \text{ [m/s]}$.

During the exploitation, bucket-wheel excavator is subjected to loads with changeable amplitudes-stochastic loads [1], which are caused by operating conditions, natural low-frequency oscillations [2] and the simultaneous influence of a large number of technological, metallurgical and structural parameters. Stochastic loads can cause unpredictable failures,

damages and breakdowns of components and assemblies. Therefore, the behaviour of the bucket-wheel excavator in real conditions of exploitation and its reliability during operation cannot be predicted by engineering methods, but only through the use of methods related to Probability Theory.

Reliability of mechanical components, assemblies and subsystems is a probability that the bucket-wheel excavator will successfully perform its operational function within the range of allowable deviations and for the designed interval of time. Development of the reliability is fundamentally based on the comparison of specified magnitudes which characterize the operational ability.

Through the use of Pareto analysis, Fault tree analysis, reliability allocation and failure intensity for the bucket-wheel excavator gearbox the data necessary for the identification of most influential components (elements, assemblies) regarding the reliability assessment, analysis of the maintenance process and refurbishment, as well as for carrying out failure prevention measures [3] were obtained.

2. BUCKET-WHEEL DRIVE GEARBOX FAILURE ANALYSIS

Data regarding the loads on the support structures of the bucket-wheel excavator, properties of base material for components and welded joints, production technologies, structural solutions for assemblies, technical and physical characteristics of recorded breakdowns and prescribed failure prevention measures are being entered into a suitable database. Nevertheless, databases should contain the data acquired during the testing of structures that proved to be adequate.

Correspondence to: Dr Miodrag Arsić, Principal Research Fellow

Institute for materials testing Belgrade
Bulevar vojvode Mišića 43, 1110 Belgrade, Serbia
E-mail: miodrag.arsic@institutims.rs

2.1 Resistance to excavation and operational stresses at the shaft of the bucket-wheel excavator drive

Measurement of resistance to excavation and calculation of torque at the shaft of the excavation subsystem of the bucket-wheel excavator SRs 470.20/3 in various environments has been performed through the use of the wattmeter method. On the basis of tensometric deformation measurements performed

through the use of 4 XY-120-HBM gauges, stresses and torque at which the plastic deformations or initial cracks may occur at the shaft of the excavation subsystem have been calculated. Through the use of the method which refers to the comparison of load and strength by maximizing the ratio of their indicators drive factor K_A at the gear with the highest number of revolutions which is a part of the bucket-wheel drive gearbox was determined.

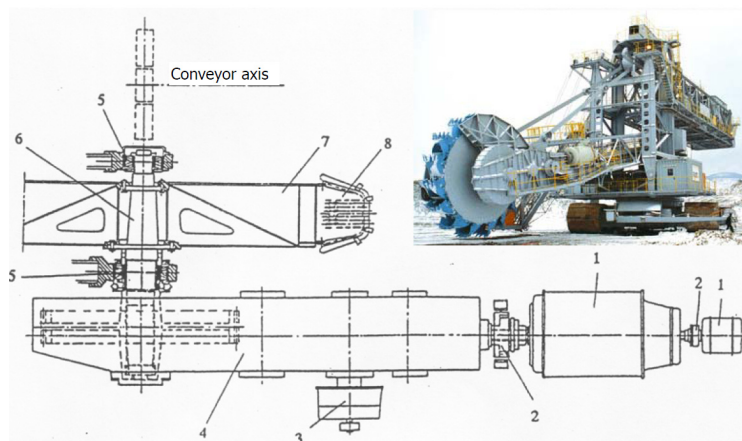


Figure 1. Appearance of the bucket-wheel excavator SRs 470.20/3 and of the excavation subsystem

2.2 Pareto Analysis

On the basis of available databases regarding the failures of the excavation subsystem the Pareto (ABC) analysis has been performed, which shows the average contribution percentage of failures of basic subsystem assemblies in correlation with the overall standstill.

2.3 Fault Tree

A fault tree presents a series of events, causes and effects which cause the failure of the specific function in relation to which the reliability of the system is being assessed. It is of utmost importance to identify the events which directly violate the considered function, as well as to identify the logical correspondence between those events. Fault Tree Analysis continues until the level of basic events which are not caused by other events is being reached by deductive analysis.

2.4 Reliability allocation and failure intensity

Most suitable for the allocation of reliability and failure intensity is the method that is based on the assessment of the relative ratio of the failure intensity of

the 'weakest' element and conditionality of possibility of system failure if that element fails. Level of conditionality ranges between 0 and 1. When the failure of an element causes the failure of the whole system $E_i = 1$.

3. RESULTS

All characteristics of the production system, taking into account their role and specified goal functions, are defined as a probability that the system will successfully operate in the moment of need and perform the predefined criterion function in projected time and under existing conditions of exploitation.

3.1 Measurement results

Stresses τ_i , resistances to excavation per knife length k_{Li} and torques T_i at the bucket-wheel shaft of excavator SRs 470.20/3 were calculated on the basis of tensometric measurements of deformations and powers measured by wattmeter at the electromotor of the bucket-wheel drive. Results of those calculations are shown in Table 1.

Table 1. Values of stress, resistance to excavation and torque at the drive shaft of a bucket-wheel excavator

Operational environment	According to tensometric measurements				According to the power variation of the electromotor			
	Maximum value		Mean value		Maximum value		Mean value	
	T_i [kNm]	τ_i [MPa]	T_i [kNm]	τ_i [MPa]	T_i [kNm]	k_{Li} [N/cm]	T_i [kNm]	k_{Li} [N/cm]
Loose soil	178	21	132	17	275	64	183	441
Transition zone	434	51	283	31	309	75	262	618
Grey clay	576	64	376	38	511	101	326	676

3.2 Pareto Analysis

Pareto analyses that refer to contribution and cause of failure during the operation of the bucket-wheel excavator SRs 470.20/3 showed that the failures of gearbox elements cause more than 40% of failures of the excavation subsystem, Figure 2.

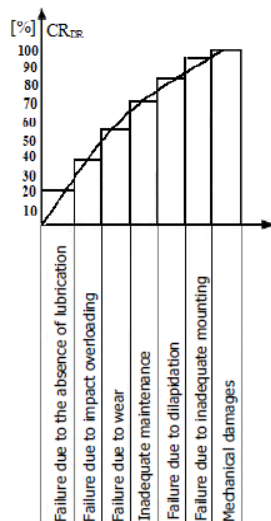


Figure 2. Pareto analyses of the contribution and causes of failure of the bucket-wheel excavator drive gearbox

3.3 Fault Tree Analysis

In Figure 3 detailed analysis of the fault tree for bucket-wheel excavator drive gearbox is shown. The cross-section of the gearbox is shown in Figure 4. Horizontal gearbox of the excavation subsystem, with nominal power $N=400$ kW and reduction ratio 135 transfers the power, or to put it differently reduces the number of revolutions from 980 to 7.25 min⁻¹ by means of the hollow shaft and bucket-wheel axle.

Basic assemblies of the gearbox are: input shaft (1), lubricating drive (2), slip coupler (3), wedges for the connection of the hollow shaft (4) and the bucket-wheel axle (6) and output gear with the hollow shaft (5), Figure 4.

3.4 Results of reliability allocation and failure intensity

Analysis of reliability and failure intensity of gearbox subassemblies was performed on the basis of their condition during operation, as well as their condition while the bucket-wheel excavator was at a standstill due to failure in the period from 2011–2016 [4], Table 2.

Table 2. Condition of gearbox subassemblies during operation and while at a standstill in the period from 2011–2016

Surface mine "Kostolac"	Time	Total time in operation	Total time at a standstill
Bucket-wheel drive gearbox	[h]	25200	5223

Reliability of the gearbox is being obtained through the use of the following equation:

$$R(t) = \frac{n(t)}{n} \quad (1)$$

Where:

n – total number of hours in operation and at a standstill

$n(t_r) = 25000$ – total number of hours in operation

$n(t_0) = 5223$ – total number of hours in standstill

$n = 25200 + 5223 = 30423$ [h]

$$R(30423) = \frac{25200}{30423} = 0.83 \quad (2)$$

Obtained value of reliability could be considered satisfiable. Experimental researches performed on this and similar systems show that reliability of bucket-wheel gearbox subassemblies lies within the range between 0.8051 and 0.8280 ($0.8051 \leq R_{bg} \leq 0.8280$). It should be emphasized that the lower limit of reliability ($R_{bg} = 0.8051$) is the lowest value of reliability of the system, below which the goal function would not be accomplished. This is a referent value of reliability, used in order to determine reliability of other elements of the system. The failure intensity of the bucket-wheel drive gearbox is being obtained through the use of the following equation, on the basis of determined reliability $R(30432) = 0.83$:

$$\lambda(t) = -\frac{\ln R_s(t)}{n} = -\frac{\ln 0.83}{30432} = -\frac{-0.1863}{30432} = 6.122 \cdot 10^{-6} [h] \quad (3)$$

On the basis of results of complete researches that refer to the reliability of subsystems and their elements in the period from 2011–2016 it was determined that buckets and bucket-wheel drive gearbox have the lowest reliability, while all elements of other subsystems of bucket-wheel excavator SRs 470.20/3 have much lower values of failure criticality.

4. DISCUSSION

On the basis of measurement results it can be concluded that torques and torsion stresses are within the projected range (bucket-wheel shaft material is 25CrMo4V), while the values of specific excavation resistances per knife length, for maximum measured loads, are close to the upper limit $k_L=700$ [kN/cm], [5].

On the basis of Pareto analyses of failures, taking into account the failure mode of the gearbox assembly shown in Figure 4b, it can be concluded that failures are, for the largest part, caused by the lack of lubrication, impact loads and wear, and to a lesser extent by inadequate maintenance, dilapidation of elements (components), inadequate mounting and the least of all by mechanical damaging.

On the basis of results of analyses that refer to reliability and failure intensity carried out for subsystems of the bucket-wheel excavator drive for the period from 2011–2016 it can be concluded that obtained value of reliability is satisfiable.

On the basis of results of analyses that refer to reliability and failure intensity carried out for subsystems of the bucket-wheel excavator drive for the period from 2011–2016 it can be concluded that obtained value of reliability is satisfiable.

5. CONCLUSION

Approach to failure analysis, carried out for the excavation subsystem of the bucket-wheel excavator SRs 470.20/3, enables the decrease of criticality, severity and effects of failure after adequate measures in the maintenance process have been taken. This approach is usable for all subsystems and all types of bucket-wheel excavators when general data necessary for the identification of most important elements for the analysis are at disposal. Data on the causes of damages and failures is valuable for the improvement of design methods, development of new technical solutions, development of testing methods in the prototype phase, improvement of properties of existing materials and technologies regarding their treatment.

ACKNOWLEDGMENT

This work is a contribution to the Project TR 35006 founded by the Ministry of Education and Science of Serbia.

REFERENCES

- [1] Limnios, N., Oprisan, G.: *Semi-Markov Processes and Reliability, Statistics for Industry and Technology*, A Birkhäuser book, 2001.
- [2] Gottvald, J., Krása, J., Helebrant, F., Fries, F. and Kraus V.: FT-TA4/018 Modern Trends in Increasing Equipment Reliability for the Open-Cast Mining of Utility Minerals, Part 6b.: In-Situ Verification of Methods and a Proposal for Their Application-Draft Methodology for Measuring, Research Report, 2009.
- [3] Ušakov, I.A.: *Handbook of Reliability Engineering*, John Wiley & Sons, 1994.
- [4] Documentation taken from the surface mine "Kostolac", TPP - SM Kostolac.
- [5] Documentation of the producer of the bucket-wheel excavator SRs 470.20/3, "Lauhhammer", Germany.

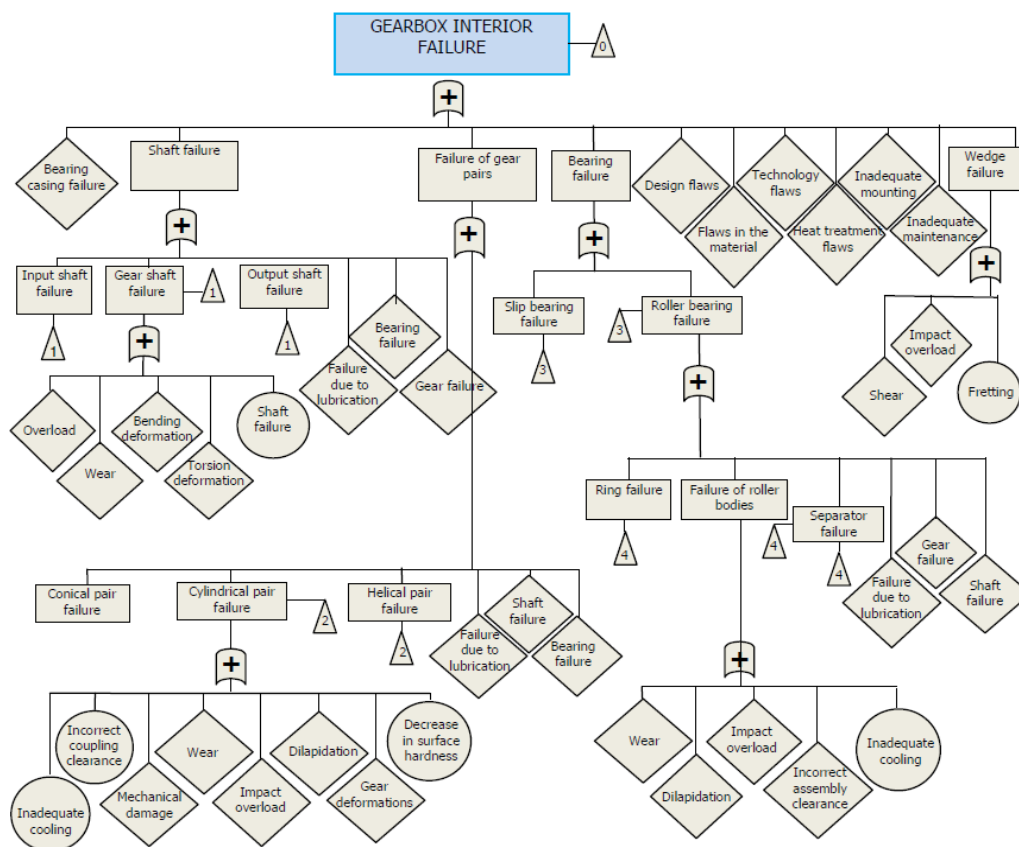


Figure 3. Fault tree analysis that refers to the bucket-wheel excavator drive gearbox

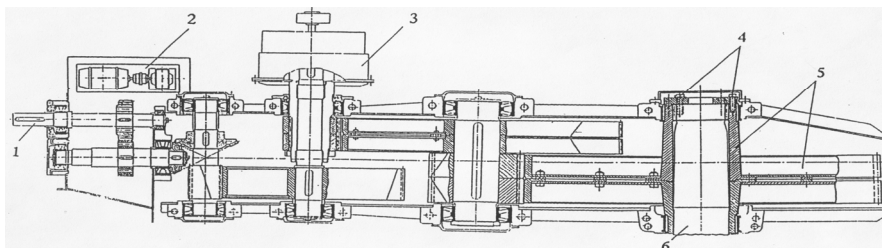


Figure 4. Schematic appearance of the bucket-wheel excavator drive gearbox cross-section

Thomas Mitterlehner

Teaching Assistant
Vienna University of Technology
Faculty of Mechanical and Industrial
Engineering
Institute for Engineering Design and
Product Development

Georg Kartnig

Professor
Vienna University of Technology
Faculty of Mechanical and Industrial
Engineering
Institute for Engineering Design and
Product Development

Markus Haider

Professor
Vienna University of Technology
Faculty of Mechanical and Industrial
Engineering
Institute for Energy Systems and
Thermodynamics

Analysis of the thermal ratcheting phenomenon in packed-bed thermal energy storage using Discrete Element Method

Packed-bed thermal energy storages (TES) play a major role in energy technology. During energy absorption, hot air flows through the content of the TES in top-down direction. During the heating process, the expansion of the heat-storing medium (bulk material) leads to a stress increase on the walls of heat-storage tanks. These occurring loads are to be considered by means of a discretized model. Furthermore, it is of interest how the loads modify during several loading and unloading processes (thermal ratcheting phenomenon). In this paper, it will be investigated how this behaviour can be modelled using the DEM approach.

Keywords: Thermal energy storage (TES), Discrete Element Method (DEM), thermal ratcheting, thermal stress, calibration

1. INTRODUCTION

In course of a NEFI (New Energy for Industry) project, the waste heat of a cement plant with a temperature of around 300-400°C shall be used for energy recovery. For this purpose, a storage in form of an air-flowed packed-bed thermal energy storage (TES) [8] has to be implemented. Since 2018, this goal has been pursued at the Vienna University of Technology in a project of the Department of Engineering Design and Material Handling (KLFT) in cooperation with the Institute for Energy Systems and Thermodynamics (IET).

In simplified terms, packed-bed TES are tanks that are filled with bulk material. The bulk material serves as a heat-storing medium. The most important goal of TES systems is to decouple the generation of thermal energy from its use, since the renewable energy can be used by a neighbouring company.

The expansion of the heat-storing medium (bulk material) during the heating process leads to a stress increase on the walls of the heat storage tank. Previous results [1], [5], [6], [7] have shown that increasing contact forces of the bulk material and the associated stress increase on the heat storage walls can lead to damage (see Figure 1).

The special feature of this project is to consider this thermal expansion of the bulk material and to investigate the thermal ratcheting phenomenon (increasing stress due to several loading and unloading cycles).

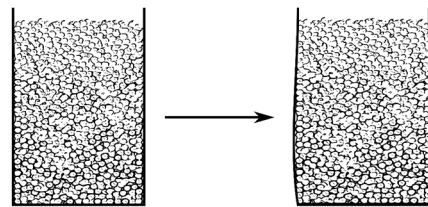


Figure 1. Damaged packed bed thermal energy storage

With increasing temperature the size of particle enlarges. The thermal expansion leads to the following effects:

- The contact forces between the individual particles rise (see Figure 2, left). This can cause damage to the bulk material.
- The contact forces between particles and the tank wall of the TES also rise (see Figure 2, right). This can cause damage to the tank wall.

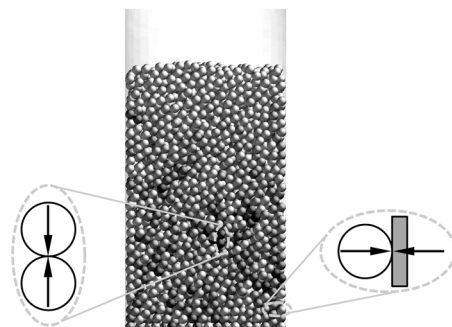


Figure 2. Contact force particle-particle, particle-wall

Under this directive, a vertical air-flowed cylindrical TES with a diameter of 17 m, a height of 15 m and filled with round gravel up to a height of 12 m shall be investigated. At the beginning, the analysis is performed on a reduced test geometry with enlarged particles. When charging (heating), air flows in top-down direction, while discharging (cooling) takes place with air flowing bottom-up.

Correspondence to: Dipl.-Ing. Thomas Mitterlehner
Technische Universität Wien,
Getreidemarkt 9/307-1, 1060 Vienna, Austria
E-mail: thomas.mitterlehner@tuwien.ac.at

Firstly, a DEM model is created with EDEM in which expansion and the stresses caused by one loading and unloading cycle can be shown. After that, several cycles are taken into consideration. The planned calibration of the particle parameters is going to be discussed at the end.

2. ANALYTICAL CALCULATION OF THE PRESSURE

In order to achieve better comparability of the stress change, the occurring normal stresses are normalized. The hydrostatic pressure (1) on the one hand and the horizontal bulk pressure (3) on the other have been taken into account (see Figure 3).

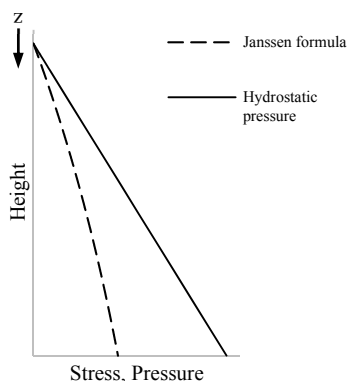


Figure 3. Hydrostatic and horizontal bulk pressure

The hydrostatic pressure is given in equation (1). z denotes the depth of the bulk material from top to bottom.

$$p_{(z)} = p_0 + \rho_b \cdot g \cdot z \quad (1)$$

In bulk material, a stress $\sigma_{h(z)}$, which is smaller than the vertical stress $\sigma_{v(z)}$, occurs due to a vertical load in horizontal direction. This relation is referred to as stress ratio λ (2).

$$\lambda = \frac{\sigma_{h(z)}}{\sigma_{v(z)}} \quad (2)$$

The horizontal bulk pressure according to Janssen [2] can be calculated with (3) using the following relation:

$$\sigma_{h(z)} = \frac{\rho_b \cdot g \cdot A}{\tan \varphi_x \cdot U} \cdot \left[1 - e^{-\frac{\lambda \cdot \tan \varphi_x \cdot U \cdot z}{A}} \right] \quad (3)$$

According to Janssen, the results of the DEM simulation are divided by the horizontal pressure on the ground in order to achieve standardized values.

3. DEM MODEL

The DEM model is constructed with the classical Hertz-Mindlin model and an implementation for thermal expansion [3]. Before the bulk material undergoes thermal expansion, the content of the TES is filled and divided into n layers.

With the loading and unloading start time t_n of the individual layers, the thermal expansion of the particles can be regulated for each layer at any time. This allows to display the temperature distribution during the loading and unloading processes of the TES.

In reality, the bulk material filled into the heat storage expands or contracts depending on the change of temperature ΔT and the coefficient of thermal expansion α_p .

The scaling velocity v_s and the time step Δt are needed in order to compute the scaling factor ψ_s , which is then used to implement this effect in the DEM model. When the TES is getting charged, the term $v_s \cdot \Delta t$ is used positively in the equation. When the TES is discharging, it is used negatively.

$$\psi_s = 1 \pm v_s \cdot \Delta t \quad (4)$$

The scaling velocity v_s can be used to set the speed at which the particles are enlarged or reduced. For the diameter D_s to increase or decrease as a function of the temperature, the original particle diameter D_p is scaled with ψ_s (5).

$$D_s = D_p \cdot \psi_s \quad (5)$$

When D_{max} is reached at the maximum temperature, the enlarging process stops (6).

$$D_{max} = D_p \cdot (1 + \Delta T \cdot \alpha_p) \quad (6)$$

Finally, the number of loading and unloading cycles can be used to simulate several runs and thus to investigate whether the load changes during several cycles or not.

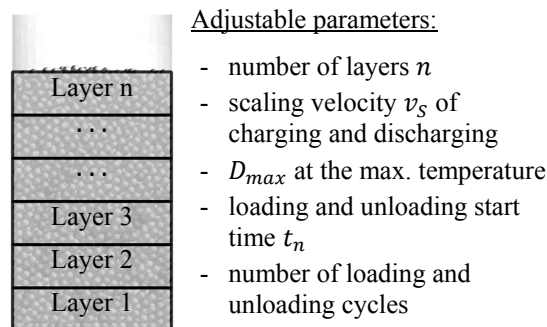


Figure 4. Structure of the DEM model with thermal expansion

Since the volume of the particles increases or decreases during the loading or unloading process, the particle mass also changes. This change in mass can be neglected because it is below 1%.

4. RESULTS OF THE DEM SIMULATION

In the simulation model a heat storage system with a reduced scale geometry of 1:10 was filled with crushed gravel, as calibrated material parameters are already available for it (properties see Table 1). Later on, the calibration for the bulk material that is actually going to be used (see Figure 8) must be carried out (see section 5). The walls are considered as rigid.

Table 1. Used properties

bulk material	geometry of the tank	number of particles	particle diameter
crushed gravel	D = 1,7 m H = 1,5 m	25.000	50 mm

Figure 5 shows the normal stress of the tank wall in the initial state (= before first heating) as a function of height (black line). Furthermore, the horizontal bulk pressure (grey dotted line) according to (3) and the hydrostatic pressure according to (1) are shown.

As you can see, the initial state matches the horizontal bulk pressure after Janssen quite well. As described in section 2, the normal pressure of the abscissa is plotted in a normalized manner (see Figure 6).

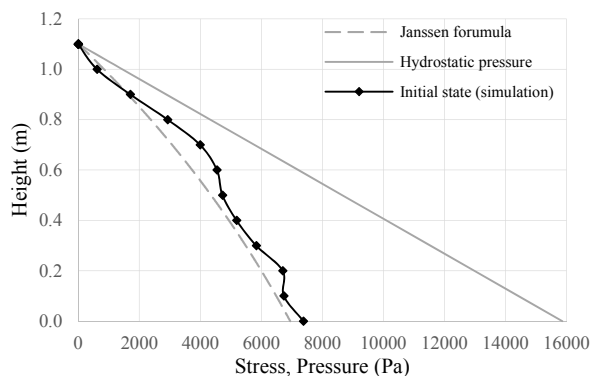


Figure 5. Normal stress in the initial state

Starting from the initial state in Figure 6, the heating of the bulk material leads to the resulting charging states 1 and 2. The line of the initial state shifts to the right with increasing loading and assumes higher stresses at any altitude (grey lines).

In charging state 1, the bulk material has already experienced a temperature change in the upper part. In the lowest layer, no temperature change has been observed yet. Therefore, the stress is the same as in the initial state. In charging state 2, the temperature has already been distributed over the entire height, but the final temperature has not been reached in the lowest layers yet.

At the end of the charging process, the load reaches its maximum (black line). When the heating is over, cooling starts. At the end of the discharge process, the horizontal pressure shifts to lower loads while unloading (black line). This shows that, after completion of the unloading process, the maximum load on the ground is slightly higher than at the beginning of the initial state.

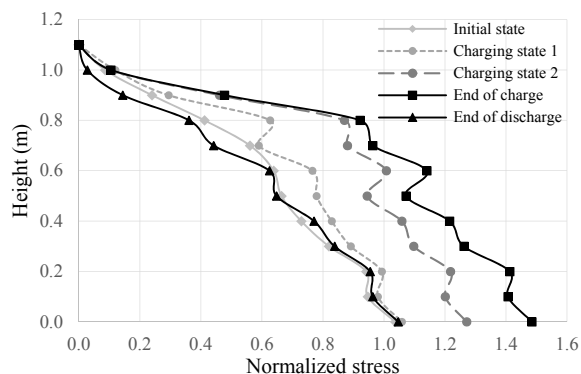


Figure 6. Normalized stress of charging and discharging

Until now, only one charging and one discharging process were considered. Furthermore, it is of interest whether the load changes in the course of several cycles or not. For this purpose, the maximum occurring

normalized horizontal pressure (normalized with the maximum horizontal pressure of Janssen) was plotted as a function of the number of loading and unloading cycles (see Figure 7). The upper line shows the maximum stresses at the end of the loading cycles ($T = 400^{\circ}\text{C}$) and the lower line the maximum stresses at the end of the discharging cycles ($T = 100^{\circ}\text{C}$). As the result shows and according to Janssen, the stresses increase to 1.5 times the horizontal pressure when loaded. With each further loading, the stresses increase only slightly.

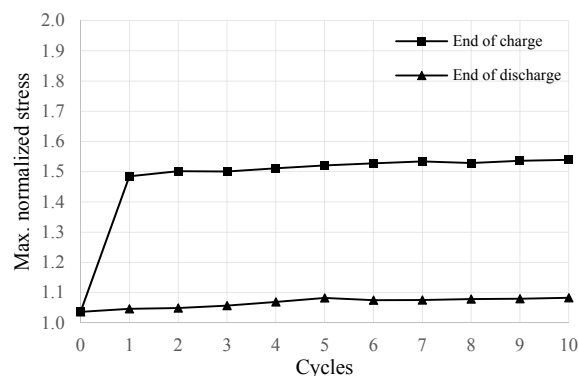


Figure 7. Multiple charging and discharging cycles

5. CALIBRATION

In order to finally use the correct material properties, the bulk material has to be calibrated. Despite the simplifications required for DEM simulation, a calibration of the bulk material parameters is necessary in order to map the bulk material behaviour correctly (see Figure 8).

These simplifications are in particular the spherical mapping of the grain shape as well as the increase of the particle size and the reduction of the particle stiffness. Thus, the computing time can be reduced considerably.



Figure 8. Bulk material (round gravel) to be calibrated

Although the simplifications mentioned usually apply to almost every DEM simulation, there is currently no standard calibration method. In most cases, the Angle of Repose (AoR) test is used for calibration. However, only one parameter in the form of this angle is considered in order to calibrate the friction parameters. To include more independent values for the determination of the two friction parameters, the draw down test according to [4] is used. Here, in addition to the AoR ($^{\circ}$), the mass flow (kg/s) and the remaining mass fraction (%) in the upper chamber are also measured.

In this project, a new device for calibration experiments according to [4] was developed and built in order to perform the planned draw down test (Figure 9).

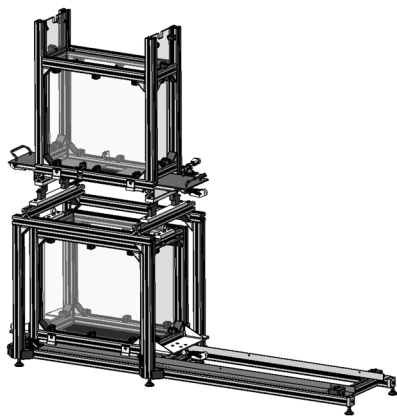


Figure 9. Calibration experiment device at KLFT, TU Wien

6. SUMMARY AND OUTLOOK

With the DEM model developed, influences of temperature effects in bulk material can be represented. The change of contact forces between the single particles and the change in the contact forces between the particles and the wall as a result of increasing and decreasing temperature play an important role in dimensioning packed-bed heat storage systems.

It is essential that the effects of several loading and unloading cycles - also known as thermal ratcheting phenomenon - are taken into account. As the investigations have shown, the load on the container walls increases with the number of cycles up to a maximum.

In further ongoing studies, the bulk material is calibrated with the draw down test. In order to validate the simulation results, experimental measurements must be carried out. Together with the IET, experimental investigations on bulk materials are carried out at the KLFT laboratory. Finally, the investigations will be transferred to the original heat storage geometry.

REFERENCES

- [1] Dreißigacker, V., Zunft, S., Müller-Steinhagen, H.: A thermo-mechanical model of packed-bed storage and experimental validation, *Applied Energy*, Elsevier, Vol. 111, pp. 1120 - 1125 2013.
- [2] Janssen, H.A.: Experiments on Corn Pressure in Silo Cells, *Ztg Ver dt Ing* 39, pp. 1045–1049, 1895.
- [3] Mitterlehner, T.: DEM modelling of charging and discharging cycles in packed bed thermal energy storage, *Verein Netzwerk Logistik, Logistik Werkstatt Graz*, ISBN 978-3-85125-673-4, pp. 155-174, 2019.
- [4] Roessler, T., Richter, C., Katterfeld, A. and Will, F.: Development of a standard calibration procedure for the DEM parameters of cohesionless bulk materials – part I: Solving the problem of ambiguous xparameter combinations, *Powder Technology*, Vol. 343, pp. 803 – 812, 2018.
- [5] Sassine, N., Donzé, F., Bruch, A. and Harthong, B.: Rock-Bed Thermocline Storage: A Numerical Analysis of Granular Bed Behavior and Interaction with Storage Tank, 22nd SolarPACES Conference, 11 – 14 October, Abu Dhabi, 2016.

- [6] Sassine, N., Donzé, F., Bruch, A. and Harthong, B.: Numerical Analysis of Granular Bed Behavior in Thermocline Storage Tank and Bed/Wall Interactions, French Alternative Energies and Atomic Energy Commission (CEA) – LITEN, Grenoble, AIP Conference Proceedings 2033, 2018.
- [7] Sassine, N., Donzé, F., Bruch, A. and Harthong, B.: Thermal stress numerical study in granular packed bed storage tank, *Granular Matter*, Springer-Verlag GmbH Germany, 2018.
- [8] Singh, H., Saini, R.P. and Saini, J.S.: A review on packed bed solar energy storage systems, *Renewable and Sustainable Energy Reviews*, Vol. 14, No. 3, pp. 1059 – 1069, 2010.

NOMENCLATURE

A	Area of the thermal energy storage
D_{max}	Maximum diameter where the enlarging process stops
D_p	Original particle diameter
D_S	Diameter to increase or decrease as a function of the temperature
g	Acceleration due to gravity
n	Number of layers
$p_{(z)}$	Hydrostatic pressure
p_0	Atmospheric pressure
t_n	loading and unloading start time t_n
U	Perimeter of the thermal energy storage
v_s	Scaling velocity
z	Depth of bulk material in thermal energy storage

Greek symbols

α_p	Coefficient of thermal expansion
λ	Stress ratio
φ_x	Wall friction angle
ψ_s	Scaling factor
ρ_b	Bulk density
$\sigma_{h(z)}$	Horizontal bulk pressure
$\sigma_{v(z)}$	Vertical bulk pressure
Δt	Time step
ΔT	Change of temperature

Alexander Haber

Research Assistant
Vienna University of Technology
Faculty of Mechanical and Industrial
Engineering
Institute for Engineering Design and
Product Development

Georg Kartnig

Professor
Vienna University of Technology
Faculty of Mechanical and Industrial
Engineering
Institute for Engineering Design and
Product Development

Development of a new DEM contact model for hygroscopic bulk solids

In this work, a contact model for the simulation of crystalline solid-bridges in discrete element method (DEM) programmes is presented and compared with previous so-called bond models. The aim of the contact model is a generally valid calibration covering all states of a hygroscopic bulk material in a silo. The developed simulation model is verified by qualitative sensitivity analysis. Furthermore, a procedure for easy calibration of the required model parameters is proposed.

Keywords: DEM, caking, solid-bridge, bonds, hygroscopic bulk solid.

1. INTRODUCTION

Even today, hygroscopic bulk solids such as fertiliser urea and other salts are mainly stored in storage sheds or domes, since their behaviour in silos remains challenging. Disadvantages often associated with dome-based storage include time-consuming dosing and mixing using the ‘last-in-first-out’ principle, sometimes carried out with wheel loaders. These issues lead to reduced product quality and significant economic losses every year. Computer-assisted analysis of bulk material behaviour by means of the discrete element method (DEM) could remedy this situation and provide the necessary data for designing process-safe silos. However, industry still lacks a suitable contact model for the simulation of hygroscopic bulk solids that can reproduce the unconfined yield strength achieved by solid-bridge formation under various operating conditions.

In [2] it is shown that a DEM contact model for hygroscopic bulk solids must reproduce the following properties in order to cover the entire parameter space of possible operating conditions for a given set of material parameters:

- strength as a function of moisture
- strength as a function of time
- strength as a function of pressure

The present article concretises and verifies the approach presented in [2]. Figure 9 illustrates this approach as a simulation scheme for the calculation of crystallisation-induced solid-bridges. In addition, we present a simple calibration procedure for determining the required model parameters.

2. EXISTING DEM COHESION MODELS FOR HYGROSCOPIC BULK SOLIDS

For the development of contact models for the DEM simulation, cohesive bulk solids can be divided into two groups based on the binding mechanism: reversible and irreversible consolidation.

Reversible and an irreversible consolidation can be distinguished based on the time it takes for the formation of tensile forces acting between two neighbouring particles with respect to the duration of the simulation. In both groups, flow of the bulk solid can be caused only by exceeding the adhesion forces. If a bulk solid with reversible consolidation starts to flow, the formation of the corresponding adhesive forces takes place continuously during the simulation between neighbouring particles. This group includes cohesive powders with particles in the micro- to nanometer range, as well as moist bulk solids with particles up to the millimetre range. Corresponding to the large number of different binding mechanisms, a large number of contact models already exist for this group. These models are comparatively easy to implement, since in most cases the size of the adhesive forces is only a function of interparticle distance.

However, in the case of bulk solids with an irreversible binding mechanism, no adhesive force is formed between other particles when the adhesive forces are exceeded. The models developed for this purpose are so-called bond models and are used, for example, for chemical compound bulk solids with sinter bridges and hygroscopic bulk solids with crystalline solid-bridges, such as urea. The implementation in DEM programmes is a bit more complicated: In addition to the size of a possible adhesive force, the possible persistence of an upright connection between neighbouring particles must be determined. It should be noted that the term ‘irreversible’ applies only to typical simulation times of DEM simulations. Over typical real-world storage timescales, which go far beyond possible simulation timescales, consolidation can certainly occur via renewed formation of adhesive forces after previous breakage. A bond model implementation commonly used in DEM programmes is that for rocks after *Potyondy and Cundall* [6]. The input parameters required for this model are listed in Table 1.

Although bond models seem to be suitable for hygroscopic bulk solids in general, the implementation according to [6] is hardly applicable to industrial applications for designing a silo for urea, for example. In contrast to the model’s workings in its original field of application, the dependence of solid-bridge strength on storage time and moisture content is strong for hygroscopic bulk solids. Therefore, the already complex

Correspondence to: Dipl.-Ing. Alexander Haber
Faculty of Mechanical and Industrial Engineering,
Getreidemarkt 9, 1060 Vienna, Austria
E-mail: alexander.e307.haber@tuwien.ac.at

calibration of the models, in particular the bond radius, must be carried out each time under new operating conditions. Furthermore, the bond radius and thus the strength among all particles is assumed to be the same size, with local particle distances not considered.

Table 1. Input parameters for the classic bond model

		symbol	unit
particle parameters	particle diameter	d_P	m
	density	ρ	kg/m ³
	elastic modulud	E	N/m ²
	Poisson ratio	ν	-
interaction parameters without cohesion	coeff. of restitution	e	-
	sliding friction coeff.	μ	-
	rolling friction ceoff.	μ_r	-
bond parameters	bond radius	r_B	m
	bond range	a_{max}	m
	bond normal stiffness	k_N	N/m ⁴
	bond shear stiffness	k_T	N/m ⁴
	normal breaking stress	σ_{max}	N/m ²
	shear breaking stress	τ_{max}	N/m ²
	time of bond creation	t_{create}	s

In the following analysis, therefore, a bond model is presented that takes into account these dependencies of bulk solid pressure, moisture and storage time during the calibration process.

3. DEVELOPMENT OF A BOND MODEL FOR HYGROSCOPIC BULK SOLIDS

The principle of the new bond model has already been described in [2] (see Figure 9) and is based on the physical processes responsible for the formation of a crystalline solid-bridge. These processes occur in the following rough order:

1. Moisture exchange between the particles and the environment across particle surfaces
2. Capillary formation of liquid-bridges at contact points
3. Dissolution of the crystalline particulate solid
4. Formation of crystalline solid-bridges through complete evaporation or local supersaturation and crystal growth

The time scale for processes 3) and 4) is many times greater than that for processes 1) and 2). For detailed information, see [2] or [3].

The bond model takes effect only at a user-selected time t_{create} . At this time there is a random bed with various particle distances a . First, temporary liquid-bridge radii are calculated on the basis of the predetermined moisture content described by the liquid saturation S , from which bond radii are subsequently determined in accordance with the storage time $t_{storage}$. The required parameters are summarised in Table 2.

3.1 Calculation of the liquid-bridge radii

Depending on the amount of liquid contained in a bulk material, different saturation regimes and different types of liquid-bridges between the particles can be distinguished. The amount of liquid is expressed in terms of the pore volume occupied by the liquid saturation S .

$$S = \frac{V_{Flüssig}}{V_{Poren}} = \frac{V_{Flüssig}}{\varepsilon \cdot V_{Gesamt}} \quad (1)$$

Table 2. Input parameters for the hygroscopic bond model

		symbol	unit
moisture parameters	bulk saturation	S	-
	bulk porosity	ε	-
	contact angle	δ	rad
	bond range	a_{max}	m
time parameters	time of bond creation	t_{create}	s
	crystallisation parameter	t_{63}	h
	Storage time	$t_{storage}$	h
material parameters	bond normal stiffness	k_N	N/m ³
	bond shear stiffness	k_T	N/m ³
	normal breaking stress	σ_{max}	N/m ²
	shear breaking stress	τ_{max}	N/m ²

In (1), ε describes the porosity of the bulk solid. In the so-called pendular-state, i.e., the range of $S_{min} < S < 0.08$, liquid-bridges occur exclusively in the form of individual annular bridges (see Figure 1). The minimum moisture at which the bulk solid loses its cohesive properties is stated in [4] as $S_{min} = 0.002$. In the funicular-state $0.08 < S < 0.24$, the bulk solid gradually achieves union of individual bridges into more complex structures. Although the global connection of liquid-bridges in both cases is interrupted by pores, liquid can be exchanged along the particle surfaces via channels in the size range of the roughness itself [4].

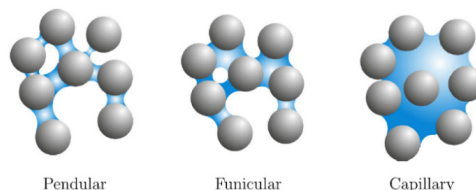


Figure 1. Liquid-bridges at different saturation regimes [11]

In the equilibrium state, therefore, capillary pressures are similar to one another across all liquid-bridges due to liquid exchange [8], if the influences of surface tension and gravitational acceleration are neglected. According to *Pietsch and Rumpf* [7], the radii, the volumes and the capillary pressures of the liquid-bridges can be calculated given known particle diameter d_P , particle distance a , filling angle β and contact angle δ (see Figure 2).

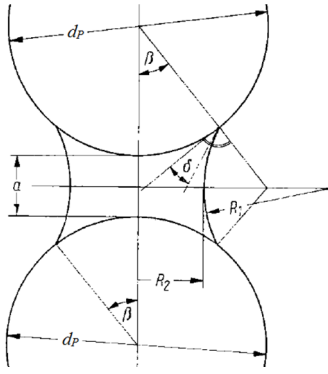


Figure 2. Liquid-bridge model [7]

With complete wetting, the contact angle δ is 0° , so the liquid-bridges connect tangentially to the particles.

In order to determine the equilibrium local liquid-bridge radii, a target value for the capillary pressure as a function of liquid saturation must be obtained. To this end, a mean filling angle $\bar{\beta}$ is first calculated on the basis of the empirical equation presented in [12]:

$$\bar{\beta} = \arcsin \left[\left(\frac{S}{0,36} \frac{\varepsilon^2}{1 - \varepsilon} \frac{1}{C_a} \frac{1}{C_\delta} \right)^{1/4} \right] \quad (2)$$

This equation provides an explicit relationship for $\bar{\beta} = f(S, \varepsilon, a, d_p, \delta)$ with the correction functions C_a and C_δ , which can be omitted for $a = 0$ and $\delta = 0$

$$C_a = 1 + 6 \frac{a}{d_p} \quad (3)$$

$$C_\delta = 1 + 1,1 \sin \delta \quad (4)$$

Eq. (2) is in good agreement with *Pietsch and Rumpf's* [7] general model, in which β cannot be represented in explicit form for a monodisperse bulk solid in the range $0.05 \leq S \leq 0.3$. Although nonpenetration of neighbouring particles ($a > 0$) is considered, several DEM simulations have shown that the average particle distance \bar{a} remains less than zero. Therefore the correction factor C_a need not be taken into account for the calculation of $\bar{\beta}$.

According to the Young-Laplace equation

$$p_K = \gamma_l \left(\frac{1}{R_1} + \frac{1}{R_2} \right) \quad (5)$$

with liquid surface tension γ_l and the required radii according to [7]

$$R_1 = \frac{d_p(1 - \cos \beta) + a}{2 \cos(\beta + \delta)} \quad (6)$$

$$R_2 = \frac{d_p}{2} \sin \beta + R_1[\sin(\beta + \delta) - 1], \quad (7)$$

the dimensionless positive capillary pressure F_{pK} can be calculated if R_2 takes a negative sign in (5):

$$F_{pK} = p_K \frac{d_p}{\gamma_l} \quad (8)$$

The liquid surface tension γ_l therefore does not need to be determined.

The local filling angles β and liquid-bridge radii R_2 are calculated as a function of the particle distance a for a given dimensionless capillary pressure F_{pK} .

Since an explicit equation for β according to *Pietsch and Rumpf* [7] is not possible, (2) would seem to be an obvious source for the calculation of the local filling angles. However, Figure 3 shows that there is not sufficient agreement between the analytic equation and the empirical equation using the correction factor C_a (3).

As can be seen in Figure 4, on the other hand, the analytic function can be very well approximated by the following cubic function:

$$\frac{a}{d_p} = A\bar{\beta}^3 + B\bar{\beta}^2 + C\bar{\beta} \quad (9)$$

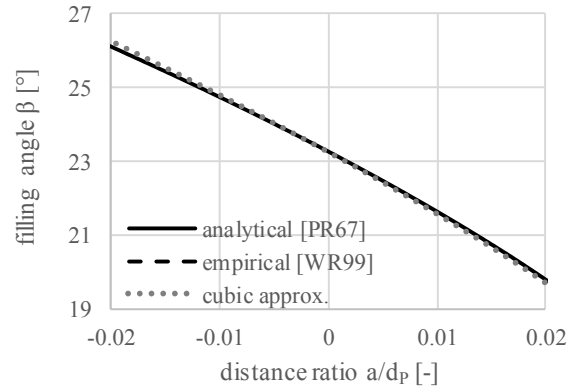


Figure 3. Dependence of the filling angle on the distance ratio for various approaches ($S=0.05$, $\varepsilon=0.34$, $\delta=0 \rightarrow F_{pK}=16.745$)

Therein, the coefficients are determined by empirical equations as functions of F_{pK} :

$$A = 2,1 \cdot 10^{-9} F_{pK}^2 + 4 \cdot 10^{-7} F_{pK} - 2,2 \cdot 10^{-6} \quad (10)$$

$$B = -1 \cdot 10^{-7} F_{pK}^3 + 3,6 \cdot 10^{-6} F_{pK}^2 \quad (11)$$

$$- 6 \cdot 10^{-5} F_{pK} - 4 \cdot 10^{-5}$$

$$C = [3,5 \cdot 10^{-5} F_{pK}^2 - 0,0097] e^{\left(-\frac{a}{6d_p} + 1\right)} - [2,1 \cdot 10^{-9} F_{pK}^2 - 2,1 \cdot 10^{-9} F_{pK}^2 - 0,0084] e^{\left(-\frac{a}{6d_p}\right)} \quad (12)$$

Eq. (9) is written by transformation as a reduced cubic equation without a quadratic term and then solved for β [°] by applying Cardano's method.

According to Figure 4, equations (9) - (12) provide a very good approximation for (5) or rather (8) in a range of $0.1 \leq F_{pK} \leq 18$. The range specified for the dimensionless capillary pressure F_{pK} covers the entire range of validity of the liquid saturation of $0.05 \leq S \leq 0.3$ for a realistic bulk solid porosity of $\varepsilon \approx 0.3 - 0.5$. The liquid saturation range is limited by the underlying model of individual annular bridge occurrences. Since the approximation currently contains no dependence on the contact angle δ , this work applies exclusively to $\delta = 0$.

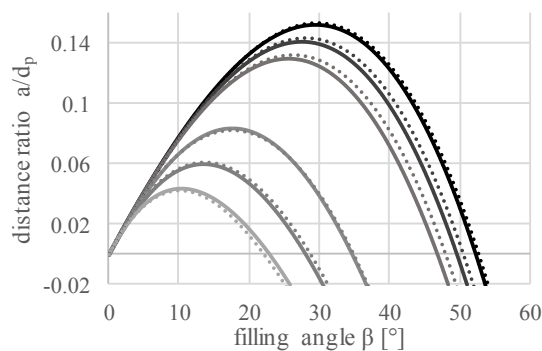


Figure 4. Curve family $f(F_{pk}, \beta, a/d_p)$. Comparison between [7] and by the cubic function (9) in the validity range of the developed contact model

With the local filling angles determined, the liquid-bridge radii R_2 are calculated according to (7).

3.2 Calculation of bond radii

On the basis of the determined liquid-bridge radii and the storage time to be investigated, the bond radii R_B can be calculated using the time parameter t_{63} according to Tomas [9]:

$$R_B = R_2 \cdot \left[1 - e^{\left(-\frac{t_{storage}}{t_{63}} \right)} \right] \quad (13)$$

According to (13), crystallisation growth is determined by an inverse exponential function. Therein t_{63} describes the time at which the crystallisation progress reaches 63%. For very long storage timescales, the bond radius corresponds to the liquid-bridge radius. Depending on the solubility L of the particulate solid in the liquid, a more or less porous bond cross-section is formed during crystallisation. This circumstance is taken into account by the calibration of the breaking stress in accordance with Chapter 4. Since the solubility L can be strongly temperature-dependent (see Table 3), a direct consideration of this parameter in (13) is possible:

$$R_B = L \cdot R_2 \cdot \left[1 - e^{\left(-\frac{t_{storage}}{t_{63}} \right)} \right] \quad (14)$$

When using (14) instead of (13), the calibrated breaking stress takes on a different value, and temperature dependence is taken into account by the actual solubility.

Table 3. Solubility of urea in water as a function of temperature [5]

	temperature [°C]					
	0	20	40	60	80	100
L [g/g]	0.65	1.07	1.65	2.53	4.05	7.40

4. CALIBRATION OF MODEL PARAMETERS

To carry out a DEM simulation with the presented contact model, the parameters listed in Table 2 must be set. As with the parameters in Table 1, the liquid saturation S and the storage time $t_{storage}$ must now be specified instead of directly defining the unknown bond radius.

The liquid saturation of the bulk solid can be determined by means of so-called sorption isotherms from the relative humidity RH and the ambient temperature T_U . Table 4 shows some values of the sorption isotherm of urea at 25 °C.

Table 4. Sorption isotherm values for urea at 25 °C [1]

	relative humidity RH [%]					
	12	33	53	76	92	97
X [%]	0.09	0.11	0.11	0.67	49.37	58.50

Therein, X is mass-based material moisture, mostly used for sorption isotherms

$$X = \frac{m_{liquid}}{m_{particle,dry}}, \quad (15)$$

which can be easily converted into the liquid saturation S required as input parameter:

$$S = X \cdot \frac{1 - \varepsilon}{\varepsilon} \cdot \frac{\rho_{particle}}{\rho_{liquid}} \quad (16)$$

The typical progression of sorption isotherms according to Table 4 shows at first a very small amount of adsorbed liquid and a strong increase in moisture from a critical relative humidity CRH .

The bulk porosity ε can be obtained in many cases from the results of a first simulation without bonds. However, if the particle size selected in the simulation does not correspond to the actual grain size, this is not possible and the parameter ε must then be calibrated. This case will not be discussed here. However, a possible procedure for its calibration could be a final comparison of the calculated liquid-bridge volume with the adjusted liquid saturation according to (1).

The physical value of the contact angle δ must be determined in accordance with the wettability of the bulk solid with the surrounding liquid. Therefore, a calibration is not required.

For the bond range a_{max} , a relatively large value can be selected. Since no unphysical results are allowed while determining the correct solution of the cubic equation, no liquid-bridge will be created unless the capillary pressure at that distance reaches the desired target value, even if the value for a_{max} is large. In this sense, a_{max} only defines the range of possible contact partners. For many cases, a_{max} can be chosen in a range of $0.02 \leq a_{max}/d_p \leq 0.05$.

The time for the creation of the bonds t_{create} is chosen by the user on the basis of the simulation process so that the particle bed has already come to rest and the kinetic energy is close to zero.

Since crystalline solid-bridges consist of the same material as the particles themselves, the same stiffness settings can be used for the bond stiffnesses k_N and k_T as for the cohesionless particle contact model. If the elastic modulus is used to quantify particle stiffness, it can be converted into the required stiffness per unit area $[N/m^3]$ as follows:

$$k = \frac{E}{L_0} \quad (17)$$

with

$$L_0 \approx d_p \quad \text{for } k_N \quad \text{and} \quad (18)$$

$$L_0 \approx 2R_B \quad \text{for } k_T \quad (19)$$

Finally, the breaking stresses σ_{max} and τ_{max} and the crystallisation parameter t_{63} remain from Table 2 for the calibration. Since studies on single grains (e.g., [10] and [3]) are generally very complex, the uniaxial compression test is used here and it must be carried out twice. For this purpose, the sample material is prepared identically in both cases with respect to liquid saturation and temperature. Subsequently, the samples are precompressed by pressure from above and stored in a climate chamber under defined conditions. In the last step, the walls of the mostly cylindrical sample geometry are removed, and the sample is crushed by loading from above. Based on the maximum applied force and the cross-section of the sample, the compressive strength σ_c is determined.

The first sample is stored as long as the crystallisation process is complete, at which point no further increase in compressive strength is to be expected with further storage (Figure 5). The stress value σ_1 determined at t_1 serves to calibrate the maximum breaking stresses σ_{max} and τ_{max} .

The heretofore unknown parameter t_{63} required for the calibration simulations must be determined first. This is done using the second sample shown in Figure 5, which is stored for only a few hours. The exact storage time t_2 depends on the bulk solid and the added liquid. The goal is the determination of a representative point σ_2 on the solidification curve for the determination of t_{63} with:

$$t_{63} = -\frac{t_2}{\ln\left(1 - \frac{\sigma_2}{\sigma_1}\right)} \quad (20)$$

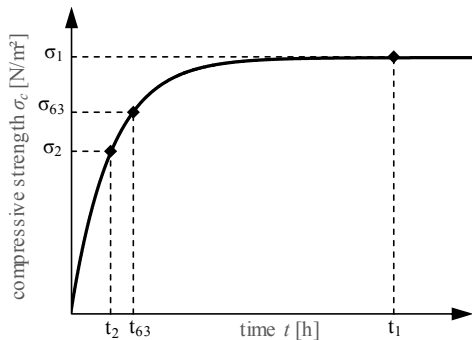


Figure 5. Consolidation curve for calibration of the bond model by means of a uniaxial compression test

5. VERIFICATION AND VALIDATION

To verify the developed contact model, we simulate a uniaxial pressure test, and we then qualitatively assess the compressive strengths achieved at different precompactions, liquid saturations and storage times. For this purpose, particles with a uniform diameter of 6 mm are filled into a virtual sample cylinder. The cylinder has a diameter of 61 mm and a height of 85

mm. Figures 6, 7 and 8 show the results of these simulations.

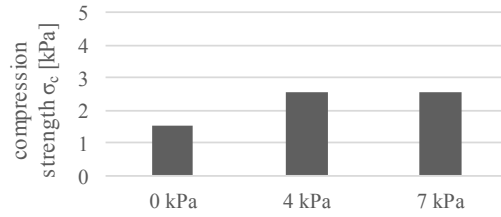


Figure 6. Compressive strength as a function of compression pressure at $t_{storage} = t_{63}$ and $S = 0.3$.

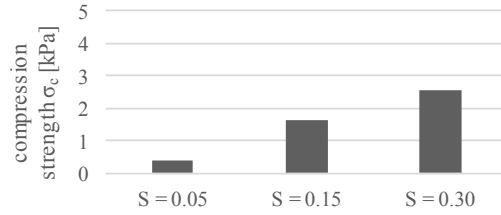


Figure 7. Compressive strength as a function of liquid saturation at 4 kPa and $t_{storage} = t_{63}$.

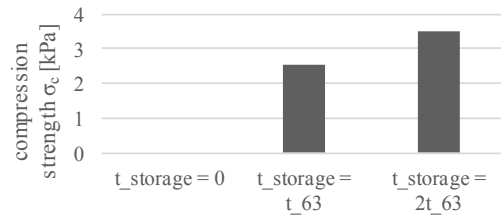


Figure 8. Compressive strength as a function of storage time at 4 kPa and $S = 0.3$.

According to Figure 6, a dependence on compression pressure is evident only at very low pressures. This restriction corresponds to the range over which particles rearrange from a loose bed to a dense packing. Further reduction of interparticle distance is relatively minor in comparison. Under typical silo pressures, this dependence is observed to be rather low, coinciding with the observations of *Wahl et al.* [10].

The trend in compressive strength as a function of liquid saturation and storage time (Figures 7 and 8) is in line with expectations. A detailed validation by comparative measurements is still pending.

6. CONCLUSION

A DEM contact model for hygroscopic bulk solids was developed. An essential feature is its dependence on storage time and moisture. With a one-time calibration, a parameter set valid for all operating conditions can be found. With the help of the presented calibration method, all required parameters can be determined with a simple test bench and little effort. Verification of the model was based on various parameter variations, yielding promising behaviour.

In the next step, the model for various hygroscopic bulk solids, such as urea, sugar, etc., is calibrated. Subsequently, the simulation results are compared with comprehensive measurement series.

Future steps also include an extension of the model with regard to the following possibilities:

- Consideration of a possible particle size distribution
- Detection of contact angles $\delta \neq 0^\circ$
- Impact of local humidity and temperature differences

REFERENCES

- [1] Bröckel, U., Kirsch, R., Wahl, M. and Feise, H. J.: Formation and strength of solid bridges in bulk solids, *Particulate Science and Technology*, Vol. 26, No. 1, pp. 23-32, 2007.
- [2] Haber, A. and Kartnig, G.: Ansätze zur Berücksichtigung der zeit- und ortsabhängigen Eigenschaften von Festkörperbrücken in DEM-Simulationen, *Logistics Journal: Proceedings*, 2018.
- [3] Kirsch, R., Williams, R., Bröckel, U., Hammond, R. and Jia, X.: Direct Observation of the Dynamics of Bridge Formation between Urea Prills, *Industrial & Engineering Chemistry Research*, Vol. 50, No. 20, pp. 11728–11733, 2011.
- [4] Lukyanov, A.V., Sushchikh, M.M., Baines, M.J. and Theofanous, T.G.: Superfast nonlinear diffusion: Capillary transport in particulate porous media, *Physical review letters*, Vol. 109, No. 21, pp. 214501, 2012.
- [5] Meessen, J. H.: Urea, *Ullmann's Encyclopedia of Industrial Chemistry*, pp. 657-695, 2012.
- [6] Potyondy, D.O. and Cundall, P.A.: A bonded-particle model for rock, *International journal of rock mechanics and mining sciences*, Vol. 41, No. 8, pp. 1329-1364, 2004.
- [7] Pietsch, W. and Rumpf, H.: Haftkraft, Kapillardruck, Flüssigkeitsvolumen und Grenzwinkel einer Flüssigkeitsbrücke zwischen zwei Kugeln, *Chemie Ingenieur Technik*, Vol. 39, No. 15, pp. 885-893, 1967.
- [8] Schaber, M: *Flüssigkeitsumverteilung in feuchten Granulaten*, *Dissertation, Universität des Saarlandes*, Fakultät für Naturwissenschaften und Technik, Saarbrücken, 2015.
- [9] Tomas, J.: Zur Verfestigung von Schüttgütern – Mikroprozesse und Kinetikmodelle, *Chemie Ingenieur Technik*, Vol. 69, No. 4, pp. 455-467, 1997.
- [10] Wahl, M., Kirsch, R., Bröckel, U., Trapp, S. and Bottlinger, M.: Caking of Urea Prills, *Chemical Engineering & Technology*, Vol. 129, No. 6, pp. 674–678, 2006.
- [11] Washino, K., Chan, E. L., Midou, H., Tsuji, T. and Tanaka, T.: Tangential viscous force models for pendular liquid bridge of Newtonian fluid between moving particles, *Chemical Engineering Science*, Vol. 174, pp. 365-373, 2017.
- [12] Weigert, T. and Ripperger, S.: Calculation of the liquid bridge volume and bulk saturation from the half-filling angle, *Particle & Particle Systems Characterization*, Vol. 16, No. 5, pp. 238-242, 1999.

NOMENCLATURE

a	[m]	particle distance
d_p	[m]	particle diameter
F_{pK}	[-]	dimensionless capillary pressure
k_N	[N/m ³]	bond normal stiffness
k_T	[N/m ³]	bond shear stiffness
L	[g/g]	solubility
p_K	[Pa]	capillary pressure
R_2	[m]	liquid-bridge radius
R_B	[m]	bond radius
S	[-]	liquid saturation
t_{63}	[h]	crystallisation parameter

$t_{storage}$	[h]	storage time
X	[g/g]	mass-based material moisture

Greek symbols

β	[rad]	filling angle
$\bar{\beta}$	[rad]	mean filling angle
δ	[rad]	contact angle
ε	[-]	bulk porosity
σ_c	[N/m ²]	compression strength
σ_{max}	[N/m ²]	normal breaking stress
τ_{max}	[N/m ²]	shear breaking stress

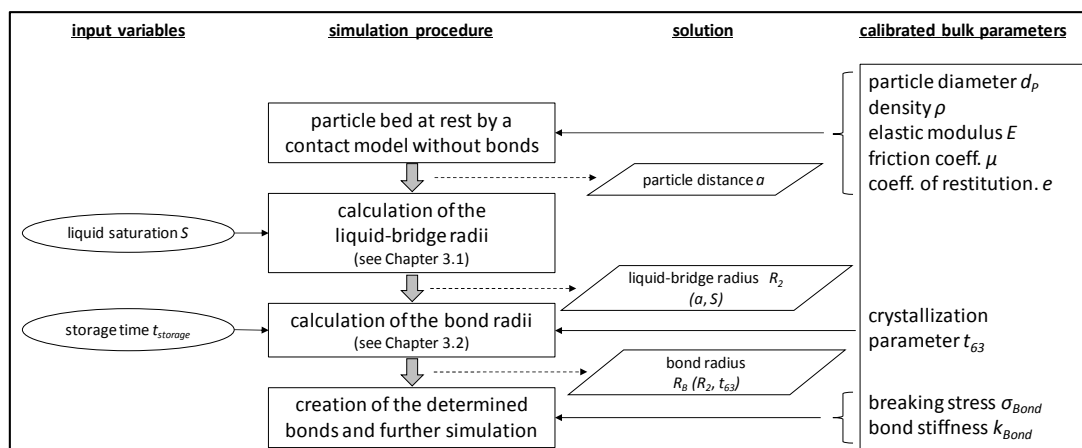


Figure 9. Simulation procedure for consideration of pressure- and time-dependent solid-state bridges [2]

Srđan BošnjakProfessor
University of Belgrade
Faculty of Mechanical Engineering**Nebojša Gnjatović**Assistant Professor
University of Belgrade
Faculty of Mechanical Engineering**Ivan Milenović**Research Assistant
University of Belgrade
Faculty of Mechanical Engineering**Aleksandar Stefanović**Research Assistant
University of Belgrade
Faculty of Mechanical Engineering**Marko Urošević**Research Assistant
University of Belgrade
Faculty of Mechanical Engineering

Modernization and Unification of the Excavating Devices of Bucket Wheel Excavators SRs 2000 Deployed in Serbian Open Pit Mines

A bucket wheel with drive represents a vital subsystem of any bucket wheel excavator. A multidecadal experience in the exploitation and maintenance of bucket wheel excavators SRs 2000 has imposed a need for modernization and unification of the excavating devices of four of such machines, used for the excavation of overburden in Serbian open pit mines. This paper presents a portion of the research dedicated to the problems of strength and dynamic properties of the bucket wheel boom, static stability of the superstructure as well as installation of the unified design solution for the bucket wheel drive of the bucket wheel excavator SRs 2000. By installing a modernized design solution of the bucket wheel with drive, i.e. by the means of partial revitalization of the bucket wheel excavator, its exploitation life span is prolonged and, additionally, the level of reliability and availability of the overburden systems is increased, and a significant reduction in maintenance expenses is achieved.

Keywords: bucket wheel excavator, excavating device, bucket wheel boom, strength, modal analysis, static stability, mounting and installation.

1. INTRODUCTION

A widespread application and multidecadal exploitation of the bucket wheel excavator (BWE) TAKRAF SRs 2000 in working environments of varying properties (coal and overburden) has imposed a need for a permanent upgrade of its subsystems. A relatively large number of studies, dealing with the vibration problems and structural strength [1,2], bucket wheel with drive [3-9], as well as problems of efficiency [10] and effectiveness [11] of this type of a BWE has been performed and published.

Since the deployment of the BWEs SRs 2000 (1970), the manufacturer (TAKRAF) has dedicated special attention to the increase of the reliability levels of the bucket wheel drive, developing a plethora of improved design solutions for the bucket wheel (a single-walled bucket wheel in place of a double-walled design solution) with drive, with various conceptions and engine power outputs [9,12-14].



Figure 1. The BWE SRs 2000x32/5+VR92 in the OP "Tamnava West Field"

Four SRs 2000-type excavators are deployed in Serbian open pit mines (OP) with the purpose of overburden excavation, three of which are being used in OP "Drmno", and one in OP "Tamnava West Field" [3], Figure 1. During 2016, TAKRAF has performed an extensive reconstruction of the excavating device on one of the BWEs in OP "Drmno": (1) a double-walled bucket wheel has been replaced with a single-walled variant; (2) a gearbox with a single 1250 kW electric motor has been introduced in place of an existing gearbox, powered by two, 670 kW, electric motors.

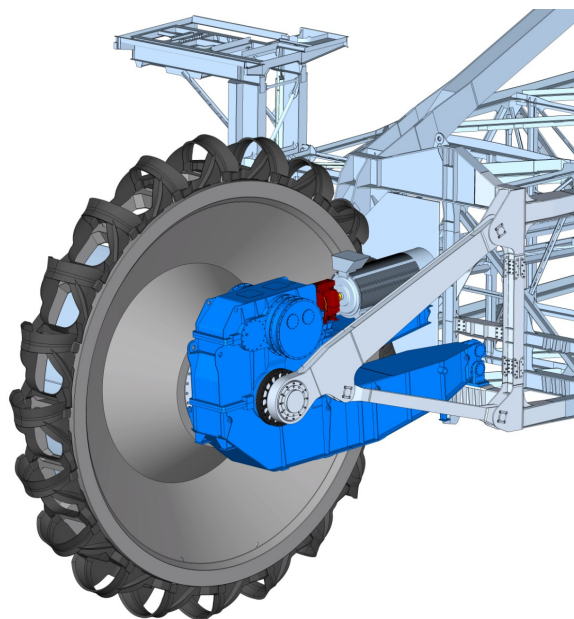


Figure 2 [15]. The single-walled bucket wheel with a single 1250 kW orbiting gearbox (manufactured by TAKRAF)

Correspondence to: Dr Nebojša Gnjatović, Ass. Professor
Faculty of Mechanical Engineering,
Kraljice Marije 16, 11120 Belgrade 35, Serbia
E-mail: ngnjatovic@mas.bg.ac.rs

Redesigning a bucket wheel with drive poses a very challenging and complex engineering task [15-17]. On the basis of a positive impression of the performance of the BWE SRs 2000 with the redesigned bucket wheel boom head, as well as a thorough study by the research team the authors of this paper are a part of [15], a unified technical solution for the bucket wheel drive for the SRs 2000 type of excavators, consisting of a single 1250 kW electric motor, fully synchronized with the single-walled bucket wheel, has been proposed as the optimal for the needs of Serbian coal mines, Figure 2. In order to make the installation of the unified bucket wheel drive possible, the first frame of the bucket wheel boom also had to be reconstructed, Figure 3, as well as locally reinforced. This paper then proceeds to present a portion of the research [15] dedicated to the problems of strength and dynamic properties of the bucket wheel boom, static stability of the superstructure and, finally, the installation of the unified bucket wheel drive solution for the BWE SRs 2000.

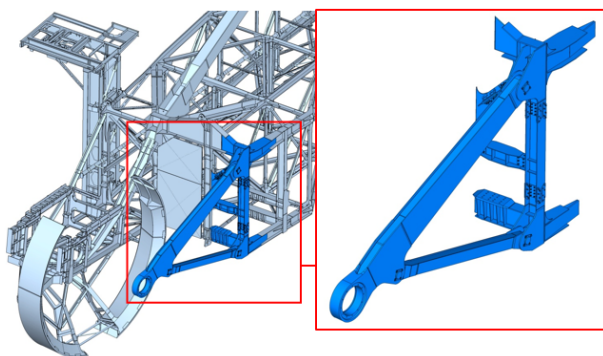


Figure 3 [15]. The redesigned first frame of the bucket wheel boom

2. STRENGTH OF THE BUCKET WHEEL BOOM SUBSTRUCTURE

BWE SRs 2000 was designed in accordance with the standard TGL 13472 [18], which was in effect at the time of its development. The differences between this standard and DIN 22261-2 [19], which is the current standard in effect, include:

the method for the calculation of the intensity of certain partial loads/influences;

the number of relevant load cases, as well as the method for forming the sets of partial loads which define them.

Validation of the redesigned structure of the bucket wheel boom has been achieved by applying a comparative analysis [16, 20, 21] of its response. For all the relevant load cases (LCs), the identification of the stress states has been performed for three representative positions of the bucket wheel boom: horizontal position - position 1; inclined position - position 2; declined position - position 3. The results of the finite element analyses of the original bucket wheel boom with the redesigned head (variant 1: V1), subjected to loads determined by the standard [19], have revealed the existence of five zones (labelled as "critical zones") in which the equivalent calculation stresses (von Mises) are higher than allowed, Figure 4. It is important to notice, Figure 5, that the critical zones appear in those subdomains of the original bucket wheel boom substructure where there was no need for reconstruction due to the installation of the redesigned bucket wheel. With the introduction of favorably-shaped reinforcements in the critical zones (variant 2: V2), the effects of the stress concentrators have been reduced significantly, bringing the stress values within the limits prescribed by the standard [17], Figure 6, for all load cases.

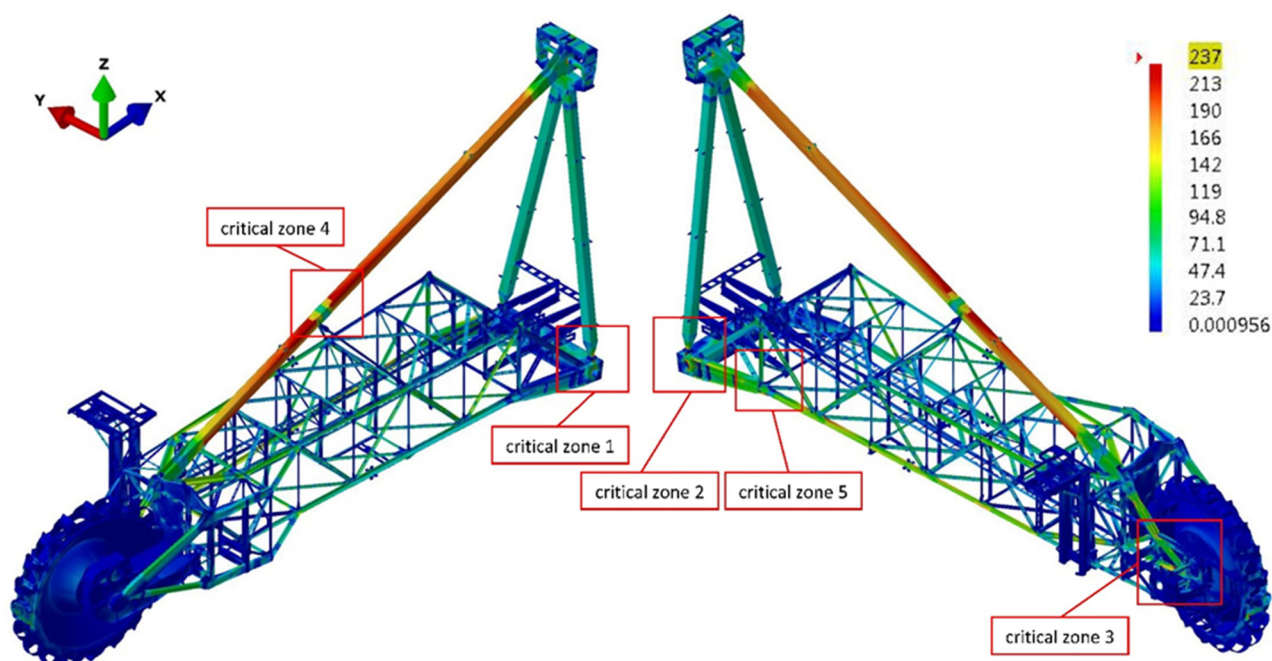


Figure 4 [15]. Critical zones of the bucket wheel boom substructure

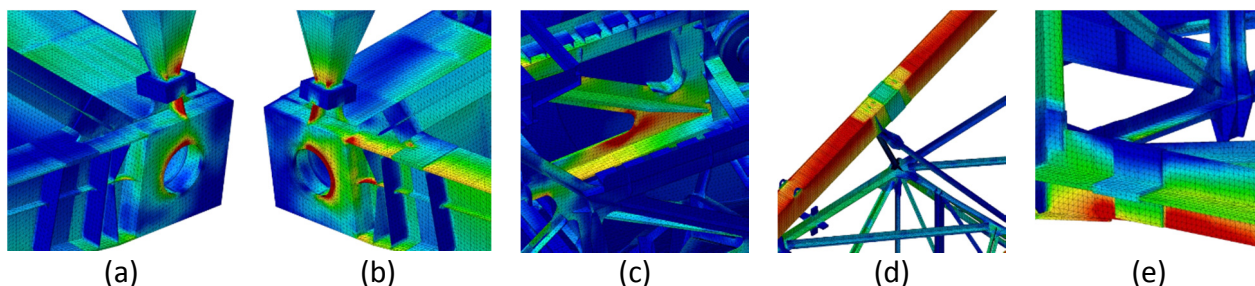


Figure 5 [15]. Von Mises stresses in BWB critical zones (LC H1.2, permissible stress value $\sigma_{per}=237$ MPa; BWB position 1; direction of the lateral loads: +y): (a) zone 1, $\sigma_{VM}=303$ MPa; (b) zone 2, $\sigma_{VM}=280$ MPa; (c) zone 3, $\sigma_{VM}=304$ MPa; (d) zone 4, $\sigma_{VM}=245$ MPa; (e) zone 5, $\sigma_{VM}=272$ MPa

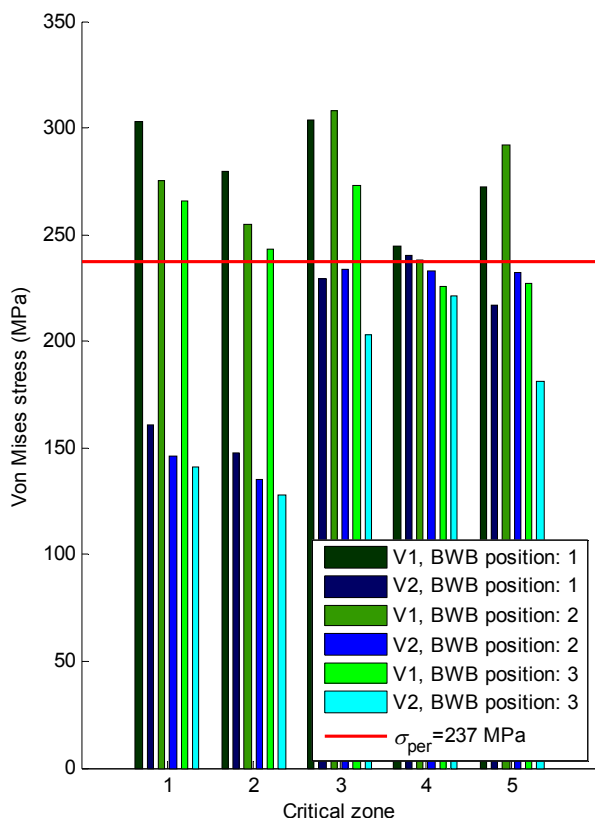


Figure 6 [15]. Von Mises stresses: V1 vs V2 in LC H1.2

3. MODAL ANALYSIS OF THE BUCKET WHEEL BOOM SUBSTRUCTURE

In order to avoid undesired dynamic effects [4,22,23], a modal analysis of the bucket wheel boom substructure has been performed for the variants V0 (state before the reconstruction) and V2 (state after the reconstruction), Figure 7, Table 1. The biggest percent differences between the natural frequencies occur in the second and third mode, when the bucket wheel boom is in position 3. In these instances, the natural frequencies of the redesigned bucket wheel boom (V2) are 12.6% and 20.0% higher, respectively. In each of the remaining cases the percent difference is less than 10%.

Numerical values of the critical excitation frequencies of the bucket wheel boom where resonant states may occur have been determined with a modal analysis of the entire superstructure. The final ranges of the electric motor frequencies that should be avoided are to be defined after the adjustments to the ballast and the control weighing of the superstructure.

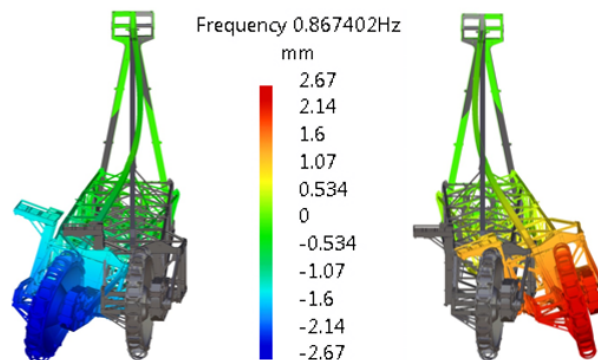


Figure 7 [15]. The fundamental mode of the redesigned bucket wheel boom substructure (V2)

Table 1 [15]. Frequencies of the first ten modes: V0 vs V2

Mode	BWB position					
	1		2		3	
	V0	V2	V0	V2	V0	V2
	Frequency (Hz)					
1	0.888	0.867	0.880	0.867	0.896	0.867
2	1.344	1.466	1.386	1.512	1.197	1.348
3	2.028	2.061	1.836	2.072	1.701	2.041
4	2.355	2.353	2.352	2.353	2.352	2.353
5	3.786	3.789	3.755	3.790	3.481	3.788
6	3.957	3.968	3.696	3.982	3.711	3.941
7	4.468	4.484	4.518	4.485	4.489	4.484
8	4.582	4.602	4.583	4.600	4.567	4.600
9	4.651	4.659	4.665	4.659	4.668	4.658
10	5.361	5.419	5.346	5.431	5.594	5.393

4. STATIC STABILITY OF THE SUPERSTRUCTURE

The superstructure of the BWE SRs 2000x32/5, Figure 8, consists of three fundamental substructures:

- substructure 1 (SuS1) - the bucket wheel boom;
- substructure 2 (SuS2) - the counterweight boom;
- substructure 3 (SuS3) - the slewing platform.

The bucket wheel boom substructure has a cylindrical joint connection to the counterweight boom

substructure, and its inclination angle is adjustable via a rope wire mechanism. The counterweight boom is loosely rested on the slewing platform substructure, meaning that the connection is lost if the counterweight boom is tilted backwards. Meanwhile, on the side of the counterweight, it is connected to the slewing platform by cylindrical joints. The numerical model for the 'a posteriori' examination of the static stability of the superstructure [24] was formed by applying the concept of corrective mass [25].

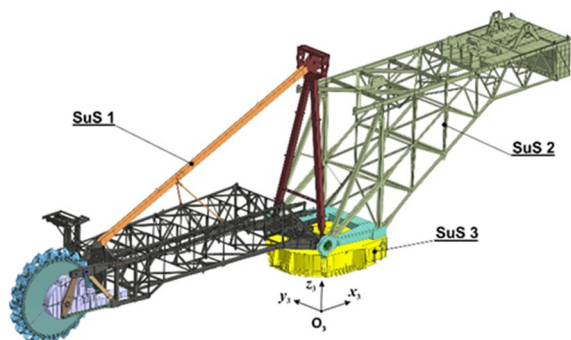


Figure 8 [15]. 3D model of the BWE SRs 2000x32/5 superstructure

According to DIN 22261-2 standard [19], the safety factor against the loss of static stability, i.e. against overturning, is determined by the ratio between the moment of stability (M_s) and the moment of overturning (M_p),

$$v = \frac{M_s}{M_p} \geq v_{\text{DIN,min}} \quad (1)$$

under the condition that its value has to be higher than the minimum prescribed value for the relevant load case.

The standard TGL 13472 [18] offers two procedures for the proof of static stability. The first fully matches the procedure prescribed by the standard DIN 22261-2 [18], expression (1), with the condition

$$v_1 = \frac{M_s}{M_p} \geq v_{1\text{TGL,min}} = 1.25. \quad (2)$$

Therefore, unlike the standard DIN 22261-2, the standard TGL 13472 treats every load case with the minimum value of the safety factor: 1.25, expression (2). The other procedure is based on factorization of the moments of stability and overturning,

$$v_2 = \frac{\varepsilon M_s}{\sum \alpha_i M_{p,i}} \geq v_{2\text{TGL,min}} = 1.0, \quad (3)$$

where the reduction factor for the moment of stability equals to $\varepsilon=0.97$, while the value of the increase factor for the moment of overturning $\alpha_i > 1$ depends on the character of the partial load. Finally, according to the standard TGL 13472, the condition for the static stability is satisfied if at least one of the criteria defined by the expressions (2) and (3) is met.

The differences in the intensities of calculated partial loads and the criteria for the proof of static stability are especially pronounced in LC H1.2. Namely, the

calculation procedure prescribed by the standard DIN 22261-2 yields twice the weight of the incrustation on the bucket wheel to that obtained in accordance with the standard TGL 13472. At the same time, for the same LC, the standard DIN 22261-2 prescribes a higher minimum value of the safety factor against overturning (1.5) than one prescribed by the standard TGL 13472 (1.25). The minimum value of the safety factor against overturning on the BW side (BWS), obtained in accordance with the standard DIN 22261-2 is 6.5% lower than the minimum value prescribed by the said standard, Figure 9. However, if the procedure for proving the static stability prescribed by the standard TGL 13472 is applied, Figure 10, then the conclusion is that the superstructure meets both criteria of static stability prescribed by this standard.

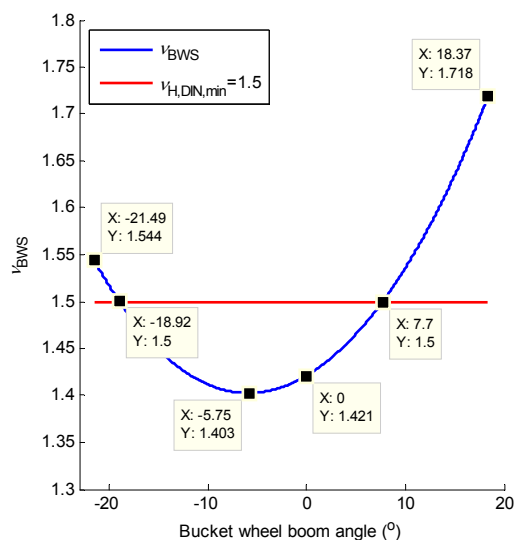


Figure 9 [15]. LC H1.2: safety factor against overturning on the BW side according to the standard DIN 22261-2

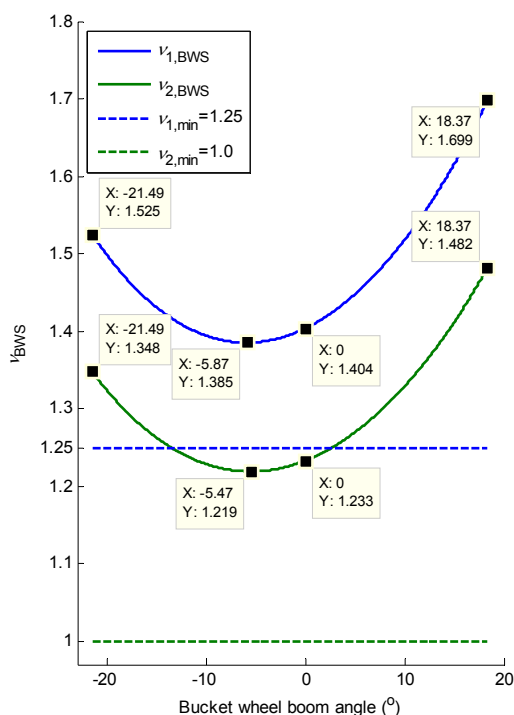


Figure 10 [15]. LC H1.2: safety factor against overturning on the BW side according to the standard TGL 13472

5. INSTALLATION OF THE UNIFIED BUCKET WHEEL WITH DRIVE

Installation of the unified bucket wheel with drive is conducted in five phases, namely:

- phase 1 – preparation of the worksite and the excavator for the reconstruction, Figures 11a,b,c;
- phase 2 – dismantling of the existing excavating device, Figures 11d,e,f;
- phase 3 – reconstruction and reinforcing of the bucket wheel boom, Figures 11g,h,i,j;

- phase 4 – installation of the unified bucket wheel with drive, Figures 11k,l;
- phase 5 – final steps before the bucket wheel excavator undergoes a test run.

In accordance with the schedule, Figure 12, the total time for the installation of the unified bucket wheel with drive, including functionality tests, amounts to 35 12-hour workdays.

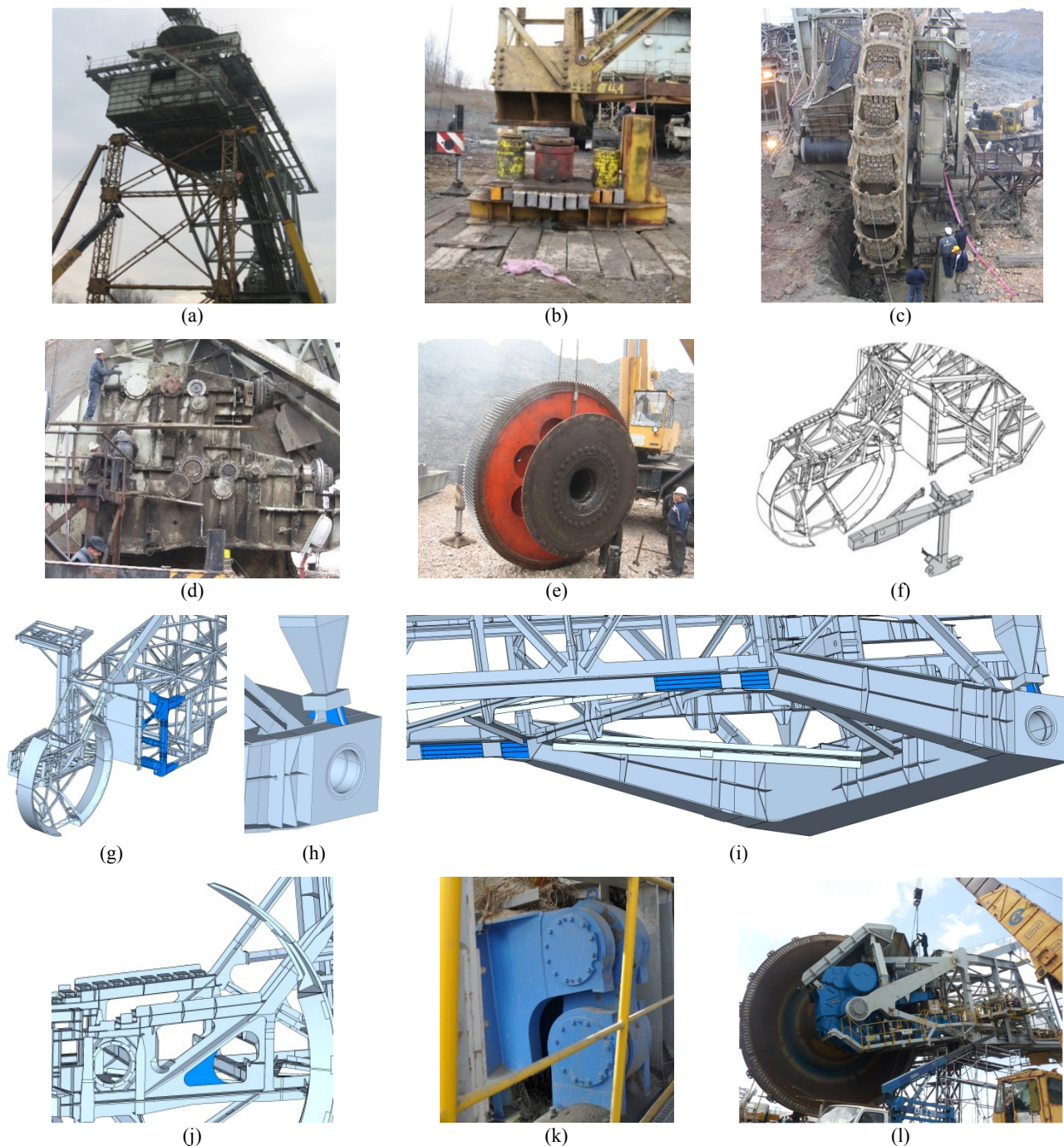


Figure 11 [15]. Phases of installation of the unified bucket wheel with drive: (a) mounting of the temporary support for the counterweight boom; (b) hydraulic cylinders for the temporary support of the counterweight boom; (c) bucket wheel being prepared for dismantling; (d) dismantling of the subassemblies of the bucket wheel drive gearbox; (e) dismantling of the output shaft of the bucket wheel drive gearbox; (f) cutting and dismantling of a segment of the first frame of the bucket wheel boom; (g) installation of the redesigned segment of the first frame of the bucket wheel boom; (h) installation of the ribs in the zone of support of the A frame; (i) reinforcing of the vertical plates on the lower girders of the bucket wheel boom; (j) reinforcing of the gusset plate in the zone of axially-constrained bearing of the bucket wheel shaft; (k) installation of the torque arm support; (l) installation of the unified bucket wheel with drive

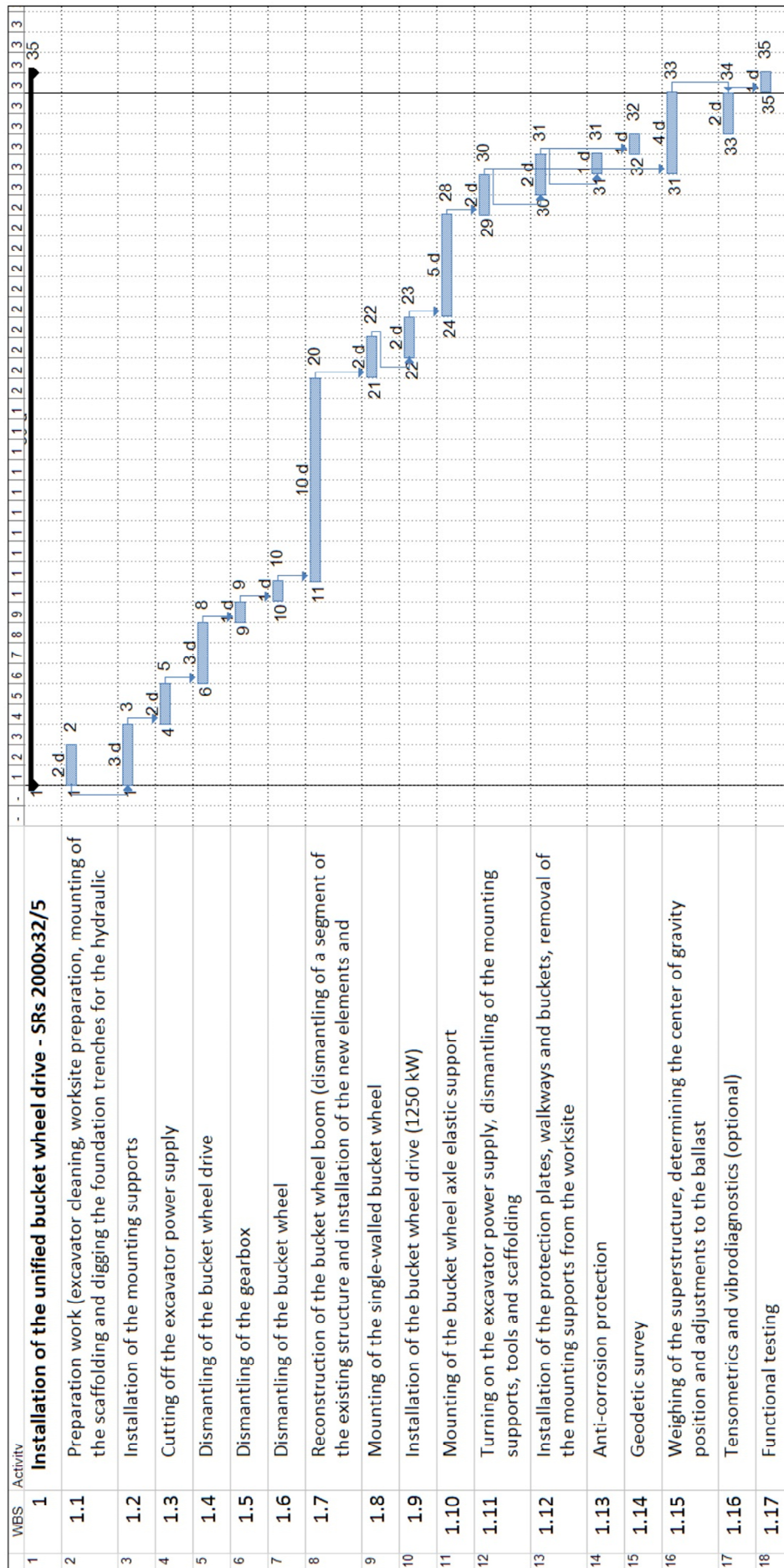


Figure 12 [15]. Schedule for the installation of the unified bucket wheel with drive

6. CONCLUSION

By modernizing the excavating devices of the bucket wheel excavators SRs 2000, the observed drawbacks of the double-walled bucket wheel (accumulation of the material on the bucket wheel body, above anything else) as well as the originally-designed support of the bucket wheel drive gearbox are eliminated. Replacement of the existing excavating device requires a detailed analysis of the influence of the newly developed solution on strength, dynamic response and static stability of the machine. Based on the results of the appropriate analyses [15], portions of which are presented in this paper, the following outcomes have been achieved:

- the local redesign of the bucket wheel boom has been fully defined, and its carrying capacity has been proven after its reconstruction;
- it is proven that the risk of occurrence of unwanted dynamic effects, i.e. resonance is eliminated after the reconstruction;
- the necessary correction of the ballast has been defined and the static stability of the superstructure after the reconstruction has been proven;
- the procedure for the installation of the newly designed excavating device has been described, along with the detailed specification of the required workforce, machinery, equipment and tools.

The installation of the newly designed bucket wheel with drive represents a partial revitalization of the bucket wheel excavator which extends its lifespan, along with increasing the reliability and availability of the overburden systems on the Serbian surface mines. Additionally, the unification of the excavating devices of the bucket wheel excavators BWEs SRs 2000 leads to a significant reduction of maintenance costs.

ACKNOWLEDGMENTS

This work is a contribution to the Ministry of Education and Science of Serbia funded project TR 35006.

The authors would like to express their gratitude to The Joint Japan-Serbia Center for the Promotion of Science and Technology for providing the resources to conduct simulations.

REFERENCES

- [1] Pietrusiak, D., Moczko, P., Rusiński, E.: Recent achievements in investigations of dynamics of surface mining heavy machines, 24th World Mining Congress Proceedings, Instituto Brasileiro de Mineração, Rio de Janeiro, pp. 295–308, 2016.
- [2] Rusiński, E., Czmochoowski, J., Moczko, P., Pietrusiak, D.: Surface Mining Machines - Problems of Maintenance and Modernization, Springer International Publishing AG, Cham, 2017.
- [3] Jovančić, P., Ignjatović, D., Maneski, T., Novaković, D., Slavković, Č.: Diagnostic procedure of bucket wheel and boom computer modeling – A case study: Revitalization bucket wheel and drive of BWE SRs 2000, Proceedings of the 14th International Scientific Conference: Computer Aided Engineering, Springer International Publishing AG, Cham, pp. 310-318, 2019.
- [4] Jovančić, P., Čelović, Š., Ignjatović, D., Maneski, T.: Redesigning components of power transmission according to numerical model and vibration diagnostics, Journal of Vibroengineering, Vol. 15, No. 3, pp. 1322-1329, 2013.
- [5] Jovančić, P., Ignjatović, D., Gnjatović, N., Bošnjak, S.: Analysis of bucket wheel drive system at SRs 2000 excavators, for the unification purpose [in Serbian], Proceedings of the 13th International Conference "OMC 2018", Yugoslav opencast mining committee, Belgrade, pp. 63-71, 2018.
- [6] Karišić, D.: UT-Excavator Working Wheel Axle Side Search Technique [in Serbian], Proceedings of the International Congress on Process Engineering – Processing, Vol. 23, No. 1, pp. 1-7, 2017.
- [7] Novaković, D., Jovančić, P.: Analysis and troubleshooting of the bucket wheel drive on bucket wheel excavators SRs 2000 – The road to modernization [in Serbian], Proceedings of the 8th International conference "COAL 2017", Yugoslav opencast mining committee, Belgrade, pp. 247-256, 2017.
- [8] Savković, M., Gašić, M., Arsić, M., Petrović R.: Analysis of the axle fracture of the bucket wheel excavator, Eng. Fail. Anal., Vol. 18, No. 1, pp. 433-441, 2011.
- [9] Savković, M., Gašić, M., Zdravković, N., Novaković, D.: Analysis of the SRs bucket wheel excavator excavation drive solutions, IMK – 14 Research&Development, Vol. 32-33, No. 3-4, pp. 69-74, 2009.
- [10] Jakovljević, I., Stepanović, S., Šubaranović, T.: Logistics approach to investigation of slice thickness-height ratio effects on excavation resistance of bucket wheel excavator, The International Journal Transport&Logistics, Vol. 10, No. 19, pp. 69-79, 2010.
- [11] Živković, L., Lazić, M., Polovina, D.: Comparative analysis of the effectiveness work of the bucket wheel excavator SRs 2000 in opencast mines EPS and MIBRAG [in Serbian], Proceedings of the 11th International Opencast Mining Conference "OMC 14", Yugoslav opencast mining committee, Belgrade, pp. 463-471, 2014.
- [12] Gnilke, M.: Intelligent retrofit solutions for bucket wheel excavators, WISSENSPORTAL baumaschine.de 1(2006), pp. 1-7, 2006.
- [13] Gnilke, M.: Aktueller Entwicklungsstand bei Schaufelradgetrieben mittlerer und großer Leistung, WISSENSPORTAL baumaschine.de 1(2006), pp. 1-8, 2006.

- [14] Mizerski, Z., Gnilke, M.: New bucket wheel drive for BWE SRs 2000 in Bełchatów opencast mine [in Polish], *Górnictwo i Geoinżynieria*, Vol. 35, No. 3/1, 189-198, 2011.
- [15] Bošnjak, S., Jovančić, P., Gnjatović, N., Ignjatović, D., Milenović, I. et al.: The Analysis of the Bucket Wheel Drivetrains on Bucket Wheel Excavators SRs 2000 with the Purpose of Unification, realized for JP „Elektroprivreda Srbije Beograd” - Beograd, Faculty of Mechanical Engineering and Faculty of Mining and Geology, Belgrade, 2019.
- [16] Bošnjak, S., Petković, Đorđević, M., Gnjatović, N.: Redesign of the Bucket Wheel Excavating Device, Proceedings of the 19th International Conference on Material Handling, Constructions and Logistics - MHCL'09, University of Belgrade - Faculty of Mechanical Engineering, Belgrade, pp. 123-128, 2009.
- [17] Durst, W., Vogt, W.: Bucket Wheel Excavator, Trans Tech Publications, Clausthal-Zellerfeld, 1989.
- [18] TGL 13472: Steel supporting structures of heavy aggregates for open mining – Calculation, structural design, VVB Tagebauausrüstungen, Krane und Förderanlagen, Amt für Standardisierung, Meßwesen und Warenprüfung, 1974.
- [19] DIN 22261-2:2016-10: Bagger, Absetzer und Zusatzgeräte in Braunkohlentagebauen - Teil 2: Berechnungsgrundlagen, Deutsches Institut für Normung, Berlin, 2016.
- [20] Bosnjak, S., Petkovic, Z., Dunjic, M., Gnjatovic, N., Djordjevic, M.: Redesign of the vital subsystems as a way of extending the bucket wheel excavators life, *Technics Technologies Education Management*, Vol. 7, No. 4, pp. 1620-1629, 2012.
- [21] Bošnjak, S., Petković, Z., Zrnić, N., Dunjić, M., Dragović, B.: Redesign of the Bucket Wheel Excavators Substructures Based on the Comparative Stress – Strain Analysis, *Advanced Materials Research*, Vol. 402, pp. 660-665, 2012.
- [22] Bošnjak, S., Oguamanam, D., Zrnić, N.: The influence of constructive parameters on response of bucket wheel excavator superstructure in the out-of-resonance region, *Archives of Civil and Mechanical Engineering*, Vol. 15, No. 4, pp. 977-985, 2015.
- [23] Gnjatović, N., Bošnjak, S., Stefanović, A.: The dependency of the dynamic response of a two mast bucket wheel excavator superstructure on the counterweight mass and the degree of Fourier approximation of the digging resistance, *Archives of Mining Sciences*, Vol. 63, No. 2, pp. 491-509, 2018.
- [24] Bošnjak, S., Gnjatović N., Milenović I.: From ‘a priori’ to ‘a posteriori’ static stability of the slewing superstructure of a bucket wheel excavator, *Eksplatacja i Niezawodność – Maintenance and Reliability*, Vol. 20, No. 2, pp. 190-206, 2018.
- [25] Bošnjak, S., Gnjatović N., Savićević S., Pantelić M., Milenović I.: Basic parameters of the static stability, loads and strength of the vital parts of a bucket wheel excavator’s slewing superstructure, *Journal of Zhejiang University-SCIENCE A (Applied Physics & Engineering)* Vol. 17, No. 5, pp. 353-365, 2016.

Vlada GašićAssociate Professor
University of Belgrade
Faculty of Mechanical Engineering**Nikola Košanin**MSc Engineer
Novelic d.o.o. Belgrade**Grzegorz Olszyna**PhD Engineer
AGH University of Science and
Technology
Faculty of Mechanical Engineering and
Robotics**Aleksandra Arsić**PhD Student
University of Belgrade
Faculty of Mechanical Engineering

FEA Aspects of the Local Bending stresses at the HEA-section Runway Beams

This paper deals with the local bending stresses at the steel runway beams made of HEA sections. Some aspects of this structural problem are considered here, with usage of finite element analysis (FEA). There are presented three different models and several load cases to obtain the values of local bending stresses which enable the comparison with the results from adopted EN regulative. Specially, it is considered the possible superposition of stresses for adjacent wheel loads. This is done due to restriction in regulative which deals with the geometry of trolley vs. beam width. It is confirmed some inconsistencies in current regulative, along with the occurrence of affected zone in section with possible higher values of stresses near the web. Without consideration of volume, it is noted that distance of adjacent wheels has influence on the level of local stresses.

Keywords : I-section, runway beam, stress, local bending

1. INTRODUCTION

Runway beams are vital parts of every industrial facility. It enables the transport of various payloads throughout the hoist with trolley or underhanging crane (fig. 1). Generally, structure of runway is made of I-section beams because they are very appropriate for bending over section major axis. Steel production process has given several types of shapes, eg. HEA, HEB, IPN, IPE, where every type has its own characteristics for usage which are related to design parameters [1].



Figure 1. Runway beam for hoist with trolley

The subject of this paper is runway beam with HEA section. This type of I-section belongs to the class of parallel, wide flange beams and stands for "strong" beam and is used for the case of heavier payloads over "longer" spans. Even considered as simple structural elements, safety requirements for the runway have to be accomplished and calculated in detail. Primarily, this

implies the design check of stresses, deflection and lateral buckling [2]. On secondary level, it is advised to check the local bending stresses in the bottom flange due to wheel loads. It is highly recommended for beams with HEA section which are more subjected to this phenomenon due to its wider flanges, when compared with other I-sections.

The method of calculation of local bending stresses is given in EC3-6-Crane supporting structures [3]. Along with other requisitions, it is given geometric restriction that distance along the runway beam between adjacent wheels is not less than $1.5b$ where b is the flange width. However, it is not explained the situation when this is not the case and there is only recommendation to adopt conservative approach by superposing the stresses calculated for each wheel load acting separately.

Nowadays, finite element analysis is standard engineering guide where is a lack of experimental results, when is needed understanding of local structural effects or to generate extensive parametric studies [4]. Therefore, the aim of this work is to perform the FEA of the local bending stresses at several cases of the runway beams which consider adjacent wheels distance and their influence on the stresses in the bottom flange.

2. THEORETICAL POSTULATION

The problem of local bending of the I-section beams was noticed since the beginning of the industrial usage of runway beams. There are several approaches for calculation of these stresses, which authors will not emphasize here because of the fact that overview is given in literature [5]. Former engineering practice in this field, on national level, was based on calculation method given by Mendel [6]. Currently, it is common to use approach given in EC3-6 for crane supporting structure or EN 15011 for cranes.

Particularly, the EC3-6 represent the phenomenon of local bending with additional stresses in two directions, σ_{ox} , σ_{oy} , fig. 2.

Correspondence to: Dr Vlada Gašić, Associate Professor
Faculty of Mechanical Engineering,
Kraljice Marije 16, 11120 Belgrade 35, Serbia
E-mail: vgasic@mas.bg.ac.rs

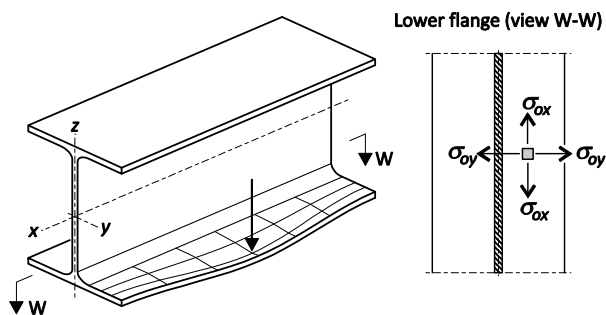


Figure 2. Local bending in the bottom flange

The wheel loads, with intensity noted as $F_{z,Ed}$, produce these stresses which are considered at three locations: 0 (the web-to-flange transition), 1 (centerline of the wheel load) and 2 (outside edge of the flange). The following picture gives general notation of the studied case, with basic parameters of the HEA section such as web thickness (t_w), flange thickness (t_f), flange width (b) and load position with the distance from the edge (n).

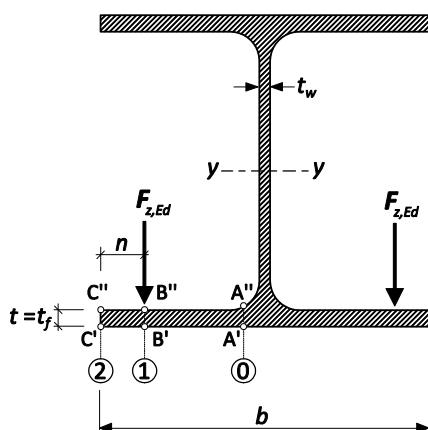


Figure 3. Geometrical postulation

The local longitudinal and transverse bending stresses should be obtained from:

$$\sigma_{ox} = c_x \cdot \frac{F_{z,Ed}}{t^2}, \quad (1)$$

$$\sigma_{oy} = c_y \cdot \frac{F_{z,Ed}}{t^2}, \quad (2)$$

where t is characteristic thickness of the bottom flange, while coefficients c_x , c_y are dependent of the ratio:

$$\mu = \frac{2 \cdot n}{b - t_w}, \quad (3)$$

and calculated for all the three locations, as follows:

$$c_{x0} = 0.050 - 0.580\mu + 0.148e^{3.015\mu}, \quad (4)$$

$$c_{x1} = 2.230 - 1.490\mu + 1.390e^{-18.33\mu}, \quad (5)$$

$$c_{x2} = 0.730 - 1.580\mu + 2.910e^{-6.000\mu}, \quad (6)$$

$$c_{y0} = -2.110 + 1.977\mu + 0.0076e^{6.530\mu}, \quad (7)$$

$$c_{y1} = 10.108 - 7.408\mu + 10.108e^{-1.364\mu}, \quad (8)$$

$$c_{y2} = 0. \quad (9)$$

The above given expressions are used in this form for bottom face of the flange and for upper face it should be used with opposite sign. For clarity purpose, it is given here notation of characteristic points of the three locations with A', B', C' for bottom face and A'', B'', C'' for upper face, fig. 3. From engineering practice, it is familiar to calculate the local stress values for bottom face of the flange due to bigger values of global bending since they are considered together in stress check.

3. FEA MODELS

The physical model is rather simple, as depicted on figure 4, where segment of the runway beam has span L . The payload is located round the mid-section as most critical case for calculation of bending for simple beams. It is assumed that capacity of payload is transmitted on the structure with 4 equal forces, considering that trolleys almost always have 4 wheels. Per each side, the adjacent forces are located with the distance of x_w .

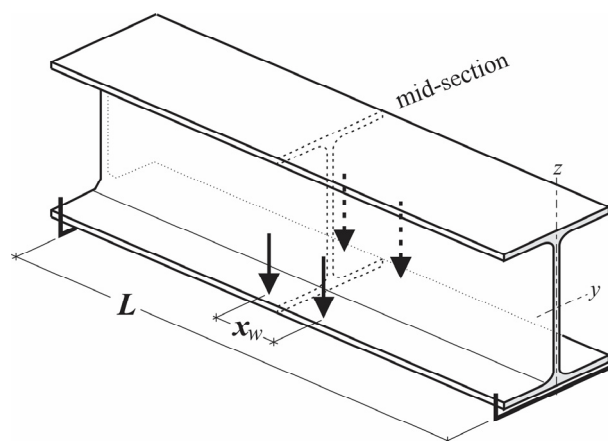


Figure 4. Physical model of the beam segment

There are considered three different models of the beam, HEA 160 (Model 1), HEA 200 (Model 2) and HEA 240 (Model 3), as runway beams are generally made of "small" I-sections. Respectively to chosen beams, the payload of 1 t, 2 t and 3 t are adopted, along with spans of 3 m, 4 m and 6 m. The payload produces forces $F_{z,Ed}$, while span has only physical characters because the intention here is to exclude the global bending. This is done in models with implementation of intermediate supports on the centroid line of the beam.

The main parameters are given in following table, where analysis cases (1 to 6) correspond to variation of the distance of adjacent wheels - x_w . The limit distance is adopted as $1.5b$, as given in standard EC3-6, while minimal distance is adopted according to adjacent wheels geometry for common types of trolleys.

Table 1. Analysis cases

Case	HEA b [mm]	$F_{z,Ed}$ [kN]	L [m]	n [mm]	x_w [mm]
1	160	2.5	3	10	240
2					100
3	200	5	4	12.5	300
4					120
5	240	7.5	6	15	360
6					150

Here, FEA is performed for the insight of the local stress state in bottom flange. All the steel members (S235) are modeled with shell (mostly quadrilateral) elements assuming ideal elastic material. The meshing is done to comply with real geometric parameters and with guidelines for aspect ratio in shell elements usage [7]. This postulation shouldn't exclude other finite elements in further modeling.

4. NUMERICAL RESULTS AND DISCUSSION

The deformation round the middle of the span, due to the title problem, is given at following figure and only has descriptive character.

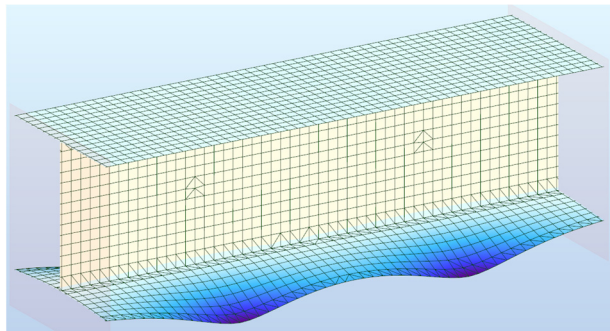


Figure 5. Deformed shape of bottom flange

The stress values are obtained for all the cases. Due to fine mesh the stress values can't be easily visible. Thus, the values are obtained in tabular form for characteristic sections (fig. 6) and corresponding points on the bottom face of flange (i.e. A', B', C'). Moreover, due to symmetry of loads the values are given only for section I and mid-section (the difference of values for section I and II are negligible). The results for Models 1,2,3 are given in following tables.

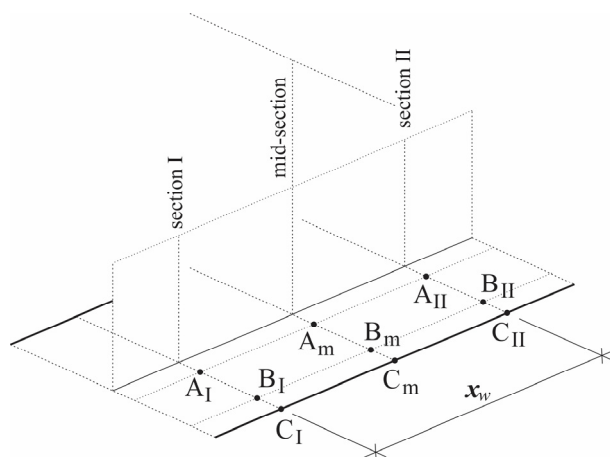


Figure 6. Characteristic points for stress values

Table 2. Model no. 1 – HEA 160

[kN/cm ²]	Case 1 – 240 [mm]		Case 2 – 100 [mm]	
	σ_{ox}	σ_{oy}	σ_{ox}	σ_{oy}
A _I	-1.47	-6.65	-2.24	-7.37
A _m	-1.09	-3.31	-2.51	-7.80
B _I	9.14	4.58	8.18	4.28
B _m	-1.77	-0.49	-0.95	-0.77
C _I	7.20	0.97	6.29	0.99
C _m	-1.89	-0.02	-0.91	-0.09

Table 3. Model no. 2 – HEA 200

[kN/cm ²]	Case 3 – 300 [mm]		Case 4 – 120 [mm]	
	σ_{ox}	σ_{oy}	σ_{ox}	σ_{oy}
A _I	-2.83	-10.92	-3.75	-12.00
A _m	-1.60	-5.28	-3.96	-13.02
B _I	14.78	7.43	13.25	7.02
B _m	-2.84	-0.90	-1.22	-1.04
C _I	11.68	1.29	9.66	1.64
C _m	-3.08	-0.01	-1.16	-0.02

Table 4. Model no. 3 – HEA 240

[kN/cm ²]	Case 5 – 360 [mm]		Case 6 – 150 [mm]	
	σ_{ox}	σ_{oy}	σ_{ox}	σ_{oy}
A _I	-2.28	-9.46	-3.28	-12.42
A _m	-1.85	-5.26	-4.02	-12.82
B _I	14.70	6.97	13.29	6.81
B _m	-2.94	-1.31	-1.64	-1.56
C _I	12.76	0.94	9.47	1.88
C _m	-3.30	0.07	-1.60	0.05

First, it is done tabular comparison of obtained FEA results with the results for local stresses calculated with EC3-6, (1) – (9). This is done for all the three basic models and given in tables 5, 6 and 7.

Table 5. Model no. 1 – HEA 160

[kN/cm ²]	EC3-6		Case 1	
	σ_{ox}	σ_{oy}	σ_{ox}	σ_{oy}
A _I	0.6	-5.7	-1.47	-6.65
B _I	6.7	2.1	9.14	4.58
C _I	5.7	0	7.20	0.97

Table 6. Model no. 2 – HEA 200

[kN/cm ²]	EC3-6		Case 3	
	σ_{ox}	σ_{oy}	σ_{ox}	σ_{oy}
A _I	1	-9.2	-2.83	-10.92
B _I	10.8	3.4	14.78	7.43
C _I	9.3	0	11.68	1.29

Table 7. Model no. 3 – HEA 240

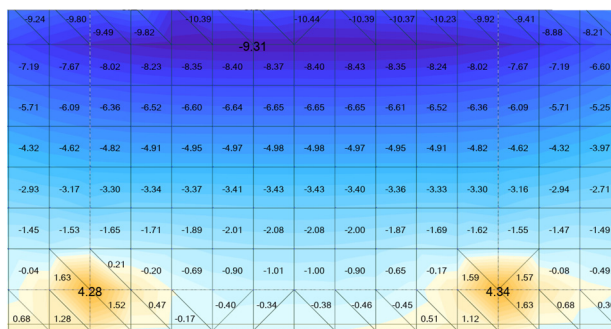
[kN/cm ²]	EC3-6		Case 5	
	σ_{ox}	σ_{oy}	σ_{ox}	σ_{oy}
A _I	1	-9.6	-2.28	-9.46
B _I	11.3	3.5	14.70	6.97
C _I	9.8	0	12.76	0.94

One may see that values obtained with two different methods are in the same range of numbers which stands for basic verification. The results from FEA have generally higher values for all the models and can be considered as the worst case of the title problem due to following: (1) – the section structural plates are modeled as plane shells which elongates the "cantilever" effects for y-direction, and the "free" zone for x-direction (2) – the intermediate supports are located in the planes of load action which disable "distribution" of the strain for x-direction.

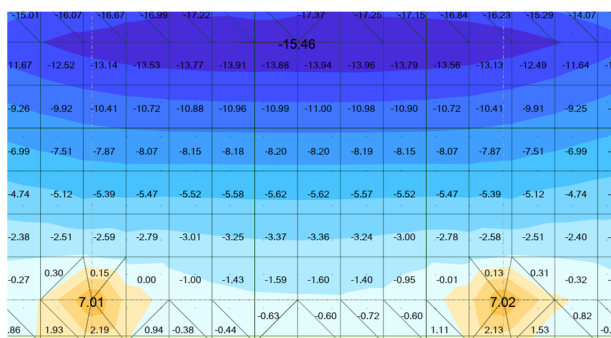
However, for all the models, there is clear difference of signs for σ_{ox} stresses at point A, when EC3-6 results is compared with values obtained with FEA. Thus, these values can't be validated which corresponds with the conclusion in [8].

With previous restrictions, the intention here is to give overview of the possible superposition of the stresses near the mid-section (tables 2 – 4). Cases 1, 3 and

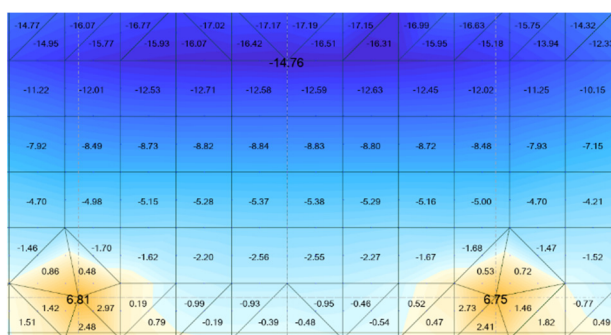
5 show that corresponding points of mid-section has lower values of stresses than for section I where load is applied. Since those cases deal with the distance of $x_w=1.5 b$, the results are preserved to comply with EC3-6. Cases 2, 4 and 6, on the other hand, show clear difference. Mainly, the stresses for points B and C has similar values (mostly lower) for both the distances. This can't be validated due to expected level of mistakes with usage of FEA. However, the difference is bigger for point A where one may find increase of stresses for lower distance of adjacent loads. The corresponding point A_m has also higher values of stresses which show that there is affected zone between the wheels, near the web of section. For example, it is illustrated on following picture for relevant cases with lower distance of adjucent wheels.



a)



b)



c)

Figure 7. Half-flange stresses σ_{oy} , : a) Case 2, b) Case 4, c) Case 6

5. CONCLUSION

FEA is performed here for calculation of local bending stresses of HEA section runway beams. With six cases included, the results are compared for two characteristic distances of adjacent wheels. Values for σ_{ox} for point near the web confirm aspect of inconsistency in EC3-6. Thus, it is advised to check results with previous method, such as given in [9]. Additional validation of this issue has to be done, preferably with theoretical background or with extensive experimental testing on several types of section.

The numerical study in this paper shows possible superposition of adjacent loads. In certain case this corresponds to restriction in EC3-6, because of the affected zone between the wheels, near the web. The authors consider this study as the first step in observing this phenomenon. The general conclusions and large numbers of given values stand for further investigation of local effects of the bottom flange subjected to wheel loads.

ACKNOWLEDGMENT

This work is a contribution to the Ministry of Education, Science and Technological Development of Republic of Serbia founded project TR 35006.

REFERENCES

- [1] Seesselberg, C.: *Kranbahnen-Bemessung und konstruktive Gestaltung nach Eurocode*, Beuth Verlag GmbH, Berlin, 2014.
- [2] Gašić, V., Zrnić, N., Milojević, G.: Loading capacity curves for design of I-section runway beams, XXI International Conference MHCL 15, Vienna, 2015.
- [3] EN 1993-6: Design of steel structures – Part 6: Crane supporting structures, European Committee for Standardization, 2007.
- [4] Kindmann, R., Kraus, M.: *Steel Structures-Design using FEM*, Wilhelm Ernst&Sohn, Berlin, 2011.
- [5] Petersen, C.: *Stahlbau*, Vieweg Verlag, 3. Auflage, Wiesbaden, 1994.
- [6] Mendel, G.: *Berechnung der Tragerflanschbeanspruchung mit Hilfe der Plattentheorie*, Fordern und Heben, 14/1972.
- [7] Spyarakos, C., Raftoyiannis, J.: *Finite Element Analysis in Engineering Practice*, Algor, Pittsburgh, 1997.
- [8] Cvijović, A., Bošnjak, S.: The impact of the transition radius lower flange-web on local stress of monorail crane girder, Trans. FME, Vol. 45, No. 4, pp. 543-547, 2017.
- [9] Gašić, V., Zrnić, N.: Comparative overview of stress field of HEA section runway beams according to bottom flange bending, IX International Conference DEMI, Banja Luka, 2009.

Validation of the number of buckets on the working device of a bucket wheel excavator from the aspect of dynamic behavior of the system

Nebojša Gnjatović

Assistant Professor
University of Belgrade
Faculty of Mechanical Engineering

Srdan Bošnjak

Full Professor
University of Belgrade
Faculty of Mechanical Engineering

Ivan Milenović

Research Assistant
University of Belgrade
Faculty of Mechanical Engineering

Aleksandar Stefanović

Research Assistant
University of Belgrade
Faculty of Mechanical Engineering

The method for validation of the number of buckets on the working device of a bucket wheel excavator from the aspect of dynamic behaviour of the system, partially presented in this paper, was developed on the basis of the original spatial reduced dynamic model of the bucket wheel excavator with two masts, which enables modal analysis and analysis of the dynamic response of the system for continuous variation of constructional parameters and parameters of excitation. The set of 16 seemingly-acceptable solutions, all of which satisfied the rigid design restrictions which were: (a) use of the same bucket wheel drivetrain, (b) preservation of the theoretical capacity, (c) possibility of the excavation of soil of the fourth category and (d) preservation of the superstructure centre of gravity position, was analyzed. On the basis of limiting vertical and lateral accelerations, derived from dynamic coefficients prescribed by the code DIN 22261-2, of the bucket wheel centre, which for a proper geometrically-designed bucket wheel excavator structure represents a well grounded indicator of its dynamic behaviour, 14 out of 16 analyzed solutions were discarded, yielding the set of possible solutions to only 2, the originally designed one (with 17 buckets) and the solution with 20 buckets installed on the bucket wheel.

Keywords: bucket wheel excavator, dynamic behaviour analysis, limiting accelerations, number of installed buckets

1. INTRODUCTION

Due to the perennial exploitation in extremely harsh working conditions (for example, more than half of the BWEs operating in open-cast mines in Serbia are in exploitation for more than 30 years [1]), failures and breakdowns of the bearing structures and mechanical subsystems [2-7] occur relatively frequently. The most important consequence of the aforementioned failures, apart from the risk for safety and life of workers, is the downtime of the machine, which accumulates extremely high financial losses. Modernization of the BWE fleet is conducted in two equally represented directions. Apart from the acquisition of new units, redesign of the dated and obsolete machines and their subsystems is also executed in order to reduce the power consumption, reduce the maintenance costs by decreasing the number of scheduled repairs and, most importantly, to increase the productivity by reducing the number of accidental stops. Apart from the age of excavating units, relatively frequent failures and accidental stops are also the consequence of the everlasting tendency towards improving the performances of BWEs, which has not been adequately supported by the calculation methods

and technical regulations, drawing a conclusion that it was practically impossible to carry out a detailed stress-strain analysis and the dynamic behaviour analysis during the stage of their design, as stated in [8]. Redesign, conducted in order to achieve modernization of the machine, is a procedure inevitably followed by the alternation of operating (constructional) parameters which strongly influence the structural behaviour of the BWEs.

The excavating subsystem, consisting of a bucket wheel (BW) with its belonging drivetrain, is the most important part of a BWE, since its construction determines the output and total behaviour of the machine. Although it is clearly stated, by the literature relevant to the field of BWEs, that the redesign of an excavating system, in order to correct the design errors, would be difficult and expensive, if at all possible after the machine has been constructed [9], in the modern engineering practice there is a rising number of scientific institutions and research and development centres dealing with this extremely complex engineering challenge. As a part of the overall modernization of the excavating units operating on the open-cast mines in the Oltenia coal basin, which represents the backbone of the lignite production in Romania, which started as early as 1995, 17 out of 33 BWEs of the same design (SchRs 1400), responsible for the 80% of total lignite and overburden exploitation on the said surface mine, have been subjected to the process of reconstruction [10], whose key aspect was based on the replacement of the existing BW drivetrain (essentially replacing the

Correspondence to: Dr Nebojša Gnjatović, Ass. Professor
Faculty of Mechanical Engineering,
Kraljice Marije 16, 11120 Belgrade 35, Serbia
E-mail: ngnjatovic@mas.bg.ac.rs

gearbox of the classical design with a planetary one) and the change in the number of buckets on the BW (9 filling + 9 cutting with 20 filling-cutting buckets) [11]. Aside from the analysis of the influence of change in the number of buckets on the BW on the modal characteristics of the bucket wheel steel structure [12], additional information on the consequences of said changes on the dynamic behaviour of the BWE were not available to the authors of this paper. Similar project, on a smaller scale, was conducted in the Kolubara open-pit mine in Serbia, when the 55-year old BWE SchRs 350 has been subjected to the process of redesign of the excavating subsystem [13], which included substituting the planetary gearbox for the existing spur-gearred one, as well as the installation of two additional buckets on the BW (increasing the total number of 8 to 10). In paper [14], the analysis of excitation due to the resistance to excavation and conclusions on the potential of a more favourable influence of the said excitation on the dynamic behaviour of the system, have been presented. Negative dynamic effects, which have been diagnosed experimentally, gave rise to the need to replace the existing bucket wheels on the two conceptually-different BWEs (SchRs 4600.50 and SchRs 4600.30), operating in the Belchatow surface mine in Poland [15]. On the basis of the experimental and numerical modal analyses of the entire structures, conclusions have been drawn on the design of a unique BW steel structure and the corresponding number of buckets which would satisfy the requirements for the safe operation of both BWEs without changes to the existing drivetrains.

To the authors' knowledge, none of the aforementioned cases provide any information regarding the influence of variation of the number of buckets on the BW on the dynamic response of the system. As it will be shown in the remainder of this paper, said variation is a key parameter because of its influence on the overall dynamic behaviour of the machine and, as such, is vital in the process of selection and validation of the appropriate design solutions. The method for validation of the number of buckets on the working device of a BWE from the aspect of dynamic behaviour, will be presented using the technical characteristics of the BWE SchRs 1600, Fig 1, as the base model.



Figure 1. BWE SchRs 1600 in operating conditions: mass (with mobile conveyor) 3345t, theoretical capacity 6600m³/h

2. REDUCED SPATIAL DYNAMIC MODEL

The analysis of the dynamic responses of large scale machines such as bucket wheel excavators can often prove difficult to perform due to several obstacles such as the extreme complexity of the corresponding dynamic system, small number of modifiable parameters after the mounting of the structure and the limitation of the finite element analysis (FEA), which is reflected on the discrete nature of the method.

The analysis of the dynamic behaviour of the BWE SchRs 1600 superstructure was performed on the basis of a reduced spatial dynamic (RD) model with 64 DOF. The model was developed and validated according to the procedures presented in [16-18]. Validation of the said procedure, which supplements the finite element method in its application in the dynamic behaviour analysis of the BWE spatial truss structures, has been performed on the basis of relevant measurements and used to develop models and conduct dynamic response analysis of excavators with different design conceptions [19,20]. The model, presented in Fig. 2, for which the development procedure is enclosed in detail in [21], enables modal analysis as well as analysis of the dynamic response in a continuous domain of both constructional and parameters of excitation variation.

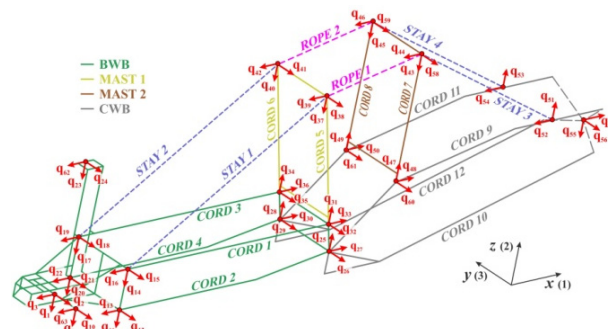


Figure 2. A reduced spatial dynamic model of the BWE SchRs 1600 [21]

Although BWEs are constructions with changeable configuration, which makes the analysis of their dynamic behaviour extremely complex [17,22,23], according to the findings presented in [18], the influence of the BW boom inclination angle on modal characteristics of the analyzed excavator is not significant. Thus, the horizontal position of the BW boom has been adopted as referent for further analysis.

3. SELECTING THE APPROPRIATE DESIGN SOLUTIONS

The choice of number of buckets, from the aspect of the dynamic behaviour of the machine, was conducted in three stages, with respect to the extremely rigid design restrictions which are, as already stated:

- use of the same drivetrain,
- preservation of the theoretical capacity,
- possibility of the excavation of soil (overburden) of the fourth category, dominantly present on the "Kolubara" open pit mine and
- preservation of the superstructure centre of gravity position.

In the first stage, the analysis was conducted for continuous variation of the number of buckets in the range from 9 to 24 buckets on the BW. Although the aforementioned parameter is of discrete nature, the analysis was conducted in a continuous domain in order to perceive the influence of the proximity of certain resonant states on the dynamic response of the construction. After defining the set of possible solutions using the limiting accelerations, derived from dynamic coefficients prescribed by the code [24] as a cut-off criterion, the influence of the adhered material (incrustation on the bucket wheel and bucket wheel chute blockage) on the modal characteristics and dynamic response of the system was analyzed. In the final stage, the mass of the bucket wheel steel structure was varied in the range of $\pm 20\%$ of the original solution, while preserving the centre of gravity position by modifying the mass of the counter-weight.

Some results of the first stage of the research will be presented in the paper. Namely, for a proper geometrically-designed BWE structure the BW centre (point of penetration of the BW shaft axis through the vertical symmetry plane of the buckets) presents a referent point whose dynamic response is a well grounded indicator of the dynamic behaviour of the superstructure. In the RD model of the BWE, motion of the BW centre (BWC) is defined with three generalized coordinates (q_1 , q_2 , q_3) [21]. Maximum vertical ($a_{1,\max}$) and lateral ($a_{2,\max}$) accelerations of the said referent point will be used for determining the appropriate design solution in terms of the dynamic behaviour.

3.1 Excitation loads assumptions

Identification of the external loads caused by the resistance to excavation was performed according to the procedures presented in [25,26]. The obtained external loads were approximated with trigonometric polynomials with five harmonics, using the Fourier coefficients, with respect to the results and conclusions made in [20].

The dependence of the moment of excavation (M_T)

on the number of buckets (n_k) on the bucket wheel is shown in Fig 3.

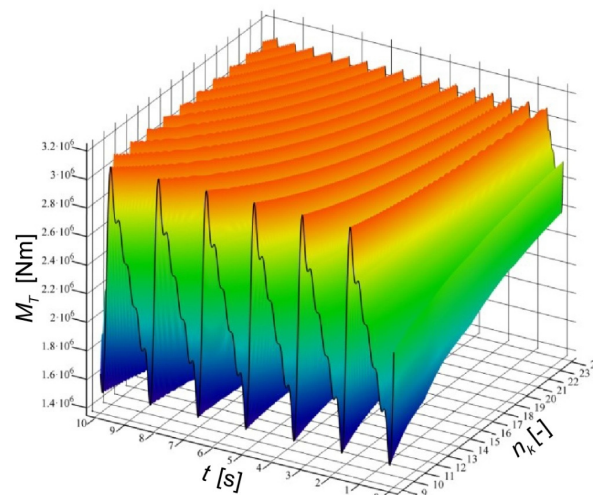


Figure 3. Moment of excavation

From the presented diagram, it is evident that the maximum values of loads caused by the resistance to excavation remain constant, which is a consequence of the adopted parameters of the BW drive, which are unchangeable. Mean values of the loads ($M_{T,m}$) rise, while the amplitude values ($M_{T,a}$) decline with the increase of the number of buckets that are in interaction with the soil, Table 1. It can also be observed that the value of the first (and therefore higher excitation frequencies) rises as the number of buckets on the BW is increased.

If the designed state of the excavator (17 buckets on the wheel) is taken as the basis for the analysis of the results presented in Table 1, it can be concluded that, for the case of 9 buckets on the BW, the mean values of loads caused by the resistance to excavation are 12.5% lower, while the load amplitudes are 65.5% higher. For the case of the bucket wheel with 24 buckets, mean values of loads are 4.7% higher, and load amplitudes are 25.5% lower than those of the designed state, Table 2. Values of excitation frequencies are in the range between -47.1% and +41.2%.

Table 1. Dependence of the moment of excavation and the first frequency of excitation on the number of buckets on the bucket wheel

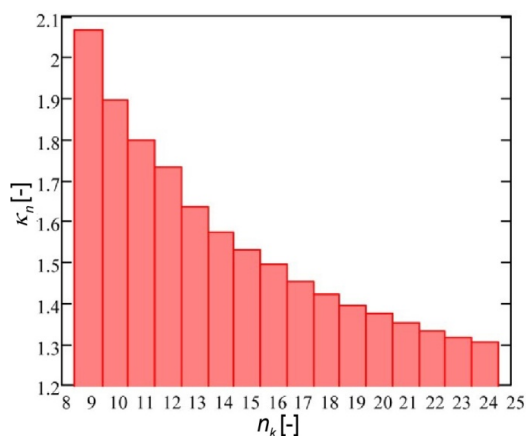
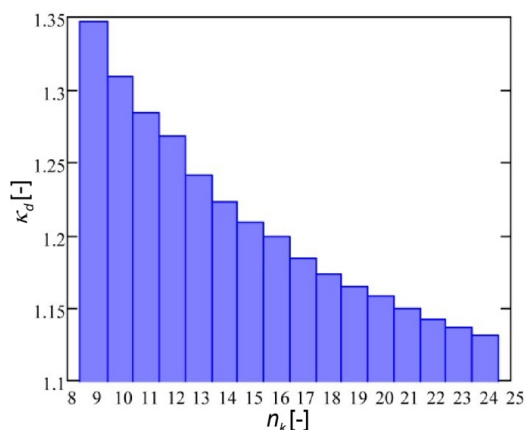
$n_k(-)$	9	10	11	12	13	14	15	16
$M_{T,m}(\text{kNm})$	2296.1	2363.2	2408.1	2439.8	2492.6	2530.4	2558.6	2580.3
$M_{T,a}(\text{kNm})$	797.4	730.3	685.4	653.7	600.9	563.1	534.9	513.2
$f_{E1}(\text{Hz})$	0.612	0.680	0.748	0.816	0.885	0.953	1.021	1.089
$n_k(-)$	17	18	19	20	21	22	23	24
$M_{T,m}(\text{kNm})$	2611.6	2635.8	2655	2670.5	2691.3	2708.1	2722	2733.6
$M_{T,a}(\text{kNm})$	481.9	457.7	438.5	423	402.2	385.4	371.5	359.9
$f_{E1}(\text{Hz})$	1.157	1.225	1.293	1.361	1.429	1.497	1.565	1.633

Table 2. Percent deviation of the moment of excavation and the frequencies of excitation

$n_k(-)$	9	10	11	12	13	14	15	16
$\left[\frac{(M_{T,m,n_k} - M_{T,m,DES^*})}{M_{T,m,DES}}\right]100 (\%)$	-12,1	-9,5	-7,8	-6,6	-4,6	-3,1	-2,0	-1,2
$\left[\frac{(M_{T,a,n_k} - M_{T,a,DES})}{M_{T,a,DES}}\right]100 (\%)$	65,5	51,5	42,2	35,6	24,7	16,8	11,0	6,5
$\left[\frac{(f_{E,j^{**},n_k} - f_{E,j,DES})}{f_{E,j,DES}}\right]100 (\%)$	-47,1	-41,2	-35,3	-29,4	-23,5	-17,6	-11,8	-5,9
$n_k(-)$	17	18	19	20	21	22	23	24
$\left[\frac{(M_{T,m,n_k} - M_{T,m,DES})}{M_{T,m,DES}}\right]100 (\%)$	0,0	0,9	1,7	2,3	3,1	3,7	4,2	4,7
$\left[\frac{(M_{T,a,n_k} - M_{T,a,DES})}{M_{T,a,DES}}\right]100 (\%)$	0,0	-5,0	-9,0	-12,2	-16,5	-20,0	-22,9	-25,3
$\left[\frac{(f_{E,j,n_k} - f_{E,j,DES})}{f_{E,j,DES}}\right]100 (\%)$	0,0	5,9	11,8	17,6	23,5	29,4	35,3	41,2

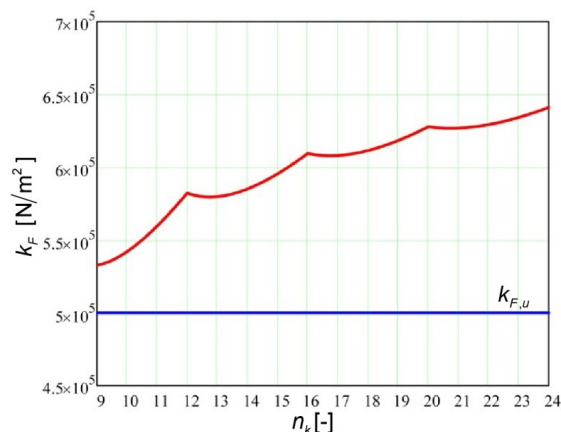
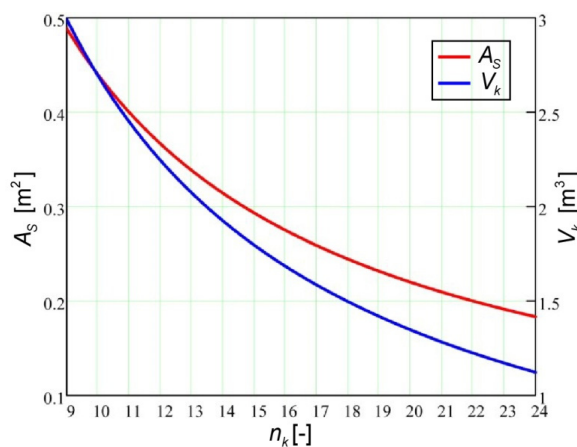
*designed state of the construction, $n_k = 17$ ** $j = 1,2...5$ – frequency of excitation

The non-uniformity of loads caused by the resistance to excavation is expressed with the non-uniformity coefficient (κ_n), which represents the ratio between the maximum and minimum load values, Fig 4, as well as with the coefficient of dynamism (κ_d), which is the ratio of maximum and mean load values, Fig 5.

**Figure 4. Coefficient of non-uniformity****Figure 5. Coefficient of dynamism**

Based on the experimental-analytical research, conducted by the Mining institute of Zemun [27], the characteristics of soil found in the open pit mines of Serbia mostly befall under the IV category. According to [27], the specific resistance to excavation reduced to the cutting surface (k_F) befalls in the range between 3.1

and 6.4 daN/cm². Papers [28,29], which simulate the loads on the bucket wheel excavators of three different designs, each operating in the open pit mine "Kolubara", adopt the average specific resistance to excavation of $k_{F,u} = 5.0$ daN/cm². Based on the presented data, it can be concluded that each of the analysed cases of the number of buckets on the BW could perform the excavation of the soil of the IV category, Fig 6.

**Figure 6. Specific resistance to excavation****Figure 7. Dependence of the chip cross section area and the capacity of the bucket of the number of buckets installed on the BW**

Chip cross section area, and therefore nominal bucket capacity, decreases with the increase of the

number of buckets on the bucket wheel, Fig 7. In order to achieve the designed theoretical capacity, which is the basic condition of the analysis, the capacity of a bucket, for cases of 9 and 24 buckets on the BW, has to be ~89% higher and ~24% lower than that of the designed state, respectively.

Reduction of the chip cross section area results in the increase of the specific resistance to excavation. Specific resistance to excavation which the system for the excavation of material with 9 buckets on the BW is able to overcome is 12.4% lower, while in the case of

24 buckets this resistance is 5.4% higher than that of the designed state.

3.2 Determining the set of possible solutions

Comparative display of the first fourteen natural frequencies and five frequencies of excitation on the range from 9 to 24 buckets is presented in Fig 8. In the analysed interval of the number of buckets, for frequency ranging up to 8 Hz, 31 resonant states are observed. The values of analyzed parameter which lead the system into resonant states are presented in Table 3.

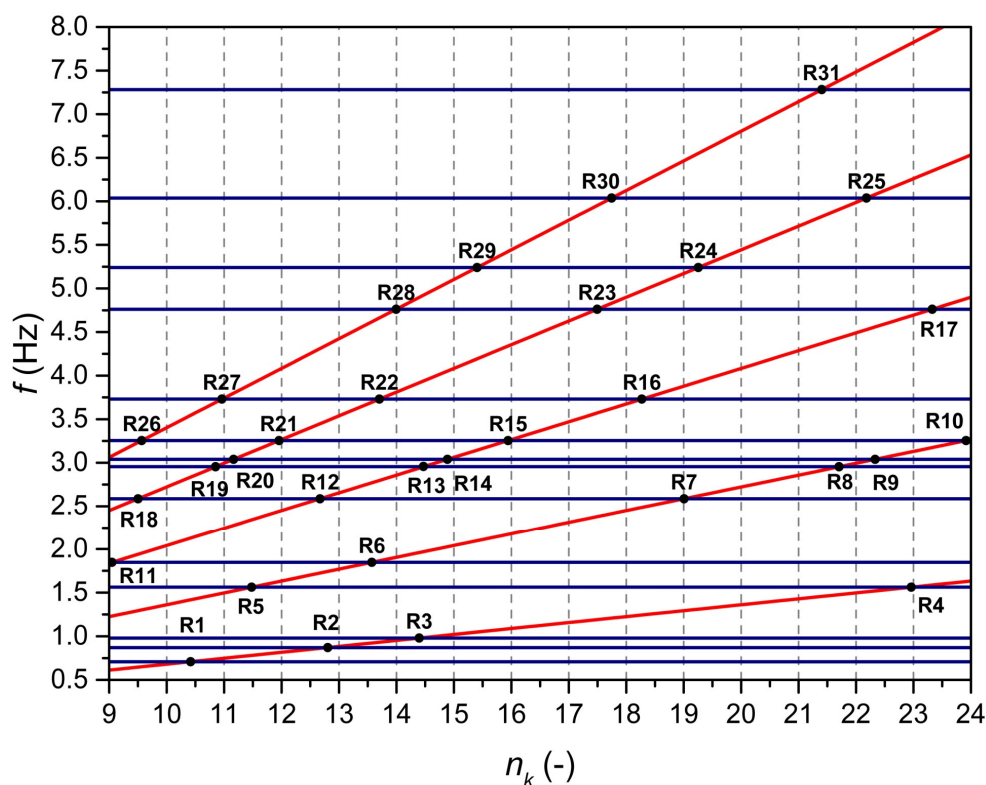


Figure 8. Comparative display of natural frequencies (blue coloured lines) and frequencies of excitation (red coloured lines) dependant on the number of buckets (resonances are marked with black dots and label R_i , $i=1,2,\dots,31$)

Table 3. The order of resonance and values of the analysed parameter

Order*	I				II			
Label	R1	R2	R3	R4	R5	R6	R7	R8
$n_k(-)$	10.42	12.8	14.4	22.96	11.48	13.57	19.01	21.71
Order	II		III					
Label	R9	R10	R11	R12	R13	R14	R15	R16
$n_k(-)$	22.33	23.92	9.05	12.67	14.47	14.89	15.94	18.27
Order	III	IV						
Label	R17	R18	R19	R20	R21	R22	R23	R24
$n_k(-)$	23.33	9.50	10.85	11.17	11.96	13.70	17.50	19.26
Order	IV	V						
Label	R25	R26	R27	R28	R29	R30	R31	
$n_k(-)$	22.18	9.57	10.96	14.00	15.40	17.75	21.40	

* the order of resonance is determined in regard to frequencies of excitation

Based on the results presented in Table 3, it can be concluded that, for the analyzed number of buckets on the BW ($n_k=9, 10, \dots, 24$), only one case leads to the appearance of a resonant state. Said resonant state occurs for the design solution which includes 14 buckets on the BW, which can be discarded based on the results of a modal analysis alone.

However, based on the presented data, comments on the effects of the proximity to certain resonant states on the response of the system cannot be made, nor can any conclusion on the quality of the adopted design be derived. This is because modal analysis, as it is well known, cannot provide any insight on the ranges of resonant areas, thus, in combination with the lack of proper recommendations by the known literature, it is necessary to perform the analysis of the dynamic system response.

German standard [24] prescribes the limiting accelerations of the referent points, which are used as a cut-off criterion for the diagnosis of negative dynamic effects during the experimental and analytical analysis of the dynamic response of BWEs [4,19,30-32].

Maximum values of the vertical and lateral accelerations of the BWC of $a_{V,zul} = 1 \text{ m/s}^2$ and $a_{Q,zul} = 0,167 \text{ m/s}^2$, respectively, are prescribed by the said standard, but it does not prescribe its maximum allowed axial acceleration. In the preliminary stage of the process of selection of the number of buckets on the BW, the maximum values of vertical and lateral accelerations of this referent point, Figs 9 and 10, have been used to determine the number of buckets which would satisfy the criteria prescribed by the standard.

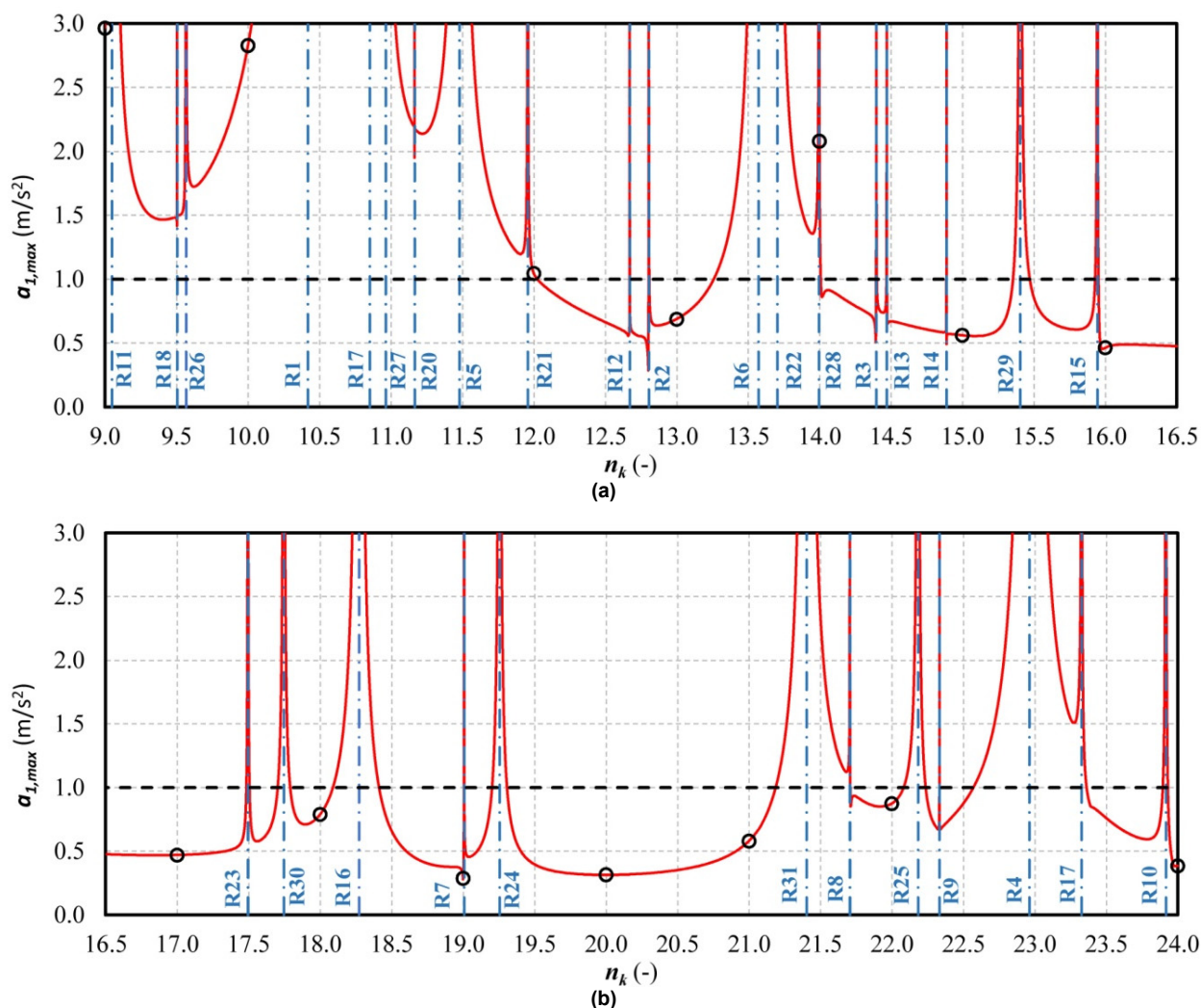


Figure 9. Maximum vertical accelerations of the BW centre: (a) $n_k = 9 \div 16.5$; (b) $n_k = 16.5 \div 24$ (red coloured line presents maximum vertical accelerations for continuous variation of n_k , blue dash-dot lines are resonances, black circles are values of maximum vertical accelerations for $n_k=9, 10, \dots, 24$, while the limiting vertical acceleration of the BWC, $a_{V,zul} = 1 \text{ m/s}^2$, is presented with black dash-dash line)

Table 4. Maximum vertical accelerations of the BWC for $n_k=9, 10, \dots, 24$

$n_k(-)$	9	10	11	12	13	14	15	16
$a_{1,max} \text{ (m/s}^2\text{)}$	2.964	2.826	3.979	1.045	0.687	2.078	0.560	0.462
$n_k(-)$	17	18	19	20	21	22	23	24
$a_{1,max} \text{ (m/s}^2\text{)}$	0.469	0.787	0.287	0.313	0.579	0.874	9.487	0.383

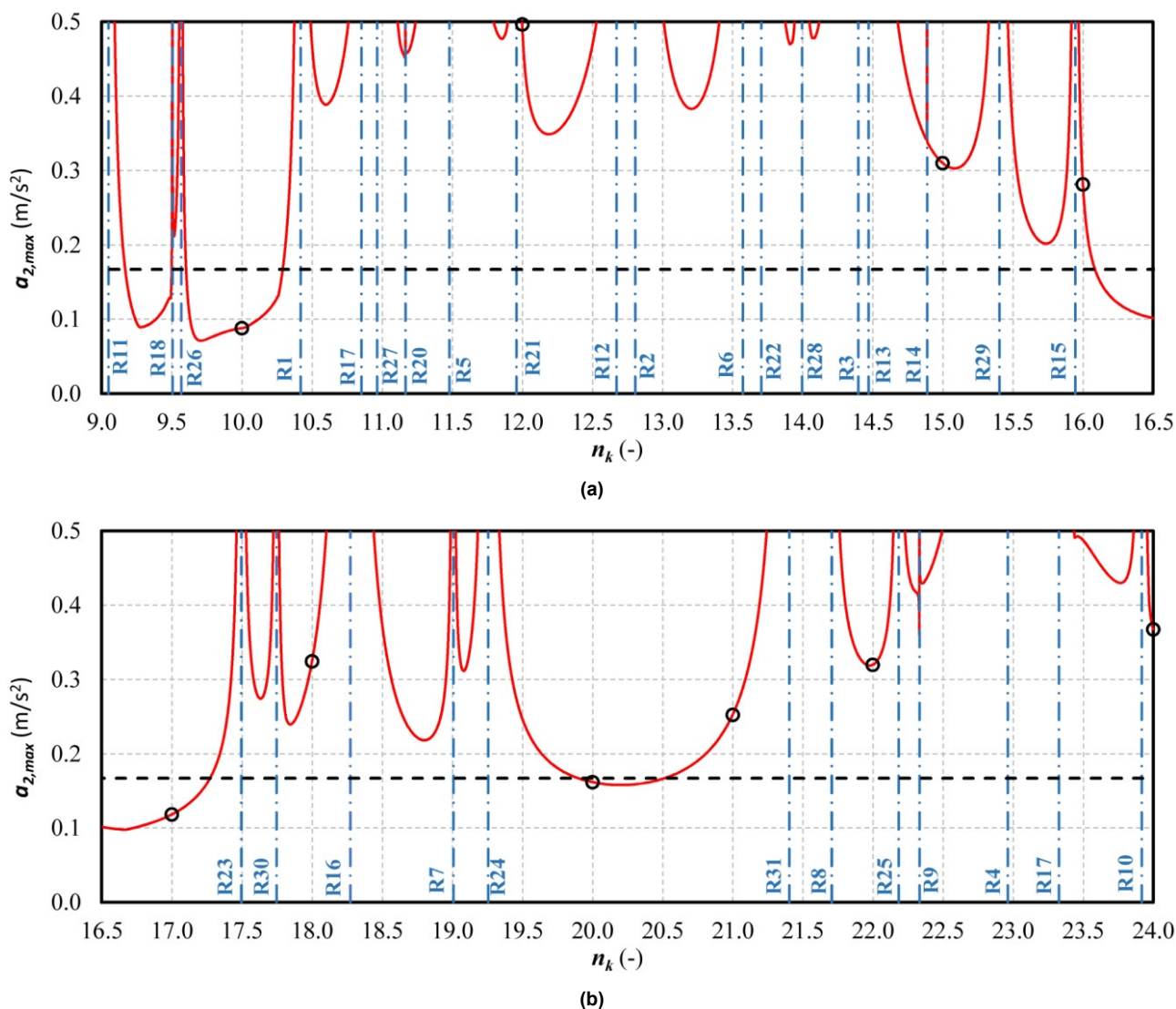


Figure 10. Maximum lateral accelerations of the BW centre: (a) $n_k = 9 \div 16.5$; (b) $n_k = 16.5 \div 24$ (red coloured line presents maximum lateral accelerations for continuous variation of n_k , blue dash-dot lines are resonances, black circles are values of maximum lateral accelerations for $n_k = 9, 10, \dots, 24$, while the limiting lateral acceleration of the BWC, $a_{Q,zul} = 0.167 \text{ m/s}^2$, is presented with black dash-dash line)

Table 5. Maximum lateral accelerations of the BWC for $n_k = 9, 10, \dots, 24$

$n_k(-)$	9	10	11	12	13	14	15	16
$a_{2,max} \text{ (m/s}^2\text{)}$	0.617	0.088	1.461	0.496	0.516	2.652	0.310	0.281
$n_k(-)$	17	18	19	20	21	22	23	24
$a_{2,max} \text{ (m/s}^2\text{)}$	0.118	0.324	1.098	0.162	0.252	0.32	5.972	0.367

Based on the data presented in Fig 9 and Table 4, it can be concluded that 6 out of 16 possible design variants do not satisfy the criterion of limiting vertical acceleration of the BWC. That includes the variant with 14 buckets on the BW, which has already been discarded after the modal analysis.

The lateral acceleration of the BWC has a significantly higher sensitivity to the proximity to the resonant states, thus resulting in only 3 out of 16 considered variants being adequate when this cut-off criterion is considered, Fig 10 and Table 5.

It is interesting to note that the design variant with 10 buckets on the BW satisfies the lateral acceleration criterion but, at the same time, this cut-off parameter has insufficient sensitivity to the appearance of the first order resonance (R1) whose modal deflection shape (see Figs 7(a) and 7(b) in [21]), singles out the vibrations of the system in the vertical plane as the dominant form of the system oscillations. With that in mind, said variant has been discarded, reducing the set of possible solutions to only 2 – the originally designed one and the variant with 20 buckets on the BW.

4. DISCUSSION AND CONCLUSION

Out of the 16 seemingly-acceptable solutions, all of which satisfied the rigid design restrictions (defined in the 3rd chapter of this paper), one was discarded based on the results of the modal analysis alone. By introducing the criterion of limiting accelerations of the bucket wheel centre, prescribed by the code DIN 22261-2, 13 more solutions were found to be unsatisfactory, thus reducing the set of possible solutions to just 2, confirming the fact that, as is also stated in the relevant literature, simultaneously reconstructing the bucket wheel and ensuring there are no changes to the safe operation of the machine is an extremely difficult task. This implies that any attempts at drawing conclusions without prior analyses of the dynamic response of the system may lead to fallacies.

Namely, the results of the modal analysis, on their own, without any additional insight such as knowing the energetic potential of the 31 resonances of the first and higher order, all of which appear in the low-frequency range (below 8 Hz), do not provide enough information for determining the appropriate variant solution. This fact is further supported by the lack of any relevant guidelines for assessing the width of the resonant areas in literature dealing with this class of machines.

The results obtained from the analysis of the dynamic response of the bucket wheel centre, lead to the following conclusions:

- Limiting vertical acceleration of the BWC cannot be the sole criterion for validation since it eliminates only 6 out of 16 possible design variants;
- When the limiting lateral acceleration of the BWC is used as the cut-off parameter, 13 out of 16 solutions are discarded, leading to a conclusion that the lateral acceleration of the BWC has a significantly higher sensitivity to the proximity to the resonant states;
- None of the analysed cut-off criteria are sufficiently sensitive to be applied on their own, and therefore have to be used in conjunction as presented in the example of 10 buckets installed on the bucket wheel.

Conclusions on the validity of the remaining two design solutions (the originally designed one and the variant with 20 buckets on the bucket wheel) can be derived only after the following additional investigations are conducted:

- the analysis of response of the remaining referent points of the dynamic system. This is required because in some modes the majority of the potential energy is generated by the substructures other than the bucket wheel boom [21];
- the analysis of the influence of the additional mass on the bucket wheel body which is the consequence of inevitable soiling. This is supported by the fact that, for the design solution with 20 buckets on the bucket wheel, the maximum lateral acceleration of the bucket wheel centre is only 3% lower than the limiting acceleration;
- the impact of differences between the masses of the reconstructed bucket wheel and the original design solution on the dynamic behaviour of the entire system, while accounting for the preservation of the position of the superstructure centre of gravity.

Just from the results presented in this paper, multiple observations have been made, all of which attest to the superiority of the 20-bucket redesign variant over the original design with 17 buckets on the bucket wheel, including:

- the first and therefore the remainder of the excitation frequencies of the 20-bucket variant are 17.6% higher than those of the original solution;
- the coefficients of dynamism and non-uniformity are 2.2% and 5.2% lower for the 20-bucket variant, respectively;
- the 20-bucket redesign variant is able to overcome 3.3% higher resistance to excavation.

Using the reduced spatial dynamic model of a bucket wheel excavator with two masts superstructure, with the introduction of the limiting accelerations of the referent system points, it is possible to avoid the appearance of negative dynamic effects as early as during the machine's design stage. This way, the risk of failures and breakdowns of substructures of the considered class of bucket wheel excavators is significantly reduced.

The results presented in this paper represent a contribution to the field of dynamic behaviour of the bucket wheel excavators, even more so having in mind the fact that, in engineering practice and the effective technical regulations, insufficient familiarity with the dynamic processes is compensated with use of the quasi-static approach.

The development of the procedure for validating the number of buckets on the bucket wheel from the aspect of the dynamic behaviour of the system, whose fundamental steps are presented in this paper, represents an important step forward in defining the constructional parameters of this class of machines for continuous excavation.

ACKNOWLEDGMENTS

This work is a contribution to the Ministry of Education, Science and Technological Development of Serbia funded project TR 35006.

The authors would like to express their gratitude to The Joint Japan-Serbia Center for the Promotion of Science and Technology for providing the resources to conduct simulations.

REFERENCES

- [1] Bošnjak, S., Arsić, M., Zrnić, N., Rakin, M., Pantelić, M.: Bucket wheel excavator: integrity assessment of the bucket wheel boom tie – rod welded joint, *Eng Fail Anal*, Vol. 18, No. 1, pp. 212-222, 2011.
- [2] Rusiński, E., Czmochocki, J., Iluk, A., Kowalczyk, M.: An analysis of the causes of a BWE counterweight boom support fracture, *Eng Fail Anal*, Vol. 17, No. 1, pp. 179-191, 2010.
- [3] Rusiński, E., Moczko, P., Kaczynski, P.: Structural modifications of excavator's bucket wheel by the use of numerical methods, *Solid State Phenomena*, Vol. 165, pp. 330-335, 2010.

- [4] Rusiński, E., Czmochoński, J., Moczko, P., Kowalczyk, M., Pietrusiak, D., Przybyłek, G., Smolnicki, T., Stańco, M.: *Assessment of the Technical Condition of Mining Machines* (in Polish), Oficyna Wydawnicza Politechniki Wrocławskiej, Wrocław, 2015.
- [5] Savković, M., Gašić, M., Arsić, M., Petrović, R.: Analysis of the axle fracture of the bucket wheel excavator, *Eng Fail Anal*, Vol. 18, No. 1, pp. 433-441, 2011.
- [6] Jovančić, P., Ignjatović, D., Tanasijević, M., Maneski, T.: Load-bearing steel structure diagnostics on bucket wheel excavator, for the purpose of failure prevention, *Eng Fail Anal*, Vol. 18, No. 4, pp. 1203-1211, 2011.
- [7] Bošnjak, S., Momčilović, D., Petković, Z., Pantelić, M., Gnjatović, N.: Failure Investigation of the Bucket Wheel Excavator Crawler Chain Link, *Eng Fail Anal*, Vol. 35, pp. 462-469, 2013.
- [8] Bošnjak, S., Zrnić, N.: Dynamics, failures, redesigning and environmentally friendly technologies in surface mining systems, *Arch Civ Mech Eng*, Vol. 12, No. 3, pp. 348-359, 2012.
- [9] Durst, W., Vogt, W.: *Bucket Wheel Excavator*, Trans Tech Publications, Clausthal-Zellerfeld, 1988.
- [10] Predoiu, I.C., Antonie, D., Pop, C.R., Teodorescu, M.A., Balacescu, S.: Current issues of the lignite deposit exploitation in Romania, *Proceedings of the 24th World Mining Congress*, Brazilian Mining Association, Rio de Janeiro, pp. 23-31, 2016.
- [11] Dumitrescu, I., Boyte, A., Ghioc, S.: Rehabilitation of the working flow line at lignite open-casts located in Oltenia, *Annals of the University of Petrosani - Mining Engineering*, Vol. 6, No. 33, pp. 177-187, 2005.
- [12] Vilceanu, F.I., Iancu, C.: Bucket wheel rehabilitation of ERC 1400-30/7 high-capacity excavators from lignite quarries, *IOP Conf Ser-Mat Sci*, Vol. 161, pp. 1-11, 2016.
- [13] Bošnjak, S., Petković, Z., Dunjić, M., Gnjatović, N., Đorđević, M.: Redesign of the vital subsystems as a way of extending the bucket wheel excavators life, *Tech Technol Educ Ma*, Vol. 7, No. 4, pp. 1620-1629, 2012.
- [14] Bošnjak, S., Petković, Z., Đorđević, M., Gnjatović, N.: Redesign of the Bucket Wheel Excavating Device, *Proceedings of the 19th International Conference MHCL*, University of Belgrade, Faculty of mechanical engineering, Belgrade, pp. 123-128, 2009.
- [15] Rusiński, E., Dragan, S., Moczko, P., Pietrusiak, D.: Implementation of experimental method of determining modal characteristics of surface mining machinery in the modernization of the excavating unit, *Arch Civ Mech Eng*, Vol. 12, No. 4, pp. 471-476, 2012.
- [16] Bošnjak, S., Oguamanam, D., Zrnić, N.: On the dynamic modelling of bucket wheel excavators, *FME Transactions*, Vol. 34, No. 4, pp. 221-226, 2006.
- [17] Bošnjak, S., Gnjatović, N.: The influence of geometric configuration on response of the bucket wheel excavator superstructure, *FME Transactions*, Vol. 44, No. 3, pp. 313-323, 2016.
- [18] Gnjatović, N.: *Influence of constructional parameters and parameters of excitation on response of the bucket wheel excavator with two masts in the out-of-resonance region*, Ph.D. dissertation, University of Belgrade, Faculty of mechanical engineering, Belgrade, 2016.
- [19] Bošnjak, S.M., Oguamanam, D.C.D., Zrnić, N.Đ.: The influence of constructive parameters on response of bucket wheel excavator superstructure in the out-of-resonance region, *Arch Civ Mech Eng*, Vol. 15, No. 4, pp. 977-985, 2015.
- [20] Gnjatović, N., Bošnjak, S., Stefanović, A.: The dependency of the dynamic response of a two mast bucket wheel excavator superstructure on the counterweight mass and the degree of fourier approximation of the digging resistance, *Arch Min Sci*, Vol. 63, No. 2, pp. 491-509, 2018.
- [21] Gnjatović, N., Bošnjak, S., Zrnić, N.: Spatial Reduced Dynamic Model of a Bucket Wheel Excavator with Two Masts, In: Rusiński, E., Pietrusiak, D. (eds) *Proceedings of the 14th International Scientific Conference: Computer Aided Engineering. CAE 2018, Lecture Notes in Mechanical Engineering*, Springer, Cham, 2019.
- [22] Gottvald J.: The calculation and measurement of the natural frequencies of the bucket wheel excavator SchRs 1320/4x30, *Transport*, Vol. 25, No. 3, pp. 269-277, 2010.
- [23] Gottvald J.: Measuring and Comparison of Natural Frequencies of Bucket Wheel Excavators SchRs 1320 and K 2000, *GEMESD'11 - Proceedings of the 4th WSEAS international conference on Energy and development - environment - biomedicine*, Corfu Island, pp. 335-340, 2011.
- [24] DIN 22261-2: Excavators, Stackers and Auxiliary Equipment in Brown Coal Open Cut Mines Part 2 Calculation Principals, German Institute for Standardization, 2016.
- [25] Rasper L.: *The Bucket Wheel Excavator Development Design Application*, Trans Tech Publications, Clausthal-Zellerfeld, 1973.
- [26] Volkov D.P., Cherkasov, V.A.: *Dynamics and strength of multi-bucket excavators and stackers*, Mašinostroenie, Moscow, 1969.
- [27] Jovanović, D.: *Research of the Rotary Excavators Loads in Dependence on Condition of Realizing Excavation Material Process on the Strip Mines*, Ph.D. dissertation, University of Belgrade, Faculty of mechanical engineering, Belgrade, 1995.

- [28] Jovković, M.: *Analysis of influence of structural parameters and working regimes parameters on loading and dynamic behaviour of bucket wheel excavators*, Magisterial thesis, University of Belgrade, Faculty of mechanical engineering, Belgrade, 2002.
- [29] Petrić, S.: *Dynamics of rope hoisting mechanism of a bucket wheel boom*, Magisterial thesis, University of Belgrade, Faculty of mechanical engineering, Belgrade, 2006.
- [30] Pietrusiak, D.: Evaluation of large-scale load-carrying structures of machines with the application of the dynamic effects factor, *Eksplot Niezawodn*, Vol. 19, No. 4, pp. 542-551, 2017.
- [31] Bošković, S., Jovančić, P., Ignjatović, D., Rakićević, B., Maneski, T.: Vibration as deciding parameter during revitalization process for replacing the bucket wheel drive, *Journal of Vibroengineering* Vol. 17, No. 1, pp. 24–32, 2015.
- [32] Pietrusiak, D., Moczko, P., Rusiński, E.: World's largest movable mining machine vibration testing - numerical and experimental approach, *Proceedings of ISMA2016 International Conference on Noise and Vibration Engineering, USD2016 International Conference on Uncertainty in Structural Dynamics*, Katholieke Universitet Leuven, Leuven, pp. 2287-2299, 2016.

SESSION C

LOGISTICS AND INTRALOGISTICS SYSTEMS

Andreas Rücker

Research Assistant
Technical University of Munich
Faculty of Mechanical Engineering
Chair of Materials Handling,
Material Flow, Logistics (fml)

Jona Rief

Student
Technical University of Munich
Faculty of Mechanical Engineering
Chair of Materials Handling,
Material Flow, Logistics (fml)

Johannes Fottner

Professor
Technical University of Munich
Faculty of Mechanical Engineering
Chair of Materials Handling,
Material Flow, Logistics (fml)

An investigation of mean energy demand, performance and reference cycles for stacker cranes

Automated storage and retrieval systems (AS-RS) are commonly used in intralogistic facilities and are often operated by stacker cranes. These stacker cranes are used in high-bay warehouses to move small load carriers, pallets and special load carriers. This paper presents an approach for the determination of the mean energy demand of stacker cranes, using a reference cycle. The examination of the reference cycles is based on a large scale simulation experiment with randomly generated stacker crane and rack configurations and operation tasks. The results permitted an analysis of the correlations between various parameters e.g. energy demand and performance of stacker cranes. Subsequently, three different reference cycles which allow an easy and fast calculation of the mean energy demand are developed and evaluated.

Keywords: Intralogistics, High-bay warehouse, Automated storage and retrieval system, Stacker crane, Energy demand.

1. INTRODUCTION

Stacker cranes (SCs) are large machines which move small load carriers and pallets in high-bay warehouses. These high-bay warehouses are one typical component of intralogistic facilities. The energy demand during the operation of SCs is influenced by a huge number of variable effects. These effects are often coupled and influence each other. Therefore the analytical calculation of the energy demand is complex and sometimes linked to detailed simulation models. The main idea is to find reference cycles which allow the calculation and evaluation of the overall mean energy demand of different SCs and storage configurations. This paper presents an approach, which determines and evaluates reference cycles. Subsequently, the reference cycles are tested for their use in the determination of the mean energy demand. Such reference cycles are already in use to calculate the mean travel time of SCs [6, 18]. In this paper we distinguish between miniload stacker cranes (MSCs) for small load carriers and pallet stacker cranes (PSCs), as they differ fundamentally in their mass ratios. Figure 1 shows a typical scheme of a rack feeder with the nomenclature used in the paper.

The main components are the base frame, the mast, the head, the lift device and the drives. A rack feeder has two main drives – for the horizontal and vertical movement of the payload. The main drives are electrically connected via an intermediate circuit.

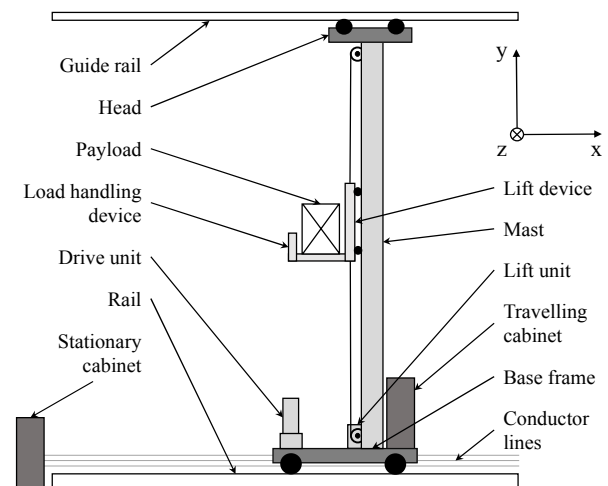


Figure 1. Scheme of a rack feeder (cf. [14])

2. LITERATURE

The determination of the travel time of SC has been the subject of a large number of investigations in the past. Starting with the basics of travel time metrics in [3], several papers have been presented in recent years. A detailed review of the literature concerning SC was presented from Roodbergen [13]. The most recent review paper, though its focus was on the scheduling task, was published in 2016 [2]. In the past, various publications have dealt with the energy demand of SCs. Meneghetti et al. performed various investigations into the strategic parameters that influence energy demand and performance [9–12]. Schulz et al. performed an investigation of isoenergetic shelves in automatic small parts warehouses [15]. Ertl presented a simplified way of calculating the mean energy demand of MSCs [5]. Lerher et al. gave an initial method for calculating the energy efficiency of MSCs [8]. A method for the benchmarking of different types of AS-RS was presented by Stöhr et al.

Correspondence to: Andreas Rücker, Research Assistant
Chair of Materials Handling, Material Flow, Logistics (fml)
Boltzmannstr. 15, 85748 Garching, Germany
E-mail: andreas.ruecker@tum.de

[17]. In their work they suggested the use of the standard double cycle from VDI 3561 [18] and other standards to compare three different types of AS-RS. PSCs have not been studied in such detail in the past. Various standards define a calculation scheme for the mean travel time and the throughput of an SC. These standards [6, 18] use reference cycles to perform a standardised calculation of the mean travel time. Azzi et al. proposed a method to calculate a reference quadruple cycle via a Monte Carlo simulation [1]. None of the existing approaches is combining the energy demand and throughput analysis of MSC and PSC with an approach for a reference cycle for the mean energy demand.

3. MATERIALS AND METHODS

SCs can be operated with different operation modes. The basic mode is the single cycle mode. In a single cycle, the SC performs a store or retrieve task regarding one item. In a double cycle, the SC performs a store task and then a retrieve task. In the complex quadruple cycle, two store and two retrieve tasks are combined into one cycle. Quadruple cycles can be performed with double load handling device SCs. Examples for the movement of the SC within different cycle types are shown in Figure 2. In our investigation, we used single and double cycles, and the Input/Output point is located in the lower left corner of the rack.

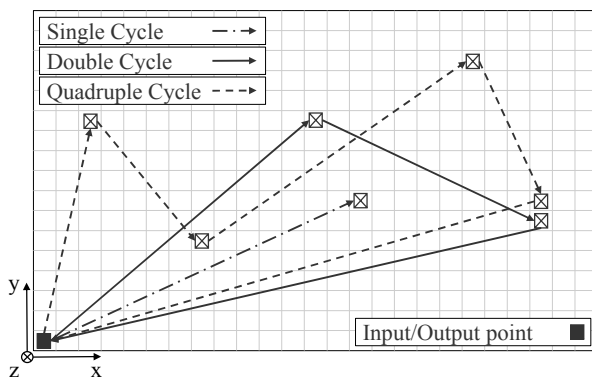


Figure 2. Examples for different cycle types (cf. [14])

In this paper, we use the basic approach from Azzi et al. of taking a large number of random cycles to investigate not the mean travel time, but the mean energy demand and the performance of various SC configurations. The goals are the investigation of the influence of different parameters and the formation of reference cycles. The reference cycles should represent the mean energy demand in the use of various types of SC. Therefore MSCs and PSCs with and without a refeed unit are investigated. The refeed unit allows an SC to feed electrical energy, released during braking, back to the supply network. We use a large-scale simulation experiment to examine the mean energy demand by simulating a large number of random cycles. The layout of the simulation experiment is pictured in Figure 3.

Initially the SC and storage configuration are randomly generated. The values for the varied parameters are selected between predefined borders via a Latin hypercube sampling (LHS) algorithm [16].

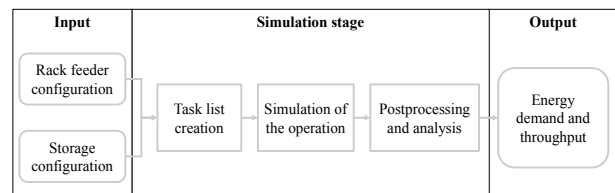


Figure 3. Layout of the simulation study

The varied parameters for MSCs and PSCs and their minimum and maximum values are listed in Table 1. The number of columns and levels defines the size of the rack.

Table 1. List of the varied parameters and their maximum and minimum values for MSCs and PSCs

Parameter	MSC min	MSC max	PSC min	PSC max
Number of columns n_{col}	30	80	20	60
Number of levels n_{lev}	20	40	8	18
Acceleration drive unit a_x	2.0 m/s ²	5.0 m/s ²	0.5 m/s ²	1.5 m/s ²
Acceleration lift unit a_y	1.0 m/s ²	3.0 m/s ²	0.2 m/s ²	1.0 m/s ²
Velocity drive unit v_x	4.0 m/s	6.0 m/s	1.5 m/s	3.5 m/s
Velocity lift unit v_y in m/s	1.5 m/s	3.0 m/s	0.5 m/s	2.0 m/s
Efficiency drive and lift unit η_x, η_y	0.4	0.7	0.4	0.7
Mass base frame m_{base}	1.2 t	2 t	8 t	20 t
Mass lift unit m_{LU}	250 kg	450 kg	2.5 t	4.5 t
Mass payload m_{load}	25 kg	75 kg	0.5 t	1.5 t
Storage occupancy Occ	0.4	0.9	0.4	0.9
Use of a refeed unit RU	0	1	0	1

The parameters include the main construction parameters such as size of the rack and the SC, the configuration of the brake-energy use, the transported load and the drive speeds. The efficiency values combine electrical and mechanical losses in the drives. Every rack feeder configuration is equipped with an intermediate circuit and is able to use the brake energy of one drive for another drive.

After the creation of the configuration, a task list with random cycles is generated. The storage occupancy is used to create a starting rack layout with stored items and the occupancy is kept relatively constant throughout the simulation. The task list and the configuration data is used to simulate the energy demand and the throughput of the SC for one configuration. For the simulation, a

simplified model is used to keep computation time as short as possible. The model is based on the analytical calculation of energy demand in terms of kinetic and potential energy, and various friction-based resistances. In order to fully parameterize the model, we have used the results of previous research. The evaluated measurement data from [7] and the results from Ertl [4] were used.

For the MSCs and the PSCs we used 10000 different configurations each. 5000 configurations are selected via the LHS and the use of a refeed unit is either on or off. For every single configuration, the number of random single and double cycles is calculated via (1).

$$N_{col} \cdot N_{lev} \cdot 1000 \quad (1)$$

Thus, in total we simulated 20000 configurations with several hundred thousand to several million cycles in each configuration. Following the simulation of energy demand and throughput for all configurations and cycles, the data was processed and analysed.

4. RESULTS

We analysed two general aspects in the calculated data. First we inspected the different effects of the varied parameters on energy demand and performance. We used the throughput of moved items per hour as an indicator for performance. Secondly the data is used to find reference cycles which meet the overall mean energy demand of the rack feeder. The mean energy demand is calculated as global mean of all drive and lift movements. We have not taken any downtime into account.

4.1 Effects of single parameters

We split the results for the MSCs and PSCs and plotted the correlations between the varied parameters and energy demand E and throughput TP . The number in every correlation field represents the correlation coefficient. This coefficient takes values between minus 1 and plus 1. The mass moved in a horizontal direction m_x comprises the overall mass of the base frame, mast and lift unit, while the moved mass in vertical direction m_y comprises the mass of the lift unit and the load-handling device. The results for the MSCs are shown in Figure 4.

The units of the variables are shown in Table 1. Drive acceleration and velocity and the moved masses show a strong dependency on E . The effect from m_x on TP is caused by the fact that the mass of the mast is scaled according to the number of levels. Therefore we have an increased m_x for higher racks and a dependency between m_x and TP . Lift acceleration a_y and velocity v_y have no significant effect on the energy demand. The number of columns and levels define the storage capacity. For increasing numbers, the mean energy demand increases and the throughput decreases.

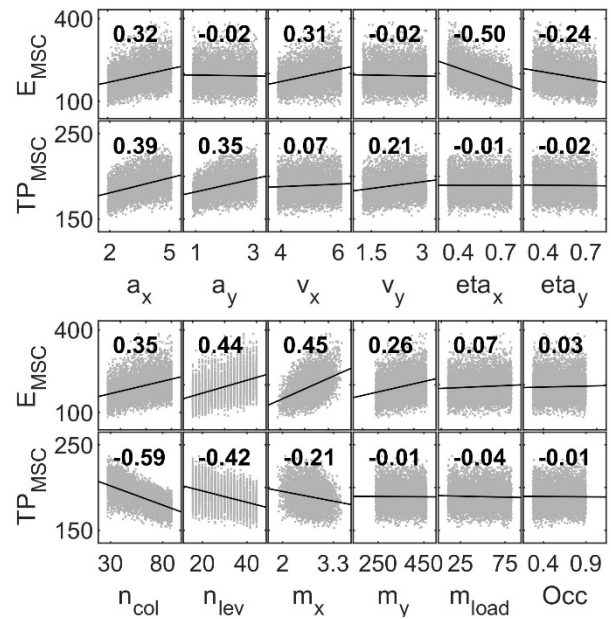


Figure 4. Correlations for the MSC double cycle configurations without refeed unit and with TP in moved items per hour and E in kJ

For the PSCs we found similar correlations which are shown in Figure 5. Due to the changed mass ratios, the sizes of the correlation coefficients change. Accelerations and velocities are smaller than the ones from the MSCs and are less significant in terms of TP and E . The ratio of maximum speed to maximum acceleration of an MSC drive can reach 1, whereas this ratio for the PSCs is around 2 and bigger. The influence of the masses on E is slightly higher compared to the MSCs. With MSCs, the influence of the efficiency of the drive unit is higher than that of the lift unit, with PSCs it is just the other way round.

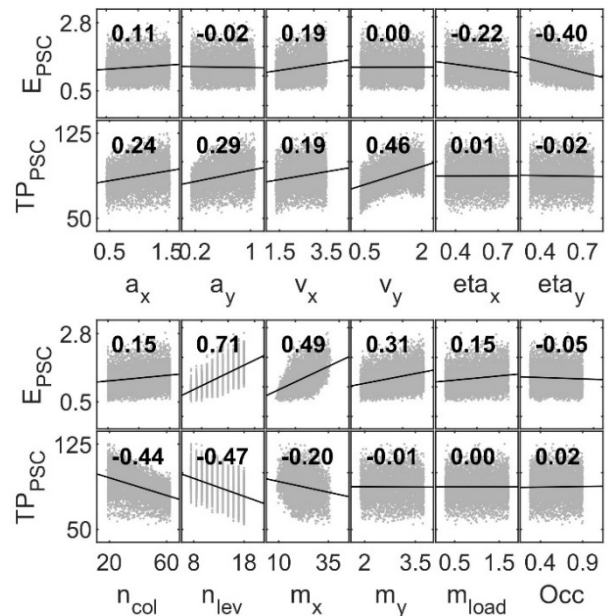


Figure 5. Correlations for the PSC double cycle configurations without refeed unit and with TP in moved items per hour and E in MJ

Occ has no influence on MSC or PSC configurations because, at occupancy levels between 40 and 90 % the

normal operation of the whole storage facility is still possible. Relocations were not taken into account during the simulation.

For the correlations, we used the 5000 configurations without a refeed unit. We also inspected the results with a refeed unit, however the general trends essentially gave a similar picture. With the use of a refeed unit we discovered a general reduction in the mean energy demand. The reduction for the MSC double-cycle configurations are shown in Figure 6. Every ring represents the results for one simulated configuration. The reduction varies between 3 and 23 %. For PSCs and single cycles we found similar results for the reduction of the energy demand.

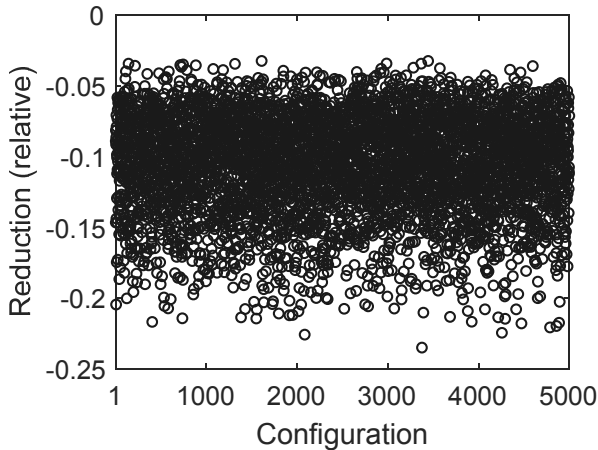


Figure 6. Reduction of the mean energy demand through the use of a refeed unit for MSC double cycle configurations

The use of a refeed unit increases the standby power of an SC. Therefore its use in a real-world application does not always lower the overall energy demand, because if the SC has a lot of downtime with no movement, then the increased standby power causes a general rise in energy demand. For our simulation with no downtime, the general reduction of the mean energy demand is hence obvious.

4.2 Reference cycles

In essence, we searched for cycles which had the same energy demand as the overall mean energy demand and called these cycles “reference cycles”. A reference cycle allows the quick calculation of the mean energy demand and is also suitable for subsequent experiments, analogously to the way reference cycles are used for the mean cycle-time calculation. Within the scope of this work, we developed the two different calculation approaches “mean” and “interpolation”. Overall, we examined three different reference cycles. The mean cycle, the interpolation cycle and the reference cycle proposed in the FEM 9.851 [6]. For the FEM cycle, we used the store and retrieve position from (2).

$$\text{Store position: } P_S \left(\frac{2}{3} \cdot L, \frac{1}{5} \cdot H \right)$$

$$\text{Retrieve position: } P_R \left(\frac{1}{5} \cdot L, \frac{2}{3} \cdot H \right) \quad (2)$$

where L is rack length and H is rack height

For the purpose of comparison, we chose the double cycle because this proved to be suitable in previous research work [7]. The presented results are focused on the MSC configurations without a refeed unit. The other configurations were also inspected, but showed no significant differences in their general trend. The overall relative error over the percentage of configurations is shown in the histograms in Figure 7 and Figure 8. Starting with the mean and the interpolation cycle in Figure 7 we see relative errors of between minus 15 and plus 60 %. Although the interpolation shows different results, neither the mean nor the interpolation cycle gave satisfying results.

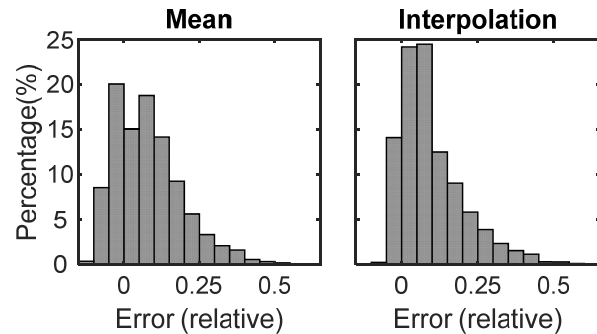


Figure 7. Relative error for the mean and the interpolation cycle for the MSC configurations

Following the results for the relative error of the FEM cycle are presented in Figure 8. Surprisingly the FEM cycle showed much better results, with a maximum relative error of between 0 and 17 %. With the FEM cycle, we were able to ensure relatively stable deviations from the mean energy demand.

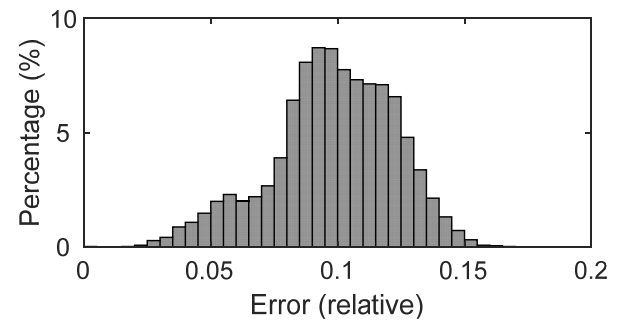


Figure 8. Relative error of the FEM cycle for the MSC configurations

Additionally, the correlation of the simulated mean energy demand and the energy demand of the mean cycle and the FEM cycle is shown in Figure 9. Every dot represents the result for one simulated configuration. The FEM cycle shows clearly lower maximum deviations and differs significantly less than the mean cycle. Using a linear fitting, it would easily be possible to recalculate the overall mean energy demand by using the FEM cycle.

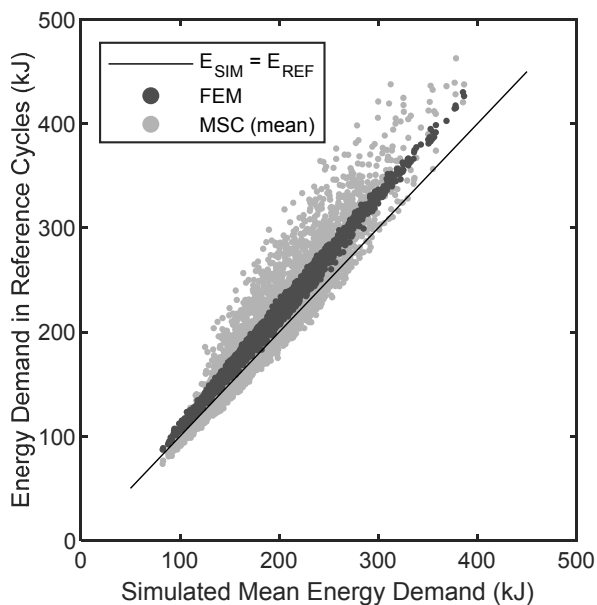


Figure 9. Correlation for the mean energy demand for MSC

5. CONCLUSION

In the simulation study we analysed single and double cycle operation for MSC and PSC with a large scale simulation experiment. The results from the simulation allowed an investigation of the varied parameters and their effect on the mean energy demand and the performance. This allowed important relationships between the parameters to be shown and existing research work was confirmed.

The reference cycles should allow an easy comparison between different types of SC and should be suitable for a good estimation of the mean energy demand. With the FEM cycle as currently best solution for the mean energy demand we found a suitable reference cycle. This cycle can also be used for real life tests of SC.

Our further research tasks in this field will be focused on the application from the gained results to an energy efficiency calculation method. Based on the work of Ertl [4] and Lerher et al. [8] a detailed energy efficiency model for MSCs and PSCs will be presented in further publications.

ACKNOWLEDGMENTS

The research has been conducted within the *Industrielle Gemeinschaftsforschung* [collective industrial research] (IGF) project “Entwicklung einer Bewertungsmethodik für die Energieeffizienz eines Regalbediengerätes” (IGF project number 18839N). This project has been funded by the Federal Ministry for Economic Affairs and Energy on the basis of a decision of the German Bundestag [Federal Parliament].

REFERENCES

- [1] Azzi, A., Battini, D., Faccio, M., Persona, A. and Sgarbossa, F.: Innovative travel time model for dual-shuttle automated storage/retrieval systems, *Computers & Industrial Engineering*, Vol. 61, No. 3, pp. 600-607, 2011.
- [2] Boysen, N. and Stephan, K.: A survey on single crane scheduling in automated storage/retrieval systems, *European Journal of Operational Research*, Vol. 254, No. 3, pp. 691-704, 2016.
- [3] Bozer, Y.A. and White, J.A.: Travel-time models for automated storage/retrieval systems, *IEE Transactions*, Vol. 37, pp. 329-338, 1984.
- [4] Ertl, R.: *Energy demand determination and energy efficiency assessment of storage and retrieval machines in automatic small parts warehouses*, (German), PhD, Technical University of Munich, 2016.
- [5] Ertl, R. and Günthner, W.A.: Meta-model for calculating the mean energy demand of automated storage and retrieval systems, *Logistics Journal*, Vol. 2016, No. 2, 2016.
- [6] European Materials Handling Federation: Performance record for storage and retrieval machines - Cycle times, FEM standard No. 9.851, 2003.
- [7] Fottner, J. and Rücker, A.: *Development of an evaluation methodology for the energy efficiency of stacker cranes* (German), Technical University of Munich, 2019.
- [8] Lerher, T., Edl, M. and Rosi, B.: Energy efficiency model for the mini-load automated storage and retrieval systems, *The International Journal of Advanced Manufacturing Technology*, Vol. 70, No. 1-4, pp. 97-115, 2013.
- [9] Meneghetti, A. and Monti, L.: Energy Efficient Dual Command Cycles in Automated Storage and Retrieval Systems, *Conference Proceedings World Renewable Energy Congress – Sweden*, 2011.
- [10] Meneghetti, A. and Monti, L.: Multiple-weight unit load storage assignment strategies for energy efficient automated warehouses, *International Journal of Logistics Research and Applications*, Vol. 17, No. 4, pp. 304-322, 2013.
- [11] Meneghetti, A. and Monti, L.: Sustainable storage assignment and dwell-point policies for automated storage and retrieval systems, *Production Planning & Control: The Management of Operations*, Vol. 24, No. 6, pp. 511-520, 2013.
- [12] Meneghetti, A., Dal Borgo, E. and Monti, L.: Rack shape and energy efficient operations in automated storage and retrieval systems, *International journal of production research*, Vol. 53, No. 23, pp. 7090-7103, 2015.
- [13] Roodbergen, K.J. and Vis, I.F.A.: A survey of literature on automated storage and retrieval systems, *European Journal of Operational Research*, Vol. 194, No. 2, pp. 343-362, 2009.
- [14] Rücker, A. and Fottner, J.: Development of a multi-component evaluation methodology for the energy efficiency of stacker cranes (German), *Logistics Journal Proceedings*, 2018.
- [15] Schulz, R., Monecke, J. and Zadek, H.: Isoenergetic shelves of automatic small parts warehouses, *Logistics Journal*, Vol. 2012, 2012.

- [16] Siebertz, K., van Bebber, D. and Hochkirchen, T.: *Statistical design of experiments* (German), 2017. MHCL 2017, 4th-6th October 2017, Belgrade, Serbia, pp. 133-138, 2017.
- [17] Stöhr, T., Schadler, M. and Hafner, N.: Energy efficiency benchmarking concept for diverse automated storage and retrieval systems, Conference Proceedings XXII International Conference on Material Handling, Constructions and Logistics – [18] VDI Verband Deutscher Ingenieure: Test cycles for performance comparison and approval of storage and retrieval machines (German), VDI guideline No. 3561, 1973.
-

RC Vehicle Fleet E-Monitoring in Practice and Future

Goran Radoičić

Scientific Associate
University of Niš
Faculty of Mechanical Engineering

Miomir Jovanović

Full Professor
University of Niš
Faculty of Mechanical Engineering

Bratislav Blagojević

Professor
Hihg Technical and Technological School
of Vocational Studies, Kruševac

Miloš Vojinović

"Mobile Solutions" Belgrade

This paper provides evidence on improvements in a waste collection and transport system using an integrated control model based on GPS, GIS and RFID technologies. The system envisages two parameters of weight monitoring: the total vehicle weight and the weight of the loaded waste from each vessel. The control system is based on the connections between the three factors: the development group, the logistical-dispatch center, the vehicle. The control system contains a module for advanced management of fuel, itineraries and route effectiveness. Some of the control methods allow diagnostics of the electric power supply in the vehicle. Others show the influence of changing the engine crankshaft speed to the occurrence of voltage amplitudes when recharging the accumulator batteries on the vehicle, etc. Good results were achieved by monitoring the change of pressure in the hydraulic installation for waste bin lifting.

Keywords: control system, fleet, monitoring, sensor, signal processing.

1. INTRODUCTION

Waste collection process implies the use of transportation machinery, which at the same time represents a vehicle in public transport and a work vehicle for self-loading, compacting and unloading the waste. Due to the complexity of the work process, it is preferable to control the process in real time. The control involves measuring the current values of characteristic operating parameters of the vehicle and comparing them with the set values. In addition to optimizing the work cycle, special attention should be paid to the safety aspects of the crew that puts the waste into the vehicle (the increased risk category). This requires the introduction of another tool - video surveillance. The task of the vehicle control becomes so complex because it needs to manage the integrated technology of remote voice, data and video transmission. Nowadays, the integration of GPS and other technologies in control systems is very current, [1-5]. The application of an integrated high-level monitoring system based on the use of new technologies influences the increase in the efficiency parameters of the utilities. The evidence on improvements in the real process of collecting and transporting waste using the original model for integrated control is given below.

2. VEHICLE TRACKING FUNDAMENTALS

If we have a known the position of the satellite and known time of the emission of the signals (the satellite time), then we can look for positions of the vehicles moving on the surface of the Earth. The positioning of the signal receiver (vehicle) is reduced to determining the difference in the time display between the receiving

(system) and satellite clock. To accurately determine the position of the vehicle, we need to receive a signal from at least four satellites. The receiver's position signal contains data on latitude, longitude, altitude and non-synchronization error between the system time used by the receiver and the GPS time of the emitter. Since satellite positions are known, by measuring the time of propagation of the GPS signal to the receiver, the receiver's position can be determined as well.

The fundamental frequency of the satellite master clock is $f_0=10.23\text{MHz}$. The error in the frequency of the receiving signal is $\varepsilon_{f_0}=(\pm 5\text{kHz})/(\pm 10\text{kHz})$. Before sending the signal to the receiver, the frequency of the wave generated in the satellite clock is multiplied using constants k_i :

$$f_i = k_i f_0, \quad (1)$$

in order to get the carrier signals from the so-called L-wave band whose frequencies are: $f_1=1.57542\text{GHz}$, $f_2=1.2276\text{GHz}$ and $f_3=1.17645\text{GHz}$. The wavelengths of these signals are: $\lambda_1=0.19\text{m}$, $\lambda_2=0.24\text{m}$ and $\lambda_3=0.255\text{m}$.

The unmodulated carrying signal has a cosine shape:

$$L_i(t) = a_i \cos(\omega_i t), \quad (2)$$

where a_i is the amplitude and ω_i is the circular frequency.

The GPS signal, structurally as an EM wave, emitted from the satellite, contains three component signals: a carrier signal, a PRN code (pseudorandom noise) and a navigation message (NAV data). The PRN (or PN) code commonly occurs in two forms depending on frequency: C/A code and P-code. The C/A code is publicly available (clear/access). The frequency of the C/A code is $f_{C/A}=0.1f_0$. The whole set of the C/A code has 1023 members (512 units and 511 zero, randomly distributed) and the repetition interval of 1ms. The wavelength of the C/A code is $\lambda_{C/A}=300\text{m}$. The frequency of the P-code (precision code) is $f_P=f_0$. The P-code repetition cycle lasts 266.4 days, or 38 segments of the cycle with 7 days per cycle, of which 32 segments

Correspondence to: Dr Goran Radoičić, scientific associate
University of Niš, Faculty of Mechanical Engineering,
Aleksandra Medvedeva 14, 18000 Niš, Serbia,
E-mail: goran.radoicic@gmail.com

are assigned to satellites in the form of unique associated security code. The wavelength of the P-code is $\lambda_p=30\text{m}$. The duration of one bit of the navigation message is 20ms, and its frequency is 50Hz.

Two methods of the extended spectrum technique are most commonly used to transmit signals: the Direct Sequence Spread Spectrum method (DSSS) and the Frequency Hopping Spread Spectrum method (FHSS). The DSSS method has a wide practical application. This method introduces a large number of bits using the pseudorandom code B in the original information signal A (Fig. 1) and then adds the signals A and B using the logical “OR” (or the addition by module 2, \oplus), and thus forms (on the transmitter) the transmit signal C of an extended spectrum. The receiver uses the same generated pseudocode B which then is added to the C signal, also using logical operation named the exclusive “OR” in order to obtain the original output data A.

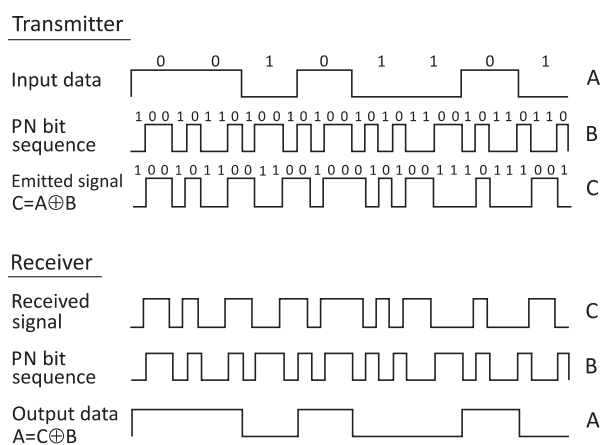


Figure 1. Direct sequence spread spectrum method

3. MODELLING THE CONTROL SYSTEM

The development concept of the system for controlling the operation of the refuse collection vehicles (hereinafter: RC vehicles) is based on the interactions of the three key carriers: the development group, the logistics dispatch center, and the vehicles (drivers). All analyses and reengineering of the transport process are carried out by the internal development group. The management, corrective actions and comparison of the set and measured parameters is carried out by the logistics dispatch center (hereinafter: LD center). Corrective orders are made via SMS or voice, and rarely through direct (dynamic) control actions. The LD center constantly receives feedback on the vehicle's work, on the basis of which it compares the execution of the plan. The LD center uses a temporary technical database that contains documents about: vehicles, drivers, travel orders, workbooks and other documents that give the proofs of the regularity of the participation of the vehicles in public transport. The knowledge basis of the control system is based on many years of experience in the performance of service. POIs (points of interest) contained in the database, represent places in the city where waste containers are placed. The control system performs a comparison of the required sizes and feedback on the sizes from the work

process. This concept, shown in Fig. 2, was realized in 2018 on the fleet of 20 RC vehicles with OBD technology in the utility company “Mediana” Niš.

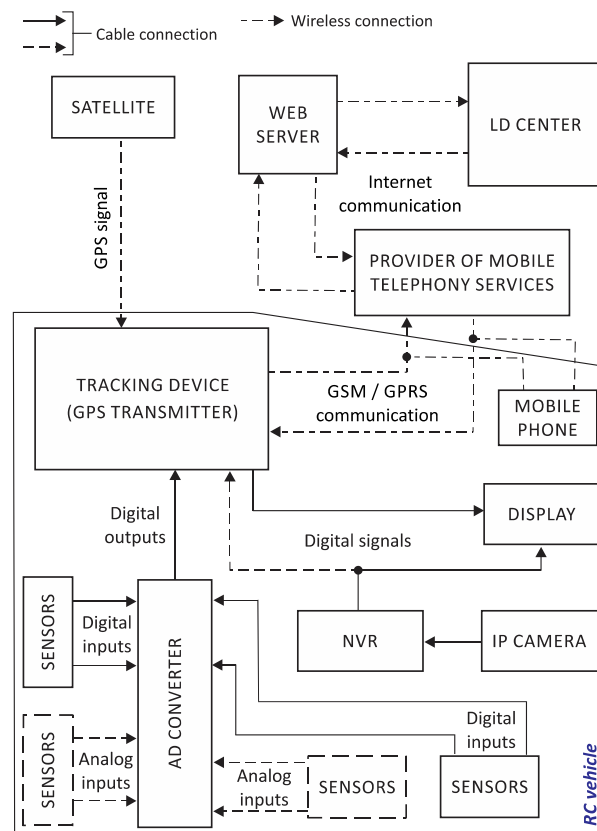


Figure 2. Scheme of the connections between the elements in an integrated RC vehicle e-monitoring system

The developed integrated system for controlling the RC vehicles has a dual function: supervisory and dynamic. Supervisory control monitors the parameters of the vehicle's operation in order to form statistics that are analyzed in post-processing, on the basis of which the conclusions about the work are drawn. Classes of these parameters are: vehicle speed, distance travelled, crankshaft speed, fuel consumption, pressure in vehicle's installations, operating fluid temperatures, battery voltage, vibration and other parameters essential for the correctness and safety of the vehicle as a system. Dynamic control is used to manage those aspects of vehicle's operation in which the state of the vehicle components itself can affect the outcome of the control activities, for example, in overloading the vehicle or the lifting mechanism. Dynamic control provides quick corrective measures to prevent against the damage (fast hydraulic stop switch, or remote stopping the engine). Analog signals from the sensors are converted to digital in the A/D converter and together with the GPS satellite signal delivered via a GPRS protocol from the transmitter integrated in the tracking device, Fig. 2. The WEB server enables acquisition and processing of the measured signals by using the appropriate software. The video signal from the IP camera is recorded with the network video recorder (NVR) and transferred to the display in the vehicle cabin, but also remotely, via the internet, to be available on-line not only to the driver, but also to the vehicle tracking center, Fig. 2. The

current on-board video surveillance system uses only one camera in the rear of the vehicle, but it is desirable to include two new cameras on the sides of the vehicle for monitoring the workers who bring the waste bins to the place of loading into the vehicle.

4. HARDWARE AND SOFTWARE SUPPORT

The appropriate sensors are used for monitoring and measuring the significant system parameters. The accuracy of the monitoring depends on the accuracy of the measured parameters, and it is conditioned by the quality of all elements of the measuring system which, first of all, consists of: sensors, amplifiers, cables and connections. Choosing whether the connection will be cable or wireless also influences on the accuracy.

The e-monitoring system model presented by the paper is based on an electronic GPS transmitter of the

FM-4200 type, [6], with a dual-band signal transmission at the frequencies of 900MHz and 1800MHz, Fig. 3. Signal transmission can be done in GPRS, SMS or Voice traffic. The device is equipped with the ARM7 TDMI processor, built-in CAN-BUS support according to the SAE J1939/FMS protocol and built-in 3-axes accelerometer. The voltage range of this device is 10÷30V DC (power of 12W), the number of digital inputs and outputs is 4 to each of them, and the number of analog inputs is also 4. GPS information is received using a 50-channel receiver of the BloxNEO-5M50 type. Particular attention has been paid to overvoltage protection and indication (OPI), Fig. 3.

The management of the selected vehicle fleet (PUC “Mediana” Niš, 2018) is done using the Mob-Track software version: 24v.2.6.1.13 by Mobile Solutions Belgrade (www.mobilesolutions.rs).

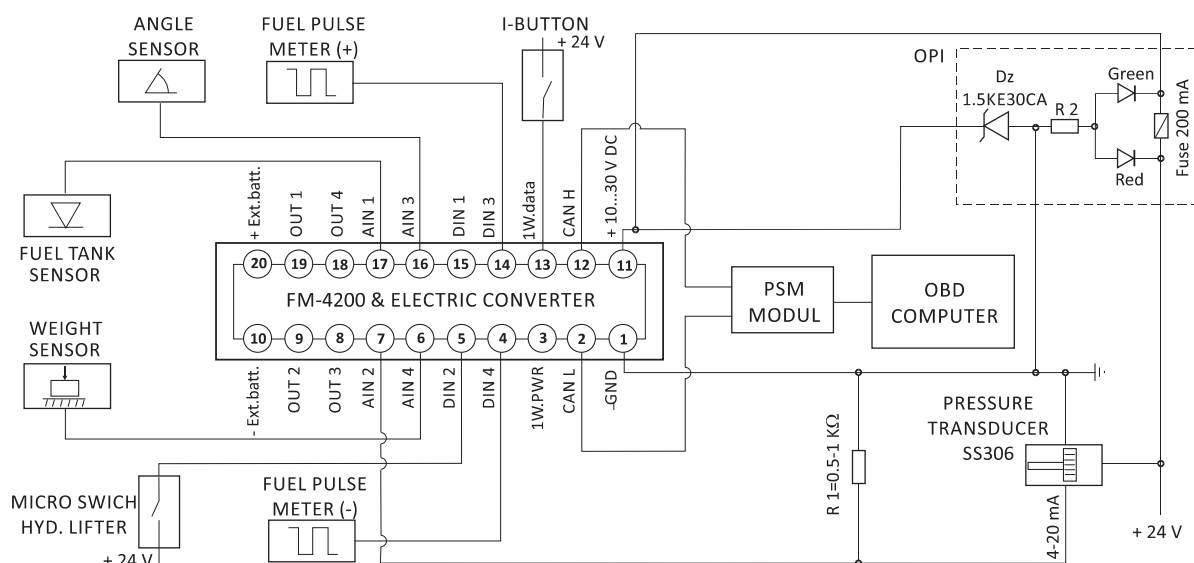


Figure 3. Electrical scheme of the connection between the tracking device and the sensors

5. FUEL CONSUMPTION CONTROL

The utility company uses data on fuel from the internal gas station and plans maintenance using of the FMS Coming Computer Engineering software platform (COMING, est. 1991, <http://www.coming.rs>). The integrated control system uses fuel control methods: the tank fuel level measurement method and the impulse counters method. The first of them is based on an analog level sensor which exists in most vehicles, and which is connected in this case via AIN1 channel with the transmission device (Fig. 4, Method-A). This method requires calibration of the obtained voltage value representing the volume of fuel in the tank. The second method is to measure fuel consumption in a vehicle engine. This method is also known as the pulse counters method. On each of the flow fuel valves, direct and return, one pulse meter is placed (Fig. 4, Method-B). On the basis of digital signals from the pulse meter, the FM-4200 device calculates the difference of DIN3-DIN4 which represents the fuel consumption in the drive motor of a RC vehicle.

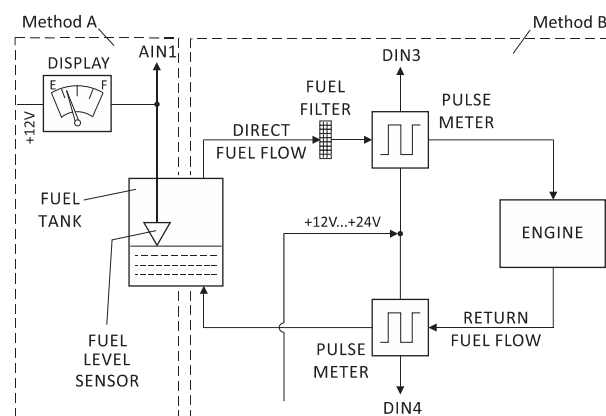


Figure 4. Fuel control methods: A - Tank fuel level measurement, B - Pulse counters method

Useful analysis can be done by comparing the results of the measurement of altitude and measurement of fuel consumption using an analog level sensor in the fuel tank, Fig. 5. The level sensor is calibrated to a minimum value of 500ml of spent fuel.

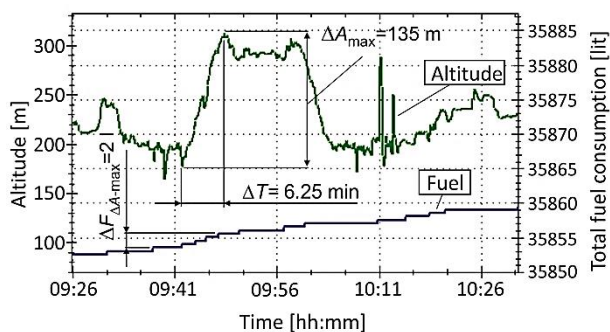


Figure 5. An authentic signal record of the total fuel consumption (vehicle reg. no. Ni 050-ČU, Niš, 17.6.2013)

6. MEASUREMENT OF COLLECTED WASTE

This control system envisages two levels of weight control: measurement of loaded waste from each individual waste bin and monitoring the total weight of the RC vehicle.

The actuator, Fig. 6, causes a rotational movement of the fork to grip and lift the waste bin changing the angle θ . A load cell sensor is located within the fork structure. Measurement of the weight (i.e. force F_D) is carried out in the movement of the lifting mechanism on two occasions: when lifting the bin (gross weight) and lowering the bin (tare). The position in which these two measurements are made must be the same, and it is determined by the angle sensor. The difference between these two discrete measured sizes represents the weight of the loaded waste.

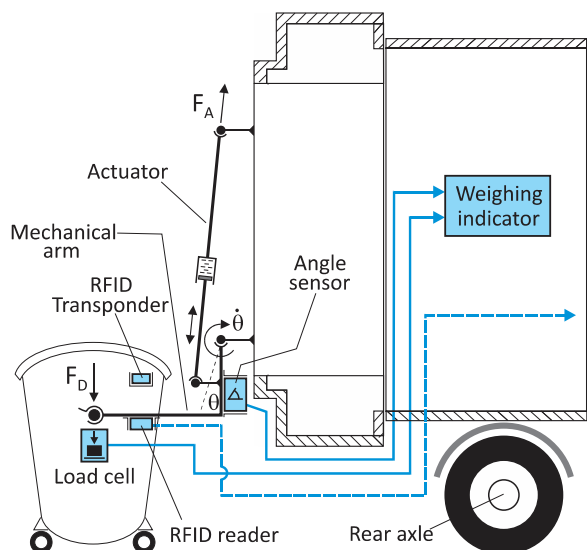


Figure 6. Part of the on-board weighing system

In this way, the conditions are created for charging the service per kilogram of collected waste. Such a system requires the introduction of Radio Frequency Identification technology, i.e. the RFID reader mounted on the vehicle and the RFID transponder on the waste bin itself. This allows identification of the waste bins and users. The integrated monitoring system has paid special attention to the analyzing and selecting the sensors for measurement of the gross vehicle weight and the weight of loaded waste in the vehicle, [7].

7. EVENT CONTROL METHOD BASED ON THE MONITORING HYDRAULIC PRESSURE

Efficiency control of the waste collection process is based on tracking of the change in oil pressure in the hydraulic installation for lifting and emptying the waste bins. The SS306 pressure transducer ("Sendo", PRC) was used in the measurement. Its position in the hydraulic installation of the direct oil flow is on the vehicle superstructure and in the immediate vicinity of the lifting mechanism. The pressure change is indicated by the V-P solid line and expressed in units of the voltage equivalent, Fig. 7. This curve has local peaks which mark events, i.e. execution of a working operation of lifting and unloading of single waste bin. Each measured local peak of the hydraulic pressure corresponds to the voltage equivalent U_j . For example, the peak no.4 has its own voltage equivalent that is $U_4=9250\text{mV}$. By calibrating the voltage equivalents, the weight of the loaded waste was determined for each event. Since the change in oil pressure in the hydraulic installation is nonlinear, this control method is not applicable with full accuracy (error of $\pm 5\%$).

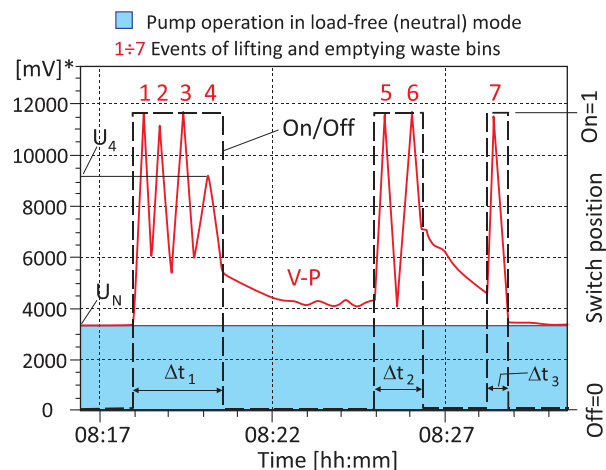


Figure 7. An authentic signal record of the hydraulic piston operation (the vehicle, reg. no. Ni166-LB, Niš, 1.8.2018); *Voltage equivalent to hydraulic pressure

Using the event control method, one can check whether the process is being realized according to the established dynamic plan, i.e. determine the number of emptied out bins. The method is also used for calculating the effective operating time of the hydraulic lifting mechanism by summing different time intervals Δt_i , Fig. 7 (On/Off line). This switch function has two values: "on"=1 and "off"=0. After lifting the bin and unloading waste into the vehicle ("on" position), the lifting mechanism returns to the lower position "off", completing one operating cycle. A rectangular impulse may have more than one operating cycle depending on the number of bins located at one stop point (POI location). The example in Fig. 7 shows three impulses with four, two and one working cycle which makes seven working cycles in the total observed time.

8. GPS APPLICATION IN VEHICLE DIAGNOSTICS

GPS technology can be used to diagnose the electrical system of the vehicle, and especially to

diagnose the part of the system for charging the vehicle battery. Simultaneous control of the voltage change in the vehicle battery and the change of the engine contact position (on/off) is shown in Fig. 8. In the diagram, one can see that the charging time of the battery coincides with the duration of the switch operation “on=1” and that the battery electric supply is stable because the voltage fluctuations slightly vary around the upper limit value of 28V. It should be noted that the electric supply system on the selected RC vehicle uses two battery units of 135Ah/12V capacity which is connected in series.

At shutdown time “off=0” there is no battery charging because the vehicle engine is not running. That is when the process of discharging of the vehicle battery takes place, because the voltage gradually decreases but does not exceed the lower allowed value of 24V. During a one-day work cycle of the RC vehicle with on-off alternating changes of operating regime, at a shift of 7-18h, the minimum voltage value of the two serial connected batteries was 25.4V, Fig. 8. This example indicates full functionality of the electrical system for charging of the vehicle battery whose structure is preserved. The high level of regularity of the electrical system on the vehicle, such as shown in this example, allows the obtaining of reliable GPS parameters and exact calculation of other derived quantities.

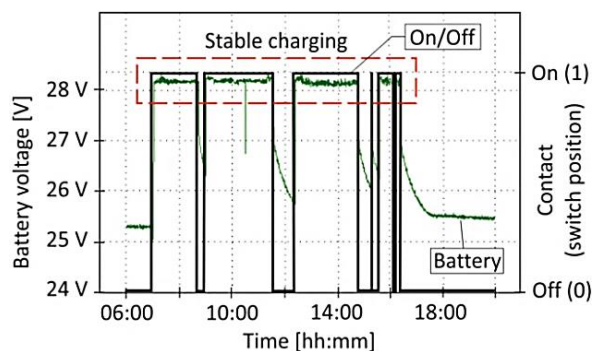


Figure 8. An authentic record of the transferred battery signal to the dispatch center (by measuring on the vehicle with registration number Ni 188-TE, Niš, 22.5.2013)

Unlike the previous one, the following two examples indicate faults in the vehicle's electrical system. The first of them introduces a very common case in practice: the unstable charging of the vehicle battery, Fig. 9. This problem implies alternative sharp increase and decrease in voltage between the battery electrodes. Practically, we have a situation where, at one point, the value of the battery voltage meets the upper limit, and at another point, it is at the lower limit. This behavior of the battery-charging system is most often the result of a failure of a controlling element that regulates the charge voltage. However, this so-called pulse charging can cause the occurrence of an error when calculating engine operating hours, because lowest limited voltage value that implies the vehicle engine operation (“contact”=“on”) has been previously software defined. All voltage values above the limited value of 26.5V (Fig. 9) can be considered as the engine operation, and those below it, the stopped engine. Thus, if the analyst in the LD center relies on the total engine operation time of 3 hours, which is obtained by summing the time parts of the “battery” curve above the value of 26.5V, then he

will not get an accurate picture of the engine's operation nor an accurate data on fuel consumption, which will be significantly higher per unit of time. However, if the analyst relies on data about the switching operations “on/off”, then he will get information about the eight-hour operation of the vehicle. Although the data based on the “on/off” impulse function is not completely accurate, it nevertheless is a much more precise criterion for calculating the engine's operating time in comparison with the “battery” criterion. A more reliable way to control the engine's operation is measuring the crankshaft rotating speed.

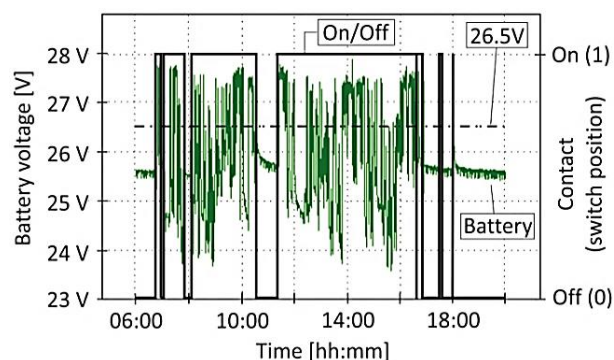


Figure 9. An authentic record of the battery signal which indicates a malfunction case: charging with high voltage fluctuation (the vehicle, reg. no. Ni 010-WD, Niš, 5.3.2013)

Figure 10 shows a malfunction of the battery-charging system during the all-day operation of the vehicle. After the first start of the engine (March 5, 2013, at 7 o'clock), the battery voltage was satisfactory (the correct system state). However, the first start of the engine had a failure that required the use of auxiliary methods which led to a sudden discharge of the battery (maximum discharge at start-up). Later, there was a serious drop in voltage in the vehicle battery, even up to a value of only 10V (operational discharge). The malfunction of the battery charge system caused a complete discharge of the battery and its replacement was required, since the measured voltage was less than 12.4V per unit battery, which represents the lower limited voltage for lead batteries. The engine's operating data in this case, as well as the previous one, are not reliable because they are calculated on the basis of the “battery” curve. The impulse function of “on/off” switch operations here also gives more precise information on vehicle operation.

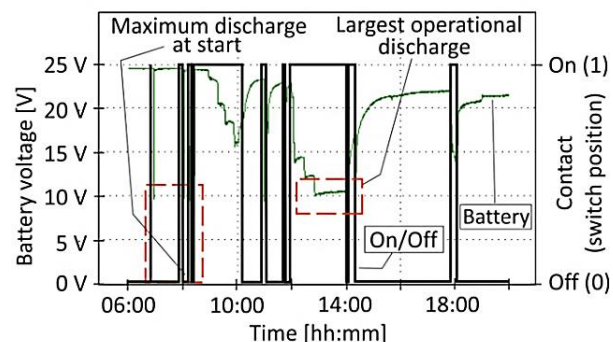


Figure 10. An authentic record of the battery signal which indicates the second malfunction case: rapid discharging the battery (the vehicle, reg. no. Ni 082-NR, Niš, 5.3.2013)

9. CONCLUSION

The research, presented briefly in this paper, provides several contributions:

1. The original model of vehicle fleet monitoring system is developed in one large utility company, which enables advanced management of a certain number of functions. The introduction of a larger number of controllable functions will be carried out at further expansion of the system according to the same model. This extension implies the introduction of new monitoring parameters, i.e. sensors and further development of a software application that will enable processing of multi-channel data in order to generate more complex graphic and numerical reports.

2. The solution for controlling the occupancy of the waste tank capacity on the RC vehicle is improved by introducing a measurement system that measure weight of unloaded waste into the vehicle in each individual emptying of waste bin. This solution created the conditions for implementation of the weighing system on all fleet's units in the next investment cycle, which will allow accurate identification of the waste weight generated by each user of the service. In perspective, this solution will allow the transition to a new method of charging service costs in relation to the previous one - billing per kilogram of generated waste.

3. The fuel consumption control solution for the vehicle fleet is improved by introducing a pulse flow measurement system on newer vehicles. So, in addition to monitoring the level of fuel in the vehicle's tank, the solution allows monitoring of effective - dynamic fuel consumption as the difference in fuel volume that is delivered to the vehicle engine and that is returned as surplus in the tank. This control method prevents misuse of fuel during operation of the vehicle on the site.

4. By this survey, the POI collections (database) were created and updated with all the necessary attributes (types of bins/waste containers, coordinates, owner's or user's name, etc.) and displayed as a special graphic layer on the operational map of the territory covered by the utility company.

5. A program procedure for controlling event that is characteristic in the waste collection process (lifting and unloading the waste bins into the RC vehicle) is developed by this investigation. The procedure controls the pressure in the hydraulic installation and checks whether the collection process takes place according to the established plan. More precisely, it can be counted how many waste containers are emptied out. The method is based on converting the measured pressure to the equivalent value of the voltage. Due to the non-linearity of the pressure change of hydraulic oil, i.e. complicated calibration of voltage equivalents, this method was avoided as the solution for determining the converted value (voltage) of the weight of the collected waste. Finding a better solution is the next research task.

6. The authors established a series of software tools for diagnostics of the waste collection and transport

process as well as individual subsystems on the vehicle, for example, for diagnostics of the battery charging system. Modern monitoring technology is already being applied in advanced companies, and development takes place in the domain of control, monitoring and expert software systems. Therefore, already specialized electronic components for tracking vehicles appear in the paper. The ultimate goal is - monitoring the fleet. The development of the communal waste management systems in the short-term future period should focus on establishing the conditions for the application of the fleet mode in the operation of RC vehicles. These conditions should define stricter requirements for the most important categories such as: planning (routing, reduction of effective operation of the vehicle and crew, monitoring of fuel consumption, etc.), technical equipment of vehicles (new and better technologies), formation of good communication systems, selection of more precise Global Positioning System, equipping with cameras for video surveillance as a general trend.

ACKNOWLEDGMENT

The paper is a part of the research performed within the project TR 35049. The authors would like to thank to the Ministry of Education, Science and Technological Development, Republic of Serbia.

REFERENCES

- [1] Bajaj, D. and Gupta, N.: GPS based automatic vehicle tracking using RFID, *Int. J. Eng. Innovative Tech.*, Vol. 1, No. 1, pp. 31-35, 2012.
- [2] Chalkias, C. and Lasaridi, K.: A GIS based model for the optimization of municipal solid waste collection - The case study of Nikea, Athens, Greece, *WSEAS Trans. Env. Develop.*, Vol. 5, No. 10, pp. 640-650, 2009.
- [3] Ghose, M.K., Dikshit, A.K. and Sharma, S.K.: A GIS based transportation model for solid waste disposal - A case study on Asansol municipality, *Waste Management*, Vol. 26, No. 11, pp. 1287-1293, 2006.
- [4] Tavares, G., Zsigraiova, Z., Semiao, V. and Carvalho, M.G.: Optimization of MSW collection routes for minimum fuel consumption using 3D GIS modeling, *Waste Management*, Vol. 29, No. 3, pp. 1176-1185, 2009.
- [5] Lia, H., Chenb, Z., Yonga, L. and Kong, S.C.W.: Application of integrated GPS and GIS technology for reducing construction waste and improving construction efficiency, *Automation in Construction*, Vol. 14, No. 3, pp. 323-331, 2005.
- [6] Teltonika, www.teltonika.eu, April, 2019.
- [7] Radoičić, G., Jovanović, M. and Arsić, M.: Experience with an on-board weighing system solution for heavy vehicles, *ETRI J.*, Vol. 38, No. 4, pp. 787-797, 2016.

Thomas KriehnTeaching Assistant
Heilbronn University
Faculty of Technical Processes**Franziska Schloz**Teaching Assistant
University of Stuttgart
Institute of Mechanical Handling and
Logistics**Robert Schulz**Full Professor
University of Stuttgart
Institute of Mechanical Handling and
Logistics**Markus Fittinghoff**Full Professor
Heilbronn University
Faculty of Technical Processes

Algorithm and analytical model to optimize class-based storage of shuttle-based storage and retrieval systems

Compared to crane-based automatic storage and retrieval systems (AS/RS), shuttle based storage and retrieval systems (SBS/RS) can often achieve higher throughput and energy demand tends to be lower due to less mass movement. As a result, SBS/RS have become widely used in recent years. They can be found in distribution centers across all industries, but can also be found in warehouses for producing companies to supply the production process. A common application is a SBS/RS, which supplies subsequent picking stations via conveyors. The throughput of a SBS/RS can be increased by the storage management policy class-based storage. This policy assigns totes to storage locations based on their frequency of requests. This leads to the definition of zones for classes of totes (or articles). This paper shows how zoning can be improved by an algorithm with use throughput as optimization criterion.

Keywords: shuttle, simulation, model, class-based-storage, throughput, storage, retrieval, algorithm, analytical, SBS/RS.

1. INTRODUCTION

SBS/RS consists of one or more shuttle carriers, at least one elevator, a rack structure and a control system [1].

Systems with aisle- and tier-captive shuttle carriers are often used for high throughput demands.

Tier-to-tier shuttle carriers cannot change the aisle, but the tiers. In such cases, the shuttle carrier uses the elevator to change to another tier. This can lead to throughput-reducing waiting times [2].

Aisle- and tier-captive SBS/RS use a shuttle carrier for each tier, which cannot leave the tier. The shuttle carrier and the elevator use buffer locations at each tier to store or retrieve totes. As a result, the horizontal and vertical transport is largely decoupled from one another. Accordingly, aisle- and tier-captive SBS/RS can often achieve a higher throughput than tier-to-tier SBS/RS [2].

The throughput of a SBS/RS can be increased by class-based storage. This raises the question of how the totes can be optimally assigned to storage locations due to their frequency of requests. This paper deals with this question.

This paper is structured as follows: Chapter 1 gives an introduction. Chapter 2 contains an explanation of the existing literature on class-based storage for the considered SBS/RS (2.1), the description of the analytical model (2.2) and the simulation model (2.3) as well as the optimization algorithm for class-based storage (2.4). Chapter 2 ends with the results received by the applied algorithm (2.5). Chapter 3 contains the summary of the article.

Correspondence to: Thomas Kriehn, Teaching Assistant
Faculty of Technical Processes, University Heilbronn,
Max-Planck-Str. 39, 74081 Heilbronn, Germany
E-mail: thomas.kriehn@hs-heilbronn.de

2. MODEL AND ALGORITHM

2.1 Literature

In [2-7] class-based storage is used for aisle- and tier-captive and in [8, 9] for tier-to-tier SBS/RS. The papers show the effect of throughput increase by class-based storage.

In [4] an ant colony clustering algorithm is used to define zones. There are no results mentioned. The SBS/RS considered does not use any buffer locations and thus deviates from aisle- and tier-captive SBS/RS used predominantly in industrial practice. Without buffer locations, the SBS/RS can only achieve a comparatively low throughput, since the elevator and shuttle carrier have to wait for the transfer of totes.

In [5] a part of the algorithm that is described in detail in this paper, is introduced for the first time by way of example, without mentioning results.

[2, 3] and [6-9] show to which extent throughput increases through class-based storage is possible. Moreover, in [2] and [6-8] principles are described to achieve a favorable definition of zones. A favorable definition of zones can be achieved by matching as close as possible the throughput of elevators and shuttle carriers in the high frequented tiers.

2.2 Analytical Model

In order to be able to calculate the impact of class-based storage on throughput, the assumptions of uniform distribution of storage locations have to be relaxed. Uniform distribution of storage locations implies that each storage location is requested with the same probability (for retrieval or storage requests). [8] describes an analytical model, that allows adjustable distribution of storage locations. The model is based on

single-depth tier-to-tier SBS/RS and is expanded in this paper to aisle- and tier-captive SBS/RS.

The definition of zones is formulated for the sides of the aisle with the matrices $Z_{LP1,k,i}$ (LP1 means left side) and $Z_{LP2,k,i}$ (LP2 means right side) whose rows represent tiers (k) and whose columns storage positions (i). i and LP1/LP2 define the storage location. The zones are numbered in ascending order ($1, 2, \dots, \max(z)$).

$$Z_{LP1,k,i} = \begin{pmatrix} Z_{LP1,1,1} & \dots & Z_{LP1,1,i} \\ \dots & \dots & \dots \\ Z_{LP1,k,1} & \dots & Z_{LP1,k,i} \end{pmatrix} \quad (1)$$

$$Z_{LP2,k,i} = \begin{pmatrix} Z_{LP2,1,1} & \dots & Z_{LP2,1,i} \\ \dots & \dots & \dots \\ Z_{LP2,k,1} & \dots & Z_{LP2,k,i} \end{pmatrix} \quad (2)$$

The vector w_z assigns the probability of requests to each zone.

$$w_z = \begin{pmatrix} w_1 \\ \dots \\ w_{\max(z)} \end{pmatrix} \quad (3)$$

The vector l_z assigns the number of associated storage positions to each zone.

$$l_z = \begin{pmatrix} l_1 \\ \dots \\ l_{\max(z)} \end{pmatrix} \quad (4)$$

$$t_{EF,y} = \begin{cases} \sum_{k=1}^{n_y} w_{k,y} \left(\frac{|l_{E,y} + (k-1)l_y|}{v_L} + \frac{v_L}{a_L} \right) \text{ for } |l_{E,y} + (k-1)l_y| \geq \frac{(v_L)^2}{a_L} \\ \sum_{k=1}^{n_y} w_{k,y} \left(2 \sqrt{\frac{|l_{E,y} + (k-1)l_y|}{a_L}} \right) \text{ for } |l_{E,y} + (k-1)l_y| \leq \frac{(v_L)^2}{a_L} \end{cases} \quad (9)$$

v_L is the maximum achievable velocity of the elevator, a_L is the acceleration of the elevator. The deceleration is assumed to be identical. $l_{E,y}$ is the distance from the input- or output-point (depending on whether storage or retrieval requests are calculated) to tier 1. The value is given a negative sign if the input-point is above tier 1 (otherwise positive). l_y is the distance between the tiers. n_y is the number of tiers. k is a variable to count tiers. Tier $k = 1, 2, \dots, n_y$.

For the mean cycle time of a single-command cycle of the elevator applies:

$$t_{ES,y} = 2(t_{EF,y} + t_{G,y} + t_{P,y}) \quad (10)$$

$t_{P,y}$ is the switching and positioning time that occurs during each braking operation until the elevator stops. $t_{G,y}$ is the time for tote handling of the elevator.

The mean throughput of the elevator [tote/h] is therefore:

$$D_{ES,y} = \frac{3600}{t_{ES,y}} \quad (11)$$

The following equations apply to the calculation of a dual-command cycle of the elevator.

The probability of requests for a storage location, based on the entire SBS/RS (or the considered subarea thereof, e.g. an aisle), results as follows:

$$w_{i(k,z),x,LP1} = w_{i(k,z),x,LP2} = \frac{w_z}{l_z} \quad (5)$$

$w_{i(k,z),x,LP1}$ is the probability for requests for the storage position i of the tier k , storage location is on the left side. $w_{i(k,z),x,LP2}$ is the probability for requests for the storage position i of the tier k , storage location is on the right side.

The probability for requests from a tier k results as follows:

$$w_{k,y} = \sum_{i=1}^{n_x} (w_{i(k,z),k,LP1} + w_{i(k,z),k,LP2}) \quad (6)$$

The probability for requests for a position i for a shuttle carrier, that is located in tier k , results as follows:

$$w_{i(k),x,LP1} = \frac{w_{i(k,z),x,LP1}}{w_{k,y}} \quad (7)$$

$$w_{i(k),x,LP2} = \frac{w_{i(k,z),x,LP2}}{w_{k,y}} \quad (8)$$

The model based on (1 - 8) for tier-to-tier SBS/RS is described in detail in [8]. For aisle and tier-captive SBS/RS, the model will be extended as follows. The mean travel time of a single travel of the elevator is:

The probability that the elevator will remain in the same tier after finishing a storage request is:

$$w_{0,y} = \sum_{k=1}^{n_y} w_{k,y}^2 \quad (12)$$

In the case of a dual-command cycle, the probability $w_{m,y}$ is the probability to travel, after finishing a storage request, to the tier with the next retrieval request. m is the number of changed tiers (eg $m = 1$, one tier has been changed). The following applies:

$$w_{m,b,y} = \sum_{k=1}^{n_y-m} 2w_{k,y}w_{k+m,y} \quad (13)$$

The mean travel time for changing the tiers between storage and retrieval is calculated as follows:

$$t_{L,y} = \begin{cases} \sum_{m=1}^{n_y-1} w_{m,y} \left(\frac{ml_y}{v_L} + \frac{v_L}{a_L} \right) \text{ for } ml_y \geq \frac{(v_L)^2}{a_L} \\ \sum_{m=1}^{n_y-1} w_{m,y} \left(2 \sqrt{\frac{ml_y}{a_L}} \right) \text{ for } ml_y \leq \frac{(v_L)^2}{a_L} \end{cases} \quad (14)$$

If the location of the input-point differs from that of the output-point, another travel time is required to calculate. After finishing the retrieval request a travel to the input-point is required. The following applies:

$$t_{EFA,y} = \begin{cases} \frac{|l_{E,y} - l_{A,y}|}{v_L} + \frac{v_L}{a_L} \text{ für } |l_{E,y} - l_{A,y}| \geq \frac{(v_L)^2}{a_L} \text{ and } l_E \neq l_A \\ 2 \sqrt{\frac{|l_{E,y} - l_{A,y}|}{a_L}} \text{ für } |l_{E,y} - l_{A,y}| \leq \frac{(v_L)^2}{a_L} \text{ and } l_E \neq l_A \\ 0, \text{ otherwise} \end{cases} \quad (15)$$

$l_{E,y}$ is the position of the input-point, $l_{A,y}$ is the position of the output-point (sign selection as described for $l_{EA,y}$).

The mean travel time of a dual-command cycle is:

$$t_{EFL,y} = t_{EF,E,y} + t_{EF,A,y} + t_{L,y} + t_{EFA,y} \quad (16)$$

The expectation value for the occurrence of the switching and positioning times takes into account the positions of the input- and output-point and the probability of the tier remaining.

$$E_{DS} = \begin{cases} (3 - w_{0,y})t_{P,y} \text{ for } l_E = l_A \\ (4 - w_{0,y})t_{P,y} \text{ for } l_E \neq l_A \end{cases} \quad (17)$$

The mean cycle time of a dual-command cycle of the elevator is:

$$t_{DS,y} = t_{EFL,y} + 2t_{G,x} + 2t_{G,y} + E_{DS} \quad (18)$$

The mean throughput of a dual-command cycle of the elevator [tote/h] is:

$$D_{DS,y} = 2 \left(\frac{3600}{t_{DS,y}} \right) \quad (19)$$

For the calculation of the cycle time of a single-command cycle of the shuttle carrier, the following equations apply.

The probability to travel to a position i in the tier k is:

$$w_{i(k),x} = w_{i(k),x,LP1} + w_{i(k),x,LP2} \quad (20)$$

For the mean travel time of the shuttle carrier applies:

$$t_{EF,x(k)} = \begin{cases} \sum_{k=1}^{n_x} w_{i(k),x} \left(\frac{(k-1)l_x}{v_s} + \frac{v_s}{a_s} \right) \text{ for } (k-1)l_x \geq \frac{(v_s)^2}{a_s} \\ \sum_{k=1}^{n_x} w_{i(k),x} \left(2 \sqrt{\frac{(k-1)l_x}{a_s}} \right) \text{ for } (k-1)l_x \leq \frac{(v_s)^2}{a_s} \end{cases} \quad (21)$$

The mean cycle time of the shuttle carrier for a single-command cycle in tier k results in:

$$t_{ES,x(k)} = 2(t_{EF,x(k)} + t_{P,x}) + t_{G,x} + t_{G,\ddot{U}P,x} \quad (22)$$

$t_{G,\ddot{U}P,x}$ is the time required for tote handling, pick-up from or set-down to a buffer location. $t_{G,x}$ is the time required for tote handling, pick-up from or set-down to a storage location.

The throughput of the shuttle carrier in the tier k results in:

$$D_{ES,x(k)} = \frac{3600}{t_{ES,x(k)}} \quad (23)$$

The mean throughput of all shuttle carriers in one aisle is:

$$D_{ES,x} = \sum_{k=1}^{n_y} D_{ES,x(k)} \quad (24)$$

For a dual-command cycle of the shuttle carrier, the following equations apply. The probability of remaining in the same position, after a storage, is:

$$w_{0,b,x(k)} = \sum_{i=1}^{n_x} w_{i(k),x,LP1} \frac{w_{i(k),x,LP2}}{1 - w_{i(k),x,LP1}} + w_{i(k),x,LP2} \frac{w_{i(k),x,LP1}}{1 - w_{i(k),x,LP2}} \quad (25)$$

The probability of a change of position is:

$$w_{m,b,x(k)} = \sum_{i=1}^{n_x-m} (w_{i(k),x,LP1} \frac{w_{i+m(k),x,LP1} + w_{i+m(k),x,LP2}}{1 - w_{i(k),x,LP1}} + w_{i(k),x,LP2} \frac{w_{i+m(k),x,LP1} + w_{i+m(k),x,LP2}}{1 - w_{i(k),x,LP2}} + w_{i+m(k),x,LP1} \frac{w_{i(k),x,LP1} + w_{i(k),x,LP2}}{1 - w_{i+m(k),x,LP1}} + w_{i+m(k),x,LP2} \frac{w_{i(k),x,LP1} + w_{i(k),x,LP2}}{1 - w_{i+m(k),x,LP2}}) \quad (26)$$

For the travel time for changing the position applies:

$$t_{L,b,x(k)} = \begin{cases} \sum_{m=1}^{n_x-1} w_{m,b,x(k)} \left(\frac{ml_x}{v_{max}} + \frac{v_{max}}{a} \right) & \text{for } ml_x \geq \frac{(v_{max})^2}{a} \\ \sum_{m=1}^{n_y-1} w_{m,b,x(k)} \left(2 \sqrt{\frac{ml_x}{a}} \right) & \text{for } ml_x \leq \frac{(v_{max})^2}{a} \end{cases} \quad (27)$$

The mean travel time for the dual-command cycle in tier k is:

$$t_{EFL,b,x(k)} = 2t_{EF,b,x(k)} + t_{L,b,x(k)} \quad (28)$$

The switching and positioning times coincide with the probability of remaining in the position $w_{0,b,x(k)}$ twice and with the probability of a position change (sum of the

probabilities over m positions) $\sum_{m=1}^{n_x-1} w_{m,b,x(k)}$ three times.

The following applies:

$$\sum_{m=1}^{n_x-1} w_{m,b,x(k)} = 1 - w_{0,b,x(k)} \quad (29)$$

The expected value of the switching and positioning times in a dual-command cycle results in:

$$E_{DS,x(k)} = 3t_{p,x} \sum_{m=1}^{n_x-1} w_{m,b,x(k)} + 2t_{p,x}w_{0,b,x(k)} = (3 - w_{0,b,x(k)})t_{p,x} \quad (30)$$

The mean cycle time for a dual-command cycle is:

$$t_{DS,x(k)} = t_{EFL,b,x(k)} + 2t_{G,ÜP,x} + 2t_{G,x} + E_{DS,x(k)} \quad (31)$$

The mean throughput of a shuttle carrier [tote/h] in the tier k is:

$$D_{DS,x(k)} = 2 \left(\frac{3600}{t_{DS,x(k)}} \right) \quad (32)$$

The mean throughput achievable by shuttle carriers for one aisle is:

$$D_{DS,x} = \sum_{k=1}^{n_y} D_{DS,x(k)} \quad (33)$$

$$D_{ES,w,y(k)} = \begin{cases} \min(D_{ES,y(k)}, D_{ES,x(k)}), & \text{one elevator used} \\ \frac{1}{2} \min(2D_{ES,y(k)}, D_{ES,x(k)}), & \text{two elevators used} \end{cases} \quad (35)$$

$$D_{ES,w,x(k)} = \begin{cases} D_{ES,w,y(k)}, & \text{one elevator used} \\ 2D_{ES,w,y(k)}, & \text{two elevators used} \end{cases} \quad (36)$$

In this context, the word "used" distinguishes between actually existing elevators in an aisle and the elevators actively used for the case in question. For example, an aisle may contain two elevators, but one elevator is responsible for storage requests, the other for retrieval requests. Then only the corresponding elevator becomes active when processing only storage or retrieval requests.

The elevator as well as all shuttle carriers in the aisle reach the following mean throughput in total, over all tiers k :

$$D_{ES,w,y} = \sum_{k=1}^{n_y} D_{ES,w,y(k)} \quad (37)$$

With this model, cycle time and throughput can be calculated without the consideration of waiting times. The calculation of waiting times is described in [8] for tier-to-tier SBS/RS and is expanded in this paper aisle- and tier captive SBS/RS.

2.2.1 Single-command cycle, elevator and shuttle carrier

The throughput that could be realized by the elevator in the tier k without consideration of a waiting time is:

$$D_{ES,y(k)} = w_{k,y} D_{ES,y} \quad (34)$$

The achievable mean throughput for the elevator $D_{ES,E,w,y}$ and for the shuttle carrier $D_{ES,w,x(k)}$ in the tier k is determined as follows:

$$D_{ES,w,x} = \sum_{k=1}^{n_y} D_{ES,w,x(k)} \quad (38)$$

2.2.1 Dual-command cycle, elevator and shuttle carrier

The throughput, which could be realized by an elevator in the tier k , without consideration of a waiting time, is:

$$D_{DS,y(k)} = w_{k,y} D_{DS,y} \quad (39)$$

The achievable mean throughput for the elevator $D_{DS,w,y(k)}$ and for the shuttle carrier $D_{DS,w,x(k)}$ in the tier k is determined as follows:

$$D_{DS,w,y(k)} = \begin{cases} \min(D_{DS,y(k)}, D_{DS,w,x(k)}), & \text{one elevator used} \\ \frac{1}{2} \min(2D_{DS,y(k)}, D_{DS,w,x(k)}), & \text{two elevators used} \end{cases} \quad (40)$$

$$D_{DS,w,x(k)} = \begin{cases} D_{DS,y(k)}, & \text{one elevator used} \\ 2D_{DS,y(k)}, & \text{two elevators used} \end{cases}$$

The elevator(s) and the shuttle carriers reach the following mean throughput in total, over all k tiers:

$$D_{DS,w,y} = \sum_{k=1}^{n_y} D_{DS,w,y(k)} \quad (40)$$

$$D_{DS,w,x} = \sum_{k=1}^{n_y} D_{DS,w,x(k)} \quad (41)$$

2.3 Simulation model

The simulation model determines the maximum average throughput for the selected parameter combination. The study relates to an aisle with two shelves with storage locations: left and right from the aisle. In each scenario, it is assumed that requests are available for processing at any time. The SBS/RS is single-deep. The capacity for totes per travel is one for the elevators and the shuttle carriers. Here, one tote corresponds to one article. Each storage location can store one tote. The capacity of the buffer locations is one. In each scenario, two elevators are used per aisle. The simulation model is used to validate the analytical model.

2.4 Algorithm to optimize class-based storage

The algorithm described below iteratively change the definition of zones. After each (valid) iteration, the throughput is determined. After all iterations have been completed, the optimal result for zoning is returned and also associated parameters for system behavior (throughput, cycle time, waiting time). Using this algorithm, the number of zones can be freely defined, up to the number of storage locations. The algorithm returns the result relatively quickly, when using an analytical model.

The algorithm starts with the definition of zone 1 with the tier closest to the midpoint between the input- and output-point. Position i starts with the value one and is incrementally increased. $i = 1$ implies that only the first two storage locations (left and right) in the permitted tiers is assigned to zone 1, $i = 2$ implies that the first and second position with their four storage locations (left and right) in the permitted tiers are assigned to zone 1. The iterations continue until, for the first time, a valid combination is achieved (all required storage locations of zone 1 can be filled).

For each valid combination, the achievable throughput is determined. Thereafter, the position i is further increased to the maximum value. In result allowed tiers near the midpoint of the input- and output-point to the position i are assigned to zone 1 and more distant allowed tiers maybe no longer be assigned to zone

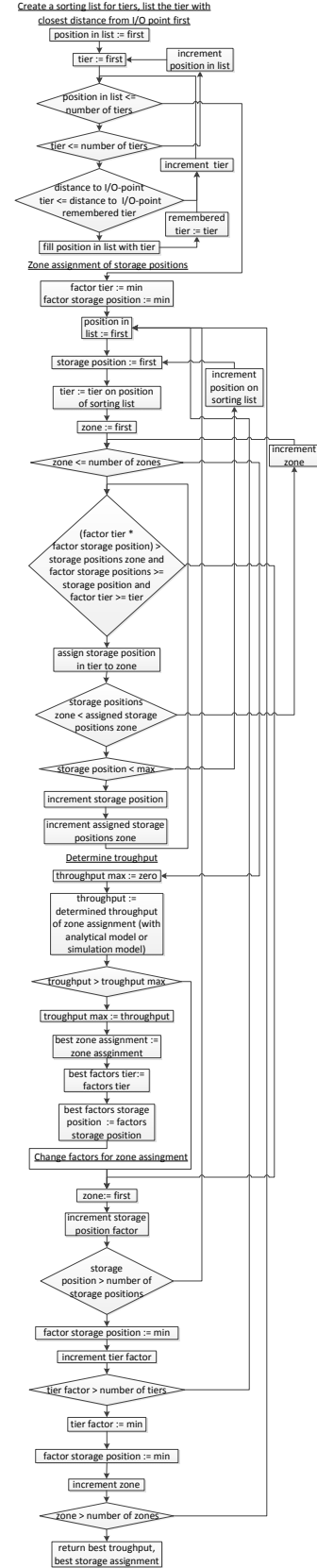


Figure 1: Algorithm

1 in the position i , since the required number of storage locations for zone 1 has already been reached. As soon as the position i corresponds to the maximum value, an additional tier for the assignment of zone 1 is released. Position i is reset to 1 and the iterations start again. All other zones are defined one after the other during these iterations, but all tiers and all storage locations are allowed for subsequent zones (except for the storage locations already assigned to the previous zone). **Figure 1** shows the algorithm.

Once all iterations have been performed for zone 1, the storage locations for zone 2 will be iteratively assigned in the same pattern. Positions are already reserved for zone 1 (the definition that previously provided the maximum throughput) can't be assigned to zone 2.

Figure 2 illustrates the approach of the algorithm using an example of three zones, six tiers, and six storage locations. The first iteration is shown (zone 1 is dark gray). $f_{k(1)}$ is the number of allowed tiers for the definition of zone 1. $f_{i(1)}$ is the number of allowed storage positions for the definition of zone 1.

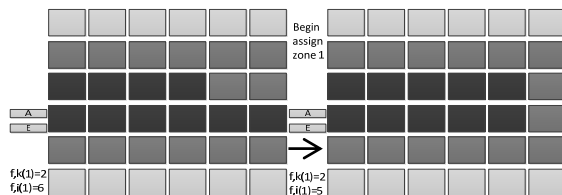


Figure 2: Iterative definition of zones, first iteration

2.5 Results

This chapter shows how to optimize throughput by using the optimization algorithm, and the accordance from the analytical and the simulation model. Table 1 shows the constant parameter values of the investigated SBS/RS.

Table 1. Constant parameter values

Parameter	Value
l_y [m] (Distance between tiers)	0.4
l_{EA} [m] (Distance between first tier and I/O-point)	-1
$n_x (= \max(i))$ (Storage positions per tier)	100
l_x [m] (Distance between storage positions)	0.5
$t_{p,y}$ [s] (Positioning and switching times Elevator)	0.5
$t_{G,x} (= t_{G,\bar{u}p,x})$ [s] (Tote handling time shuttle-carrier)	3
$t_{p,x}$ [s] (Positioning and switching times shuttle-carrier)	0.5
SBS/RS	Aisle- and tier-captive

Table 2 shows the variable parameter values (variants). Table 3 shows the parameter values for different zones. Tables 4 - 10 show the results of the investigated variants. The values written in cursive were determined by the simulation model, while the rest were calculated by the analytical model. Zones = 1 implies

random storage assignment. Variants 1 - 3 show the definition of zones and the potential of optimization for different values of acceleration and velocity for elevators and shuttle carriers. Variant 4 shows the possibility of taking account of a lower storage ratio by a zone that is not requested (variant 4 deviates from variant 1 only with a lower storage ratio). Variation 5 shows the effect of zoning for a higher SBS/RS (variant 5 deviates from variant 2 only with 36 tiers). The throughput results in the following tables refer to the throughput of one elevator. In the scenarios shown here, two elevators are used per aisle. Thus, twice the throughput can be achieved per aisle.

Table 2. Variable parameter values

Variant	1	2	3	4	5
n_y (Tiers)	12				36
v_L (Velocity elevator)	1	4	7	1	4
a_L (Acceleration elevator)	2	4	7	2	4
$t_{p,y}$ (Pick-up and set-down time elevator)	1	4	3	1	4
v_S (Velocity shuttle carrier)	5	3.5	2	5	3.5
a_S (Acceleration shuttle carrier)	5	3.5	2	5	3.5
Storage ratio [%]	95		50		95

Table 1. Parameter values for different zones

Zones	1	2	3	4	6
l_z (Storage positions per zone)	1200	400 800	240 360 600	120 180 300 600	100 140 160 200 280 320
w_z (Probability of request per zone)	1	0.6 0.4	0.6 0.3 0.1	0.6 0.3 0.1 0	0.3 0.25 0.2 0.15 0.06 0.04

Table 2: Results variant 1

	Throughput elevator			
Cycle	Single-command			
Zones	1	2	3	6
Variant 1	494.01 (494.75)	565.11 (552.42)	632.19 (616.23)	627.98 (615.84)

Table 3: Results variant 2, single-command cycle

	Throughput elevator			
Cycle	Single-command			
Zones	1	2	3	6
Variant 2	319.34 (319.7)	331.71 (332.67)	343.83 (341.52)	344.14 (341.14)

Table 4: Results variant 2, dual-command cycle

Variant 2	Throughput elevator			
Cycle	Dual-command			
Zones	1	2	3	6
Variant 2	344.89 (344.08)	353.9 (350.93)	365.64 (358.15)	365.89 (357.75)

Table 5: Results variant 3, single-command cycle

	Throughput elevator			
Cycle	Single-command			
Zones	1	2	3	6
Variant 3	466.41 (466.59)	482.46 (480.49)	491.64 (490.82)	487.08 (485.44)

Table 6: Results variant 3, dual-command cycle

	Throughput elevator			
Cycle	Dual-command			
Zones	1	2	3	6
Variant 3	512.75 (510.84)	526.65 (522.21)	539.86 (532.53)	528.94 (524.25)

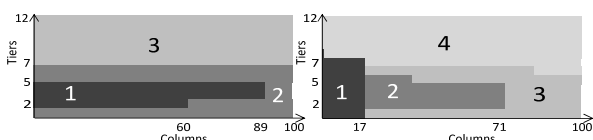
Table 7: Results variant 4

	Throughput Elevator	
Cycle	Single-command	
Zones	1	4
Variant 4	494.01 (494.75)	659.40 (645.32)

Table 8: Results variant 5

	Throughput Elevator			
Cycle	Single-command		Dual-command	
Zones	1	3	1	3
Variant 5	259.16 (260.64)	304.41 (303.64)	294.10 (297.98)	328.24 (327.22)

The optimal definition of zones at increased acceleration and velocity of the elevator tends to increase the number of frequently used tiers. The optimal definition of zones at increased acceleration and velocity of the shuttle carriers tends to decrease the number of frequently used tiers, see also [3]. **Figure 3** shows two examples of defined zones by the algorithm.

**Figure 3: Optimal zones defined by algorithm, left variant 3, right variant 4**

The results show the potential of optimization for defined zones. Also it can be shown, that the analytical model has only slight deviations from the simulation model for the calculated variants (highest deviation is 2.52 %).

All of the following mentioned percentage increases in throughput refer to the comparison between the zone definition of a variant and random storage assignment.

For variant 1, the throughput can be increased by 27.97%, for variants 2 - 3 between 5.29% and 7.77%. The slower the elevator moves (and the faster the tote handling time), the stronger the effect of reducing the path is due to zone formation. Therefore the throughput in variant 1 can be increased significantly more as for variant 2 and 3.

The consideration of a lower storage ratio results in a significant increase in throughput of 33.48% (variant 4).

The farther the elevator has to travel, the higher the potential for optimization. Variation 5 increases throughput by defined zones up to 17.46%. This is a much higher increase than with variant 2, which has the same parameter values as variant 5 with the exception of the number of tiers (variant 5 has 36 tiers, variant 2 has 12 tiers).

3. CONCLUSION

In this paper, an analytical model for calculating the throughput of aisle- and tier-captive SBS/RS is presented. The model allows the consideration of any probabilities of requested storage locations. Hence, modelling the storage management policy class-based storage is possible. The analytical model has a high accordance with the simulation model for the calculated and simulated variants.

Furthermore, an algorithm was presented, that optimize the definition of zones. The algorithm optimize according to the criterion of maximum throughput. The results show the potential of optimization by the application of the algorithm.

Further interesting topics for future work may be:

- Finding optimal zones with evolutionary algorithms (is currently being researched at Heilbronn University).
- Methods of artificial intelligence, e.g. for deep reinforcement learning to solve control and optimization problems (is currently being researched at the Institute for Mechanical Handling and Logistics at the University of Stuttgart).

ACKNOWLEDGMENT

This work was supported by the Industrial Community Research (IGF) of Germany under the Number 19508N.

REFERENCES

- [1] VDI-2692: *Automated vehicle storage and retrieval systems for small unit loads*, Berlin: Beuth-Verlag, 2015.
- [2] Kriehn, T., Schloz, F., Wehking, K.-H. and Fittinghoff, M.: Storage management policies for throughput optimization of shuttle-based storage and retrieval systems, Proceedings of the XXII International Conference on Material Handling, Constructions and Logistics, Belgrade, Serbia, 4-6 October 2017, pp. 177-184, 2017.

- [3] Ekren, B.Y., Sari, Z. and Lerher, T.: Warehouse design under class-based storage policy of shuttle-based storage and retrieval system, IFAC-PapersOnLine, Vol. 48, No. 3, pp. 1152-1154, 2015.
 - [4] Wang, Y., Mou, S. and Wu, Y.: Storage Assignment Optimization in a Multi-tier Shuttle Warehousing System, Chinese Journal of Mechanical Engineering, Vol. 29, No. 2, pp. 421-429, 2016.
 - [5] Schloz, F., Kriehn, T., Fittinghoff, M. and Wehking, K.-H.: Development of situation-based storage strategies for autonomous vehicle storage and retrieval systems, Logistics Journal: Proceedings, Vol. 2017, 2017.
 - [6] Kriehn, T., Schloz, F., Wehking, K.-H. and Fittinghoff, M.: Generation of simulation models to detect the system behavior of shuttle based storage and retrieval systems, Proceedings of ASIM/GI, STS and GMM Conference, Heilbronn, pp. 119-124, 2018.
 - [7] Kriehn, T., Schloz, F., Wehking, K.-H. and Fittinghoff, M.: Impact of Class-Based Storage, Sequencing of Retrieval Requests and Warehouse Reorganisation on Throughput of Shuttle-Based Storage and Retrieval Systems, FME Transactions, Vol. 46, No. 3, Serbia, Belgrad, pp. 320-329, 2018.
 - [8] Kriehn, T.: *Development of an analytical model for determining the system behavior of tier-to-tier shuttle based storage and retrieval systems*, University Stuttgart, Master-Thesis, 2018.
 - [9] Kaczmarek, S., Goldenstein, J. and ten Hompel, M.: Performance Analysis of Autonomous Vehicle Storage and Retrieval Systems Depending on Storage Management Policies, Proceedings of the 21st International Conference on Industrial Engineering and Engineering Management 2014, 9-12 December 2014, Bandar Sunway, Malaysia, pp. 1424-1428, 2015.
-

Material flow systems and intralogistics components for a non-sequential, flexibly timed automobile production – First prototypes

Matthias Hofmann

Institute of Mechanical Handling and
Logistics - University of Stuttgart
Department Machine Design / Material
Flow Automation

Since the introduction of assembly lines by Henry Ford and Frederick Taylor, the principles of automobile production have been maintained nearly unchanged. The underlying principle still builds on sequential synchronized production patterns, even though the products have radically changed. Because of model policy and the successive digressing from fossil fuel powered mobility, the variance between models is currently escalating even more. From the present point of view, the production of automobiles with such varying technical specifications requires a flexible production system with individually adjustable cycle times and a non rigid sequence of processing steps. A new concept for production logistics, designed by the Institute for Mechanical Handling and Logistics at the University of Stuttgart aims to enable an efficient production of batch size one due to flexible and convertible material flow systems. The key elements of this completely new concept are disruptive intralogistics components.

Keywords: automobile industry, batch size one, product diversity, efficient series production, Just-In-Real-Time

1. MOTIVATION AND STATEMENT OF THE PROBLEM

In light of the background of the parallel production of passenger vehicle model ranges with hybrid drives or purely electrical drives next to conventional internal combustion models from an assembly line with comprehensive and individualized equipment packages, the possibilities for a more efficient design of the classic assembly line production seem exhausted, in spite of advances in automation. As a result, the abandonment of well-known production principles is coming to the fore in mid-term and long-term corporate planning. Abandoning assembly lines would present no less than a paradigm shift in automotive production, the more so as production without belts and precise timing requires the development of disruptive support, warehousing and handling machines, because the available inflexible continuous conveyors in the final assembly lines, e.g. electric monorail conveyors or thruster platforms, are opposed to the desire for flexible, convertible and scalable assembly and production logistics systems.

1.1 Variant diversity

The great range of workloads which already exist in in a vehicle model line primarily demand, in terms of the production technology, customized individual cycle times for each vehicle configuration, which is impossible to

harmonize with the current strict cycle times for the traditional assembly line principles. As a result, a required average for the cycle time of the so-called model mix is ensured. A particularly high degree of complexity can be found in the production of hybrid and electric vehicles.

These vehicles are fundamentally different from conventional vehicles with internal combustion engines, which makes itself felt in the sequence and scope of the assembly process. Ensuring the strict cycle times can only be achieved by actively generating the necessary head start for the elaborate hybrid and electric vehicles using previous and following vehicle configurations with lower assembly time requirements. It can be seen from the decidedly comprehensive data collection generated in the course of the “FlexProLog – Realignment of Production Logistics for affordable Electromobility” survey project, that there can be only a certain percentage of the total production of hybrid and electric vehicles in such manufacturing lines, cf. [1]. Not only the capacity limits, but also the minimal time span within which two hybrid or electric vehicles can be built, are considerable. These restrictions arise solely due to the cycle times and the sequence of the material flow chain. As the data involved from the automobile manufacturers must be handled with discretion, a detailed discussion is not possible here. The results of the survey suggest, however, that – measured by the current situation – not only is action necessary for the output of electric cars to grow along with the expansion of the market, but also to increase productivity to maintain competitiveness. This topic does not only pertain to vehicles with alternative drive systems, but more to all vehicle configurations with a broad range of extra features, as well as those with certain technological features, e.g. a sun roof, which are complicated to install. To the extent that it is this result that has fundamentally

Correspondence to: Dipl.-Ing. Matthias Hofmann
Institute of Mechanical Handling and Logistics,
University of Stuttgart
Holzgartenstraße 15 B, 70174 Stuttgart,
E-mail: matthias.hofmann@ift.uni-stuttgart.de

changed the principles to the assembly line production of vehicles in this field, it is aimed at the strict cycle systems of the assembly of the vehicles in greater numbers. These conflicting priorities do not only hold business-relevant aspects, but also those of the customer, in that the hitherto limited production capacities and the additional expense related to cycle systems for hybrid and electric vehicles lead to higher costs and longer delivery times which are closely related to customer acceptance.

1.2 Volatile Demand and Supplier Bottlenecks

The strong differentiation of the product portfolio in connection with specific production lines holds a high vulnerability to capacity fluctuations in certain lines due to volatile demand within a manufacturer's product spectrum. This was especially apparent after the onset of the financial crisis of 2008 and the economic crisis it entailed in the form of massive declines in sales in the automobile industry. The industry is also currently confronted with volatile markets, which are caused by political policy parameters connected to measures to combat air pollution in European conurbations and city centers. These have resulted in unavoidable capacity fluctuations in factories, as the predominant production structures are unable to adjust their capacities up or down to meet the changing situation. It is thus neither possible to react to sudden changes in demand, nor is it possible to effectively master the supply bottlenecks at short notice. This often results in factory closure days.

There are thus a variety of reasons for luxury automobile manufacturers to be increasingly interested in taking a new direction for their production processes in order to be able to manufacture a broader and more strongly differentiated product spectrum more efficiently in the future. The Board of Directors of the European division of General Motors proclaimed in 2007: "we want to increase the flexibility between the different models, and our goal is to be able to make as many different models in one plant as possible", cf. [2]. Due to the demonstrable product diversification over the last ten years, and the anticipated continuation of this market development, it will simply no longer be possible to create an assembly line for each model as has been done up to now. In light of the investment costs of approx. 50 to 200 million EUR per assembly line, cf. [3], this would not be economically feasible in the end, also due to the immense space requirements.

Remarks have been made in connection to the foregoing that the problems described in the context of the automobile industry are of cross-sectoral relevance, and extend well beyond the same areas of tension between production, market and/or buying habits and the wide variety of various areas of engineering and construction, and differ from one another only in their company-specific forms.

2. OBJECTIVES AND DESIGN

A new logistics concept for flexible and convertible automobile production was developed at the Institute of Mechanical Handling and Logistics (IFT) with funding of the Federal State of Baden-Württemberg. In addition to

systems for parts provision and material flow, the conceptual development of an innovative assembly and logistics large automated guided vehicle (AGV) to be used as workpiece carrier for automobile final assembly. The objective in the first step was to conceptually develop production logistics systems for manufacturing without a belt and cycle system and to investigate their suitability and performance for a concrete application in automobile production by means of simulations.

By eliminating the strict frequency and the firmly linked sequence of processing steps, not only are new mounting supports with related conveyor technology required, but also quicker-reacting material flow systems for the parts provision due to the pearl chain of the parts supply being dissipated by the elimination of the timed sequence, cf. [4]. Whereas the pearl chain had previously constituted the most effective method to deal with the wide variety of situations in series production, the production program and the assembly stations in a flexible and convertible production system no longer constitute fixed points on which the pearl chain can be organized. In a classic conveyor-belt production, the strict adherence to the production program, as well as the precise timing and sequencing from the exact point in time when a part can be assigned to a concrete customer order – precisely quantified – allows it to be planned in advance. In this respect, the material flow and the supply specifically for the prearranged needs for each station ultimately occurs. On the other hand, there are no strict time or location constraints on the assembly scope in a flexible and convertible production, so that instead of a station-specific rather an object-specific delivery oriented on real-time requirements, is required. Real-time requirements, therefore, because the independent workpiece carriers, like those of the mobile assembly islands described in Chapter 3, enable a pass through the assembly oriented on the technical production requirements, which can also be changed at short notice while the part is being produced. This can occur, among other reasons, because of events like, for example, assembly errors or the detection of defective components at the point of use. The real-time need of a specific workpiece could be, in this case, to such an extent that a replacement part would be needed and/or at least an assembly time requirement over the cycle time could arise.

Greater flexibility in the assembly thus requires less reaction time in the parts provisioning. The principles and the related hardware of the material flow systems for the supply of preassembled component, module and assembly materials constitute a central element of the disruptive production logistical concept developed at the Institute of Mechanical Handling and Logistics.

An assembly and logistical platform was conceived for the physical implementation of the logistical concept, in order to perform all the steps in the final assembly – beginning with the floor module or the chassis – directly on this platform. By basing the platform on a large automated guided vehicle (AGV), a per se decoupling of the workpiece carriers is achieved.

The assembly and logistical AGV consists primarily of an omnidirectional freely navigating AGV with integrated handling technology and a circumferential work platform for the personnel while carrying out the

scope of the project while driving. In this respect, the assembly and logistical AGV does not only constitute a workpiece carrier, but more a mobile assembly island on which the complete vehicle final assembly can be carried out without the aid of external lifting or handling equipment. This is made possible by integrated handling equipment which constantly brings the objects to be assembled into an ergonomic position. The 3,500 x 6,000 mm mobile assembly island thus replaces the relevant workpiece carrier and conveyor systems in the form of monorail overhead conveyors and thruster platforms as have been used in classic assembly systems to date.

The transfer of the final assembly from classic materials handling to AGV entails the elimination of the rigid pacing and sequentially immovable progression of the cycling of the individual stations, as there is no mechanical links between the workpiece carriers. This

constitutes more of a self-sufficient system with individual pathway options and speed. As a direct consequence, the stations actually required for the assembly of each vehicle model only have to be started or gone through. Final assembly lines are currently comprised of approx. 150 to 200 stations where the stations are allocated to specific assembly tasks and installations. Depending on the specific product configuration, the workpiece also consequently goes through stations where no value is added because the conveyor system does not permit differentiated pathway options. The application of layout-flexible conveyor systems makes a sort of production possible where not the conveyor system, but the manufacturing needs resulting from the characteristics of the product set the pathway within the assembly layout.

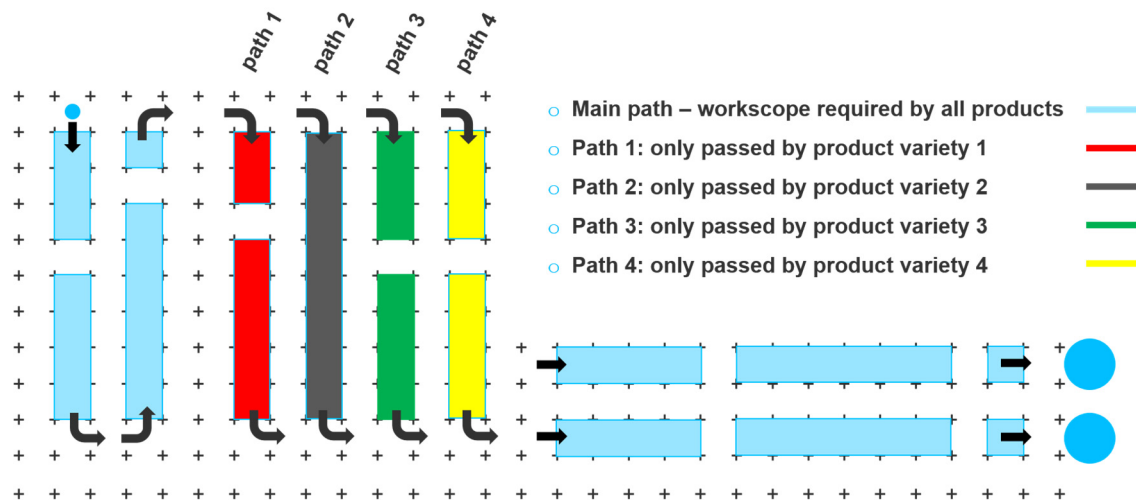


Figure 1. Production layout with individual pathway

The mobile assembly island also creates the possibility of carrying out assembly processes independent of a specific place when parts or components need to be installed whose deployment, handling and assembly are not particularly dependent on a stationary facility, and the parts in question can be delivered using a delivery AGV for the assembly and logistical AGV cf. Figure 2. Accordingly, the causal connection for work scopes at fixed stations is eliminated.

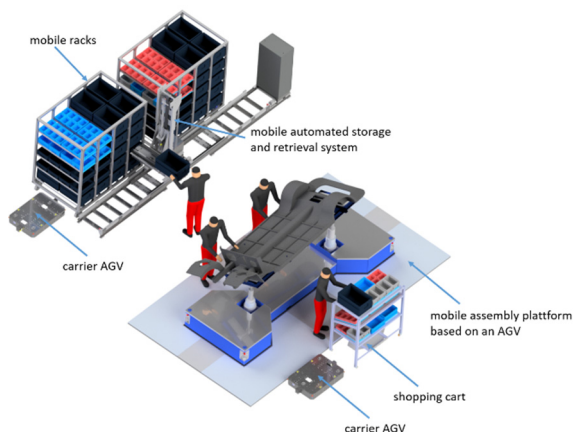


Figure 2. Supply chain and material flow systems based on mobile intralogistics components

The potential for improving efficiency connected to the deployment of the mobile assembly island is, however, seriously broadened when the possibility of unloading and reloading of a partially assembled vehicle can be implemented in the manufacturing process. While every workpiece carrier constitutes an autonomous system, this holds the technical requirement to interrupt the production process of an individual object to be assembled at the point in time of a fault event in any particular part of the layout, without adversely affecting the assembly process of the other workpieces.

3. PROTOTYPE “MOBILE ASSEMBLY ISLAND”

Compared to AGV-based assembly carriers, of the sort found in current small-batch production and assembly, the mobile assembly island constitutes a disruptive technology, because it connects transport means, assembly supports, handling and working platform. The AGV can be divided into 3 main structural components, cf. Figure 3.

The chassis, together with the drive unit and power unit make up the vehicle body. The drive train consists of a combination of the drive and steering units, whose swiveling range make omnidirectional driving, particularly turning in place, possible. In consideration of the total dimensions of 3,500 mm x 6,000 mm, this is an essential prerequisite to be able to maneuver efficiently.

A further primary requirement concerning the drive train is the expansion of the driving speed range, for a high variability in the sense of the “individual cycle time”. With the mobile assembly island in its current prototype stage, speeds between 0.05 m/s and 1.5 m/s can be achieved. The vehicle body is surrounded by the circumferential work and standing platform. The fully variable load carrier, attached to the lifting device, which constitute the superstructure, is located above the vehicle body.

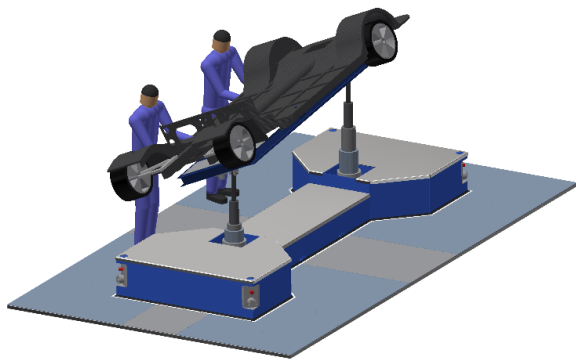


Figure 3. Concept of the mobile assembly and logistical platform based on an AGV

The hoist concept is conceived in such a way that the load carrier, by means of two telescoping hydraulic cylinders cf. Figure 4, can be lifted upon a maximum of 1,500 mm above the initial position, which is located 500 mm above the working and standing platform.



Figure 4. Prototype of the Mobile Assembly Island

By differentially extending the lift cylinders, a pitch in the traverse axis of the superstructure can be achieved, whilst the swiveling on the longitudinal axis is carried out by two additional hydraulic cylinders. The superstructure, which functions as the workpiece carrier, is the primary component with regard to the flexibility and versatility of the mobile island. Only the fully automatic adjustment of the superstructure ensures adaptability and usability across all models within an automobile manufacturer's complete product range. This is the central component and basic prerequisite if one wishes to produce fundamentally different vehicle models in terms of design and dimensions in a factory with one and the same conveyor, warehousing and handling technology machines in the shape of a mobile assembly island in the future.

In order to satisfy the layout flexibility requirements, the AGV has a free, non-track bound navigation system based on laser scanners and an indoor navigation system with ultra-wideband technology. In this way, the AGV has the necessary prerequisites to reach absolute coordinates within a variable layout without assistance from fixed points like magnetic markers or RFID tags installed in the building structure.

4. PROTOTYPE “MOBILE SUPERMARKET”

In order to implement a flexible production system without a fixed cycle sequence, material flow systems with a high degree of responsiveness are needed. The classic pearl chain is based on a production program planned many days in advance. Should there be changes at short notice in the production program due to interruptions in the assembly process or a postponement of the workpiece, the pearl chain will be broken.

The material flow system must be synchronized with the actual production program at the point where there is a physical need. Since the need in flexible production in regard to forms, time and location can vary, the assembly supply has to be oriented towards the real time needs – Just-In-Real-Time – of the individual workpieces. In consequence, completely new principles are required for the supply chain and its material flow systems, to establish such a decoupled process without fixed locations or times.

One such system called “Mobile Supermarket”, developed at the IFT, specializes on the supply characteristics of frequently needed parts with high variety, e.g. mirrors, headlights, steering wheels, etc. The complete system consists of three individual components that can also be independently operated, but only together form a sort of small scale mobile automated mini-load system in whose rack modules a variant parts portfolio can be found. The mobile supermarket is thus comprised of a compact AGV which transports mobile shelf modules as well as a non-stationary picking unit for handling the loading and unloading of small load carriers (VDA-KLT) from the mobile shelf modules cf. Figure 2 and Figure 5.



Figure 5. Prototype of the Mobile Supermarket

The compact AGV constitutes a proprietary concept and construction of the IFT. As the AGV does not lift the shelf modules, whose load capacity is 1,200 kg, but only drags them, it is, on the one hand, extremely compact and

cost-effective, and, on the other hand, an unspecified design can be used. Unspecified in the sense that the AGV is not specifically designed for transporting the shelves, but can also be used in its basic form for transporting baskets of goods, special load carriers and small load carriers. Additionally, the compact AGV is suitable, because of its “carrier vehicle with accessory equipment” modularity, for additional application scenarios, whereby the type diversity of the AGV used can be reduced.

The picking unit consists of a semi-stationary mini storage and retrieval system (Mini-ASRS), specifically developed at the IFT for this concept use-case, which hands the employee the material needed in a direct man-machine collaboration cf. Figure 6.



Figure 6. Hand out of needed material in direct man-machine collaboration at the Mini-ASRS

The Mini-ASRS was primarily designed to provide a non-stationary piece of equipment which only requires a power source as infrastructure. In order to further expand the layout flexibility, the Mini-ASRS can be operated using a battery storage device. For this reason, all the technology is on board, and the design is self-supported, without interference with the floor structure of the factory or warehouse area, so that the equipment can be moved about by means of a forklift or hand pallet truck. The Mini-ASRS is a completely proprietary design of the IFT, from the complex double-deep extendable telescopic table to the pulleys and drive rollers of the belt drive. This makes double-deep (1,200 mm) loading and unloading possible, as the necessary aisle width of the Mini-ASRS is only approx. 660 mm. The universality of this equipment is ensured to the effect that the loading and unloading unit can be utilized independently of the specifications of the small load carrier (VDA-KLT system) and trays with basic measurements of 600 x 400 or 400 x 300 mm. No specific gripper bags are necessary in handling the load carrier.

To meet the needs of a load of 60 kg (corresponding to 2 VDA-KLT 400 x 300 with maximum allowable

loading) with a higher handling capacity, and the unsupported design which functions without floor anchoring, particular attention must be paid to the ASRS's center of gravity. In this respect, all axes are implemented with weight-saving timing belt drive and the drive unit positioned centrally. The unit has a track length of 5,000 mm making it suitable for the simultaneous loading and unloading of two of the mobile rack modules, each having 40 VDA-KLT places with basic dimensions of 600 x 400 mm. Due to the design of the horizontal drive with endless timing belts in an omega configuration and onboard drive system, the track length can be varied at will and expanded to accommodate a larger number of rack modules. In the current design, the horizontal axis can reach a maximum velocity of 2m/s, whereby the vertical axis can be run at 1 m/s. The maximum storage height is currently 1,800 mm, whereas the minimum achievable shelf height is 320 mm above ground level. Due to the strong dynamics of the axes' motions, 4 carriers in the configuration with double-deep shelf modules can be ready in only 90 seconds, even at the maximum travel distance.

The mobile supermarket system is not only characterized by a fast reaction velocity, but also its utilization makes reductions in manual picking and turnover processes, as employees can always be handed the materials needed for the pending task. This makes it possible to target reductions in potential error sources, while simultaneously reducing the workload of the assembly worker.

5. CONCLUSION

Between 2014 and 2017, the IFT was not only able to develop the concept for the convertible and flexible automobile production of the future with the help of subsidies from the state of Baden-Württemberg, but rather also implemented primary components necessary for the realization of the prototypes. This includes a mobile assembly island based on an AGV whose deployment in automotive final assembly makes production independent of fixed cycle times. Besides the implementation of an “individual cycle time” as a function of the specific vehicle design, a disruption of the assembly process and deferment of a workpiece are made possible by the decoupling of the individual workpiece carriers. Reworking costs can be significantly reduced as a result, as the correction of defects and the production status connected to them can be carried out at the point of the error. Material supply concepts needing a number of days of advance planning are thus obsolete, as the production program and the sequence of the material retrieval can be changed at short notice, not only in response to removal. The mobile supermarket developed at the IFT targets the provision of parts and assembly materials connected to real-time needs – Just-in-Real-Time. The IFT is carrying out trials of the individual prototypes as well as the further development in cooperation with their interaction on the research campus ARENA2036 at the University of Stuttgart.

REFERENCES

- [1] Popp, J.: *Neuartige Logistikkonzepte für eine flexible Automobilproduktion ohne Band*, Dissertation Universität Stuttgart, 2018.
- [2] Götz, A.: *Zukunftsstandort Deutschland, Automobilproduktion*, pp. 16-19, Ausgabe, 02/2007.
- [3] Roscher, J.: *Bewertung von Flexibilitätsstrategien für die Endmontage in der Automobilindustrie*, Dissertation Universität Stuttgart, 2008.
- [4] Wehking, K.-H. and Popp, J.: *Automobilproduktionslogistik – heute, morgen und übermorgen*, 32. Logistik-Kongress der Bundesvereinigung Logistik (BVL) e.V.
- [5] Wehking, K.-H., Hofmann, M., Korte, D., Hagg, M. and Pfleger, D.: *Automobilproduktionslogistik im Wandel*, Bundesvereinigung Logistik (BVL) e.V. (Hg.): *Digitales trifft Reales, Kongressband - 35. Deutscher Logistik-Kongress, 2018, Hamburg: DVV Media Group*, 2018.
- [6] Hofmann, M. and Wehking, K.-H.: *Mobile Montageinsel für die Automobilproduktion ohne Band und Takt*. In: Bruns, R., Ulrich, S.: *Forschungskatalog Flurförderzeuge 2018*, Helmut-Schmidt-Universität Hamburg, Lehrstuhl MTL, 2018, Hebezeuge Fördermittel, Huss Medien GmbH, 10400 Berlin, 2018

Travel Time Prediction for Multimodal Freight Transports using Machine Learning

N. Servos

PhD Student
Robert Bosch Manufacturing Solutions
GmbH
Bosch Connected Industry

M. Teucke

Research Assistant
BIBA - Bremer Institut für Produktion und
Logistik GmbH at the University of Bremen

M. Freitag

Professor
University of Bremen
Faculty of Production Engineering
BIBA - Bremer Institut für Produktion und
Logistik GmbH at the University of Bremen

Predicting an accurate travel time for freight transports provides a significant value to supply chain participants, including e.g. improved capacity planning. The basic requirement is a continuous monitoring of freight transports by using mobile sensors. Despite the superior capabilities of Machine Learning (ML) methods for solving non-linear problems, only a minority of recent publications applied ML for travel time prediction in freight transports. We have selected ExtraTrees, AdaBoost and Support Vector Regression (SVR) as learning algorithms, as these can deal with a low volume of data and high complexity while requiring low processing times. Using features derived from the data, several travel time prediction models have been built. The models have been evaluated using real world data of multimodal container transports from Germany to the USA and compared to historical approaches. We show that compared to other approaches machine learning yields improved predictions of travel times.

Keywords: Logistics, Supply Chain Management, Freight Transports, Travel Time Prediction, Machine Learning

1. INTRODUCTION

Predicting accurate travel times for freight transports offers significant value to supply chain participants and their logistics quality [1-3]. As an example, a material planner can identify delayed deliveries in advance, adapt material stocks or adjust staff and machinery capacities. Furthermore, logistic service providers benefit from more accurate capacity planning at their warehouses and improved transport planning. Consequently, manufacturers and logistic service providers can enhance their efficiency, optimise their processes and increase planning accuracy. [1, 3, 4] To do so, a continuous monitoring of freight transports is required, e.g., by using mobile sensors attached to transported goods [5].

Currently, the majority of the published literature deals with short term forecasting, rather than long term forecasting [6, 7]. In most cases the field of research relates to bus arrival times or highway travel times, using historical [8, 9], statistical [10, 11], Kalman filter [11-15] or machine learning (ML) approaches [16-24]. The authors of [6] claim that only ML models can adequately deal with the dynamic situations during transports. This statement can be confirmed by the literature as ML approaches usually perform better than historical and statistical approaches [12, 16, 17].

For instance, ML can deal better with complex and non-linear relationships between predictors and process complex and noisy data [7]. Nevertheless, only a minority of recent publications deal with the travel time

prediction in freight transports using ML methods, such as Support Vector Regression (SVR) or Artificial Neuronal Networks (ANN) [2, 3, 25, 26]. In long term forecasting of multimodal freight transports, only very limited research has been conducted, which mainly uses historical approaches [27]. Consequently, this paper focuses on the application of ML for long term forecasting to predict travel times of multimodal freight transports.

2. METHODOLOGY

2.1 Choice of Models

Based on a literature review, the methods ExtraTrees and AdaBoost as well as SVR, have been selected for modeling, as those methods can deal with a low volume of data and a high complexity while requiring low processing times [2, 3, 22, 23, 26].

Support Vector Machine (SVM) is a classification technique that aims to separate two groups of data points using an optimally derived hyperplane having the maximum margin and has also been adopted to Regression Problems (SVR) [22]. To deal with non-linear problems the so called kernel trick has been introduced [22]. In the literature, the radial basis function (RBF) is proposed as a kernel function for travel time estimation [28]. Further important parameters are ϵ and C . The parameter ϵ describes an insensitive loss function that penalizes prediction residuals larger than the value specified by it. The parameter C acts as a regularization parameter which describes the tolerance towards prediction errors. [28]

Models including SVR have recently shown many improvements and reasonable performances in Time Series Analysis. In sum, SVRs have the ability to generalize data and guarantee global minima while

Correspondence to: Nikolaos Servos
Bosch Connected Industry,
Leitzstrasse 47, 70469 Stuttgart
E-mail: nikolaos.servos@de.bosch.com

having a low processing time given the constraints of low training data and high problem complexity. [22, 28] For this reason, SVR has been chosen for this study.

ExtraTrees are extremely randomized decision trees used on various sub-samples of data [29]. They introduce randomness to the process of bagging to create a number ($n_{estimators}$) of independent decision trees. Thus, the variance of the models is reduced. The algorithm also uses a regularisation parameter $random_states$. AdaBoost is an adaptive boosting technique where several weak learners (decision trees in this case) are converted into a strong learner using a weighted sum of their predictions. In addition to the number of estimators, the learning rate is also a relevant parameter for AdaBoost. In [25] and [26] ExtraTrees and AdaBoost are used for travel time estimation where both methods prove their ability of low prediction errors. Furthermore, those methods provide information regarding the importance scores of the features used to train and test the models.

2.2 Framework

Based on the Knowledge Discovery in Databases (KDD) Data Mining process flow, the framework shown in Figure 1 has been derived [30]:

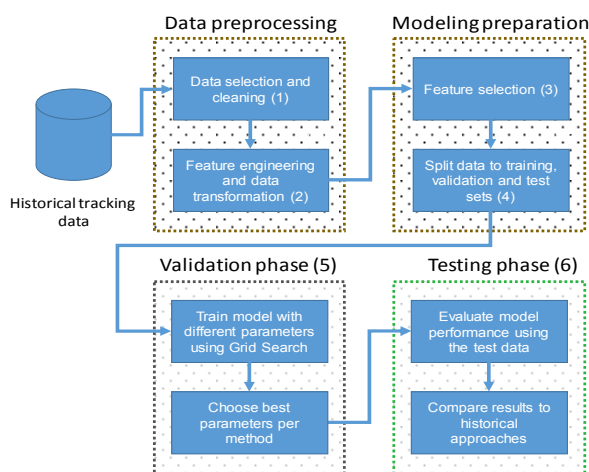


Figure 1. Framework used for travel time prediction

Our approach is based on historical tracking data of transports of the same route and involves six steps: (1) Relevant data for modelling is selected and cleansed to eliminate outliers. (2) Literature and domain knowledge are used to engineer appropriate features for travel time estimation and to transform the data [2, 3]. (3) Based on domain knowledge, relevant features are selected and (4) the data is split into training, validation and test sets. (5) Using a grid search with the training and validation set. The best parameters for each learning algorithm are determined, resulting in one model per learning algorithm. (6) Finally, the test set is used to identify the best model and to compare the results with historical approaches applicable to freight transports.

3. USE-CASE AND DATA GENERATION

The following chapter shortly introduces the use-case and describes the data generation.

3.1 Use-Case Description

We have used real-life data derived from a multimodal supply chain extending from Bremen in Germany to Vance in the United States, which includes multi-modal transports by truck, vessel and train. At a logistics service hub in Bremen a container is packed with the required goods for the destination Vance and subsequently picked up by truck. The container is transported to the port of Bremerhaven and stored there for four to seven days. From there the container is transported by vessel to the port of Charleston via the port of Norfolk. In Charleston, the container is loaded onto a train driving to a train yard in Bessemer, where it is picked up by truck and transported to its final destination in Vance.

3.2 Data Generation

Over a period of seven weeks, seven container shipments have been equipped with a hybrid sensor system for tracking purposes. Hereby, a sensor has been attached to each pallet and associated with the serial number of the transport load unit. This process is called pairing and is concluded with a scan after attaching the sensor. The sensor itself is transmitting its ID and quality related values, e.g., temperature or humidity, via Bluetooth Low Energy (BLE) to a telematics unit called Gateway. [5] One such Gateway has been attached to each container and collects all sensor transmissions in reachable distance, adds the Global Positioning System (GPS) position to each tracking point and sends it to a data cloud via Global System for Mobile Communications (GSM). Due to the use of a mobile sensor system and a restricted battery life time, GPS data are generated every 30 minutes and transmitted in the same interval. If there is no connection available, the data is buffered and transmitted once a GSM connection is available again. At the end of the transport the association to the transport load unit is removed automatically (un-pairing) via BLE using a stationary Gateway with a special configuration.

3.3 Data Description

The previously described system basically provides a table of sensor traces from the time of pairing till the time of un-pairing with the columns described in Table 1:

Table 1. Extract of the relevant data collected by the used track and trace system

Column	Description
unitloadId	Unique identifier of paired transport load unit
start/ end of tracking	Pairing and un-pairing unix time in seconds
gatewayId	Unique identifier of transmitting gateway
lastUpdate	Unix time of trans-mission in milliseconds
latitude, longitude	Geo-location of the last update
temperature, humidity	Quality related data of sensor of last update

In addition to the sensor data, the system also provides the transport origin and destination, each as a geo-fence in the form of a cycle with a radius and a coordinate.

4. DATA PRE-PROCESSING

Data cleansing and feature engineering are major tasks in this research. GPS data can often be quite noisy. High data quality and relevant features are needed for a good prediction model.

4.1 Data Cleansing

Based on a qualitative analysis of the raw data, the following rules have been applied to cleanse the data:

- Test pairings with no GPS transmissions in the destination geo-fence have been removed.
- Transmissions with latitude and longitude set to 0° due to absence of a GPS signal have been removed.
- Outliers where the speed to bridge the distance to the previous two points exceeds 120 kmph, as shown in Figure 2, case 1 and 2, have been removed.
- Due to consideration of the transport time between the origin and destination, data points other than the last transmission in the start geo-fence and the first transmission in the destination geo-fence have been removed, as shown in Figure 2, case 3:

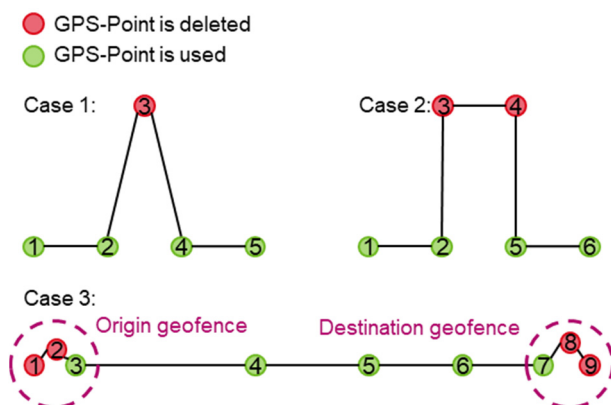


Figure 2. Deletion of outlier GPS-Points

Furthermore, only one unit load per ride has been kept to avoid using the same ride in the training and test set.

4.2 Feature Engineering and Data Transformation

Based on the business context and a literature review the raw data has been transformed into several features where we assume that they can model the travel time well. Assuming that a low amount of data is available, a pre-selection of features has been conducted. Features that consider the issue in a more complex way are initially deferred. The relevant features are shown in Table 5 in the appendix and can be categorized as follows:

The departure time indicates the corresponding timestamp on the basis of the last data point in the origin geo-fence. The timestamp has been transformed into

hours of the day and day of the week as numerical values, so that the learning algorithms can process them. [2]

The actual status provides information on the number of data points, the geo coordinates of the current position and the time stamp, transformed into various features [2]. In addition, the current country has been identified based on latitude and longitude using an API.

To represent the relation of each data point to the origin and destination the distance, time and average speed to origin and destination has been calculated. In particular, the distance values are seen as very relevant features for the arrival time prediction [2, 8, 27]. Here, the destination driven time is the target.

Some additional features have been developed in this research to describe the driving behaviour and the traffic conditions on a trip without using additional data sources. This is approximated on the basis of counters of the average speed between the transmission points, without necessarily including the traffic data. In addition, a simplified assumption of intermediate stops is made at this point. If the average speed between the data points is less than one kmph for at least two hours, a stop is assumed.

5 MODELLING

5.1 Modelling Preparation

In this study the feature selection process has been performed based on business knowledge so that no further feature selection has been conducted.

Before starting the modelling phase, the cleansed and pre-processed data set with 5823 data points has to be divided into a training and a test set, in order to gain an unknown data set to evaluate the generated model. As some features depend on the value of the previous data point in a ride, we consider the unit load for splitting the data set. Previous experiments have already shown that the prediction error is quite small when having data points of the same unit load in the training and the test set. Based on seven rides, two rides have been randomly chosen for testing the models.

5.2 Validation Phase

The validation phase deals with choosing the best parameters for the applied learning algorithms. Therefore, usually the training data set is split again into a training and a validation data set. Due to the low number of remaining unit loads in the training set, a cross validation has been applied by randomly creating ten different combinations of training and validation sets, whereby the validation set includes two unit loads.

Using the training and validation sets, a grid search has been conducted determining the best parameters for each learning algorithm based on the best average Mean Absolute Error (MAE; see section 5.3) over the ten validation sets. The chosen parameters and values of the grid search are shown in Table 2. The chosen range has been defined based on previously conducted experiments.

Table 2. Parameter values chosen for the grid search

Learning algorithm	Parameters
Support Vector Regression (SVR)	Kernel = 'rbf' C = 0.001, ..., 5.001, increment of 0.02 ϵ = 0.001, ..., 0.1 split into 30 values
ExtraTrees	n_estimators = 1, 2, 3, 4, 5, 6, 7, 8, 9, 10 random_state = 6, 7, 8, 9, 10, 11, 12, 13, 14, 15, 16, 17, 18
AdaBoost	n_estimators = 1, 2, 3, 4, 5, 6, 7, 8, 9, 10 learning_rate = 0.0001, ..., 1,0001, increment of 0.025

5.3 Testing Phase

The models created based on SVR, ExtraTrees and AdaBoost are finally evaluated using the test set. To get an average estimate of the performance of the model, the Mean Absolute Error (MAE) and Root Mean Square Error (RMSE) are chosen as evaluation metrics. [3]

The Mean Absolute Error is an error metric used to calculate how close or far the predictions are to the actual outcome. It is an average of all forecast errors and is located on the same scale as the data that is measured [3]. The formula to calculate the MAE is shown below (the parameter n describes the number of observations).

$$MAE = \frac{1}{n} \sum_{i=1}^n |actual_i - prediction_i| \quad (1)$$

The Root Mean Square Error is a very common error metric to evaluate numerical predictions [3]. The RMSE weights the errors with respect to how large the errors are and provides information about the variance of errors of a model.

$$RMSE = \sqrt{\frac{1}{n} \sum_{i=1}^n (actual_i - prediction_i)^2} \quad (2)$$

Table 3 shows the results of the tested learning algorithms. The best result has been obtained with SVR. With an MAE of 17 hours, the result is surprisingly good, if you consider the small training set of five transports and an average transport time of 25 days.

Table 3. Prediction results of machine learning methods

Model	MAE	RMSE	Best Parameters
ExtraTrees	29.47 h	33.08 h	N_estimators: 7 RandomState: 18
AdaBoost	38.91 h	41.15 h	N_estimators: 14 Learning rate: 0.9751
SVR	17.16 h	27.59 h	C: 3.801 ϵ : 0.01

6. EVALUATION

To evaluate the developed model a comparison to historical approaches has been conducted as shown in Table 4.

The easiest approach is using the average travel time for travel time estimation, without updating it based on current position of the transport.

In [9] the average travel time is also used, but updated based on the percentage of distance remaining to the destination from the current transmission.

In [27], the prediction is based on the current GPS position of the delivery vehicle. Therefore, the average travel time of historical data points to the destination within a sensitivity radius from the current position is determined.

In [8], the prediction of travel time is based on the current and average speed of the current ride as well as the distances to the origin and destination.

Table 4. Prediction results of the machine learning methods compared to historical methods

Model	MAE	RMSE
SVR	17.16 h	27.59 h
Average Time	52.64 h	52.65 h
Celan [9]	88.65 h	108.10 h
Heywood [27]	42.02 h	52.20 h
Singla [8]	224.84 h	247.86 h

The results show that the prediction based on machine learning is considerably more accurate. Especially the SVR algorithm outperforms the historical approaches. While evaluating those results, one should also consider that the high errors of the historical approaches occur due to the use of a sporadic transmission in a 30 minutes interval, a low amount of data and absence of information about the trans-loading points.

7. CONCLUSION

The study has shown that even with a small amount of data of complex supply chains, machine learning provides the ability to perform a relatively good prediction compared to historical approaches.

Nevertheless, some more research work is required. First of all, more data and other use cases have to be evaluated to confirm the current results. Furthermore, features related to the trans-loading points and route should be added. Methods to determine relevant features and to derive experiments with different feature combinations should also be considered.

ACKNOWLEDGMENT

This work is funded by the German Federal Ministry for Economic Affairs and Energy (BMWi) as part of the collaborative research and development project 01MA16004 "SaSch – Digital Services for Shaping agile Supply Chains".

REFERENCES

- [1] Schuh, G. and Stich, V.: Smart-Logistic-Grids. Anpassungsfähige multimodale Logistiknetzwerke durch integrierte Logistikplanung und -regelung, FIR-Edition Forschung Band 18, by FIR e.V. an der RWTH Aachen, Aachen, 2016.
- [2] Masiero, L. P., Casanova, M. A. and de Carvalho, M. T. M.: Travel time prediction using machine learning, Proceedings of the 4th ACM SIGSPATIAL International Workshop on Computational Transportation Science, pp. 34–38, by ACM. Chicago, Illinois, 2011.
- [3] Parolas, I., Tavesszy, L., et.al.: Prediction of Vessels' estimated time of arrival (ETA) using machine learning, A port of rotterdam case study, In Proceedings of the 96th Annual Meeting of the Transportation Research, pp. 8-12, Washington, DC, USA, 2017.
- [4] Lin, H.-E. and Zito, R.: A review of travel-time prediction in transport and logistics. Proceedings of the Eastern Asia Society for Transportation Studies 5, pp. 1433–1448, 2005.
- [5] Sommerfeld, D., Teucke, M. and Freitag M.: Identification of Sensor Requirements for a Quality Data-based Risk Management in Multimodal Supply Chains, Procedia CIRP, Vol. 72, pp. 563-568, 2018.
- [6] Vlahogianni, E. I., Karlaftis, M. G. and Golias, J.C. Short-term traffic forecasting: Where we are and where we're going, Transportation Research Part C: Emerging Technologies, Vol. 43, No. 1, pp. 3–19, 2014.
- [7] Altinkaya, M. and Zontul, M.: Urban bus arrival time prediction: A review of computational models. International Journal of Recent Technology and Engineering (IJRTE), Vol. 2, No. 4, pp. 164-169, 2013.
- [8] Singla, L. and Bhatia, P.: GPS based bus tracking system. International Conference on Computer, Communication and Control (IC4), by IEEE, pp. 1-6, 2015.
- [9] Čelan, M. and Lep, M.: Bus arrival time prediction based on network model. Procedia computer science, Vol. 113, pp. 138-145, 2017.
- [10] Idé, T. and Kato, S.: Travel-time prediction using Gaussian process regression: A trajectory-based approach. Proceedings of the 2009 SIAM International Conference on Data Mining, by Society for Industrial and Applied Mathematics (SIAM), pp. 1185-1196, 2009.
- [11] Kwon, J. and Petty, K. A.: Travel time prediction algorithm scalable to freeway networks with many nodes with arbitrary travel routes. Transportation Research Board 84th Annual Meeting, pp. 147–153, Washington, DC, 2005.
- [12] Shalaby, A. and Farhan, A.: Prediction model of bus arrival and departure times using AVL and APC data. Journal of Public Transportation, , Vol. 7, No. 1, pp. 41-61, 2004.
- [13] Chen, M., Liu, X., Xia, J. and Chien, S. I.: A dynamic bus arrival time prediction model based on APC data. Computer-Aided Civil and Infrastructure Engineering, Vol. 19, No. 5, pp. 364-376, 2004.
- [14] Vanajakshi, L., Subramanian, S. C. and Sivanandan, R.: Travel time prediction under heterogeneous traffic conditions using global positioning system data from buses. IET intelligent transport systems, Vol. 3, No. 1, pp. 1-9, 2009.
- [15] Chien, S. I. J. and Kuchipudi, C. M.: Dynamic travel time prediction with real-time and historic data. Journal of transportation engineering, Vol. 129, No. 6, pp. 608-616, 2003.
- [16] Fan, W. and Gurmu, Z.: Dynamic travel time prediction models for buses using only GPS data. International Journal of Transportation Science and Technology, Vol. 4, No. 4, pp. 353-366, 2015.
- [17] Yu, B., Lam, W. H. and Tam, M. L.: Bus arrival time prediction at bus stop with multiple routes. Transportation Research Part C: Emerging Technologies, Vol. 19, No. 6, pp. 1157-1170, 2011.
- [18] Chen, M., Liu, X., Xia, J. and Chien, S. I.: A dynamic bus arrival time prediction model based on APC data, Computer-Aided Civil and Infrastructure Engineering, Vol. 19, No. 5, pp. 364-376, 2004.
- [19] Ramakrishna, Y., Ramakrishna, P., Lakshmanan, V. and Sivanandan, R.: Bus Travel Time Prediction Using GPS Data. Proceedings Map India, 2006.
- [20] Chien, S. I.-J., Ding, Y. and Wei, C.: Dynamic bus arrival time prediction with artificial neural networks, Journal of Transportation Engineering, Vol. 128, No. 5, pp. 429–438, 2002.
- [21] Jeong, R. and Rilett, R.: Bus arrival time prediction using artificial neural network model. Proceedings of the 7th International IEEE Conference on Intelligent Transportation Systems (IEEE Cat. No. 04TH8749), by IEEE, pp. 988-993, 2004.
- [22] Wu, C.H., Ho, J.M. and Lee, D.T.: Travel-time prediction with support vector regression. IEEE transactions on intelligent transportation systems, Vol. 5, No. 4, pp. 276-281, 2004.
- [23] Kee, C.Y., Wong, L.P., Khader, A.T. and Hassan, F.H.: Multi-label classification of estimated time of arrival with ensemble neural networks in bus transportation network. 2017 2nd IEEE International Conference on Intelligent Transportation Engineering (ICITE), by IEEE, pp. 150-154, 2017.
- [24] Gurmu Z.K. and Fan, W.D.: Artificial neural network travel time prediction model for buses using only GPS data. Journal of Public Transportation, Vol. 17, No. 2, pp. 45-65, 2014.
- [25] Sun, X., Zhang, H., Tian, F. and Yang, L.: The use of a machine learning method to predict the real-time link travel time of open-pit trucks. Mathematical Problems in Engineering, Vol. 7, pp. 1-14, 2018.
- [26] van der Spoel, S., Amrit, C. and van Hillegersberg, J.: Predictive analytics for truck arrival time estimation: a field study at a European distribution

centre. International journal of production research, Vol. 55, No. 17, pp. 5062-5078, 2017.

- [27] Heywood, C., Connor, C., Browning, D., Smith, M.C. and Wang, B.: GPS tracking of intermodal transportation: System integration with delivery order system. IEEE Systems and Information Engineering Design Symposium: [SIEDS 2009], by University of Virginia. Charlottesville, VA, USA, pp. 191–196, 2009.
- [28] Barbour, W., Martinez Mori, J.C. and Kuppa, S.: Prediction of arrival times of freight traffic on US

railroads using support vector regression. Transportation Research Part C: Emerging Technologies, Vol. 93, pp. 211–227, 2018.

- [29] Geurts, P., Ernst, D. and Wehenkel, L.: Extremely randomized trees. In Machine learning, Vol. 63, No. 1, pp. 3–42, 2016.
- [30] Swamynathan, Manohar.: Mastering machine learning with Python in six steps. A practical implementation guide to predictive data analytics using Python, 2017.

NOMENCLATURE

C	Regularisation parameter SVR
ε	Loss function
$n_estimators$	Number of trees

$random_state$	Regularisation parameter for ExtraTrees
$learning_rate$	Gradient for adjusting weights
n	Number of observations

Table 5. List of features used

Feature	Description
AbsoluteDistanceToPrevious	Absolute distance in km from the current GPS transmission to the previous GPS transmission.
AvgSpeedPrevious	Average speed from previous GPS transmission to current GPS transmission as quotient of AbsoluteDistanceToPrevious and DrivenTimePrevious.
CounterAvgSpeed0_1, CounterAvgSpeed1_30, CounterAvgSpeed30_60, CounterAvgSpeed_above_60	Counter of the number of AvgSpeedPrevious from departure to the current GPS transmission from 0 to 1 kmph, 1 to 30 kmph, 30 to 60 kmph and over 60 kmph derived from the data. Those features are based on business knowledge to represent traffic conditions.
CounterStops	Number of detected stops, a stop is detected only if the speed 0 to 1 kmph is detected for 2 hours.
Current_DayOfWeek	Day of the current GPS transmission from 1 to 7.
Current_Lat/ Current_Long	Latitude and longitude of the current GPS transmission.
Current_TimeInHours	Hour from 0 to 23 of the current GPS transmission.
CurrentCountry	Country based on the current GPS position encoded according to ISO-3166 ALPHA-3 (3-letter encoding) using the geo-coder API of HERE.
Departure_DayOfWeek	Departure day from 1 to 7 based on the last GPS transmission in the geofence of the place of origin.
Departure_TimeInHours	Hour of departure from 0 to 23 based on the last GPS transmission in the geo-fence of the place of origin.
DestinationAbsoluteDistance	Absolute distance in km from the current GPS transmission to the arrival at the destination.
DestinationDrivenTime	Time in hours from the current GPS transmission to arrival at the destination, variable to predict .
DrivenTimePrevious	Time in hours from the previous GPS transmission to the current GPS transmission.
No_of_Transmission	Counter of data transmission from departure.
PastActualDistanceToOrigin	Sum of absolute distances between each GPS transmission in km.
PastAvgAbsoluteSpeed	Average speed from departure at the point of origin to the current GPS transmission as a quotient of PastActualDistanceToOrigin and PastDrivenTimeToOrigin.
PastDrivenTimeToOrigin	Time in hours from departure at the place of origin to the current GPS transmission.
TotalDurationOfStops	Sum of the length of all stops at a given time.

Rafael Mortensen Ernits

Research Scientist
University of Bremen
Bremer Institut für Produktion und
Logistik - BIBA

Thies Beinke

Research Scientist
University of Bremen
Bremer Institut für Produktion und
Logistik - BIBA

Michael Freitag

Full Professor
University of Bremen
Bremer Institut für Produktion und
Logistik - BIBA

Moritz Rohde

Technology Manager
Vollers GmbH

Automatic Unloading of Coffee Sacks out of Sea Containers – Special Pile Situations and Challenges for Gripping

The automated unloading of coffee sacks out of a sea container is a complicated task, mainly due to the non-predictable environment and piling situation of the container content. Gripping systems for this task have to be able to grasp sacks reliably out of every position in the container. This includes the challenges of clamped sacks; sacks fell from piles, or sacks, which are piled chaotically.

The purpose of this paper is to review pile situations and suitable gripping strategies for unloading coffee sacks from sea containers. A special needle chain gripper will be presented and evaluated with a focus on special pile situations. The paper will present the design and functionality of the gripper as well as its evaluation by test cases. As a result, the benefits and drawbacks of this gripper system will be derived, and possible application fields will be discussed.

Keywords: End effector, industrial engineering, logistics, system testing

1. INTRODUCTION

Green coffee beans are transported from the origin country to Europe, mainly in containers. Due to the long distance and low amount of coffee compared to, e.g. cocoa, transportation of loose sacks collected in slings, as common in the past or still conventional for cocoa, is not anymore state of the art. Coffee is still transported in sacks but collected in standard oversea containers.

Coffee in sacks is still a usual way of transporting coffee, even though the majority of green coffee is transported as bulk in containers – for mainstream coffee approximately 70 % is imported as bulk in containers. The coffee transported in sacks is usually of better quality or even speciality coffees. The trend towards smaller private roasters benefits from this, as they usually buy smaller quantities of speciality or certified coffees rather than whole containers [1] [2].

Furthermore, there is a change toward a wider variety of coffees due to the demand for certified or sustainable coffees. From 2008 to 2016, the demand for sustainable coffee tripled. It now represents more than 25% of the world's coffee harvest [3][4].

Coffee sacks are made out of jute or sisal or a mixture of both. Even though more sacks out of polypropylene or grainpro sacks (jute sacks with a synthetic inlet) are used, the natural fibre sacks have the desired mechanical properties for bulky packaging goods and their price is still an advantage comparing to synthetic fibres [5]. The tensile strength of natural fibres, jute and sisal, can vary significantly as verified by [6].

Usually, the capacity of a sack is designed for 60kg of coffee, but sacks of 70-75 kg may also occur, depending on the country of origin. The dimensions of a sack differ as well; still, the majority is by 800 mm x 550 mm x 220 mm (length, width, height). At the short edges, the sacks are sewn together. As one side is sewn together manually after filling the sack with coffee, this side often has a more substantial material slope [7].

Coffee sacks are usually loaded manually inside a container in origin country. The packing strategy differs: sometimes the sacks are aligned lengthwise and sometimes crosswise. In general, however, saddle stow filing is used to keep air circulation and thus condensation to a minimum and to make maximum use of space in the container, as shown in **Figure 1**. In most cases, 20 to 40 cm free space remains above the sacks. Furthermore, the side walls of the container, as well as the ceiling, is covered with craft paper or carton in order to reduce condensation and mould. Often dry sacks are placed within the container to keep the moisture in the air on a low level.



Figure 1. Saddle stow piling of jute coffee sacks

Correspondence to: Rafael Mortensen Ernits, research scient.
University of Bremen
Bremer Institut für Produktion und Logistik - BIBA
Hochschulring 20, 28209 Bremen, Germany
E-mail: mor@biba.uni-bremen.de

Depending on the mechanical strain of the container during transport, an orderly piling situation also exists at the destination. In most cases, however, it can be assumed that sacks slip or have fallen off the pile, especially in the area of the door. In this case, there is often a shift in the centre of gravity within the sack; while a properly piled coffee sack usually strives for an even distribution of the beans and thus has an almost centrally arranged centre of gravity, slipping or falling of the coffee sacks usually leads to a one-sided shift in the centre of gravity.



Figure 2. Seam excess and yarns/strings

Another issue regarding the sack material, which can interfere in the unloading process, is the seam excess. The coffee sacks are filled and sewn up in the country of origin. Individual sewing machines are applied for this purpose, and they need a surplus of material to ensure a durable sewing seam. Depending on the filling level of the sack, this excess fabric will vary in size. **Figure 2** shows an example of excess fabric and sewing material.

2. UNLOADING PROCESS

2.1 Manual process

The usual manual unloading process is performed in most of the container handling cases by two people using special hooks. It results in four gripping points distributed at the corners of the sack dividing its weight. The sack is lifted until it reaches the height of a conveyor belt or a pallet, a horizontal movement is necessary to move the sack over the conveyor or a pallet. The last step is to lay the sack over the conveyor or a pallet and release the hooks.

This approach works very well for humans. The 7 degrees of freedom of each human arm allows very complex movements, but it does not mean that a robot system must necessarily mimic this method. Besides, this approach could face some disadvantages, as the use of robot arms with 7 degrees of freedom may imply in an oversized system, as the constant movement of the sack does not demand a high number of degrees of freedom. Another possible disadvantage could be the choice of the four gripping points on the corners of the sack. Those points are not always visible, and the decision of balancing the sack's weight is dependent of the worker's experience, which could result in a lack of robustness for

an automatic system, damaging the sacks during the unloading process.

Besides the operational issues, the manual unloading process is a strenuous task due to the weight of the sacks and amount inside of a container. The automatic approach has been already considered by [7], and according to the market potential analysis performed by [8], there is a demand for autonomous unloading systems for bulky deformable goods, as coffee sacks.

2.2 Automatic process

An automated system for unloading sacks out of sea containers must be able to unload the sacks in the middle, near the container's ceiling, as well as the sacks which are directly in contact with the walls and on the floor. The boundaries of the container are intrinsic constraints for unloading as they may imply in a collision with walls depending on how the system is going to grasp the coffee sacks.

For unloading coffee sacks automatically, the calculation of the gripping point is required, this can be performed through an object recognition system. Based on this data, a collision-free trajectory calculation takes place. Also, a meaningful sequence of sack unloading must be determined in order to ensure that the piling situation is as stable as possible [9].

The height of the pile is relevant for the automatic unloading process. Since space is not always available above the sacks, gripping from the top cannot be carried out continuously. An orderly pile of sacks can facilitate automatic unloading; however, due to unforeseeable events during transport, this cannot be guaranteed.

3. GRIPPING

3.1 General principles

The grasping principle can be defined as "the physical principle which causes the force effect necessary to get and maintain the part in a relative position concerning the gripping device" [10].

In robotic systems, the element that interacts with the environment is called end-effector [11]. The end-effector may consist of a gripper like a manipulator, or a tool like a welding gun [12].

This contribution follows the classification done by [13] separating the gripping principles in 1. impactive, 2. ingressive, 3. astrictive and 4. contigutive.

Considering the impactive grippers, prehension occurs due to mechanical forces acting on the object surface. Ingressive grippers permeate the object surface and by the use of astrictive grippers a binding force is generated in a single direction. Within contigutive grippers there is direct contact with the object, but the acting force is non-impactive [13].

3.2 Gripping methods

[14] developed a method for selecting gripping principles after a series of interactions with the user. The method supports the selection mostly concerning the object and the handling operations. [15] also proposed an

automated selection and dimensioning of gripper systems. Hereafter the pre-selection is performed, taking into consideration the part to be grasped, the handling device, the process, and the environment.

3.3 Grippers for sacks

[16] derived many principles for gripping bulky and deformable goods, especially the handling of jute coffee sacks.

[17] presented a robotic end effector for grasping sacks. By the movement sack material is dragged between the rollers as the rollers are covered with a gripping material for increasing the friction, the sack is squeezed and stays tight to the rollers. The “Traction Gripper” consists of two conveying units; the grasping object is put in contact with the conveyors, by activating the conveyor belts in the opposite direction the object is forwarded to the middle of the gripper and sustained by friction forces [18].

[19] also proposed an automatic system for unloading coffee sacks, which grasps the sacks by rotating needles. With this gripper, coffee sacks can only be grasped from the top. [20] developed an automatic unloading system for coffee sacks, the developed gripper is called “Spider Gripper” and is based on an ingressive method with multiple needles grasping the sack from above.

3.4 Evaluation of gripping principles for unloading coffee sacks

The two principles that most meet the requirements of unloading coffee sacks are the impactive and ingressive principles. At the best of our knowledge, there are no contiguous nor adhesive grippers for grasping heavy textile sacks. [21] synthesized the main influence factors for the choice of a gripper system. The presented chart in **Figure 3** is an adaptation for the studied case of unloading coffee sacks.

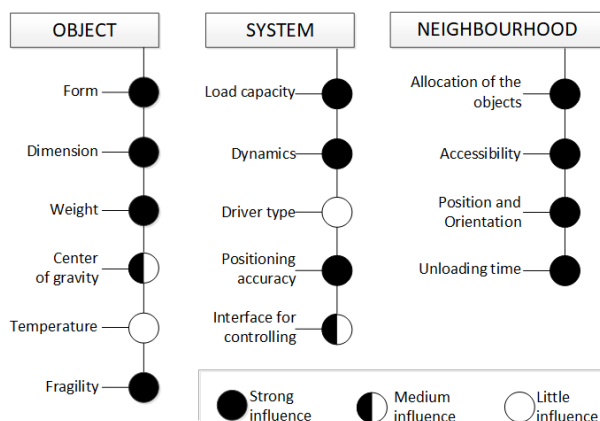


Figure 3. Influence factors for gripper choice.

Although the criterion from [21] is mostly applied for manipulator robots used for pick and place tasks, it can be adapted for unloading tasks, following the problem division in “Object”, “System” and “Neighbourhood”. The form, dimension, weight and fragility of the sack are considered the most impacting components related to the object for grasping. For the system hardware, the load capacity and dynamics associated to velocity and

acceleration during the unloading procedure together with the positioning accuracy at the gripping point are the most relevant issues for the unloading system (gripper/kinematic). The neighbourhood concerns the container and the way the sacks were loaded and the intended time for unloading the coffee sacks.

[22] presented a study about selecting grippers for grasping coffee sacks. Following this approach and after pondering the restrictions arrived from other principles; a concept with the following categories was pursued: ingressive, form closure, continuous and hook.

According to the method, several requirements with weights defined after expert interviews were determined, and the grippers were correspondingly classified. The following requirements were chosen:

- R1. Weight: 70kg.
- R2. Dimension: 600x300x900[mm].
- R3. Material: sisal or jute.
- R4. Content: coffee beans(deformable).
- R5. Maximum admitted damage: 200mm².
- R6. Surface: irregular, mesh.
- R7. Position and orientation: undefined.
- R8. Space around the sacks: limited.
- R9. Time for grasping and release: 5s.
- R10. Gripping point: individual for each sack.

A combination of gripper principles was done in order to evaluate potentials for overcoming principles drawbacks; the combination is presented in a simplified form in **Figure 4**.

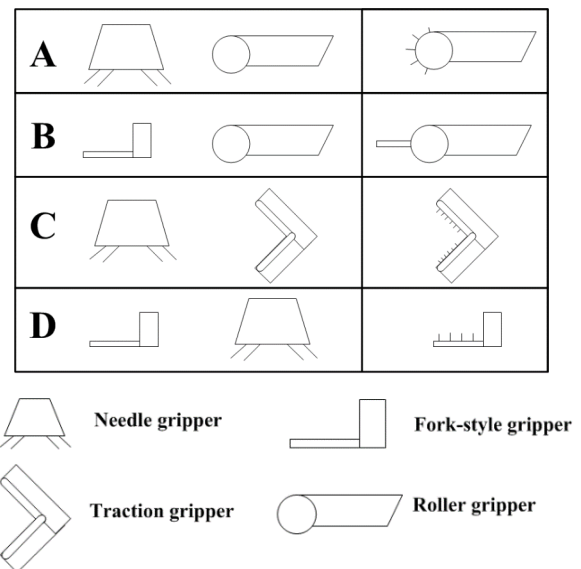


Figure 4. Gripper principles combination.

After an evaluation with experts, the combination of the needle principle with the roller principle was the most profitable. The approach has many attractive features, as it provides a continuous flux of the unloaded object, and the position and orientation of the sacks do not play a significant role compared to other concepts. As the sack is not going to be lifted entirely, the issues involved by grasping objects in the surroundings of the centre of gravity and the dynamics of moving large loads reduce their importance. A challenge is to assure the needles do not significantly damage that coffee sacks during the unloading process. Therefore the combination of a roller gripper with a needle gripper was chosen for developing

a gripper for automatically unloading coffee sacks from sea containers.

3.5 Analysis of gripping

The analysis used simplified models for understanding the behaviour of the sack, forces and textile while gripping.

Three different cases were considered for understanding the gripping force/pull force. By the principle, the upper coffee sack is separated from the lower coffee sack by pulling the first one.

The model is very simplified; it considers that the sacks are not deformable and the centre of gravity is defined in the middle of the sack. Another reduced proposition is that all the forces are applied directly at the centre of gravity.

The analysis contemplates the pull force (F_p) from the gripper, the normal force (F_n), the weight force (F_w) and the friction force (F_f). The angle of the sack inclination is given by α .

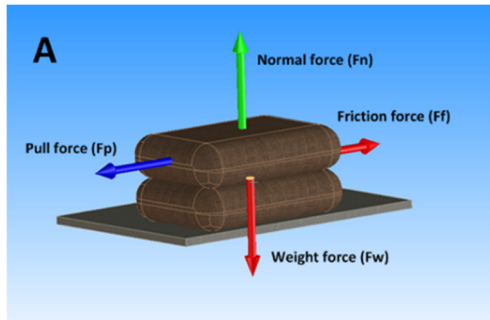


Figure 5. Simplified force analysis, case A

The pull force for moving the sack must be greater than the friction force, for case A:

$$F_p > F_f$$

$$\text{where } F_f = F_n * \mu \quad (1)$$

$$\mu = \text{friction coefficient}$$

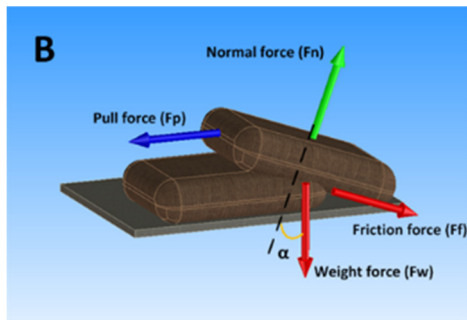


Figure 6. Simplified force analysis, case B.

For case B:

$$F_p > F_f$$

$$F_n = F_w$$

$$F_p > F_w * \frac{\sin \alpha * \mu + \cos \alpha}{\sin \alpha - \mu * \cos \alpha} \quad (2)$$

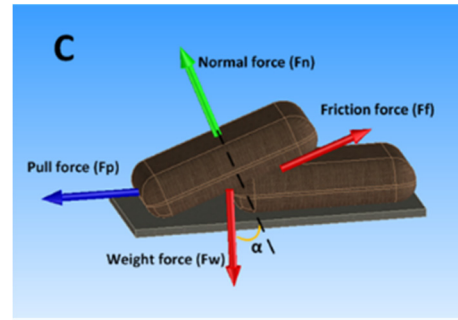


Figure 7. Simplified force analysis, case C.

For case C:

$$F_p > F_f$$

$$F_f = F_w \quad (3)$$

$$F_p > F_w * \frac{\sin \alpha * \mu - \cos \alpha}{\cos \alpha + \mu * \sin \alpha}$$

The inclination angle and friction coefficient mostly influence the pull force behaviour. According to the supposition presented by the model, case B could be critical for the pulling force. The inclination angle of the sack represents strong efforts for a gripping system, as forces could achieve high values depending on the way the coffee sack lays.

4. PROTOTYPES

After the choice and analysis of the gripping principle, two prototypes were subsequently developed, the NeedleRollGripper and the NeedleChainGripper; both using the combination of needle and roller principles. The main difference between the prototypes was the conveying principle. While the NeedleRollGripper (Figure 8) uses rollers for transferring the sacks over the gripper surface, the NeedleChainGripper (Figure 9) applies chains for transporting the sacks to a conveyor belt [23] [9].

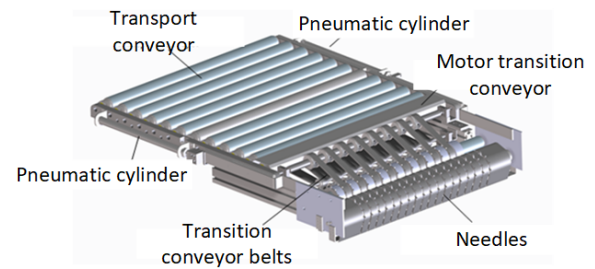


Figure 8. NeedleRollGripper.

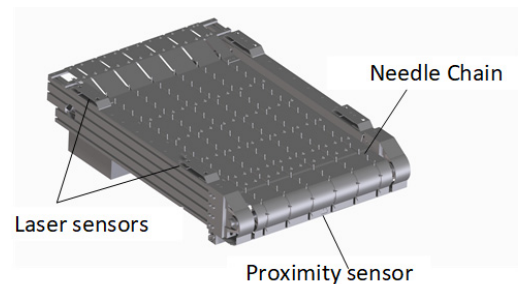


Figure 9. NeedleChainGripper.

5. EVALUATION

The evaluation presented in this paper concerns the tests performed with the NeedleChainGripper, as its conveying principle showed better results than the NeedleRollGripper. The most relevant factors for achieving a successful unloading process are shown in **Figure 10**. An accurate gripping point was stated as the primary factor for successfully unloading the coffee sacks. By using an unprecise gripping point, more than one sack could be grasped and therefore be damaged.

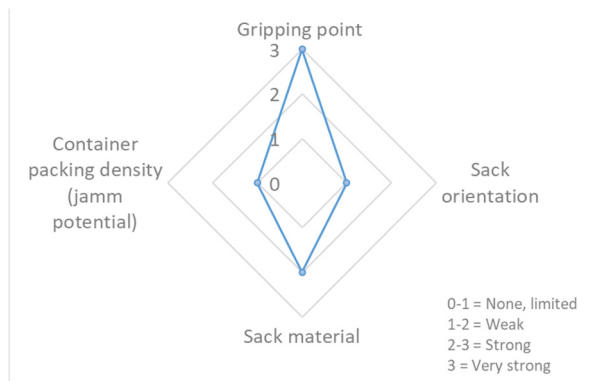


Figure 10. Impact factors.

The container packing density interfered in the unloading process as jammed sacks required a higher pulling force, which in some cases, damaged the sacks. The sack material was also an important factor; it was stated that sisal sacks were more robust for this specific case than jute sacks. The NeedleChainGripper could not guarantee a proper gripping if the sack's orientation horizontally exceeded 20° . Some examples of the damage occurred during successful unloadings are presented in **Figure 11**.



Figure 11. Examples of damage after unloading coffee sacks.

In order to reduce the influences experienced with the impact factors, the gripper was modified, as shown in **Figure 12**. The previous form of the gripper's tip was changed in order to achieve a better clearance between sacks and to give more flexibility regarding the gripping point. Also, longer needles were designed in order to achieve a safer grip. The performed tests showed that the best results achieved with the NeedleChainGripper were with the pile situations A and C presented in **Figure 13**.



Figure 12. NeedleChainGripper modifications.



Figure 13. Special pile situations.

The case B was partly possible with accurate gripping points but the risk of damaging the sacks due to jamming was still present. The case D could not be unloaded, especially because the gripper was rigid in shape and could not adapt to particular sack orientation, so the gripper could not guarantee a secure grip for the sacks in chaotic pile situations.

6. CONCLUSION

This paper analysed principles and state of the art for grasping coffee sacks. The task of automatically unloading coffee sacks of sea containers was delimited by showing the environment conditions, the characteristics of the unloading procedure and object for gripping.

An analysis of the gripping principles derived from the evaluated principles was presented for the choice of a gripping principle to develop a gripper for the task. Coffee sacks that were not perfectly neatly oriented could be unloaded after an adapted strategy. Coffee sacks which were completely chaotic loaded, require a different unloading strategy from the one followed in this paper.

Tests were performed for investigating the behaviour of the sacks fabrics while gripping with the chosen principle. The behaviour of the natural fibres was a challenging task and a more accurate model from the coffee sack mesh would help improve the gripping capabilities. Also more robust sacks could contribute for using the developed gripper.

The NeedleChainGripper was tested in a real scenario with coffee sacks lying in different pile situations. The major advantage of this approach is the increase of grasping stability, as the needles stay in contact with the coffee sack until it leaves the conveying area of the gripper to the next conveyor. The final industrial demonstration at Vollers GmbH was documented in video and can be seen at [24].

ACKNOWLEDGMENT

The research leading to the results presented here has received funding from the European Community's Seventh Framework Programme (EU FP7 ICT-2) within the project "Cognitive Robot for Automation Logistics Processes (RobLog)".

REFERENCES

- [1] ITC: The Coffee exporter's guide, Third edition ed. International Trade Centre, xvi, 247, Geneva, 2011.
- [2] Giovannucci, D. and Ponte, S.: Standards as a new form of social contract? Sustainability initiatives in the coffee industry, Food Policy, Vol. 30, No. 3, pp. 284–301., 2005.
- [3] Lernoud, J., Potts, J., Sampson, G., Schlatter, B., Huppe, G., Voora, V., Willer, H., Wozniak, J.: The state of sustainable markets 2018 - Statistics and emerging trends. ITC, Geneva, 198 pp., 2018.
- [4] Panhuysen, S. and Pierrot, J.: Coffee Barometer 2018. https://www.hivos.org/sites/default/files/coffee_barometer_2018.pdf. Accessed 1 July 2019.
- [5] Alves Fidelis, M.E., Pereira, T.V.C., Gomes, Otávio da Fonseca Martins, Andrade Silva, F. and de Toledo Filho, R.D.: The effect of fiber morphology on the tensile strength of natural fibers, Journal of Materials Research and Technology, Vol. 2, No. 2, pp. 149–157., 2013.
- [6] Müssig, J.: Industrial application of natural fibres: Structure, properties, and technical applications, Wiley, Chichester, 538 pp., 2010.
- [7] Kirchheim, A., Burwinkel, M. and Echelmeyer, W.: Automatic unloading of heavy sacks from containers, IEEE International Conference on Automation and Logistics, ICAL 2008 ; 1-3 Sept. 2008, Qingdao, China.
- [8] Urru, A., Bonini, M., Burbach, T., Hong, E., Stein, P. and Echelmeyer, W.: Autonomous unloading of heavy deformable goods: Market opportunities, Service Operations And Logistics, And Informatics (SOLI), IEEE International Conference on Service Operations And Logistics, And Informatics (SOLI), Yasmine Hammamet, Tunisia. 11/15/2015 - 11/17/2015. IEEE, [S.l.], pp. 54–59., 2015.
- [9] Stoyanov, T., Vaskevicius, N., Mueller, C.A., Fromm, T., Krug, R., Tincani, V., Mojtahedzadeh, R., Kunaschk, S., Mortensen Ernits, R., Canelhas, D.R., Bonilla, M., Schwertfeger, S., Bonini, M., Halfar, H., Pathak, K., Rohde, M., Fantoni, G., Bicchi, A., Birk, A., Lilienthal, A.J. and Echelmeyer, W.: No More Heavy Lifting: Robotic Solutions to the Container Unloading Problem, IEEE Robot. Automat. Mag., Vol. 23, No. 4, pp. 94–106, 2016.
- [10] Tichem, M., Lang, D. and Karpuschewski, B.: A classification scheme for quantitative analysis of micro-grip principles, Assembly Automation, Vol. 24, No. 1, pp. 88–93, 2004.
- [11] Kurfess, T.R.: *Robotics and automation handbook*, CRC Press, Boca Raton, 1 p., 2005.
- [12] Hesse, S. and Malisa, V.: Taschenbuch Robotik - Montage - Handhabung, 2., neu bearbeitete Auflage ed. Fachbuchverlag Leipzig im Carl Hanser Verlag, München, 614 pp., 2016.
- [13] Monkman, G.J.: Robot grippers, Wiley-VCH, Weinheim, Chichester, 452 pp., 2007.
- [14] Fantoni, G., Capiferri, S. and Tilli, J.: Method for Supporting the Selection of Robot Grippers. <https://www.sciencedirect.com/science/article/pii/S2212827114006945?via%3Dihub>. Accessed 23 May 2019.
- [15] Schmalz, J. and Reinhart, G.: Automated Selection and Dimensioning of Gripper Systems, Procedia CIRP 23, pp. 212–216, 2014.
- [16] Tilli, J., Brando, A. and Fantoni, G.: Gripping Device for Heavy and Deformable Materials Handling. Concept, Design, Selection and Test, Procedia CIRP 21, pp. 373–378, 2014.
- [17] Kazerooni, H. and Foley, C.: A robotic end-effector for grasping postal sacks, 2003.
- [18] Wohlfahrt, A.: Reibschlüssige Greifsysteme für die automatische Handhabung im Materialfluss. Logistics Journal: nicht-referierte Veröffentlichungen 2005 (April).
- [19] Burwinkel, M., Echelmeyer, W., Kirchheim, A. and Steiner, P.: Automatische Entladung schwerer Kaffeesäcke. wt Werkstattstechnik online, Vol. 98, No. 9, pp. 706–710, 2008.
- [20] Copal Handling Systems. Container unloading and palletizing. <https://www.copalhandlingsystems.com/>. Accessed 1 July 2019.
- [21] Seliger, G., Szimmat, F., Niemeier, J. and Stephan, J.: Automated Handling of Non-Rigid Parts, CIRP Annals, Vol. 52, No.1, pp. 21–24, 2003.
- [22] Fantoni, G., Gabelloni, D. and Tilli, J.: Concept design of new grippers using abstraction and analogy. Proceedings of the Institution of Mechanical Engineers, Part B: Journal of Engineering Manufacture, Vol. 227, No. 10, pp. 1521–1532, 2013.
- [23] Mortensen Ernits, R., Kunaschk, S., Rohde, M. and Freitag, M.: Autonome Entladung von Kaffeesäcken aus Überseecontainern durch ein innovatives Greifverfahren. Industrie 4.0 Management, Vol. 31, No. 6, pp. 51–55, 2015.
- [24] RobLog Consortium, 2015. RobLog - Autonomous Robot for Unloading of Sacks - Final Industrial demonstration - YouTube. https://www.youtube.com/watch?v=U7_lxH-qB5I&. Accessed 1 July 2019.

Alexander Ortner-Pichler

Research Assistant
Graz University of Technology
Faculty of Mechanical Engineering

Christian Landschützer

Associate professor
Graz University of Technology
Faculty of Mechanical Engineering

Concepts for the use of knowledge-based engineering in intralogistics system planning

The planning process of intralogistics systems is characterised by a complex set of interdependencies of various conditions and specifications to be fulfilled. Within the planning process a huge source of existing knowledge in the form of various 3D-CAD machinery designs or information found within PDM-systems is only used sparingly. The newly developed knowledge-based engineering methodology to be shown states concepts for the formalization, enrichment and use of this existing knowledge in order to assist in intralogistics system planning and thus increasing its efficiency.

Keywords: Intralogistics, system planning, knowledge-based engineering, methodology development, CAD.

1. INTRODUCTION

System planning in the field of intralogistics is a very manifold topic. Complex interdependencies [1, 2] in terms of material flow, cost estimation, process optimization and many more between the various system's sections need to be considered. This complexity meets a rather straightforward design processes regarding the choice and adaptation of the needed machinery caused by long product life cycles and mostly using variant designs [3].

Considering the numbers of newly build intralogistics systems and the growth rates especially in the e-commerce sector [4 - 6], it can be assumed, that even small increases of the cost and time based efficiency in system planning may have good impacts.

When investigating potentials for possible increases of the efficiency in the planning process within its practical realization, differences to the theoretically stated planning processes [7 - 9] can be observed. One major difference can be found within rough planning as it is mostly done by the combination of existing machinery and subsystems in order to fulfil the needed logistics performance in a - by a huge set of boundary conditions - often widely predefined material flow layout and the ideal planning even fully skipped. In addition to this, modern software technologies are not fully utilized as the layout planning of intralogistics systems is usually done using 2D-CAD tools even though most machinery is designed using 3D-CAD tools [3].

This article shows the main idea and the key concepts of a newly developed methodology utilizing knowledge-based engineering in intralogistics system planning. Details on the used data structures and the prototype implementation will be published in further articles.

2. UTILISATION OF KNOWLEDGE-BASED ENGINEERING IN INTRALOGISTICS SYSTEM PLANNING

The combination of existing information and knowledge to a highly interdependent system - especially when carried out within the CAD domain - can be supported by the use of knowledge-based engineering (KBE) [10, 11]. This discipline can be defined (depending on the various, rather blurry definitions) as the "use of knowledge processing systems in product development" [10] or the "cross point of diverse fundamental disciplines, such as artificial intelligence (AI), computer aided design (CAD) and computer programming" [11]. In opposite to most definitions, a huge source of knowledge is not accessible out of existing full KBE methodologies (see [12] for the differentiation of full-KBE and augmented CAD-KBE), as there is no possibility to use existing 3D-CAD models or designs to create an overall systems based on these designs [13 - 16].

As there is no methodology available focusing on these demands, a new concept for a KBE methodology was developed that focuses on the specific characteristics of intralogistics system planning in order to increase the efficiency of the planning process. Main idea of the methodology to be described, is to access the unused information, which can be found in the form of various 3D-CAD machinery designs or information found within PDM-systems.

The concept to be shown, states a way how to markup and enrich the existing information in a way, so that an intralogistics systems can be created generically in a first step and then easily derive various variants of different technical characteristics and thus reducing the gap between ideal and rough planning.

3. KEY CONCEPTS

The methodology grounds on five key concepts to be shown in the following. Possibilities arising by the use of the key concepts are described in the next section.

Correspondence to: Alexander Ortner-Pichler, Research Assistant, Graz University of Technology, Faculty of Mechanical Engineering, Institute of Logistics Engineering
Inffeldgasse 25/E, 8010 Graz, Austria
E-mail: alexander.ortner-pichler@tugraz.at

3.1 Export & Re-import

Most information used in intralogistics system planning is available in the concerning companies, but it's spread in different departments or hidden within proprietary software solutions. In order to handle this problem the approach was chosen to collect all information used within an separated layer. This means that the used information in form of geometry, performance data and further more needs to be exported, marked up and enriched, to later be used within the methodology. After the use of the information - i.e. the system planning - generated information will be re-imported into the designated target locations (for example another software solution that is needed for the detail planning).

3.2 Black-box encapsulation

Within the methodology, existing machinery is described as an encapsulated black-box. These black-boxes are specified by a set of parameters, holding information about geometry, logistics performance and other data used in the planning process as well as a logic core, that can perform analytic or algorithmic calculations within the encapsulated system. This representation is mainly chosen in order to reduce the system's complexity, as on a basic level e.g. a steady conveyor can be specified by its width, length and height as well as the conveyor's throughput and availability.

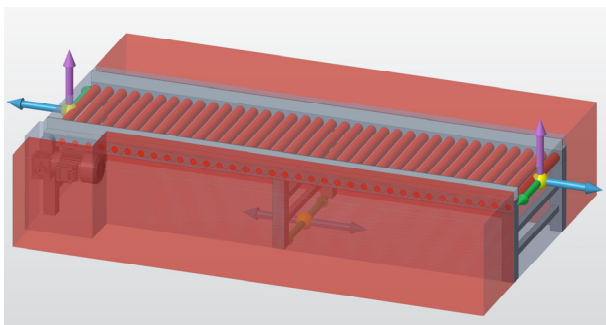


Figure 1. Visual representation of a roller conveyor encapsulated in a black-box

As shown in figure 1 on an abstract level, the black-boxes can be represented by a rough geometry in the form of the machinery's bounding geometry, extended by prohibited spaces, needed for the machinery's operation or maintenance. A detailed system configuration of the machinery can be done asynchronously using a 3D-CAD system based on the black-boxes parameter setting (see [17] for details). By choosing this separation of rough and detailed machinery configuration, an implementation of the methodology may provide fast variant generation, but still maintaining the complete technical data of the machinery.

3.3 Interface connection

As the black-boxes themselves are actually fully encapsulated against their environment, they are extended by interfaces in order to be connected to any other black-box. These interfaces provide the possibility

to match parameters held by the black-boxes being connected.

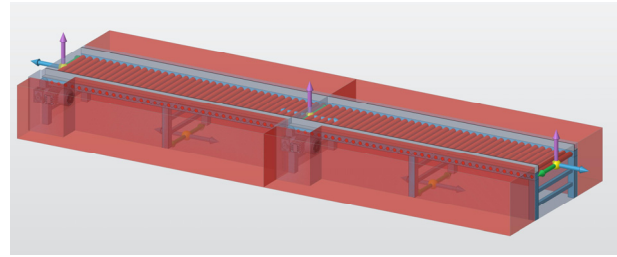


Figure 2. Two roller conveyors linked to each other by an interface connection

On a basic level of system generation, these interconnections of black-boxes can be used to e.g. set the position of different conveyors following each other and simultaneously generating the routes of the material flow within the overall system as seen in figure 2. For illustration purposes the interfaces are represented within the figure as a coordinate cross. Figure 1 shows two interfaces, representing the points of entry and leave of the conveyed goods and one interface shown in the middle, to connect the conveyor to the ground.

3.4 Object-oriented structuring

All machinery used by the methodology within the black-boxes is structured in an object-oriented hierarchy. The root classes of this hierarchy are mainly differentiated by the count of points (or interfaces) describing the point of entry and leave of the conveyed goods, as well as the kind of positional displacement (1D, 2D or 3D) between point of entry and leave. This leads to the fact, that e.g. a roller conveyor and a belt conveyor are represented by the same class, if the abstraction of the class is high enough, allowing them to be easily exchanged during the planning process.

3.5 Grouping

The fifth key concept states, that a black-box can group any number of other black-boxes and thus integrating them into its own encapsulation, allowing it to create, replace or delete them. By the use of this grouping concept a black-box's logic core can programmatically choose between e.g. a belt or a roller conveyor based on specific parameters or create a conveyor line of varying length stringing together conveyors of fixed length, but still reducing the system's complexity by the encapsulation of the subsystem.

4. NETWORK DESIGN & NETWORK ANALYSATION

When using machinery, marked up the way described in the last section, network design appears to be rather easy and efficient. Machinery can be placed in the surrounding space (e.g. a simple room or an existing factory building layout) either by an absolute coordinate reference or relatively to another machinery's interface. Keeping in mind, that by connecting two interfaces various parameters can be matched, network information of an intralogistic system can be generated en passant, when matching parameters describing the geometric

placement as well as parameters describing the direction of the material flow or the simple occurrence of a material flow. This way various possibilities to describe the so generated network arise by deriving a network graph or an adjacency, a distance or a transportation matrix.

Based on the object-oriented structuring this can either be done by an instantiated object (e.g. a roller conveyor of 2 meters in length) or a more abstract instances (e.g. a conveyor with a one-dimensional translational displacement between point of entry and leave). This results in the possibility to generically design an intralogistic material flow layout as a set of 1D, 2D or 3D displacements queued one after another. The material flow layout can thus be designed without technical restrictions of the machinery specifications on an abstract level, later be specified as a technical variant (e.g. roller or belt conveyor) and compared to each other. Within this process boundary conditions caused by the machinery's geometry or the building structure are still considered.

Considering the other key concepts of the methodology can, most remarkably, lead to one

possibility: network design feedback - i.e. information of generated networks can be used in the configuration or parametrization of the machinery used. On a simple level this can be used to notify a user that a conveyor line delivers too little logistic performance and request a modification of the machinery's parameters. On a more sophisticated level the methodology can be used to assist a user by a (semi-)automated machinery selection and configuration as well as routing or subsystem design or even use the network information in an optimization cycle for the specification and parametrization of the used machinery.

Another example of the network feedback can be, that the geometric position can be analysed or modified programmatically, when geometric collisions of a machinery's bounding geometry against another machinery prohibited maintenance space is detected. This can be useful when using the grouping structure to create a programmatically generated conveyor line between a source and a sink.

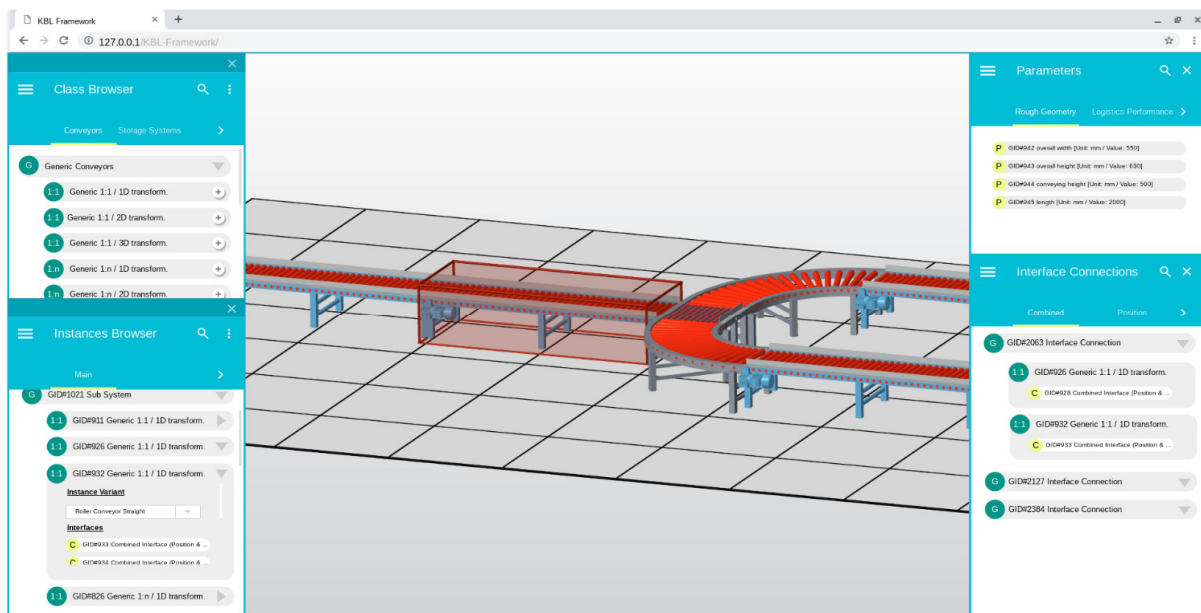


Figure 3. Prototype implementation of a web-based interface using the developed methodology

5. PROTOTYPE IMPLEMENTATION

Figure 3 shows a web-based user interface of a prototype implementation using the developed KBE methodology. In the center of the image a 3D visualization can be seen, showing the conveyor in the middle being selected. On the left side the class browser and instanced objects browser can be seen. The right side shows a dialog to edit parameters and system interconnections. The methodology core is implemented using an object-oriented approach in JavaScript and provides the object-oriented structuring as well as the logic cores of the used black-boxes. The used geometry of the roller conveyors was modelled using PTC Creo and is being visualized using three.js (a webGL framework in JavaScript) after a sequence of export, conversion and optimization processes.

In order to provide real time collaboration functionality, the prototype implementation uses the Google Realtime API. As this API is unfortunately deprecated an upgraded version is planned utilizing the Google Firebase. This implementation of the methodology can be seamlessly integrated in an existing IT environment as it considers the key concept of export and re-import. That means that when system planning within the web-based interface is done, a 3D model of the whole intralogistic system can be generated in PTC Creo.

6. CONCLUSION

In this paper a concept for a new knowledge-based engineering methodology is described, that tries to utilize existing information. The developed methodology focuses on the boundary conditions considering the planning of intralogistic systems, but it is usable in a wide

spread field of applications especially in systems based on networks.

Most notable the methodology extends related research done [18 - 20] by the possibility to generically design an intralogistics system thus allowing to easily compare system variations of different technical characteristics. This process tries to help to bring the ideal and rough planning closer to each other. In addition to that the methodology reduces system complexity by the encapsulation of subsystems but still maintaining the option to use generated material flow network information within machinery specification and configuration and thus generated encapsulated optimization cycles.

REFERENCES

- [1] Crostack, H.A., Mathis, J. and Noll, K.: Components of A Requirement of An Intralogistics Facility, 11th QMOD Conference. Quality Management and Organizational Development, 2008.
- [2] Schuhmacher, J., Baumung, W. and Hummel V.: An Intelligent Bin System for Decentrally Controlled Intralogistic Systems in Context of Industrie 4.0, Procedia Manufacturing, Vol. 9, pp. 135-142, 2017.
- [3] Landschützer C.: Methoden und Beispiele für das Engineering in der Technischen Logistik (Habilitationsschrift): Schriftenreihe des Instituts für Technische Logistik, Verlag der Technischen Universität Graz, 2016.
- [4] BIEK. (n.d.): Erwartetes durchschnittliches jährliches Wachstum der Sendungsvolumina in der Kurier-, Express- und Paketbranche in Deutschland im Zeitraum der Jahre 2017 bis 2022 nach Marktsegmenten. In Statista - Das Statistik-Portal. Retrieved Februar 19, 2019, from <https://de.statista.com/statistik/daten/studie/219462/umfrage/prognose-zu-den-kep-sendungsvolumina/>.
- [5] BNP Paribas Real Estate. (n.d.): Transaktionsvolumen am Investmentmarkt für Logistikimmobilien in Deutschland von 2005 bis 2018 (in Millionen Euro). In Statista - Das Statistik-Portal. Retrieved Februar 19, 2019, from <https://de.statista.com/statistik/daten/studie/302663/umfrage/transaktionsvolumen-auf-dem-investmentmarkt-fuer-logistikimmobilien/>.
- [6] BNP Paribas Real Estate. (n.d.): Investments in Gewerbeimmobilien in Deutschland in den Jahren von 2011 bis 2018 nach Art des Objekts (in Millionen Euro). In Statista - Das Statistik-Portal. Retrieved Februar 19, 2019, from <https://de.statista.com/statistik/daten/studie/278479/umfrage/investments-in-gewerbeimmobilien-in-deutschland-nach-objektart/>.
- [7] Martin, H.: *Praxiswissen Materialflußplanung: Transportieren, Handhaben, Lagern, Kommissionieren*, Springer-Verlag, 2013.
- [8] Gudehus, T.: *Logistik: Grundlagen - Strategien – Anwendungen*, Springer Berlin Heidelberg, 2005.
- [9] ten Hompel, M., Schmidt, T. and Nagel, L.: *Materialflusssysteme: Förder- und Lagertechnik*, Springer Berlin Heidelberg, 2007.
- [10] Vajna, S., Weber, C., Zeman, K., Hehenberger, P., Gerhard, D. and Wartack, S.: *CAX für Ingenieure: Eine praxisbezogene Einführung*, Springer-Verlag, 2018.
- [11] La Rocca, G.: Knowledge based engineering: Between AI and CAD. Review of a language based technology to support engineering design, Advanced Engineering Informatics, Vol. 26, No. 2, pp. 159–179, 2012.
- [12] Landschützer, C., Jodin, D.: Knowledge-based methods for efficient material handling equipment development, Progress in Material Handling Research 2012.
- [13] Verhagen, W.J.C., Bermell-Garcia, P., van Dijk, R.E.C. and Curran, R.: A critical review of Knowledge-Based Engineering: An identification of research challenges, Advanced Engineering Informatics, Vol. 26, No. 1, pp. 5–15, 2012.
- [14] Stokes, M. (Hrsg.): Managing engineering knowledge: MOKA - methodology for knowledge based engineering applications, Professional Engineering Publishing, 2001.
- [15] Lovett, P.J., Ingram, A. and Bancroft, C.N.: Knowledge-based engineering for SMEs - a methodology, Journal of Materials Processing Technology, Vol. 107, No. 1-3, pp. 384-389, 2000.
- [16] Curran, R., Verhagen, W. J.C., van Tooren, M. J.L. and Van der Laan, T.H.: A multidisciplinary implementation methodology for knowledge based engineering: KNOMAD, Expert Systems with Applications, Vol. 37, No. 11, pp. 7336-7350, 2010.
- [17] Ortner-Pichler, A., Landschützer, C.: Improving geometry manipulation capabilities of knowledge-based engineering applications by the versatile integration of 3D-CAD systems, The Publications of the MultiScience - XXX. microCAD International Multidisciplinary Scientific Conference University of Miskolc, 2017.
- [18] Ghoofrani, M.: *Entwicklung und Einführung eines flexiblen Softwaresystems zur Konfigurierung virtueller Produkte*, Shaker, 2008.
- [19] Kipouridis, O., Günthner, W.A., Roidl, M., ten Hompel, M.: Kollaborative Planung dezentral gesteuerter Materialflusssysteme in der Intralogistik, Logistics Journal, 2013.
- [20] Fonseca, D.J., Uppal, G., Greene, T.J.: A knowledge-based system for conveyor equipment selection. In Expert Systems with Applications, Vol. 26, No. 4, pp. 615-623, 2004.

Artificial Intelligence methods for solving Product Allocation Problem (PAP)

Augustyn Lorenc

Assistant Professor
Cracow University of Technology
Institute of Rail Vehicle, Poland

Małgorzata Kuźnar

Research Assistant
Cracow University of Technology
Institute of Rail Vehicle, Poland

Tone Lerher

Professor
University of Maribor
Slovenia

For many companies, proper planning of a warehouse layout and the distribution of products in it, constitute major challenges. Many companies do not think about product allocation and focus on improving the efficiency of the currently used system. From the perspective of optimization, apart from improving the processes of handling goods in the warehouse, it is also important to properly plan the warehouse structure and to distribute goods accordingly inside it. Product Allocation Problem (PAP) in warehouses plays a significant role in the effectiveness of product picking process.

To reduce the distance of picking a route, there is a need to classify the products by pickup density, and then plan their allocation. Currently, in order to plan the distribution of products in a warehouse, products classifications methods like ABC, XYZ, Index COI are used. This means that different products are ascribed to groups of different ranks, and then they are distributed in the warehouse in such a way to ensure the shortest access time to products of the highest importance. The problem is complex because many products have a short lifetime on the market, so after a few weeks or months, the product can be replaced by a new one. Because of that the Product Allocation Problem (PAP) should be solved each day.

In the paper, the new approach for the classification of the problem is presented. Authors used real picking data from the Warehouse Management System (WMS) from peak season from September to January. Artificial Neural Network (ANN) and Machine Learning (ML) were used to develop a new classification method. Base on the picking list the clients' orders were prepared. These orders were used as input data to ANN and ML. This method base on the orders for each day and the previous class of the product returns the optimal classification. The developed method is based on the actual and past situation for predicting the importance of each product. In the research over 380000 picks for almost 1600 locations were used. In the paper, the architecture of the system module for solving the PAP problem is presented.

By the presented research, it was confirmed that Artificial Intelligence methods can be used to increase the efficiency of the order picking process.

Keywords: Product Allocation Problem, Artificial Intelligence, Artificial Neural Network, Clustering, Picking list analysis

1. INTRODUCTION

Product Allocation Problem (PAP) is one of the major challenges for a number of warehouses and logistic centres. It would appear that it is a quite plain problem, however, for many companies storage of products is not currently sufficient [1]. The modern market force companies to compete not only on a local but also on a global scale [2]. From the perspective of the global market, it is not so important where the product was produced, but how much time and money cost the

transport and logistics operations. The costs of transport are often a significant part of the total cost of a product, especially for products of relatively small value [3].

In the transport system, a warehouse is very often a bottleneck that raises total delivery costs. Consequently,

if product allocation planning is made randomly, it may increase the distance during picking - the higher demand products will be located far from picking and packing zone. Thus, loss of time, the increase of needed employees and means of transport may occur. The different methods of items classification are used in order to plan product allocation in the warehouse. Items are identified and clustered, then they are distributed in the warehouse area in such a way as to ensure the shortest time to access products of the highest importance. Typical methods of items classification are ABC, XYZ, EIQ, AHP, and COI Index analyses [4], [5], [6], [7].

Correspondence to: Dr Augustyn Lorenc, Assistant Professor
Cracow University of Technology
al. Jana Pawła II 37, 31-864 Cracow, Poland
E-mail: alorenc@pk.edu.pl

Although these methods are still widely used, they do not satisfy the requirements placed on the warehouses. These analyses are most often performed for just one criterion, sometimes repeated for another's criterion and averaged according to obtained results. However, the mentioned approach allows to take into account several criteria at the same time but doesn't allow to include correlations between classified items [8], [9], [10], [11], [12], [13].

According to insufficient methods of items classification, companies are increasingly looking for new methods by combining those already used or refining them. Each company, by its nature, may have different expectations[14]. An example can be a company producing bulk/granular goods packed in cartons and bags. For this type of business, it will be important for the products to be picked according to the type of packaging and weight which describes stacking resistance. It is to avoid the necessity to rearrange products placed on the order picking truck in a sequence, where small items can be damaged by heavier and larger items located above [15], [16]. Therefore, by distributing products only according to their demand, completion according to the type of packaging and weight would cause a number of problems – it would be necessary to cross the warehouse several times to revisit the places in the same area [2]. On the other hand, it cannot ignore the importance of the demand, seasonality, value of the product [17]. One might also ask themselves what about the relationships between products, e.g. frequency of certain product groups on picking lists? Due to an amount of input data of this type, problems cannot be solved by methods of classical classification. Because of that, the artificial intelligence method like Machine Learning and Artificial Neural Networks were examined to find new method taking into account many criteria at the same time.

The warehouse used for the case study stock the electronics home appliances, computers and computer accessories.

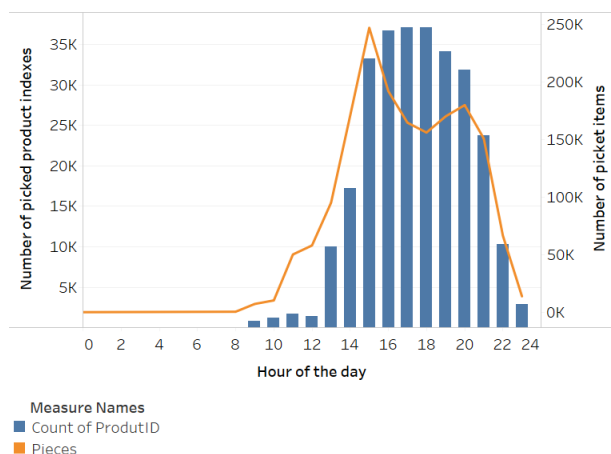


Figure 1. The picking of the product by the hour of the day

The picking of a product by the hour of the day is presented on image 1. The storekeepers work in two work shifts, from 8 am to 4 pm, and from 4 pm to midnight. The product dispatch is done by the 12 gates, and most of the transports are sent at the 3 pm.

The total area of the warehouse is about 5400 m² (90x60m). In the warehouse, there is 96 forklifts and picking trolleys for the small orders.

The warehouse is divided into two main areas: an area for small products marked with “T” prefix for location number, and the area for big products stock on pallet unit marked with prefix “P”. The number of shelves in the “T” area is 22 000 for average 30 tier, the number of shelves for the standard tier is 740. The number of pallet socket in the racks is 3060 for the average of 3 tier, the number of the socket is 1160.

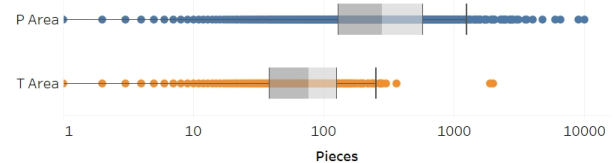


Figure 2. The picking items for the “P” and “T” area

The pick by order policy is generally used, but for big orders, the picking list is divided into few storekeepers and picked simultaneously. The relocation of the product is done during normal day picking.

The analysis was done for the period from October to December – the busiest period of the year. In the analysed period was stock 22586 of the product indexes.

2. METHODOLOGY AND GENERAL ASSUMPTIONS

The data from the WMS system was cleaned from useless information. After that base on each housekeepers activities, the client's orders were formed. In the next step, the general statistics were done. Base on the warehouse plan (Autocad) the location for each shelf and pallet racks were measured.

For making product classification model the Matlab and Tableau software was used. After a few iterations, the most promising model was chosen. The training process for the ANN was base on the data from October and November. And for simulation the data from November to December was used. The visualisation of the results was done in the Tableau software.

The method of evaluating the Product Allocation Problem taking into account the developed predictive model of the technical condition is shown in Figure 2.

2.1 Classification base on the Artificial Neural Network

A feed-forward network was used for the simulation. The selection of an artificial neural network structure was based on the method of subsequent approximations. The 10 different structures were examined. The network structure selection was made on the basis of the mean square error (MSE). The created artificial neural network (ANN) consists of one hidden with 8 neurons and one output layer (Fig. 4). As an activation, the tangensoidal function was used. The Levenberg-Marquardt backpropagation method was used as the learning algorithm.

As the input data, the 22 586 cases were used. The data was divided into three sets: for training: 15810

samples, for validation: 3388 samples and for a test: 3388 samples.

Fig. 4 shows the structure of the network. Fig. 5 shows the best validation performance.

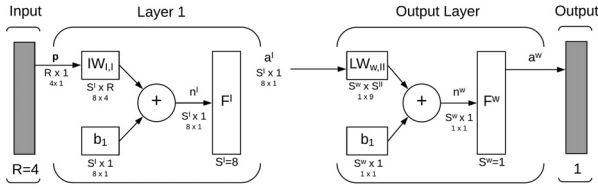


Figure 4. Structure of chosen artificial neural network

$$a^w = f^3(LW_{3,2}f^2(LW_{2,1}f^1(IW_{1,1}p + b_1) + b_2) + b_3 = y \quad (1)$$

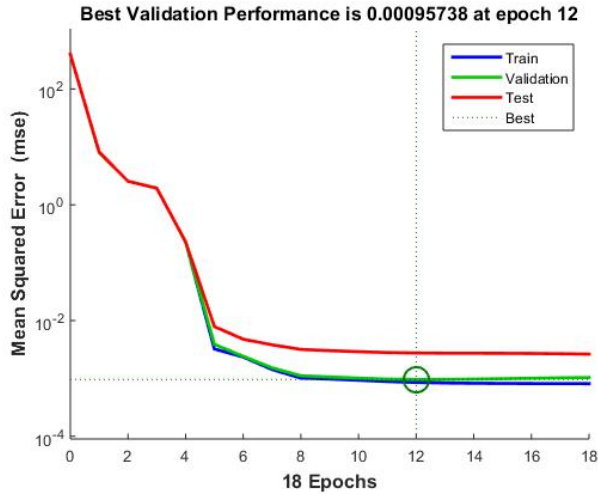


Figure 5. Best validation performance

For the ANN structure with best results, the MSE of 0.00095738 was achieved at the 12 epoch. After 12 epoch the results are worst. It could be also noticed by the learning factors changed in the epochs. The gradient, damping factor - training gain (μ), and validation check is presented in figure 6.

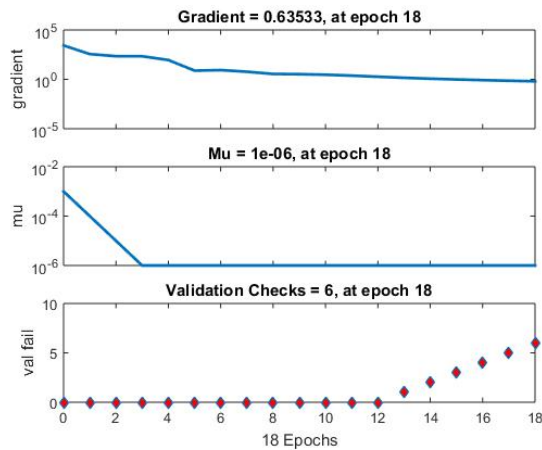


Figure 6. Learning factors by the epochs

The results achieved in the training, the validation and testing of neural network processes are presented in Fig. 7.

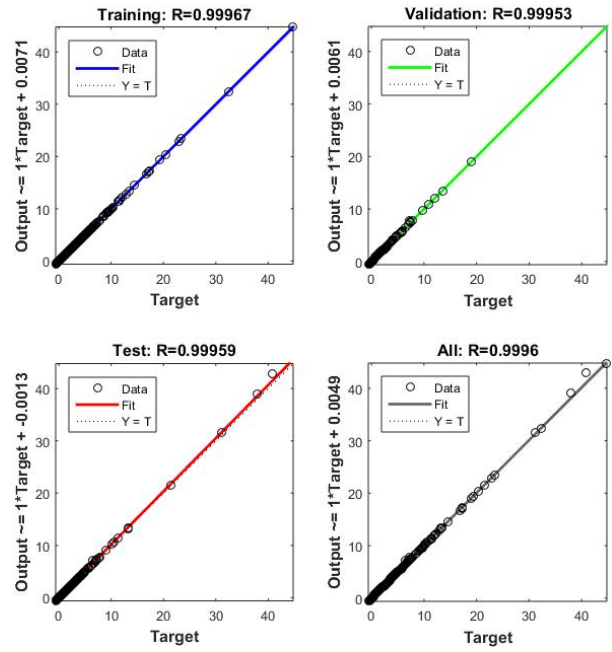


Figure 7. Regression plot for training, validation and testing of ANN

The error analysis is presented by the histogram chart in figure 8.

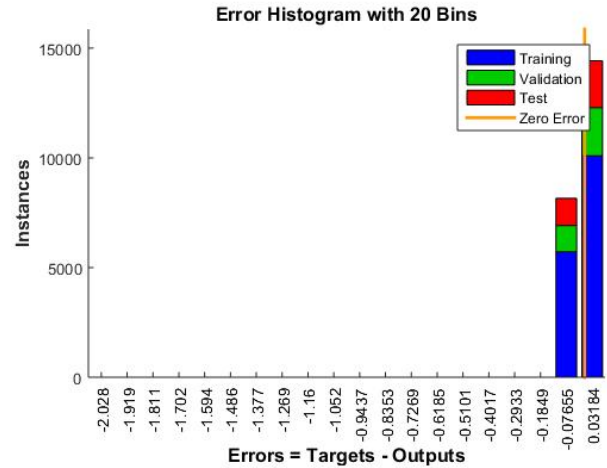


Figure 8. Histogram of the error for the best network structure

Figure 5 and 6 shows the good quality of the model results.

2.2 Classification model base on Machine Learning

For making the classification model the 22586 input data was used. As the criteria for each product index where defined: the number of orders in which it occurs, the number of items, the difference between actual and previous months of the number of orders and items.

To avoid empty cluster, and cluster with just one product the appropriate number of the cluster was found – 6 clusters. For finding the number of clusters the Calinski-Harabasz criterion was used to assess cluster quality.

$$CL = \frac{SS_B}{SS_W} \cdot \frac{N - k}{k - 1} \quad (1)$$

The data diagnostics for the generated by Machine Learning model are presented below:

- between-group Sum of Squares: 58.673,
- within-group Sum of Squares: 35.912,
- total Sum of Squares: 94.585.

For ML classification model was used the k-means algorithm. For a given number of clusters k , the algorithm partitions the data into k clusters. Each cluster has a centre (centroid) that is the mean value of all the points in that cluster. K-means locates centres through an iterative procedure that minimizes distances between individual points in a cluster and the cluster centre.

K-means requires an initial specification of cluster centres. Starting with one cluster, the method chooses a variable whose mean is used as a threshold for splitting the data in two. The centroids of these two parts are then used to initialize k-means to optimize the membership of the two clusters. Next, one of the two clusters is chosen for splitting and a variable within that cluster is chosen whose mean is used as a threshold for splitting that cluster in two. K-means is then used to partition the data into three clusters, initialized with the centroids of the two parts of the split cluster and the centroid of the remaining cluster. This process is repeated until a set number of clusters is reached.

Table 1. Centres of the cluster by each criterion

Cluster	Number of Items	Count of Orders	Change by Pieces	Change by Order	Count of Pieces
CL1	18353	3.86	0.14	-0.02	15.61
CL2	2611	27.59	0.32	0.10	145.30
CL3	357	88.31	0.41	0.18	592.11
CL4	1211	9.12	7.16	3.77	35.75
CL5	45	219.24	0.19	0.18	2080.80
CL6	9	57.11	0.46	0.54	13274.00

The Lloyd's algorithm with squared Euclidean distances to compute the k-means clustering for each k was used. Combined with the splitting procedure to determine the initial centres for each $k > 1$, the resulting clustering is deterministic, with the result depends only on the number of clusters.

The analysis of variance for the model was done. The results are presented in Table 2.

Table 2. Result for analysis of variance for the clustering model

Variable	F-statistic	p-value	Sum of Squares	Sum of Squares
Count of Orders	3834.0	0.0	36.52	43.02
Count of Pieces	3072.0	0.0	5.03	7.39
Change by Order	1845.0	0.0	17.02	41.66
Change by Pieces	205.3	0.0	0.11	2.52

The F-statistic for one-way, or single-factor, ANOVA is the fraction of variance explained by a variable. It is the ratio of the between-group variance to the total variance. The larger the F-statistic, the better the corresponding variable is distinguishing between clusters.

The p-value is the probability that the F-distribution of all possible values of the F-statistic takes on a value greater than the actual F-statistic for a variable. If the p-value falls below a specified significance level, then the null hypothesis (that the individual elements of the variable are random samples from a single population) can be rejected. The degrees of freedom for this F-distribution is $(k - 1, N - k)$, where k is the number of clusters and N is the number of items (rows) clustered. The lower the p-value, the more the expected values of the elements of the corresponding variable differ among clusters.

The Model Sum of Squares is the ratio of the between-group sum of squares to the model degrees of freedom. The between-group sum of squares is a measure of the variation between cluster means. If the cluster means are close to each other (and therefore close to the overall mean), this value will be small. The model has $k-1$ degrees of freedom, where k is the number of clusters.

The Error Sum of Squares is the ratio of the within-group sum of squares to the error degrees of freedom. The within-group sum-of-squares measures the variation between observations within each cluster. The error has $N-k$ degrees of freedom, where N is the total number of observations (rows) clustered and k is the number of clusters. The Error Sum of Squares can be thought of as the overall Mean Square Error, assuming that each cluster centre represents the "truth" for each cluster.

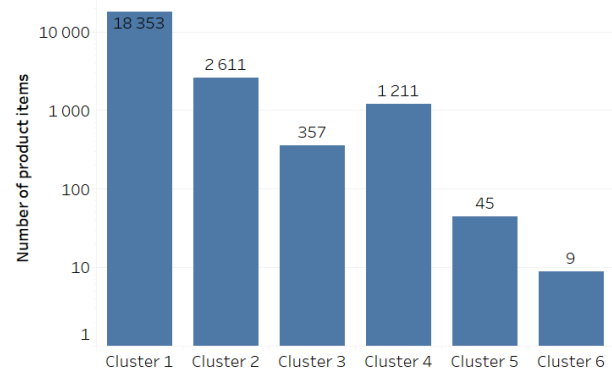


Figure 9. Summary statistic for clustering results

For compare the results, the simulations of product allocation regarding the results of ANN and clustering were done. The simulation results were compared by Boc-Whisker plot and Heat Map for both areas: small products "T" area, and pallet unit "P" area. The results of visualisation are presented in the figures 10a-10c.

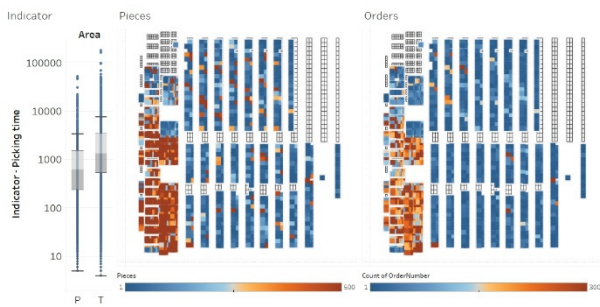


Figure 10a. Box-Whisker plot and Heat Map for reference product allocation

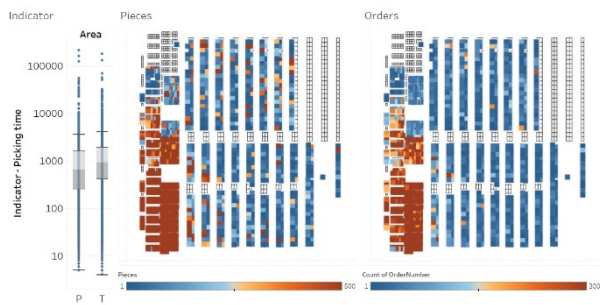


Figure 10b. Box-Whisker plot and Heat Map for product allocation by ANN results

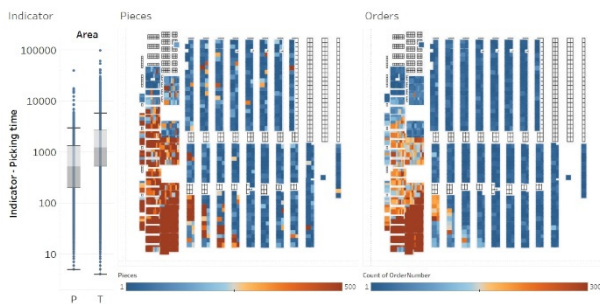


Figure 10c. Box-Whisker plot and Heat Map for product allocation by Clustering results

The results also are presented in table 3 – comparison for each area and product allocation method.

Table 3. Comparison statistic for the direct picking time [min]

Area	Reference		ANN		Clustering	
	P	T	P	T	P	T
Upper Whisker	57,2	126,3	60,0	68,0	49,9	97,8
Upper Hinge	25,4	55,9	26,9	31,4	22,0	44,6
Median	10,3	22,5	10,9	15,7	8,8	20,8
Lower Hinge	3,9	8,7	4,2	6,9	3,3	8,8
Lower Whisker	0,1	0,1	0,1	0,1	0,1	0,1

It could be seen, that best results were achieved for clustering. The product of the highest pickup density for orders and products picks are located in the nearest area of orders packing. For the actual (real) product allocation, the products with similar pickup density are placed in distant places. It is an unprofitable situation. The ANN

method helps to find a better solution but not as good as clustering.

3. CONCLUSION

The presented research proves that it is possible to improve the warehouse picking process by shorting the picking distance and reduce the time of this process.

The research base on the real data, and prove that achieving results could be useful and can be implemented by the company.

In future research, the comparison with the classic method will be done. What is more, the presented method of clustering product will be upgraded by taking into account the relation between the products on the same picking list. The research with the own product Correlation Searching Algorithm (CSA) gave promising results. Because of that in the future, the CSA algorithm will be combined with clustering method.

REFERENCES

- [1] Roodbergen, K.J., Vis, I.F.A. and Taylor G.D.: Simultaneous determination of warehouse layout and control policies, *International Journal of Production Research* 53, pp. 3306–3326, 2015.
- [2] Li, M.L.: Goods classification based on distribution center environmental factors, *International Journal of Production Economics*, Vol. 119, No. 2, pp. 240–246, 2009.
- [3] van Gils, T., Ramaekers, K., Caris, A. and de Koster, R.B.M.: Designing efficient order picking systems by combining planning problems: State-of-the-art classification and review, *European Journal of Operational Research*, Vol. 267, No. 1, pp. 1–15, 2018.
- [4] Larco, J.A., de Koster, R.B.M, Roodbergen, K.J. and Dul, J.: Managing warehouse efficiency and worker discomfort through enhanced storage assignment decisions, *International Journal of Production Research*, Vol. 55, No. 21, pp. 6407–6422, 2017.
- [5] Lorenc, A.: Method of effectiveness evaluation of products picking process for pick by order type in warehouse on basis of a picking list, 13th International Conference on Industrial Logistics, ICIL 2016 - Conference Proceedings, 2016.
- [6] Lorenc, A., Jacyna-Golda, I. and Szarata, A.: Assessment of the impact of products classification methods onto the efficiency of order picking process, in *IEEE ICALT'2016 : 2016 5th IEEE Int. Conf. on Advanced Logistics and Transport*, June 1-3, 2016, Krakow, Poland : conference guide, pp. 129–134, 2016.
- [7] Zhao, Z. and Yang, P.: Improving order-picking performance by optimizing order batching in multiple-cross-aisle warehouse systems: A case study from e-commerce in China, in *2017 4th International Conference on Industrial Engineering and Applications (ICIEA)*, pp. 158–162, 2017.

- [8] Subramanian, N. and Ramanathan, R.: A review of applications of Analytic Hierarchy Process in operations management, *International Journal of Production Economics*, Vol. 138, No. 2, pp. 215–241, 2012.
- [9] Henn, S.: Algorithms for On-line Order Batching in an Order Picking Warehouse, *Compututer & Operations Research*, Vol. 39, No. 11, pp. 2549–2563, 2012.
- [10] Chen, F.-L., Chen, Y.-C. and Kuo, J.-Y.: Applying moving back-propagation neural network and moving fuzzy neuron network to predict the requirement of critical spare parts, *Expert Systems with Applications*, Vol. 37, No. 6, pp. 4358–4367, 2010.
- [11] Rao, S.S. and Adil G.K.: Class-based storage with exact S-shaped traversal routeing in low-level picker-to-part systems, *International Journal of Production Research*, Vol. 51, pp. 4979–4996, 2013.
- [12] Hadi-Vencheh, A. and Mohamadghasemi, A.: A fuzzy AHP-DEA approach for multiple criteria ABC inventory classification, *Expert Systems with Applications*, Vol. 38, No. 4, 2011.
- [13] Moeller, K.: Increasing warehouse order picking performance by sequence optimization, *Procedia - Social and Behavioral Sciences*, Vol. 20, pp. 177–185, 2011.
- [14] Karkula, M.: *Badania symulacyjne procesów transportowych realizowanych w obiektach logistycznych*, Logistyka, 2014.
- [15] Vis, I.F.A. and Roodbergen, K.J.: Layout and control policies for cross docking operations, *Computers & Industrial Engineering*, Vol. 61, No. 4, pp. 911–919, 2011.
- [16] Faber, N., de Koster, R.B.M and Smidts, A.: Organizing warehouse management, *International Journal of Operations & Production Management*, Vol. 33, pp. 1230–1256, 2013.
- [17] Boysen, N. and Stephan, K.: The deterministic product location problem under a pick-by-order policy, *Discrete Applied Mathematics*, Vol. 161, No. 18, pp. 2862–2875, 2013.

NOMENCLATURE

R	number of elements in input vector
S	number of neurons in layer
a	neuron output vector
IW	initial weights
LW	layer weights
p	vector of R input elements
f	sigmoid transfer function
b	bias value
y	output vector of ANN
CL	number of clusters
SS_B	overall between-cluster variance
SS_W	overall within-cluster variance
k	number of clusters
N	number of observations

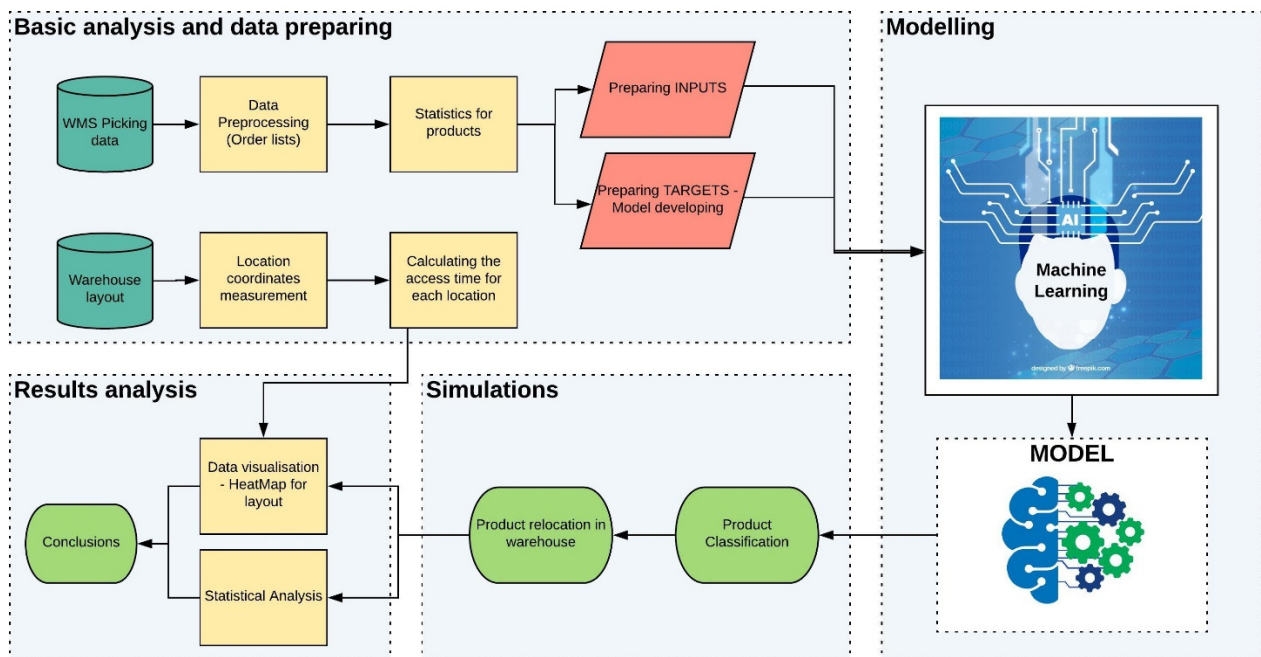


Figure 3. Research methodology

Tone LerherProfessor
University of Maribor
Faculty of Logistics
Celje, Slovenia**Teodor Hliš**M.Sc. student
University of Maribor
Faculty of Logistics
Celje, Slovenia**Jakob Marolt**Research assistant
University of Maribor
Faculty of Logistics
Celje, Slovenia**Bojan Rupnik**Research assistant
University of Maribor
Faculty of Logistics
Celje, Slovenia**Miha Kovačič**Technical Development Manager
Štore Steel d.o.o.
Štore, Slovenia

Design of automated warehouse for long and heavy load steel bars

In this paper, design of automated warehouse for long and heavy load steel bars is presented. Because of the required conditions, that the warehouse should be technically highly efficient and that it should be designed at reasonable expense, the objective function is represented by maximum throughput performance. The objective function combines elements of the static (storage rack construction) and dynamic (travel time model) parts of the warehouse. Due to the nonlinear, multi-variable and discrete shape of the objective function, the method of genetics algorithms (GA) by using an open source software OptiMax was used for the optimization process of the decision variables. An analysis of the chosen automated warehouse for long and heavy load steel bars has been presented. It was established that the optimum solutions regarding throughput performance of the warehouse can be found in the area of large values of ratio between single and double command cycles along with the kinematic properties of the S/R machine. The presented model is useful and flexible tool for choosing a particular set of kinematic properties of the S/R machine when designing automated warehousing systems for long and heavy load steel bars.

Keywords: Material Handling Systems, Automated Warehouses, Design, Analytical and Simulation Modelling, Performance Analysis.

1. INTRODUCTION

A steel production company produces steel bars and has a large assortment of the end products with several dimensions and material properties. The steel bars are stored on the floor in a stacking frame (Figure 1).



Figure 1. Transport of steel bars [source: Štore Steel; <http://www.storesteel.si/EN/enDefault.aspx>]

For the order picking of steel bars, an overhead (bridge) crane is used mainly for reshuffling all the necessary steel bars to get access to the required product ([1] – [3]).

While the production schedule allows for anticipating the storage occupancy, a stochastic transport arrival prevents optimal product stacking for efficient order-

picking operation. Accordingly, any order-picking sequence may result in reshuffling of the stacked material, which increases labour cost, order-picking times, and complicates material traceability.

In order to decrease the labour costs, order-picking times and to improve material traceability steel bars can be stored in a fully automated honeycomb system (AS/RS) with the use of automated storage and retrieval machine (Figure 2).

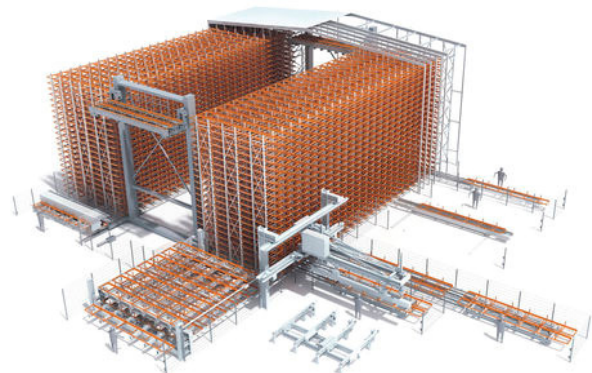


Figure 2. AS/RS for steel bars [source: KASTO storage system; <https://www.kasto.com/en/home.html>]

In the past few decades, the share of AS/RS in steel production companies, which in comparison with conventional warehouses provides a higher level of technological efficiency, has increased expressively. The use of the AS/RS in general already received consideration decades ago, when in 1962 the company Demag created the first AS/AR [4]. The aforementioned AS/RS was the first high-bay warehouse measuring 20 meters in height, which marked the beginning of a new era in the development of material handling equipment in Europe.

Correspondence to: Dr. Tone Lerher, Professor
University of Maribor, Faculty of Logistics
Mariborska c. 7, 3000 Celje, Slovenia
E-mail: tone.lerher@um.si

The AS/RS consists of storage racks (SRs), a storage and retrieval machine (SR machine), accumulating conveyors, an input and output location (I/O location) and a computer system for managing and organizing the activities in the warehouse.

In comparison with conventional warehousing systems, the key advantages of the ASRS are: (i) high throughput capacity Pf , (ii) high warehouse volume Q (rack capacity), (iii) high reliability and better control of the warehousing process, (iv) improved safety conditions and (v) a decrease in the amount of damage and the loss of goods. Due to advanced technology and the complete automation of the system, the AS/RS demands extensive investment.

Estimating the throughput performance of the AS/RS is an essential step in AS/RS design. One way to improve the throughput performance of the AS/RS is to reduce the dimensions of the SR along with the kinematic properties of the S/R machine, which will be introduced and discussed in this paper.

2. AUTOMATED STORAGE AND RETRIEVAL SYSTEMS FOR LONG AND HEAVY LOAD STEEL BARS

AS/RS for long and heavy steel bars (Figure 2) consist of the S/R machine with a hoisted carriage that is moving in the vertical direction and is feeding the storage rack with steel cassettes. The hoisted carriage has its own drive for the vertical movement. The storage rack consists of columns in the horizontal direction and tiers in the vertical direction for storing cassettes with steel bars. At the beginning of the SR is a buffer position, where cassettes with steel bars are delivered by the roller conveyor. Delivered cassettes with steel bars wait for an S/R machine to be transferred in the SR. The S/R machine is an automatic vehicle on rails and has its own drive for the horizontal movement. The S/R machine operates on a single command (SC) and on a double command (DC) sequence, as well ([5] – [11]).

The storage and retrieval sequencing take place is based on the following transactions:

Storage Transaction

- The S/R machine starts from the ground floor, i.e., the first tier of the SR.
- The S/R machine picks up the cassette with steel bars and moves to the designated location in the SR.
- When the S/R machine reaches its destination in the SR, it releases the cassette with steel bars in the storage location.
- The SR machine travels simultaneously with a hoisted carriage in the horizontal direction (x) and the vertical direction (y).

Retrieval Transaction

- The S/R machine moves to the retrieval location to pick-up the cassette with steel bars and then travels to the ground floor.
- The S/R machine releases the cassette with steel bars in the buffer position.
- The SR machine travels simultaneously with a hoisted carriage in the horizontal direction (x) and the vertical direction (y).

The assumptions that were used in the AS/RS modelling are summarized as follows ([5] – [11]):

- The AS/RS is divided into SR on both sides (left and right), therefore cassette with steel bars can be stored at either side in i^{th} storage location of the SR.
- The I/O location of the SR is located at the first tier of the SR.
- The SR is divided by columns and tiers.
- The S/R machine works on a Single Command (SC) and on Double Command (DC) modes.
- The sequences of (i) Acceleration, constant velocity and deceleration has been used.
- The drive characteristics of the S/R machine, as well as the height H_{SR} and the length L_{SR} of the SR, are known in advance.
- The height H_{SR} of the SR is large enough for the S/R machine to reach its maximum velocity v_{max} in the vertical direction.
- The length L_{SR} of the SR is large enough for the S/R machine to reach its maximum velocity v_{max} in the horizontal direction.
- A randomized assignment policy is considered, which means that any storage location is equally likely to be selected for storage or retrieval location to be processed.

3. DESIGN OF AS/RS FOR LONG AND HEAVY LOAD STEEL BARS

The model for designing the AS/RS for long and heavy load steel bars (Figure 3), is based on the structured approach where all the parameters influencing the warehouse volume Q (SR rack capacity) and the throughput capacity Pf have to be taken into account.

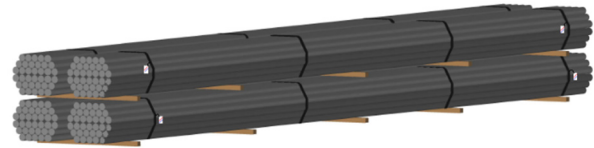


Figure 3. Sets of steel bars

3.1 Transport unit load

Includes the design of the steel cassette along with steel bars (Figure 4), which forms the basic transport unit load (TUL).

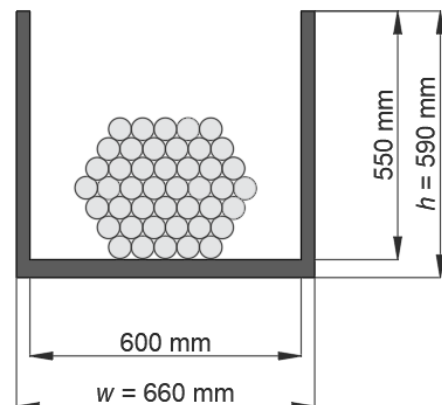


Figure 4. Transport unit load

3.2 Storage compartment

On the basis of the basic transport unit load, the storage compartment (Figure 4), which forms the basis for setting up the SR, is determined.

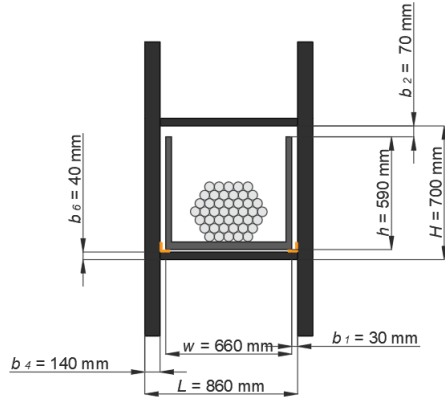


Figure 5. Storage compartment

3.3 Storage rack

When designing the SR structure, upright frames and rack beams, has to be selected. The type of SR structure (Figure 6) is selected in accordance with the weight of the cassette with steel bars and their arrangement in the horizontal (x) and vertical (y) directions. On the basis of the required warehouse volume Q , the geometry of the warehouse and the form of SR, have been determined.

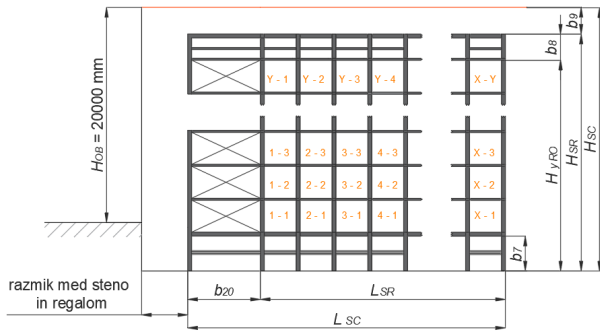


Figure 6. Storage rack structure

3.4 Layout of the storage rack

Based on the design of the basic transport unit load, storage compartment and the SR, the layout of the AS/RS for 6 meters and 10 meters cassettes is presented on Figures 7 and 8.

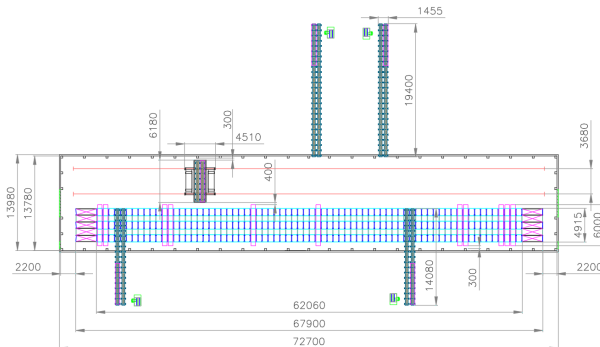


Figure 7. Layout of the storage rack 1 – 6 meters cassettes

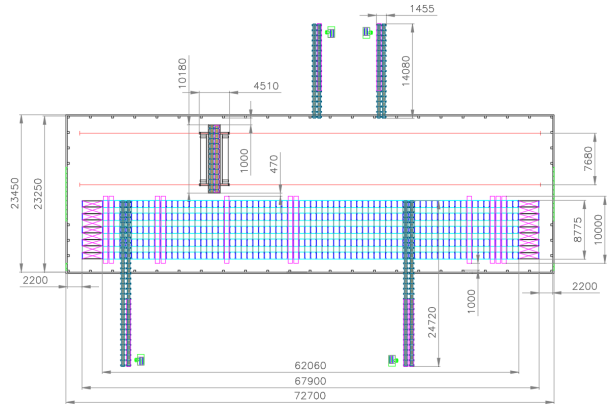


Figure 8. Layout of the storage rack 2 – 10 meters cassettes

4. THROUGHPUT PERFORMANCE CALCULATION

Throughput performance of the AS/RS is inversely dependant from the cycle time of the S/R machine. Cycle time of the S/R machine is based on the analytical travel-time model from Gudehus [12], which is based on the assumption on a non-constant velocity time distribution and the probability theory.

4.1 Shape factor

The shape factor (w) depends on the geometry of the SR along with the kinematic property of the S/R machine and is calculated by (1):

$$w = \frac{H_{SR}}{L_{SR}} \cdot \frac{v_x}{v_y} \quad w \leq 1, w > 1 \quad (1)$$

4.2 Single and double command cycle

The average single command cycle time $T(SC)$ of the S/R machine is calculated by (2) [12]:

$$T(SC) = \left(2 \cdot t_{p/s} + \left(\frac{v_x}{a_x} + \frac{v_y}{a_y} \right) + \frac{4}{3} \cdot \frac{L_{SR}}{v_x} \right) \cdot w \quad (2)$$

The average double command cycle time $T(DC)$ of the S/R machine is calculated by (3) [12]:

$$T(DC) = \left(4 \cdot t_{p/s} + \frac{3}{2} \cdot \left(\frac{v_x}{a_x} + \frac{v_y}{a_y} \right) + \frac{4}{3} \cdot \frac{L_{SR}}{v_x} \right) \cdot w + \frac{14}{30} \cdot \frac{L_{SR}}{v_x} \quad (3)$$

4.3 Performance measure

By considering (2) and (3) the throughput performance Pf of the AS/RS for long and heavy load steel bars is calculated by (4) [9]:

$$Pf = \frac{2 \cdot T}{r \cdot T(DC) + 2 \cdot (1 - r) \cdot T(SC) + 2 \cdot t_{p/s}} \cdot \eta \quad (4)$$

5. OPTIMIZATION OF AS/RS FOR LONG AND HEAVY LOAD STEEL BARS

For the optimization of decision variables of AS/RS for long and heavy load steel bars, we have used the open source software called OptiMax. OptiMax is an optimization package with graphical user interface for Windows platform. OptiMax enables single and multi-objective optimization, enables design of experiments (DOE), runs different applications as components including console application, enables recording of workflow data and files, supports scalars and arrays, supports simple mathematical expressions between scalars and arrays, save and open projects (source: <http://lace.fs.uni mb.si/wordpress/borovinsek>).

OptiMax is a tool that analyses the relation between constant, input and output variables in order to identify the significant factors affecting the output.

For the input variables, the following variables were used: velocity, acceleration/deceleration, ratio between SC and DC.

For the constant variables, the following variables were used: length and height of the SR.

For the output variables (performance measures), the following variables were used: cycle time and throughput capacity of the AS/RS.

In our model, the GA randomly creates the required number of subjects in a generation called organism. The subject refers to the AS/RS, whereas genes in the organism are demonstrated by the input variables. Based on the max. performance and project constraints, the GA evaluates each subject in the generation and arranges them with regard to their evaluation - the max. performance. The rest of the generations in the GA (e.g. 95%) are created by crossover, reproduction and mutation. The optimization process of GA and the meaning of individual genetic and evolutionary operators are presented in detail in [13] and [15].

OptiMax optimization package with graphical user interface for Windows platform looks as follows (Figure 9).

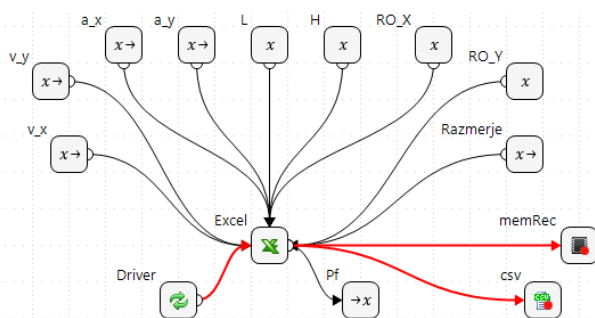


Figure 9. Design of Experiments with OptiMax [source: <http://lace.fs.uni mb.si/wordpress/borovinsek>]

5.1 Case study

In the present section a case study by using OptiMax with GA analysis, will be presented and discussed. The case study is based on a SC and DC sequence.

Table 1. Levels of (input and constant) variables

Factors	Codes	Levels
Height of the SR	Low level	$H_{SR} = 4 \text{ m}$
	High level	$H_{SR} = 26 \text{ m}$
Warehouse volume	Low level	500 cassettes
	High level	8000 cassettes
Horizontal velocity	Low level	$v_x = 1.33 \text{ m/s}$
	High level	$v_x = 2 \text{ m/s}$
Horizontal acceleration	Low level	$a_x = 0.5 \text{ m/s}^2$
	High level	$a_x = 1.5 \text{ m/s}^2$
Vertical velocity	Low level	$v_y = 0.4 \text{ m/s}$
	High level	$v_y = 1.17 \text{ m/s}$
Vertical acceleration	Low level	$a_y = 0.6 \text{ m/s}^2$
	High level	$a_y = 1.8 \text{ m/s}^2$

In continuation, some print screens from our knowledge-based engineering tool will be provided on Figures 10, 11, 12 and 13.

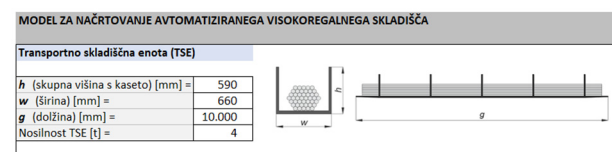


Figure 10. Definition of a transport unit load

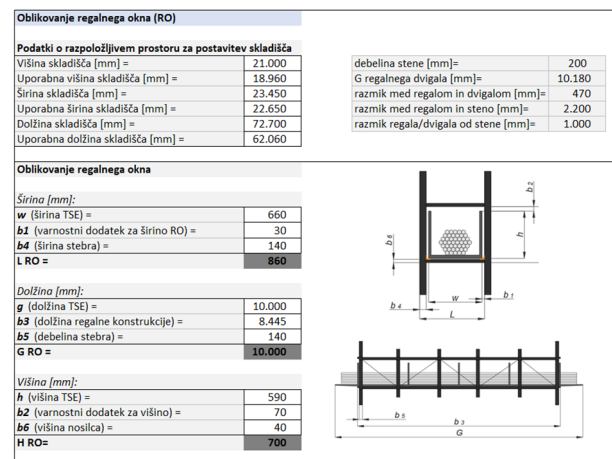


Figure 11. Definition of a storage compartment

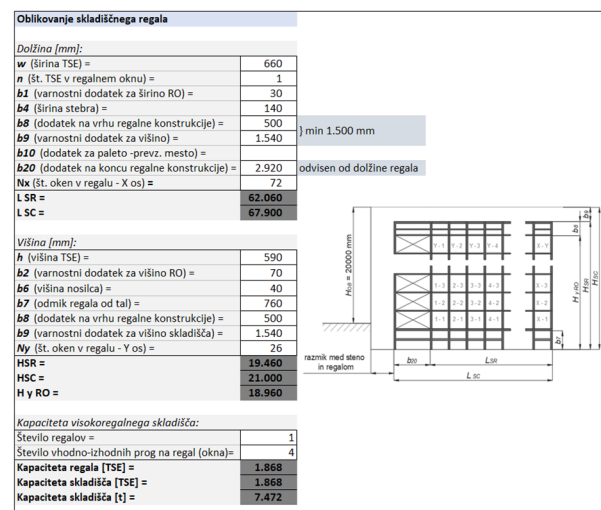


Figure 12. Definition of a storage rack

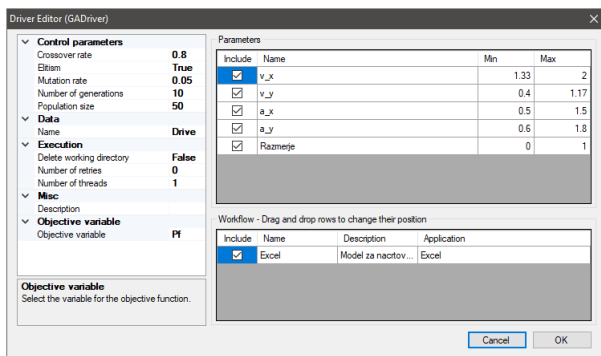


Figure 13. Definition of set of data for GA

Table 2. AS/RS scenarios

ID	v_x	v_y	a_x	a_y	Ratio	Pf
38	1.44	1.12	0.80	0.89	0.89	816.50
2	1.38	1.13	1.19	1.01	0.77	814.41
13	1.49	1.16	0.90	1.76	0.68	802.65
29	1.41	0.98	1.11	0.90	0.99	770.82
17	1.56	1.16	1.26	0.72	0.54	764.81
6	1.33	1.09	1.28	1.71	0.96	841.13
17	1.51	1.05	1.50	1.24	0.91	784.36
62	1.51	1.03	0.75	1.42	0.87	759.25
40	1.96	1.15	0.66	1.24	0.84	751.13
46	1.51	1.05	1.00	1.06	0.74	747.68
16	1.34	1.13	1.44	0.99	0.79	825.30
47	1.76	1.12	1.06	0.99	0.97	792.43
32	1.56	1.10	1.28	1.58	0.79	785.19
66	1.61	1.04	1.27	1.46	0.98	773.78
23	1.44	1.16	1.14	1.56	0.41	766.58
33	1.47	1.16	1.46	1.28	0.96	856.69
40	1.35	1.16	1.44	1.65	0.74	834.41
42	1.43	1.12	1.46	0.61	0.83	808.59
46	1.55	1.16	1.20	1.62	0.68	795.95
92	1.46	1.09	0.93	1.07	0.73	777.19
31	1.39	1.17	1.33	1.48	0.85	851.66
20	1.34	1.09	0.86	0.99	0.90	821.79
33	1.66	1.13	0.86	1.76	0.94	807.60
10	1.86	1.14	0.79	1.09	0.88	768.15
62	1.61	1.08	1.05	1.41	0.78	763.01

Five (5) successive simulations with results according to velocity profile of the S/R machine and the hoisted carriage are presented in Table 2. The warehouse volume Q is constant, since the length (L_{SR}) and the height (H_{SR}) of the SR are known in advance.

According to results in Table 2, the AS/RS performs well in the case of relatively large ratio between SC and DC cycles ($\gg r$). The highest throughput performance of

the AS/RS would be between 816 and 856 cassettes with steel bars per shift.

The proposed model proves to be useful when designing AS/RS for long and heavy load steel bars and could help the warehouse designer to analyse the efficiency of SR layout along with the kinematic properties of the S/R machine in the early stage of project.

6. CONCLUSION

In this paper, a design model of the ASRS for long and heavy load steel bars is presented. Due to the high complexity of the warehouse, the conventional design process rises to higher and more demanding levels, in the form of the computer aided design and optimization of warehousing systems. The presented design model is based on the structured approach and refers to the ASRS for long and heavy load steel bars. Due to requirements for the most economical design and at the same time technically highly efficient warehouse, the objective function maximum Pf has been formed.

The objective function is represented by a mathematical model, which includes the decision variables (velocity, acceleration/deceleration, ratio between SC and DC) along with all the relevant operational and physical parameters. Due to the non-linearity of the maximum Pf , discrete shape of the objective function and proposed decision variables, the method of genetics algorithms (GA) has been applied in our analysis. On the basis of the results of the optimization of the decision variables in the maximum Pf , the AS/RS performs well in the case of relatively large ratio between SC and DC cycles ($\gg r$). The highest throughput performance of the AS/RS would be between 816 and 856 cassettes with steel bars per shift.

This study can be extended with (i) Different velocity and acceleration/deceleration scenarios for the S/R machine, (ii) Different layout configurations of AS/RS, (iii) Application of the environment aspects like energy consumption and CO₂ emissions may also be considered in the analysis.

7. ACKNOWLEDGEMENT

This work was supported by Slovenian Research Agency (ARRS) [Methodology for Building an Integral Model of Transport-Warehouse Processes to Enhance Intralogistics System Efficiency; grant number: L5-8237].

REFERENCES

- [1] Kim, K.H. and Hong, G.P.: A heuristic rule for relocating blocks, Computers & Operation Research, Vol. 33, No. 4, pp. 940-954, 2006.
- [2] Tang, L.X., Liu, J., Rong, A. and Yang, Z.H.: Modelling and a genetic algorithm solution for the slab stack shuffling problem when implementing steel rolling schedules, International Journal of Production Research, Vol. 40, No. 7, pp. 1583-1595, 2002.
- [3] Tang, L., Zhao, R. and Liu J.: Models and algorithms for shuffling problems in steel plants,

- Naval Research Logistics, Vol. 59, No. 7, pp. 502-524, 2012.
- [4] Scheid W.M.: 40 Jahre Hochregallager - ein vergessener Geburtstag, Förderung und Heben - Marktbild Lager, pp. 10-13, 2002.
- [5] Lerher, T., Šraml, M., Potrč, I. and Tollazzi, T.: Travel time models for double-deep automated storage and retrieval systems, International Journal of Production Research, Vol. 48, No. 11, pp. 3151-3172, 2010.
- [6] Hausman, H. W., Schwarz, B. L. and Graves, C. S.: Optimal storage assignment in automatic warehousing system, Management Science, Vol. 22, No. 6, pp. 629-638, 1976.
- [7] Graves, C. S., Hausman, H. W., Schwarz, B. L.: Storage retrieval interleaving in automatic warehousing system, Management Science, Vol. 23, No. 9, pp. 935-945, 1976.
- [8] Bozer, A. Y., White, A. J.: Travel-time models for automated storage and retrieval systems, IIE Transactions, Vol. 16, No. 4, pp. 329-338, 1984.
- [9] Hwang, H. and Lee, S.B.: Travel time models considering the operating characteristics of the storage and retrieval machine, International Journal Production Research, Vol. 28, No. 10, pp. 1779-1789, 1990.
- [10] Lerher, T.: *Model for designing automated storage and retrieval systems*, PhD dissertation, Faculty of Mechanical Engineering, University of Maribor, 2005.
- [11] Lerher T. and Potrč I.: The Design and Optimization of Automated Storage and Retrieval Systems, Strojniški vestnik, Journal of Mechanical Engineering, Vol. 52, No. 5, pp 268-291, 2006.
- [12] Gudehus, T.: *Principles of order picking: Operations in distribution and warehousing systems*, Essen, Germany: W. Girardet Verlag, 1973.
- [13] Diao, X., Li, H., Zeng, S., WY Tam, V. and Guo, H.: A Pareto multi-objective optimization approach for solving time-cost-quality tradeoff problems, Technological and Economic Development of Economy, Vol. 17, No. 1, pp. 22-41, 2011.
- [14] Lerher T., Borovinšek, M. and Šraml, M.: A multi objective model for optimization of automated warehouses. Logistics: perspectives, approaches and challenges, Nova Publishers, Inc., New York, pp. 87-110, 2013.
- [15] Bekker, J.: Multi-objective Buffer Space Allocation with Cross-entropy Method, International Journal of Simulation Modelling, Vol. 12, No. 1, pp. 50-61, 2013.

Simulation analysis and performance measurement of a heavy load transport vehicle in a steel plant company

Tone Lerher

Professor
University of Maribor
Faculty of Logistics
Celje, Slovenia

Jakob Marolt

Research assistant
University of Maribor
Faculty of Logistics
Celje, Slovenia

Bojan Rupnik

Research assistant
University of Maribor
Faculty of Logistics
Celje, Slovenia

Matjaž Štor

Logistic Manager
Štore Steel d.o.o.
Štore, Slovenia

Miha Kovačič

Technical Development Manager
Štore Steel d.o.o.
Štore, Slovenia

In this paper simulation analysis and performance measurement of a heavy load transport vehicle in a steel production company are presented. A steel production company produces two main products, known as rolled round steel bars and flat steel bars. One of the most important material handling devices in their facility are overhead (bridge) cranes, which are used for handling material and are often very highly utilized. Due to increasing trend of production capacities in the following years different means of transporting of material (steel bars) from the production site to the product warehouse is needed.

For this reason, a heavy load transporter with a special cassette for carrying 50 tons of materials (steel bars) in one ride will be used. In order to test the utilization and system performance of a heavy load transporter discrete event simulation has been applied. The logistics (i.e. availability of the crane for loading and unloading the vehicle, transport between production site and the product warehouse) and technological process (throughput performance of the production plant) were analysed. Location of workstations and workplaces as well as loading/unloading places for the transporter was defined by the layout. From the layout, distances between workstations, equipment, buffers and the warehouse can be defined, as well. For the simulation analysis of a heavy load transport vehicle the following methods have been used: observation, measurements, non-structured interviews (to obtain data from practice), modelling, optimization, statistical analysis, etc.

Keywords: *Material Handling Systems, Heavy Machinery, Internal Transport, Discrete Event Simulation, Performance Analysis.*

1. INTRODUCTION

In a steel plant company, a vast variety of different steel bars can be manufactured by changing the shape and dimensions of a profile, increasing or decreasing the length of the bars, and by altering the chemical compound of the steel.

However, two profile shapes of steel bars are being mainly produced: circular (rolled round steel bars) and rectangular (flat steel bars). Each profile type demands different production technology and consequently different machinery.

Steel bars with rectangular shape flows through production towards the product warehouse. Steel bars with circular shape flows away from the product warehouse, because the layout configuration of the machinery for this shape cannot be placed parallel to the machinery of a rectangular shape.

The company is therefore forced to transport the circular shape steel bars from point A to point B (Figure 1).

Currently this task is being solved with a combination of overhead (bridge) cranes and tractors with small load capacity. Overhead cranes are primarily meant for handling material for the needs of production and are often very highly utilized.

The company decided to look for a new solution, to solve the transportation of heavy material, from the end of the production line of a circular shape steel bars to the final warehouse.

They decided to invest into a heavy transport vehicle (Figure 2), with a larger capacity of 50 tons, that will replace the current means of transport and to ease the usage of overhead cranes. The problem this paper analyses is the transport of a heavy load vehicle that conveys circular shape steel bars with the usage of special cassettes. The circular shape profile production workers load the finished steel bars bundles into an empty cassette at the point A. The vehicle operator then loads a full cassette onto the vehicle, without the need of an overhead crane, and drives them to the point B. When the driver arrives to the point B with a full cassette, the driver must also empty the sets of steel bars from the cassette. The operator cannot empty the bundles of steel bars, if an overhead crane is being utilized by the rectangular shape profile production workers. Therefore, the operator has two options. He can unload a full cassette into a buffer at point B, if there are any empty slots, or he can wait for the overhead crane to become available.

Correspondence to: Dr. Tone Lerher
University of Maribor, Faculty of Logistics
Mariborska c. 7, 3000 Celje, Slovenia
E-mail: tone.lerher@um.si

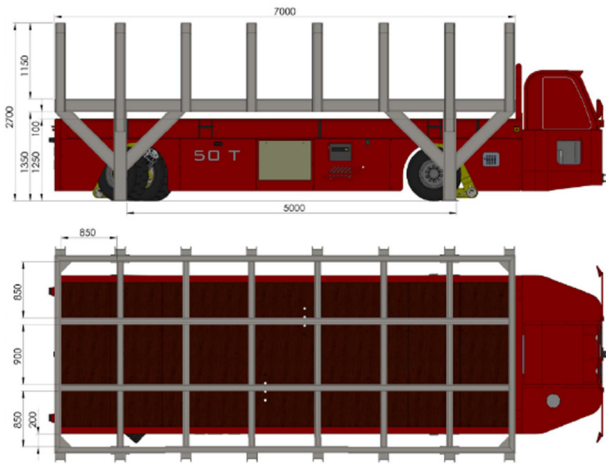


Figure 1. Heavy load transport vehicle with an empty cassette

The goal of this paper is to present all possible decisions an operator can make and to present a model for overhead crane utilization. Furthermore, we tested different waiting times of the operator using discrete event simulation, to present, what are the best decisions of the operator to either maximize the throughput performance or to minimize the number of trips ([1] – [7]).

2. METHODOLOGY AND GENERAL ASSUMPTIONS

To complete this research study, we must describe both aspects that intertwine in our discrete event simulation. First, the choices of the operator in a form of deterministic process flow diagram decisions and second, the stochastic behaviour of an overhead crane utilization. In the proposed model the assumption is made, that the occupation distribution of the crane utilization by production is normal.

In this study the following parameters were considered: occupation of an overhead crane by production workers, number of times an overhead crane is available and different waiting times of an operator upon arrival with the vehicle from point A to point B. The simulation results are given by the throughput performance and number of trips of the heavy load vehicle [3], [5], [6].

2.1 Process flow diagram of a heavy load vehicle

The following subsection explains the interactions on Figure 3. Based upon this process flow algorithm, the discrete event simulation has been developed [1], [2], [4], [7].

The operator starts in a point A, where the operator has to load a full cassette of steel bars onto the heavy load vehicle. If there is no full cassette, the operator must wait until a full cassette appears. Then the operator moves to point B and checks, if an overhead crane is available. If the crane is available, the operator first empties the material (sets of steel bars) from the loaded cassette. If the production worker does not require the overhead crane the operator can continue to unload sets of steel bars from any other full cassette in the buffer. Once the operator either emptied all the cassettes in point B or had

to stop, because of the production needs, the operator drives an empty cassette back to point A where the process from the start is repeated.

Upon arrival to point B, there is another possibility, that the overhead crane is not available. The operator now has to wait for some time with the maximum waiting time being T_w . While the operator waits, he constantly checks if the overhead crane becomes available. If the crane becomes available, the operator continues the process previously described. If the crane does not become available, the operator checks if there are any empty slots in the buffer. If there are no empty slots in the buffer, the operator waits until the crane becomes available again. Otherwise, if there is a free slot in the buffer, the operator has to unload the full cassette to a free slot. Afterwards, the operator must check, if there are any empty cassettes in the buffer. If there are none, the operator drives back to point A without any cassette. Otherwise the operator loads the empty cassette and returns to point A, where he has to unload an empty cassette and repeat the process from the start.

2.2 Overhead crane utilization model

The overhead crane is primarily used for the material handling needs of the production. When the crane becomes available the operator of a heavy load vehicle can utilize it to either unload sets of steel bars from a full loaded cassette or from one of the full cassettes waiting in the buffer.

If the production needs the crane, while the operator is unloading sets of steel bars, they let him finish the current task and then the operator has to return the crane controller to production workers upon completion.

To simulate the crane utilization, we used the model based upon Gaussian normal distribution [3], [4]. Parameters symbols and their clarification are summed in Table 1.

Table 1. Parameters and their description

Parameter	Description
D	Number of downtimes
O	Occupancy of an overhead crane
r	Randomness factor
T	Time of observation
i	Phase
t_{d-min}	Minimum time of downtime
t_{u-min}	Minimum time of up state
Δt_d	Length of downtime
Δt_u	Length of uptime
t_i	Time of an up/downtime in phase i
μ_d	Average time of downtime
μ_u	Average time of uptime
σ_d	Standard deviation of downtime
σ_u	Standard deviation of uptime

The length of the observation example has to be selected. This can either be one shift, two shifts, a complete day or some longer period. If the time of the observation is divided with the number of a crane downtimes and multiplied with an average occupancy of a crane, an average time of downtime can be calculated (time period when an overhead crane is not available).

With a similar process an average time of uptimes can be calculated (overhead crane is available).

$$\mu_d = \frac{T}{D} \cdot (1 - O) \quad (1)$$

$$\mu_u = \frac{T}{D} \cdot O \quad (2)$$

The Gaussian normal distribution model also requires a standard deviation. To calculate a standard deviation of up and downtime, an average time of each state has to be multiplied by the randomness factor r . The larger r is, more sporadic the length of time phases become.

$$\sigma_d = r \cdot \mu_d \quad (3)$$

$$\sigma_u = r \cdot \mu_u \quad (4)$$

With both, the average time of up and downtime and standard deviation of up and downtime, the length of each phase can be determined as:

$$\Delta t_d = \text{Gauss}(\mu_d, \sigma_d) \quad (5)$$

$$\Delta t_u = \text{Gauss}(\mu_u, \sigma_u) \quad (6)$$

To generate data for the whole period of observation T , every next phase is calculated by adding time of current phase t_i to a previous phase t_{i-1} .

$$t_i = t_{i-1} + \Delta t_d \quad (7)$$

$$\forall i \in \{2, 4, 6 \dots (2 \cdot D)\}$$

$$\forall \Delta t_d > t_{d-\min}$$

$$t_i = t_{i-1} + \Delta t_u \quad (8)$$

$$\forall i \in \{1, 3, 5 \dots (2 \cdot D - 1)\}$$

$$\forall \Delta t_u > t_{u-\min}$$

Because of the normal distribution, the last time phase can either be over or under our time period T . That is why we have to normalize the times by:

$$t_i = \frac{t_i \cdot T}{t_{(2 \cdot D)}} \quad (9)$$

$$\forall i \in \mathbb{N}$$

$$i < (2 \cdot D)$$

The result of this approach is a dataset of time phases that simulate the occupation and availability of the overhead crane (Figure 4).

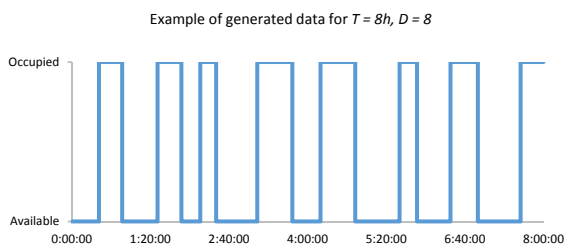


Figure 2. Example of dataset for one shift

3. CASE STUDY

The proposed model was tested with data from the steel plant company. With some help of the factory workers, we were able to estimate the unloading time of a full cassette, which was set to the mean of 30 minutes, and standard deviation of 5 minutes.

Also, the transport time from point A to point B was approximated with the known distance and speed of a heavy load vehicle. Transport time from point A to point B was therefore set to 6 minutes and standard deviation of 1 minute. There was always a full cassette in point A, ready to be taken and transported to point B. In this way we could also compare the throughput at maximum load. At point B there are three available slots in the buffer area for storing the cassettes. Each observation example was set to one (1) day, which corresponds to three (3) shifts.

Simulations were made on two different levels of overhead crane occupation (70% and 80%) and three different levels of down times state (20, 25 and 30). Waiting times varied from one (1) min to fifteen (15) min. In Tables 2 and 3 the simulation results are presented of two different overhead crane occupation levels and three different downtimes number.

The simulation results are given by the average number of emptied cassettes and the number of required trips after 10,000 iterations.

Table 2. Results of the simulation study with overhead crane occupancy set to 70%

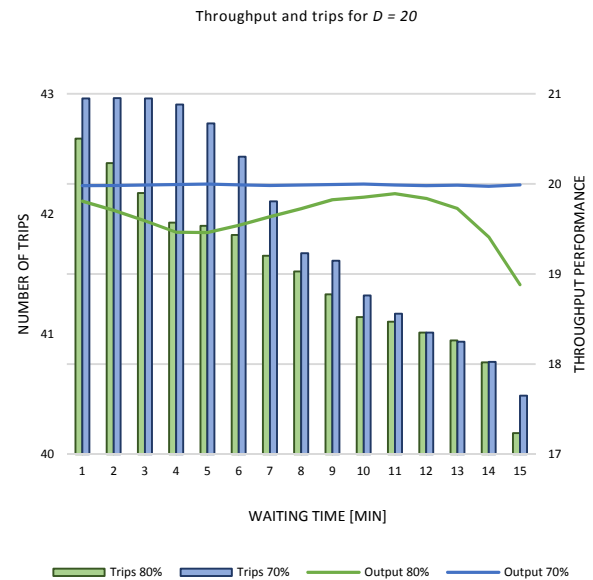
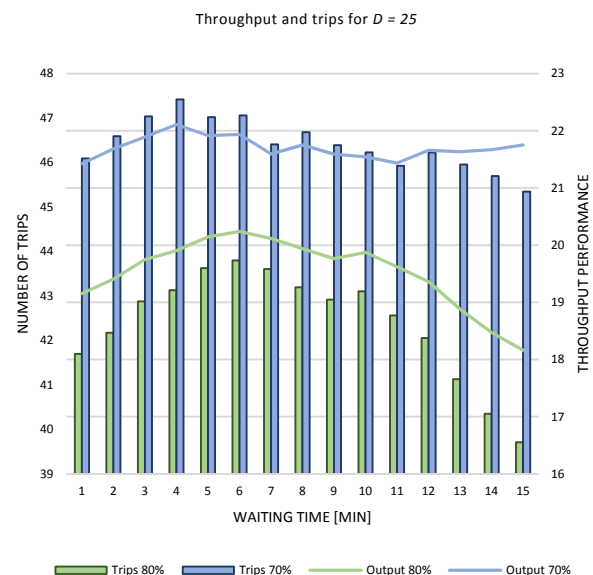
	$D = 20$		$D = 25$		$D = 30$	
T_w [min]	Through- put	Trips	Through- put	Trips	Through- put	Trips
1	19.98	42.96	21.42	46.09	17.70	39.05
2	19.98	42.96	21.68	46.59	17.63	38.92
3	19.99	42.96	21.89	47.04	17.53	38.67
4	19.99	42.91	22.109	47.42	17.38	38.42
5	20.00	42.75	21.92	47.02	17.27	38.18
6	19.99	42.48	21.94	47.06	17.16	38.04
7	19.98	42.11	21.59	46.41	17.24	38.06
8	19.99	41.67	21.75	46.68	17.21	37.99
9	19.99	41.61	21.59	46.39	17.12	37.84
10	20.00	41.32	21.54	46.23	16.89	37.46
11	19.99	41.17	21.44	45.93	16.82	37.14
12	19.98	41.01	21.66	46.23	16.76	36.97
13	19.99	40.94	21.63	45.96	16.92	36.75
14	19.97	40.77	21.67	45.69	16.98	36.16
15	19.99	40.49	21.75	45.35	17.08	35.89

Table 3. Results of the simulation study with overhead crane occupancy set to 80%

	$D = 20$		$D = 25$		$D = 30$	
T_w [min]	Throughput	Trips	Throughput	Trips	Throughput	Trips
1	19.81	42.63	19.15	41.70	16.11	35.86
2	19.71	42.42	19.40	42.17	16.13	35.88
3	19.59	42.17	19.75	42.88	16.05	35.72
4	19.46	41.93	19.90	43.13	16.01	35.67
5	19.46	41.90	20.15	43.63	15.85	35.29
6	19.54	41.83	20.24	43.80	15.82	35.25
7	19.64	41.65	20.12	43.61	15.66	34.91
8	19.72	41.52	19.94	43.20	15.39	34.95
9	19.82	41.33	19.76	42.92	15.33	34.35
10	19.85	41.14	19.87	43.10	15.41	34.41
11	19.89	41.10	19.62	42.56	15.27	34.18
12	19.84	41.01	19.36	42.06	14.80	33.23
13	19.73	40.95	18.88	41.13	14.52	32.71
14	19.41	40.76	18.47	40.35	14.22	32.15
15	18.88	40.18	18.16	39.71	13.86	31.46

On the following graph (Figure 5) simulation results of our study case with 20 downtimes are presented. With an overhead crane occupation of 70%, the throughput performance is independent on different waiting times. If this was the case the operator should wait at point B full 15 minutes to reduce the number of trips as much as possible. With an overhead crane occupation of 80%, the throughput differs slightly at different waiting times, and starts declining after 13 minutes. In this case the operator should not wait more than 13 min on each trip, because the overall number of trips is lowest with the same throughput.

The results of 25 downtimes are presented on Figure 6. With an overhead crane occupation set to 70% the throughput performance varies from approximate 21.5 cassettes to 22.1 cassettes. The maximum is reached at $T_w = 4$ minutes. To minimize the required number of trips the operator should wait full 15 minutes. With an overhead crane occupation set to 80%, there is a reduction in the throughput performance compared to 70% occupation. The maximum is reached at $T_w = 6$ minutes. The lowest number of trips from point A to point B is at the waiting time of 15 minutes, but consequently the throughput performance is also decreased.

**Figure 3. Graph displaying number of trips and throughput performance for the case with 20 downtimes****Figure 4. Graph displaying number of trips and throughput performance for the case with 25 downtimes**

The results of 30 downtimes are given on Figure 7. The maximum throughput performance for both 70% and 80% occupation level appear at waiting time $T_w = 1$ min. Once again, the difference in throughput between 70% and 80% is quite expressive. With the increase of the waiting time the number of trips decreases. There is an interesting point at 70% occupation level and 15 min of waiting time, where the number of required trips still decreases, compared to 14 minutes of waiting time, but the throughput increases.

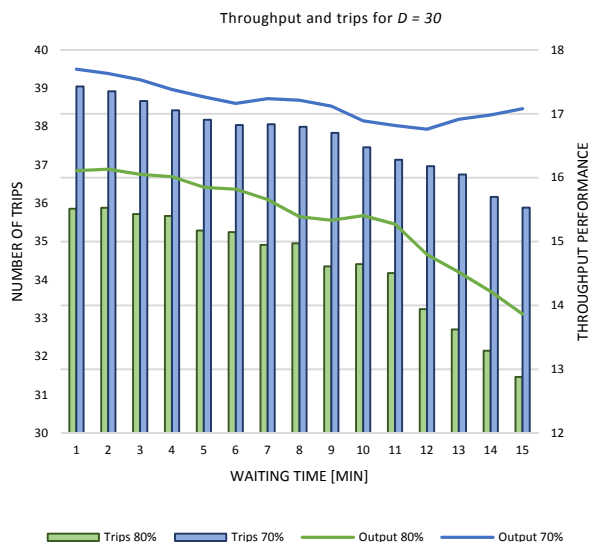


Figure 5. Graph displaying number of trips and throughput performance for the case with 30 downtimes

The simulation results can also be observed from another perspective. If we know the demanded throughput performance of cassettes from point A to point B, we can set some rules how the crane utilization should be set. In this way the objective function of the heavy transport vehicle could just be the minimization of required trips. With the reduction of one (1) trip per day we can yearly save approximately 130 km of a heavy transport vehicle travel distance.

4. CONCLUSION

In this paper a throughput performance analysis of a heavy load vehicle transport has been analysed. All possible decisions of the vehicle operator were showed with a process flow diagram. Upon arrival of the heavy load vehicle to the product warehouse an overhead crane, that is primarily utilized by the production workers, is required to empty the sets of steel bars from the cassette.

A proposed model of crane utilization was based upon Gaussian normal distribution. With an operator of a heavy load vehicle aspect and overhead crane utilization model, a discrete event simulation was applied.

In our study case, the following parameters were considered: occupancy needs of an overhead crane by production workers, number of times an overhead crane is available in a period T and different waiting times of the operator upon arrival to product warehouse (point B).

The simulation results considered both the maximization of the throughput performance and minimization of required trips of a heavy load vehicle.

ACKNOWLEDGEMENT

This work was supported by Slovenian Research Agency (ARRS) [Methodology for Building an Integral Model of Transport-Warehouse Processes to Enhance Intralogistics System Efficiency; grant number: L5-8237].

REFERENCES

- [1] Gudehus, T.: *Principles of order picking: Operations in distribution and warehousing systems*, Essen, Germany: W. Girardet Verlag 1973.
- [2] Bartholdi, J.J., Hackman, S.T.: *Warehouse and distribution science*, USA: Georgia Institute of Technology, <http://www.warehouse-science.com/>, accessed 22.04.2019.
- [3] Zrnić, Đ., Savić, D.: *Simulation of processes in material handling (Simulacija procesa unutrašnjeg transporta)*, Faculty of Mechanical engineering, University of Belgrade, Belgrade, 1987, ISBN: 86-7083-166-X.
- [4] Banks, Y., Carson, S.J.: *Discrete-Event System Simulations*, Georgia Institute of Technology, 1984.
- [5] Dieter, A.: *Materialflusslehre-Grundlagen der Fördertechnik, Transport und Logistik*, Karlsruhe, 1995.
- [6] Heinrich, M.: *Transport- und Lagerlogistik: Systematik, Planung, Einsatz und Wirtschaftlichkeit*, Springer Vieweg, 2016.
- [7] Kay, M.: *Production system design*. Department of Industrial and Systems Engineering, North Carolina State University, USA, 2016.

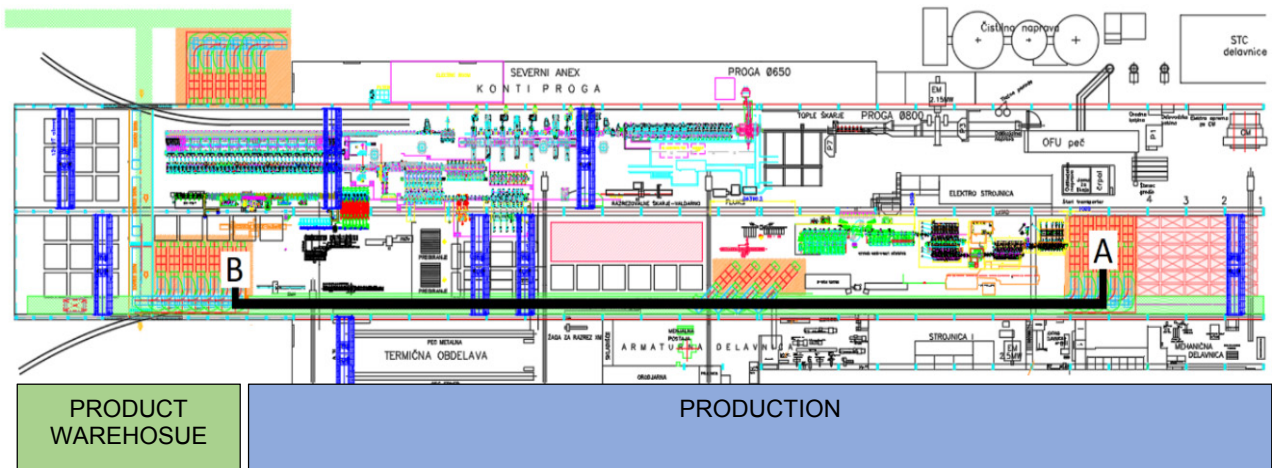


Figure 6. Layout of steel plant company

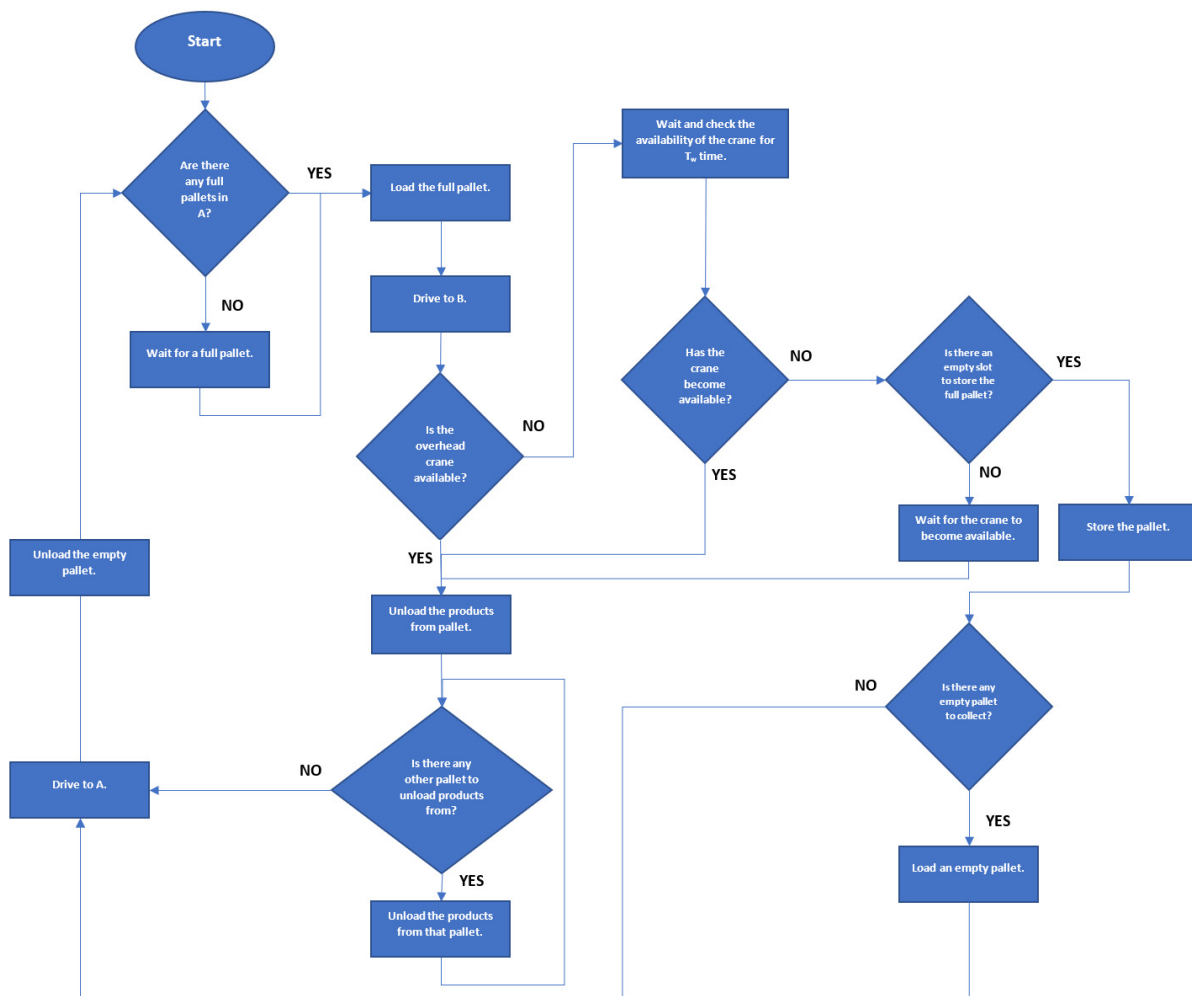


Figure 7. Process flow diagram of all possible decisions a heavy load vehicle operator must make

Etsuko Nishimura

Associate Professor
Kobe University
Graduate School of Maritime Sciences

Aomi Kutsuna

Undergraduate Student
Kobe University
Faculty of Maritime Sciences

Zhujun Wei

Graduate Student
Kobe University
Graduate School of Maritime Sciences

A heuristic approach for operating the marine container drayage using dummy node concept

From the point of view about giving consideration to the environment and performing logistics activities efficiently, this study proposes the mathematical model for operating marine container drayage. This study consider the tractor head assignment to trailers with full/empty container with considering the precedence constraints for visiting customers, in order to minimize CO₂ emissions. We propose the heuristic approach based on Ant Colony Optimization using a dummy node concept, in order to find feasible solutions. From the computational results, CO₂ emissions by the proposed approach are reduced 20 % from those of the conventional operation.

Keywords: Freight transportation, Container drayage, Global warming countermeasure, Ant colony optimization

1. INTRODUCTION

CO₂ occupies over 90% of artificially emitted the Greenhouse Gas (GHG). It has the most hazardous impact on the environment. CO₂ is mainly emitted by the factory, road traffic and thermal power plant and so on. As related in road traffic that we described above, we focus on inland transport of marine containers. In Japan, in the inbound operation, after the full container arrives at a specific consignee point, it is needed to the time spent for making an empty container, which can be supplied to a intermodal terminal after devanning operation. On the contrary, a shipper gets an empty container from the terminal, and the container is loaded for outbound trip. As well, it is needed that the time for vanning container and so on. Under such a situation, "Round use of containers" is promoted by Ministry of Economy, Trade and Industry in Japan as one of the projects. To be concrete, inbound or outbound full container transport is combined with empty container transport at the inland depot, and the objective is to reduce the through-put of empty containers in an internal area. We focus on a vehicle routing for container transport on this project, there are three conditions for containers: inbound trip, outbound trip and empty condition, and there are two situations for vehicles: trailer truck (with full or empty container loaded), empty truck (as tractor only). The change of situation at each one customer is dealt with two different points: (a) a delivery point and a point with an empty container supplied at a consignee, (b) a point with an empty container demanded and a pickup point at a shipper. On the conventional operation, a truck is assigned to points before and after the situation

change at one customer. On the proposed operation, one or more trucks can be assigned to points before and after the situation changes at one customer.

Therefore, in this study, we consider the vehicle routing problem taking container conditions and vehicle situations into account without the inland depot but with the precedence constraints between two situations at a customer. We propose the heuristic approach based on Ant Colony Optimization (ACO) in order to find feasible solution in this problem.

2. LITERATURE REVIEW

This problem is closely related to the vehicle routing problem (VRP) with back hauls, that finds an optimal set of paths visiting delivery points and pick-up points after leaving a particular depot in each route, any load is carried on the return trip after delivery operation. There are so many studies related VRP. Jula *et al.* [5] treat that the multi-traveling salesman problem with time windows for container's movement. In their study, a lot of container transports are performed by multiple trailers, each of undertakes a series of two types of container moves: one from an intermodal facility such as port, etc. to a customer and the other vice versa. As each delivery has a pickup interrelated, a pickup & delivery pair is regarded as a corresponding node. That study is similar to our study, in that each trailer has the time limit for working, and it must return to the depot as its time limit is not exceeded.

Imai *et al.* [4] consider the problem of vehicle routing that arises in pickup & delivery full container loaded from/to an intermodal terminal. As most shippers and consignees are located close to in a distribution area near a terminal in Japan, they assume that the requests to a container, such as the time of shipment and the container suitability to goods like type and size, are satisfied. The objective is, that an empty container move is reduced by a merged route consisted of both delivery and pickup trips. Then the related cost of the vehicle fleet is minimized. Their study consider the full/empty container transport, however, an empty truck travel is not

Correspondence to: Dr. Etsuko Nishimura, Associate Prof.
Graduate School of Maritime Sciences, Kobe University
5-1-1 Fukae-minami, Higashinada, Kobe 658-0022, JAPAN
E-mail: e-nisi@maritime.kobe-u.ac.jp

considered. And as they described, a trailer-truck consists of a tractor and a trailer, normally they can be uncoupled. In Japan, the shuttle service is operated between the intermodal terminal and customers once or twice a day. Thus a tractor uncouples a trailer as a chassis with a container on it, and it leaves it at a customer site, so that the truck can be assigned to the next shipment. Therefore, this study considers the tractor assignment to trailer with full and empty containers.

Cheung *et al.* [2] consider the cross-border drayage problem and show how the regulatory policy impacts the system. In Hong Kong, the container drayage has very low productivity in terms of drivers' time, trip time and tractor time. In a trip, a full container is taken in one direction, and the relevant container returns as an empty in another direction. Therefore they use the approach as a policy evaluator to quantify the benefit of relaxing the 1st policy which the driver, tractor, chassis and container have to be operated simultaneously, and the 2nd policy which a tractor can be operated by one particular driver only. It is shown that their proposed approach provides the good solutions.

Breakers *et al.* [1] study a full truckload vehicle routing for transporting loaded and empty containers in drayage operation. This study is so closely related to our study, which considers customer locations, including empty supply and demand locations. However, a full container pickup location as a shipper is not considered. That study considers that the empty containers can be stored at several vehicle depots. However, in Japan, those containers are stored at a container terminal. Thus in our study, the vehicle depot is the same as a relevant container terminal.

Nishimura *et al.* [6] proposed the mathematical model for marine container drayage. The change of situation at each one customer is dealt with two different points, such as (a) a delivery point and a point with an empty container supplied at a consignee, (b) a point with an empty container demanded and a pickup point at a shipper. It is given that the handling time between different points at one customer with considering the precedence constraints. From computational results in small size problem by CPLEX, it is clear that the CO₂ emissions reduction depends on handling time length. Comparing with the conventional operation, our proposed model can reduce CO₂ emissions.

Therefore, we assume that each truck can serve a single load at a time, and a driver can assign to customers in the network during a single working time limit. This study consider the location type and the expression of conventional operation by ACO as shown in Fig. 1. In the ACO based heuristic, dummy nodes located at the intermodal terminal, consignee or shipper are needed in order to find the feasible solution for large size problem in Nishimura *et al.* [6]. We address the tractor head assignment to trailers with full/empty container with considering the precedence constraints for visiting customers, in order to minimize CO₂ emissions.

3. PROBLEM DEFINITION AND FORMULATION

3.1 Problem definition

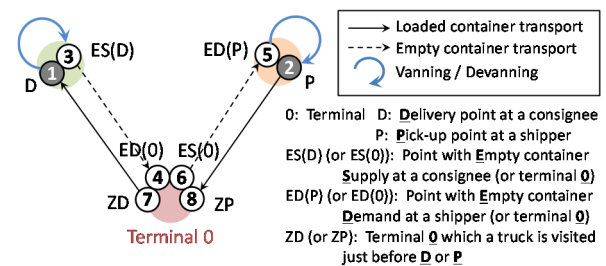


Figure 1. Conventional operation by ACO representation

This vehicle dispatch problem (VDP) is defined on a graph $G = (N, A)$ with N is a node set representing the marine terminal and customers, and A is the arc set. Fig. 2 shows the locations and routes for container transport in the target area as an example. We express the terminal as "0", the shippers where a full container is picked up as "P" and an empty container is demanded as "ED", the consignees where a full container is delivered as "D" and an empty container is supplied as "ES". Arrows between locations mean as follows. A black colored one means container transport, dotted one empty container transport, blue colored one means the time passed before and after vanning/devanning at a customer. One customer has two locations with different situations. Allow from D to ES means the time passed by an empty container can be supplied after devanning operation at a consignee. Allow from ED to P also means the time passed by an empty container can be demanded after vanning operation at a shipper. And grey arrow means empty truck (with trailer head only).

Fig. 2 (a) shows the conventional operation of the VDP is a shuttle trip between the depot and a customer site (shipper or consignee), whether containers transported are full or empty ones, called individuals trips. Fig. 2 (b) shows our proposed concept, on back-ward way, a truck does not always return to the origin point of the forward way. A truck does not always return to the origin point of the forward way. In other words, a truck transports an empty container to the other customer without visiting the terminal 0, or a trailer head is separated from a chassis, and then the trailer head goes to receive a container at another customer. The above flexible operation is supposed. Because there are different CO₂ volumes emitted by among a full container transport and empty container transport and empty truck movement, in order to get the total CO₂ emissions, which multiply each condition distance moved by CO₂ emission per its distance unit as weight. Then we will compare CO₂ emissions by the conventional operation with that by our proposed operation.

3.2 Problem formulation

It minimizes CO₂ emitted by truck travels for container transport as the objective function value. We assume that a kinds of truck is one, each customer is serviced by each one truck. Each truck has the working time limit, without considering the overtime work.

Parameters used in VDP are defined as follows:

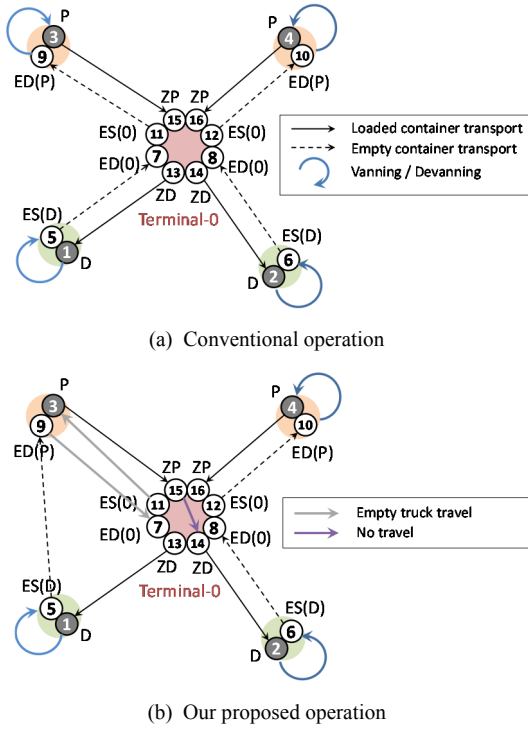


Figure 2. Concept of vehicle dispatch problem

$N (= N^D \cup N^P \cup N^{ES} \cup N^{ED} \cup \{0\})$ set of locations that consists of customers and terminal “0” ;
 $i, j (\in N)$ index of location number;
 $(i, j) (\in A)$ index of arc (A : set of arcs);
 $k (\in V)$ index of truck number (V : set of trucks);
 l loaded condition of the relevant truck (fc : a full container is loaded, ec : an empty container is loaded, et : empty truck);
 N^D set of locations where a full container is delivered;
 N^P set of locations where a full container is picked up;
 N^{ES} set of locations where an empty container is supplied;
 N^{ED} set of locations where an empty container is demanded;
 A^{fc} set of arcs that a full container is delivered;
 A^{ec} set of arcs that an empty container is delivered;
 $A^{et} (\in A \setminus \{A^{fc} \cup A^{ec}\})$ set of arcs that an empty truck is traveled;
 $CO2_l$ CO_2 emissions per one kilometre for traveling under loaded condition l of the relevant truck;
 $CE_{ij} = \begin{cases} CO2_{fc} & \forall (i, j) \in A^{fc} \\ CO2_{ec} & \forall (i, j) \in A^{ec} \\ CO2_{et} & \forall (i, j) \in A^{et} \end{cases}$
 CO_2 emissions per one kilometre for traveling from location i to location j ;
 D_{ij} traveled distance from location i to location j (Note that it assumed that $D_{ij} = \infty$.) ;
 T_{ij} traveled time(or handling time) from location i to location j ;
 TL_k working time limit for truck k ;
 AL_i actual location index for location i being belong to set N^{ES} or N^{ED} ;
 M very large constant.
And variables used in VDP are defined as follows:
 $x_{ijk} = 1$ if truck k travels from location i to location j ,

$= 0$ otherwise (0-1 decision variable);
 $y_{ik} = 1$ if truck k visits to location i , $= 0$ otherwise (0-1 decision variable);
 u_{ik} visiting order which truck k visits to location i ;
 a_i^+ time when any truck arrives location i except the terminal 0;
 h_i = time when an empty container can be served after the devanning operation at location i in N^D , or = time when a full container can be completed after the vanning operation at location i in N^{ED} ;
 a_i^- = later time between arrival time of a full container to location i and leaving time of an empty container from location i if location i is included in N^D , or = later time between arrival time of an empty container to location i and leaving time of a full container from location i if location i is included in N^P ;
 b_i time when one truck arrives at location i .

This problem VDP will be formulated as follows:

$$[VDP] \text{ Minimize } \sum_{i \in N} \sum_{j \in N} \sum_{k \in V} CE_{ij} D_{ij} x_{ijk} \quad (1)$$

Subject to

$$\sum_{j \in N} x_{ijk} = y_{ik} \quad \forall i \in N, k \in V \quad (2)$$

$$\sum_{i \in N} x_{ijk} = y_{jk} \quad \forall j \in N, k \in V \quad (3)$$

$$\sum_{k \in V} y_{ik} \begin{cases} \leq |N| - 1 \\ = 1 \end{cases} \quad \begin{matrix} \forall i \in \{0\} \\ \forall i \in N \setminus \{0\} \end{matrix} \quad (4)$$

$$u_{ik} - u_{jk} + 1 \leq N(1 - x_{ijk}) \quad \forall i, j \in N \setminus \{0\}, k \in V \quad (5)$$

$$u_{jk} - u_{ik} - 1 \leq N(1 - x_{ijk}) \quad \forall i, j \in N \setminus \{0\}, k \in V \quad (6)$$

$$y_{ik} \leq u_{ik} \leq N y_{ik} \quad \forall i \in N \setminus \{0\}, k \in V \quad (7)$$

$$\sum_{k \in V} x_{0jk} = 1 \quad \forall j \in N^D \quad (8)$$

$$\sum_{k \in V} x_{i0k} = 1 \quad \forall i \in N^P \quad (9)$$

$$\sum_{j \in N^{ED}} \sum_{k \in V} x_{ijk} = 1 \quad \forall i \in N^{ES} \quad (10)$$

$$\sum_{i \in N^{ES}} \sum_{k \in V} x_{ijk} = 1 \quad \forall j \in N^{ED} \quad (11)$$

$$\sum_{j \in N} x_{ijk} - \sum_{j \in N} x_{jik} = 0 \quad \forall i \in N, k \in V \quad (12)$$

$$b_0 = 0 \quad (13)$$

$$a_j^+ \geq b_0 + T_{0j} - (1 - \sum_{k \in V} x_{0jk})M \quad \forall j \in N \setminus \{0\} \quad (14)$$

$$a_j^+ \geq b_i + T_{ij} - (1 - \sum_{k \in V} x_{ijk})M \quad \forall i, j \in N \setminus \{0\} \quad (15)$$

$$a_{N+1}^+ \geq b_i + T_{i0} - (1 - \sum_{k \in V} x_{i0k})M \quad \forall i \in N \setminus \{0\} \quad (16)$$

$$h_i \geq \min \{ (\sum_{i' \in N \setminus N^D} \sum_{k' \in V} x_{i'jk'} - \sum_{k \in V} x_{ijk})M, a_i^+ + T_{ij} \max \{0, 1 - |i - AL_j| M\} \} \quad \forall i \in N^D, j \in N^{ES} \quad (17)$$

$$h_i \geq \min \{ (\sum_{i' \in N \setminus N^{ED}} \sum_{k' \in V} x_{i'jk'} - \sum_{k \in V} x_{ijk})M, a_i^+ + T_{ij} \max \{0, 1 - |AL_i - j| M\} \} \quad \forall i \in N^{ED}, j \in N^P \quad (18)$$

$$a_j^- \geq \min \{ (\sum_{i' \in N \setminus N^D} \sum_{k' \in V} x_{i'jk'} - \sum_{k \in V} x_{ijk})M, \max \{h_i, a_j^+ - |i - AL_j| M\} \} \quad \forall i \in N^D, j \in N^{ES} \quad (19)$$

$$a_j^- \geq \min \{ (\sum_{i' \in N \setminus N^{ED}} \sum_{k' \in V} x_{i'jk'} - \sum_{k \in V} x_{ijk})M, \max \{h_i, a_j^+ - |AL_i - j| M\} \} \quad \forall i \in N^{ED}, j \in N^P \quad (20)$$

$$a_i^- = a_i^+ \quad \forall i \in N \cup \{|N|+1\} \setminus \{N^{ES} \cap N^P\} \quad (21)$$

$$b_i = \max\{0, a_i^+, a_i^-\} \quad \forall i \in N \cup \{|N|+1\} \quad (22)$$

$$b_i \leq TL_k \quad \forall i \in N \cup \{|N|+1\}, k \in V \quad (23)$$

$$x_{ijk} = \{0, 1\} \quad \forall i, j \in N, k \in V \quad (24)$$

$$y_{ik} = \{0, 1\} \quad \forall i \in N, k \in V \quad (25)$$

$$u_{ik} \geq 0 \quad \forall i \in N, k \in V \quad (26)$$

$$a_i^+, a_i^-, b_i \geq 0 \quad \forall i \in N \cup \{|N|+1\} \quad (27)$$

$$h_i \geq 0 \quad \forall i \in N^D \cup N^{ED} \quad (28)$$

where the objective function (1) minimizes the total CO₂ emissions by truck traveling for container transport. Constraint sets (2) and (3) show the relationship between x_{ijk} and y_{ik} . Constraint set (2) ensures that truck k must travel to any one location from location i . Constraint set (3) also ensures that truck k must travel to location j from any one location.

Constraints (4) ensure that any one truck must visit customer location i exactly once, except for the terminal 0. Constraints (5) and (6) mean that a sub-tour visited only customer locations except the terminal 0 is forbidden. Constraints (5) and (6) guarantee the relationship among u_{ik} , u_{jk} and x_{ijk} . If $x_{ijk} = 1$, constraints (5) and (6) become $u_{ik} - u_{jk} + 1 \leq 0$ and $u_{jk} - u_{ik} - 1 \leq 0$, respectively. This means that $u_{jk} = u_{ik} + 1$ if $x_{ijk} = 1$. If $x_{ijk} = 0$, constraints (5) and (6) become $u_{ik} - u_{jk} + 1 \leq \infty$ and $u_{jk} - u_{ik} - 1 \leq \infty$, respectively. Therefore, there is the relationship of visit-ing order between u_{ik} and u_{jk} . Constraint set (7) guarantees the relationship between y_{ik} and u_{ik} . If $y_{ik} = 1$, it becomes $1 \leq u_{ik} \leq \infty$, then variable u_{ik} is not zero. If $y_{ik} = 0$, it becomes $0 \leq u_{ik} \leq 0$, then variable u_{ik} is zero.

Constraint sets (8) to (11) mean the precedence constraint. Constraint sets (8) and (9) guarantee that any one truck must visit a location of N^D immediately after it visits the terminal 0, and any one truck must visit a location of N^P just before it visits the terminal 0. Constraint sets (10) and (11) guarantee that any one truck visits a location of N^{ES} just before it visits a location of N^{ED} .

Constraint set (12) means the flow conservation constraint, it guarantees the number of times a truck arriving at a location is same as the number of times the relevant truck leaving from the relevant location. A truck arrives and leaves each customer only once. Trucks can arrive and leave the terminal 0 more than once. The constraint set (13) defines the time when any truck leaves the terminal 0 as zero.

Constraint sets (14) to (16) define variable a_j^+ by using variables x_{ijk} and b_i . Constraint (14) defines variable a_j^+ for the terminal 0 where is visited just before location j . If $x_{0jk} = 1$, it defines as $a_j^+ = b_0 + T_{0j}$. If $x_{0jk} = 0$, it becomes $a_j^+ \geq -\infty$, then it defines as $a_j^+ \geq 0$. Constraints (15) define variable a_j^+ for any location except the terminal 0 which is visited just before location j . If $x_{ijk} = 1$, it defines as $a_j^+ = b_i + T_{ij}$. If $x_{ijk} = 0$, it becomes $a_j^+ \geq -\infty$, then it defines as $a_j^+ \geq 0$. Constraints (16) define variable a_j^+ for the relevant location j which is the terminal 0. If $x_{i0k} = 1$,

it defines as $a_{N+1}^+ = b_i + T_{i0}$. If $x_{i0k} = 0$, it becomes $a_{N+1}^+ \geq -\infty$, then it defines as $a_{N+1}^+ \geq 0$.

Constraints (17) to (20) define the time at the point which means before a situation changes, and the time at the point which means after a situation changes in a relevant customer. Constraints (17) define the variable h_i as the time when can supply the empty container, that means after a full container arrives at the point in N^D and the devanning work is completed. Constraints (18) define the variable h_i as the time when it can supply the full container, that means after an empty container arrives at the point in N^{ED} and the vaning work is completed. Constraints (19) compare the time h_i when an empty container can be supplied with the time a_j^+ when a truck arrives to N^{ES} , and define the variable a_j^- as the later time. Constraints (20) compare the time h_i when a full container can be supplied with the time a_j^+ when a truck arrives to N^P , and define the variable a_j^- as the later time. Constraints (19) and (20) mean the following. That is, if it is not in the condition that a scheduled container goes to the next at the time when a truck arrives, the truck must wait for the container.

Constraints (21) define the variable a_j^- for other locations except the above definitions. Constraints (22) define variable b_i by using variables a_i^+ and a_j^- . Constraints (23) guarantee that each truck must service its assigned workload within its work time limit.

4. SOLUTION PROCEDURE

As shown in the previous section, it is clear that there are many constraints in this problem. From the previous study, It is clear that it is difficult to obtain the problem of a realistic scale in suitable computation time. Then, we propose the heuristic approach by Ant colony optimization (ACO) shown by Dorigo and Stutzle [3], in order to find the feasible solution of VDP.

4.1 ACO algorithm

ACO algorithms can be used to solve both static and dynamic combinatorial problems. This problem as a static problem are given once and for all when the problem is defined, and do not change while the problem is being solved. As shown in [3], the main tasks to be considered in ACO are (a) the data initialization, (b) the solution construction, (c) the pheromone trails update.

(a) Initialize the data: Set the number of ants as ANT , the distance matrix D_{ij} and time matrix T_{ij} between location i and location j are given in advance. And the initial pheromone matrix τ_0 obtained by move from location i to location j by the Ant System rule as follows.

$$\tau_0 = ANT / (\rho \cdot OBJ^{best}) \quad (29)$$

$$\tau_{ij} = \tau_0 \quad \forall (i, j) \in T^{ANT} \quad (30)$$

where $0 < \rho \leq 1$ is the pheromone evaporation rate, OBJ^{best} is the best objective function value of among a solution generated by each ant, because we consider that the nearest-neighbor heuristic cannot be used to this problem with some precedence constraints.

(b) Construct the solution: The solutions are constructed by the probability for selecting the next visiting location shown in the following 4.2 section.

(c) Update the pheromone trails: MAX-MIN Ant System (MMAS) proposed by Stutzle and Hoos [8] introduces VDP in order to avoid a stagnation situation in which all the ants follow the same solution. To counteract this effect, MMAS limits the possible range of pheromone trail value τ_{ij} at an iteration to the interval $[\tau_{MIN}, \tau_{MAX}]$. After all the ants have constructed their solutions, the pheromone trails are updated.

$$\tau_{ij} = (1 - \rho)\tau_{ij} + \Delta\tau_{ij}^{best}, \quad (31)$$

$$\Delta\tau_{ij}^{best} = \begin{cases} 1/OBJ^{best} & \text{if } (i, j) \in T^{best} \\ 0 & \text{otherwise} \end{cases}, \quad (32)$$

where ρ is the pheromone evaporation rate, which is used to avoid unlimited accumulation of the pheromone trails. T^{best} is set of paths included in the best solution at each iteration. OBJ^{best} is the objective function value of the best solution at each iteration.

Firstly, the pheromone trail limits are

$$\tau_{MAX} = 1/(\rho \cdot OBJ^{best}), \quad (33)$$

$$\tau_{MIN} = \{\tau_{MAX} \cdot (1 - \sqrt[ANT]{0.05})\} / \{(ANT/2 - 1) \cdot \sqrt[ANT]{0.05}\}. \quad (34)$$

Then the pheromone trail is

$$\tau_{ij} = \begin{cases} \tau_{MAX} & \text{if } \tau_{ij} < \tau_{MAX} \\ \tau_{ij} & \text{if } \tau_{MIN} \leq \tau_{ij} \leq \tau_{MAX} \\ \tau_{MIN} & \text{otherwise} \end{cases}. \quad (35)$$

However, this process remains that we may find the solution's pheromone trail value which is less than the lower pheromone trail limits. Therefore the pheromone trail is reinitialized used by λ -branching factor, Λ as follows.

$$\tau_{max}(i) = \max_{1 \leq l \leq N, l \neq i} \tau_{il}, \quad (36)$$

$$\tau_{min}(i) = \min_{1 \leq l \leq N, l \neq i} \tau_{il}, \quad (37)$$

$$\varepsilon(i, j) = \begin{cases} 1 & \text{if } \tau_{ij} > \lambda \cdot \{\tau_{max}(i) - \tau_{min}(i)\} + \tau_{min}(i) \\ 0 & \text{otherwise} \end{cases}, \quad (38)$$

$$\Lambda = 1/N \cdot \sum_{1 \leq l \leq N} \sum_{1 \leq j \leq N, j \neq i} \varepsilon(i, j), \quad (39)$$

Where N is the number of locations. λ is 0-1 real number given as parameter. If Λ is threshold value given in advance, the pheromone trail value is adjusted by

$$\tau_{ij} = \tau_{ij} + a \cdot (\tau_{MAX} - \tau_{ij}) / \sum_{k=1, k \neq i}^N (\tau_{MAX} - \tau_{ik}). \quad (40)$$

This process can avoid the stagnation behavior.

4.2 Solution construction procedure for VDP

Multiple ants build solutions of VDP as the traveling salesman problem instance. Initially, ants are put on randomly chosen locations. At each construction step, ant k applies a probabilistic action choice rule to decide which location to visit next. The probability with which ant k currently at location i , chooses to go to location j is

$$p_{ij}^k = [\tau_{ij}]^\alpha [\eta_{ij}]^\beta / \sum_{l \in N_i^k} [\tau_{il}]^\alpha [\eta_{il}]^\beta \quad \text{if } j \in N_i^k \quad (41)$$

where $\eta_{ij} = 1 / (D_{ij} \cdot CE_{ij})$ is a heuristic value that is available a priori, α and β are two parameters which determine the relative influence of the pheromone trail and the heuristic information, and N_i^k is the feasible neighbor-hood of ant k when being at location i , that is, the set of locations that ant k has not visited yet.

Table 1 shows the example of each location's number and its attribute in Fig. 2. Point 5, 6, 9, 10, 13 to 16 are located in the terminal 0. There are different attributes as ES(0), ED(0), ZD and ZP in their points. From this example, Table 2 shows the truck condition and the condition change from location i to location j . From Table 2, the travel distance, handling time, and CO₂ emission from location i to location j can be obtained. The use of the dummy nodes located at terminal 0 can simplify judgment whether the arc (i, j) has already chosen or not.

Table 1. Example of location number and its attribute

Node #	1	2	3	4	5	6	7	8	9	10	11	12	13	14	15	16
Attrib	D		P		ES(D)		ES(0)		ED(P)		ED(0)		ZD		ZP	
Actual location	1	2	3	4	1	2	0	0	3	4	0	0	0(1)	0(2)	0(3)	0(4)

Table 2. Truck condition and condition change from location i to location j

i \ j	D		P		ES(D)		ES(0)		ED(P)		ED(0)		ZD		ZP	
	1	2	3	4	5	6	7	8	9	10	11	12	13	14	15	16
D	1	-	-	ET	ET	H	ET	ET	ET	-	-	-	-	ET	-	-
	2	-	-	ET	ET	ET	H	ET	ET	-	-	-	-	ET	-	-
P	3	-	-	-	-	-	-	-	-	-	-	-	-	-	FC	-
	4	-	-	-	-	-	-	-	-	-	-	-	-	-	-	FC
ES(D)	5	-	-	-	-	-	-	-	EC	EC	EC	EC	-	-	-	-
	6	-	-	-	-	-	-	-	EC	EC	EC	EC	-	-	-	-
ES(0)	7	-	-	-	-	-	-	-	EC	EC	0	0	-	-	-	-
	8	-	-	-	-	-	-	-	EC	EC	0	0	-	-	-	-
ED(P)	9	-	-	H	ET	ET	ET	ET	-	-	-	-	-	-	ET	ET
	10	-	-	ET	H	ET	ET	ET	-	-	-	-	-	-	ET	ET
ED(0)	11	-	-	ET	ET	ET	ET	0	-	-	-	-	-	-	0	0
	12	-	-	ET	ET	ET	ET	0	-	-	-	-	-	-	0	0
ZD	13	FC	-	-	-	-	-	-	-	-	-	-	-	-	-	-
	14	-	FC	-	-	-	-	-	-	-	-	-	-	-	-	-
ZP	15	-	-	-	ET	ET	ET	0	-	-	-	-	0	0	-	-
	16	-	-	ET	-	ET	ET	0	-	-	-	-	0	0	-	-

FC : Full container transport EC : Empty container transport

ET : Empty truck travel

H : Handling operation (van/devan) including cleaning and arranging

0 : No travel because actual position of i is the same as j , but path (i, j) can be chosen

- : No travel because of constraints which path (i, j) cannot be chosen

5. COMPUTATIONAL EXPERIMENTS

5.1 Computational design

The problem was modeled in the ACO on a workstation. Problems used in these experiments were generated randomly, but systematically, in order to obtain problems with differing levels of customer location or handling time length.

The number of locations are set to 40 and 80. First and second of one eighth are delivery and pickup locations, respectively. Third and forth of one eighth are where empty containers are supplied, and also are same as delivery locations or the terminal 0. Fifth and sixth are where empty containers are demanded, and are same as pickup or the terminal 0. Seventh and the remaining of one eighth are where the terminal 0 just before a delivery

location and the terminal 0 immediately after a pickup location. As introduced in Imai *et al.*[4], the coordinates of customer points P_i were defined as

$$P_i = (R1_i \times 100 - 50)(r + R2_i \times 0.4) \quad (42)$$

where r is a parameter of 0.2, 0.4, or 0.6, and $R1_i$ and $R2_i$ are two series of random numbers both from a uniform distribution between 0 and 1. By changing r , we can determine the range of customer's location from the terminal. $R1_i$ defines a basic location for each point, while $R2_i$ gives a variance of the location for a particular range of a customer's location set. A fleet of trucks is given the working time limit as 8 hours. Handling time length included vanning/devanning operation, cleaning the container or arranging before next situation is given as 2 to 6 hour at interval of one hour.

We can obtain the way to calculate CO₂ emissions in proportion to the travel distance as the following definition (43) from the guideline for calculating CO₂ emissions in logistics fields [7]:

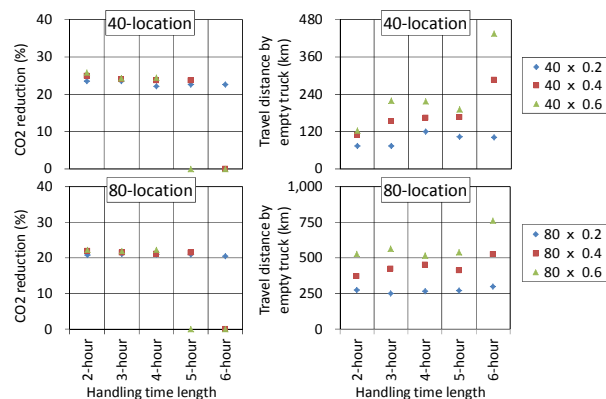
$$CO2_i = W_i / 10^3 \times EF_i / 10^3 \times CV \times CEF \times CO2_i / C \quad (43)$$

where $CO2_i$ CO₂ emissions per one kilometre in truck condition i (t-CO₂/km); W_i weight of relevant container loaded on truck in truck condition i (kg); W_{fc} = weights of chassis, container and load; W_{ec} = weight of chassis & container; W_e = weight of chassis*10%; EF_i fuel cost in truck condition i (km/kL); CV heat value per a kilo litre of fossil fuel used by a truck (GJ/kL); CEF coefficient of C emissions for fossil fuel used by a truck (t-C/GJ); $CO2_i/C$ coefficient of CO₂ emissions for fossil fuel used by a truck (t-CO₂/t-C).

5.2 Computational results

Fig.3 shows the CO₂ reduction (%) from the conventional operation, and the travel distance by empty truck which is operated by the proposed approach. As empty truck travel does not occur in the conventional operation, we investigate the effect on CO₂ emission by empty truck travel.

From the computational results, CO₂ emissions by the proposed approach are reduced 20 % from the conventional operation in any customer location distribution and any handling time length. The travel distance by empty truck depends on number of locations, customer location distribution and handling time length.



(a) CO₂ reduction (%) (b) Travel distance by empty truck
Note) CO₂ reduction 0% means the case that the working time by a truck in the conventional operation exceeds the time limit.

Figure 3. Computational results

In order to reduce CO₂ emissions, empty truck travel occurs. Then the wider customer distribution is located, the longer travel distance by empty truck becomes. In the case of 6-hour handling time, the long travel distance by empty truck can reduce CO₂ emissions.

6. CONCLUSION

This study addresses the vehicle dispatch problem for marine container drayage, in order to reduce CO₂ emissions. The change of situation at each one customer is dealt with two different points. It is given that the handling time between different points at one customer with considering the precedence constraints. We propose the heuristic approach based on ACO using a dummy node concept, in order to find feasible solutions. From computational results, it is clear that the long travel distance by empty truck can reduce CO₂ emissions in long handling time.

ACKNOWLEDGMENT

This work was supported by JSPS KAKENHI 18K04618 and 17H02039. This financial support is gratefully acknowledged.

REFERENCES

- [1] Breakers, K., Caris, A. and Janssens, G.K.: Integrated planning of loaded and empty container movements, *OR Spectrum*, Vol.35, pp. 457-478, 2013.
- [2] Chueng, R.K., Shi, N., Powell, W.B. and Simao, H.P.: An attribute-decision model for cross-border drayage problem, *Transportation Research Part-E*, Vol.44, pp. 217-234, 2008.
- [3] Dorigo, M. and Stutzle, T.: Chapter 3: Ant Colony Optimization Algorithms for the Traveling Salesman Problem, *Ant Colony Optimization*, pp.65-119, The MIT press, 2004.
- [4] Imai, A., Nishimura, E. and Current, J.: A Lagrangian relaxation-based heuristic for the vehicle routing with full container load, *European Journal of Operational Research*, Vol. 176, pp. 87-105, 2007.
- [5] Jula, H., Dessouky, M., Ioannou, P. and Chassiakos, A.: Container movement by trucks in metropolitan networks: modelling and optimization, *Transportation Research Part-E*, Vol. 41, pp. 235-259, 2005.
- [6] Nishimura, E., Shintani, K. and Imai, A.: Vehicle dispatch problem with precedence constraints for marine container drayage, *Proceedings of 2018 IEEE International Conference on Industrial Engineering and Engineering Management*, pp. 56-60, 2018.
- [7] The guideline for calculating CO₂ emissions in logistics fields, Website of Agency for Natural Resources and Energy : Ministry of Economy, Trade and Industry, Japan. (<http://www.greenpartnership.jp/co2brochure.pdf>), accessed in 28 June 2019. (in Japanese)
- [8] Stutzle, T. and Hoos, H.H.: MAX-MIN Ant System and local search for combinatorial optimization problems, *Proceedings of 2nd International Conference on Metaheuristics*, pp.1-15, 1997.

Conceptual design of a modular, hybrid sensor system (*Duck Box*) for the implementation of location-based material flow analyses

Rainer Pascher

PhD Student
Vienna University of Technology
Institute of Management Science
Industrial and Systems Engineering

Christoph Ecker

PhD Student
Vienna University of Technology
Institute of Management Science
Industrial and Systems Engineering

Wilfried Sihm

Professor
Vienna University of Technology
Institute of Management Science
Head of Department Industrial and Systems Engineering

Intralogistics show great potential for increasing efficiency in many companies. For this purpose, material flow analyses are used. The underlying data basis can be provided by Indoor Positioning Systems (IPS) or Real Time Location Systems (RTLS). Due to poor user-friendliness and the influence of company-specific factors, such systems are usually not used. The aim of this paper is to develop the conceptual design of a modular, hybrid sensor system (project name: Duck Box) to enable complete material flow analyses. Based on the state of the art, the paper describes the general requirements for such a system, the selection of components, the calculation of the required power supply as well as the construction of a housing. In contrast to other systems, the developed modular hybrid sensor system acts as an enabler for holistic location-based material flow analyses.

Keywords: *Intralogistics, IPS, Material flow analyses, Sensors, Duck Box, ultrasonic, forklifts*

1. INTRODUCTION

Intralogistics, which include all internal material storage, handling and transport costs, accounts for 25 % of the total personnel input, 55 % of the space required and 87 % of the actual throughput time. These percentages show the great potential of an efficient implementation [3].

An essential component of intralogistics are the material flow transports that are required in the context of value creation. Despite increasing automation, these are usually carried out manually and are associated with high personnel and cost input. The distances covered by industrial trucks or forklift trucks vary, among other things, in terms of their distance, intensity and relevance for the actual value-added process. These and other properties are investigated within the framework of a material flow analysis [7-9].

2. MATERIAL FLOW ANALYSIS

The current state of the art for the analysis of intralogistics material flows are a large number of visualization and modelling tools. For the underlying database, so-called Indoor Positioning Systems (IPS) or Real Time Location Systems (RTLS) are used. To locate transport vehicles and to draw conclusions about the existing traffic the positioning data is analysed. By using these systems for further optimisation, an efficiency increase of 15-20 % can be achieved in the picking area of a warehouse [2, 4, 6, 8, 10].

The advancing digitalization with a seemingly infinite number of different technologies and sensors is currently used by companies inadequately or not at all. A lack of standardisation, poor user-friendliness and a myriad of influencing factors do not permit a specific application for location-based material flow analyses in an industrial environment [1, 5, 11].

3. OVERALL NEEDED SOLUTION

The target is to link company-specific requirements and technological framework conditions, in order to make the use of modular, hybrid sensor technology possible as well as to create the basis for the analysis of material flows.

Due to the different requirements resulting from the respective company's conditions and processes, individualization is usually necessary. Therefore, different technologies and sensors must be combined into a hybrid overall concept. In addition, the user-friendliness of the system is to be made possible by variable mounting options on different means of transport as well as the simple adaptability of the software.

The use of a modular, hybrid sensor technology enables the company to carry out a complete material flow analysis. [12]

4. CONCEPTUAL MEASURING UNIT (PROJECT NAME: DUCK BOX)

This paper describes the development of a conceptual measuring unit (project name: Duck Box). It essentially has a mobile battery powered processor which connects and controls various modules and sensors. All components have been selected for the highest possible economic efficiency and can be

Correspondence to: DI Rainer Pascher, Researcher
Vienna University of Technology Research GmbH,
Theresianumgasse 7, 1040 Vienna, Austria
E-mail: rainer.pascher@fraunhofer.at

obtained easily and inexpensively from independent retailers.

An ultrasonic sensor is used to record the loading condition. Depending on a company's requirements, the position data, the distance travelled and the associated dwell times can be recorded alternately using an active RFID tag, UWB, WLAN or Bluetooth. Depending on the selected IPS and sensor technology, the generated data is recorded locally on a storage medium or alternatively transmitted via wireless connection to a database positioned in the analysis area.

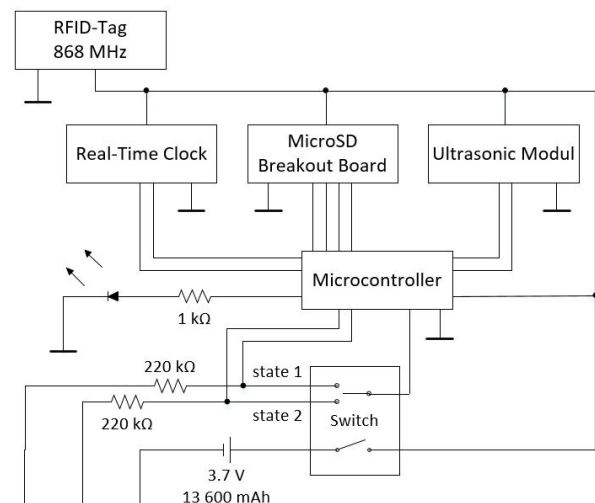


Figure 1. Circuit diagram of the components used

All components are accommodated in a compact and also robust housing suitable for industrial use. The housing is manufactured using the 3D printing process and has various mounting options for industrial forklifts.

4.1 Processor and Programming

A microcontroller is used as the computing processor. The processor handles the programming code and controls the interaction of all components. The programming is done in the programming language C++ and is structured in the following steps:

1. Definition of the variables and assignment of the outputs
2. Definition of the power saving mode and measuring cycle
3. Initialization of the storage medium
4. Initialization of time
5. Creation of a separate record for each recording period
6. Measurement of the transport movements
7. Measurement of further transport parameters
 - a. Measurement of the loading condition
 - b. Temperature measurement
 - c. Measurement of vibrations
8. Saving the data sets

4.2 Time Measurement

The time module is installed in order to always be able to assign the exact time to each data record. Each data record is provided with the current time and stored

on an SD module. By means of a separate power supply, the correct time can still be called up after a temporary non-use of the measuring equipment. The module must be set to the correct time zone once by programming.

4.3 Ultrasonic Sensor

The ultrasonic sensor is selected for the identification of loading conditions. Using the ToA (time of arrival) method, the distance of the object can be calculated. Additionally conclusions about the loading condition can be drawn. The sensor emits ultrasonic waves at a specified interval. If an object is located in a specified transport area (e.g. forklift fork, loading area of a truck, etc.), the ultrasonic waves are reflected at this object and returned to the sensor. The distance of the object can then be determined on the basis of the speed of sound. The sensor is designed for five volts and has a trigger and an echo port which is connected to the processor.

4.4 SD Module and Storage

The recorded measurement results of the ultrasonic sensor are stored as a text file on a Micro-SD memory card. The SD module ensures continuous data readings and writings.

The first two columns show the exact time of the measurement. In the distance column, the measured distance from the measuring unit to any load carrier on the load handling attachment is entered. Depending on the mounting position, column 4 can be used to determine whether the forklift is loaded (defined with the value "1") or unloaded (defined with the value "0").

4.5 Indoor Positioning System

Depending on the selected IPS, the corresponding technology is to be implemented in the measuring unit. The modularity of the measuring unit theoretically allows any extension by various positioning systems. Prerequisite is a mobile power supply or the possibility to connect the mobile power supply integrated in the measuring system. Based on the current state of the art and considering the material flow-specific requirements of IPS, the integration can be explained using the example of RFID:

To determine the position an active RFID tag is integrated and connected to the integrated battery. The tag operates at a frequency of 868 MHz and transmits a programmable ID at a programmable interval. The ID as well as the transmission strength can be read out by means of appropriate RFID receivers.

UWB, Bluetooth and WLAN systems can be integrated in the Duck Box analogous to RFID. The resulting changes based on the current state of science and technology are shown in the following table:

Table 1. Characteristics of tracking technologies

Characteristics	Technology			
	RFID	UWB	Blue-tooth	WLAN
Frequency	868 MHz	3.1-10.6 GHz	2.4 GHz	2.4 GHz
Power supply Tag	Duck Box	Duck Box	Duck Box	Duck Box
Power supply infrastructure	battery	socket	socket	socket
Data logging	local	network	network	network
Position-ing	RSSI	ToF	RSSI	RSSI

4.6 Power Supply

A mobile power supply provides the sensor with energy for the duration of the analysis. All components have a common resistance of about 139 Ohm. The ohmic law is used to calculate the optimum voltage:

$$I = \frac{U}{R} \quad (1)$$

This means that at constant resistance R a lower operating voltage U also enables a lower current consumption I and thus a more energy-efficient operation. With this in mind all components are selected and optimized. The voltage of 3.7 volts corresponds to the lowest limit value at which available processors, SD reader modules and ultrasonic sensors operate reliably. 3.7 Volt also correspond to the commercially available 18650 lithium-ion batteries which already have a PCB protection circuit. Standard cells have a maximum capacity of around 3,400 mAh. To increase this capacity, it is necessary to connect several cells in parallel. This also enables a voltage of 3.7 volts with increased battery capacity.

In order to calculate the expected battery life, the derated capacity and the average current requirement have to be calculated first:

$$c = C * \frac{85}{100} \quad (2)$$

$$I_{average} = \frac{(I_{awake} * t_{awake} + I_{sleep} * t_{sleep})}{3,600} \quad (3)$$

The current requirement of the components used is measured at this operating voltage over the course of several measurements. This result is 20 mA for the current while sleeping and 40 mA for the current while awake when the ultrasonic measurement is performed. The expected battery life can be calculated by using four 18650 cells with 3,400 mAh each and a measuring interval of three seconds:

$$battery\ life = \frac{c}{I_{average} * 24} \quad (4)$$

By using the values, a battery life of about 19 days results.

4.7 Housing

The construction of the housing can be divided into three stages:

1. Feasibility study: To check the general feasibility of the sensor, all components were plugged onto a so-called developer board. This was integrated into a cardboard packaging for demonstration purposes. The aim of the feasibility study has been to check the functionality of the selected components and evaluate the stored data. The recorded measurement results and the associated accuracy have been validated and adjusted for the planned application.

2. Prototype: A functioning prototype has been produced for use in an industrial environment. In order to be able to realize a setup as realistic as possible, it was equipped with the final components with the exception of the power supply, the housing and the processor (due to the faster adaptability of an Arduino Uno). The prototype was then mounted on a manual hand pallet truck at the pilot factory of the Vienna University of Technology and put into operation over a period of 3 weeks. After successful completion of this test phase, all components have been transferred to an industrial housing.

3. Final housing: After completion of the prototype phase, a final housing has been constructed. The design is engineered for additive manufacturing methods. The following aspects have been taken into account:

- Wall thicknesses: The housing should be robust due to the industrial environmental conditions.
- Modular design: All components and parts should be exchangeable and controllable. The power supply should be easily replaceable.
- Separation of components: Sensors and various cabling should not come into direct contact with the power supply in the housing. This should make it easier to replace the batteries and prevent short circuits. A separate partition wall is designed to meet these requirements.
- Size: In order to be able to mount the unit as simply and universally as possible in the front area of an industrial truck, attention should be paid to a compact design.
- Mounting options: The primary mounting option is magnetic. For this purpose, M6 threads are inserted on all sides, which should enable problem-free screwing of various pot magnets as well as other fastening solutions such as screw or clamp connections.
- Connection and configuration options: In order to be able to install different and company-specific software versions on the measuring equipment, a USB port with direct connection to the processor and a 3-way toggle switch for selecting different operating modes should be provided.
- LED-Diode: In order to be able to check the correct operating status, an LED diode should be visible.

The construction was carried out using the Catia V5 construction program, the production was conducted by Fraunhofer Austria using a 3D printer.

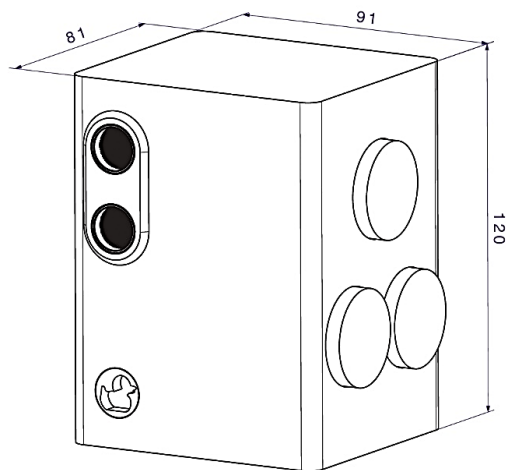


Figure 2. Isometric view of the Duck Box

5. CONCLUSION

Depending on the existing infrastructure, the state of digitisation and the specific requirements of the companies, different factors and therefore technologies have to be taken into account when carrying out a location-based material flow analysis. Within the current state of the art with the material flow-specific criteria analysed, no suitable sensor system can be identified on the market that meets all the requirements of the companies.

A novel hybrid sensor system has been developed which functions as an enabler of a location-based material flow analysis under consideration of company-specific boundary conditions. With this developed sensor system for internal means of transport, transport distances and intensities can be linked to the loading conditions, as well as the length of stay and also driving and handling times can be determined.

The use of this modular, hybrid sensor technology enables the company to carry out a complete material flow analysis.

ACKNOWLEDGEMENT

The modular, hybrid sensor system was originally developed within the research project “SEMPRE”, funded by the *The Austrian Research Promotion Agency (FFG)*.

REFERENCES

- [1] Al Nuaimi, K., Kamel, H.: A survey of indoor positioning systems and algorithms, In 2011 International Conference on Innovations in Information Technology, pp. 185–190, 2011.
- [2] Dieter, A., Furmans, K.: *Materialfluss in Logistiksystemen*, Springer-Verlag, Berlin Heidelberg (VDI-Buch), 2005.

- [3] Bortolini, M., Gamberi, M., Piana, F. and Regattieri, A.: Industrial application of UWB real-time location system technology to increase inbound logistic performances, 23rd International Conference for Production Research, pp. 1-13, 2015.
- [4] Chow, H., Choy, K., Lee, W. and Lau, K.: Design of a RFID case-based resource management system for warehouse operations, *Expert Systems with Applications* Vol. 30, No. 4, pp. 561–576, 2006.
- [5] Deak, G., Curran, K. and Condell, J.: A survey of active and passive indoor localisation systems, *Computer Communications*, Vol. 35, No. 16, pp. 1939–1954, 2012.
- [6] Gladysz, B., Santarek, K. and Lysiak, C.: Dynamic Spaghetti Diagrams. A Case Study of Pilot RTLS Implementation, *Intelligent Systems in Production Engineering and Maintenance – ISPEM 2017*, Vol. 637. Cham: Springer International Publishing (Advances in Intelligent Systems and Computing), pp. 238–248, 2018.
- [7] VDI 2689, 05.2010: Leitlinie für Materialflussuntersuchungen.
- [8] Heinrich, M.: *Transport- und Lagerlogistik. Systematik, Planung, Einsatz und Wirtschaftlichkeit*, Springer Vieweg, Wiesbaden, 2016.
- [9] Pfohl, H.C.: *Logistiksysteme. Betriebswirtschaftliche Grundlagen*, Springer, Berlin, 2010.
- [10] Ruppert, T., Jaskó, S., Holczinger, T. and Abonyi, J.: Enabling Technologies for Operator 4.0: A Survey, *Applied Sciences*, Vol. 8, No. 9, 1650, 2018.
- [11] Sakpere, W., Adeyeye Oshin, M. and Mlitwa, N.B.W.: A State-of-the-Art Survey of Indoor Positioning and Navigation Systems and Technologies, *SACJ*, Vol. 29, No. 3., 2017.
- [12] Wannenwetsch, H.: *Integrierte Materialwirtschaft, Logistik und Beschaffung*, Springer Vieweg (Springer-Lehrbuch), pp. 289, Berlin, 2014.

NOMENCLATURE

c	derated capacity
C	capacity rating of battery
I	current
$I_{average}$	average current
I_{awake}	current when awake
I_{sleep}	current when sleeping
R	resistant
t_{awake}	wake time per hour
t_{sleep}	sleep time per hour
U	Voltage

Model for the conceptual design of unit load warehouse systems through the integrated solution of five sub-problems

Philip Ramprecht

PhD Student
Vienna University of Technology
Institute of Management Science
Industrial and Systems Engineering

Martin Riester

PhD Student
Vienna University of Technology
Institute of Management Science
Industrial and Systems Engineering

Wilfried Sihh

Full Professor
Vienna University of Technology
Institute of Management Science
Industrial and Systems Engineering

Warehouses play a major role in modern supply chains concerning performance and costs. These factors are largely determined during the planning phase of these systems. The conceptual design is very complex and the outcome depends strongly on the planner's individual knowledge. Science mostly addresses isolated sub-planning-problems, which have low relevance for designers in practice.

This paper presents a model to aid the conceptual design of unit load warehouses. This approach consists of three modules. The data integration module is described in detail. It can process large amounts of data and is adaptable to individual data structures. Automatically generated key metrics are provided to the second module. Here the five sub-problems in warehouse design are addressed in iterative solving circles. This way different solutions are created. The last module estimates the performance and costs for each option from module two. Including quantitative factors, a single conceptual design is then suggested to the user based on a scoring system.

Keywords: warehouse system, warehouse design, design steps, planning problems, key figures, big data

1. INTRODUCTION

Warehouses and distribution centers are often considered as major bottlenecks in modern supply chains with regards to the performance [1]. In addition, warehouse systems are a crucial factor for defining expenses within the logistics network. In Europe, estimations reveal that warehousing and inventory carrying costs make up over 40 % of a company's total logistics costs [1, 2, 3, 4].

[2, 5, 6, 7, 8] state that the performance and cost effects of a warehouse are largely determined in the design phase. The design of warehouse systems is generally regarded as highly complex [9, 10]. This is due to high degrees of freedom, few fixed restrictions, internal and external factors as well as interdependent design problems [11]. Data volumes, data quality and frequent changes to the underlying data further complicate the design [12]. The planning of warehouse systems is therefore not only associated with high risk, but also with time and resource expenditure [13]. However, today's business environment does not allow sufficiently long design phases. Time periods for the conceptual planning phase of only two weeks are not unusual for warehouse designers [14].

2. CONCEPTUAL DESIGN OF UNIT LOAD WAREHOUSE SYSTEMS

In the conceptual stage of design, the issues are to meet storage and throughput requirements as well as minimizing costs [15]. This design phase strongly depends on the way the goods are packed and stored (e. g. whether they are palletized). Most designs are carried out on the basis of unit loads in order to create a more flexible system. A unit load is a group of items or bulk materials arranged in a way, that the load can be picked up and transported as a single unit [16].

2.1 Five sub-problems in the conceptual design phase

Roughly 900 academic contributions were identified during the underlying literature research, which are related to the topic of warehouse design. The majority of the research is limited to the consideration of isolated sub-design-problems [17]. [15] divide the conceptual planning phase for warehouse systems into five sub-design-problems as shown in figure 1.

These individual aspects are strongly interdependent and the isolated consideration leads to suboptimal overall solutions [5, 15, 18, 19]. Nevertheless, no scientific paper was found, which investigates all five sub-problems in order to create a comprehensive conventional design model for unit load warehouse systems [2, 3, 4, 19, 21, 22, 23].

The isolated approach to warehouse design, which is most common in science, leads to a high discrepancy between research and practice. Real problems are too complex to be described by linking individual,

Correspondence to: Philip Ramprecht, PhD Student
Vienna University of Technology, Theresianumgasse 7, 1040
Vienna, Austria
E-mail: philip.ramprecht@fraunhofer.at

independently solved sub-problems [24]. In addition, a strong tendency in the investigation of classical, manual person-to-good systems can be observed in science.

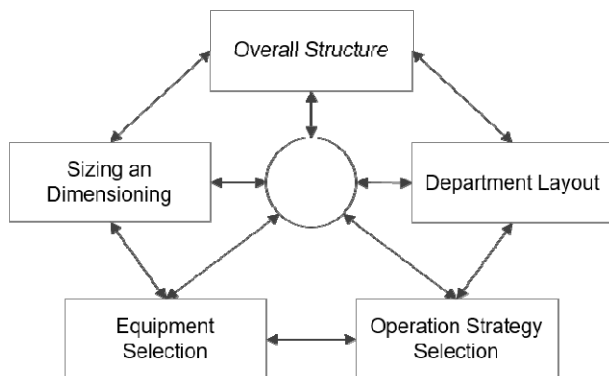


Figure 1. Five sub-problems in warehouse design [15]

In Europe, a trend towards automated storage solutions is emerging due to high personnel costs and land prices [25, 26]. The inadequate exchange between science and practice further increases the existing gap. Field-tested methods and findings have no influence on research regarding the planning of warehouse systems. Scientific results, on the other hand, are not appropriately translated into practice [15]. This leads to the fact that in the practical design of warehouses, recourse is made to old, proven solutions, regardless of the current state of research [27].

2.2 Model description

Addressing the stated problem, a model for the conceptual design of unit load warehouse systems is presented as shown in figure 2.

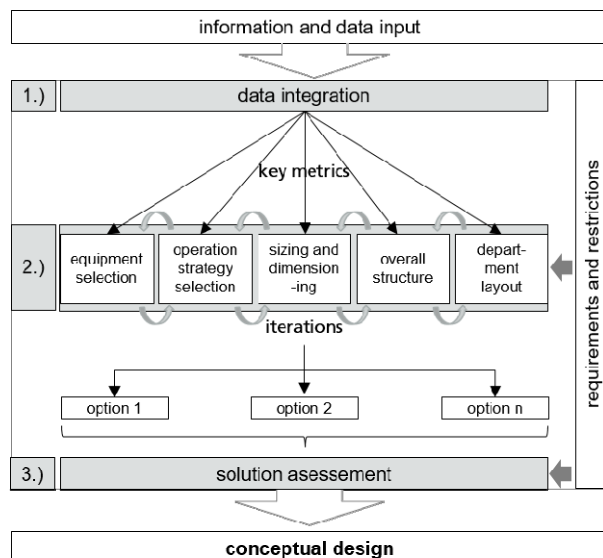


Figure 2. Conceptual warehouse design model divided into 3 modules (own figure)

The shown model describes a new, non-purely hierarchically approach to the problem. Beforehand the needed information and data requirements must be defined. The model itself consists of three individual modules:

Module 1 is called “Data Integration”. In this design step the available data is loaded into a developed software tool. Unique data structures are taken into account by using a translator, which the user can adapt to the individual needs. After loading and translating the data, errors within the structure are identified and reports are created automatically. The remaining data is then used to calculate certain key values as a basis for the following design step.

Module 2 is addressing the five sub-problems described beforehand. These problems are not dealt with sequentially, but are solved interdependently. The key figures derived from step 1 are the basis for finding possible solutions. Iterative steps are used to consider the impact, the individual sub-problems have on each other. Requirements and restrictions, which were defined beforehand, also have a high impact on this stage. In the end a number of possible options are created and form the input for the following design step.

Module 3 evaluates the performance, the capacity and the costs of each design option based on a data base with performance indicators and pricelists. Qualitative facts such as flexibility or reliability can also be considered. The importance of each requirement can be weighted individually by the user. The output of this step is a suggestion for the best design option based on a scoring system.

If more than one option seems very plausible, the designer has the choice to elaborate them in the detailed design phase, which follows the conceptual design. Here it might be useful to use simulation tools to specify the performance indicators, especially for highly automated systems.

3. DATA INTEGRATION

This paper will present the data integration model in more detail. The quality of the final warehouse design strongly depends on the underlying data. Today’s data volumes tend to grow rapidly and the quality of real life data is often quite poor. Almost every company has a very unique data structure. In addition, the databases can sometimes be changed in the course of a planning project. In order to create a comprehensive model for warehouse design, real life data has to be loaded, checked and transformed easily, regardless of the individual data structure. Errors within the underlying data have to be identified right away, since single values can affect the analysis quite strongly. Especially the design of highly automated systems is very sensitive to the accuracy of certain key values (e. g. picks per orderline) [12].

In order to create an easy to use data integration module, which addresses the problems stated beforehand, a certain number of ETL (Extract Transform, Load) tools were examined. In the course of a master thesis, these tools were evaluated concerning certain aspects like: user-friendliness, processing time, costs, community support etc. [28]. In the end the Java-based application *Pentaho Data Integration* (former *Kettle*) was chosen.

3.1 Data integration module

This module was built in a way, that the user does not need any knowledge about how to use the *Pentaho Data Integration* software. Therefore the model derives all the information needed from an *Excel* file. In a number of spreadsheets the user chooses what kind of data sources are available. He then defines the headers of each data source. The name of each header must then be assigned to predefined fieldnames. Obligatory fields are marked. After “translating” the data structure for the model, the user has to provide the filenames, for each data source. Multiple files can be read at once and even be added later on. The user can now start the transformation shown in figure 3. This transformation injects all needed input, which the user specified in the *Excel* sheets, into the actual data integration model.

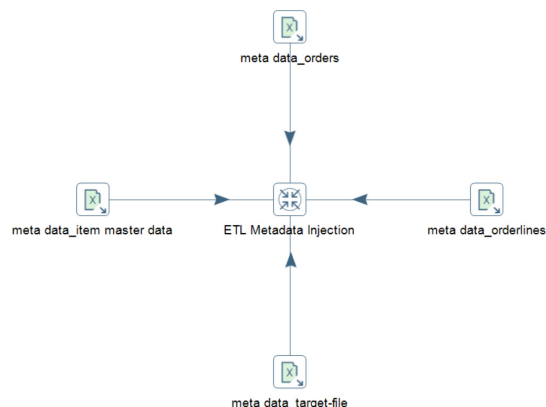


Figure 3. Metadata Injection from Excel sheet (own figure)

The actual data integration model (as shown in figure 4) automatically reads in all the files, which were defined beforehand. It then tries to convert all the rows according to the user’s definition. The amount of items picked has to be a number type for example. In the next step the model reads all the errors into separate files. These files can then be used to correct incorrect datasets. After testing every cell from every data source according to the previously specified metadata, all flows are merged into one single data stream. Physical dimensions of each SKU (Stock Keeping Unit) are added to the orderlines for example. In case no match is found the model creates another error file, for the user to analyze and correct.

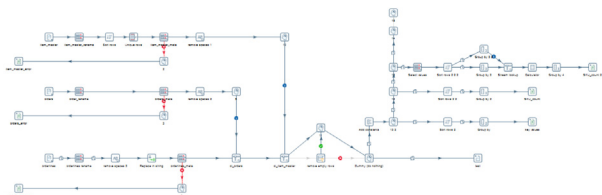


Figure 4. Actual data integration model

The model uses the validated data stream to perform certain analysis and generate key values automatically. In order to reduce calculating time, the user can deactivate certain calculations. At the current stage the model is able to carry out the following tasks:

- Calculate the amount of active SKU (Stock Keeping Unit)
- Calculate the pieces per storage unit

- Calculate the picks per orderline in average
- Calculate the picks per day in average
- Perform an ABC analysis
- Perform an COI (Cube-per-Order-Index) analysis

3.2 Use case

The data integration module was used to validate new warehouse design concepts based on existing data for a real life company. Each week more than 1 Mio. Orderlines were created and stored in separate csv files. Picking time and amount of picks were stored in separate files. Since the amount of items sold was strongly seasonal, an entire year had to be analyzed in order to create a solid planning base. Instead of reading 3 different sources with 52 single files each, the user just had to state the pathways in the models Excel sheets. After defining the data structure, the data integration tool performed an ABC analysis automatically. The output was a list with each SKU active throughout the entire year, including the amount of picks, the percentage of the picks in total and the ABC classification. This information was then used to assign each SKU to one of three picking techniques. In addition the models output was a couple of data files with individual errors within the given data set. This way the item stem data for individual SKUs could be corrected in an optimizing step. The analysis was then carried out again with the improved data set.

4. CONCLUSION

In this paper a new approach for the design of warehouse systems was presented. The basis of this approach is the data integration module. It allows the user to read in large amounts of data, independent of the individual data structure, in a standardized way. Errors within the dataset are recognized automatically and stored in separate error handling files. In the use case, an ABC analysis was done for approximately 50 Mio. Orderlines and 5 000 different items. The result was used to optimize the picking techniques for each SKU.

ACKNOWLEDGEMENT

The data integration modul was originally developed within the research project “SEMPRE”, funded by the *The Austrian Research Promotion Agency (FFG)*. It is used to consolidate data from different sources and of different quality as an input for machine learning algorithms helping with logistical planning tasks.

REFERENCES

- [1] Gue, K.R., Ivanović, G. and Meller, R.D.: A unit-load warehouse with multiple pickup and deposit points and non-traditional aisles, *Transportation Research Part E: Logistics and Transportation Review*, Vol. 48, No. 4, pp. 795–806, 2012.
- [2] Baker, P., Canessa, M.: Warehouse design: A structured approach, *European Journal of Operational Research*, Vol. 193, No. 2, pp. 425–436, 2009.

- [3] Kostrzewski, M.: In Search of Unified Warehouse Designing Method, Research in Logistics and Production, Vol. 3, No. 2, 2014.
- [4] Roodbergen, K.J., Vis, I.F.A. and Taylor, G.D.: Simultaneous determination of warehouse layout and control policies, International Journal of Production Research, Vol. 53, No. 11, pp. 3306–3326, 2014.
- [5] Rouwenhorst, B., Reuter, B., Stockrahm, V., van Houtum, G.J., Matel, R.J. and Zijm, W.H.M.: Warehouse design and control: Framework and literature review, European Journal of Operational Research, Vol. 122, pp. 515–533, 1999.
- [6] Abdoli, S., Kara, S.: A Review of Modelling Approaches for Conceptual Design of Complex Engineering Systems (CESSs), Proceedings of the 2017 IEEE IEEM, pp. 1266–1270, 2017.
- [7] Caridade, R., Pereira, T., Pinto Ferreira, L. and Silva, F.J.G.: Analysis and optimisation of a logistic warehouse in the automotive industry, Procedia Manufacturing, Vol. 13, pp. 1096–1103, 2017.
- [8] Kucharavy, D., Damand, D., Barth, M. and Derrouiche, R.: Collaborative Design of Warehousing 4.0 Using the Concept of Contradictions, 19th IFIP WG 5.5 Working Conference on Virtual Enterprises, pp. 396–405, 2018.
- [9] Thomas, L.M., Meller, R.D.: Analytical models for warehouse configuration, IIE Transactions, Vol. 46, No. 9, pp. 928–947, 2014.
- [10] McGinnis, L., Sprock, T.: Toward an Engineering Discipline of Warehouse Design, 14th IMHRC Proceedings, 2016.
- [11] Murrenhoff, A., McGinnis, L.F. and Sprock, T.: Toward a Tool Chain for Warehouse Design Decision Support, Proceedings of the 2015 Industrial and Systems Engineering Research Conference, 2015.
- [12] Staab, T., Günther, W.A.: *OptiMAL - Optimale Planung manueller Lagersysteme. Forschungsbericht zu dem IGF-Vorhaben der Forschungsstelle Lehrstuhl für Fördertechnik Materialfluss Logistik, Technische Universität München.*, Technische Universität München. Garching: Lehrstuhl für Fördertechnik Materialfluss Logistik Technische Universität München, 2016.
- [13] Dallari, F., Marchet, G. and Melacini, M.: Design of order picking system, Int J Adv Manuf Technol Vol. 42, No. 1-2, pp. 1–12, 2009.
- [14] Goetschalckx, M., McGinnis, L., Sharp, G., Bodner, D., Govindaraj, T. and Huang, K.: Development of a design methodology for warehousing systems, School of Industrial and Systems Engineering Georgia Institute of Technology, Atlanta, 2001.
- [15] Gu, J., Goetschalckx, M. and McGinnis, L.F.: Research on warehouse design and performance evaluation: A comprehensive review, European Journal of Operational Research, Vol. 203, No. 3, pp. 539–549, 2010.
- [16] Moran, S.: *Warehouse Storage. In: Process Plant Layout*, 2nd edition, Elsevier, pp. 179–186, 2017.
- [17] Boysen, N., De Koster, R.B.M. and Weidinger, F.: Warehousing in the e-commerce era: A survey, European Journal of Operational Research, Vol. 277, No. 2, pp. 396–411, 2018.
- [18] De Koster, R.B.M., Johnson, A.L.; Roy, D.: Warehouse design and management, International Journal of Production Research, Vol. 55, No. 21, pp. 6327–6330, 2017.
- [19] McGinnis, L.F.: An object oriented and axiomatic theory of warehouse design, 12th IMHRC Proceedings, 2012.
- [20] Kembro, J.H., Norrman, A., Eriksson, E.: Adapting warehouse operations and design to omni-channel logistics, Int Jnl Phys Dist & Log Manage, Vol. 48, No. 9, pp. 890–912, 2018.
- [21] Thomas, L.M., Meller, R.D.: Developing design guidelines for a case-picking warehouse, International Journal of Production Economics, Vol. 170, pp. 741–762, 2015.
- [22] Sprock, T., Murrenhoff, A. and McGinnis, L.F.: A hierarchical approach to warehouse design, International Journal of Production Research, Vol. 55, No. 21, pp. 6331–6343, 2016.
- [23] van Gils, T., Ramaekers, K., Caris, A. and De Koster, R.B.M.: Designing efficient order picking systems by combining planning problems. State-of-the-art classification and review, European Journal of Operational Research, Vol. 267, No. 1, pp. 1–15, 2018.
- [24] Gerales, C.A.S., Carvalho Sameiro, M. and Pereira, G.A.B.: A Warehouse Design Decision Model – Case Study, Engineering Management Conference, Piscataway, NJ, 2008.
- [25] Arnold, D.: *Intralogistik. Potentiale, Perspektiven, Prognosen*, Springer, Berlin, Heidelberg, 2006.
- [26] Azadeh, K., De Koster, R.B.M. and Roy, D.: Robotized Warehouse Systems: Developments and Research Opportunities, SSRN Electronic Journal, 2017.
- [27] Apple, J.M., Jr., Meller, R.D. and White, J.A., Jr.: Empirically-Based Warehouse Design: Can Academics Accept Such an Approach?, 11th IMHRC Proceedings, 2010.
- [28] Knödgen, P.: *Erstellung eines Werkzeugs zur Integration großer Datenmengen für die Lagerplanung*, Diplomarbeit, TU Wien, 2017.

Goran Dukic

Professor
University of Zagreb
Faculty of Mechanical Engineering and
Naval Architecture

Tihomir Opetuk

Assistant Professor
University of Zagreb
Faculty of Mechanical Engineering and
Naval Architecture

Hrvoje Cajner

Assistant Professor
University of Zagreb
Faculty of Mechanical Engineering and
Naval Architecture

Brigita Gajsek

Assistant Professor
University of Maribor
Faculty of Logistics

Influence of pick time distribution on expected throughput of dual-tray VLMs

The efficiency of an order-picking operation both in manufacturing and distribution environment can be enhanced with AS/RSs, which can provide an alternative picker-to-parts solution for small objects picking from small racks where the products are stocked in cartons, totes, boxes or on trays. One of them is Vertical Lift Module (VLM) in which insertion/extraction (I/E) device is traveling vertically and extracts trays or totes from the shelves and brings them to the operator putting it on pick shelf. While usual VLM systems have only one picking place, recently some producers of VLMs offer solution with two pick places, naming it dual-tray VLM or dual-bay VLM. To design order-picking systems with dual-tray VLM, analytical throughput model is developed. However, model assumes pick time by human operator either deterministic or exponentially distributed. So in this paper different pick time distributions are analysed using simulations and compared with analytical solutions.

Keywords: Vertical lift module systems, Throughput model, Order-picking, Pick time distribution.

1. INTRODUCTION

Automated storage and retrieval systems (AS/RS) have been widely used in manufacturing and warehousing/distribution environments for a more than half a century. Despite higher investments costs and less flexibility, the usage of AS/RSs provide several advantages over non-automated systems, like labour costs and floor space savings, increased reliability and better accuracy [1]. Those advantages create benefits of using AS/RSs both for storage and order-picking operations in warehouses. Order-picking process is the most laborious and the costliest activity in a typical warehouse. With up to 55% of warehouse total operating costs [2], it is obvious why many companies are improving their order picking operations by using more efficient systems. In the case of a traditional low-level picker-to-parts warehouse, the items to be picked are positioned on the lower stocking locations of the shelves. The pickers usually use electric pallet trucks to move along the aisles and to transport one or more mixed pallets, composed of the items collected during their order picking activity [3]. Since in those cases traveling amounts for around 50% of total picking time [2], the logical way of improving it is to reduce or eliminate unproductive walking time.

The efficiency of an order-picking operation both in manufacturing and distribution environment can be enhanced with AS/RSs, which can provide an alternative picker-to-parts solution for small objects picking from small racks where the products are stocked in cartons, totes, boxes or on trays. Also called dynamic solutions, such systems as vertical carousels, horizontal

carousels, vertical lift modules, mini-load AS/RS systems, A-frames and picking machines, as well as the robots that have been recently employed, can assure higher space utilization and reduced travel distances [4]. In the focus of this paper is Vertical Lift Module (VLM), illustrated in Figure 1, in which insertion/extraction (I/E) device is traveling vertically and extracts trays or totes from the shelves and brings them to the operator putting it on pick shelf (or pick window) [5,6].

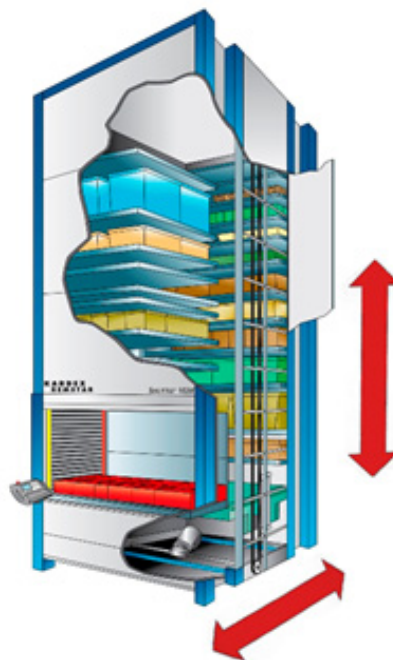


Figure 1. Vertical Lift Module (VLM) with motion directions of I/E device

Usual VLM systems have only one picking place, however recently some producers of VLMs offer solution with two pick places, naming it dual-tray VLM or dual-bay VLM. With the appearance of dual-tray

Correspondence to: Dr Goran Dukic, professor
Faculty of Mechanical Engineering and Naval Architecture,
Ivana Lucica 5, 10000 Zagreb, Croatia
E-mail: goran.dukic@fsb.hr

VLM, logical consequence was to develop throughput model for it, as an aid to warehouse designers and managers in determination of expected throughput. Such model was developed in [7]. However, developed analytical model assumes pick time by human operator either deterministic or exponentially distributed. It is unlikely that pick time in practice will be exactly deterministic or stochastic with exponential distribution, more likely it will follow some other theoretical distribution or adequate empirical distribution.

Analytical throughput model for dual-tray VLM with human picker is shortly presented in next section. Developed simulation model used to simulate closed-loop system with VLM extractor and human picker as servers is presented in section 3, together with the results obtained by applying various distributions of service time of pickers. Last section gives conclusions.

2. ANALYTICAL THROUGHPUT MODEL FOR DUAL-TRAY VLM WITH HUMAN PICKER

While literature addressed models to design most types of AS/RSs, dual-tray VLMs are still relatively new in this arena. Not many papers deal with the VLM systems although they are in use in practice since early 1970's, both in warehouse and manufacturing applications. The most important paper that presented throughput model for single-tray VLM with human order-picker is [8].

Based on that model and models of mini-load AS/RS [9, 10], the throughput model for dual-tray VLM is presented in [7]. This model assumes single VLM device with one crane and two pick places (for two trays in VLM's window), one above another, as illustrated schematically in Figure 2.

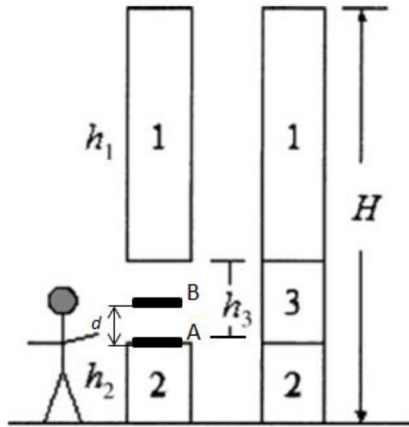


Figure 2. Side view of dual-tray VLM with typical sections, taken from [7]

While human picker is picking item(s) from one tray, I/E crane of VLM is able to store previous tray and retrieve next tray. Storage and retrieval of trays is done by I/E crane doing dual commands, alternatively from lower and upper pick position. The throughput model is based on cycle of the system. I/E device is doing dual command cycles (storing previous tray and delivering next one in one such cycle), while expected dual command cycle time could be calculated as average of two expected dual command time based on models from [8] (for more details please refer to the [7]).

With the similarity of dual-tray VLM operating characteristics and mini-load AS/RS operating characteristics, the same idea for used to develop throughput model. Due to complex form of the probability distribution for dual command cycles, storage/retrieval travel time was approximated with a uniform distribution. Limits of uniform distribution of expected dual command travel time depend on expected dual command travel time $E(DC)$ and its standard deviation $S(DC)$ (which is presented as the fraction of dual command travel time and could be approximated as $S(DC) \approx 0.383 E(DC)$). So the limits of uniform distribution of dual command cycle time are

$$\begin{aligned} t_1 &= E(DC) - 1.7321 \cdot S(DC) + C \\ t_2 &= E(DC) + 1.7321 \cdot S(DC) + C \end{aligned} \quad (1)$$

where C is constant tray handling time per dual command cycle. C consists of four times to pickup and deposit a tray (two pickups and two deposits) and four times to accelerate and decelerate.

Pick time was assumed either deterministic or exponentially distributed. If the pick time per delivered tray p_T is deterministic, expected system cycle time is

$$E(CT) = \begin{cases} E(DC) + C & \text{for } 0 < p_T \leq t_1 \\ \frac{p_T^2 - 2p_T t_1 + t_2^2}{2(t_2 - t_1)} & \text{for } t_1 < p_T \leq t_2 \\ p_T & \text{for } t_2 < p_T \end{cases} \quad (2)$$

while in case pick time is exponentially distributed, expected system cycle time is

$$E(CT) = E(DC) + C + \frac{p_T^2}{t_2 - t_1} [\exp(-t_1 / p_T) - \exp(-t_2 / p_T)] \quad (3)$$

From the calculated expected system cycle time one can calculate expected picker's utilization $E(PU)$ and system's throughput R_T as

$$E(PU) = p_T / E(CT) \quad (4)$$

$$R_T = 3600 / E(CT) \quad \text{or} \quad R_T = 3600 \cdot E(PU) / p_T \quad (5)$$

Accuracy of analytical model was tested using comparison with results obtained by simulation models, confirming proposed model satisfactory accurate for estimating throughput of system with single dual-tray VLM and human order-picker.

Apart from papers presenting above mentioned models, only few more papers are dealing with VLMs. In [11] simulation-based approach to estimate the performance of single-bay VLM is presented for various configurations. In [12] authors focus on order batching optimization, considering single-tray VLM but with assumed constant pick time and constant storage/retrieval time. In [13] authors are considering dual-tray VLM order picking system under different configurations. Unlike in previous models with assumed random storage policy, they are considering different storage policies and retrieval sequencing policies. The

same authors in [14] compare dual-bay VLM to a carton racks warehouse. Those two storage solutions are analysed from an economic and a performance point of view.

3. SIMULATION MODEL FOR DUAL-TRAY VLM WITH HUMAN PICKER AND RESULTS

Simulation model was build in Enterprise Dynamics 10.2 simulation software. It is simulation software tool for 2D and 3D simulation modelling of discrete-event simulations using so-called atoms as entities. In this case system with dual-tray VLM and human picker was modelled as closed, two server cycling system with trays as customers, circulating in the loop and served alternately by the human picker and VLM's I/E device. Model with its entities and connections is shown in Figure 3.

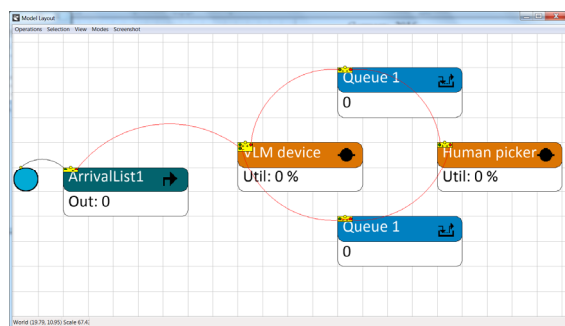


Figure 3. Simulation model of dual-tray VLM with human picker

VLM device and Human picker are server entities representing the system. Two “customers” (entities *Product* created at the start) are circulating in the loop between servers. Two queue entities are representing both A and B places of trays, where either delivered tray is waiting on human picker (*Queue 1*) or another tray is waiting on I/E device (*Queue 2*) to be taken back into shelving position.

Important attributes of servers are cycle times (service times), being uniform distribution of expected dual command cycle time of VLM device (therefore “customer” being served by this server represent actually two trays – one being taken back to the shelf and another being retrieved from the shelf and delivered to the pick window) and selected distribution of expected pick time per tray of Human picker. Capacity of queues is set to one. Utilisation of the server Human picker corresponds to the expected picker’s utilization $E(PU)$ from Eq. (4), which value is then simply used to calculate expected system cycle time and corresponding system’s throughput using Eq. (5).

Simulation model was verified using deterministic service times and observations in real-time using software’s animation, while validated comparing results for deterministic and exponentially distributed pick times for known configurations presented in [7]. Those configurations are with 4 different heights of VLM device (H in mm), 3 different speeds of I/E device (v in cm/s) and three different average pick times per tray for each configuration (p_T in s). Values of pick time are corresponding to the lower limit, upper limit and average value of uniformly distributed dual command

cycle of VLM. Constant C was set to 24 seconds. Calculated expected dual command cycle times used to determine uniformly distributed cycle time of VLM device are given in Table 1.

Table 1. Analytical results for dual-tray VLM expected dual command cycle times, $E(DC) + C$, (in seconds)

H [mm]	$v=50$ cm/s	$v=100$ cm/s	$v=150$ cm/s
4500	33.88	28.94	27.29
6000	37.64	30.82	28.55
7500	41.50	32.75	29.83
9000	45.40	34.70	31.13

Average service time of Human picker was selected from the Table 2 and used with different distributions for the purposes of validation and analysis.

Analysis of different pick time distributions on expected dual-tray VLM throughput was done with arbitrary chosen two uniform distribution of pick time (one with small and one with large range) and 3 normal distributions (with small, medium and large standard deviation).

Results are presented in Table 3 only for the case of VLM with $H=7500$ mm due to the clarity of the presentation, while results for other VLM heights are quite similar in terms of conclusions.

4. CONCLUSION

In this paper different distributions of pick time in dual-tray VLM with human order-picker were analyzed, in order to see influence of different distributions (and deviations) on resulting throughput, in the same time compared to the previously available analytical solutions for deterministic and exponentially distributed pick times only.

Simulation analysis showed that expected system cycle time (therefore resulting throughput) depends on the pick time distribution. Results for distributions with smaller deviations are closer to the analytical deterministic solutions, while distributions with larger deviations are getting closer to the analytical exponential distribution. This was of course expected, however one should be aware of real practice pick time distribution and it’s influence on the resulting throughput.

Simulation results presented here contribute to the understanding and design of order-picking with dual-tray VLM systems in practice. In the further research more empirical distributions (possibly taken from practice) will be tested.

REFERENCES

- [1] Roodbergen, K.J., Iris, F.A.V.: A survey of literature on automated storage and retrieval systems, *European Journal of Operational Research*, Vol. 194, pp. 343-362, 2009.
- [2] Tompkins, J.A., White, J.A., Bozer, Y.A., Frazelle, E.H., Tanchoco, J.M.A. and Trevino, J.: *Facilities Planning*, 2nd ed. John Wiley & Sons, Inc., 1996.

- [3] Battini, D., Calzavara, M., Persona, A. and Sgarbossa, F.: A method to choose between carton from rack picking or carton from pallet picking, *Computers & Industrial Engineering*, Vol. 126, pp. 88-98, 2018.
- [4] Battini, D., Calzavara, M., Persona, A. and Sgarbossa, F.: Dual-tray Vertical Lift Modules for Fast Order Picking, 14th IMHRC Proceedings, Karlsruhe, Germany, 2016.
- [5] Romaine, E.: *Dynamic Storage Systems, The Essentials of Material Handling: part 2 –The Basic Product Knowledge Program*, Material Handling Industry of America, Charlotte, North Carolina, 2004.
- [6] Romaine, E.: *Vertical Lift Modules and Carousels AS/RS Systems & Material Handling Equipment Helps Translate Productivity into Prosperity*, 2011.
- [7] Dukic, G., Opetuk, T. and Lerher, T.: A throughput model for a dual-tray Vertical Lift Module with a human order-picker, *International Journal of Production Economics*, Vol. 170, pp. 874-881, 2015.
- [8] Meller, R.D., Klote, J.F.: A throughput model for carousel/VLM pods, *IIE Transactions*, Vol. 36, pp. 725-741, 2004.
- [9] Bozer, Y.A., White, J.A.: Travel-time models for automated storage/retrieval systems, *IIE Transactions*, Vol. 16, No. 4, pp. 329-338, 1984.
- [10] Bozer Y.A., White J.A.: Design and performance models for end-of-aisle order pick-ing systems, *Management Science*, Vol. 36, No. 7, pp. 852-866, 1990.
- [11] Rosi, B., Grasic, L., Dukic, G., Opetuk, T. and Lerher, T.: Simulation-based performance analysis of automated single-tray vertical lift module, *International journal of simulation modelling*, Vol. 15, No. 1, pp. 97-108, 2016.
- [12] Lenoble, N., Frein, Y. and Hammami, R.: Order batching in an automated warehouse with several vertical lift modules: Optimization and experiments with real data, *European Journal of Operational Research*, Vol. 267, No. 3, pp. 958-976, 2018.
- [13] Sgarbossa, F., Calzavara, M. and Persona, A.: Throughput models for a dual-bay VLM order picking system under different configurations, *Industrial Management & Data Systems*, Vol. 119 No. 6, pp. 1268-1288, 2019.
- [14] Calzavara, M., Sgarbossa, F. and Persona, A.: Vertical Lift Modules for small items order picking: an economic evaluation, *International Journal of Production Economics*, Vol. 210, pp. 199-210, 2019.

Table 2. Average pick time per delivered tray for various tested VLM configurations (in seconds)

H [mm]	v [cm/s]								
	50			100			150		
	p_{T1}	p_{T2}	p_{T3}	p_{T1}	p_{T2}	p_{T3}	p_{T1}	p_{T2}	p_{T3}
4500	27	34	41	25	29	33	25	27.5	30
6000	28	37.5	47	26	31	36	25	28.5	32
7500	29	41.5	54	26	32.5	39	25	29.5	34
9000	31	45.5	60	27	34.5	42	26	31	36

Table 3. Average system cycle times by simulation model and analytical model for different distributions of pick time per tray (in seconds)

H [mm]	Pick time distribution	v [cm/s]								
		50			100			150		
		$E(CT)_1$	$E(CT)_2$	$E(CT)_3$	$E(CT)_1$	$E(CT)_2$	$E(CT)_3$	$E(CT)_1$	$E(CT)_2$	$E(CT)_3$
7500	Deterministic, analytical	41.50	44.40	54.00	32.75	34.08	39.00	29.83	30.64	34.00
	Deterministic, simulation	41.49	44.39	54.00	32.75	34.10	39.00	29.83	30.63	34.00
	Uniform (0.75 pT , 1.25 pT)	43.74	48.71	56.60	32.91	35.02	39.59	30.08	31.69	34.69
	Uniform (0.25 pT , 1.75 pT)	44.96	51.30	60.40	34.99	38.83	43.62	32.51	35.24	38.51
	Normal (pT , 0.1 pT)	43.61	48.54	56.31	32.83	34.54	39.27	29.94	31.15	34.31
	Normal (pT , 0.5 pT)	45.17	51.81	61.02	35.28	39.11	43.97	32.72	35.46	38.77
	Normal (pT , pT)	45.60	54.75	65.30	37.09	42.15	47.74	34.72	37.87	42.08
	Exponential, simulation	48.66	56.93	66.75	40.19	44.64	49.48	37.43	40.58	43.98
	Exponential, analytical	48.62	56.96	66.73	40.19	44.68	49.65	37.44	40.60	44.00

Automated Storage and Retrieval Systems as Lightweight Design

Martin Egger

Professor
Upper Austria University of Applied
Sciences
Department Mechanical Engineering

Karl Angleitner

CEO
Angleitner Entwicklungsdienstleistungen

Wolfgang Steiner

Professor
Upper Austria University of Applied
Sciences
Department Mechanical Engineering

Current Automated Storage and Retrieval Systems (ASRS) use heavy designs. Usually 90% is dead weight, the payload is only about 10%. The shape of the structure as well as material used influence strongly the total weight. A mechanical model of a single mast stacker crane allows to investigate, to value and to compare the varieties of designs for this important machine type. The different designs lead to different dimensions, load situations and hence to different material input and further to different dead weights. Mechanical stresses in the relevant components, mass and space requirement are used as valuation measures. An optimized design in form of a self-supporting mast, where the bottom carriage can be reduced to a minimum can be identified. Strain gauge and acceleration measurements confirm the mechanical model and its underlying assumptions. Furthermore the measurements capture the driving dynamics of the optimized vehicle. Both, driving dynamics, and safety go hand in hand with lightweight construction.

Keywords: storage and retrieval system, lightweight construction, weight reduction, jerk, vibrations.

1. INTRODUCTION

Current Automated Storage and Retrieval Systems (ASRS) use heavy designs. Usually 90% is dead weight; the payload is only about 10%. This strategy of a robust design has certain disadvantages such as high material- and manufacturing costs. High operating costs and poor driving dynamics result from the high mass of the structure. It is assumed, that the reduction of the amount of materials will improve the reliability and the overall safety too.

The shape of the structure as well as material used influence strongly the total weight. In this article the very popular type of the single mast stacker crane is investigated. A variety of designs is principally possible. Single-mast cranes are designed for storing small items, for bigger and heavier parts double-mast cranes are used. Lifting heights up to 46 meters are possible [1].

Figure 1 shows the components of a single mast stacker crane [2]. The entire unit moves horizontally within an aisle, while the load handling device is able to elevate up the mast to the necessary height to reach the load, and can extend and retract to store or retrieve loads. The electric drives accelerate the bottom carriage up to 4m/s^2 and subject the individual parts of a vehicle to high stress. [3], [4] and [5] give calculation rules taking into account overstraining of materials beyond the elastic limit, overstraining of structure beyond the critical buckling stresses as well as overstraining of material beyond the fatigue strength.

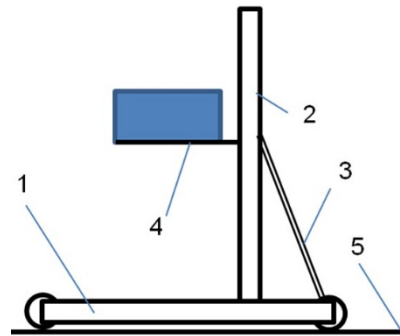


Figure 1. Components of a single mast crane: 1: Bottom Carriage, 2 Mast, 3 Supporting Rod, 4 Load Handling Device, 5 Bottom Travel Rail

2. TOPOLOGY OF SINGLE MAST STACKER CRANES

Three different design types of single mast stacker cranes can be distinguished.

2.1 Type 1: Free standing Mast

A typical design is to apply a free standing mast as a profile construction with large cross sectional area to gain the torsional and flexural rigidity as depicted in Figure 2. There are no additional elements to stabilize the mast. The restraining torque has to be transmitted through the bottom carriage to the wheels. In addition to a robust and heavy mast an equally strong and heavy bottom carriage is necessary to clamp the mast and to withstand the high loads induced by this construction type.

2.2 Type 2: Guyed Mast

To reduce the weight of the mast and to increase stability guys are used. To realize a short length l of the stacker crane supporting rods instead of cables are used,

Correspondence to: Professor Dr. Martin Egger
Upper Austria University of Applied Sciences,
Stelzhamerstraße 23, 4600 Wels, Austria
E-mail: martin.egger@fh-wels.at

figure 3. Supporting rods are able to transmit both tensile and compression forces whereas cables can transmit tensile stresses only. But long rods are themselves subject to instability and overstraining beyond the critical buckling stresses has to be taken into account! Due to the the supporting rod, one fraction of the load is transmitted directly from the mast to the back wheel of the bottom carriage. Hence, both the mast and the bottom carriage are relieved that means that significantly lighter construction is possible.

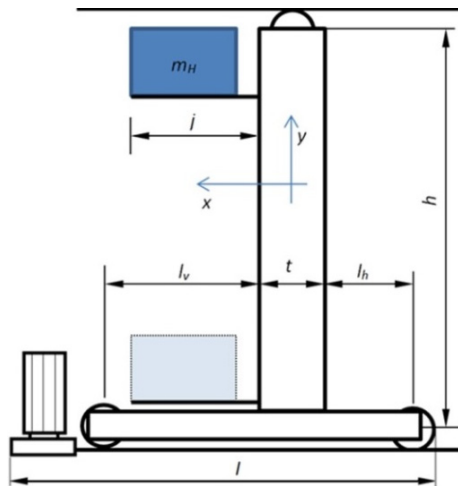


Figure 2. Type 1: Free standing Mast

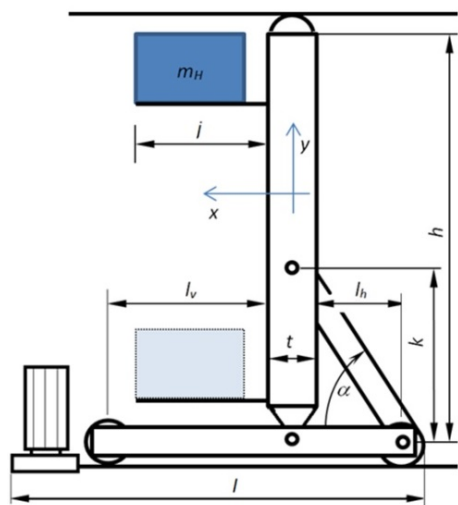


Figure 3. Type 2: Guyed Mast

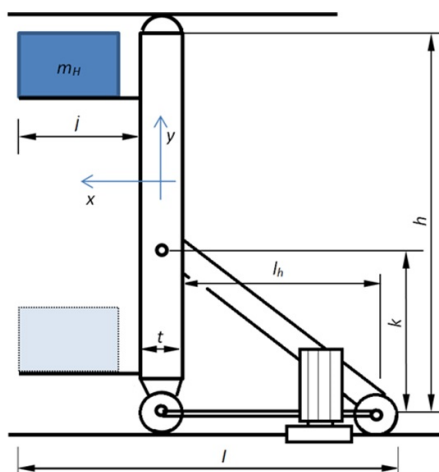


Figure 4. Type 3: Self-Supporting Mast

By uncompromisingly implementing the strategy of a guyed mast the bottom carriage can be reduced to a minimum, figure 4. The mast is positioned directly above the front wheel of the bottom carriage. The mast itself has the compressive strength to support the weight (y-direction), but does not have the flexural strength to stand unsupported. It requires long supporting rods to resist inertial forces induced by acceleration (x-direction) as well as lateral forces (z-direction) from the load handling device due to the retrieval process. The supporting rods keep the mast upright. The whole design is something like a truss. A triangular unit constructed with three members mast, supporting rod and bottom carriage that create a rigid structure. Assuming straight members and assuming that only the main loads due to the payload and acceleration are taken into account, structural components can be considered where force is applied to only two points that means that bending moments can be excluded, in particular for the bottom carriage. The carriage can be designed as a simple and lightweight tensile rod. Compared to other designs the load handling device is outside the wheels where the drive unit can be positioned between the wheels which results in an optimized wheel base.

3. MECHANICAL MODEL

A mechanical model of the single mast stacker crane is developed to calculate mechanical stresses, factoring in compression, bending and buckling. The guyed mast design according to figure 3 represents the general design of single mast stacker crane which covers the two special cases, free standing mast where $k=0$, as well as the self-supporting mast where $l_v=-0,5 \cdot t$. Assuming that a certain stress limit must not be exceeded, the mechanical model yields the dimensions of the components used and hence the performance characteristics, like the total weight of each type can be calculated. The calculations are based on the geometrical and mechanical parameters given in table 1. Table 2 shows interesting calculation results and presents a comparison between the three design types.

Table 1. Fixed parameters for the comparison between the three design types

Acceleration SRS a [m/s ²]	Mass of load m_H [kg]	Height of mast h [m]	total Length of SRS l [mm]	Length of lever arm j [mm]
4	475	11,5	3000	750

Table 2: Performance characteristics of the different construction designs: Type 1: Freestanding Mast, Type 2: Guyed Mast, Type 3: Self-Supporting Mast

	Type 1	Type 2	Type 3
Length of the front l_v [mm]	1150	1150	-98
Length of the back l_h [mm]	500	805	1655
Height of the connection k [mm]	0	9000	9000
Stress mast σ_M [N/mm ²]	50	48	48
Stress bottom carriage σ_F [N/mm ²]	50	50	49
Stress supporting rod σ_S [N/mm ²]	0	18	14
Wheel load A [kN]	27	22	28
Total weight of the SRS m [kg]	2300	1970	1610

According to table 3 a weight reduction of 30% can be expected from the lightweight construction type 3,

Self-Supporting Mast. Figure 5 shows a quite detailed assembly of the vehicle.



Figure 5. Type 3: Self-Supporting Mast

4. DYNAMIC OSCILLATION COEFFICIENTS

Acceleration acting on an elastically deformable structure will affect a deformation which depends on its mass distribution, stiffness and the acceleration applied. Due to the high mast its flexural stiffness is quite low. Depending on the machine type, the position of the lifting carriage and the applied acceleration the mast will be bended opposed to the direction of acceleration, see figure 6. But not only the amount of acceleration a is of interest, also its rate of change, the jerk j , plays an important role.

$$j = \frac{da}{dt} \quad (1)$$

If the change in acceleration is slow, the jerk j is small, and the propagation of this deformation through the body may be considered instantaneously. It is a discontinuity of the acceleration which causes vibrations. Since vibrations significantly impair the quality of transportation, there is good reason to simply minimize jerk in vehicles. Figure 6 and 7 show the influence of the jerk j to the propagation of acceleration through the structure. In the shown example a maximum acceleration of 4m/s^2 is applied to the bottom carriage. In this example the jerk can easily be calculated as the ratio between the applied acceleration a_b and the rise time ta of the acceleration:

$$j = \frac{\text{MAX}(a_b)}{ta} \quad (2)$$

A simple spring-mass-model is used to calculate the acceleration in the top carriage as a function of the jerk. The mechanical behaviour (eigenfrequency, damping) of the real stacker crane according to figure 5 has been measured (figure 9) by accelerometers. A high jerk (acceleration bottom carriage a_b , graph_3 and the amplified acceleration top carriage a_t , graph_4: $j=40\text{m/s}^3$) causes double acceleration in the top carriage. A moderate jerk does not cause a significant amplification of acceleration due to wave propagation (acceleration bottom carriage a_b , graph_1 and acceleration top carriage a_t , graph_2: $j=8\text{m/s}^3$).

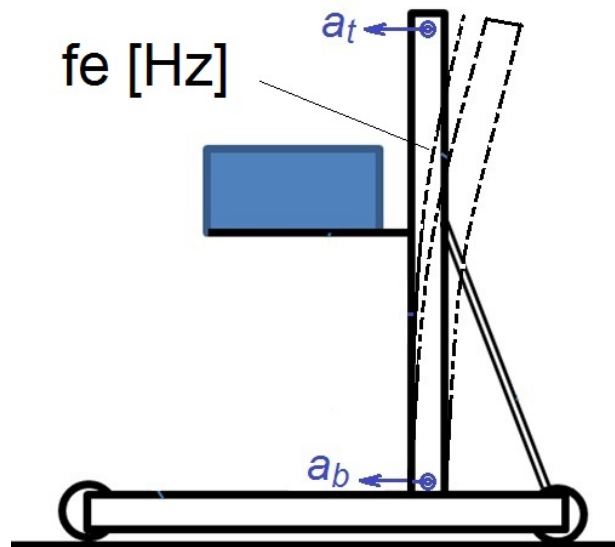


Figure 6. Propagation of deformation through the structure of an SRS, where fe is the first eigenfrequency of the mast, a_b : acceleration bottom carriage, a_t : acceleration top carriage

The amplification of acceleration due to wave propagation through the structure depends on both, the jerk j and the eigenfrequency fe . A dimensionless parameter can be found as relationship between the jerk, the eigenfrequency of the structure and the applied acceleration at the bottom carriage a_b . η can be considered as a frequency rate, the ratio of the applied acceleration frequency over the undamped natural frequency.

$$\eta = \frac{j}{fe \cdot a_b} = \frac{1}{fe \cdot ta} \quad (3)$$

The oscillation coefficient S_w [2] is defined as acceleration bottom carriage a_b caused by the drive units divided by acceleration top carriage a_t due to oscillations caused by travel motions.

$$S_w = \frac{MAX(a_t)}{MAX(a_b)} \quad (4)$$

Figure 8 shows the relation between oscillation coefficient S_w and the frequency rate η according to equation (5).

$$S_w(\eta) = \frac{\eta}{2 \cdot \pi} \cdot \sqrt{2 - 2 \cdot \cos\left(\frac{2 \cdot \pi}{\eta}\right)} \quad (5)$$

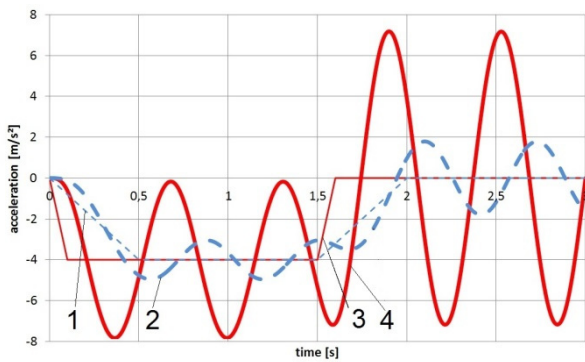


Figure 7. Simulation results based on a simple spring-mass-model, $fe=1,45\text{Hz}$: Influence of the jerk to the vehicles driving dynamics: 1. acceleration bottom carriage a_b , $j=8\text{m/s}^3$ 2. acceleration top carriage a_t , $j=8\text{ m/s}^3$ 3. acceleration bottom carriage a_b , $j=40\text{ m/s}^3$ 4. acceleration top carriage a_t , $j=40\text{ m/s}^3$

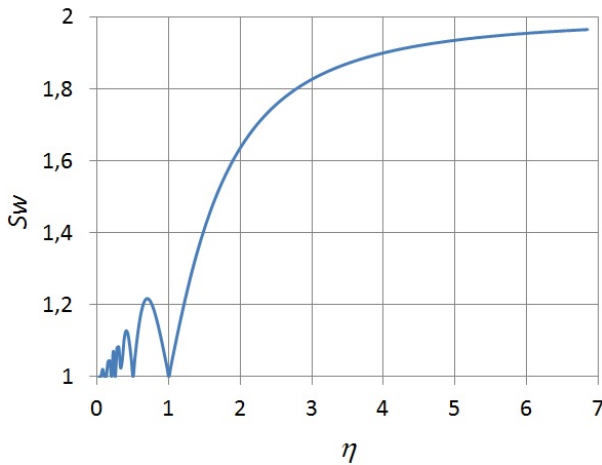


Figure 8. Amplification of acceleration due to wave propagation

The analysis according to [2] takes into account the drive forces but also the vibrations of the stacker cranes themselves.

$$a_t(t) = a_b \cdot (\cos(\omega \cdot t) - 1) \quad (6)$$

Stress reaches its maximum if the parenthesized expression assumes the value (-2) hence the oscillation coefficient $S_{w,max} = 2$ must be used for calculations [2]. Obviously an infinite jerk is assumed.

5. MEASUREMENT RESULTS

Measurements of acceleration in the bottom carriage a_b as well as in the top carriage a_t according to figure 6 yield the dynamic behavior of the structure. Eigenfrequency fe and damping behavior are the quantities of interest. The measurement results of figure 9 show a very good accordance with the simulation results of figure 7 which are based on a simple spring-mass-model where damping has still been neglected.

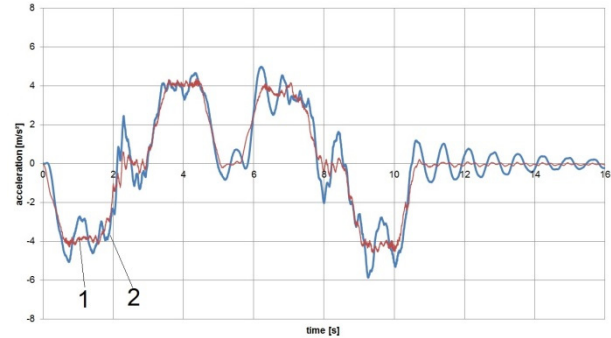


Figure 9. Measurement Results: 1. acceleration bottom carriage a_b , $j=8\text{ m/s}^3$ 2. acceleration top carriage a_t , $j=8\text{ m/s}^3$

6. CONCLUSION

An optimized design in form of a self-supporting mast, where the bottom carriage can be reduced to a minimum can be identified by the mechanical model of a single mast stacker crane. A weight reduction of 30% can be expected according to the model. The reduction of the cross section of main components opens additional production technologies which furthermore reduces weight. The high mast is object to low damped vibrations. The amplification of acceleration due to wave propagation through the structure depends on both, the jerk j and the eigenfrequency fe and it is limited to the factor 2. It can be stated that both, driving dynamics, and safety go hand in hand with lightweight construction.

REFERENCES

- [1] Scheffler, M., Feyrer, K. and Matthias, K.: *Fördertechnik und Baumaschinen*, Vieweg 1997.
- [2] FEM 9.001: Terminologie / Wörterbuch Regalbediengeräte, 1997.
- [3] FEM 9.311: Rules for the Design of Storage and Retrieval Machines, Structures, 1978.
- [4] FEM 9.831: Berechnungsgrundlagen für RBG im HRL-Bereich: Toleranzen, Verformungen, Freimaße im Hochregallager, 1995.
- [5] DIN EN 13001-3-1: Krane - Konstruktion allgemein, Teil 3-1: Grenzzustände und Sicherheitsnachweis von Stahltragwerken, 2015.

Ola Hassan

Teaching Assistant
Alexandria University
Faculty of Engineering
Transportation Department

M. Hamdy Elwany

Professor
Alexandria University
Faculty of Engineering
Production Engineering Department

M. El Naggar

Professor
Alexandria University
Faculty of Engineering
Transportation Department

Adel M. Fahiem

Assistant Professor
Alexandria University
Faculty of Engineering
Transportation Department

Modelling of Highly Congested Container Terminals

As a result of the increase in container transport rates, container terminals suffer from congestion. Congestion features appear in different forms; e.g. ships waiting for a berth, operation disruption in storage yard and truck queues at gates. The paper proposes a conceptual framework for developing the logistics system at the strategic level. Based on real statistical data and field surveys, a comprehensive analysis is carried out using logical and probabilistic models to identify the source of terminal congestion, predict efficiency performance indicators and compare them with international recommendations. Sensitivity analysis is also conducted to investigate relationships between resources and factors affecting performance indicators. A goal-oriented process is prepared to formulate and evaluate scenario options, exploring whether it is necessary to expand the terminal, a new terminal is needed, or just to update its infrastructure and operation systems. The methodology is applied to a container terminal at Alexandria Port, Egypt.

Keywords: Container Terminal, Congestion, Capacities, Performance Indicators, Logistics Centre.

1. INTRODUCTION

The capacity of a container terminal with its specific resources should, normally, match the throughput; however, sometimes there is excess in the terminal capacity, while in other cases there is a shortage, causing congestion. As a result of the continuous rapid increase in rates of containerization, a lot of container terminals suffer from congestions with significant delays.

Congestion occurs generally when the throughput exceeds the terminal design capacity. Congestion may also be a result of limited internal road area, causing bottlenecks due to dense use of trucks, handling equipment and random stacking of containers on the ground. Furthermore, customs inspection and security checks may obstruct a smooth flow of containers through the terminal. Congestion features appear in various forms: ships waiting in queues in anchorage area, a ship waiting at berth for assigning cranes, operation disruption due to delays of transfer vehicles, and interruption in the storage yard. In addition, congestion can be observed on internal roads, at the gates, and even around its boundary, in the form of truck queues.

Congestion has unpleasant consequences on terminal productivity, efficiency, on shipping and inland transport companies as well as importers and exporters. The consumption of additional fuel in these queues leads to significant increase of greenhouse gases. Otherwise, ship delays in a terminal may have a direct impact on the schedule of ships, and accordingly, on the operation programs in other ports [1].

A container terminal is a multi-dimensional logistics system with several interrelated subsystems managing the bi-directional flow of export and import containers between waterside and landside. These subsystems (berths, QCs, storage yard, and gates) interact to move containers delivered by ships inland as well as export containers transported by trucks and rail onto ships.

2. CONCEPTUAL FRAMEWORK

Improving the situations in a congested terminal can be achieved in physical and operative planning tasks. The constraints can follow an imbalance between supply and demand, and when there are differences between capacities of the terminal subsystems. To face these challenges and extend terminal productivity with appropriate service quality, a methodology is proposed. The sequence of its steps is arranged in the following conceptual framework (Figure 1):

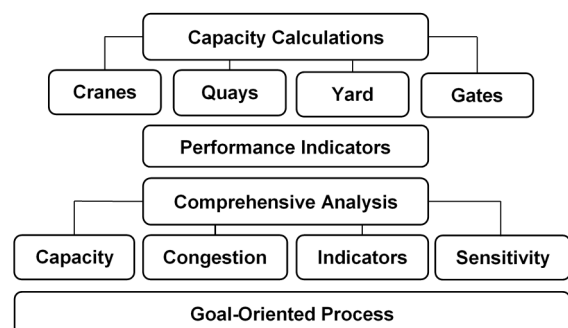


Figure 1. Conceptual framework

(a) calculating the capacity of terminal subsystems related to their influencing factors, (b) identifying and evaluating the operational performance indicators that reflect the efficiency of use of the resources, (c) comprehensive analysis of the subsystems capacities, congestion phenomena and sensitivity analysis of

Correspondence to: Ola Hassan, teaching assistant
Alexandria University, Faculty of Engineering,
Transportation Department ,
Lotfy El-Sied st. off: Gamal Abd El-Nasir, Alexandria
Governorate 11432, Egypt
E-mail: olahassans@gmail.com

operational performance indicators, and (d) preparing a goal-oriented process in a hierarchical structure.

3. TERMINAL CAPACITY ASSESSMENT

The container terminal design capacity can be defined as the maximum number of TEUs that can be handled over a time period without experiencing bottlenecks.

However, the terminal capacity has no rigid value. It is very sensitive to the management strategies and the human resources (experiences and qualifications of the operating team). In addition, technical equipment over the course of time will no longer be able to operate at its designed capacity. Thus, the terminal actual capacity is the maximum number of TEUs produced per time taking into consideration the real efficiency of the resources, and the idle time due to weather conditions, holidays and equipment maintenance.

The berth capacity represents the annual capacity of the mooring quay (TEUs/year). It can be calculated based on the number of berth places on the quay, average annual berth occupancy ratio as a proportion of mooring times of all ships to the total times during their existence in the terminal, average annual downtime days, daily operating hours and average annual productivity of ship at berth over a year in TEUs per hour. The number of berth places depends on the mooring quay length, as well as ship's length and a safety clearance between ships [2].

The gantry quay cranes capacity is defined by the operation potential of a set of cranes equipped on container quay. The annual capacity of QCs in TEUs per year is determined taking into consideration the depending factors; i.e. the number of container cranes, the capacity of a crane multiplied by an efficiency coefficient (obtained from field observations), and crane utilization (average crane service time divided by daily terminal operating time).

The storage yard capacity can be computed according to the number of TEU slots, average stacking height of containers per slot, average dwell time of containers in the storage yard in days, and percent of the yard utilization. This time is the duration for which a container stays between delivery and dispatch in the terminal for service. It depends on the type of container (import, export, or transit).

One of the main terminal resources is the gates. The traffic capacity of a gate (trucks/year) can be determined by dividing the operating time on the average service time at the gate. Disruption often occurs as a direct result of insufficient number of gates and/or increasing service time, arrival with improper documents. However, increasing gates capacity can lead to a low utilization level of the gate system in non-peak periods. In addition, enough lands in a container terminal for additional gates are often not possible [3].

4. PERFORMANCE INDICATORS

The terminal should expect rapid growth in container flow and at the same time increase competitiveness among other terminals. Thus, the interest of terminal management is to achieve competitive fares with proper productivity, efficiency and service quality. Reliable

performance indicators (EPIs) should be sensibly formulated to reflect the effectiveness of asset use [4]. The indicators are classified in categories; i.e. productivity, utilization and level of service.

The productivity-oriented indicators include: (a) terminal area productivity (TEUs/m² of terminal land). It detects the efficiency of the terminal area to achieve proper productivity, (b) berth productivity (TEUs/berth length). It indicates capability of allocated cranes for loading/unloading, combined with service time and idle time, and (d) quay crane productivity (TEUs/hour) that affects handling rates and ship turnaround time. In addition, terminal annual throughput (TEUs/time) is also a useful measure for official purposes to observe variations of throughput and analyse their causes.

Utilization indicators expressed in percentage form can identify the intensity level of using a resource of the terminal over a time period. High utilization is a sign of congestion, while low occupancy denotes under-utilisation of resources. Yard utilization identifies the severity of congestion, the yard begins with congestion by more than 70% utilization, and it is considered highly congested with significant delays by 80% [2].

Quality standards of a terminal refer to customer satisfaction with the level of services provided. Service quality indicators are related to the fast processing of transport modes and containers. For shipping lines, the indicators widely used are ship productivity at berth and ship turnaround time expressed as the relative waiting time ϵ between waiting time in anchor area and berth time. For inland transport, the most significant indicator is the truck turnover, while reducing container dwell time is important for cargo owner.

5. COMPREHENSIVE ANALYSIS

5.1 Capacity analysis

A comparison of the capacity of each terminal subsystem separately can enable identifying source of capacity deficiency and detecting the congestion spots. The advantage is multi-dimensional, the most important of which, it is a flexible mechanism for defining the highest realistic value of the terminal capacity as a whole and examining whether there is still available excess capacity in some subsystems not been fully used.

Moreover, the scope of conceivable actions needed to meet expected container flow can be decided; e.g. the comparison starts with the storage yard, if its capacity exceeds the capacity of both quay cranes and berths, it can attract more container traffic [5]. Conversely, it is necessary to investigate the plausible possibilities for expanding the storage capability.

5.2 Congestion analysis

Queuing theory is an important tool to investigate queuing performance [6], based on a statistical analysis of real data. It can be employed to describe the congestion phenomena that might occur in a container terminal in terms of queuing length, waiting time and traffic intensity. The objective of the application is not only to

determine the performance characteristics of a system but also to define different options to ease congestions.

The analysis investigates the relation between two probability distributions; the customer arrival rate λ (ship/truck) and service time μ with several servers (berths/gates). It should be subjected to the following assumption: arrival and service times follow the pattern of random occurrences and the operation is processed on the "first-come-first-served" discipline.

The distributions of arrival time and service time should first be constructed and matched into the closest theoretical statistical distribution, and then the appropriate formulas will be applied to expect the queuing performance system. This compatibility analysis can be performed through the well-known Goodness of Fit Test. If the appropriate formulas are not obtainable, this process is to be simplified. For this purpose, two types of queuing theory models are most practical to explain ship movements in port; (M/M/n) and (M/E_k/n) models. In both models, the first letter M indicates ship or truck arrival time probabilities, the second M in the earliest model refers to the service time distribution, the E_k in the last model fitted to the degree of Erlang multiple exponential service time distribution, and the n denotes the number of available servers.

5.3 Indicators analysis

The efficiency performance indicators should be measured up with performance benchmarks to assess their actual efficiency. The comparison is an important instrument to assess whether the optimal use of available resources is reached, before deciding how to increase terminal productivity and efficiency [7].

5.4 Sensitivity analysis

Sensitivity analysis is needed to identify, understand and determine the relationships between EPIs and the relevant influencing factors; such as: berth throughput and ship waiting time, berth occupancy and the relative waiting time, productivity of ship call and handled containers, and dwell time and storage capacity.

The core of the sensitivity analysis is to change input variables, and then to re-estimate the EPIs under different combination patterns of modifications. The analysis is subject to a "what-if" approach to determine how a change in a variable affects the outcome.

6. GOAL-ORIENTED PROCESS

A goal-oriented process is set up in a hierarchical structure to form four consecutive levels in a systematic and logical manner (Figure 2). It starts from the first level (main goal) and passes through the second intermediate level (sub-goals) and the third level (actions) to the fourth lowest level (scenarios).

Main Goal: Develop terminal productivity and efficiency and relieve congestions

Sub-Goals: The sub-goals are specifically arranged based on the comprehensive analysis, including:

- Expand and harmonise the physical infrastructure capacity of terminal subsystems

- Improve productivity and utilization of subsystems
- Enhance service quality (minimizing ship/truck turnaround and container turnover)

Actions: An action can be defined as a measure that can be taken to reach the desired sub-goals. Thus, a lot of specific actions can be proposed, such as: technological improvement, extend terminal facilities, intensive use of rail transport, improve operating regulations, introduce automation.

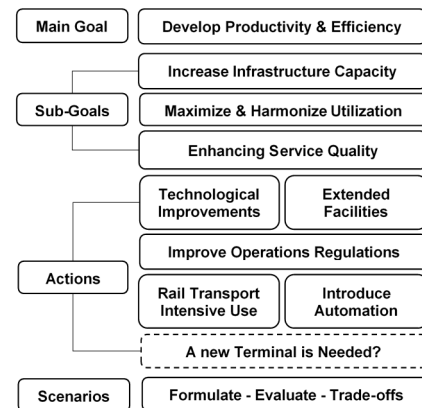


Figure 2. The goal-oriented process

Scenarios: A scenario is a combination of feasible actions that may lead to a vision for the future. The object of the formulation of a scenario is to draw attention to congestion causes and decisions required. Given the complex nature of the main goal, the evaluation could be subject to trade-offs analysis between advantages and disadvantages of action options.

7. CASE STUDY

In 1984, the Alexandria Container and Cargo Handling Company established the Alexandria Container Terminal (ACT). It is the first specialized container terminal in Egypt. In the middle of Alexandria Port, ACT covers a gross area of 163,000 m² designed to handle 160,000 TEUs per year. The quay of 531-meter-long and two 25-meter-long RO-RO berths, with 12.00 meters water depth can accommodate several ships according to the sizes of arriving ship. The terminal is well connected to both national road and rail networks.

With the rapid increase in container flow, several attempts are made to improve its productivity; e.g. upgrading handling equipment, creating new facilities and expanding storage capacity. Figure 3 illustrates the yearly distribution of terminal productivity between 2008 and 2018; the ACT achieved its highest throughput in 2015. The development represents a 200% growth compared with the 1984 design capacity.

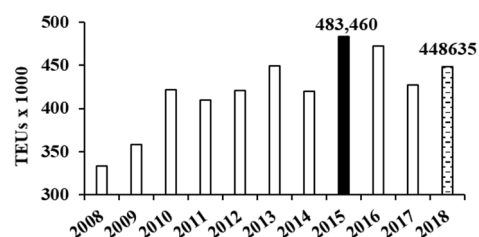


Figure 3. Yearly frequency distribution of terminal productivity

The quay and the QCs work 24 hours a day, except on public holidays and days with improper weather conditions. Based on terminal statistics of 2018, the monthly distribution of productivity shows the variation in trade volumes with average monthly productivity of 37386 TEUs. It reached its highest value in April (42078 TEUs), and the lowest levels during winter months.

7.1 Capacity and productivity assessment

The quay received 516 container ships in 2018, with an average of 1.41 ships per day, handled 285755 container boxes. With a ratio of 1.57 between TEUs and container boxes, the volume was 448635 TEUs. Table 1 presents the calculation of berth productivity.

Table 1. Berth productivity assessment, 2018

Quay	
Average Number of Berths	2.8
Available Quay Working Hours	8,520
Average Occupancy Rate	46.20%
Average Ship Productivity (TEUs/Hour)	40.706
Berth Productivity (TEUs/Year)	448,635
Berth Productivity (TEUs/Meter/Year)	845

The reached ships spent 18914 hours in the terminal, 7890 anchor hours waiting for a berth (41.72%) and 11024 hours service time at berth (58.28%). The berth time was divided into (a) pre-service time to set the required number of QCs with an average of 0.88 hours/ship, (b) service time of 17.99 hours/ship, and (c) post-service time of 2.82 hours/ship before departure.

In an interview with terminal operators, it is explained that one of the reasons for long anchor times is the extension of berth time due to the limited yard storage capacity. All import containers must be stacked in the yard for customs clearance before leaving. They also stated that non-completion of export documents at the right time increases the post-service time.

Figure 4 displays the frequency distribution of anchor times; an asymmetrical pattern that tends to the right.

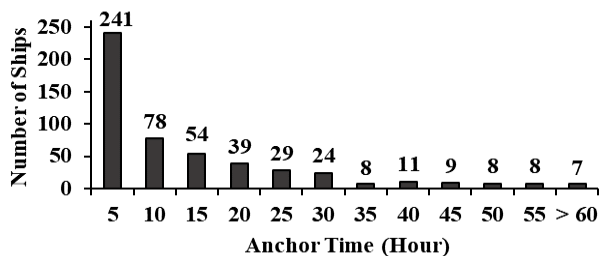


Figure 4. Distribution of anchor time, ACT 2018

The quay is equipped with four gantry rail-mounted of a total of 105 containers/hour nominal capacity. The QCs were operated 355 days, and the maintenance required 14.5% downtime of the total operating hours. According to field surveys, the average operating efficiency is about 79%. Terminal operators are authorized to assign an adequate number of cranes per ship based on its size and number of containers handled.

The QCs productivity assessment can be obtained in Table 2.

Table 2. Berth productivity assessment, 2018

QCs	
Annual Available Cranes-Hours	7,285
Capacity of Cranes (Box/Hour)	83
Annual Capacity of all Cranes (TEUs)	949,308
Utilization of all Cranes	47.26%
Cranes Productivity (TEUs/Year)	448,635

The surface area of the storage yard is 110,000 m², including ground slots and traffic lanes. To expand the storage capacity, containers in the yard were gradually rearranged; (a) utilizing the two RO-RO berths as storage areas, (b) decreasing the width of internal traffic lanes, (c) constructing a railway crossing through the railway station to create a new entrance gate, (d) randomly extending internal blocks, and (e) leasing 9 external storage spots. It should be noted that the railway facilities have not been regularly operated for the past decades.

The analysis indicated that the average container dwell time in the terminal and the external spots ranged from 7.00 days for export and 14.80 days for import; 40% export and 60% import. Thus, the container turnover was 30.80 days on average. Table 3 describes productivity in three container storage facilities.

Table 3. Storage facilities productivity assessment, 2018

Storage Facilities	Yard	Random Storage	External Storage
Storage Area (m ²)	52,915	7,290	34,536
No. of Ground Slots	2,940	212	2,125
Avg. Stacking Height	4.53	3.67	4.00
Storage Capacity (TEUs)	13,320	778	8500
Capacity (TEUs/Year)	410,256	23,962	261,800
Productivity(TEUs)	274,460	11,335	162,840
Utilization	66.9%	47.5%	62.2%

The ACT gate system consists of two truck entrance gates (gate 1 for export & gate 2 for empty trucks) and one exit gate, in addition to a private gate for the company staff. The terminal gates are equipped with the Optical Character Recognition system, which uses to automatically detect, record and process the necessary data of each container and truck entering or leaving a gate. Data collected from ACT is analysed around the service time per truck at gates in 2018. The results present that during 18 hours of daily active gate operation, the average service times are 1.56 for each entrance gate and 1.44 minutes for the exit gate. Thus, the annual capacity for the two entrance gates together is 386,362 and 418,666 trucks for the exit gate.

Terminal productivity may be constrained by the insufficient capacity of any subsystem, a plotted graph is designed to determine the capacity and productivity of

the subsystems (Figure 5). It explains that both QCs and entrance gates have excess capacity, while the yard can achieve the current productivity only by extending its capacity through the internal and external storage facilities. Moreover, the exit gate capacity is less than the system's productivity, leading to heavy gate congestion.

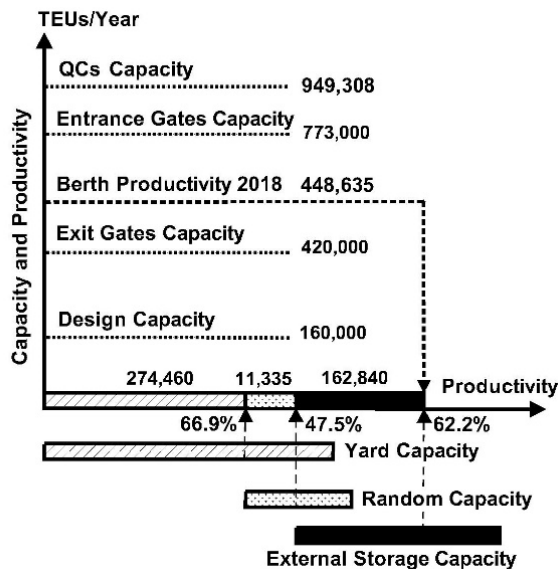


Figure 5: Capacity and productivity of ACT subsystems

7.2 Congestion analysis

Queuing theory is applied to analyse ship-shore congestion. The analysis confirms that the arrivals match a Poisson distribution at a λ rate of 0.0589 ships/hour, and the service time follows an exponential distribution at a μ rate of 0.0473 ships/hour, with the chi-square test at 95% confidence level. The results of employing the M/M/n model can be summarized as follows:

- Berth utilization = 44.5%
- Average queue length in line = 0.74 ship
- Average queue length in terminal = 1.98 ship
- Average waiting time in line = 12.50 hrs/ship
- Average waiting time in terminal = 33.70 hrs/ship

The queuing theory is also used to investigate the traffic severity at the gates based on detailed actual statistics between the 1st and 14th of April 2018. The daily truck activity indicates that Wednesday is the weekly peak day and a significant downward trend on weekends (Fridays).

According to Egypt's traffic control regulations, heavy trucks are prohibited from driving daily between 6:00 am to 11:00 pm on major congested urban roads and highways. Thus, truck long-distance trips to and from Alexandria are carried out overnight. Truck drivers spend the prohibited hours in port parking spaces or outside for rest, and prepare required documents.

An analysis is concerned with the behaviour of trucks in four consecutive hours at the gates on Wednesday, the 4th of April. Figure 6 displays that mornings the entrance gates are active with light traffic; (peak periods 3:00 pm - 7:00 pm for gate 1 and from 11:00 am - 3:00 pm for gate 2). It also shows that traffic at the exit gate mornings is almost busy, and then and until late at night the trucks become very dynamic (peak period: 18:00 - 22:00).

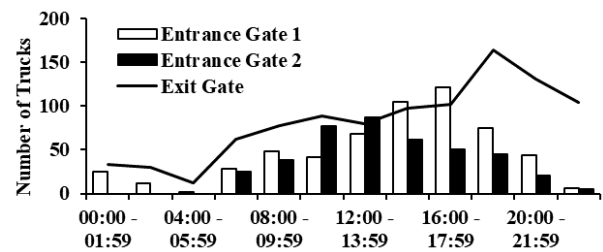


Figure 6. Hourly distribution of traffic at the gates, 2018

The analysis screens the attitude at peak periods of 230 trucks (gate 1), 170 trucks (gate 2) and 295 trucks (exit gate), account for 40%, 42% and 30% of the total daily traffic volumes, respectively. The ACT data is then investigated with respect to the truck inter-arrival and gate service times at the peak periods. The results reveal that the truck inter-arrival times corresponds to the exponential distribution and the service time follows a poisson distribution for all gates with the chi-square test at a confidence level of 90%. Table 4 features the queue performance at the different gates obtained through the application of the M/M/n model.

Table 4. Congestion phenomena at gates, April 14th, 2018

Queuing Performance (Averages)	Gate 1	Gate 2	Exit Gate
Arrival Rate λ (truck/min.)	0.552	0.601	0.665
Service Rate μ (truck/min.)	0.652	0.643	0.695
Gate Utilization	85%	93%	96%
Queue Length in line; truck	5	14	22
Queue Length at Gate, truck	6	15	23
Waiting Time in Line; min.	8.47	22.25	31.89
Waiting Time at Gate; min.	10.00	23.81	33.33

Field surveys revealed a disturbance within the yard; crowded trucks and handling equipment were moving with stop/go tempo on the narrow roads between blocks. This phenomenon affects the turnaround time of trucks within the yard. Statistical analysis shows that the truck's turn-time distribution corresponds to an asymmetric, left-leaning pattern, averaging 2.47 hours per truck.

7.3 Indicators analysis

The ACT performance indicators are formulated and compared with those in performance benchmarks. Practical information related to benchmarks is provided in several reports, such as UNCTAD, Review of Maritime Transport 2017/2018, Port Benchmarking Report: SA Terminals 2015/16, and UNCTAD Expert Meeting on Assessing Port Performance 2012.

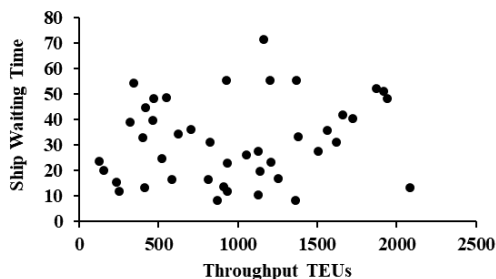
By assessing productivity and utilization indicators in ACT, Table 5 highlights slight differences within the minimum limits of the corresponding benchmarks, while time-related indicators exceed widely the acceptable ranges. This result means that ACT is experiencing delays and congestions in its operating system.

Table 5. Efficiency performance indicator analysis, 2018

Performance Indicators		ACT	Benchmarks
Area productivity	TEUs/m ²	2.75	2.63
Berth productivity	TEUs/m.	845	850 - 1700
QCs productivity	TEUs/hr.	20.70	25 - 40
Berth utilization	%	46.20	50 - 70
Storage utilization	%	64.46	70 - 80
Ship productivity	TEU/hr.	40.71	35 - > 65
Relative waiting time		0.74	0.05 - > 0.2
Ship turnaround time	Hours	37.30	22.08
Truck turnover time	Hours	2.47	0.5 - 1
Export dwell time	Days	7.00	3 - 5
Import dwell time	Days	14.80	5 - 7

7.4 Sensitivity analysis

To explore the relations between selected EPIs and the relevant influencing factors, the analysis indicates that there are no reliable statistical relationships with appropriate accuracy between them; i.e. as if they have nothing to do with each other. Figure 7 reveals, for example, the relation between throughput and ships waiting time. The distorted scatterplots may be a result of unexpected delays that leads to a misleading relationship. The results require further in-depth analysis.

**Figure 7: Relationship between throughput and ship waiting time**

However, relationships can be calculated assuming that the unexpected delays have only a slight effect on the performance. For example, the storage calculation expects that if the dwell time for import and export containers is reduced to 9 and 5 days respectively, yard capacity can cover the current throughput with 75.69% utilization, without the need to expand storage areas.

Shuttle trucks between the terminal and the external storage zones worsen congestion at gates; as each truck requires about one hour round trip on average. These trucks represent 36.27% of the daily traffic at the gates.

The analysis also shows, if the terminal rail is activated to transport only 10% of the terminal throughput (one train per direction daily), the average utilization of the exit and entrance gates can be reduced to 74% and 78%, correspondingly.

8. CONCLUSION

The annual design capacity of the ACT, established in 1984, is 160,000 TEUs, but now deals with more than 450,000 TEUs, suffering from harmful congestion. One of the obvious problems today is the insufficiency of yard

capacity, so relying on internal random and external storage zones that are served by transport shuttle trucks.

The ACT system is mainly based on road transport, producing severe gate bottlenecks and disruptions in the yard with heavy utilization of trucks, handling equipment and stacking of containers at the same time. The result is an expansion of the truck time spent in the yard.

Although the ACT is well connected to the national rail network, rail transport is neglected and have not been regularly operated for several years.

The long dwell time of containers due to customs regulations has negative impacts not only on storage capacity but also on terminal service quality. Thus, the container dwell time values require further investigation.

One of the results of scenario assessment is the importance of connecting ACT to a dry logistics centre in the Alexandria region, where the import containers are transported by rail for customs inspection there.

The application in this paper is an attempt to highlight the practicality of the proposed conceptual framework for the modelling of highly congested container terminals, such as ACT.

ACKNOWLEDGEMENT

The authors wish to express their deep appreciation to the Chairman and members of the ACT Board for the valuable cooperation and authorizing data collection.

REFERENCES

- [1] Nze, I. C. and Onyemechi, C.: Port congestion determinants and impacts on logistics and supply chain network of five African ports, *Journal of Sustainable Development Transport and Logistics*, Vol. 3, No. 1, pp. 70–82, 2018.
- [2] González, R.: *A Methodology Proposal to Obtain Operational Parameter Forecasts and Operational Risk Assessment in Container Terminals*, Caminos, 2015.
- [3] Minh, C. C. and Huynh, N.: Optimal design of container terminal gate layout, *International Journal of Shipping and Transport Logistics*, Vol. 9, No. 5, pp. 640–650, 2017.
- [4] Pham, T.Y. and Yeo, G.T.: Evaluation of Transshipment Container Terminals' Service Quality in Vietnam: From the Shipping Companies' Perspective, *Sustainability*, Vol. 11, No. 5, pp. 1503, 2019.
- [5] Zhen, L.: Modeling of yard congestion and optimization of yard template in container ports, *Transportation Research Part B: Methodological*, Vol. 90, pp. 83–104, 2016.
- [6] Saeed, N. and Larsen, O.: Application of queuing methodology to analyze congestion: A case study of the Manila International Container Terminal, Philippines, *Transport on Policy*, Vol. 4, No. 4, 2016.
- [7] Ningning, L., Jingjing, Y., Guolei, T., Da, L and Yong, Z.: Container terminals capacity evaluation considering port service level based on simulation, *ECMS*, 2017.

Branislav DragovićProfessor
University of Montenegro
Maritime Faculty**Vassilis Tselentis**Professor
University of Piraeus Department of
Maritime Studies**Nenad Zrnić**Professor
University of Belgrade
Faculty of Mechanical Engineering**Radovan Orlandić**Executive Director
AD Marina Bar**Zdravko Paladin**Young Researcher
Bar, Montenegro**Kenan Perazić**Executive Director
Agent Plus

Environmental and operational risk assessment procedures for Sustainable Marina: The case of Marina Bar

In this paper are presented environmental and operational risk assessment procedures for sustainable marina with regards to the case of Marina Bar, Montenegro. We begin with the environmental and operational risk determination process which is suitable for analyzing the environmental and operational risk assessment procedures for sustainable marina. Then, methodological approach and procedures for environmental and operational risk assessment are presented. The study approach to life risk assessment: the case of the Marina Bar is elaborated with some numerical results which are followed by specific comments. This study has been done through investigation project entitled "Applying and promoting the concept of sustainable development to AD Marina Bar (SUST-MARINA)".

Keywords: Sustainable marina, environmental and operative management, environmental aspects, risk assesment and evaluation, ISO procedures

1. INTRODUCTION

Environmental and operational issues are one of the most important problems in contemporary business and management operations, which need to be adequately identified, monitored, and appropriately assessed in order to improve its performance and risk management. Being the fact that contemporary economy strives towards implementation of sustainable development concept in every field, it is necessary to analyze the environmental and operational protection possibilities and adopt the international institutions development strategy plans, recommendations and suggestions regarding the environmental and risk management.

Therefore, the International Standards Organization, as well as other institutions relevant for maritime affairs and marine ecology such as ESPO (The European Sea Ports Organisation), Gold Anchor Award Scheme and Blue Flag ([9], [18], [21], [32]) provide the wide range of regulative documents, recommendations, requirements and marine strategy framework for most important business activities and operations, especially regarding quality and environmental protection for marine ecosystems [4].

It is necessary to make a comprehensive methodological approach that will be a framework for valuation of environmental aspects, impacts, operative risks and externalities, in order to help maritime industry related decision-makers to improve, develop and implement their environmental and risk management policy efficiently. Also, waterfront redevelopment and its

features must be considered in order to improve environmental performance ([11], [19]). In this purpose, various methodological approaches have been introduced and conducted in the way to describe, monitor, register, classify, and find solution for operational risk level decreasing and potential environmental issues.

Firstly it is necessary to implement the analytical approaches of the Key Environmental Performance Indicators (EPI) for port and marinas sustainable development. In the recent studies this is usually made by selection of the appropriate survey sample of about more than 100 ports and marinas. There were examined various aspects of EPI with regards to concept, benefits and types. Environmental and risk indicators have been collected, filtered and analyzed through specific criteria within environmental and operative management. Special theoretical and practical assessment using Delphi method has been used regarding port authority and port related stakeholders. Environmental indicators have been classified in three main categories: Management Performance, Operational and Environmental Condition Indicators. This methodological approach is very useful for ports and marinas because of its consistent application over time and environmental trends dynamics. Therefore, improvements of environmental management system can be assessed by this estimation tool ([27]-[29], [36]).

Also, sustainability regarding organizational and environmental issues in ports and marinas are analyzed with methodological approach based on review of current state of all facilities, its technical capacities and reports in official regulatory and institutional frames. Discussions within the planning development process in marinas, regulatory environmental framework, risk reduction management plans and sustainable marina design contributed to specification of goals that one marina should put in order to become successful in marina market and be in the environmental compliance with standards ([7], [8], [13], [39]).

Correspondence to: Dr Branislav Dragovic, Professor
Maritime Faculty, University of Montenegro,
Dobrota 36, 85330 Kotor, Montenegro
E-mail: branod@ac.me

In that sense, every marina should make efforts and attention regarding the environmental and risk matters since the key processes need to be appropriately operated with as much as possible lower level of identified risks realization.

The remainder of the paper is organized as follows. In Section 2, the environmental and operational risk determination process in sustainable marina is presented. This process is suitable for analyzing the environmental and operational risk assessment procedures for sustainable marina, while methodological approach and procedures for environmental and operational risk assessment are given in Section 3. The study approach to life risk assessment: the case of the Marina Bar is elaborated in Section 4 with some numerical results which are presented in Appendix I followed by specific comments. In Section 5, concluding remarks are given.

2. ENVIRONMENTAL AND OPERATIONAL RISK DETERMINATION PROCESS IN SUSTAINABLE MARINA

It is important to note that environmental aspects represent the essential part of Environmental Management System (EMS), based on ISO 14001:2015, (Environmental management systems – Requirements with guidance for use) which are defined within basic terminology as [21]:

ENVIRONMENT

Surroundings in which an organization operates, including air, water, land, natural resources, flora, fauna, humans and their interrelationships. Surroundings can extend from within an organization to the local, regional and global system. Surroundings can be described in terms of biodiversity, ecosystems, climate or other characteristics.

ENVIRONMENTAL ASPECT

Element of an organization's activities or products or services that interacts or can interact with the environment. An environmental aspect can cause (an) environmental impact(s). A significant environmental aspect is one that has or can have one or more significant environmental impact(s). Significant environmental aspects are determined by the organization applying one or more criteria."

Environmental aspects are related with many operational marina activities and they can have various positive or adverse impacts, that can be identified as risk and threats to marina operations and facilities.

Therefore, environmental risk management is an essential issue for most marina managers and operators. A collision or an explosion of equipment or a boat in a port and marina area does not only affect workers, boaters and personnel in that area but might also have influences and adverse impacts to other parties such as nearby-residents, industries located in the marina territory, etc. Since all stakeholders of marina are aware of this issue and the contents of marina operation and maneuvering aquatorium area is not a risk-free zone, risk management is therefore a sensible matter for any marina operator. To conduct a good risk management, risk assessment as its pre-requisite must be well prepared and accomplished [40].

For that reason, it is important to discuss the environmental risk assessment as main tool for resolving the quality and environmental problems. The term "risk assessment" refers to both the risk assessment process and documents that result from that process. Procedurally, risk assessment is an organized process used to describe and estimate the likelihood of adverse health outcomes from environmental exposures to chemicals ([6], [33]-[36]). The four steps of risk assessment are:

1. hazard identification,
2. dose-response assessment,
3. exposure assessment,
4. risk characterization.

In risk assessment, risk assessors and evaluators use data of known quality in a standardized analytical framework to estimate type and degree of risks posed by environmental contaminants. Risk characterization, the fourth (and final) step in risk assessment, involves calculation of various risks by combining exposure intake and uptake levels with, for example, toxicity and other values. Numerical results of a risk characterization and environmental impacts must be accompanied by text and suggestions to fully explain risk assessment findings, ecological and biological monitoring, relevant parameters and environmental aspect impact estimation ([24], [25], [34]).

New trends in risk management lead to application of automatic, online monitoring and web-based platforms and softwares provided as guidance tool for port operators and personnel dealing with safety issues. Therefore, it is designed the special platform *RAPORT* (Risk Assessment for PORT) with aim to support the risk assessment according to Formal Safety Assessment (FSA) as recommended by the International Maritime Organization (IMO) [40].

3. METHODOLOGICAL APPROACH AND PROCEDURES FOR ENVIRONMENTAL AND OPERATIONAL RISK ASSESSMENT

Marinas and ports, within the IMS implementation should conduct continual monitoring of their activities and operational processes as well as traffic intensity of boats and ships, their frequency, types, speed, time of arrival and departure in order to manage the traffic and water area. In order to manage the both environmental and operational risks, there have to be made adequate procedures for monitoring and control of local ecosystems, service areas, possible pollutions from boats and from land, environmental and biological monitoring, equipment maintenance.

Here it is assumed that procedure has the defined subject, objectives, area of implementation, the scope of activities and boat risk assessment. Also this must be related with online and software based platform for automatic monitoring and precise risk assessment [20].

It is necessary to mention that risk assessment procedures are in compliance with ISO standard required principle Plan-Do-Check-Act (PDCA cycle), given as follows [22]:

- Planning phase consists of design risk assessment framework (Identification of risks, review database),

- Risk analysis and mitigation (assess and priorities, mitigation measures, implementation of results),
- Checking and monitoring of aspects and risks, review and update, tracking performance metrics,
- Continuous improvement of the risk frameworks.

It is very important to note, that risk analysis and assessment is done with priority to manage human risk in order to protect human lives in the whole marina or port area. In that reason, Chlomudis et al. [10] have proposed the special port risk assessment methodology for human accident with aim to anticipate hazards, make proactive approach to safety and classify risk assessment steps and processes.

Risk identification is the first and in many ways the most important step in risk assessment. An overlooked risk is likely to introduce more error into the overall risk estimate than an inaccurate consequence model or frequency estimate ([10], [30]).

It is imperative to evaluate the treats and environmental aspects and impacts and determine which safety and security measures are required to manage risks. Therefore, a risk assessment approach needs to be conducted involving every aspect related to this industry; such as boats, facilities, infrastructure, water area, gates, service and dock areas and other objects. Particularly, marinas and seaports possess an extraordinary amount of hazards, which will lead to different types of risks that can be categorized into: environmental, natural, operational, security, technical and organizational ([5], [26]).

4. STUDY APPROACH TO LIFE RISK ASSESSMENT: THE CASE OF THE MARINA BAR

The case study analyzed in this paper comprehends realization of the international project “Applying and promotion of the sustainable development concept in AD Marina Bar” (SUST-MARINA) within the Montenegrin south coast marina in Bar ([1], [21], [31]). During this project realization it have been made a significant effort in modernizing the marina system by implementing the ISO, Blue Flag and Gold Anchor Award Scheme recommendations and requirements, ecological investigations, environmental aspects and parameters monitoring and reporting, modeling the marina operations, facilities, berths and IMS activities, procurement of eco-friendly technologies within the sustainable development concept ([12]-[17], [33]-[39]).

Therefore, as one of the main project goals, it is made comprehensive Integrated Management System (IMS) which consists of Quality Management System (QMS) (ISO 9001:2015) and Environmental Management System (EMS) (ISO 14001:2015) ([3], [4], [12]-[17], [33]-[39]). Within the part of EMS it have been defined the IMS manual and system of procedures which regulate the environmental activities conduction, measurements, monitoring of aspects, risk assessment, ecological investigations, reporting, indicators measurements and classification, ecological activities effectiveness assessment, quality and environmental policy, compliance with national legislative framework and international standards ([13]-[15], [23], [34]).

Therefore it has been made the analysis of threats and dangers – risks identified within marina regular processes and operational activities, in order to comprehensively manage the risk realisation possibility in emergent situations, according to implemented IMS.

Marina has already done security and safety system by professional licensed firm for safety and security of port and marina. Consequently, “International Ship and Port Facility Security (ISPS) Code” – Safety and Security system in marina consists of all procedures with regards to:

- a) Life risk assessment,
- b) Port facility security assessment.

Health care and first aid procedure in AD Marina Bar is also part of Safety and Security assessment and Security Plan. We would like to point out that procedure for health care and first aid is based on the principles of health care law in Montenegro.

First aid in marina can be applied during some injuries, using some parts of sanitary materials allocated on fourteen different positions in first aid cabinets. Each gate in marina has first aid cabinets plus some other selected points ([2], [3], [21]).

The following analysis represents the addition of Safety assessment of AD Marina Bar, and it is made according to IMO/ILO matrix (Threat and Risk Analysis Matrix - TRAM).

General note in relation to score distribution and method of risk calculation:

1. Threat – risk:

- 3 = big,
- 2 = moderate,
- 1 = negligible – small

2. Harming of the port/facility

- 4 = without implementation of protection measures,
- 3 = minimal implementation of protection measures,
- 2 = appropriate implementation of protection measures,
- 1 = full implementation of protection measures,

3. Consequences:

- 5 = heavy consequences with numerous human victims,
- 4 = significant consequences with human victims, numerous injuries and significant material damage,
- 3 = economic damage for port, environment and significant consequences for business image,
- 2 = damages in relation with particular assets, loading/unloading mechanization and infrastructure
- 1 = damage of port services customers' property – in small size, which can be solved by port in direct contact
- 0 = negligible or without consequences

Therefore, we give overall risk in marina (ORM) area calculation formula (1):

$$R \cdot H \cdot C = ORM \quad (1)$$

Where, the component symbols stand for R – risk, H – harming, and C – consequences. As mentioned, these components can take the following values, $R \in \{1,2,3\}$, $H \in \{1,2,3,4\}$, $C \in \{1,2,3,4,5\}$, respectively. Maximal number of score of estimated risk is 60, and minimal 1 (see Appendix I, Table I.1).

Safety management plan comprehend several key phasis and parts, whose symbols in register table represent:

- A* – Scenario (possibility of realization of various risks and its related impacts),
- B* – Specification (description) of threat (register of heavy risk that can lead to emergencies),
- C* – Level of risk estimation,
- D* – Level of harming,
- E* – Consequences consideration and analysis of its impacts on environment and humans,
- F* – Summa in level of security 1,
- G* – Summa in level of security 2,
- H* – Summa in level of security 3,
- I* – Applied contra measures (corrective measures and emergency plan actions provided by IMS and ISPS risk procedures)
- J* – Summa in level of security 1 after CM (contra measure),
- K* – Summa in level of security 2 after CM (contra measure).

These criteria/specifications are applied on estimated risk level for different threats in port/marina and some examples of these threats are related with the following:

- potential threat destroying the Petrol station on the Secondary breakwater with explosive material,
- Suspicion for taking in the explosive material in the marina area – onboard (boat) on the berth; attack with detonation agent.
- Potential threat that member of ship/boat crew or member of staff in the marina takes drugs in the marina and delivers it on the boat in the purpose of further distribution; illegal pass of state boundary with (without) help of the member of ships' crew.

These examples are provided in the attachment of this risk assessment document.

In the Table I.1 (see Appendix I, Table I.1) it has been given risk assessment matrix for mentioned three categories of risk level:

- Threat – risk,
- Harming of the port/facility,
- Consequences.

Therefore, calculation of the level of the risk for every possible case is made according to already established formula (1) (see Appendix I, Table I.1).

Safety conditions in marina regarding the risk of falling in the water and other accidents related to injuries of boaters, visitors and workers in the water is improved by installation of 12 safety equipment sets on marina main gates, pontoon and secondary breakwater (see Appendix I, Figure I.2a and Figure I.2b). This safety installation boxes consist of following elements:

- Safety ladders,
- Life belts,
- Life jackets,
- First Aid cabinets,
- Rope for belt,
- Grapnels

Allocation of safety boxes is given on the following figure – Layout of AD Marina Bar with safety and fire fighting equipment plan (see Appendix I, Figure I.1.)

During the first half of September, 2017, in order to reduce the overall risk level for boats damage, there have

been procured and installed special bitts for boats on gates, with same design and various dimensions depending on their location and purpose. Therefore, the bigger bitts are installed on secondary breakwater because of common practise of berthing the biggest yachts on this part of Marina Bar. The smaller bitts have been put on gates 1-8 and they are suitable for boats with maximum length 15m (see Appendix I, Figure I.2.d).

Also, in the AD Marina Bar it has been made a special document *Project/elaborate on facilities maintenance* in national language, which contents a study and calculation of optimal mooring of the boats in marina. On the following figures it is given a front page of the plan, short description of organization of berths and the schedule of boats moorings, as well as some graphical scheme of mooring system with ropes, bitts, underwater mooring blocks and fairways. There have been shown dimensions of underwater concrete blocks and its features as well as mathematical formulae for calculation of physical aspects of underwater blocks and its technical conditions, too.

In AD Marina Bar it is launched a process of procurement of special equipment for dry dock: Moveable 'T' Form Cradles, Static Yard Cradles and Yacht Stands, which are like the following figure represents (see Appendix I, Figure I.2.c).

Together with mentioned ORM calculation as well as Overall Risk Rating calculation for environmental aspects register and management (EAR) ([3], [4], [12]-[17], [24], [25], [33]-[39]), in AD Marina Bar within the IMS has been made comprehensive analysis and all significant risk identification and classification. The part of that list (13 from 48 identified risk) is given on the end, in Appendix I, Table I.2.

5. CONCLUSIONS

Harmful outcomes of identified risk realization withih the operative processes can significantly affect the marina facilites, boats, as well as personel and indanger their lives and property. The risks are generally classified and managed by their group characteristics, such as natural hazards (natural conditions, environmental issues, weather situation) and hazrads in infrastructure context (built environment, human factors, technical capacities, equipement delay). Risk assessment is necessary instrument for risk mitigation, anticipation and management and should be included in operational and environmental procedures within IMS. In that sense, risk assessment approach can suggest different policy implications in environmental and business policy for sustainable marina.

The concept of environmental and operational risk determination process which is suitable for analyzing the environmental and operational risk assessment procedures for sustainable marina consists of several stages with identification of environmental effects from existing activities, objectives and targets, environmental policy, planning, application and control. One of the goals of the this concept, presented in this paper, is to ensure continuous improvement after the completion of its environmental and operational risk assessment procedures for sustainable marina, in various fields

including the implementation of joint action plans addressing both commercial viability, as well as the responsibilities concerning maintenance and its upgrade using environmental management system principles.

The main aim of this approach is to make sustainable marina and bring positive feedback to the top management. This means that a marina should have firstly adopted specific goals of Integrated Management System (IMS) and policy of IMS as well as policy of environmental protection if marina implements the Environmental Management System.

ACKNOWLEDGEMENTS

The study was carried out within the Project MNE-HERIC-81180, “Applying and promoting the concept of sustainable development to A.D. Marina Bar (SUST-MARINA)”, financed within the scope of “Higher Education and Research for Innovation and Competitiveness in Montenegro” — (“HERIC”) project, from the International Bank for Reconstruction and Development loan, in accordance with the Decision of the Ministry of Science of Montenegro on awarding the grant: Number: 01-1062 from 29th May 2014.

REFERENCES

- [1] AD MARINA BAR (ADMB): Annual report of 2018, Issued by AD Marina Bar, 2019.
- [2] AD Marina Bar Integrated Management System (Quality Management System and Environmental Management System – ISO 9001:2015 and ISO 14001:2015), Procedure 11 - “Environmental aspects identification“, Internal documnetation of AD Marina Bar, 2017.
- [3] AD Marina Bar Integrated Management System (Quality Management System and Environmental Management System – ISO 9001:2015 and ISO 14001:2015), Procedure 4 - “Equipment maintenance“, Internal documnetation of AD Marina Bar, 2017.
- [4] ASCE MANUALS AND REPORTS OF ENGINEERING PRACTICE No. 50 (ASCE), Planning and Design Guidelines for Small Craft Harbors (3rd ed.), Published by American society of Civil Engineering, 2012.
- [5] Audigier, M., Kiremidjian, A., Chiu, S. and King, S.: Risk Analysis of Port Facilities, Stanford University, 12th World Conference on Earthquake Engineering, Auckland, New Zealand, 2000.
- [6] Benjamin, S.; Belluck, D. *A practical Guide to Understanding, Managing and Reviewing Environmental Risk Assessment Reports*, Lewis Publishers, New York, USA, 2001.
- [7] Biondi, E.: A sustainable approach to marina development, Caribbean Compass, pp. 21-23, 2017.
- [8] Biondi, E., Lara, A., 2015, Sustainable marinas – Institutional framework of sustainability, “SMART RIVERS 2015” Buenos Aires, Argentina, 7-11 September 2015, www.pianc.org.ar/sr2015
- [9] CALIFORNIA DEPARTMENT OF BOATING AND WATERWAYS (CDBW), Layout and design guidelines for marina berthing facilities, 2005.
- [10] Chlomoudis, C., Pallis, P. and Tzannatos, E.: Port Risk Assessment Methodology for Human Accidents in Container Terminals: Evidence from the Port of Piraeus – Greece, International Journal for Traffic and Transport Engineering, Vol. 6, No. 4, pp. 368 - 377, 2016.
- [11] del Saz-Salazar, S., García-Menéndez, L. and Merk, O.: The port and its environment: Methodological approach for economic appraisal, OECD Regional Development WorkingPapers, 2013/24, OECD, 2013.
- [12] Dragović, B.: *Marinas - Small Craft Harbors and Recreational Ports: Sustainable Development*, 1st ed., SaTCIP, in Serbia and Montenegro, 2015.
- [13] Dragović, B., Papadimitriou, S., Tselentis, V. and Tzannatos, E.: Study of sustainable marina development performance: Environmental implications, Proceedings of XXI Triennial International Conference MHCL 2015, Vienna University of Technology, Vienna, Austria, September 2015, pp. 263–268, 2015.
- [14] Dragović, B., Tselentis, V., Orlandić, R. and Paladin, Z.: Environmental Management Concept Implementation with Regards to Marina Bar, Proceedings of the XXI International Conference MHCL 2017, 2017.
- [15] Dragović, B., Tselentis, V., Orlandić, R. and Paladin, Z.: Environmental Implications to Sustainable Marina: The Case of Marina Bar, Proceedings of the XXI International Conference MHCL 2017, 2017
- [16] Dragović, B. and Tselentis, V.: Applying and promoting of marina sustainable development concept: The case of Marina Bar, Montenegro, Journal of Business and Economics, Vol. 6, No. 12, pp. 2097–2108, 2015.
- [17] Dragović, B. and Tselentis, V.: Some approaches to the sustainable marina concept, Proceedings of 3rd International Conference on Production and Supply Chain Management, Athens, Greece, December 2014, pp. 11–19, 2014.
- [18] FEE International: Blue flag marina criteria and explanatory notes, <http://www.blueflag.org>
- [19] Heron, R. and Juju, W.: *The Marina-Sustainable Solutions for a Profitable Business*, Create Space Independent Publishing Platform, 2012.
- [20] Introduced Marine Species Risk Assessment Procedure Port of Port Hedland, No. A232514, Pilbara Port Authority, North Australia, 2014.
- [21] ISO (International Organization for Standardization), ISO 14001:2015 Environmental Management Systems and Requirements with Guidance for Use, 2015.
- [22] Janowicz, K. and Pauling J.: Risk Assessment, Management, and Mitigation for Port and Marine Terminals Projects, presentation at AAPA Cargo Optimization June 8, 2016.

- [23] Kuznetsov, A., Dinwoodie, J., Gibbs, D., Sansom, M. and Knowles, H.: Towards a sustainability management system for smaller ports, *Marine Policy*, Vol. 54, pp. 59-68, 2015.
- [24] Orlandić, R. and Paladin, Z.: Sustainable development improvements and Environmental Management trends with regards to AD Marina Bar, *Proceedings of the Maritime and Port Logistics of the MHCL 2019 – Bar Conference*, pp. 170-174, 2019.
- [25] Paladin, Z., Orlandić, R. and Karanikić, P.: Environmental Management instruments and improvement of marina performance – Case study: AD Marina Bar, *Proceedings of the Maritime and Port Logistics of the MHCL 2019 – Bar Conference*, pp. 204-207, 2019.
- [26] Parra, N.M., Nagi, A. and Kersten, W.: *Risk Assessment Methods in Seaports: a Literature Review*, Publications of the HAZARD PROJECT 24:2018, University of Turku, Finland, 2018.
- [27] Puig, M., Pla, A., Segui, X. and Darbra R.M.: Tool for the identification and implementation of Environmental Indicators in Ports (TEIP), *Ocean and Coastal Management*, Vol. 140, pp. 34-45, 2017.
- [28] Puig, M., Wooldridge, C.F., Casal, J. and Darba, R.M.: Tool for the identification and assessment of Environmental Aspects in Ports (TEAP), *Ocean and Coastal Management*, Vol. 113, pp. 8-17, 2015.
- [29] Puig, M., Wooldridge, C.F., Mihail, A. and Darba, R.M.: Current status and trends of the environmental performance in European ports, *Environmental Science & Policy*, Vol.48, pp. 57-66, 2015.
- [30] Siu Lee Lam, J. and Lassa, J.: Risk assessment framework for exposure of cargo and ports to natural hazards and climate extremes, *Maritime Policy & Management*, 2016.
- [31] SUST-MARINA Project Team: Periodical report, AD Marina Bar, Internal project document, 2017.
- [32] The Yacht Harbour Association: The Gold Anchor Award Scheme, <http://www.tyha.co.uk>
- [33] Tselentis, V., Dragović, B., Nikitakos, N., Škurić, M. and Ćorić, A.: Integrative model of sustainable development for marinas and nautical ports, *Proceedings of European Conference on Shipping, Intermodalism & Ports – ECONSHIP 2015*, June 2015, pp. 1–10, 2015.
- [34] Tselentis, V., Dragović, B., Tzannatos, E. and Paladin, Z.: A practical monitoring approach in marinas: A case study of Marina Bar, *Proceedings of 5th Mediterranean Conference on Embedded Computing, MECO 2016*.
- [35] Tselentis, V. and Dragović, B.: Analysis of vessel traffic indicators and performances in marina, *Proceedings of 3rd International Conference on Production and Supply Chain Management*, Athens, Greece, December 2014, pp. 51–61, 2014.
- [36] Tselentis, V., Michail, A., Darbra, R.M., Marti, P. and Wooldridge, C.F.: Evidence-based monitoring for sustainable development in port and chain operations, In: *Sustainable Development of Sea-Corridors and Coastal Waters, The TEN ECOPORT project in South East Europe*, (Eds. C. Stylios, T. Floqi, J. Marinski, L. Damiani), Springer, pp. 177–184, 2015.
- [37] Tselentis, V., Papadimitriou, S., Tzannatos, E. and Dragović, B.: An analysis of sustainable development framework of marina, *Proceedings of 34th International Conference on Organizational Science Development, ICOSD 2015*, Portorož, Slovenia, March 2015, pp. 1178–1183, 2015.
- [38] Tselentis, V.: Marina environmental review system: A methodology to assess environmental management in recreational ports, *European Research Studies*, Vol. 11, No. 1-2, pp. 47–56, 2008.
- [39] Wooldridge, C. and Stojanovic, T.: *Integrated environmental management of ports and harbours. The European experience – from policy to practice*. Routledge, New York, 2004.
- [40] Zuesongdham, P., Noce, E., Salaris, M.V., Gómez Arche, A.M. and Antao, P.: *RAPORT – Guidance for Port Risk Assessment*, Conference Paper, Technical University of Lisbon, 2018.

Appendix I

Table I.1. Risk assessment matrix for AD Marina Bar in respect to life of berth users, visitors, dock masters, marina personnel, and other people

		Consequences							
		0	1	2	3	4	5		
Threat - risk	1	0	1	2	3	4	5	1	Harming the port / marina / facility
		0	2	4	6	8	10	2	
		0	3	6	9	12	15	3	
		0	4	8	12	16	20	4	
	2	0	2	4	6	8	10	1	
		0	4	8	12	16	20	2	
		0	6	12	18	24	30	3	
		0	8	16	24	32	40	4	
	3	0	3	6	9	12	15	1	
		0	6	12	18	24	30	2	
		0	9	18	27	36	45	3	
		0	12	24	36	48	60	4	

Note: We would like to point out that AD Marina Bar already has very detailed Security and Safety Plan according to ISPS and SOLAS written in national language according to national laws.

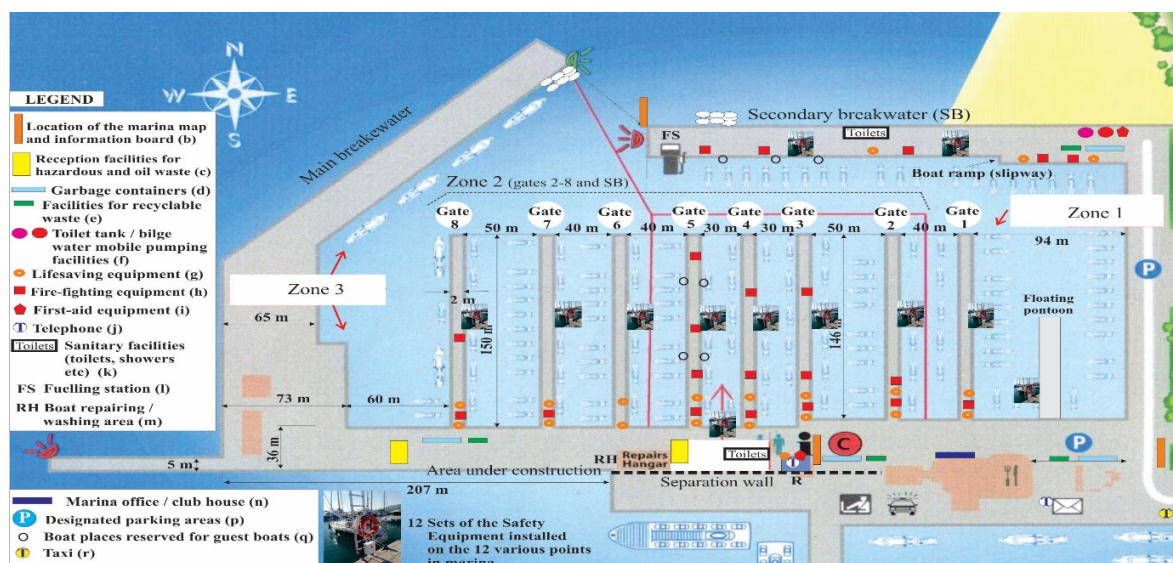
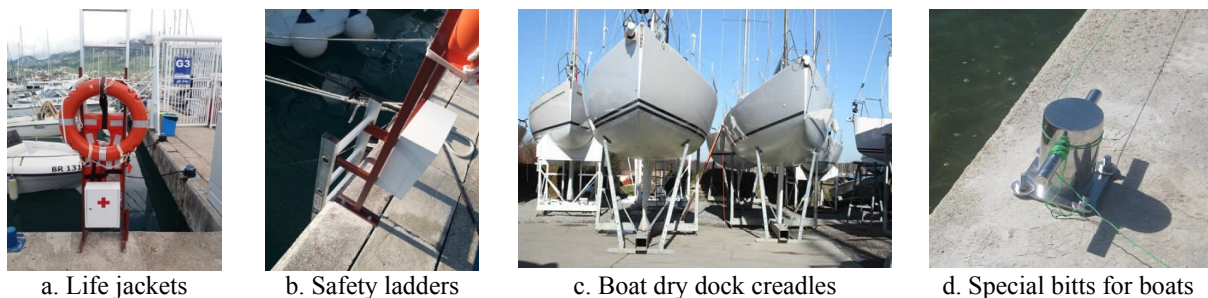
**Figure I.1.** Layout of AD Marina Bar with safety and fire fighting equipment plan ([13]-[17])**Figure I.2.** New safety equipment introduced in order to decrease technical and operational risks

Table I.2. List of some identified risks and opportunities in AD Marina Bar from 48 all identified and assessed risks

Ref	Risk category	Risk/ opportunity description	Cause of risk/ opportunity	Likelihood / Frequency	Harm / Danger / Severity	ORM – Overall Risk in Marina	Allowable level of risk	Responsible for risk monitoring	Necessary corrective measures
1	Meteoro-logical and weather risks	Elementary accidents	Storm wind, extreme weather, temperature earthquake	5	5	25	15	Management	It is not possible to prognose and work on risk apperance
2		Exploitation of weather risks for obtaining additional resources and raising company image	Timely appropriate and adequate measures and reactions	2	3	6	15	Management	Reporting by means of public information service and social media
3	Ecological risks	Pollution materials discharge rom boats	Human factor, boat breakdown, damage na failure	2	4	8	15	Boat owner and sailors	Surveilance
4		Wildfire emergence – impact on human health and safety of workers and tourists/ Environmental pollution/ Damage of property	Human factor	2	5	10	15	Safety and security personnel	Trainings of workers and education on guidances/ instructions at key postions in marina
5	Financial risks	Planning and financial management	Exploitation of public function and position; bribery; unallowable lobbying	5	5	25	15	Management	Regular conduction of internal financial audits and controls
6		Constraints in procurement realization	Obligations commanded by legislative body, senate	3	3	9	15	Management	Adequate and timely appropriate planning
7	Safety risks	Work injuries	Everyday work at the places with high risk	3	5	15	15	Safety and security personnel	Trainings of workers and guidances/ instructions at marina
8		Unappropriate usage of personal protection equipement (PPE)	Negligence/ recklessness of workers	2	4	8	15	Safety and security personnel	Control of worker about usage of PPE
9	Operation-technical risks	Quality of services and repair areas	Coodrination between sector organization al functions and marina management	3	5	15	15	Management	Control and Integrated Managemnt System implementation
10		Operating delay due to the machines and devices failures	Inadequate maintenance, accidents, averages	2	5	10	15	Maintenance service	Regular maintenace procedure within IMS
11		Windshield establishment	Property and boat protection	2	5	10	15	Management	Resources provision
12	Admini-strative risks	Continual care for berth users and other customers	Often changes in service and relations quality	4	4	16	15	Management	Adequate marketing sector and activities
13		Inadequate implementation of IMS documentation by employees	Outset of management system principles	3	4	12	15	IMS responsible person	Training of employees with IMS procedures and manual

Nenad ZrnićProfessor
University of Belgrade
Faculty of Mechanical Engineering**Sanja Bojić**Associate Professor
University of Novi Sad
Faculty of Technical Sciences**Milosav Georgijević**Professor
University of Novi Sad
Faculty of Technical Sciences**Marko Urošević**Research Assistant
University of Belgrade
Faculty of Mechanical Engineering

Analysis of the potential of the Port of Novi Sad to become a new container terminal on Danube

This paper discusses the possibility the establish and construct a new container terminal in the Port of Novi Sad which has regional and international importance and good geographical position, located in the Serbian Autonomous Province of Vojvodina. The provided analysis presents current container flows in Serbia and the forecast for the next 5 and 10 years (including three scenarios: realistic, pessimistic and optimistic), at first for the whole country, but later on the analysis was focused on the Danube gravitating regions in Serbia and finally to the existing Port of Novi Sad in order to evaluate its potential to become a logistics center. It was concluded that the construction of a new container terminal in the Port of Novi Sad on the Danube aims to bring about a significant change in the container transport system in Serbia, but also in the region or the Danube countries.

Keywords: container terminal, port, logistics, Novi Sad, Danube.

1. INTRODUCTION

Serbia, officially the Republic of Serbia (RS), is a country situated at the crossroads of Central and Southeast Europe in the southern Pannonia Plain and the central Balkans. The sovereign state borders Hungary to the north; Romania and Bulgaria to the east; Macedonia to the south; Croatia, Bosnia and Herzegovina, Montenegro to the west and claims a border with Albania through the disputed territory of Kosovo (Figure 1). Serbia numbers around 7 million residents. Its capital, Belgrade (2 million residents), ranks among the oldest and largest cities in southeastern Europe.



Figure 1. Geographical position of the Republic of Serbia

The Republic of Serbia has a favorable traffic - geographical, but at the same time very sensitive geostrategic position. The significance of this position is reflected in the passage of the corridor across the territory of the Republic of Serbia from the ancient times of Via Militaris, by which the shortest terrestrial connection is realized between Europe and Asia or the Middle East.

Correspondence to: Dr Nenad Zrnić, Professor
University of Belgrade, Faculty of Mechanical Engineering,
Kraljice Marije 16, 11120 Belgrade 35, Serbia
E-mail: nznric@mas.bg.ac.rs

The Republic of Serbia is in contact with the major European regions, that is, at the intersection of the roads towards Central Europe - the Danube River, the Mediterranean - the South Adriatic and the Alps.

There are three corridors across the Balkans, while two corridors pass through Serbia. The first is the river corridor of the Rhine - Main - Danube that connects Rotterdam to the Black Sea. On the TEN - T map, the Danube Corridor through Serbia is marked with a broken line, which means that there will be no funding from the European funds until 2030. It should be mentioned that regarding the surrounding countries, Serbia has the least navigation problems. The EU and other funds finance the maintenance of locks and removal of submerged ships from the II World War in Prahovo. The second corridor is Orient/East Mediterranean, which, in its greatest part, follows the route of the former Pan-European Corridor X. Figure 2 shows the TEN - T corridors defined by the new TEN - T policy.

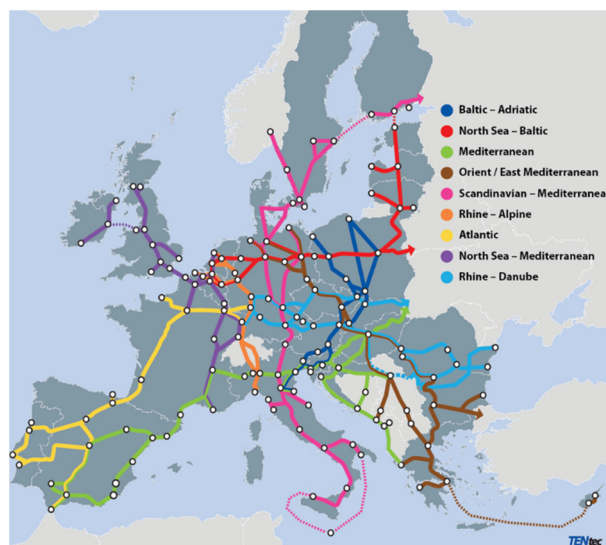


Figure 2. TEN - T corridors

The General Master plan of traffic in Serbia until 2027 is support for making the right decisions in development. It is an instrument of strategic planning that should be constantly used and improved. It provides for the establishment of good legislative procedures and the modernization of the institutional framework in the field of transport. He also gave directions for the strategy of development of water transport of the Republic of Serbia from 2015 - 2020. The results of the EU DAHAR project (Danube Inland Harbor Development) - Transnational program of development (SEE) related to the development of ports as logistics centers and their integration into the Danube logistics network were taken into account when drafting the Strategy in the form of recommendations to competent state authorities. The goal of the project is to align the long-term logistic development of the small and medium - sized port on the Danube, which would result in the establishment of a common development strategy. Position of the Republic of Serbia in relation to the Danube basin is given in Figure 3.



Figure 3. Position of the Republic of Serbia in relation to the Danube basin

Figure 4 shows the forecast of the volume of traffic on inland waterways of the Republic of Serbia (in thousands of tonnes) realized by domestic and foreign ships (inland transport, import and export) [1].

Bearing in mind that multimodal traffic allows the rapid and safe transportation of large quantities of goods, as well as directly affecting the reduction of traffic congestion and pollution reduction, the increase in the volume of goods transported by inland waterways is a direct consequence of accepting the principles of multimodality.

Table 1. Participation of exports by ports in the listed cities of the Republic of Serbia (in tonnes) in total exports

Ports and docks	Quantity of freight (t)	%
Pančevo	743394	34.41
Smederevo	352041	16.30
Belgrade	72927	3.38
Novi Sad	619837	28.69
Prahovo	-	-
Other	371964	17.22
Total	2160163	

2. STATE-OF-THE-ART AND POTENTIALS OF THE PORT OF NOVI SAD

The Port of Novi Sad (Luka Novi Sad A.D.) is situated at 45°20'N and 19°51'E, in the central part of the Autonomous Province of Vojvodina in northern Serbia.

The Port of Novi Sad is located at km 1254 at the left bank of the Danube, in the Novi Sad – Savino Selo Canal (part of the Danube - Tisa - Danube - DTD Canal network) at its km 0.4 - 1.2. It covers an area of 24 ha.



Figure 5. Danube Region [2]

Port is situated at the TEN-T Rhine - Danube Corridor (former Pan-European Corridor VII), as well as at former Pan - European Corridor X, which is projected to be a part of the TEN-T Orient/East - Med Corridor, Figure 6, and it is an important transport and cargo handling center of the Central Europe.



Figure 6. Position of the Port of Novi Sad

This position clearly indicates a good geographical position of the port and determines the direction of development in order to meet the needs of the local economic environment and international flows of goods, with particular attention to the development of multimodal transport.

The distance between the Port and the corridors:

- 300 m to the railway corridor Xb,
- 3 km to the road corridor Xb.

The Port of Novi Sad is located in the Novi Sad city which belongs to a group of Danube cities. The Novi Sad city, thanks to its geographical position in Province of Vojvodina and good traffic connections, represents the economic and business center of Vojvodina. The Port of

Novi Sad serves a region with a diameter of 60 km in which live approximately 600,000 inhabitants. Although the port handles several dominant types of goods, where each of them has specific origin and destination of their flows which implies that the size and shape of hinterland is different in relation to the type of transported goods, however it could be said that the basic hinterland of the Port of Novi Sad is South Bačka district (region within 60 km), while the competition margin cover almost the whole range of Vojvodina (Figure 2.4.). The Port of Novi Sad is mainly port for bulk cargo where the main exporting goods are cereals (mostly transported to Constanta and to a lesser extent to Germany) and scrap iron transported to Constanta. Transport activities in the port hinterland are realized mostly by road transport. The imported goods are coal and coke (import from Russia), fertilizers (import from Russia, Romania and Austria) and road salt (import from Egypt).

The direction Danube - east provides links with:

- All international ports along the Danube, downstream from Novi Sad. In addition to the ports in Serbia, those are: Bulgarian ports (Vidin, Lom, Ruse, Silistra,...), Romanian ports (Cernavoda, Braila, Galati, Giurgiu, a canal and Constanta) and Ukrainian ports (Reni and Izmail).
- Black Sea ports Varna, Burgas, Constanta.
- Over the Black Sea ports, the port has a direct connection with the Mediterranean Sea, Atlantic and Indian oceans.

The direction Danube - west provides links with:

- All international ports along the Danube upstream of Novi Sad, as are: Hungarian ports (Baja, Dunaujvaros, Budapest,...), Slovak ports (Komarno, Bratislava), Austrian port (Vienna, Linz, Enns) and German ports (Passau, Regensburg, Kelheim)
- Rhine region over the Rhine - Main - Danube Canal with Germany, Switzerland, France and the Netherlands, which provides way to the North Sea and Atlantic Ocean.

2.1 Infrastructure and equipment

The port disposes of a water area of 6 ha, with a depth of 4 - 10 m and 5 mooring places for the simultaneous accommodation of ships. The total length of the quay is 800 m.

The port has 6,000 m of operational railway tracks.

The port disposes of following equipment:

- Portal cranes, capacity 5 t to 27.5 t,
- 7 forklifts with a capacity of 3 t, 1 forklift with a capacity of 5 t, 2 forklifts with a capacity of 12.5 t, 1 forklift with a capacity of 28 t,
- 2 wheel loaders, 3 skid - steer loaders,
- 2 weighbridges, of which one is for road and rail with a measuring range of 100 t,
- 3 telescopic funnels for bulk cargo handling, with capacity of up to 500 t/h per funnel,
- 2 packaging machines (packing of bags of 50 kg and big bags of 1,000 kg),
- Pump for oil products with a storage capacity of 270,000 m³.



Figure 7. Port of Novi Sad surroundings infrastructure

The Port of Novi Sad disposes of 44,000 m² of closed and 100,000 m² of open storage areas in the function of public and customs warehouses. These storages offer storage services for domestic and export and import goods.

2.2 Cargo handling in the port

The port handles and stores:

- Bulk cargo,
- General cargo,
- Containers and
- Liquid cargo.

The most common handled and stored cargoes are bulk and general cargoes.

2.3 Containers handling

The Port of Novi Sad can handle 20' and 40' (and 45') containers of maximum gross weight up to 27 t. In recent years, the port handles containers arriving by road and rail from the Adriatic ports Koper and Rijeka. Transshipment of containers arriving on the Danube is unfortunately rare.

2.4 Port development plans

The long - term development of the Port of Novi Sad would have the following point:

- Short - term development in an existing location that should become a logistics center and
- Long - term development into so - called Asia logistics center with the relocation of all bulk cargo (and silo) and "dirty goods" to a new location, and at the existing location, which is an integral part of the urban zone of the City, to build warehouses with additional logistical services.

3. CONTAINER FLOWS AND FORECASTED VOLUME OF CONTAINERIZED TRANSPORT

Regarding the available data for Serbia, obtained by interviewing leading containers forwarding companies operating in Serbia, container throughput is around 75,000 containers): 45,000 containers - import / 30,000 containers - export

Main ports for Serbian container export/import are:

- Rijeka, Croatia: (40,000 containers),
- Bar, Montenegro: (20,000 containers),
- Koper, Slovenia: (10,000 containers),

- Piraeus, Greece: (3,000 containers),
- Thessaloniki, Greek/North EU ports (Rotterdam, Hamburg, Antwerp): (2,000 containers).

Total imports and exports from the customs offices that gravitate to the Danube Region and in the reviewed period from 2015 - 2017 (Figure 8) are given in Table 2 and on the chart (Figure 9). [3]

Table 2. Total imports and exports from the customs offices that gravitate to the Danube Region in the TEUs in the period 2015 - 2017. [3]

	2015	2016	2017
Export	24,470	24,756	30,055
Import	61,124	68,804	76,329
Total	85,594	93,560	106,384

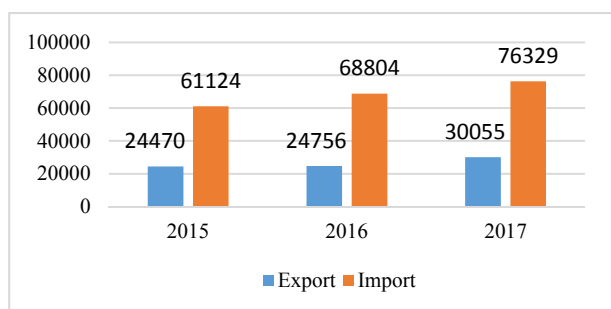


Figure 8. Total imports and exports from the customs offices that gravitate to the Danube region in the period 2015 - 2017. [3]

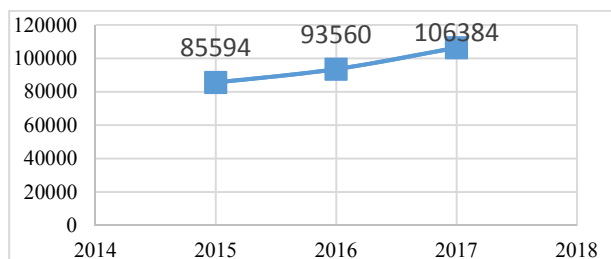


Figure 9. Total imports and exports from the customs offices that gravitate to the Danube region [3]

The overall export and import of containers in the Republic of Serbia, as well as the export and import realized through the customs offices that gravitate to the Danube region, is given in the following chart (Figure 10). [3]

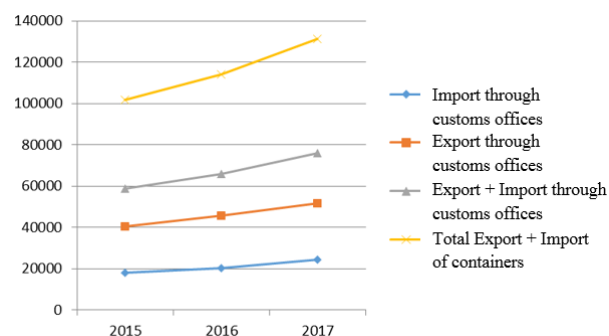


Figure 10. Export, import of containers, export and import realized through the customs offices that gravitate to the Danube region [3]

The increase in the number of containers in the Danube Region is: 9.3% for 2015 - 2016, and 13.7% for 2016 - 2017, and as a basis for the assessment of growth can be taken:

- 10% as the expected annual increase (medium scenario),
- 5% as a pessimistic option (low scenario),
- 15% as an optimistic option (high scenario).

For containers and container transport in the Danube Region, regarding Serbia and from the previous analysis, on the basis of 106,338 TEUs from 2017, follows: The increase in the number of containers, according to data from the Customs of Serbia, can be approximately estimated to 10% per year.

If in Serbia, related to the Danube region, the increase in the number of containers in the next 5 years would be at the level of:

- 0%, this would mean over 60% of TEUs for the next 5 years, which is 171,278 TEUs,
- 5% (pessimistic variant) for the next 5 years would mean about 28% TEUs, which is 136,171 TEUs,
- 15% (optimistic variant), this would mean over 100% TEU for the next 5 years, which is about 212,768 TEUs.

For the next 10 years (until the end of 2027), during which the cost of investing in the container terminal should be demanded, the number of containers in Serbia - the Danube region would be with a factor of annual increase of:

- 10% the number of containers would increase by a factor of 2.6, or around 276,598 TEUs,
- 5% (a pessimistic variant) would for the next 10 years amount to about 63% TEU, which is 173,405 TEU,
- 15% (optimistic variant), the number of containers would increase by factor 4 or about 425,536 TEU (optimistic forecast).

Of the total number of containers in Serbia, it can be taken with great reliability that

- One third belongs to the region of Vojvodina,
- One third to the region of Belgrade,
- One third in the region of southern Serbia (south of Belgrade).

Customs data of Serbia show that over 80% of the total container transport expressed in TEUs gravitates to the Danube region. [3]

If the base is taken as a rounded figure for 2017 of 105,000 TEUs that is for the increase in the number of containers of 10% per year in the Danube region:

- 169,000 TEU for 5 years,
- 273,000 TEU for 10 years (until the end of 2027). [3]

For the region of Vojvodina, which conditionally tends to the port in Novi Sad, the number of containers could be at the level of 1/3 of the total number of TEUs for the Danube Region (estimated by the number of TEUs by customs offices), which means for 2017 from the current around 35,000 TEU, for 5 years:

- With a 10% increase of 56,000 TEUs,
- With a 5% increase of 45,000 TEUs (pessimistic option),

- With a 15% increase of 70,000 TEUs (optimistic option).

And in 10 years, the expected number of containers in the Port of Novi Sad could be:

- With 10% increase: 91,000 TEU,
- With a 5% increase of 57,000 TEUs (pessimistic option),
- With 15% increase: 140,000 TEU (optimistic variant).

Such a forecast indicates that there is sufficient justification for the design and construction of a container terminal on the Danube and the expectation that the Danube will be a carrier or at least a significant factor in container transport.

For containers that could gravitate towards the Port of Novi Sad, the number of means of transport for previous data for 2017, forecasts for 2027 and for the increase in the number of containers of 10%, provided all containers are transported with the respective modes of transport is:

- 17,500 to 45,500 trucks for the transport of containers in an ideal combination of 2 TEUs/semitrailers (half of the designated numbers for TEUs),
- 583 compositions with 60 TEUs/composition, up to 1,517 compositions,
- 437 ships or barges (with 80 TEUs/barges), up to 1,137 barges for 2027.

If navigation on the Danube would be at least 300 days a year, it would appear that under ideal logistics conditions, if all the containers were transported by the Danube, it could be one to two self-propelled ships daily on the Danube.

In real terms, the number of containers that can be transported by the Danube is primarily associated with containers that come from the east and are unloaded in Constanta and a smaller number of containers circulating from and towards central Europe along the Danube. For these analyses, global movements of goods must also be taken into account, since the transport of the containers by the Danube implies liner services from Constance to at least Enns or Regensburg.

If the situation arises that the North Ports are overloaded with containers as it was before 2008, world operators will look for more favorable variants with ports on the Adriatic Sea and with the Constanta port for containers coming from the Far East, which in that period favored the activation of container terminal in Constanta, but also in Koper, Rijeka, etc. [3]

Since this analysis is restricted to the Port of Novi Sad, it appears that, with 10% growth, container terminals from the current potential of 35,000 TEU (up to 91,000 TEU in 2027) could have been a railway or railroad-road terminal for the transshipment of containers that arrive with wagons and ships, because truck transport from the Adriatic ports means door-to-door transport and does not require reloading.

If for reasonable 5 - 10 years the Serbian Railways are brought into the state of acceptable use and increase the environmental awareness of unacceptable environmental pollution from truck transport, at least half of these containers could be railways (including Luka Piraeus). The Danube remains a potential not only for Serbia, but also for EU countries.

Following this ecological principle for the transport of goods, for the Danube and for the Port of Novi Sad, the targeted number of containers in the Port of Novi Sad in 2027, therefore with a ten-year delay in applying EU environmental rules, would be: About 41,000 TEUs in 2027 would have to be transported by the Danube and unloaded in the Port of Novi Sad, while the rest to 91,000 TEU by rail (18,200 TEU) and road transport (over 31,000 TEUs).

At the level of 5 years, with a 10% increase, this figure gives 25,200 TEUs for the transport by the Danube and 11,200 TEUs by rail transport, which involves cargo handling in the port.

Based on these presented data, it is obvious that there is a need for the creation of a modern container terminal in Serbia, in this case it should be the new container terminal in the Port of Novi Sad.

The above data will be a basis for further work on the design of the container terminal in the Port of Novi Sad.

4. CONCLUSION

The aim of this paper was to analyze possibility of construction of the new container terminal in the Port of Novi Sad which has regional and international importance and good geographical position, located in the Serbian Autonomous Province of Vojvodina.

The basic goal was to identify container volumes in the region and estimate feasibility for the logistics center.

For the predicted volume of containerized transport in the Danube Region and Vojvodina province three assumptions have been analyzed, for the next periods of 5 years and respectively 10 years:

- 10% as the expected annual increase (medium scenario),
- 5% as a pessimistic option (low scenario),
- 15% as an optimistic option (high scenario).

For the economic hinterland of the Port of Novi Sad, in the foreseen conditions could be expected a realistic increase of the container flows by 10 %.

Based on the analyses and the current location of the Port of Novi Sad, it is assumed that the container terminal handles only containers with goods that are not in the category of dangerous goods.

It is as a final point conclusive that the construction of a new container terminal in the Port of Novi Sad on the Danube aims to bring about a significant change in the container transport system in Serbia, but also in the region or the Danube countries as the development of containerization is a prerequisite for the development of economy. It is obvious from this paper that the transport of goods to the Danube should be significantly more economical in order to gain an advantage in the supply chain. Also, as the follow-up effects of the new container terminal in the Port of Novi Sad and its transformation in the logistics center, in addition to all other effects, will generate new jobs and enable integration of the Port into the EU intermodal transport network.

Finally, it should be mentioned that the expected level and type of activities in the area of the Port of Novi Sad regarding the development of the new container terminal won't affect the environmental and health impacts, if the

proper and well planned measures are carried out. Furthermore, there will be no additional impact on cultural heritage and historical heritage within the new terminal location.

ACKNOWLEDGMENT

The presented research was done within the INTERREG project DBS Gateway Region, Regional and Transport Development in the Danube-Black Sea Region towards a Transnational Multiport Gateway Region, 2017-2019.

REFERENCES

- [1] Waterway Transport Development Strategy of the Republic of Serbia for the period 2015-2025 (Strategija razvoja vodnog saobraćaja Republike Srbije od 2015. do 2025. godine), "Sl. glasnik RS", br. 3/2015.
- [2] <https://www.danube-region.eu/about/the-danube-region>
- [3] Zrnić, N., Bojić, S., Georgijević, M., Urošević, M.; Analysis of the potential of Serbia to transport containers on Danube, XXIII International Conference on Material Handling, Constructions and Logistics, Maritime and Port Logistics – Bar Conference, pp. 32-37, Bar, Montenegro, 2019.

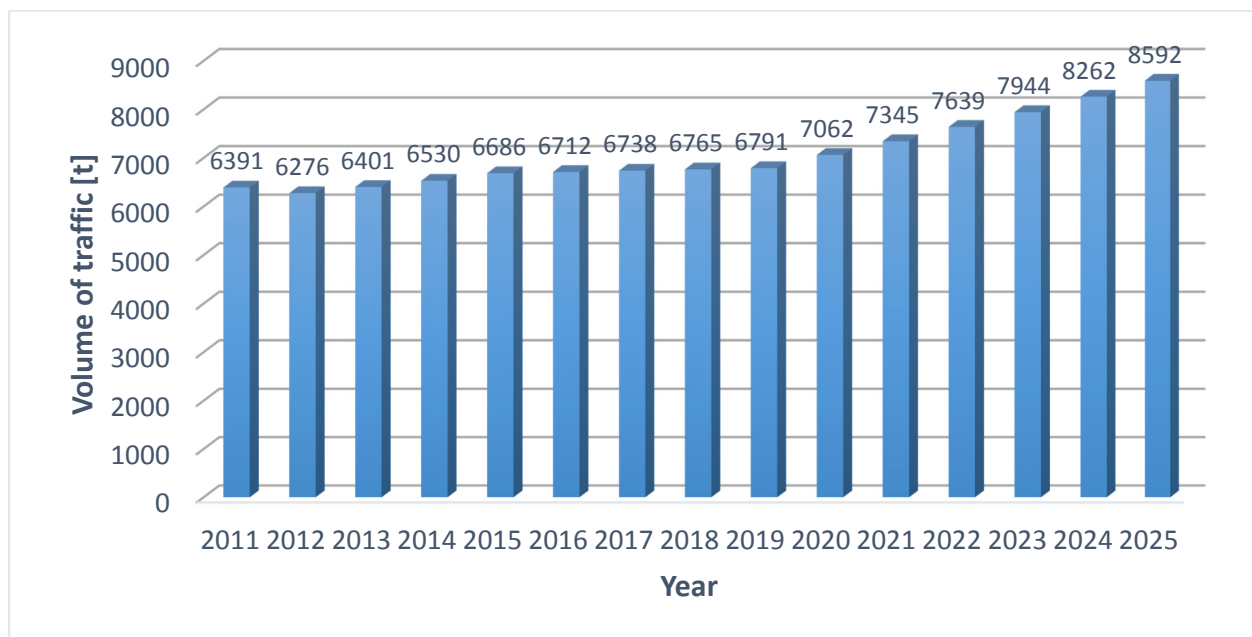


Figure 4. Forecast of traffic volume on the inland waterways of the Republic of Serbia

I. Dafnomilis

Postdoctoral Researcher
Delft University of Technology
Faculty of Mechanical, Maritime and
Materials Engineering
Department of Maritime and Transport
Technology

M. B. Duinkerken

Assistant Professor

D. L. Schott

Associate Professor

J. Ley

Design and Simulation Engineer
Development Centre for Ship Technology
and Transport Systems

G. Assbrock

Design Engineer

Optimization design of a floating modular port terminal

This paper presents a mathematical programming model for planning investment strategies in a modular floating terminal. The model is developed with the objective of minimizing the net present costs of a terminal's investments, equipment selection and operational costs over a long term future. The problem formulation evaluates time dependent parameters, such as container throughput forecasts, and performance, quality and availability of equipment over time. The results provide a visualization of investments for a modular floating terminal design, and are geared towards assisting stakeholders in strategic level planning – the optimal way to invest in new terminal setups, infrastructure and equipment selection.

Keywords: terminal design, terminal logistics, floating platform, modular terminal

1. INTRODUCTION

Global trade is increasing continuously in all dimensions like tonnage, number of containers, number and size of vessels and port size. The expansion of container handling capacity is a major issue for many sea ports because of limited space and water depths restrictions in adjacent rivers or channels. Similarly, the need for affordable renewable energy, agricultural land and even living space becomes increasingly more important, especially in populated regions like Central and North Europe. Innovative solutions are required to overcome these problems [1].

Combining several activities such as renewable energy, aquaculture, maritime transport and related services in the same marine space, including in multi-use plat-forms, can serve to divide and reduce the costs of offshore operations and the demand on the space needed for different activities. Research on multi-use platforms has already provided promising designs, technological solutions and models for combining activities in terms of economic potential and environmental impact [2]. However, before reaching a demonstration pilot stage, further technological research and innovations are needed to reduce risks for operators and investors.

1.1 Research objective

Research attempting to address the aforementioned concepts should develop combinations of innovative, cost-effective technologies and methods including automation and remote monitoring technologies, flexible structures and facilities in order to test concepts of multi-use platforms leading to pilot demonstration phases [3].

Correspondence to: Ioannis Dafnomilis PhD, Postdoctoral Researcher, Department of Maritime and Transport Technology, Mekelweg 2, 2628CD Delft, The Netherlands
E-mail: I.Dafnomilis@tudelft.nl

In light of the above, a multi-period optimization model has been developed in order to optimize the strategic level design of such a modular floating logistic hub, focusing in relieving some of the strain from congested ports in mainland Europe.

1.2 Methodology

The strategic logistic optimization is based on the assumption of increasing global trade, thus a growing demand for future terminal concepts. Such new terminals are meant to meet expectations of larger vessels and progressing number of traded goods. Defining demand scenarios, the optimization is performed for multi-period as well as steady-state scenarios. This way, terminal concepts can be evaluated for their performance in a variety of boundary conditions and demands. The optimization is specific for a cargo type and tailored for one location. The defined approach for the terminal design is:

- Creation of a database of all potential equipment that is considered for use in an modular floating terminal
- Literature survey and expert input covering equipment logistics (capital and operational expenses)
- Development of an optimization model aiming at minimizing the total costs of terminal logistic operations
- Results that provide optimal equipment and module selection and utilization, as well as dimensioning the island in relation to logistics

2. CONTAINER TERMINAL OPTIMIZATION – PARAMETERS AND ASSUMPTIONS

For the construction of the optimization model, two prerequisites need to be met: 1) A database that contains details on all the available equipment and infrastructure under consideration – capital and operational costs, productivity, storage capacity and 2) an extensive set of assumptions that describe the proposed container terminal operations as realistically as possible. These assumptions will form the constraints of the mathematical model in section 3.

2.1 Equipment and module database

Table 2 presents an aggregation of all the equipment under consideration for the floating terminal, along with their performance, as well as data related to their costs. While the productivity of container handling equipment is usually measured in moves/hour, it is important to transform this into TEU/hour (twenty-foot equivalent unit), as the use of a single metric makes interactions between functions of the model, e.g. between loading and storage, easier.

2.2 General modelling assumptions

- **Throughput:** Several throughput scenarios have been developed in order to assess the design and performance of the platform under different assumptions. The goal is to select suitable equipment on a strategic level, which can handle the expected demand. Due to space restrictions, only 2 of the 5 developed scenarios are presented, in the Appendix of this work.

- **Cargo breakdown:** The TEU factor is 1.5, i.e. 60% FEU (forty-foot equivalent unit) and 40% TEU containers respectively [1].

- **Operational steps:** The basic functions of a container terminal are broken down in 3 discrete operational steps – unloading of vessels, storage, and loading of containers to vessels for further transport. Each operational step is associated with specific container handling equipment and module types.

- **Loading/Unloading:** Both processes are assumed to be performed in a similar manner. The unloading equipment is chosen as large STS cranes able to handle ultra-large container vessels that can handle 4TEU/move when equipped with a double spreader. Only the largest size barges are chosen as loading vessels for inland transportation (Feeder type, 734 TEU/barge). Loading equipment is chosen as smaller STS (ship-to-shore) cranes that can handle 4TEU/move when equipped with a double spreader.

- **Equipment Capacity:** The average annual productivity of each equipment and the total number of hours the terminal operate have been estimated based on literature data:

310 days of operations/year

20 hours of operation/day

6200 hrs of operation/year in total

30 moves/hour nominal productivity for the unloading STS cranes

20 moves/hour nominal productivity for the loading smaller STS cranes

25 moves/hour nominal productivity for the RMG (rail mounted gantry) cranes

Productivity performance is further affected by the container handling efficiency due to wave and wind conditions at the selected location.

- **The technical and economic lifetime of each equipment type** are assumed to be the same. Economic

lifetime is the expected period of time during which a unit of equipment is useful to the average owner. The economic life of an asset could be different than its actual technical life. The values related to the lifetime of equipment are based on relevant literature.

2.3 Specific modelling assumptions

1. Two 45m modules rigidly connected are used per STS crane for the unloading berth, since large STS cranes to service the ULCV (ultra-large container vessels) require the length.

2. The outreach of the RMGs located on the storage modules adjacent to the unloading modules is enough to pick up the container(s) and transfer it to the storage modules, as well as between storage modules.

3. Combinations of 45m and 90m modules are used for the storage function of the platform.

4. 45m modules are used for the loading function of the platform.

5. One RMG crane for each 45m storage module and 2 RMGs for each 90m storage module are required since there are no rigid interconnections between modules.

6. Smaller STS cranes on the loading side to load the containers on the barges for further inland transportation.

7. A uniform equipment discount rate (or interest rate) of 0.06 (or 6%) is used throughout the model.

8. Maintenance costs of equipment are set to 3% of their respective capital costs.

3. MATHEMATICAL MODEL FORMULATION

The optimization approach presented in this chapter is formulated as an MILP (mixed-integer linear programming) problem that minimizes terminal logistics on a normal-ized annual basis. The cost function is minimized respecting certain system constraints. The output of the model is the optimal terminal configuration with specific installed capacities for the chosen equipment in terms of overall costs. The optimization performed by the model is an overall terminal logistics optimization and not a step-specific one.

3.1 Indices

i	Type of equipment	$i \in [1, \dots, 9]$
j	Operational step of terminal	$j \in [1, 2, 3]$
k	Type of module	$k \in [1, 2]$
t	Time period	$t \in [1, \dots, 12]$

3.2 Decision variables

n_{ijt} Number of equipment i used at step j at time period t

x_{ijt} Utilization of equipment i used at step j at time period t

p_{ijt} Purchased equipment i used at step j at time period t

m_{kjt} Type and number of module k used at step j at time period t

y_{kjt} Utilization of module k used at step j at time period t

3.3 Parameters

CT_t [TEU]

Container throughput per scenario

EC_i [TEU/y]

Equipment capacity for equipment i

$$EC_i = ENC_i * OPH * cte * oee_{it}$$

ENC_i [TEU/y]

Equipment nominal capacity for equipment i

cte [-]

Container transfer efficiency based on environmental conditions

OPH [h]

Operational hours of the terminal

oee_{it} [%]

Overall equipment effectiveness of equipment i at time period t

$$oee_{it} = a_{it} * p_{it} * q_{it}$$

a_{it} [%]

Availability of equipment i at time period t

p_{it} [%]

Performance of equipment i at time period t

q_{it} [%]

Quality of equipment i at time period t

SC_{kj} [TEU]

Storage capacity of modules

CC_i [€]

Capital costs of equipment i

r [-]

Interest rate of equipment

LT_i [y]

Lifetime of equipment i

MC_i [€]

Maintenance costs of equipment i

OC_{it} [€/TEU]

Operational costs of equipment i at time period t

$$OC_{it} = ep_t * elc_i$$

ep_t [€/kWhr]

Industrial electricity price for the Netherlands at time period t

elc_i [kWhr/TEU]

Electricity consumption of equipment i

3.4 Objective function

Minimize the total capital costs incurred as a result of selected equipment:

$$Z = \sum_{ijt} (p_{ijt} * NPCC_{it} + x_{ijt} * NPOC_{it} * CT_t + n_{ijt} * NPMC_{it})$$

Capital expenses CC_i only incur when the equipment is purchased. Any capital expenses incurred in a future time period t are discounted to the present via the commonly used discount factor $\frac{1}{(1+dr)^t}$, where dr is the discount rate used in this work and is equal to equipment interest rate r . Thus, the net present capital costs for the purchasing of each equipment i used in step j are given as:

$$NPCC_{it} = CC_i * \frac{1}{(1+r)^t} \quad (1)$$

Similarly, the operational and maintenance costs of the terminal for each time period are discounted to the present with the same discount factor as above, and have the following expression:

$$NPOC_{it} = OC_{it} * \frac{1}{(1+r)^t} \quad (2)$$

$$NPMC_{it} = MC_i * \frac{1}{(1+r)^t} \quad (3)$$

3.5 Constraints

- Equipment capacity demand: All TEU demand should be satisfied by the selected equipment at each

function (unloading, inter-terminal transport, loading) at each time period

$$\sum_i x_{ijt} * EC_{il} \geq CT_t, \quad \forall j, t \quad (4)$$

- The required storage capacity should be covered by the modules at the storage step for each time period

$$\sum_k y_{kjt} * SC_{kj} \geq CT_t / \text{daysperyear}$$

$$j = 2, \quad \forall k, t, \text{ 1 day dwell time} \quad (5)$$

or

$$\sum_k y_{kjt} * SC_{kj} \geq 3 * CT_t / \text{daysperyear}$$

$$j = 2, \quad \forall k, t, \text{ 3 days dwell time} \quad (6)$$

- Due to the nature of optimization, the absolute preferable scenario for the storage step would be to purchase a small number of equipment with the highest capacity, and use those to satisfy all the demand. Then, the cheapest possible equipment would be purchased and not operated to satisfy the need for equipment presence on each module. However, in reality we need all the equipment on the storage modules to operate, since all modules are used for the container storage. Thus, we need to enforce that all equipment selected in the storage step should be used for a certain amount of TEU handled

$$x_{ijt} \geq 3 * n_{ijt} * CT_t / \text{daysperyear}$$

$$i = [3, 4], j = 2, \forall t \quad (7)$$

$$x_{ijt} \geq 2 * n_{ijt} * CT_t / \text{daysperyear}$$

$$i = [5, 6, 7], j = 2, \forall t \quad (8)$$

- For each time period t , the number of selected equipment must be equal to the number of selected equipment in time period $(t - 1)$, plus any new equipment that is purchased at the start of period t . Additionally, we need to purchase equipment at the first time period:

$$n_{ijt} = n_{ij,t-1} + p_{ijt}, \quad \forall i, j, t > 0 \quad (9)$$

$$n_{ijt} = p_{ijt}, \quad \forall i, j, t = 0 \quad (10)$$

- Number of 45m modules used for unloading needs to be twice the number of units of large STS crane number and number of 45m modules used for

loading needs to be equal to the number of units of small STS cranes respectively (see section 2.3)

$$m_{kjt} = \sum_{i=3}^4 n_{ijt}, \quad j = 1, k = 1, \forall t \quad (11)$$

$$2 * m_{kjt} = \sum_{i=5}^7 n_{ijt}, \quad j = 3, k = 1, \forall t \quad (12)$$

- Number of RMG cranes is 1 per 45 and 2 per 90m module respectively (see section 2.3)

$$\sum_{i=3}^4 n_{ijt} = m_{kjt}, \quad j = 2, k = 1, \forall t \quad (13)$$

$$\sum_{i=5}^7 n_{ijt} = m_{kjt}, \quad j = 2, k = 2, \forall t \quad (14)$$

- Utilization of equipment cannot exceed the maximum utilization of selected units of equipment and utilization of modules must be lower than the respective units of modules

$$x_{ijt} \leq n_{ijt} * EC_i, \quad \forall i, j, t \quad (15)$$

$$y_{kjt} \leq m_{kjt}, \quad \forall k, j, t \quad (16)$$

4. RESULTS

4.1 Time series throughput

In this section, the results of the application of the multi-period optimization model introduced in chapter 3 are presented. The model provides the optimal equipment selection and utilization, in terms of TEU handled per year, which results in the minimization of the total floating platform logistics. A sensitivity analysis is also performed by adjusting the dwell time (DS) of the containers, as well as their stacking height (SH) on the storage modules.

Table 3 presents the results of the optimization process for the multi-period approach. It is worth noting that although the final amount of containers handled in year 2030 is very similar to that of scenario A (5.53 vs 5.64 * 10⁶ containers) which is presented in the following section, the terminal sizes are different for all combinations. This is due to the difference in the objective of optimization between the 2 models. The given throughput model optimizes the terminal design for a static throughput that is assumed to be certain and unchanging, while the multi-period model optimizes the design for a time-series throughput, that requires much more flexibility and has to take into account expansions in handling and storage capacity at each given time period.

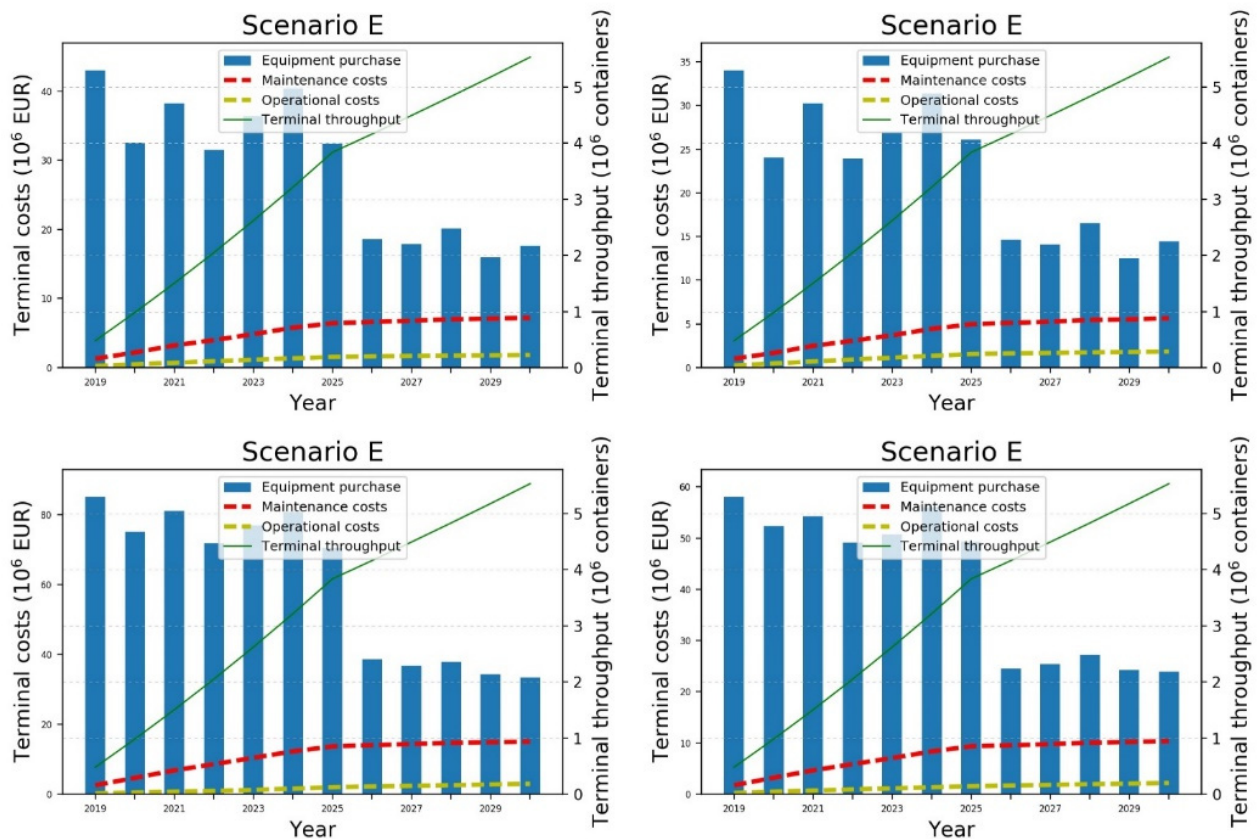


Figure 1: Total annual terminal costs, scenario E, all cases

Figure 1 presents the necessary equipment purchase strategy, alongside the maintenance and operational costs of selected equipment throughout the whole time period into consideration. On the top left is the case for 1 day dwell time and 3 container stack height, and the bottom right is the case for 3 days dwell time and 5 container stack height. The constantly increasing throughput requires constant purchase of equipment, the overwhelming majority of which is tied to the constant need for new storage modules, in order to satisfy the storage constraints. As such, while the operational costs increase as well, since more containers are handled every year, the rate of increase is low, since the new equipment is not used to a high degree of its capacity.

4.2 Steady state throughput

If we remove the time dependent elements of the modelling approach, we are able to have results catering to steady-state throughput terminals, i.e. terminals designed to handle a specific throughput. For each scenario, the model provides the optimal equipment selection and utilization as presented above, which results in the minimization of the logistics. Only the results for one of the steady-state scenarios are presented in this work. The breakdown of the equipment selection and utilization for scenario A can be seen in Table 34, and a visualization of the terminal costs can be found in Figure 2 and Figure 3.

Additionally, several other important parameters such as the split between capital and operational costs,

the number of each container type handled and the berth lengths can be found in Table 4.

Table 3 presents the equipment selection and utilization as well as the module selection that achieves the minimum annual costs for scenario A, for the specific parameters mentioned in the table title. The term utilization in the context of this work refers to the amount of TEU that the equipment handles within a 1 year period.

In Table 5, several other direct and indirect (pre- or post-processing) results of the modelling approach can be found. The information presented here are of significant importance to be used as terminal performance indicators (such as the cost/TEU or cost/container handled), and can be used as input in further research – hinterland optimization, vessel routing simulation etc..

The decision to have a 3 day dwell time has a massive effect on all the related terminal costs, which increase by 100% or more compared to the 1 day dwell time, and the size of the terminal, which behaves accordingly. As is evident in Figure 2, the increase in the costs comes from the increase in storage costs, mainly capital costs for the additional equipment needed on each additional storage module.

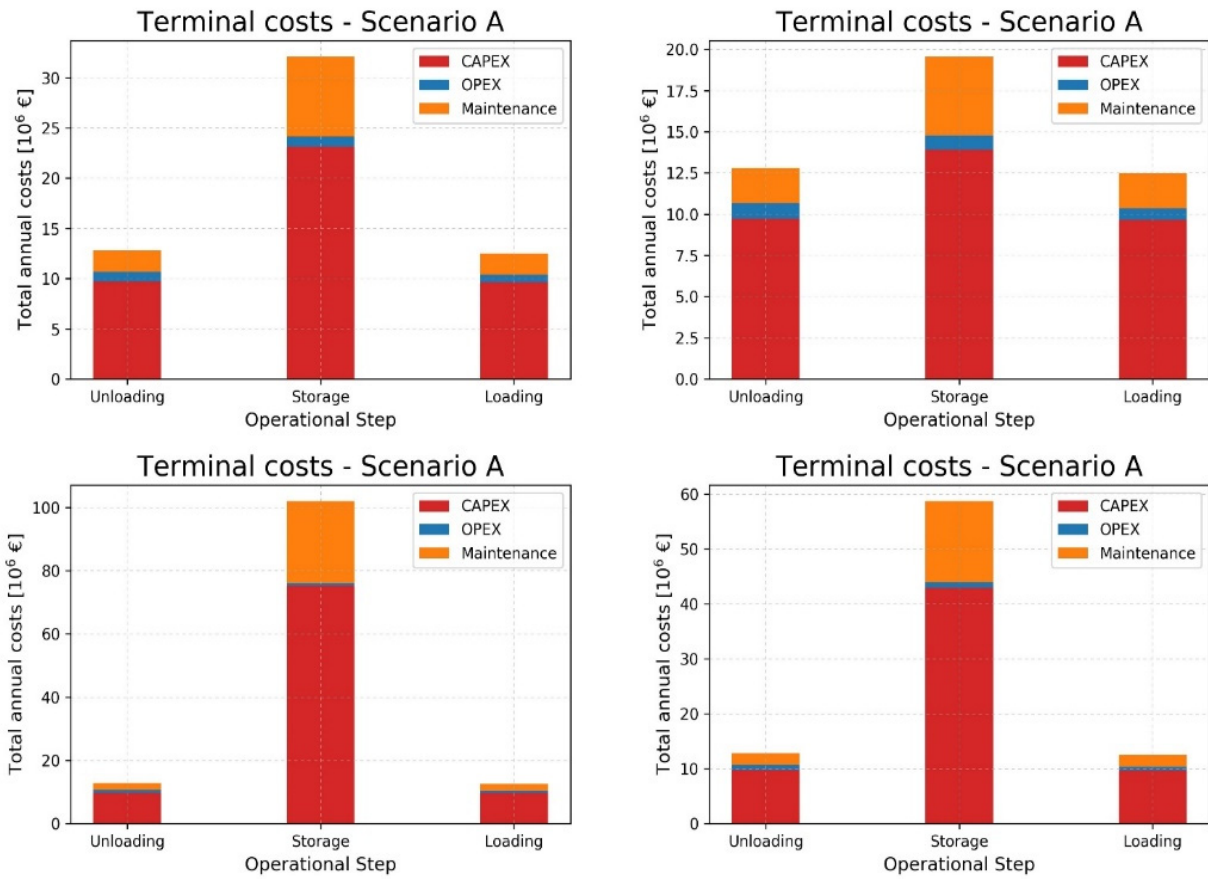


Figure 2: Total annual terminal costs, scenario A, all cases

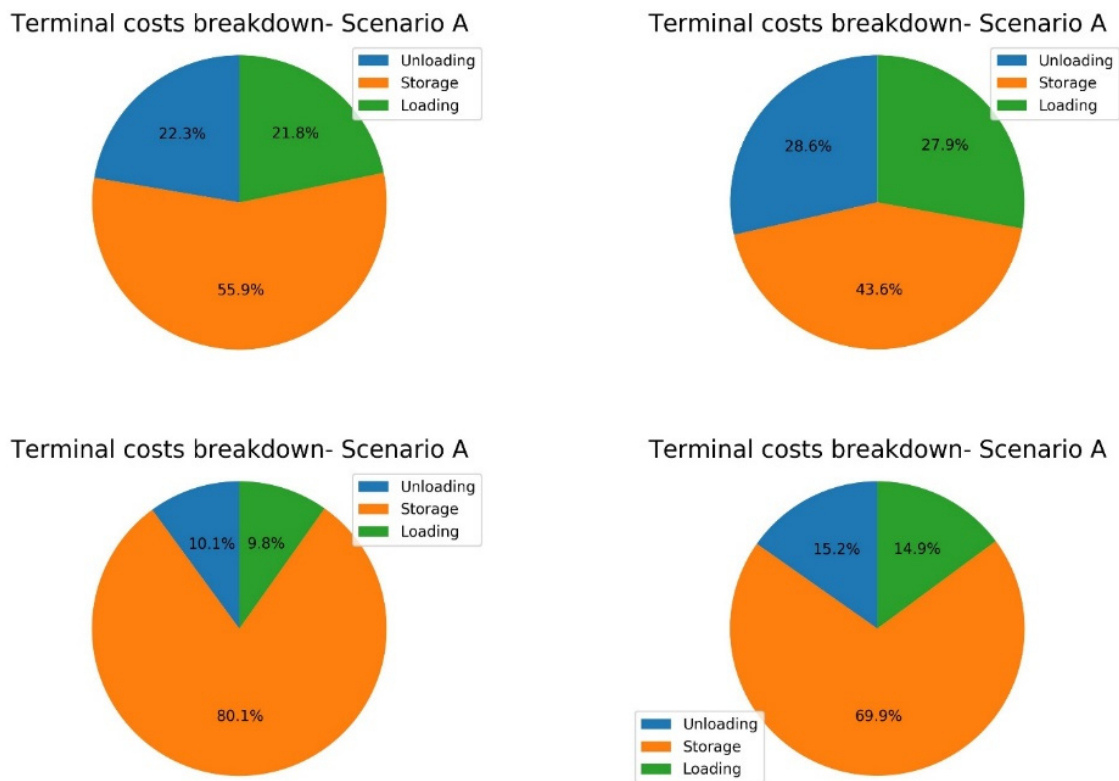


Figure 3: Terminal costs breakdown, scenario A, all cases

Figure 2 and Figure 3 provide a visualization of the costs per operational step, and the percentage of these costs in terms of total costs, respectively. On the top left is the case for 1 day dwell time and 3 container stack height, and the bottom right is the case for 3 days dwell time and 5 container stack height. Storage incurs by far the greater costs for the floating platform, as the nature of a floating terminal demands rail-mounted gantry cranes present on all storage modules, which leads to proportionally significant capital and maintenance costs. At the same time, the cranes on each storage module are used far less individually than the STS cranes in the (un)loading procedures, which leads to low utilization rates and low operational costs.

5. CONCLUSIONS

Using layout concepts developed in previous research [4], gantry crane and rail mounted crane only are used for (un)loading of vessels and for storage respectively. The optimization approach developed provides the optimal equipment and module selection and utilization in order to minimize the total net present floating terminal logistics for both a multi-period and a steady-state approach.

The scenarios, as well as the different storage periods and cargo stream details are used as a sensitivity analysis of the optimization model, in order to assess the different options for the final platform setup. As expected, the decision to go for low dwell times and higher stacking of containers provides the most economically favorable option for the terminal design, both in terms of total costs and island size, while ensuring that the throughput in every case is efficiently handled.

The main contributor to the terminal costs is the storage function, as due to the inability of rigid connections between modules forces the use of rail mounted gantry cranes on each individual storage module, leading to disproportionally high capital and maintenance costs, while incurring low operational costs.

Along the optimization-related results, many more data is provided during the pre- or post-processing of the modelling approach. The information presented here are of significant importance to be used as terminal performance indicators (such as the cost/TEU or cost/container handled), or will be used as input in further research - number of each type of container, terminal size, berth lengths etc.

For the current version of this model, the module construction and installation costs are not taken into account, since the boundaries of the work performed are limited to the actual equipment used in the container handling. In reality however, these costs will be an important factor as well in affecting decision making and may alter the optimization results to a significant degree. A further expansion of the modelling approaches will need to take these costs into account. Similarly, if information is available regarding the profits expected to be generated from the terminal's operation, the total project's net present value (NPV) can be calculated, which will provide more information

on the economic viability of a floating terminal, than just the net present costs calculation that is now performed.

Moreover, the time period we are looking into is quite short (12 years), shorter than the lifetime of all equipment that we are taking into consideration. The reason for this is that the reliable availability of data is limited to this time period only. This means that no equipment is salvaged or decommissioned due to reaching the end of its lifetime or having a significantly reduced productivity due to aging. If we need to look into a longer time period, the models will need to be adjusted to take this into account as well, and as above, this will produce different optimization results.

Finally, in order to have a more precise sizing of the terminal, more aspects than purely the size of modules as a result of the optimization of logistics needs to be taken into account. One of the more important aspects is the wave and wind effect on the motion of the modules, as the forces created from environmental conditions may prohibit the connection of certain types of modules, or may require the rigid connection of others in order to counteract them.

APPENDIX

Demand scenarios

Scenario A: 6 MTEU platform

We assume that the demand, is known beforehand, as a percentage of the total TEU of the Antwerp port. We assume a container terminal that can handle $6 \cdot 10^6$ TEU. Due to lower dwell times and added infrastructure for storage, we assume that the 6% reefer container split goes straight to the port of Antwerp. That leaves us with $5.64 \cdot 10^6$ TEU/year in total. The ratio of FEU/TEU is 1.5 (60%/40%).

This leads to the following storage capacity:

1-day dwell time = 18193 TEU

3-day dwell time = 54579 TEU

Scenario E: Dynamic growth

A multi-period scenario is developed, where the mobile platform takes up all the expected increase in the Antwerp port (see Table 1 below). This will provide a dynamic design, starting from a small platform that can handle ~500 kTEU and slowly expanding to the size of 6 MTEU by 2030.

Table 1. Forecast of handled TEU in the port of Antwerp until 2030 [1]

Year	Number of TEU	Growth Rate
2017	10,450,900	4.4 %
2018	10,910,740	4.4 %
2019	11,390,812	4.4 %
2020	11,892,008	4.4 %
2021	12,415,256	4.4 %
2022	12,961,527	4.4 %
2023	13,531,835	4.4 %
2024	14,127,235	4.4 %
2025	14,748,834	4.4 %
2026	15,073,308	2.2 %
2027	15,404,921	2.2 %
2028	15,743,829	2.2 %
2029	16,090,193	2.2 %
2030	16,444,178	2.2 %

ACKNOWLEDGMENTS

This project has received funding from the European Union's Horizon 2020 research and innovation programme under grant agreement No 774253. The opinions in this document reflect only the authors' view and in no way reflect the European Commission's opinions. The European Commission is not responsible for any use that may be made of the information it contains.

REFERENCES

- [1] Assbrock G, Ley J, Dafnomilis I. Strategic Logistic Optimisation - Deliverable 9.3. Horizon2020 Space@Sea Project. 2019.
- [2] European Commission (EC). The Ocean of Tomorrow Projects (2010-2013) - Joint Research Forces to Meet Challenges in Ocean Management. 2013. doi:10.2777/34369.
- [3] European Commission (EC). Multi-use of the oceans marine space, offshore and near-shore: Enabling technologies 2016. <https://ec.europa.eu/info/funding-tenders/opportunities/portal/screen/opportunities/topic-details/bg-04-2017> (accessed June 12, 2019).
- [4] Schott DL. Design of transshipment and storage concept for regular port services - Deliverable 9.2. Horizon2020 Space@Sea Project. 2019.
- [5] Achterberg FF. Trends in ship-to-shore container cranes. 2012. doi:2012.TEL.7720.
- [6] Zenzerovic Z, Vilke S, Antonini N. Cost Model in Function of Optimal Capacity Planning of Port Container Terminal 2013:1–13.
- [7] Tran T, Nahavandi S, Reid R. Power demand and energy usage of container crane - Comparison between AC and DC drives. Proc Univ Power Eng Conf 2008. doi:10.1109/UPEC.2008.4651655.
- [8] Wilmsmeier G, Spengler T. Energy consumption and container terminal efficiency. FAL Bull 2016:10.
- [9] Yang YC, Lin CL. Performance analysis of cargo-handling equipment from a green container terminal perspective. Transp Res Part D Transp Environ 2013;23:9–11. doi:10.1016/j.trd.2013.03.009.
- [10] Mbiydzanyuy G. An Optimization Model for Sea Port Equipment Configuration. Blekinge Institute of Technology, 2007. doi:MCS-2006:18.
- [11] Wilmsmeier G, Spengler T. Energy consumption and container terminal efficiency. FAL Bull 2016:10.
- [12] Huang W, Chu C. A selection model for inter-terminal handling systems. J Mar Sci Technol 2004;12:159–70.

Table 1. Equipment and module database

Quay cranes	Costs			Productivity	
Large Automated Ship-to-Shore Cranes (STSS)	<i>Capital:</i> 7.5-8*10 ⁶ EUR [5,6]			60 - 120	TEU/hour
	<i>Operational:</i> 8-8.2 kWh/move [7,8]			30	Moves/hour [9,10]
Small Automated Ship-to-Shore Cranes (STSS)	<i>Capital:</i> 5-5.5*10 ⁶ EUR [5,6]			40 - 80	TEU/hour
	<i>Operational:</i> 6-6.2 kWh/move [7,11]			20	Moves/hour [9,10]
Rail mounted gantry cranes (RMGs)	<i>Capital:</i> 3-3.5*10 ⁶ EUR [12]			50 - 100	TEU/hour
	<i>Operational:</i> 5.5-6 kWh/move [12]			25	Moves/hour [9]
				Storage capacity [TEU]	
Modules	Side [m]	Area [m ²]	Max TEU slots	3 stack	5 stack
Module, 1 RMG	45	2025	90	216	360
Module, 2 RMG	90	8100	360	756	1260

Table 2. Terminal logistics, scenario E, all cases

Year	Container throughput [TEU]	Terminal size [m ²]			
		1 DS 3 SH	1 DS 5 SH	3 DS 3 SH	3 DS 5 SH
2019	480072	24300	18225	52650	34425
2020	981268	44550	32400	103275	68850
2021	1504516	68850	50625	159975	105300
2022	2050787	91125	66825	214650	141750
2023	2621095	117450	85050	275400	180225
2024	3216495	147825	107325	342225	224775
2025	3838094	174150	127575	405000	267300
2026	4162568	190350	139725	441450	289575
2027	4494181	206550	151875	477900	313875
2028	4833089	224775	166050	516375	340200
2029	5179453	240975	178200	554850	366525
2030	5533438	259200	192375	593325	392850
Total terminal costs [10 ⁶ €]		422.27	332.54	873.71	601.62
Total capital costs [10 ⁶ €]		344.7	269.01	721.76	495.35
Total operational costs [10 ⁶ €]		15.1	15.1	20.03	16.11
Total maintenance costs [10 ⁶ €]		62.45	48.41	131.91	90.15

Table 3. Equipment and module selection and utilization, scenario A, 1 day dwell time, 3 containers stacking height

Terminal operation	Module type	Equipment	Units		Utilization [TEU/y]
			Equipment	Modules	
Unloading	45m * 2	STS cranes, single spreader	1	2	164160
	45m *2	STS cranes, double spreader	8	16	5475840
Storage	45m	RMG cranes, single spreader	60	60	3274839
	45m	RMG cranes, double spreader	21	21	2292386
	90m	RMG cranes, single spreader	2	1	72775
Loading	45m	STS cranes, single spreader	1	1	164160
	45m	STS cranes, double spreader	12	12	5475840

Table 4. Terminal logistics, scenario A, all cases

	1 DS 3 SH	1 DS 5 SH	3 DS 3 SH	3 DS 5 SH
Total annual costs [10^6 €]	57.41	44.86	127.27	84.01
<i>Annual capital costs</i>	42.51	33.27	94.69	62.26
<i>Annual operational costs</i>	2.66	2.53	2.39	2.72
<i>Annual maintenance costs</i>	12.24	9.06	30.2	19.04
Costs/TEU [€]	10.18	7.95	22.57	14.9
Containers handled	3.525* 10^6			
<i>20ft containers</i>	1.41* 10^6			
<i>40ft containers</i>	2.115* 10^6			
Costs/container [€/unit]	16.29	12.73	36.11	23.83
Barges serviced hinterland side				
<i>Annual basis</i>	7684			
<i>Daily basis</i>	25			
Terminal size [m^2]	234900	166050	645975	394875
Quay length [m]				
<i>Unloading quay</i>	810			
<i>Loading quay</i>	585			

AUTHORS INDEX

Anders M.	17	Hinckeldeyn J.	7	Qiu J.	65
Andruszko J.	141	Hladnik J.	99, 157	Radoičić G.	45, 203
Angleitner K.	275	Hliš T.	245	Ramprecht P.	267
Arsić A.	183	Hofmann M.	217	Richter C.	1
Arsić M.	117, 161	Jerman B.	99, 157	Rief J.	197
Assbrock G.	299	Jojić T.	147	Riester M.	267
Baucal S.	35	Jokić V.	35	Rohde M.	229
Beinke T.	229	Jovanović M.	45, 203	Rupnik B.	245, 251
Bizjak L.	99, 157	Kaczor G.	135	Rücker A.	197
Blagojević B.	203	Kamps R.	1	Savić Z.	161
Bojić S.	293	Karliński J.	151	Savković M.	59
Bona M.	127	Kartnig G.	105, 165, 169	Schloz F.	209
Bošnjak S.	117, 175, 187	Katterfeld A.	1	Schmidt T.	87
Braun P.	7	Kleeberger M.	69	Schott D. L.	299
Bulatović S.	161	Kondralis F.	39	Schulz R.	209
Burić M.	35	Košanin N.	183	Schyga J.	7
Cajner H.	271	Kovačić M.	245, 251	Sekulić A.	35
Dafnomilis I.	299	Kreutzfeldt J.	7	Servos N.	223
Dentsoras A. J.	39	Kriehn T.	209	Sihn W.	263, 267
Dragović B.	285	Kutsuna A.	257	Solazzi L.	75, 81
Duinkerken M. B.	299	Kužnar M.	135, 239	Stefanović A.	175, 187
Dukić G.	271	Landschützer C.	235	Steiner W.	275
Działak P.	151	Lerher T.	23, 239, 245, 251	Stölzner M.	69
Đorđević M.	111	Ley J.	299	Supej M.	157
Đokić R.	147	Liu E.	51	Šarkočević Ž.	161
Ecker C.	263	Lorenc A.	135, 239	Štor M.	251
Egger M.	275	Lučić M.	35	Tang X.Y.	51, 123
Eiwan C.	17	Lüdemann L.	127	Tao J.	55
El Naggar M.	279	Marković G.	59	Teucke M.	223
Ernits R.M.	229	Marolt J.	245, 251	Tong Y.	65
Fahiem A.	279	Maximow I.	31	Tselentis V.	285
Fittinghoff M.	209	Milenović I.	117, 175, 187	Vladić J.	147
Fottner J.	69, 197	Milić P.	45	Vodičar J.	157
Freitag M.	223, 229	Milojević G.	111	Vojinović M.	203
Gajić A.	147	Mitterlehner T.	165	Vujičić A.	111
Gajsek B.	271	Mladenović M.	161	Wei D.X.	123
Gašić M.	59	Moczko P.	141	Wei Z.	257
Gašić V.	183	Müller T.	87	Weise S.	31
Georgijević M.	293	Nishimura E.	257	Wen X.	123
Gnjatović N.	117, 175, 187	Novak G.	17	Wu F.	51
Golder M.	17, 31, 127	Opetuk T.	271	Xu H.	51
Grabulov V.	117	Orlandić R.	285	Yang Y.Q.	123
Guangjun L.	55	Ouyang W.	65	Urošević M.	175, 293
Günthner W.A.	69	Ortner-Pichler A.	235	Zdravković N.	59
Haber A.	169	Olszyna G.	183	Zeyu D.	55
Haider M.	165	Paladin Z.	285	Zrnić N.	111, 285, 293
Hailei R.	55	Pascher R.	263		
Hamdy Elwany M.	279	Paulschin F.	105		
Hassan O.	279	Pavlović N.	45		
Helbig M.	31	Pavlović G.	59		
Hilbrich S.	7	Perazić K.	285		
		Pietrusiak D.	141		



FULLY AUTOMATED WAREHOUSING

STACKER CRANES • CONVEYOR SYSTEMS • SOFTWARE •
ADDITIONAL SERVICES • SERVICE • RETROFIT

LTW Intralogistics GmbH
Achstrasse 53, 6922 Wolfurt
www.LTW.at

A Doppelmayr-group company

LTW
INTRALOGISTICS

ISBN: 978-86-6060-020-4



9 788660 600204